

AD _____

Award Number: DAMD17-02-2-0025

TITLE: Cholinesterase Structure: Identification of Mechanisms and Residues Involved
in Organophosphate Inhibition and Enzyme Reactivation

PRINCIPAL INVESTIGATOR: Palmer W. Taylor, Ph.D.

CONTRACTING ORGANIZATION: The University of California
La Jolla, CA 92093-0934

REPORT DATE: May 2005

TYPE OF REPORT: Final

PREPARED FOR: U.S. Army Medical Research and Materiel Command
Fort Detrick, Maryland 21702-5012

DISTRIBUTION STATEMENT: Approved for Public Release;
Distribution Unlimited

The views, opinions and/or findings contained in this report are those of the author(s) and should not be construed as an official Department of the Army position, policy or decision unless so designated by other documentation.

20060110 120

REPORT DOCUMENTATION PAGEForm Approved
OMB No. 0704-0188

Public reporting burden for this collection of information is estimated to average 1 hour per response, including the time for reviewing instructions, searching existing data sources, gathering and maintaining the data needed, and completing and reviewing this collection of information. Send comments regarding this burden estimate or any other aspect of this collection of information, including suggestions for reducing this burden to Department of Defense, Washington Headquarters Services, Directorate for Information Operations and Reports (0704-0188), 1215 Jefferson Davis Highway, Suite 1204, Arlington, VA 22202-4302. Respondents should be aware that notwithstanding any other provision of law, no person shall be subject to any penalty for failing to comply with a collection of information if it does not display a currently valid OMB control number. **PLEASE DO NOT RETURN YOUR FORM TO THE ABOVE ADDRESS.**

1. REPORT DATE (DD-MM-YYYY) 01-05-2005		2. REPORT TYPE Final		3. DATES COVERED (From - To) 15 Apr 2002 – 14 Apr 2005	
4. TITLE AND SUBTITLE Cholinesterase Structure: Identification of Mechanisms and Residues Involved in Organophosphate Inhibition and Enzyme Reactivation				5a. CONTRACT NUMBER	
				5b. GRANT NUMBER DAMD17-02-2-0025	
				5c. PROGRAM ELEMENT NUMBER	
6. AUTHOR(S) Palmer W. Taylor, Ph.D. E-mail: pwtaylor@ucsd.edu				5d. PROJECT NUMBER	
				5e. TASK NUMBER	
				5f. WORK UNIT NUMBER	
7. PERFORMING ORGANIZATION NAME(S) AND ADDRESS(ES) The University of California La Jolla, CA 92093-0934				8. PERFORMING ORGANIZATION REPORT NUMBER	
9. SPONSORING / MONITORING AGENCY NAME(S) AND ADDRESS(ES) U.S. Army Medical Research and Materiel Command Fort Detrick, Maryland 21702-5012				10. SPONSOR/MONITOR'S ACRONYM(S)	
				11. SPONSOR/MONITOR'S REPORT NUMBER(S)	
12. DISTRIBUTION / AVAILABILITY STATEMENT Approved for Public Release; Distribution Unlimited					
13. SUPPLEMENTARY NOTES					
14. ABSTRACT Studies on the structural of acetylcholinesterase (AChE) as a target of organophosphate toxicity continue and have yielded several leads of significance and practical outcomes. First, studies on oxime reactivation reveal the importance of achieving a suitable angle of attack for the oxime within the confines of the active center gorge. Through the use of mutant AChE-oxime combinations, oxime-assisted catalytic turnover of organophosphates can be achieved such that mutant AChE can be employed with oximes as a catalytic scavenger. Second, through cysteine substitution mutagenesis and acrylodan labeling we have developed a fluorescent enzyme whose emission spectrum changes upon conjugation with organophosphate. These enzymes are now being immobilized and developed as remote sensors for AChE inhibition. Third, we have developed mass spectrometry methods to detect directly the organophosphate conjugates with AChE. Lastly, we have developed several transgenic (knock-out) animal strains that enable us to study the roles cholinesterase inhibition centrally and in the periphery play in organophosphate toxicity and whether the antidotal actions of oximes arise solely through reactivation.					
15. SUBJECT TERMS acetylcholinesterase, nerve agent antidotes and prophylaxis, organophosphate scavenging , oxime reactivation fluorescence spectroscopy, exposure detection					
16. SECURITY CLASSIFICATION OF:			17. LIMITATION OF ABSTRACT UU	18. NUMBER OF PAGES 166	19a. NAME OF RESPONSIBLE PERSON USAMRMC
a. REPORT U	b. ABSTRACT U	c. THIS PAGE U			19b. TELEPHONE NUMBER (include area code)

Table of Contents

Cover.....	1
SF 298.....	2
Table of Contents.....	3
Introduction.....	4
Body.....	4 - 19
Key Research Accomplishments.....	19
Reportable Outcomes.....	20
Conclusions.....	20
References.....	20 - 21
Appendices.....	22-166

INTRODUCTION

Our overall objective of understanding the structure and function of acetylcholinesterase (AChE) as the target of organophosphate poisoning remains the same. This approach has several positive outcomes. First, AChE can be modified in its structure such that when the mutant enzyme is combined with oximes *in vitro*, it becomes a catalytic scavenger of organophosphates. Second, acrylodan or other fluorophore modification of AChE yields a fluorescent conjugate that can be used as a remote sensor for organophosphate exposure. Third, AChE conjugates can be detected directly by MALDI mass spectrometry, enabling us to characterize organophosphate exposure directly through detection of the conjugate, rather than indirectly through reduction of catalytic activity. Fourth, transgenic animal strains have been developed that should enable us to examine further the central or peripheral loci of organophosphate toxicity and understand the mechanism of action of oxime antidotes. Fifth, in new experiments we are employing a novel chemistry to synthesize oximes that cross the blood-brain barrier and have greater selectivity as antidotes. Sixth, the combination of these new approaches to the AChE oxime field has spawned new approaches for therapy for the organophosphates more refractory to antidotal therapy.

As an overarching theme, we have modified the very target of organophosphate toxicity so that the target becomes beneficial in scavenging (oxime-assisted catalytic turnover of organophosphates), the target can be used for organophosphate detection (fluorescently conjugated AChE and mass spectrometric characterization of the organophosphate conjugates), and the target in the animal through homologous recombination (AChE knock-out mice) becomes a means for ascertaining the tissue origins of toxicity.

BODY

The individual areas in which progress has been made are enumerated below.

1. *Development of an Oxime-Mutant Acetylcholinesterase System for Catalytic Scavenging of Organophosphates.* In the last project period, we presented detailed kinetics on the rates of inactivation by cycloheptyl, isopropyl and 3,3-dimethylbutyl methylphosphonyl thioesters and the reactivation of the conjugates by two oximes, 2-PAM and HI-6. Reactivation studies showed the following:
 - a. Efficient reactivation requires a phosphonate orientation where the phosphonyl (phosphoryl) oxygen is in the oxyanion hole. Hence, those S_p enantiomers that are the most reactive and toxic are also the ones most susceptible to reactivation (1).
 - b. The narrow confines of the gorge ensure that the conjugated organophosphate is sterically impacted at its base where the active center serine and conjugated organophosphate reside. Hence, the efficiency of the reactivation reaction is limited by the angle of access of the oxime to the phosphonyl phosphorus (1,2).
 - c. Opening the gorge dimensions within prescribed limits enhances the rate of reactivation by the oxime. Each oxime has slightly different attack directions, hence the mutations that enlarge gorge dimensions have a differential effect on reactivation. Thus, reactivation efficiency depends on: the organophosphate structure, the structure of the attacking oxime, and the enzyme template (2,3).

- d. Optimization of the reaction, to date, has yielded a 120-fold increase in reactivation rate for the more bulky cycloheptyl methylphosphono-AChE conjugate. Enhancement rates are not as large for the isopropyl- and the 3,3dimethylbutyl methyl phosphonate conjugates (1-3).
- e. In several cases, we have been able to deconstruct the overall catalytic rate, k_r , into an apparent dissociation constant, K_{ox} , a maximal rate for reactivation, k_{+2} .
- f. Structural determinants and gorge dimensions influencing reactivation of various organophosphate conjugates by 2-Pam and HI-6 have been analyzed.

Data described in items *a* through *e* are found in Tables 1 through 6.

Table 1: Reactivation of Recombinant DNA-Derived Mouse Cholinesterases Phosphonylated with *S*_P-Cycloheptyl Methylphosphonyl Thiocholine^a

reactivator (mM)	enzyme	k_{+2} (min ⁻¹)	K_{ox} (mM)	k_r (min ⁻¹ M ⁻¹)	% react _{max}	time
HI-6 (0.2-20)	AChE wt	0.60 ± 0.04	5.4 ± 0.8	112 ± 19	90	5 min
HI-6 (0.02-0.5)	Y337A			2000 ± 90	80	1 min
HI-6 (0.002-0.1)	F295L/Y337A			13180 ± 1414	80	3 min
HI-6 (0.01-5)	F297I/Y337A	6.0 ± 0.5	2.6 ± 0.4	2300 ± 400	100	1 min
HI-6 (0.2-10)	Y337A/F338A	0.051 ± 0.003	0.50 ± 0.12	102 ± 26	80	30 min
HI-6 (10)	F295L/F297I/Y337A ^b			≥24	80	20 min
HI-6 (1, 30)	BChE wt				<10	48 h
2-PAM (1-20)	AChE wt	0.0040 ± 0.0007	6.1 ± 3.0	0.66 ± 0.34	70	15 h
2-PAM (0.1-40)	Y337A	0.0025 ± 0.0001	0.62 ± 0.14	4.1 ± 1.0	80	5 h
2-PAM (0.4-20)	F295L/Y337A	0.016 ± 0.003	10 ± 3	1.7 ± 0.5	70	3 h
2-PAM (2-30)	F297I/Y337A	0.018 ± 0.002	2.7 ± 1.2	6.9 ± 3.3	70	2 h
2-PAM (1-60)	Y337A/F338A	0.00035 ± 0.00002	0.75 ± 0.45	0.47 ± 0.29	40	25 h
2-PAM (40)	F295L/F297I/Y337A ^b			≥0.12	100	5 h
2-PAM (5, 40)	BChE wt				<5	48 h

^a Constants (±standard errors) are calculated from k_{obs} constants (8-16 values) obtained in two to seven experiments. The maximal percent of reactivation (% react_{max}) measured within the specified time of the experiment is also given. ^b Only one k_{obs} was determined (0.24 ± 0.04 min⁻¹ with HI-6 and 0.0048 ± 0.0011 min⁻¹ with 2-PAM).

Table 3: Reactivation of Recombinant DNA-Derived Mouse Cholinesterases Phosphonylated with *S*_P-Isopropyl Methylphosphonyl Thiocholine^a

reactivator (mM)	enzyme	k_{+2} (min ⁻¹)	K_{ox} (mM)	k_r (min ⁻¹ M ⁻¹)	% react _{max}	time (min)
HI-6 (0.05-1)	AChE wt	0.20 ± 0.03	0.15 ± 0.09	1330 ± 780	90	10
HI-6 (0.2-20)	Y337A	1.13 ± 0.08	4.7 ± 0.8	240 ± 47	100	2
HI-6 (0.5-30)	F295L/Y337A	0.27 ± 0.01	0.37 ± 0.09	730 ± 180	80	10
HI-6 (0.05-1)	F297I/Y337A	0.95 ± 0.13	0.41 ± 0.14	2330 ± 844	100	5
HI-6 (1-20)	Y337A/F338A	0.26 ± 0.02	1.5 ± 0.6	178 ± 74	90	15
HI-6 (0.05-5)	BChE wt	0.014 ± 0.001	0.064 ± 0.024	215 ± 70	80	90
2-PAM (0.1-10)	AChE wt	0.095 ± 0.013	0.088 ± 0.075	1080 ± 940	100	30
2-PAM (0.2-40)	Y337A	0.21 ± 0.01	2.6 ± 0.3	82 ± 11	80	20
2-PAM (1-40)	F295L/Y337A			3.5 ± 0.4	90	30
2-PAM (0.1-40)	F297I/Y337A	2.9 ± 0.2	5.5 ± 1.3	534 ± 133	90	1
2-PAM (1-40)	Y337A/F338A	0.072 ± 0.004	1.5 ± 0.5	46 ± 14	90	30
2-PAM (0.05-10)	BChE wt	2.98 ± 0.01	2.39 ± 0.02	1250 ± 9	90	1

^a Constants (±standard errors) are calculated from k_{obs} constants (6-19 values) obtained in two to five experiments. The maximal percent of reactivation (% react_{max}) measured within the specified time of the experiment is also given.

These studies continue, and we have examined whether aging affects the reactivation rates for these methylphosphonates. We find that it does not, and we have also found that spontaneous hydrolysis of the phosphonate conjugated enzyme is slow relative to oxime induced reactivation (1-3). Some of the R_p compounds are extremely resistant to reactivation, (cf: Tables 4-6) and we have begun to examine structure-activity relationships for achieving more rapid reactivation. Similar considerations apply to tabun and related phosphoramidates, as well as the non-volatile VX compounds. Currently, we are studying reactivation of a tabun modified enzyme, but have yet to develop a complete structure-activity profile.

Table 4: Reactivation of Recombinant DNA-Derived Mouse Cholinesterases Phosphonylated with R_P -Cycloheptyl Methylphosphonyl Thiocholine^a

reactivator (mM)	enzyme	k_{+2} (min ⁻¹)	K_{ox} (mM)	k_r (min ⁻¹ M ⁻¹)	% react _{max}	time (h)
HI-6 (1, 40)	AChE wt				<15	50
HI-6 (0.3-20)	Y337A	0.00042 ± 0.00002	1.0 ± 0.2	0.41 ± 0.06	50	85
HI-6 (1-30)	F295L/Y337A				<25	40
HI-6 (10-40)	F297I/Y337A				<25	72
HI-6 (0.2-2)	Y337A/F338A				<15	40
HI-6 (10-30)	BChE wt				<15	50
2-PAM (1, 40)	AChE wt				<25	50
2-PAM (0.3-5)	Y337A	0.00047 ± 0.00004	0.36 ± 0.16	1.3 ± 0.6	50	85
2-PAM (20-40)	F295L/Y337A				<25	40
2-PAM (5-40)	F297I/Y337A				<40	60
2-PAM (0.3-5)	Y337A/F338A	0.00040 ± 0.00010	0.99 ± 0.87	0.40 ± 0.37	40	20
2-PAM (20-40)	BChE wt			0.027 ± 0.001	70	25

^a Constants (±standard errors) are calculated from k_{obs} constants (4-8 values) obtained in one to three experiments. The maximal percent of reactivation (% react_{max}) measured within the specified time of the experiment is also given.

Table 5: Reactivation of Recombinant DNA-Derived Mouse Cholinesterases Phosphonylated with R_P -3,3-Dimethylbutyl Methylphosphonyl Thiocholine^a

reactivator (mM)	enzyme	k_{+2} (min ⁻¹)	K_{ox} (mM)	k_r (min ⁻¹ M ⁻¹)	% react _{max}	time (h)
HI-6 (0.2-2)	AChE wt				<15	40
HI-6 (0.2-40)	Y337A	0.00040 ± 0.00002	0.54 ± 0.14	0.74 ± 0.19	70	35
HI-6 (1,10)	F295L/Y337A				<25	60
HI-6 (10-40)	F297I/Y337A				<25	60
HI-6 (0.2-2)	Y337A/F338A	0.00014 ± 0.00001	0.076 ± 0.051	1.8 ± 1.2	50	40
HI-6 (1-10)	BChE wt				<25	50

2-PAM (0.3-5)	AChE wt				<15	40
2-PAM (0.5-5)	Y337A	0.0007 ± 0.0000	0.38 ± 0.08	1.8 ± 0.4	60	35
2-PAM (5, 30)	F295L/Y337A				<25	60
2-PAM (20-60)	F297I/Y337A				<25	60
2-PAM (0.3-5)	Y337A/F338A				<15	60
2-PAM (3-30)	BChE wt	0.0079 ± 0.0011	13 ± 4	0.62 ± 0.22	80	20

^a Constants (\pm standard errors) are calculated from k_{obs} constants (4-8 values) obtained in one or two experiments. The maximal percent of reactivation (% react_{max}) measured within the specified time of the experiment is also given.

Table 6: Reactivation of Recombinant DNA-Derived Mouse Cholinesterases Phosphonylated with *R*_p-Isopropyl Methylphosphonyl Thiocholine^a

reactivator (mM)	enzyme	k_{+2} (min ⁻¹)	K_{ox} (mM)	k_r (min ⁻¹ M ⁻¹)	% react _{max}	time (h)
HI-6 (0.2-40)	AChE wt	0.0075 ± 0.0003	4.3 ± 0.7	1.7 ± 0.3	70	10
HI-6 (0.2-30)	Y337A	0.0071 ± 0.0004	0.97 ± 0.23	7.3 ± 1.8	80	8
HI-6 (1-30)	F295L/Y337A	0.0013 ± 0.0001	0.95 ± 0.56	1.3 ± 0.8	70	16
HI-6 (5-40)	F297I/Y337A	0.0021 ± 0.0003	16 ± 8	0.13 ± 0.07	50	16
HI-6 (1-30)	BChE wt	0.00035 ± 0.00004	1.1 ± 0.9	0.23 ± 0.25	40	25
2-PAM (0.3-40)	AChE wt	0.0029 ± 0.0004	1.9 ± 1.1	1.5 ± 0.9	70	20
2-PAM (0.3-40)	Y337A	0.0026 ± 0.0001	0.60 ± 0.21	4.3 ± 1.5	80	8
2-PAM (5-30)	F295L/Y337A	0.0096 ± 0.0039	10 ± 11	0.95 ± 1.09	80	10
2-PAM (5-60)	F297I/Y337A			0.041 ± 0.003	100	25
2-PAM (5-30)	BChE wt	0.024 ± 0.006	27 ± 13	0.88 ± 0.47	100	4

^a Constants (\pm standard errors) are calculated from k_{obs} constants (6-10 values) obtained in two to four experiments. The maximal percent of reactivation (% react_{max}) measured within the specified time of the experiment is also given.

We have also noted that excessive enlargement of the active center gorge, such as is seen for butyrylcholinesterase, actually reduces oxime efficiency for reactivation. A more vacuous gorge may yield a condition where the conjugated phosphate may be buried in a crevice within the gorge and hence not accessible to the attacking oxime. Accordingly, precise predictions on how to enhance further reactivation rates may be problematic. Accordingly, we have taken our best double mutant, Y295L-Y337A, and developed a continuous colorimetric assay for oxime turnover using the substituted alkyl methylphosphonothiocholines as reacting ligands. Turnover yields the corresponding thiocholine that can be reacted with dithiodinitrobenzoate to form a yellow color. In figure 1, we examine the hydrolytic rate of one of the mutant enzymes. This assay has enabled us to measure the pH dependence and the catalytic parameters of oxime-assisted organophosphate hydrolysis. The kinetics reveal that the reaction is rate limited by oxime mediated dephosphorylation of the serine rather than the phosphorylation step. Thus, a suitable continuous assay applicable to multiwell, high throughput endeavors is now available for selecting mutants with enhanced organophosphate hydrolysis capacity. A mutant selection strategy has been devised, but the study has yet to be undertaken. The starting point is the corresponding mutations in human AChE.

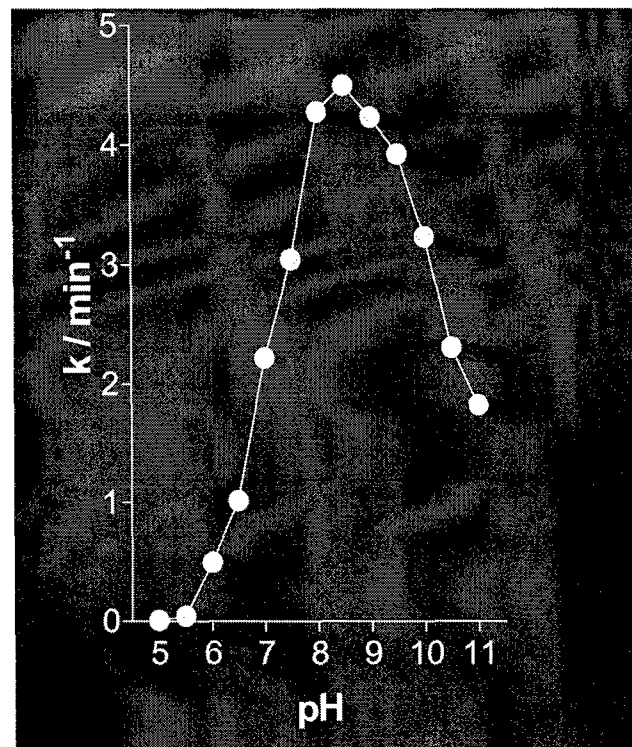
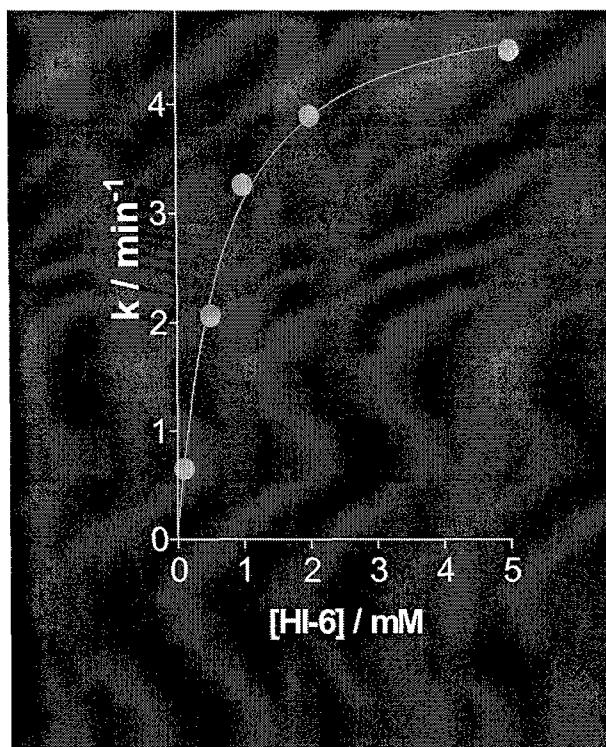
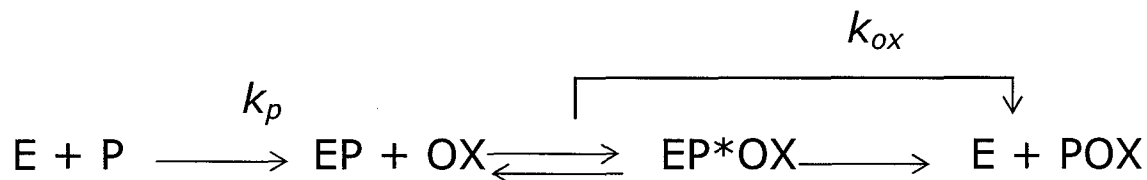
Future studies with human AChE conjugates carry the advantage that immunologic cross reactivity would be minimized. Thus, we have prepared F295L, F297I, Y337A as single mutants with the human enzyme and F295L/Y337A and F297I/Y337A as double mutants. These would be starting points in a mutation selection scheme for enhancing oxime assisted catalysis.

Table 2: Reactivation of Recombinant DNA-Derived Mouse Cholinesterases Phosphonylated with Sp-3,3-Dimethylbutyl Methylphosphonyl Thiocholine^a

reactivator (mM)	enzyme	k_{+2} (min ⁻¹)	K_{ox} (mM)	k_r (min ⁻¹ M ⁻¹)	% react _{max}	time
HI-6 (0.05-5)	AChE wt	0.39 ± 0.09	3.8 ± 1.8	102 ± 53	80	10 min
HI-6 (0.05-5)	Y337A	3.2 ± 0.5	2.8 ± 1.0	1200 ± 490	100	2 min
HI-6 (0.01-1)	F295L/Y337A			1300 ± 60	100	2 min
HI-6 (0.01-10)	F297I/Y337A	1.4 ± 0.1	1.9 ± 0.5	720 ± 180	100	5 min
HI-6 (1-40)	Y337A/F338A	0.10 ± 0.01	2.1 ± 1.2	47 ± 28	80	20 min
HI-6 (10)	F295L/F297I/Y337A ^b			≥31	80	10 min
HI-6 (0.5-20)	BChE wt	0.73 ± 0.14	7.1 ± 3.2	103 ± 51	100	10 min
2-PAM (1-40)	AChE wt			0.18 ± 0.01	90	8 h
2-PAM (5-40)	Y337A			0.041 ± 0.003	80	33 h
2-PAM (0.5-40)	F295L/Y337A	0.0018 ± 0.0002	2.8 ± 1.1	0.66 ± 0.27	90	25 h
2-PAM (10-60)	F297I/Y337A	0.0025 ± 0.0002	9.0 ± 3.6	0.27 ± 0.11	80	15 h
2-PAM (5-60)	Y337A/F338A	0.00023 ± 0.00001	0.54 ± 0.85	0.42 ± 0.65	60	70 h
2-PAM (40)	F295L/F297I/Y337A ^b			≥0.22	90	6 h
2-PAM (3-30)	BChE wt	0.028 ± 0.003	3.2 ± 1.7	8.7 ± 4.6	100	3 h

^a Constants (±standard errors) are calculated from k_{obs} constants (5-15 values) obtained in two to four experiments. The maximal percent of reactivation (% react_{max}) measured within the specified time of the experiment is also given.^b Only one k_{obs} was determined (0.31 ± 0.06 min⁻¹ with HI-6 and 0.0088 ± 0.0021 min⁻¹ with 2-PAM).

**Rate Constant (*k*) of *S*_P-Cycloheptyl Methylphosphonyl Thiocholine
Hydrolysis by mAChE Mutant F295L/Y337A^{Taylor, Palmer}**



F295L/Y337A

[HI-6] / mM	<i>k</i> [*] / min ⁻¹
0.1	0.65
0.5	2.1
1	3.3
2	3.9
5	4.5

*0.5 μM Enzyme
20 μM S-CHMPTCh
100 mM Phosphate Buffer pH 7.4

1 mM HI-6	F295L/Y337A	Y337A	F297I/Y337A	AChE w.t.
<i>k</i> [*] / min ⁻¹	3.3	0.69	0.34	0.15

Fig. 1: pH Dependence and Oxime Concentration Dependence for Cycloheptyl
Methylphosphonylthiocholine Hydrolysis in the Presence of HI-6.

2. *Studies with a Fluorescently Modified Acetylcholinesterase to Examine Conformation and Molecular Fluctuations in Enzyme Structure.* In the last project period, we showed that cysteine substitution mutagenesis at residues 81 and 84 followed by acrylodan labeling at these positions resulted in a fluorescent enzyme where excitation at 380nm yielded an emission peak residing between 470 and 525nm. The emission spectrum of acrylodan is very sensitive to its immediate dielectric constant. Thus, the immediate microenvironment around this introduced side chain can be ascertained. Several positions at the rim and just within the active center gorge and around the outside of the molecule were labeled (4, 5). Residues within the gorge and near its rim where ligands bind show a decrease in dielectric constant as would be expected from the ligand excluding the H₂O molecules upon binding. What was more surprising are the residues on the outer edge of the omega loop, residue 84, at some distance from the binding site showed a red shift to longer wavelength with the binding of ligands. This change in fluorescence results from the acrylodan side chain becoming exposed to solvent upon ligand binding. We interpret this to result from the omega loop closing down on the bound ligand, increasing the curvature on the outer portion of the loop and causing the side chain to move into the solvent. Some plasticity of the omega loop must exist and is reflected in the emission changes seen at residue 81 where the S_p-organophosphates and the reversibly bound ligand show the typical red shift to longer wavelength, whereas the R_p compounds, when conjugated, cause a blue shift. The differences between enantiomers depend on whether the organophosphate can fit into the oxyanion hole; the bulky R_p compounds do not allow such a fit. If this fit does not occur, then the acyl pocket and base gorge structure are perturbed resulting in a distinctive positioning of the acrylodan at residue 81. (Figs. 2 and 3).

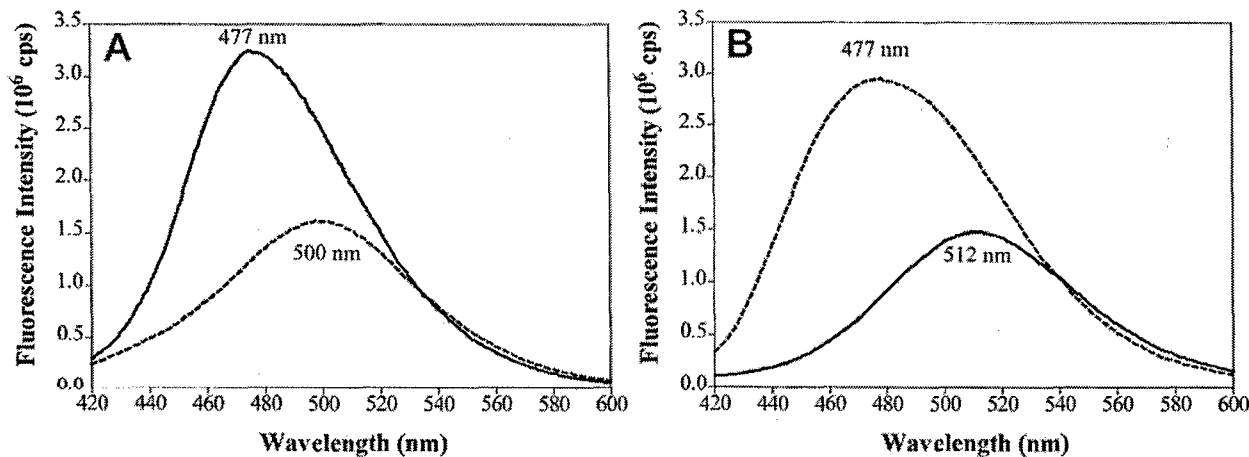


Fig. 2. Fluorescence emission spectra of acrylodan-labeled Y124C (*A*) and E84C (*B*) AChE free in solution (*dashed line*) and complexed with fasciculin (*solid line*). *A*, for acrylodan-labeled Y124C, fasciculin produces a hypsochromic shift and enhancement of fluorescence quantum yield. The large shift for Y124C reveals a clear isoemissive point indicative of the two (free and fasciculin bound) species. Equivalent concentrations of enzyme (215 nM) were present for all conditions. The concentration of fasciculin was 215 nM. *B*, for acrylodan labeled E84C fasciculin produces a bathochromic shift and reduction of fluorescence quantum yield. Equivalent concentrations of enzyme (270 nM) were present for all conditions. The concentration of fasciculin was 800 nM.

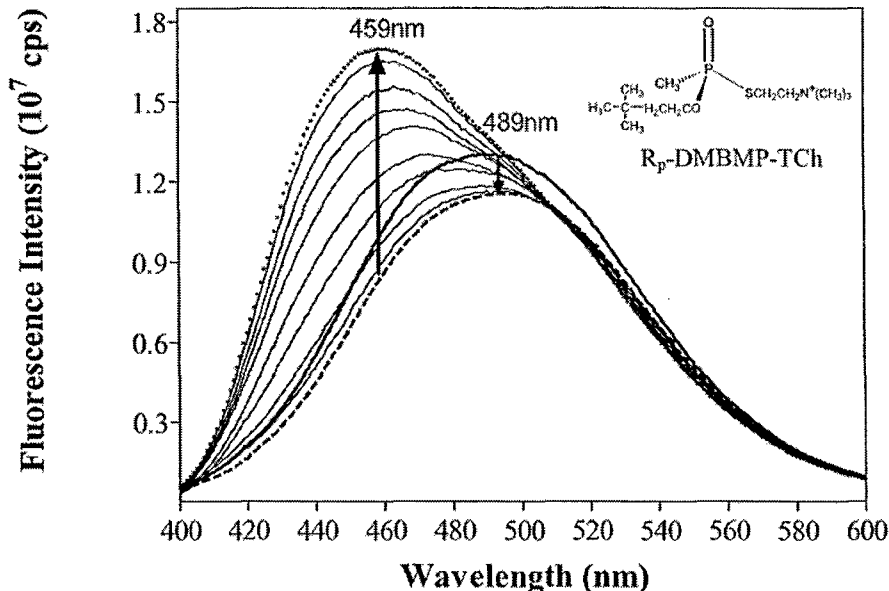


Fig. 3. Fluorescence emission spectra of acrylodan-labeled E81C AChE following addition of (*R_p*)-dimethylbutyl methylphosphonothiocholine (*R_p*-DMBMP-TCh). We observed a reduction in quantum yield immediately following addition of (*R_p*)-DMBMP-TCh, followed by a progressive hypsochromic shift and enhancement in quantum yield. Equivalent concentrations of enzyme (300 nM) were present for all measurements. A stoichiometric amount of (*R_p*)-DMBMP-TCh (340 nM) was added, and fluorescence spectrum was taken at following time points: 0, 1, 2, 8, 20, 53, 74, 89, 100, 115, and 150 min. The large shift for E81C reveals a isoemissive point at 510 nm, indicative of two (reversible DMBMP-TCh ... AChE complex and conjugated DMBMP-AChE) discrete species in the progressive reaction. Acrylodan-labeled E81C AChE free in solution (*solid line*), reversibly bound with (*R_p*)-DMBMP-TCh (*dashed line*), and covalently conjugated DMBMP-AChE (*dotted line*). (*R_p*)-DMBMP-AChE yields an emission maximum of 459 nm, a difference of 30 nm from the (*S_p*)-DMBMP-AChE

The practical outcome of these studies is that the Cys81 and Cys84 conjugated acrylodans then can report on the exposure to organophosphate by the wavelength shift. Moreover, if the 81 residue is mutated and conjugated, the enzyme can distinguish between *S_p* and *R_p* methylphosphonates and between the phosphorates that have a dimethoxy moiety (malathion, metrifonate, methylparathion-oxon, DDVP) and those that have a diethoxy or larger moiety (paraoxon, diisopropylfluorophosphate). The *S_p* methylphosphonates and methoxyphosphorates produce a red shift, while the *R_p* methylphosphonates and the ethoxy and larger phosphorates produce a blue shift. The direction of the shift depends on whether the acyl pocket on the enzyme is perturbed.

These studies over the past 18 months have been followed up using fluorescence lifetime analysis and decay of fluorescence anisotropy (5-7). These studies reveal two important points. First, differences in molecular motional fluctuations can be mapped at the various sites in the molecule as torsional, segmental and global motion. Second, the active center gorge exists in a dynamic equilibrium with rapid opening and closing of the gorge presumably on a nanosecond to picosecond time frame. This time frame is short relative to the diffusional translation time of the diffusing ligand.

Current efforts are devoted to examining other residues on the non-omega loop side of the gorge, residues 341 and neighbors, that reveal fluctuations in structure around the gorge rim. These studies were initiated by Leo Pezzementi, a sabbatical visitor from Alabama and are continuing in the laboratory (8). Here again, we notice considerable fluctuations in this region with diminished motion as we descend into the gorge base. A second set of studies examines omega loop conformation when the active center serine has been removed or the histidine in the catalytic triad has been replaced by a isoleucine. Since substrate hydrolysis is obviated, this approach has enabled us to distinguish perturbations of structure involving the formation of the initial complex and formation of the covalent conjugate.

As an aside, we found through these methods that the trifluoroacetophenones that form a hemiketal linkage with the active site serine do not require the complete catalytic triad. Isoleucine can be substituted for histidine 447 and a hemiketal conjugate forms with *m*-trimethylammonio trifluoroacetophenone, whereas the same mutant enzyme will not form conjugates with organophosphates and catalyze ester hydrolysis. These data tend to alter ones view on the importance of the catalytic triad, Glu 337, His 447 and Ser 203, in rendering the serine nucleophilic relative to the polarization induced by insertion of the keto oxygen moiety into the oxyanion hole.

Current endeavors are directed to using the fluorescent enzymes in a remote sensing device to detect organophosphate exposure. The approach has a three-fold advantage. First, detection of organophosphate inhibition of enzyme activity depends on the reduction from full or endogenous AChE activity, and full activity is subject to considerable biological variation between individuals and over time. Hence, 10 to even 30% differences in activity cannot necessarily be ascribed to organophosphate inhibition. On the other hand, measurement of the actual organophosphate conjugate by the wavelength shift and wavelength ratio is easier to detect as a significant change relative to exposure. Second, the use of the fluorescent enzyme is the very target of organophosphate toxicity and far less susceptible to false inhibition seen with simple colorimetric or fluorometric compounds. Third, detection does not require reagent addition for it is only the organophosphate conjugation that causes the fluorescence change. Hence, this system is well suited for remote sensing and a laser light source and photomultiplier detection.

Current studies are directed to placing the enzyme in a polyvinyl pyrrolidone or hydrated silicon matrices that keeps it hydrated but non-diffusible. These studies are being developed with Dr. Michael Sailor at UCSD, who has considerable experience with hydrated matrices for high through-put detection. Should this approach not be successful, we have discussed alternative experiments with Dr. John G. Reynolds of the Lawrence Berkeley laboratories, who has been studying phosphatases in immobilized matrices.

3. *Analysis of Organophosphate Conjugation by Mass Spectrometry Analysis of the Conjugates of the Active Center Serine.* These studies have now come to fruition for the phosphorate insecticides where we have been able to follow simultaneously the kinetics of inactivation by the organophosphate, ageing and spontaneous reactivation by isolating the active center tryptic peptide and determining its mass using a MALDI source (9). Moreover, the method is quite sensitive for we have been able to measure the conjugated organophosphate, dimethoxyphosphoryl serine peptide, and aged species in single brain samples after exposure to

two doses of metrifonate (Fig. 4). Current studies are directed to methylphosphonate detection *in vitro*, and following *in situ* exposure, to sarin and cyclosarin analogs. Second, we have begun to add oximes to these studies in order to ascertain the conjugate products after oxime exposure. In particular, we are measuring whether in some cases the oxime does not reactivate, but rather promotes aging. This is quite possible since the leaving group would be the serine alkoxy moiety or the alkoxy moiety on the methylphosphonate. The studies should be facilitated by our recent acquisition of a ABI Qstar XL quadrupole-time of flight mass spectrometer with both electrospray ionization (ESI) and Matrix-assisted Laser Desorption Ionization (MALDI) sources available. The nanoflow liquid chromatography capacity also enhances our sensitivity, and our preliminary runs suggest that the enhancement in sensitivity is about an order of magnitude.

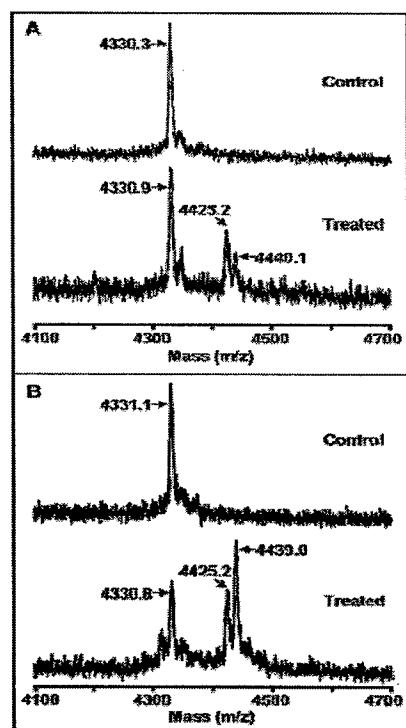


Figure 4. Endogenous mouse brain AChE. Mass spectra were acquired from AChE purified from mouse brain, digested with trypsin, and fractionated by reverse-phase resin. (A) Saline-injected control and mouse treated with 200 mg/kg metrifonate. (B) Control and 400 mg/kg metrifonate-treated mouse. Animals were sacrificed 45 min after ip injection. Unmodified ACP (4331.0 Da) of endogenous AChE from control and OP exposed mice is observed. OP-AChE conjugates are observed in metrifonate-treated animals that correspond to inhibited and aged enzyme, dimethyl and monomethyl phosphoryl ACP adducts (4439.0 and 4425.0 Da), respectively. Representative mass spectra from three independent experiments are shown.

We have also employed mass spectrometry analysis of the tryptic peptides in AChE to analyze whether methionine oxidation correlates with inactivation of the enzyme. Indeed that seems to be the case, and we find that methionine 222 is the offending residue. Its oxidation to the corresponding sulfoxide and perhaps the sulfone correlates with the inactivation process. To confirm this, we are currently mutating the methionine to a leucine, a substitution that should yield a more oxidation resistant enzyme.

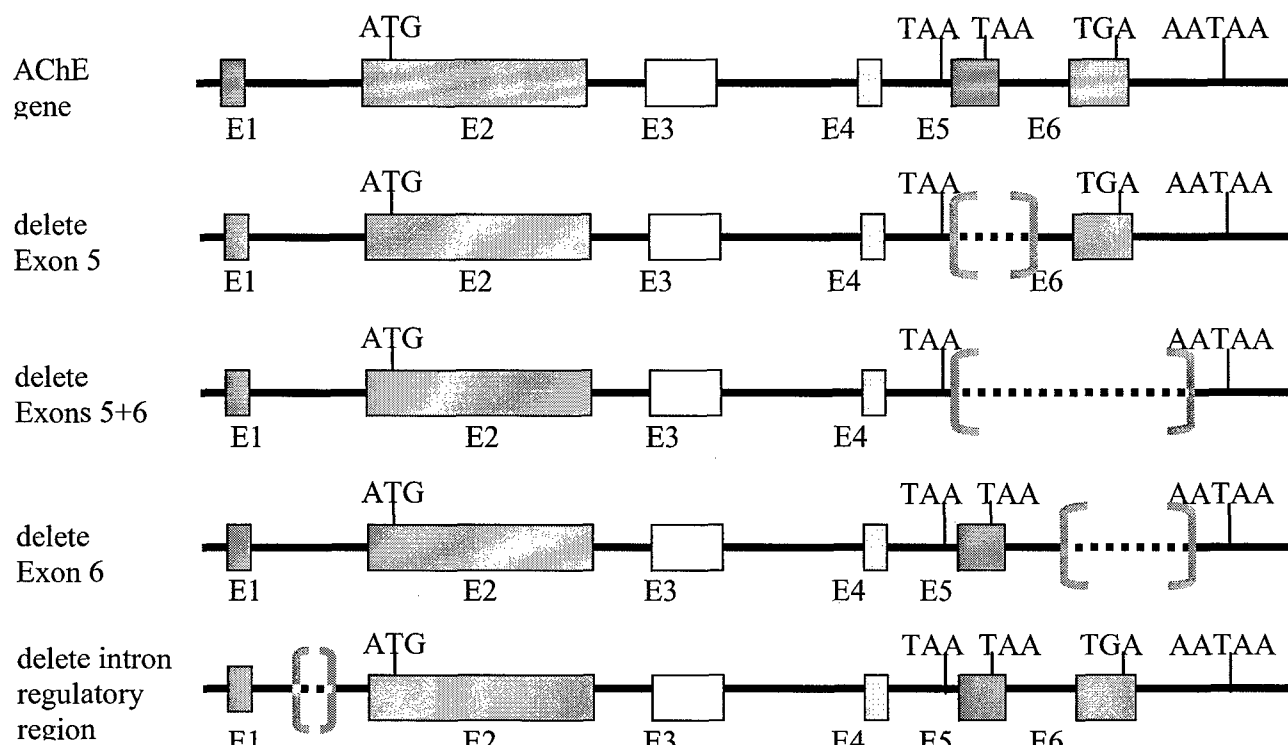


Fig. 5. Structure of the Mouse Acetylcholinesterase Gene. The 7.5 kb region from promoter to the second 3' polyadenylation signal is shown.

4. *Studies of Organophosphate Toxicity with Transgenic (Knock-out) Animal Strains.* Although the initial work was supported by a grant from the National Institute of Environmental Health Sciences, we have produced a series of transgenic mice strains that should prove useful in the study of susceptibility to organophosphate exposure (10). The various mouse strains are outlined in Figure 5. They include: (a) deletion of exon 5, a deletion that prevents formation of glycosylphosphatidyl-linked AChE, a form that resides primarily in hematopoietic cells, (b) deletion of exon 6, a deletion which precludes the expression of the major form of AChE in nerve and muscle and the splice variant that tethers to the plasma or basal lamina membranes, (c) deletion of exons 5 and 6, a deletion that will eliminate all membrane associated forms of AChE giving rise to only a soluble form of the enzyme, and (d) deletion of an upstream intron between exons 1 and 2. The later knock-out has been done with the Cre-lox system so that developmentally and tissue-selective knock outs are possible.

The homologous recombinant inbred, knock-out strains are being characterized phenotypically in terms of multiple parameters (10). The biochemical parameters include expression levels in brain, blood, liver and skeletal muscle, identification of molecular forms in the tissues of interest: skeletal muscle, regional areas of brain, cerebral spinal fluid, erythrocyte membranes and platelet membranes and interiors. Behavioral, muscle strength, physiologic and metabolic parameters are also being assessed. Once complete, we will then assess susceptibility to organophosphates and to oxime reactivation. Such animals will prove of considerable value since they will help us ascertain the extent to which toxicity is central or peripheral and what tissues are most involved. In addition, a non-chemical means of controlling AChE activity should tell us whether certain

oximes have therapeutic value arising from mechanisms other than reactivation. The most exciting development comes from the deletion of 250 bp from the upstream intron region. We observe that these animals have normal brain and spinal cord levels of AChE, but they completely lack skeletal muscle AChE as measured biochemically or by histochemical assay. Moreover, their erythrocyte AChE is normal, but they are devoid of platelet AChE. End-plate structure in the new born is normal, but with time (2-3 months), structure changes from having discrete synaptic invaginations to punctate areas of receptor density. Such changes in synaptic structure are likely to benefit the animal since, in the absence of catalysis, diminution of acetylcholine concentrations can only occur by diffusion from these punctuate areas.

AChE concentrations in organs innervated by the autonomic nervous system (post-ganglionic parasympathetic innervation) are reduced, but not to nearly the same levels as seen in skeletal muscle. Although the animals live with continuous tremors and do not reach the full body weights of their homozygous controls, compromise of function is substantially less than seen in the total knock-out produced by Dr. Oksana Lockridge and colleagues. For example, these nullizygotes will breed and reproduce colonies of nullizygotes.

Two principal conclusions come from these observations:

- (1) In the motor endplate of skeletal muscle in the intact animal, all of the AChE is derived from muscle rather than nerve origin.
- (2) A discrete intronic region of the AChE gene interacts with the endogenous promoter to control tissue specific AChE expression. This is evident in both muscle and hematopoietic cells. This behavior suggests that this intronic region behaves as an "enhanceosome," interacting with the specific promoter region.

5. Development of a New Generation of Reactivating Nucleophiles. Our recent studies with Dr. Barry Sharpless' group has led to a new approach to structure-guided drug design, where the drug target itself becomes a mini-reaction vessel in which the two precursor molecules are induced to react on the macromolecular template by virtue of the unique environment on the enzyme surface and proximity of reactive moieties (11). We have shown proof of principle using inhibition of AChE. Building blocks were originally designed from tethering points using tacrine analogues as the active center anchor and propidium as the peripheral site tether. An intervening methylene chain sequence of variable chain length terminates in either an azide or an acetylene. The biorthogonal, cycloaddition reaction forms a triazole on the very surface of the target (Fig. 6) the selectivity of the reaction is very high in terms of congeners of intervening chain length and regioisomerism in the triazole moiety. This approach has yielded compounds of extremely high affinity in some cases in the femtomolar range for dissociation constants.

The vessel: Acetylcholinesterase

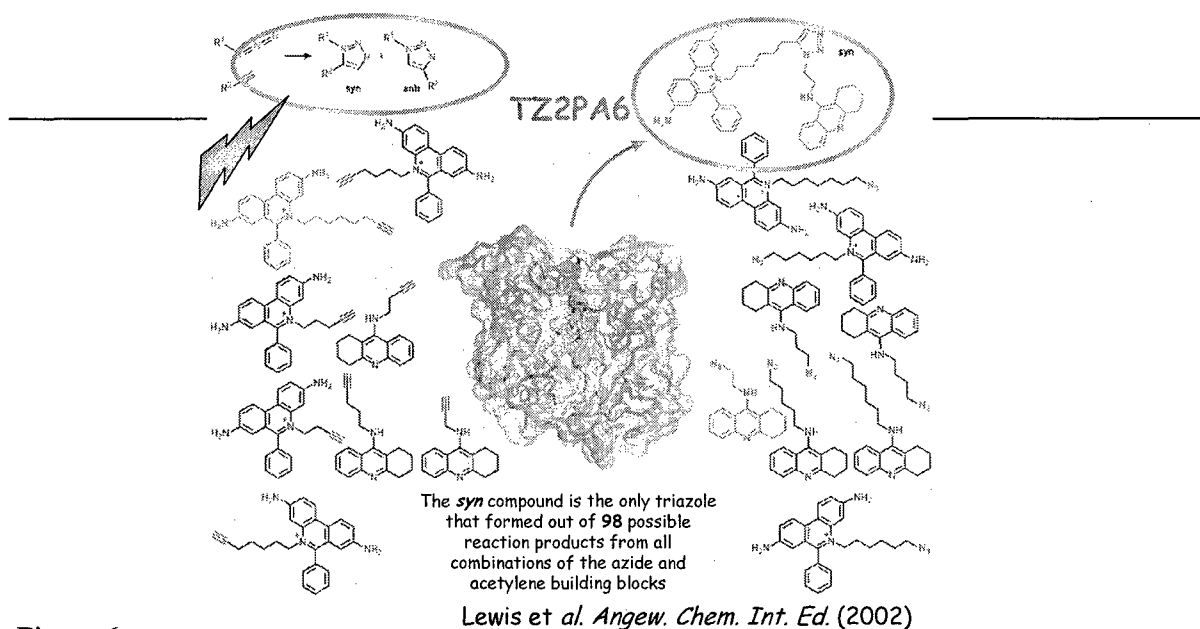


Figure 6.

Kinetic parameters for the two TZ2PA6 regioisomers

k_{on} $10^{10} \text{M}^{-1} \text{min}^{-1}$	k_{off} min^{-1}	K_d nM	Enzyme source	k_{on} $10^{10} \text{M}^{-1} \text{min}^{-1}$	k_{off} min^{-1}	K_d nM
1.5	0.0015	99	<i>E. electricus</i> AChE	1.8	0.25	14 000
1.3	0.0011	77	<i>T. californica</i> AChE	3.2	0.026	720
1.3	0.0071	410	mouse AChE	2.4	0.30	8 900

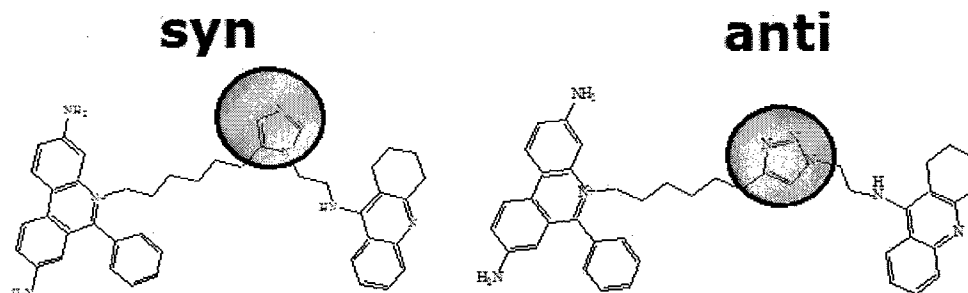


Figure 7

The template guided synthesis approach has yielded the following results:

1. Selectivity in formation of single cycloaddition products from large libraries has been demonstrated (11).
2. The complexes formed, as assessed by X-ray crystallography, show that the higher affinity regioisomer, the *syn*-form, selects out a unique conformation of the target, not seen in the lower affinity *trans* form (12).
3. Building blocks that lack quaternary groups and are simpler in structure can be used to synthesize *in situ* on the enzyme surface high affinity compounds (13). Hence, such compounds have the potential to cross the blood-brain barrier.
4. The approach has been also used with the *Drosophila* enzyme and different congeners are formed. This demonstrates the selectivity of the reaction and shows its template discrimination capacity (13, 14).

Currently, we are developing the methods so that selective reactivating, instead of inhibitory, compounds can be generated. One approach involves the conventional click chemistry where the active center ligand is a nucleophile of the oxime or hydroxamic acid type and the second building block is based on a peripheral site ligand, too bulky to enter to the base of the gorge. In this case the critical element in design is to employ an alkylphosphorylated or phosphonylated enzyme as the template for synthesis.

A second approach entails the development of new site directed nucleophiles, and our initial approach has employed the Banaert reaction that produces self-generating nucleophiles.

KEY RESEARCH ACCOMPLISHMENTS

Our overall approach has been to use AChE itself the very target of toxicity, and modify it so that it becomes a useful tool to understand and prevent toxicity from nerve agents. This approach has been used *in vitro* and *in vivo* as follows:

1. By mutating AChE, we can enhance the rate at which oximes will reactivate the alkyl phosphorylated enzyme. Thus, the combination of an oxime and a modified AChE becomes a catalytic scavenger and oxime-assisted catalysis is a prudent direction for developing prophylactic and therapeutic approaches to nerve agent toxicity.
2. Fluorophore conjugation to introduced cysteines in recombinant DNA derived AChE has yielded an enzyme that shows substantive wavelength shifts and changes in quantum yield upon reaction with organophosphates. The emission spectra can distinguish certain types of organophosphates. Since reagents do not have to be added for detection, the approach can be used in remote sensing.
3. To distinguish the precise organophosphate conjugates, we have developed a mass spectrometric means for detection and quantitation of the organophosphate conjugated tryptic peptides. Sensitivity is sufficient for detection in a single mouse brain hemisphere *in situ*.

4. Homologous recombinant mouse (knock-out) strains have been developed. They lack the exons (5 and 6) that control oligermization and cellular disposition of acetylcholinesterase. This enables us to control expression and cellular localization of AChE in various tissues. Removal of an intronic region of the gene can very selectively control tissue specific expression in skeletal muscle and hematopoietic cells. These animals become valuable models for assessing toxicity to nerve agent and insecticide exposure.
5. A new chemistry, template guided drug design, has been adopted to AChE, and we are now applying this to the development of new reactivating agent antidotes.

REPORTABLE OUTCOMES

Reportable outcomes are described in the Key Research Accomplishments section and the Publications listed in the Appendix.

CONCLUSIONS

Significant strides have been made in understanding the fundamental kinetics and mechanism of organophosphate inhibition and oxime reactivation of outcomes in assessing toxicity, developing antidotes and prophylactic agents and in detection of exposures. Substantially more needs to be done in this area to minimize threats from chemical terrorism. This research provides several new leads to pursue.

REFERENCES

1. *Kovarik, Z., Radic, Z., Berman, H.A., Simeon-Rudolf, V., Reiner, E., and Taylor, P., Acetylcholinesterase Active Center and Gorge Conformations Analysed by Combinatorial Mutations and Enantiomeric Phosphonates. *Biochem. J.*, 373:33-40 (2003).
2. Wong, L., Radic, Z., Bruggemann, R.J.M., Hosea, N., Berman, H.A. and Taylor, P., Mechanism of Oxime Reactivation of Acetylcholinesterase Analyzed by Chirality and Mutagenesis. *Biochemistry*, 39:5750-5757 (2000).
3. *Kovarik, Z., Radic, Z., Berman, H.A., Simeon-Rudolph, V., Reiner, E., and Taylor, P., Mutant Cholinesterases Possessing Enhanced Capacity for Reactivation of Their Phosphonylated Conjugates. *Biochemistry*, 43:3222-3229 (2004).
4. *Shi, J., Radic, Z. and Taylor, P. Inhibitors of Different Structure Induce Distinguishing Conformations in the Omega Loop, Cys⁶⁹-Cys⁹⁶, of Mouse Acetylcholinesterase. *J. Biol. Chem.*, 277:43301-43308 (2002).
5. *Shi, J., Boyd, A.E., Radic, Z. and Taylor, P. Reversibly Bound and Covalently Attached Ligands Induce Conformational Changes in the Omega Loop, Cys⁶⁹-Cys⁹⁶, of Mouse Acetylcholinesterase. *J. Biol. Chem.*, 276:42196-42204 (2001).

6. * Shi, J., Tai, K., McCammon, J.A., Taylor, P. and Johnson, D.A. Nanosecond Dynamics of the Mouse Acetylcholinesterase Cys⁶⁹-Cys⁹⁶ Omega Loop. *J. Biol. Chem.*, 278:30905-30911 (2003).
7. * Boyd, A.E., Dunlop, C.S., Wong, L., Radic, Z., Taylor, P. and Johnson, D.A. Nanosecond Dynamics of Acetylcholinesterase Near the Active Center Gorge. *J. Biol. Chem.*, 279:26612-26618 (2004).
8. Pezzementi, L., Taylor, P., and Johnson, D.A., Fed. Proc. Abstract (2004).
9. * Jennings, L.L., Malecki, M., Komives, E.A., and Taylor, P, Direct Analysis of the Kinetic Profiles of Organophosphate-Acetylcholinesterase Adducts by MALDI-TOF Mass Spectrometry. *Biochemistry*, 42:11083-11091 (2003).
10. * Camp, S., Zhang, L., Marquez, M., de la Torre, B., Long, J., Bucht, G., and Taylor, P. Acetylcholinesterase Gene Modification in Transgenic Animals. *Chemico-Biol. Interactions* (2005) In Press.
11. * Lewis, W.G., Green, L., Grynszpan, F., Radic, Z., Carlier, P.R., Taylor, P., Finn, M.G., and Sharpless, K.B. Click Chemistry In Situ: Acetylcholinesterase as a Reaction Vessel for the Selective Assembly of a Femtomolar Inhibitor from an Array of Building Blocks. *Angewandte Chemie*, 41:1053-1057 (2002).
12. * Bourne, Y., Kolb, H.C., Radic, Z., Sharpless, K.B., Taylor, P., and Marchot, P., Freeze-frame Inhibitor Captures Acetylcholinesterase in a Unique Conformation. *Proc. Natl. Acad. Sci.*, 101:1449-1454 (2004).
13. * Manetsch, R., Krasinski, A., Radic, Z., Raushel, J., Taylor, P., Sharpless, K.B. and Kolb, H.C. In Situ Click Chemistry: Enzyme Inhibitors Made to Their Own Specifications. *J. Amer Chem Soc.* 126:12809-12818 (2004).
14. * Krasinski, A., Radic, Z., Manetsch, R., Raushel, J., Taylor, P., Sharpless, K.B. and Kolb, H.C. In Situ Selection of Lead Compounds by Click Chemistry: Target-guided Optimization of Acetylcholinesterase Inhibitors. *J. Amer. Chem. Soc.* 127:6686-6692 (2005).

* Are included as Appendices

Acetylcholinesterase active centre and gorge conformations analysed by combinatorial mutations and enantiomeric phosphonates

Zrinka KOVARIK*^{†1}, Zoran RADIĆ*, Harvey A. BERMAN[‡], Vera SIMEON-RUDOLF[†], Elsa REINER[†] and Palmer TAYLOR*

*Department of Pharmacology, University of California at San Diego, La Jolla, CA 92093-0636, U.S.A., [†]Institute for Medical Research and Occupational Health, Ksaverska cesta 2, POB 291, HR-10000 Zagreb, Croatia, and [‡]Department of Pharmacology and Toxicology, School of Medicine, University at Buffalo, Buffalo, NY 14214, U.S.A.

A series of eight double and triple mutants of mouse acetylcholinesterase (AChE; EC 3.1.1.7), with substitutions corresponding to residues found largely within the butyrylcholinesterase (BChE; EC 3.1.1.8) active-centre gorge, was analysed to compare steady-state kinetic constants for substrate turnover and inhibition parameters for enantiomeric methylphosphonate esters. The mutations combined substitutions in the acyl pocket (Phe²⁹⁵ → Leu and Phe²⁹⁷ → Ile) with the choline-binding site (Tyr³³⁷ → Ala and Phe³³⁸ → Ala) and with a side chain (Glu²⁰² → Gln) N-terminal to the active-site serine, Ser²⁰³. The mutations affected catalysis by increasing K_m and decreasing k_{cat} , but these constants were typically affected by an order of magnitude or less, a relatively small change compared with the catalytic potential of AChE. To analyse the constraints on stereoselective phosphorylation, the mutant enzymes were reacted with a congeneric series of S_P - and R_P -methylphosphonates of known absolute stereochemistry. Where possible, the overall reaction

rates were deconstructed into the primary constants for formation of the reversible complex and intrinsic phosphorylation. The multiple mutations greatly reduced the reaction rates of the more reactive S_P -methylphosphonates, whereas the rates of reaction with the R_P -methylphosphonates were markedly enhanced. With the phosphonates of larger steric bulk, the enhancement of rates for the R_P enantiomers, coupled with the reduction of the S_P enantiomers, was sufficient to invert markedly the enantiomeric preference. The sequence of mutations to enlarge the size of the AChE active-centre gorge, resembling in part the more spacious gorge of BChE, did not show an ordered conversion into BChE reactivity as anticipated for a rigid template. Rather, the individual aromatic residues may mutually interact to confer a distinctive stereospecificity pattern towards organophosphates.

Key words: acetylcholinesterase mutation, butyrylcholinesterase mutation, organophosphate inhibition, stereoselectivity.

INTRODUCTION

Acetylcholinesterase (AChE; EC 3.1.1.7) and butyrylcholinesterase (BChE; EC 3.1.1.8) are serine hydrolases that structurally belong to the class of proteins known as the esterase/lipase family within the α/β -hydrolase-fold superfamily [1]. AChE and BChE display substantial similarity in their structures, yet differ in substrate specificities and sensitivities to a wide range of inhibitors [2–4]. The available three-dimensional structures of AChE coupled with kinetic studies of the AChE mutants with substrates and inhibitors delineate domains within the active site [3,5,6]. Besides the catalytic triad Ser²⁰³-His⁴⁴⁷-Glu³³⁴, the active site includes the oxyanion hole consisting of Gly¹²¹, Gly¹²² and Ala²⁰⁴, the choline binding site Trp⁸⁶, Tyr³³⁷, Phe³³⁸, and the acyl pocket Phe²⁹⁵ and Phe²⁹⁷ (throughout the present paper, numbers refer to the numbering of amino acid residues in mouse AChE). In BChE, which, unlike AChE, can efficiently catalyse hydrolysis of larger molecules such as butyrylcholine and benzoylcholine, modified substrate selectivity was shown to result mainly from differences in the acyl-pocket structure between the two enzymes [3,5,7]. Aliphatic residues of smaller dimensions are found at positions corresponding to Leu²⁹⁵ and Ile²⁹⁷ in BChE allowing larger substrates to fit into the active site in an orientation appropriate for efficient catalysis [1,8]. Cholinesterases also catalyse phosphorylation of the catalytic serine by organophosphonates. However, unlike carboxyl ester substrates, the phosphorylated enzyme reacts slowly with water,

rendering long-lasting conjugation and inhibition of the enzyme. Furthermore, the AChE reaction with organophosphates displays marked stereoselectivity that can also be utilized for investigation of the steric interactions with structural elements of the active centre [9–12]. The tetrahedral organophosphates contain substituents on the phosphorus atom with ideal bond angles of 109°. Therefore their substituent groups will project differently in the active site from those in planar substrates with trigonal, ideally 120°, bond angles. In the case of the organophosphate–AChE interaction the three-point attachment comes from (i) a conjugating bond distance between the active site serine and the phosphoryl phosphorus, (ii) entry of the phosphoryl oxygen into the oxyanion hole, and (iii) the thiocholine leaving group directed towards the gorge exit [13].

Because the cholinesterases contain the inherent power of stereoselectivity, and because their interaction with organophosphates enables one to deconstruct steady-state catalysis, in order to examine the transesterification step directly, we have examined the influence of multiple site-directed mutations in AChE on substrate turnover and active-centre serine phosphorylation. Mutants were subjected to phosphorylation by a series of enantiomeric pairs, S_P and R_P , of alkyl methylphosphonates in which the structure of the alkoxy group was varied: isopropyl, 3,3-dimethylbutyl and cycloheptyl methylphosphonyl thiocholine (iPrMPTCh, DMBMPTCh and CHMPTCh respectively; Figure 1). Double and triple mutants of mouse AChE with residue substitutions at selected positions

Abbreviations used: AChE, acetylcholinesterase; ATCh, acetylthiocholine iodide; BChE, butyrylcholinesterase; CHMPTCh, cycloheptyl methylphosphonyl thiocholine; DEPQ, 7-(*O*,*O*-diethylphosphinyloxy)-1-methylquinolinium methyl sulphate; DMBMPTCh, 3,3-dimethylbutyl methylphosphonyl thiocholine; DTNB, 5,5'-dithiobis(2-nitrobenzoic acid); iPrMPTCh, isopropyl methylphosphonyl thiocholine; MEPQ, 7-(methylethoxyphosphinyloxy)-1-methylquinolinium iodide.

¹ To whom correspondence should be sent, at the Croatian address (zrinka.kovarik@imi.hr).

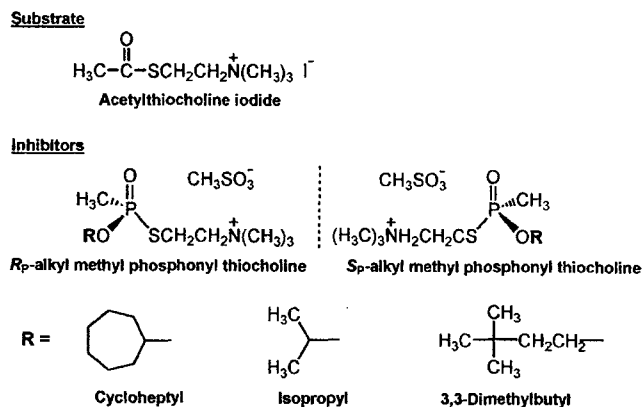


Figure 1 Structures of the substrate and inhibitors employed in the present study

in the active-centre gorge (Figure 2) were prepared to correlate, through structural perturbations, the functional architecture of the AChE gorge with the reactivity and stereoselectivity of the chiral phosphonates. Catalytic constants for acetylthiocholine iodide (ATCh) hydrolysis and rates of phosphorylation of mutant enzymes were evaluated with respect to the structure and steric orientation of the substrate and selected amino acid residues within the active-centre gorge of the enzyme. Multiple mutants of AChE containing F295L (Phe²⁹⁵ → Leu), F297I and Y337A have enabled us to dissect the structural basis for the divergence between AChE and BChE inhibitor specificity and kinetics.

MATERIALS AND METHODS

Chemicals

S_P- and *R_P*-alkyl methylphosphonyl thiocholines (Figure 1) were synthesized and isolated as resolved *S_P* and *R_P* enantiomers [9]. Stock solutions in acetonitrile were kept at -20 °C, and aliquots were diluted in water immediately before use. MEPQ [7-(methylethoxyphosphinyloxy)-1-methylquinolinium iodide] and DEPQ [7-(*O,O*-diethylphosphinyloxy)-1-methylquinolinium methyl sulphate] prepared by Dr H. Leader and Dr Y. Ashani (Israel Institute for Biological Research, Ness Ziona, Israel) were gifts from Dr B. P. Doctor (Walter Reed Army Research Center, Washington, DC, U.S.A.). MEPQ dissolved in acetone and DEPQ dissolved in acetonitrile were kept at -20 °C. ATCh, DTNB [5,5'-dithiobis-(2-nitrobenzoic acid)] and BSA were purchased from Sigma Chemical Co., St. Louis, MO, U.S.A.

Production and purification of AChE

Preparation of the cDNA that encodes mouse AChE truncated at position 548, which yields a monomeric form of the enzyme, has been described previously in [14] and was used in mutagenesis as the template wild-type cDNA. Mutant mouse AChE cDNAs were generated by PCR-mediated standard mutagenesis procedures (QuikChange® Kit; Stratagene, San Diego, CA, U.S.A.). Multiple mutants were generated by combined subcloning of DNA fragments containing single mutations, or by performing mutagenesis using mutant DNA templates. Finally, cassettes of mutant constructs were subcloned into the mammalian expression vector, pCDNA3 (Invitrogen, San Diego, CA, U.S.A.). The nucleotide sequences of the cassettes were confirmed by double-stranded sequencing.

Transfection of HEK-293 cells (purchased from American Type Culture Collection, Atlanta, GA, U.S.A.), as well as selection of expressing cells by aminoglycoside resistance conferred by co-transfection of a neomycin acetyltransferase gene, were described previously in [10]. Stable transfectants were grown to confluence in either 10-cm-diameter dishes or three-tiered flasks with a cell growth surface area of 500 cm² (Nalge Nunc International, Rochester, NY, U.S.A.) before replacement of the foetal-bovine-serum-supplemented Dulbecco's modified Eagle's medium with serum-free medium, Ultraculture cell culture medium (BioWhittaker, Walkersville, MD, U.S.A.). Harvests of the medium containing the soluble monomeric form of AChE were performed at 2–3 day intervals; by replacement of medium on the cell monolayers, cultures could be continued for several weeks.

Several litres of media were subjected to affinity chromatography to purify the mutant enzymes, typically in amounts of 2–10 mg. Procainamide affinity resin utilized CNBr-activated Sepharose CL-4B resin with a hexanoic alkyl chain [15]. Harvested ultraculture medium containing the expressed enzyme was centrifuged (2000 g for 15 min at 4 °C), and was assayed for AChE activity. MgCl₂ was added to a final concentration of 40 mM, then the resin suspension (1 ml for each 2 mg of AChE) and the mixture were allowed to stir in a spinner flask (Bellco, Vineland, NJ, U.S.A.) overnight at 4 °C in the presence of 0.02 % (w/v) NaN₃. The medium was poured into a Bio-Rad Econo-column (Bio-Rad, Hercules, CA, U.S.A.), was allowed to pack by sedimentation, and then washed with equilibrating buffer [at 50–100 times the bed volume; 10 mM NaHCO₃, 100 mM NaCl, 40 mM MgCl₂ and 0.02 % (w/v) NaN₃, pH 8]. The enzyme was subsequently eluted by competition with 100 mM decamethonium bromide, at a low flow rate (1–1.5 ml · h⁻¹). The purified enzyme was dialysed using the 14–16 kDa cut-off dialysis tubing (Spectrapore, Houston, TX, U.S.A.) against 4 litres of dialysis buffer [10 mM Tris/HCl, 100 mM NaCl, 40 mM MgCl₂ and 0.02 % (w/v) NaN₃, pH 8.0] four times for 6 h. Pools of purified enzyme were stored at 4 °C.

AChE activity measurements

Enzyme activities were determined at 22 °C by the Ellman method using ATCh as substrate [16]. Reactions were started by adding substrate to 100 mM phosphate buffer, pH 7.0, containing 0.01 % (v/v) BSA, 0.33 mM DTNB and enzyme. The linear increase of absorbance was monitored from 15 s to 2 min against a blank containing buffer, BSA and DTNB. Maximum concentrations of ATCh did not exceed 100 mM. Whenever ATCh concentrations were greater than 1.0 mM, enzyme activity was corrected for spontaneous non-enzymic substrate hydrolysis.

Known concentrations of MEPQ or DEPQ were utilized to titrate the number of active sites, according to procedures described previously in [17,18].

AChE inhibition by organophosphates

In the inhibition experiments, enzyme samples were incubated for > 30 min with organophosphonates [in 100 mM phosphate buffer, pH 7.0, containing 0.01 % (v/v) BSA] in the absence of substrate; typically, three to five inhibitor concentrations were used. The inhibition reaction was stopped by the addition of ATCh (1.0 mM final concentration), and the extent of inhibition was determined by measuring the residual activity. To obtain the enzymic activity at time-zero inhibition, the enzyme was added to the reaction medium containing inhibitor and substrate.

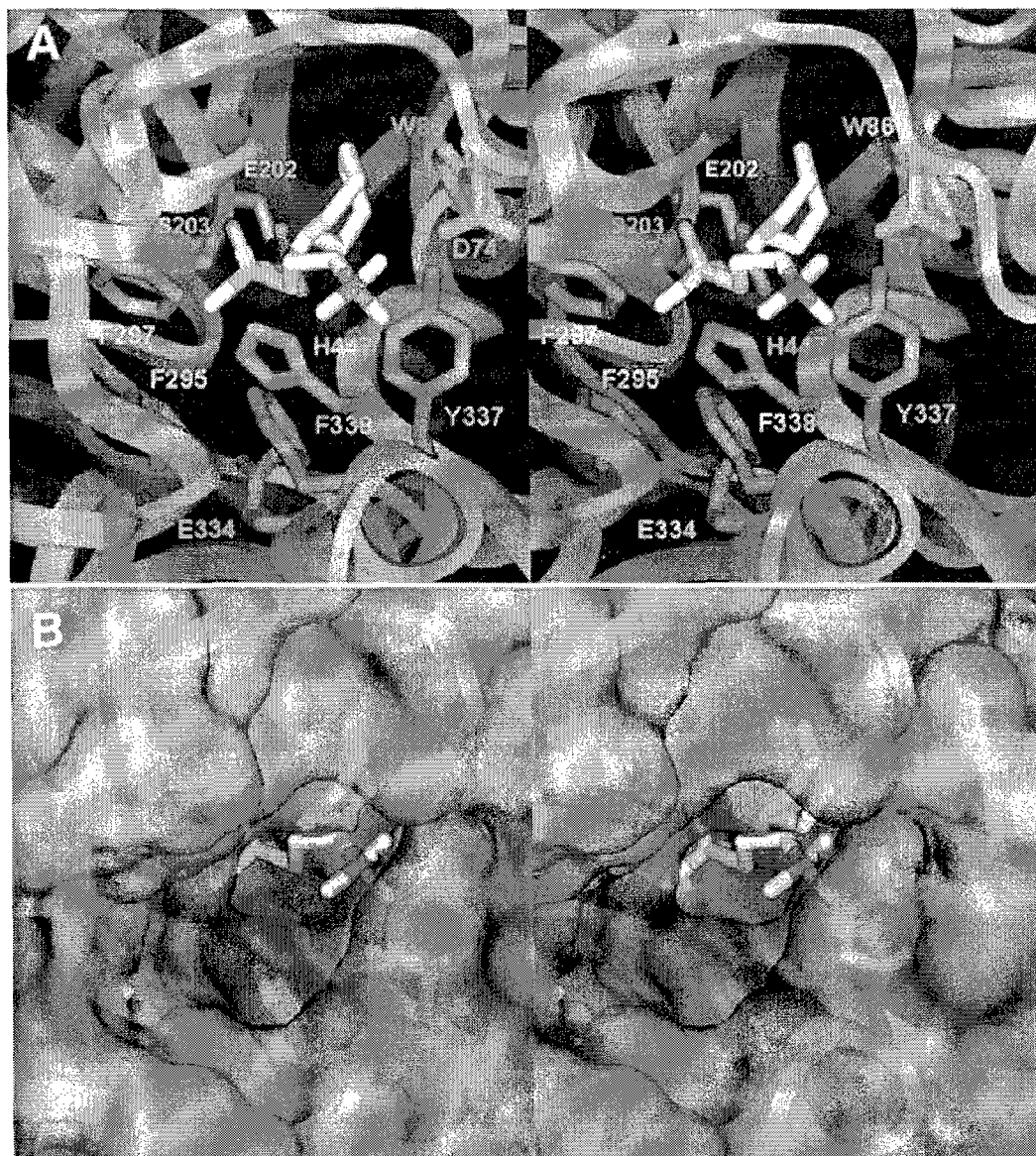


Figure 2 Stereo image of S_p -CHMPTCh bound in the active centre of wild-type mouse AChE in the form of a Michaelis-type complex (cf. Scheme 2)

The image is based on computational analysis of the organophosphate binding in the AChE active centre described previously by Hosea et al. [21]. (A) The organophosphate is represented by white (carbon), red (oxygen), blue (nitrogen) and green (phosphorus) sticks. The five AChE side chains where mutations were made are represented by orange sticks, while the catalytic triad residues (Ser²⁰³, Glu³³⁴ and His⁴⁴⁷) are coloured blue. Two additional AChE residues important for interaction with ligands, Trp⁸⁶ and Asp⁷⁴, are also displayed. The protein α -carbon backbone of mouse AChE (taken from Protein Data Bank entry 1maa) is displayed as a blue ribbon. (B) Transparent, solvent-accessible Connolly AChE surface, for the complex shown in (A). The shape of the surface illustrates spatial restrictions in the enzyme active-centre gorge imposed by the mutated and neighbouring residues.

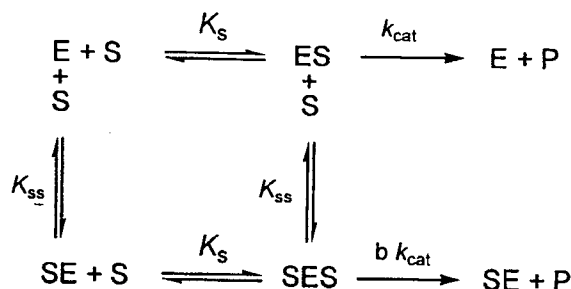
Kinetic equations

The evaluation of catalytic parameters was based on Scheme 1 (compare with [19]). According to this scheme, the enzyme (E) associates reversibly with substrate (S) forming two binary complexes: the ES complex in the active site and the SE complex in a secondary peripheral site. The complex ES results in substrate hydrolysis with the rate constant k_{cat} , whereas the SE complex is inactive. The ternary complex SES leads to substrate hydrolysis with a rate constant $b k_{cat}$. Scheme 1 assumes that S has equal affinity for the active site of E and SE as does S for a peripheral site of E and ES. Constants K_s and K_{ss} are the respective ES and SE dissociation constants. The K_s constant approximates to the Michaelis constant K_m . Throughout the present paper the symbol

K_m will therefore be used instead of K_s . Eqn (1) describes catalysis in Scheme 1:

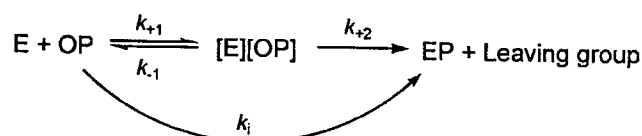
$$v_0 = \frac{e_0 \cdot k_{cat}}{1 + \frac{K_m}{[S]}} \cdot \frac{1 + b \frac{[S]}{K_{ss}}}{1 + \frac{[S]}{K_{ss}}} \quad (1)$$

where v_0 is the initial steady-state rate of ATCh hydrolysis and e_0 is the total enzyme active-site concentration. The catalytic parameters were calculated by fitting experimental data to eqn (1) [3,19].



Scheme 1 Reaction scheme for substrate hydrolysis by acetylcholinesterase

Modified from [19].



Scheme 2 Progressive inhibition of acetylcholinesterase by organophosphates

Modified from [20].

Progressive inhibition of AChE by organophosphates is defined by Scheme 2 (cf. [20]). Enzyme (E) and organophosphate (OP) form a reversible Michaelis-type complex ([E][OP]) from where the covalently phosphorylated enzyme (EP) and the leaving group of the organophosphate arise; k_{+2} is the first-order inhibition rate constant and k_i is the overall second-order rate constant of inhibition. Scheme 2 is defined by eqn (2):

$$\ln \frac{v_0}{v_i} = \frac{k_{+2} \cdot [\text{OP}]}{K_i + [\text{OP}]} \cdot t = k_{\text{obs}} \cdot t \quad (2)$$

where v_0 and v_i stand for the enzyme activity in the absence and in the presence of inhibitor (OP) respectively at the time of inhibition (t). K_i approximates to the dissociation constant of the [E][OP] complex, and k_{obs} is the first-order rate constant of inhibition determined at any given inhibitor concentration. The k_{+2} and K_i constants were calculated from eqn (2).

When $[\text{OP}] \ll K_i$, constants k_{+2} and K_i cannot be separately evaluated, because eqn (2) reduces to eqn (3):

$$\ln \frac{v_0}{v_i} = \frac{k_{+2}}{K_i} \cdot [\text{OP}] \cdot t = k_i \cdot [\text{OP}] \cdot t = k_{\text{obs}} \cdot t \quad (3)$$

from which k_i was calculated. The k_i constant corresponds to the ratio k_{+2}/K_i .

RESULTS AND DISCUSSION

Effect of mutations on catalytic constants of ATCh hydrolysis

All multiple AChE mutants contain mutations inside the active-centre gorge of mouse AChE, and many resemble the residue replacements in the mouse BChE active site (F295L, F297I and Y337A). The activity of the enzymes for ATCh is shown in Figure 3. The bell-shaped pS-curve of wild-type AChE activity reached an optimum at about 1 mM ATCh. Only the mutants, F295L/Y337A and F295L/Y337A/F338A, exhibited bell-shaped pS-curves similar to that of wild-type AChE, but reached a

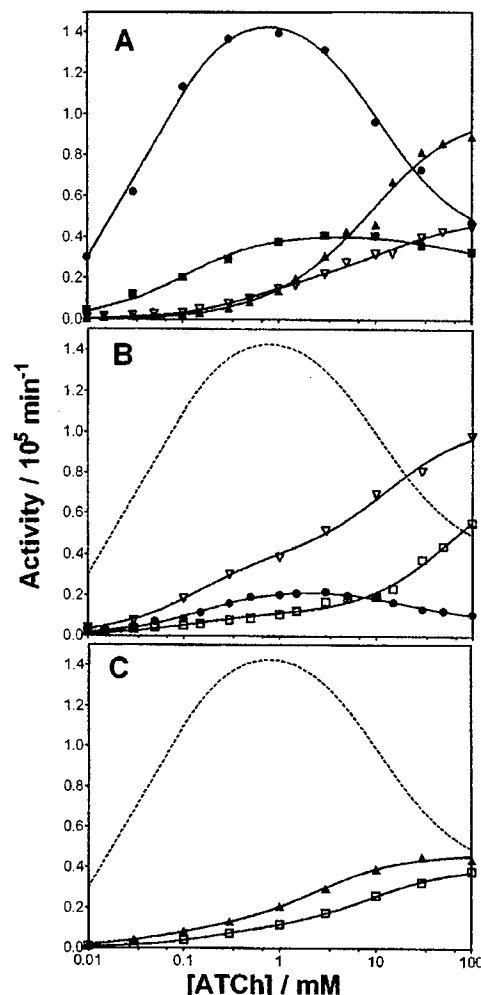


Figure 3 Concentration dependencies of ATCh hydrolysis by wild-type and mutant AChEs

Activities are expressed in moles of hydrolysed substrate per mole of enzyme active sites per minute. The curves were generated using eqn (1). (A) Wild-type AChE (●) and mutants with mutations progressing from AChE to BChE: F295L/Y337A (■), F297I/Y337A (▲) and F295L/F297I/Y337A (▽). (B) Wild-type AChE (---) and mutants with E202Q and F338A substitutions: Y337A/F338A (▽), F295L/Y337A/F338A (●) and E202Q/F295L/Y337A (□). (C) Wild-type AChE (---) and mutants with alanine substitutions: F295A/Y337A (▲) and F295A/F297A/Y337A (□).

maximum at higher ATCh concentrations, whereas pS-curves of the other mutants resembled that of BChE [21–23].

All mutations studied revealed an increase of K_m and a decrease of k_{cat} compared with AChE (Table 1). Two mutants, F295L/Y337A and Y337A/F338A, had a k_{cat} similar to that of BChE. As a result of both a higher K_m and lower k_{cat} , the efficiency of catalysis (k_{cat}/K_m) of the mutants at low substrate concentrations is less than that of wild-type AChE. Alanine at positions 295 and 297 resulted in a reduction of k_{cat} , and compared with the corresponding mutants F295L/Y337A and F295L/F297I/Y337A, alanine substitution led to a further reduction in catalytic constants (cf. Table 1). In contrast, the single mutants, F295A and F297A, showed greater catalytic rates than the F295L and F297I mutants [10]. This combinatorial behaviour might be a consequence of altered structural integrity of the acyl pocket in the mutant enzyme. Replacement of the large phenylalanine residue with alanine can be expected to yield a void area, which should be

Table 1 Catalytic constants for ATCh catalysis by recombinant DNA-derived mouse cholinesterases

Constants were obtained by non-linear regression analysis of data from pS-curves according to Scheme 1 and eqn (1). Results are means \pm S.D. ($n = 3-5$).

Enzyme	K_m (μ M)	K_{ss} (mM)	b	k_{cat} (10^4 min^{-1})	k_{cat}/K_m ($10^7 \text{ min}^{-1} \cdot \text{M}^{-1}$)
AChE wild-type	47 \pm 7	9.6 \pm 2.0	0.20 \pm 0.04	15 \pm 4	320
BChE wild-type*	35 \pm 2	1.3 \pm 0.5	3.6 \pm 0.2	4.0 \pm 0.7	110
F295L/Y337A	100 \pm 7	62 \pm 30	0.62 \pm 0.07	4.0 \pm 0.2	40
F297I/Y337A	340 \pm 100	5.5 \pm 3.4	5.7 \pm 2.1	1.4 \pm 0.4	4.1
F295A/Y337A	76 \pm 20	2.4 \pm 0.2	3.3 \pm 0.6	2.0 \pm 0.2	26
Y337A/F338A	150 \pm 80	14 \pm 8	2.6 \pm 0.9	3.9 \pm 0.5	26
F295L/F297I/Y337A	69 \pm 30	21 \pm 19	3.2 \pm 0.5	1.5 \pm 0.5	22
F295A/F297A/Y337A†	190	9.1	3.6	1.1	5.8
F295L/Y337A/F338A	150 \pm 20	14 \pm 7	0.33 \pm 0.07	1.7 \pm 0.1	11
E202Q/F295L/Y337A	100 \pm 40	38 \pm 10	7.1 \pm 5.3	1.0 \pm 0.1	10

* Radić et al. [3].

† One experiment only.

occupied with water or result in collapse of the α -carbon chain. For the F295L and F297I substitutions, the volume reduction and structural perturbation is smaller and less impacted by the concomitant Y337A substitution on the opposite face of the gorge. The aromatic residues F295, F297 and Y337 may serve to stabilize and orient ATCh for efficient catalysis. It should be noted that no natural cholinesterase identified at the present time contains alanine at positions corresponding to 295 and 297 in mouse AChE [1,24].

Inhibition by excess substrate, resulting in bell-shaped pS-curves, is explained by the binding of a substrate molecule to the peripheral site of the enzyme [19,25]. Residues in the acyl pocket and choline-binding site do influence K_{ss} and b values, demonstrating that these residues are linked to the catalytic influence of the binding of a second substrate molecule. The F295L substitution in the Y337A mutant shows a catalytic profile that resembles AChE in that this double mutant displays substrate inhibition ($b < 1$), whereas the F297I substitution in Y337A resembles BChE, where the double mutant shows apparent substrate activation ($b > 1$). The single mutants F295L and F297I show similar changes in the b parameter to those of the double mutant [3,10], showing that the Y337A substitution is not involved in the inhibition/activation process. Substitution F295L in the triple mutant F295L/Y337A/F338A also prevents the apparent substrate activation seen in Y337A/F338A (Figure 3). On the other hand, comparison of catalytic parameters of F295L/Y337A and E202Q/F295L/Y337A gives rise to the conclusion that the E202Q mutation is responsible for the apparent substrate activation ($b > 1$, cf. Table 1). Previous results showed that the single mutation E202Q of mouse AChE only slightly altered K_m and k_{cat} , but changed the K_{ss} and b values [21], and that the charge on Glu²⁰² probably has a role in stabilization of the transition state [26–28].

Conformational changes of the acyl-pocket loop following conjugation of a large organophosphate and aging of the conjugate were reported in crystal-structure analysis of *Torpedo californica* AChE [29]. It is therefore reasonable to assume that mutations of phenylalanine residues to isoleucine, leucine or alanine could affect flexibility of the loop that encompasses peripheral site residues and may link the active site with the peripheral site. The concept of a functional linkage was first suggested by Changeux [30] to explain allosteric binding of certain inhibitors to AChE; later it was demonstrated directly with fluorescence spectra of ligands bound at the peripheral site or active centre [31,32].

Table 2 Constants (\pm S.E.M.) for inhibition of recombinant-DNA-derived mouse cholinesterases by chiral thiocholine methylphosphonates

The first-order inhibition constant (k_{+2}) and enzyme–inhibitor equilibrium dissociation constant (K_i) were determined by non-linear regression of eqn (2) from k_{obs} constants (9–14 values) obtained from at least three experiments.

Enzyme	Inhibitor	k_{+2} (min^{-1})	K_i (nM)	k_i ($10^6 \text{ min}^{-1} \cdot \text{M}^{-1}$)
F297I/Y337A	R_p -iPrMPTCh	0.6 \pm 0.2	220 \pm 130	2.8 \pm 1.8
F295L/F297I/Y337A	S_p -CHMPTCh	1.1 \pm 0.3	36 \pm 15	32 \pm 17
F295L/F297I/Y337A	R_p -CHMPTCh	0.6 \pm 0.2	74 \pm 49	8.1 \pm 6.0
F295L/Y337A/F338A	S_p -CHMPTCh	1.3 \pm 0.4	83 \pm 49	16 \pm 11
E202Q/F295L/Y337A	S_p -DMBMPTCh	3.8 \pm 1.1	12 \pm 5	330 \pm 180

With the exception of F295L/Y337A/F338A, all other AChE mutants retained substantial catalytic capacity irrespective of whether their pS-profiles mimicked that of AChE or BChE.

Mutation analysis and phosphorylation of AChE

Mouse cholinesterases were phosphorylated by S_p and R_p enantiomers of CHMPTCh, iPrMPTCh or DMBMPTCh (Figure 1). The phosphonate concentration was in excess of the enzyme concentration, and the inhibition followed first-order kinetics. The constants k_{+2} , K_i and k_i were evaluated from the dependence of k_{obs} on the concentration of inhibitor [cf. eqns (2) and (3)]. Three different patterns for inhibition kinetics were obtained, as shown in Figures 4(A)–4(C). For most reactions (32 out of 43) a linear dependence of k_{obs} on the phosphonate concentration was obtained (Figure 4A), which did not allow the distinction of individual constants k_{+2} and K_i . The same applies to the reactions (6 out of 43) presented in Figure 4(B). The y-axis intercepts in Figures 4(B) and 4(C) are probably due to the formation of a reversible enzyme–inhibitor complex in which the inhibitor was not fully displaced by 1 mM ATCh that was used in the activity assay. This initial complex was not studied further. In Figure 4(C), a non-linear dependence of k_{obs} on the inhibitor concentration enabled us to calculate the primary constants for formation of the reversible complex (K_i) and the intrinsic phosphorylation constant (k_{+2}) using eqn 2 (Table 2). The k_{+2} values for R_p compounds were typically less than one-half of k_{+2} for the S_p compounds, whereas K_i ranged between 12 and

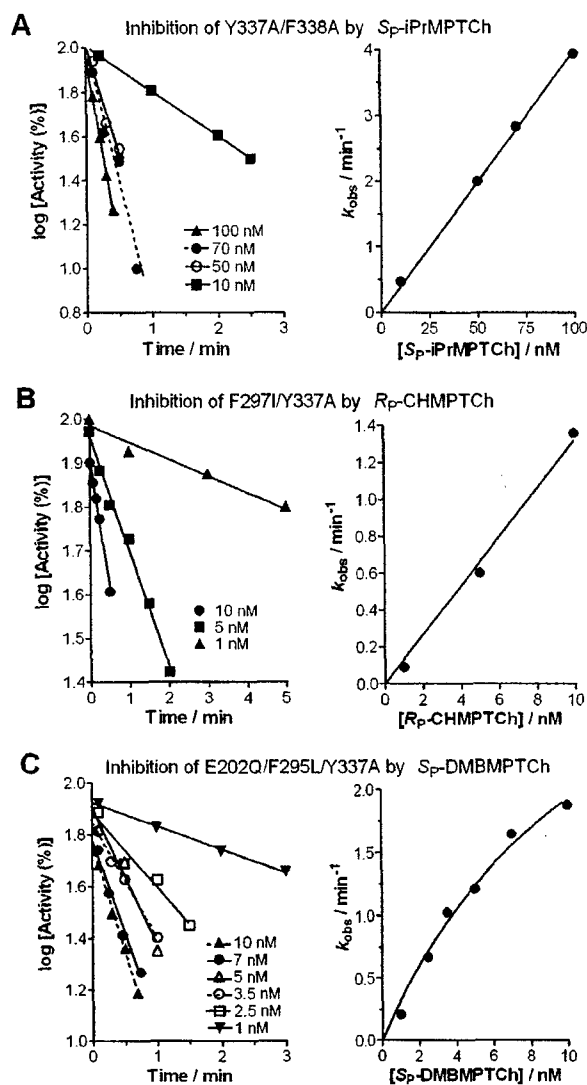


Figure 4 Representative inhibition experiments of AChE mutants by alkyl methylphosphonyl thiocholines

From the analysis of inhibition at zero time (i.e. intercept on the y-axis), and from the relationship between k_{obs} and inhibitor concentrations, inhibition kinetics displayed three different patterns: (A) all inhibition lines pass through $\log[\text{Activity} (\%)] = 2.0$, and k_{obs} was linearly dependent on inhibitor concentration; (B) the y-intercept is below 100% activity, whereas k_{obs} and inhibitor concentration still show a linear relationship; (C) the inhibition lines also intercept the y-axes below 100% activity, but k_{obs} against inhibitor concentration deviates from linearity and approaches a limiting value at high inhibitor concentrations. This indicates that an appreciable concentration of enzyme-inhibitor complex is accumulating.

220 nM. A two orders of magnitude range of second-order rate constants (k_i) for the phosphonates is primarily due to variation in K_i , the dissociation constant. Hence, K_i appears to be the major determinant of AChE reactivity toward organophosphates [9,20,33].

The high enantiomeric stereoselectivity of wild-type AChE with a preference for S_P over R_P enantiomers was decreased by mutations in the choline-binding site and acyl pocket (Tables 3–5). Generally, the mutations reduced inhibition rates by S_P enantiomers, whereas inhibition rates by R_P enantiomers were enhanced. The most dramatic change in rates was obtained in the inhibition of F297I/Y337A by R_P -CHMPTCh, where the rate was

Table 3 Rate constants (k_i) for the inhibition of recombinant-DNA-derived mouse cholinesterases by S_P - and R_P -CHMPTCh enantiomers

Eqn (3) was applied to calculate k_i (\pm S.E.M.) from k_{obs} constants (6–10 values) obtained from at least three experiments.

Enzyme	k_i ($10^6 \text{ min}^{-1} \cdot \text{M}^{-1}$)		$k_i(S_P)/k_i(R_P)$
	S_P	R_P	
AChE wild-type*	190 ± 30	0.81 ± 0.09	230
F295L*	66 ± 9	8.7 ± 1.1	7.6
F297I*	16 ± 3	62 ± 3	0.26
Y337A†	120 ± 10	0.84 ± 0.04	140
E202Q†	21 ± 2	0.13 ± 0.01	160
F295L/Y337A	140 ± 5	25 ± 2	5.6
F297I/Y337A	8.1 ± 0.7	130 ± 6	0.062
Y337A/F338A	160 ± 4	2.0 ± 0.2	80
F295L/F297I/Y337A	32 ± 17 ‡	8.1 ± 6.0 ‡	4.0
F295L/Y337A/F338A	16 ± 11 ‡	4.5 ± 0.4	3.6
E202Q/F295L/Y337A	64 ± 2	19 ± 1	3.4
BChE wild-type*	470 ± 90	6.7 ± 0.7	70

* [10].

† [21].

‡ From Table 2.

Table 4 Rate constants (k_i) for the inhibition of recombinant DNA-derived mouse cholinesterases by S_P - and R_P -iPrMPTCh enantiomers

Eqn (3) was applied to calculate k_i (\pm S.E.M.) from k_{obs} constants (7–14 values) obtained from at least three experiments.

Enzyme	k_i ($10^6 \text{ min}^{-1} \cdot \text{M}^{-1}$)		$k_i(S_P)/k_i(R_P)$
	S_P	R_P	
AChE wild-type*	16 ± 1	0.14 ± 0.03	110
F295L*	3.4 ± 0.1	1.2 ± 0.1	2.8
F297I*	0.95 ± 0.46	1.2 ± 0.1	0.79
Y337A†	24 ± 3	0.34 ± 0.04	71
E202Q†	0.49 ± 0.02	0.038 ± 0.002	13
F295L/Y337A	7.3 ± 0.2	1.8 ± 0.3	4.1
F297I/Y337A	0.47 ± 0.01	2.8 ± 1.8 ‡	0.17
Y337A/F338A	41 ± 1	0.28 ± 0.01	150
F295L/F297I/Y337A	0.48 ± 0.03	0.26 ± 0.03	1.8
F295L/Y337A/F338A	0.40 ± 0.01	0.46 ± 0.04	0.87
E202Q/F295L/Y337A	2.9 ± 0.3	0.68 ± 0.05	4.3
BChE wild-type*	10 ± 1	3.3 ± 0.1	3.0

* [10].

† [21].

‡ From Table 2.

increased 160-fold compared with the k_i of the wild-type AChE (cf. Table 3). Moreover, the mutant F297I/Y337A was inhibited 16-fold more rapidly by R_P - than S_P -CHMPTCh, showing inverted stereospecificity, greatly exceeding the ratio of rates for the single mutant F297I [10].

S_P - and R_P -DMBMPTCh showed the most rapid inhibition rates of the three enantiomeric phosphonate pairs, whereas the enantiomeric selectivity for this pair with wild-type AChE was the lowest of the three (Table 5). Inhibition rates with both DMBMPTCh enantiomers for all other multiple mutants (except Y337A/F338A) slightly decreased compared with that of wild-type AChE. The 3,3-dimethylbutyl moiety, being a primary

Table 5 Rate constants (k_i) for the inhibition of recombinant DNA-derived mouse cholinesterases by S_P - and R_P -DMBMPTCh enantiomers

Eqn (3) was applied to calculate k_i (\pm S.E.M.) from k_{obs} constants (6–9 values) obtained from at least three experiments.

Enzyme	k_i ($10^6 \text{ min}^{-1} \cdot \text{M}^{-1}$)		$k_i(S_P)/k_i(R_P)$
	S_P	R_P	
AChE wild-type*	360 \pm 10	19 \pm 9	19
F295L*	140 \pm 10	10 \pm 5	14
F297I*	56 \pm 4	12 \pm 4	4.7
Y337A†	750 \pm 20	19 \pm 1	39
E202Q†	120 \pm 10	2.7 \pm 0.1	44
F295L/Y337A	220 \pm 20	13 \pm 1	17
F297I/Y337A	28 \pm 2	12 \pm 1	2.3
Y337A/F338A	890 \pm 120	39 \pm 1	22
F295L/F297I/Y337A	32 \pm 2	4.6 \pm 0.2	7
F295L/Y337A/F338A	160 \pm 7	8.3 \pm 0.3	19
E202Q/F295L/Y337A	330 \pm 180‡	18 \pm 1	18
BChE wild-type*	500 \pm 150	32 \pm 16	16

* [10].
† [21].
‡ From Table 2.

instead of a secondary alkoxy moiety, has additional degrees of torsional freedom over the cycloheptyl and isopropyl groups. The flexibility conferred from bond rotation, along with the hydrophobicity, may contribute to the greater reactivity of the R_P -DMBMPTCh organophosphate over the other R_P -methylphosphonates. The flexibility of this group may also enhance the S_P reaction through its fit in the choline subsite.

Although the Y337A mutation had a small effect on the rate of phosphorylation, the rate for the Y337A/F338A mutant increased two-fold for all S_P and R_P enantiomers, except for S_P -CHMPTCh, showing a stereoselectivity similar to, or slightly greater than, that of the wild-type AChE (Tables 3–5). Enlargement of the choline-binding site by mutations Y337A and F338A may provide a preferable orientation for organophosphate reactivity in the active centre.

Since the absolute stereochemistry of these phosphonates is known, molecular-dynamics analysis of energy-minimized conformations for S_P - and R_P -methylphosphonates in the active site of mouse AChE revealed the probable arrangement of substituent groups [21,34]. In case of the S_P enantiomer, the methylphosphonyl moiety can fit within the space constraints of the acyl pocket, the phosphonyl oxygen enters the oxyanion hole and the leaving group can fit into the space forming the choline subsite, close to the gorge exit (Figure 2). For the R_P enantiomer, placement of the phosphonyl oxygen and the leaving group at these positions confronts a steric constraint of the alkoxy group in the acyl pocket. Alternatively, placement of the methyl group in the acyl pocket requires that either the phosphonyl oxygen is oriented out of the oxyanion hole or the leaving group is directed away from the gorge exit. By enlarging the acyl pocket so that the R_P -alkoxy group orients in that direction, both positioning criteria for efficient phosphorylation can be satisfied and the rates are accelerated. Stabilization of the S_P -methyl group within the confines of the acyl pocket by Phe²⁹⁵ and Phe²⁹⁷ (Figure 2) is also critical for efficient reactivity, since rates of phosphorylation by the S_P enantiomers are diminished for the acyl-pocket mutants, especially if Phe²⁹⁷ is mutated. Furthermore, decreased reactivity of S_P enantiomers, due to replacement of residues at either the

acyl pocket or choline-binding site, is seen in the triple mutant F295L/F297I/Y337A.

Although the F295L/F297I/Y337A mutant resembles mouse BChE in composition of the acyl pocket and choline binding site, its reactivity toward S_P enantiomers is approx. 20-fold lower than that for the mouse wild-type BChE (cf. Tables 3–5). On the other hand, the reactivity of the triple mutant toward R_P enantiomers approached that of BChE, except for R_P -DMBMPTCh, which phosphorylated both AChE and BChE at slower rates. Thus comparison of k_i constants for AChE and BChE with AChE mutants gives rise to the conclusion that the difference between AChE and BChE is not dictated solely by residues in the acyl pocket and the choline-binding site. Despite the 'equivalence' of residues in these regions of the two enzymes, their architectures are different. One difference not inherent in considerations of aromaticity and volume of the active centre is the flexibility of the α -carbon backbone surrounding the acyl pocket. For example, Arg²⁹⁶ in AChE may be anchored by interactions with Pro²³⁵, Gln⁴⁶⁹ and His⁴⁰⁵, imparting stability to the pocket, whereas in BChE, the residue at position 296 is serine. The smaller side chain and diminished interactions may be factors in conferring additional flexibility to the BChE acyl pocket. A recent study on a hexa-substituted mutant of human AChE that resembled residues of human BChE showed that this mutant did not mimic the reactivity of human BChE toward substrates and other covalent ligands, and it was suggested that the catalytically productive orientation of the catalytic triad histidine in BChE is maintained by a somewhat different array of interactions than that in AChE [35].

General conclusions

The combinatorial approach to altering the dimensions of the active centre through mutation, when coupled with the greater discriminatory power of a congeneric series of enantiomeric methylphosphonates, reveals several characteristics of the AChE active centre. The overall dimensions of the acyl pocket are the critical determinant in maintaining stereoselectivity. Mutations enlarging the dimensions of the choline subsite, do not, in themselves, reduce stereoselectivity or reactivity. It is only when mutations in the choline subsite are combined with the acyl-pocket mutation at residue 297 that the most dramatic inversion in stereoselectivity is seen. Enhanced reactivity cannot be predicted simply on the basis of the enlarged volume of the gorge, since the favourable characteristics of elimination of steric occlusion may be offset by formation of non-productive complexes in the enlarged gorge. Enlarging the acyl pocket diminishes the reactivity of all of the S_P -methylphosphonates, suggesting that positioning the methyl group within the confines of a small acyl pocket bordered by the two phenylalanine residues optimizes the position of the phosphorus for reaction in AChE. Simple partitioning of volume increases by side-chain removal does not give an ordered increase in reactivity of the R_P compounds.

We thank B. P. Doctor (Walter Reed Army Research Center, Washington, DC, U.S.A.), H. Leader and Y. Ashani (Israel Institute for Biological Research, Ness Ziona, Israel) for providing the MEPQ and DEPQ for our experiments. The assistance of Mr Si-Khanh Nguyen and Ms Esther Kim in generating some of the double-mutant DNA constructs is appreciated. This work was a portion of the Ph.D. thesis of Z. K. conducted, in part, at the Department of Pharmacology, University of California at San Diego, La Jolla, CA, U.S.A. The work was supported by the one-year fellowship of the Ministry of Science and Technology of the Republic of Croatia and by the Wood-Whelan Research Fellowship, International Union of Biochemistry and Molecular Biology, U.S.A. (to Z. K.), and by DAMD17-18014 grant (to P. T.) and grant No. 0022014 of Ministry of Science and Technology of the Republic of Croatia (to V. S.).

REFERENCES

- Cygler, M., Schrag, J. D., Sussman, J. L., Harel, M., Silman, I., Gentry, M. K. and Doctor, B. P. (1993) Relationship between sequence conservation and three-dimensional structure in a large family of esterases, lipases, and related enzymes. *Prot. Sci.* **2**, 366–382.
- Taylor, P. and Radić, Z. (1994) The cholinesterases: from genes to proteins. *Annu. Rev. Pharmacol. Toxicol.* **34**, 281–320.
- Radić, Z., Pickering, N. A., Vellom, D. C., Camp, S. and Taylor, P. (1993) Three distinct domains in the cholinesterase molecule confer selectivity for acetylcholinesterase and butyrylcholinesterase inhibitors. *Biochemistry* **32**, 12074–12084.
- Kovarik, Z., Radić, Z., Grgas, B., Škrinjaric-Špoljar, M., Reiner, E. and Simeon-Rudolf, V. (1999) Amino acid residues involved in the interaction of acetylcholinesterase and butyrylcholinesterase with the carbamates Ro 02-0683 and bambuterol, and with terbutaline. *Biochim. Biophys. Acta* **1433**, 261–271.
- Ordentlich, A., Barak, D., Kronman, C., Flashner, Y., Leitner, M., Segall, Y., Ariel, N., Cohen, S., Velan, B. and Shafferman, A. (1993) Dissection of the human acetylcholinesterase active center determinants of substrate specificity. Identification of residues constituting the anionic site, the hydrophobic site, and the acyl pocket. *J. Biol. Chem.* **268**, 17083–17095.
- Bourne, Y., Taylor, P. and Marchot, P. (1995) Acetylcholinesterase inhibition by fasciculins: crystal structure of the complex. *Cell* **83**, 503–512.
- Vellom, D. C., Radić, Z., Li, Y., Pickering, N. A., Camp, S. and Taylor, P. (1993) Amino acid residues controlling acetylcholinesterase and butyrylcholinesterase specificity. *Biochemistry* **32**, 12–17.
- Harel, M., Sussman, J. L., Krejci, E., Bon, S., Chanal, P. and Massoulié, J. (1992) Conversion of acetylcholinesterase to butyrylcholinesterase, modeling and mutagenesis. *Proc. Natl. Acad. Sci. U.S.A.* **89**, 10827–10831.
- Berman, H. A. and Leonard, K. (1989) Chiral reactions of acetylcholinesterase probed with enantiomeric methylphosphonothioates. *J. Biol. Chem.* **264**, 3942–3950.
- Hosea, N. A., Berman, H. A. and Taylor, P. (1995) Specificity and orientation of trigonal carboxylesters and tetrahedral phosphonyl esters in cholinesterase. *Biochemistry* **34**, 11528–11536.
- Ordentlich, A., Barak, D., Kronman, C., Benshop, H. P., De Jong, L. P. A., Ariel, N., Barak, R., Segall, Y., Velan, B. and Shafferman, A. (1999) Exploring the active center of human acetylcholinesterase with stereoisomers of an organophosphorus inhibitor with two chiral centers. *Biochemistry* **38**, 3055–3066.
- Shi, J., Radić, Z. and Taylor, P. (2002) Inhibitors of different structure induce distinguishing conformations in the omega loop, Cys⁶⁹-Cys⁹⁶, of mouse acetylcholinesterase. *J. Biol. Chem.* **277**, 43301–43308.
- Taylor, P., Hosea, N. A., Tsigelny, I., Radić, Z. and Berman, H. A. (1997) Determining ligand orientation and transphosphorylation mechanism on acetylcholinesterase by R_p, S_p enantiomer selectivity and site-specific mutagenesis. *Enantiomer* **2**, 249–260.
- Marchot, P., Ravelli, R. B. G., Raves, M. L., Bourne, Y., Vellom, D. C., Kanter, J., Camp, S., Sussman, J. L. and Taylor, P. (1996) Soluble monomeric acetylcholinesterase from mouse: expression, purification, and crystallization in complex with fasciculins. *Prot. Sci.* **5**, 672–679.
- Ralston, J. S., Main, A. R., Kilpatrick, B. F. A. and Chasson, L. (1983) Use of procainamide gels in the purification of human and horse serum cholinesterases. *Biochem. J.* **211**, 243–250.
- Ellman, G. L., Courtney, K. D., Andres, Jr, V. and Featherstone, R. M. (1961) A new and rapid colorimetric determination of acetylcholinesterase activity. *Biochem. Pharmacol.* **7**, 88–95.
- Levy, D. and Ashani, Y. (1986) Synthesis and *in vitro* properties of a powerful quaternary methylphosphonate inhibitor of acetylcholinesterase. *Biochem. Pharmacol.* **35**, 1079–1085.
- Luo, C., Saxena, A., Smith, M., Garcia, G., Radić, Z., Taylor, P. and Doctor, B. P. (1999) Phosphoryl oxime inhibition of acetylcholinesterase during oxime reactivation is prevented by edrophonium. *Biochemistry* **38**, 9937–9947.
- Webb, J. L. (1963) General principles of inhibition. *Enzyme and Metabolic Inhibitors*, p. 188. Academic Press, New York.
- Reiner, E. and Radić, Z. (2000) Mechanism of action of cholinesterase inhibitors. In *Cholinesterases and Cholinesterase Inhibitors* (Giacobini, E., ed.), pp. 103–119. Martin Dunitz, London.
- Hosea, N. A., Radić, Z., Tsigelny, I., Berman, H. A., Quinn, D. M. and Taylor, P. (1996) Aspartate 74 as a primary determinant in acetylcholinesterase governing specificity to cationic organophosphates. *Biochemistry* **35**, 10995–11004.
- Masson, P., Froment, M.-T., Bartels, C. F. and Lockridge, O. (1996) Asp70 in the peripheral anionic site of human butyrylcholinesterase. *Eur. J. Biochem.* **235**, 36–48.
- Simeon-Rudolf, V., Reiner, E., Evans, R. T., George, P. M. and Potter, H. C. (1999) Catalytic parameters for the hydrolysis of butyrylthiocholine by human serum butyrylcholinesterase variants. *Chem. Biol. Interact.* **119–120**, 165–171.
- Cousin, X., Hotelier, T., Giles, K., Lievin, P., Toutant, J.-P. and Chatonnet, A. (1997) AChEdb: the database system for ESTHER, the α/β fold family of proteins and the cholinesterase gene server. *Nucleic Acids Res.* **25**, 143–146.
- Aldridge, W. N. and Reiner, E. (1972) Enzyme Inhibitors as Substrates: Interaction of Esterases with Esters of Organophosphorus and Carbamic Acids. North-Holland, Amsterdam.
- Shafferman, A., Velan, B., Ordentlich, A., Kronman, C., Grosfeld, H., Leitner, M., Flashner, Y., Cohen, S., Barak, D. and Ariel, N. (1992) Substrate inhibition of acetylcholinesterase: residues involved in signal transduction from the surface to the catalytic center. *EMBO J.* **11**, 3561–3568.
- Malany, S., Sawai, M., Sikorski, R. S., Seravalli, J., Quinn, D. Q., Radić, Z., Taylor, P., Kronman, C., Velan, B. and Shafferman, A. (2000) Transition state structure and rate determination for the acylation stage of acetylcholinesterase catalyzed hydrolysis of (acetylthio)choline. *J. Am. Chem. Soc.* **122**, 2981–2987.
- Millard, C. B., Koellner, G., Ordentlich, A., Shafferman, A., Silman, I. and Sussman, J. L. (1999) Reaction products of acetylcholinesterase and VX reveal a mobile histidine in the catalytic triad. *J. Am. Chem. Soc.* **121**, 9883–9884.
- Millard, C. B., Kryger, G., Ordentlich, A., Greenblatt, H. M., Harel, M., Raves, M. L., Segall, Y., Barak, D., Shafferman, A., Silman, I. and Sussman, J. L. (1999) Crystal structures of aged phosphorylated acetylcholinesterase: nerve agent reaction products at the atomic level. *Biochemistry* **38**, 7032–7039.
- Changeux, J.-P. (1966) Responses of acetylcholinesterase from *Torpedo marmorata* to salts and curarizing drugs. *Mol. Pharmacol.* **2**, 369–392.
- Epstein, D. J., Berman, H. A. and Taylor, P. (1979) Ligand-induced conformational changes in acetylcholinesterase investigated with fluorescent phosphonates. *Biochemistry* **18**, 4749–4754.
- De Ferrari, G. V., Mallender, W. D., Inestrosa, N. C. and Rosenberry, T. L. (2001) Thioflavin T is a fluorescent probe of the acetylcholinesterase peripheral site that reveals conformational interactions between the peripheral and acylation sites. *J. Biol. Chem.* **276**, 23282–23287.
- Ordentlich, A., Barak, D., Kronman, C., Ariel, N., Segall, Y., Velan, B. and Shafferman, A. (1996) The architecture of human acetylcholinesterase active center probed by interactions with selected organophosphorus inhibitors. *J. Biol. Chem.* **271**, 11953–11962.
- Wong, L., Radić, Z., Brüggemann, R. J. M., Hosea, N. A., Berman, H. A. and Taylor, P. (2000) Mechanism of oxime reactivation of acetylcholinesterase analyzed by chirality and mutagenesis. *Biochemistry* **39**, 5750–5757.
- Kaplan, D., Ordentlich, A., Barak, D., Ariel, N., Kronman, C., Velan, B. and Shafferman, A. (2001) Does "butyrylization" of acetylcholinesterase through substitution of the six divergent aromatic amino acids in the active center gorge generate an enzyme mimic of butyrylcholinesterase? *Biochemistry* **40**, 7433–7445.

Received 29 November 2002/17 March 2003; accepted 28 March 2003

Published as BJ Immediate Publication 31 March 2003, DOI 10.1042/BJ20021862

Mutant Cholinesterases Possessing Enhanced Capacity for Reactivation of Their Phosphonylated Conjugates[†]

Zrinka Kovarik,^{‡,§} Zoran Radić,[‡] Harvey A. Berman,^{||} Vera Simeon-Rudolf,[§] Elsa Reiner,[§] and Palmer Taylor^{*,‡}

Department of Pharmacology, University of California at San Diego, La Jolla, California 92093-0636,
Institute for Medical Research and Occupational Health, HR-10000 Zagreb, Croatia, and Department of Pharmacology and
Toxicology, School of Medicine, University at Buffalo, Buffalo, New York 14214

Received December 5, 2003; Revised Manuscript Received January 12, 2004

ABSTRACT: Selective mutants of mouse acetylcholinesterase (AChE; EC 3.1.1.7) phosphonylated with chiral *S*_P- and *R*_P-cycloheptyl, -3,3-dimethylbutyl, and -isopropyl methylphosphonyl thiocholines were subjected to reactivation by the oximes HI-6 and 2-PAM and their reactivation kinetics compared with wild-type AChE and butyrylcholinesterase (EC 3.1.1.8). Mutations in the choline binding site (Y337A, Y337A/F338A) or combined with acyl pocket mutations (F295L/Y337A, F297I/Y337A, F295L/F297I/Y337A) were employed to enlarge active center gorge dimensions. HI-6 was more efficient than 2-PAM (up to 29000 times) as a reactivator of *S*_P-phosphonates (*k*_r ranged from 50 to 13000 min⁻¹ M⁻¹), while *R*_P conjugates were reactivated by both oximes at similar, but far slower, rates (*k*_r < 10 min⁻¹ M⁻¹). The Y337A substitution accelerated all reactivation rates over the wild-type AChE and enabled reactivation even of *R*_P-cycloheptyl and *R*_P-3,3-dimethylbutyl conjugates that when formed in wild-type AChE are resistant to reactivation. When combined with the F295L or F297I mutations in the acyl pocket, the Y337A mutation showed substantial enhancements of reactivation rates of the *S*_P conjugates. The greatest enhancement of 120-fold was achieved with HI-6 for the F295L/Y337A phosphonylated with the most bulky alkoxy moiety, *S*_P-cycloheptyl methylphosphonate. This significant enhancement is likely a direct consequence of simultaneously increasing the dimensions of both the choline binding site and the acyl pocket. The increase in dimensions allows for optimizing the angle of oxime attack in the spatially impacted gorge as suggested from molecular modeling. Rates of reactivation reach values sufficient for consideration of mixtures of a mutant enzyme and an oxime as a scavenging strategy in protection and treatment of organophosphate exposure.

Organophosphates are potent inhibitors of acetylcholinesterase (AChE; EC 3.1.1.7) and butyrylcholinesterase (BChE; EC 3.1.1.8). The progressive inhibition of cholinesterases by organophosphates is due to phosphorylation (denotes phosphorylation and phosphorylation) of their active center serine characterized by the formation of conjugates, which react very slowly with water. Inhibition of AChE is the main cause of organophosphate toxicity (1). Early studies on reactivation of the enzyme by Wilson and colleagues showed that, by directing nucleophiles to the active site, conjugated organophosphates could be released, regenerating the active enzyme (2, 3). Strong nucleophiles such as oximes are particularly effective in reactivating organophosphate—

cholinesterase conjugates. Nucleophilic strength, the orientation of the nucleophile with respect to the conjugated organophosphate, and the rate of aging (postinhibitory dealkylation) are three factors well-known to affect reactivation. During the past several decades, effective oximes have been developed as antidotes to cholinesterase poisoning that greatly improve efficacy of treatment of acute organophosphate poisoning (4). The monopyridinium oxime, 2-PAM, and bispyridinium oxime, HI-6, are the most potent reactivating agents in use in antidotal therapy (Figure 1). The effectiveness of oxime reactivators is primarily attributed to the nucleophilic displacement rate of the organophosphates, but efficiency varies with the structure of the bound organophosphate, the source of enzyme and the oxime.

The crystal structures of AChE (5–7) provide templates for detailed structural studies on ligand access to the impacted enzyme active center gorge and steric constraints within the active center gorge that govern selectivity in organophosphate inhibition (8–13) and oxime reactivation (14–18). The site of conjugation by organophosphates lies at the base of a narrow and 18–20 Å deep gorge. The gorge wall of AChE is lined largely by aromatic side chains contributing to a well-defined acyl pocket and choline binding site at the base of the gorge (19, 20). Therefore, the orientation of the associated

[†] This work was supported by Grants DAMD17C8014 and R37-GM18360 to P.T., Grant 0022014 to V.S.-R., and fellowships of the Ministry of Science and Technology of the Republic of Croatia and the Wood-Whelan Research Fellowship (IUBMB) to Z.K.

* To whom correspondence should be addressed. Telephone: 858-534-1366. Fax: 858-534-8248. E-mail: pwtaylor@ucsd.edu.

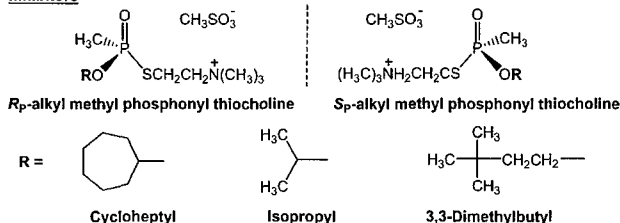
[‡] University of California at San Diego.

[§] Institute for Medical Research and Occupational Health.

^{||} University at Buffalo.

¹ Abbreviations: AChE, acetylcholinesterase; ATCh, acetylthiocholine iodide; BChE, butyrylcholinesterase; 2-PAM, 2-(hydroxyimino-methyl)-1-methylpyridinium iodide; HI-6, 1-(2'-hydroxyiminomethyl-1'-pyridinium)-3-(4''-carbamoyl-1''-pyridinium)-2-oxapropane dichloride.

Inhibitors



Reactivators

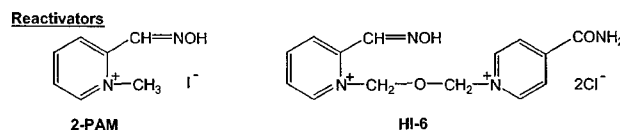


FIGURE 1: Structures of the organophosphonates and oximes used in this study.

and conjugated ligands within narrow confines of the gorge and the rates of nucleophilic attack by oxime at the conjugated phosphorus atom become important determinants of the reactivation mechanism.

In this study, we investigated structural and kinetic bases for reactivation of the enzyme conjugates by oximes using a combined structure–activity approach where both inhibitor and enzyme were modified systematically. Mouse AChE was modified within the choline binding site (Y337A, F338A) and the acyl pocket (F295L, F297I) in various mutation permutations. The mutant AChE species, except for F338A, contained mutations that resemble residues found at structurally equivalent positions in BChE (residue numbering corresponds to mouse AChE). This enabled us to examine the basis of the divergence between oxime reactivation of phosphonylated AChE and BChE. By using a congeneric series of *S_p* and *R_p* enantiomeric pairs of alkyl methylphosphonates and two related oximes of different dimensions, HI-6 and 2-PAM (Figure 1), subtle differences in reactivation capability have been analyzed with the objective of enhancing reactivation rates.

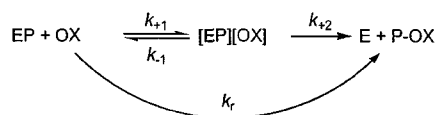
MATERIALS AND METHODS

Chemicals. *S_p*- and *R_p*-alkyl methylphosphonyl thiocholines were synthesized and isolated as resolved *S_p* and *R_p* enantiomers (8). Stock solutions in acetonitrile were kept at -20°C , and aliquots were diluted in water immediately before use. HI-6 was a gift of B. P. Doctor at Walter Reed Army Research Center, Washington, DC. 2-PAM, acetylthiocholine iodide (ATCh), 5,5'-dithiobis(2-nitrobenzoic acid), and bovine serum albumin (BSA) were purchased from Sigma Chemical Co., St. Louis, MO. Both oximes, HI-6 and 2-PAM, were kept at -20°C , and they were dissolved and diluted in water immediately before use.

Enzymes. Preparation, expression, purification, and characterization of recombinant wild-type mouse AChE and wild-type mouse BChE and AChE mutants were described in detail in previous studies (9, 13, 19, 21).

Oxime Reactivation of the Phosphonylated Enzyme. Wild-type and mutant enzymes (concentrations between 0.01 and 1.0 μM) were reacted with an $\sim 10\%$ molar excess of the corresponding alkyl methylphosphonate until inhibition was greater than 90%. Typical inhibition times were 30 min to 2 h, except for the case of slower inhibition with *R_p* enantiomers, when the required time was up to 6 h. The inhibited enzyme was passed through a Sephadex G-50 spin column

Scheme 1



(Pharmacia) to remove excess unconjugated organophosphate and incubated with specified concentrations of oxime in 10 mM Tris-HCl buffer, pH 8.0, containing 0.01% BSA, 40 mM MgCl_2 , and 100 mM NaCl. At specified time intervals, 5–10 μL of the reactivation mixture was diluted up to 100-fold, and residual activity was measured at 22°C by the Ellman method using ATCh as substrate (1.0 mM final concentration) (22). An equivalent sample of uninhibited enzyme was passed through a parallel column, diluted to the same extent as the inhibition mixture, and control activity was measured in the presence of oxime at concentrations used for reactivation. Both activities of the control and reactivation mixture were corrected for oxime-induced hydrolysis of ATCh, whenever oxime concentrations were greater than 1.0 mM.

Kinetics of Oxime Reactivation. Oxime reactivation of phosphylated cholinesterases proceeds according to Scheme 1. In this scheme EP is the phosphorylated enzyme, [EP][OX] is the reversible Michaelis-type complex between EP and the oxime (OX), E is the active enzyme and P–OX the phosphonylated oxime, k_{+2} is the maximum first-order rate constant, and k_r is the overall second-order rate constant of reactivation.

Scheme 1 is defined by the equation:

$$\ln \frac{[\text{EP}]_0}{[\text{EP}]_t} = \frac{k_{+2}[\text{OX}]}{K_{\text{OX}} + [\text{OX}]} t = k_{\text{obs}} t \quad (1)$$

where $[\text{EP}]_0$ and $[\text{EP}]_t$ are the concentrations of the phosphorylated enzyme at time zero and at time t , respectively. K_{OX} is equal to the ratio $(k_{-1} + k_{+2})/k_{+1}$, and it typically approximates the dissociation constant of the [EP][OX] complex. k_{obs} is the observed first-order rate constant of reactivation at any given oxime concentration.

When $K_{\text{OX}} \gg [\text{OX}]$, eq 1 simplifies to

$$\ln \frac{[\text{EP}]_0}{[\text{EP}]_t} = \frac{k_{+2}}{K_{\text{OX}}} [\text{OX}] t = k_r [\text{OX}] t = k_{\text{obs}} t \quad (2)$$

where from it follows that

$$k_r = \frac{k_{+2}}{K_{\text{OX}}} \quad (3)$$

Experimental data were presented as percent of reactivation

$$\% \text{ reactivation} = \frac{v_{(\text{EP}+\text{OX})_t}}{v_{(\text{E}+\text{OX})}} \times 100 \quad (4)$$

where $v_{(\text{EP}+\text{OX})_t}$ denotes the activity of the reactivated enzyme at time t and $v_{(\text{E}+\text{OX})}$ stands for the activity of the unmodified enzyme incubated with oxime. Both activities were corrected for oxime-induced hydrolysis of ATCh. If the enzyme was not completely inhibited prior to reactivation, both activities in eq 4 were also corrected for the enzyme activity at time

zero. Since $(100 - \% \text{ reactivation})$ is equal to $100[\text{EP}]_t / [\text{EP}]_0$, one can relate the experimental data to eqs 1 and 2.

At each oxime concentration, k_{obs} was calculated from the slope of the initial portion of $\log(100 - \% \text{ reactivation})$ vs time of reactivation plot as $k_{\text{obs}} = -2.303 \times \text{slope}$, assuming an approach to 100% reactivation. When reactivation followed eq 1, k_{+2} and K_{ox} were obtained by the nonlinear fit of the relationship between k_{obs} vs $[\text{OX}]$; k_r was calculated from eq 3. When reactivation followed eq 2, k_{obs} vs $[\text{OX}]$ was linear, and the slope corresponded to k_r ; in this case constants k_{+2} and K_{ox} could not be determined.

Molecular Modeling. Molecular modeling analysis was performed in order to ascertain probable HI-6 orientations inside the active center gorges of S_{P} -cycloheptyl methylphosphonylated wild-type mouse AChE and F295L/Y337A mouse AChE, where the HI-6 oxime group was facing the phosphorus conjugated to the AChE active center serine. The model of HI-6 was built as described earlier (14, 18) and docked manually inside active center gorges of either S_{P} -cycloheptyl wild-type mouse AChE (taken from ref 18) or S_{P} -cycloheptyl F295L/Y337A mutant mouse AChE (generated from phosphonylated wild-type mouse AChE using the Insight II program suite, Accelrys, San Diego) to achieve starting structures of the complex. Molecular dynamics of the complex was then performed using the procedure described earlier (14) and repeated 20 times for both wild-type and mutant complexes. During the computation the conformation of the HI-6 molecule was unrestricted, as were the side chains of AChE residues at positions 295, 297, 338, and phosphonylated serine at 203. The resulting 20 conformers of the complex were analyzed for their total energy and distance between the oxime group oxygen and phosphonate phosphorus.

RESULTS

Oxime Reactivation Kinetics. Recombinant DNA-expressed mouse cholinesterases phosphonylated with S_{P} - and R_{P} -alkyl methylphosphonyl thiocholines were subjected to reactivation by HI-6 and 2-PAM. The series of reactivation reactions were run over a wide concentration range of oximes to determine constants k_{+2} , K_{ox} , and k_r (Figure 2). The results for the 74 distinct oxime-enzyme combinations are listed in Tables 1–6. In 18 reactions, the rates of reactivation were so slow that rate constants could not be reliably determined. For these reactions only the maximum percent of reactivation obtained within the stated time is listed in the tables. For reactivation of the triple mutant F295L/F297I/Y337A only limiting values of constants were calculated because reactivation was measured at one oxime concentration only. For 8 reactions the k_{obs} values were a linear function of the oxime concentration; consequently, only the bimolecular k_r constants could be calculated. For 44 reactions, all three constants (k_{+2} , K_{ox} , k_r) were obtained as presented in Figure 2 and are displayed in the tables including the maximum percent of reactivation obtained with the highest oxime concentration after the indicated time of reaction. The mean relative standard error of k_{+2} was 11%, while the corresponding errors of K_{ox} and k_r were larger, 43% and 39%, respectively.

All k_{obs} constants were calculated from the initial slope of the reactivation profile. For some of the reactions, typically those where the reactivation was not complete (cf. Tables

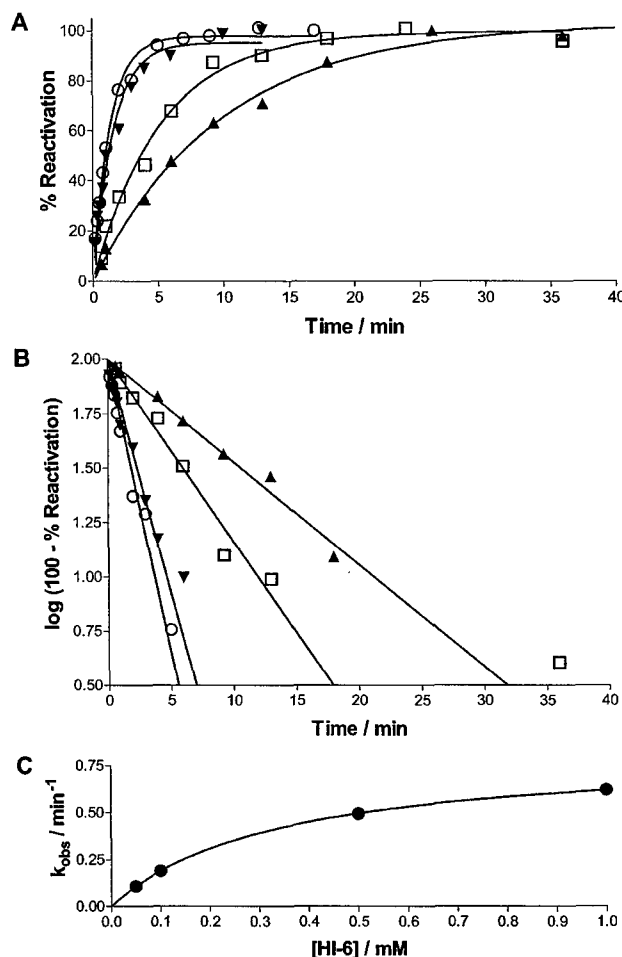


FIGURE 2: Reactivation of the S_{P} -isopropyl methylphosphonyl F297I/Y337A conjugate by HI-6. (A) Single datum points indicate calculated percent reactivation by eq 4 after the designated time of reactivation with (○) 1, (▼) 0.5, (□) 0.1, and (▲) 0.05 mM HI-6. (B) Slopes of the reactivation curve yield k_{obs} constants. (C) k_{obs} is plotted as a function of HI-6 and the line fitted using eq 1.

1–6), the kinetics at the longer time intervals deviated from the first-order process described in eqs 1 and 2. This deviation could be due to a fraction of the phosphonylated enzyme aging with the loss of the alkoxy group, reinhibition of the active enzyme by the phosphonylated oxime, the presence of a minor abundance oxime-resistant conformation, and/or spontaneous reactivation of the phosphonylated conjugates.

Aging of the three S_{P} -phosphonate-conjugated Y337A mutants was examined by measuring the extent of reactivation with high HI-6 concentrations added at designated intervals after inhibition with the phosphonate and removal of excess inhibitor. Aging of S_{P} -isopropyl and S_{P} -3,3-dimethylbutyl methylphosphonyl Y337A conjugates was not detected over 36 h, while the aging rate constant of S_{P} -cycloheptyl methyl conjugated Y337A was 0.005 min^{-1} . This is faster than the reported aging rate constant of S_{P} -cycloheptyl methyl conjugated wild-type AChE (0.0004 min^{-1} ; 18).

In a previous study it was shown that spontaneous reactivation of phosphonylated *Torpedo californica* AChE and human plasma BChE by cycloheptyl, isopropyl, and 3,3-dimethylbutyl methylphosphonyl thiocholine enantiomers

Table 1: Reactivation of Recombinant DNA-Derived Mouse Cholinesterases Phosphorylated with *S*_P-Cycloheptyl Methylphosphonyl Thiocholine^a

reactivator (mM)	enzyme	k_{+2} (min ⁻¹)	K_{ox} (mM)	k_r (min ⁻¹ M ⁻¹)	% react _{max}	time
HI-6 (0.2–20)	AChE wt	0.60 ± 0.04	5.4 ± 0.8	112 ± 19	90	5 min
HI-6 (0.02–0.5)	Y337A			2000 ± 90	80	1 min
HI-6 (0.002–0.1)	F295L/Y337A			13180 ± 1414	80	3 min
HI-6 (0.01–5)	F297I/Y337A	6.0 ± 0.5	2.6 ± 0.4	2300 ± 400	100	1 min
HI-6 (0.2–10)	Y337A/F338A	0.051 ± 0.003	0.50 ± 0.12	102 ± 26	80	30 min
HI-6 (10)	F295L/F297I/Y337A ^b			≥24	80	20 min
HI-6 (1, 30)	BChE wt				<10	48 h
2-PAM (1–20)	AChE wt	0.0040 ± 0.0007	6.1 ± 3.0	0.66 ± 0.34	70	15 h
2-PAM (0.1–40)	Y337A	0.0025 ± 0.0001	0.62 ± 0.14	4.1 ± 1.0	80	5 h
2-PAM (0.4–20)	F295L/Y337A	0.016 ± 0.003	10 ± 3	1.7 ± 0.5	70	3 h
2-PAM (2–30)	F297I/Y337A	0.018 ± 0.002	2.7 ± 1.2	6.9 ± 3.3	70	2 h
2-PAM (1–60)	Y337A/F338A	0.00035 ± 0.00002	0.75 ± 0.45	0.47 ± 0.29	40	25 h
2-PAM (40)	F295L/F297I/Y337A ^b			≥0.12	100	5 h
2-PAM (5, 40)	BChE wt				<5	48 h

^a Constants (±standard errors) are calculated (eqs 1–3) from k_{obs} constants (8–16 values) obtained in two to seven experiments. The maximal percent of reactivation (% react_{max}) measured within the specified time of the experiment is also given. ^b Only one k_{obs} was determined (0.24 ± 0.04 min⁻¹ with HI-6 and 0.0048 ± 0.0011 min⁻¹ with 2-PAM).

Table 2: Reactivation of Recombinant DNA-Derived Mouse Cholinesterases Phosphorylated with *S*_P-3,3-Dimethylbutyl Methylphosphonyl Thiocholine^a

reactivator (mM)	enzyme	k_{+2} (min ⁻¹)	K_{ox} (mM)	k_r (min ⁻¹ M ⁻¹)	% react _{max}	time
HI-6 (0.05–5)	AChE wt	0.39 ± 0.09	3.8 ± 1.8	102 ± 53	80	10 min
HI-6 (0.05–5)	Y337A	3.2 ± 0.5	2.8 ± 1.0	1200 ± 490	100	2 min
HI-6 (0.01–1)	F295L/Y337A			1300 ± 60	100	2 min
HI-6 (0.01–10)	F297I/Y337A	1.4 ± 0.1	1.9 ± 0.5	720 ± 180	100	5 min
HI-6 (1–40)	Y337A/F338A	0.10 ± 0.01	2.1 ± 1.2	47 ± 28	80	20 min
HI-6 (10)	F295L/F297I/Y337A ^b			≥31	80	10 min
HI-6 (0.5–20)	BChE wt	0.73 ± 0.14	7.1 ± 3.2	103 ± 51	100	10 min
2-PAM (1–40)	AChE wt			0.18 ± 0.01	90	8 h
2-PAM (5–40)	Y337A			0.041 ± 0.003	80	33 h
2-PAM (0.5–40)	F295L/Y337A	0.0018 ± 0.0002	2.8 ± 1.1	0.66 ± 0.27	90	25 h
2-PAM (10–60)	F297I/Y337A	0.0025 ± 0.0002	9.0 ± 3.6	0.27 ± 0.11	80	15 h
2-PAM (5–60)	Y337A/F338A	0.00023 ± 0.00001	0.54 ± 0.85	0.42 ± 0.65	60	70 h
2-PAM (40)	F295L/F297I/Y337A ^b			≥0.22	90	6 h
2-PAM (3–30)	BChE wt	0.028 ± 0.003	3.2 ± 1.7	8.7 ± 4.6	100	3 h

^a Constants (±standard errors) are calculated (eqs 1–3) from k_{obs} constants (5–15 values) obtained in two to four experiments. The maximal percent of reactivation (% react_{max}) measured within the specified time of the experiment is also given. ^b Only one k_{obs} was determined (0.31 ± 0.06 min⁻¹ with HI-6 and 0.0088 ± 0.0021 min⁻¹ with 2-PAM).

Table 3: Reactivation of Recombinant DNA-Derived Mouse Cholinesterases Phosphorylated with *S*_P-Isopropyl Methylphosphonyl Thiocholine^a

reactivator (mM)	enzyme	k_{+2} (min ⁻¹)	K_{ox} (mM)	k_r (min ⁻¹ M ⁻¹)	% react _{max}	time (min)
HI-6 (0.05–1)	AChE wt	0.20 ± 0.03	0.15 ± 0.09	1330 ± 780	90	10
HI-6 (0.2–20)	Y337A	1.13 ± 0.08	4.7 ± 0.8	240 ± 47	100	2
HI-6 (0.5–30)	F295L/Y337A	0.27 ± 0.01	0.37 ± 0.09	730 ± 180	80	10
HI-6 (0.05–1)	F297I/Y337A	0.95 ± 0.13	0.41 ± 0.14	2330 ± 844	100	5
HI-6 (1–20)	Y337A/F338A	0.26 ± 0.02	1.5 ± 0.6	178 ± 74	90	15
HI-6 (0.05–5)	BChE wt	0.014 ± 0.001	0.064 ± 0.024	215 ± 70	80	90
2-PAM (0.1–10)	AChE wt	0.095 ± 0.013	0.088 ± 0.075	1080 ± 940	100	30
2-PAM (0.2–40)	Y337A	0.21 ± 0.01	2.6 ± 0.3	82 ± 11	80	20
2-PAM (1–40)	F295L/Y337A			3.5 ± 0.4	90	30
2-PAM (0.1–40)	F297I/Y337A	2.9 ± 0.2	5.5 ± 1.3	534 ± 133	90	1
2-PAM (1–40)	Y337A/F338A	0.072 ± 0.004	1.5 ± 0.5	46 ± 14	90	30
2-PAM (0.05–10)	BChE wt	2.98 ± 0.01	2.39 ± 0.02	1250 ± 9	90	1

^a Constants (±standard errors) are calculated (eqs 1–3) from k_{obs} constants (6–19 values) obtained in two to five experiments. The maximal percent of reactivation (% react_{max}) measured within the specified time of the experiment is also given.

proceeded very slowly, if at all (rate constants less than 0.001 min⁻¹) (23). In initial studies, we did not observe spontaneous reactivation with return of AChE activity in several of the methylphosphonyl conjugates studied as we have observed for the dimethyl, diethyl, and diisopropylphosphoryl conjugates of mouse AChE (24). The phosphonyl oxime (product of reactivation) could reinhibit the free enzyme (2, 25, 26),

but we have yet to identify the inhibitory potency and the stability of these reactivation products.

Oxime Reactivation of the *S*_P-Alkyl Methylphosphonylated Cholinesterases. The kinetic parameters for reactivation of the *S*_P-cycloheptyl, *S*_P-3,3-dimethylbutyl, and *S*_P-isopropyl methylphosphonylated cholinesterases by HI-6 and 2-PAM are presented in Tables 1–3. All *S*_P conjugates were

Table 4: Reactivation of Recombinant DNA-Derived Mouse Cholinesterases Phosphorylated with *R*_P-Cycloheptyl Methylphosphonyl Thiocholine^a

reactivator (mM)	enzyme	k_{+2} (min ⁻¹)	K_{ox} (mM)	k_r (min ⁻¹ M ⁻¹)	% react _{max}	time (h)
HI-6 (1, 40)	AChE wt	0.00042 ± 0.00002	1.0 ± 0.2	0.41 ± 0.06	<15	50
HI-6 (0.3–20)	Y337A				50	85
HI-6 (1–30)	F295L/Y337A				<25	40
HI-6 (10–40)	F297I/Y337A				<25	72
HI-6 (0.2–2)	Y337A/F338A				<15	40
HI-6 (10–30)	BChE wt	0.00047 ± 0.00004	0.36 ± 0.16	1.3 ± 0.6	<15	50
2-PAM (1, 40)	AChE wt				<25	50
2-PAM (0.3–5)	Y337A				50	85
2-PAM (20–40)	F295L/Y337A				<25	40
2-PAM (5–40)	F297I/Y337A				<40	60
2-PAM (0.3–5)	Y337A/F338A	0.00040 ± 0.00010	0.99 ± 0.87	0.40 ± 0.37	40	20
2-PAM (20–40)	BChE wt				0.027 ± 0.001	70

^a Constants (±standard errors) are calculated (eqs 1–3) from k_{obs} constants (4–8 values) obtained in one to three experiments. The maximal percent of reactivation (% react_{max}) measured within the specified time of the experiment is also given.

Table 5: Reactivation of Recombinant DNA-Derived Mouse Cholinesterases Phosphorylated with *R*_P-3,3-Dimethylbutyl Methylphosphonyl Thiocholine^a

reactivator (mM)	enzyme	k_{+2} (min ⁻¹)	K_{ox} (mM)	k_r (min ⁻¹ M ⁻¹)	% react _{max}	time (h)
HI-6 (0.2–2)	AChE wt	0.00040 ± 0.00002	0.54 ± 0.14	0.74 ± 0.19	<15	40
HI-6 (0.2–40)	Y337A				70	35
HI-6 (1, 10)	F295L/Y337A				<25	60
HI-6 (10–40)	F297I/Y337A	0.00014 ± 0.00001	0.076 ± 0.051	1.8 ± 1.2	<25	60
HI-6 (0.2–2)	Y337A/F338A				50	40
HI-6 (1–10)	BChE wt				<25	50
2-PAM (0.3–5)	AChE wt	0.0007 ± 0.0000	0.38 ± 0.08	1.8 ± 0.4	<15	40
2-PAM (0.5–5)	Y337A				60	35
2-PAM (5, 30)	F295L/Y337A				<25	60
2-PAM (20–60)	F297I/Y337A	0.0079 ± 0.0011	13 ± 4	0.62 ± 0.22	<25	60
2-PAM (0.3–5)	Y337A/F338A				<15	60
2-PAM (3–30)	BChE wt				80	20

^a Constants (±standard errors) are calculated (eqs 1–3) from k_{obs} constants (4–8 values) obtained in one or two experiments. The maximal percent of reactivation (% react_{max}) measured within the specified time of the experiment is also given.

Table 6: Reactivation of Recombinant DNA-Derived Mouse Cholinesterases Phosphorylated with *R*_P-Isopropyl Methylphosphonyl Thiocholine^a

reactivator (mM)	enzyme	k_{+2} (min ⁻¹)	K_{ox} (mM)	k_r (min ⁻¹ M ⁻¹)	% react _{max}	time (h)
HI-6 (0.2–40)	AChE wt	0.0075 ± 0.0003	4.3 ± 0.7	1.7 ± 0.3	70	10
HI-6 (0.2–30)	Y337A	0.0071 ± 0.0004	0.97 ± 0.23	7.3 ± 1.8	80	8
HI-6 (1–30)	F295L/Y337A	0.0013 ± 0.0001	0.95 ± 0.56	1.3 ± 0.8	70	16
HI-6 (5–40)	F297I/Y337A	0.0021 ± 0.0003	16 ± 8	0.13 ± 0.07	50	16
HI-6 (1–30)	BChE wt	0.00035 ± 0.00004	1.1 ± 0.9	0.23 ± 0.25	40	25
2-PAM (0.3–40)	AChE wt	0.0029 ± 0.0004	1.9 ± 1.1	1.5 ± 0.9	70	20
2-PAM (0.3–40)	Y337A	0.0026 ± 0.0001	0.60 ± 0.21	4.3 ± 1.5	80	8
2-PAM (5–30)	F295L/Y337A	0.0096 ± 0.0039	10 ± 11	0.95 ± 1.09	80	10
2-PAM (5–60)	F297I/Y337A	0.024 ± 0.006	27 ± 13	0.041 ± 0.003	100	25
2-PAM (5–30)	BChE wt			0.88 ± 0.47	100	4

^a Constants (±standard errors) are calculated (eqs 1–3) from k_{obs} constants (6–10 values) obtained in two to four experiments. The maximal percent of reactivation (% react_{max}) measured within the specified time of the experiment is also given.

reactivated nearly completely with the exception of *S*_P-cycloheptyl methylphosphonylated BChE (cf. Table 1). The *S*_P-cycloheptyl methylphosphonylated F295L/F297I/Y337A mutant, structurally the most similar to BChE in substituted active center gorge residues, was reactivated between 80% and 100% by both oximes.

Reactivation of all *S*_P-phosphonylated AChE and mutant conjugates by HI-6 was appreciably faster than by 2-PAM. The difference in k_r between oximes is primarily dictated by the unimolecular reaction step, k_{+2} , which is more than 100-fold slower for 2-PAM than HI-6. Single or double substitutions involving F295L, F297I, and Y337A within the AChE gorge enhanced the k_r in reactivation of mutants phosphorylated with bulky methylphosphonates (cycloheptyl

and 3,3-dimethylbutyl; Tables 1 and 2), while only the F297I/Y337A double mutation enhanced reactivation of all three *S*_P conjugates. The greatest enhancement of k_r (about 120-fold) over the wild-type AChE was obtained in reactivation of *S*_P-cycloheptyl methylphosphonyl F295L/Y337A AChE by HI-6 (cf. Table 1); the determined k_r was the greatest for all reactions reported in this paper.

Both wild-type AChE and BChE phosphorylated with *S*_P-isopropyl methylphosphonate were reactivated by both oximes more rapidly (higher k_r value) than the wild-type enzymes phosphorylated by the more bulky *S*_P-3,3-dimethylbutyl and *S*_P-cycloheptyl methylphosphonates (cf. Table 3 vs Tables 1 and 2). Although k_r for 2-PAM reactivation of wild-type AChE and BChE was similar, the component K_{ox}

and k_{+2} constants differed by 30-fold where phosphonylated AChE had a higher affinity (i.e., lower K_{ox}) and lower k_{+2} for 2-PAM, and on the other hand, phosphonylated BChE had a higher maximum reactivation rate constant (k_{+2}).

Oxime Reactivation of the R_p -Alkyl Methylphosphonylated Cholinesterases. Tables 4–6 present results for reactivation of the R_p -cycloheptyl, R_p -3,3-dimethylbutyl, and R_p -isopropyl methylphosphonylated enzymes. HI-6 and 2-PAM showed similar but low reactivation efficiency (from 34 conjugates only 18 were reactivated). For the bulky R_p -cycloheptyl (Table 4) and R_p -3,3-dimethylbutyl (Table 5) methylphosphonylated wild-type AChE reactivation was not evident with either HI-6 or 2-PAM, while the corresponding BChE conjugates were reactivated by 2-PAM nearly completely albeit at slow rates. Hence, 2-PAM reactivation showed an inverted stereoselectivity for the cycloheptyl methylphosphonyl BChE conjugate: the S_p conjugate was resistant to reactivation (cf. Table 1), while the R_p conjugate was reactivated.

Reactivation kinetics of mouse single residue mutants of AChE conjugated with these methylphosphonates was previously studied by Wong et al. (18). Data given in the present paper agree with the reported results except for the reactivation of wild-type AChE conjugated with R_p -3,3-dimethylbutyl methylphosphonate (Table 5). In the present experiments this conjugate was found not to be reactivable, while in previous experiments substantial reactivation was observed by both oximes (18). In the previous study inhibition was carried out at a 14-fold excess of organophosphate, on average (range of 4-fold to 22-fold), and inhibition by a minor abundance of the S_p contaminant may have predominated under this condition. This situation was avoided in the current studies by using inhibitors in only 10% stoichiometric excess.

Reactivation rates of the less bulky R_p -isopropyl methyl phosphonylated enzymes presented in Table 6 were generally more rapid than the conjugates phosphonylated with the larger two R_p -phosphonates. The highest bimolecular reactivation rate for the R_p conjugate of Y337A was $7.3 \text{ min}^{-1} \text{ M}^{-1}$ for HI-6 and $4.3 \text{ min}^{-1} \text{ M}^{-1}$ for 2-PAM. Comparing these reactivation rates with the rates of R_p -Y337A conjugates in Tables 4 and 6, it follows that R_p -isopropyl methyl phosphonylated Y337A had the highest k_{+2} value. The Y337A mutation coupled with F338A also showed appreciable rates of reactivation of R_p -cycloheptyl methylphosphonyl Y337A/F338A AChE by 2-PAM and R_p -3,3-dimethylbutyl methylphosphonyl Y337A/F338A AChE by HI-6, but reactivation was not complete.

Molecular Modeling. Models of the reversible Michaelis-type complexes (Figure 3; [EP][OX] in Scheme 1) between HI-6 and either S_p -cycloheptyl methylphosphonylated wild-type mouse AChE or F295L/Y337A mouse AChE resulting from molecular dynamics calculation indicate that, with the wild-type enzyme, HI-6 can assume only one distinct productive orientation with the slender molecule extended through the narrow gorge (Figure 3B). Within the enlarged gorge of the F295L/Y337A mutant AChE additional orientations appear likely. The HI-6 chain coils back into the enlarged choline binding site where the nonreactive carbamoyl pyridinium moiety is stabilized (cf. Figure 3A,C). The distance between the oxime oxygen and the phosphorus in wild-type conformations ($4.2 \pm 1.0 \text{ \AA}$, $n = 20$) and mutant

gorge conformations ($4.5 \pm 0.9 \text{ \AA}$, $n = 20$) appeared very similar and consistent with distances found for similar oxime–AChE complex models obtained by other authors (about 4.4 \AA measured for the structure deposited by Pang et al.: PDB accession codes 1JGA and 1JGB; 27).

DISCUSSION

Reactivation by the two oximes demonstrates the superiority of HI-6 over 2-PAM for reactivation of wild-type AChE and mutant S_p -phosphonate conjugates. Moreover, the enzyme conjugates showed a high degree of stereoselectivity for HI-6 reactivation, with preference of S_p over R_p enantiomers. Taken together with previous findings on organophosphate inactivation (9, 10, 13) and reactivation (18, 25, 28), oxime-mediated reactivation is governed by several principles.

Similar to inhibition by phosphonates, reactivation efficiency is enhanced by phosphonyl oxygen insertion into the oxyanion hole in the presumed transition state. Owing to the spatial constraints of the acyl pocket, the bulky R_p -methylphosphonates cannot achieve optimal positioning of alkoxy groups without distortion of structure. Accordingly, just as the R_p inhibitors react far more slowly with AChE (9, 10, 13), they are either resistant to reactivation or reactivate slowly (18). For R_p conjugates suboptimal positioning of the phosphonyl oxygen in the oxyanion hole and limitations on oxime access to the phosphonate both slow reactivation rates. However, a single mutation of the choline binding site, Y337A, enabled reactivation of the R_p conjugates. Reactivation was increased presumably because of an improved clearance in the formation of the pentacoordinate transition state and the reduction in steric constraints around residue 337. The tetrahedral phosphonate may move slightly toward the vacant area created by removal of the aromatic side chain at position 337, allowing a more favorable angle of oxime attack.

The spatial constraints of the gorge give rise to a dimensionally impacted organophosphate with a limited angle of access for the attacking nucleophile. Our previous studies of acyl pocket mutations suggest a nucleophilic attack route to the phosphorus atom coming from the acyl pocket direction (18). We show in this paper that enhancing clearance in the vicinity of Y337 has an influence on reactivation rates. Indeed, the double mutation involving F295 and Y337 yields the greatest rate enhancement. This suggests that the route of oxime attack still occurs from the acyl pocket side, but the tethered phosphonate is able to adopt an exposed position more amenable to attack, or new orientations of the attacking oxime allowed by the vacant area created near residue 337 optimize the attack angle.

The likely position of HI-6 in the mutant F295L/Y337A for the attack on phosphonylated serine is shown in Figure 3A. Simply opening the AChE choline binding site in all dimensions to enhance access of the oxime group to the phosphorus atom is not sufficient to increase reactivation. Additional substitution by F338A leading to a more open gorge appeared counterproductive for reactivation (cf. Table 1). Certain aromatic residues may be required in order to stabilize the oxime in the proper orientation between F338 and F297 as shown in Figure 3. Hence, reactivation of S_p -cycloheptyl methylphosphonyl Y337A/F338A conjugate was



FIGURE 3: (A) Stereo image of an energy-minimized HI-6 conformation (carbon atoms in yellow, nitrogen in blue, oxygen in red) in the F295L/Y337A mouse AChE (in blue ribbon) *S_P*-cycloheptyl methylphosphonylated active center gorge. The active center is viewed through the gorge opening. The lowest energy conformer is shown, out of a cluster of 20 similar resulting conformations. The dotted white line indicates the direction of nucleophilic attack of HI-6. Only selected AChE residues are displayed in blue, white (catalytic triad), and orange (residues mutated in this study). (B, C) Cutaway diagrams at identical angles of the HI-6 complex with wild-type mouse AChE (panel B) and in the F295L/Y337A mutant mouse AChE (panel C). The AChE represented by Connolly solvent-accessible surface was cut approximately in half to reveal the position, size, and depth of the active center gorge in the wild-type and mutant AChE. The orange arrow indicates the position of the F297 side chain hidden behind a surface.

not as efficient as was reactivation of the F295L/Y337A conjugate.

While opening of the gorge can greatly enhance oxime efficacy, a gorge devoid of critical aromatic residues or a tethered phosphonate with many degrees of freedom and torsional movement, as found for BChE, yields an environment not conducive to efficient reactivation by HI-6, whereas reactivation by the smaller, but less efficient, 2-PAM molecule is less influenced by this difference. Hence, efficacy of oximes is dependent not only on the oxime structure but also on the position of the conjugated phosphorus residue. Attack by the oxime is believed to proceed through a pentavalent (trigonal bipyramidal) intermediate and formation of the phosphorylated oxime. Both 2-PAM and HI-6 have their oxime groups in the *ortho* position to the cationic pyridinium nitrogen, and their attacking orientations should have distinctive steric constraints. Hence, the inability of 2-PAM and HI-6 to cause reactivation of certain conjugates, particularly *R_P* conjugates, may not prevail for all oximes. Obidoxime and TMB-4, two symmetric dioximes with oxime

groups *para* to the pyridinium ring, reactivate *R_P* conjugates to near completion although at very slow rates (18, 23). Fortunately, the *R_P* enantiomers that are resistant to oxime reactivation are also less reactive as phosphonylation agents (9, 10, 13). Hence, they will be the less reactive and toxic of the chiral pair.

A practical outgrowth of these studies is the application of mutant AChE–oxime combinations to catalyze the hydrolysis of organophosphates both *in vitro* and *in vivo*. Cholinesterases in the plasma are efficient scavengers of organophosphates in terms of reactivity; however, their capacity is limited by virtue of the 1:1 stoichiometry between the small organophosphate (100–200 Da) and the ~70 kDa subunit bearing the catalytic serine. Hence, an enzyme–reactivator combination catalytic to the organophosphate hydrolysis, rather than stoichiometric to conjugation, would greatly reduce doses needed for scavenging.

Lockridge et al. (17) generated mutations in butyrylcholinesterase that catalyze the hydrolysis of organophosphates. However, mutations that enable organophosphate turnover

also compromise its capacity to react initially with the organophosphate, thus limiting the potential of butyrylcholinesterase in vivo. By contrast, the mutations described here that enhance oxime reactivation react efficiently with the methylphosphonates as described previously (13), and the limitations in scavenging capacity then depend on efficiency of the oxime to continually regenerate active AChE. By enhancing the rate some 120-fold, we approach a range where scavenging efficiency has a practical outcome. Efficiency of scavenging is also a pharmacokinetic consideration since the introduced organophosphate must be scavenged in the plasma before it distributes into extracellular space and/or accesses the blood-brain barrier. As shown here, the enhanced scavenging capacity is manifested to the greatest extent in those bulky *S_P* enantiomers that are most intractable to reactivation. Of the offending methylphosphonates, cyclosarin and soman would fall into this category.

REFERENCES

- Chambers, H. W. (1992) Organophosphorus compounds: An Overview, in *Organophosphates: Chemistry, Fate, and Metabolism* (Chambers, J. E., and Levi, P. E., Eds.) pp 3–17, Academic Press, San Diego, CA.
- Wilson, I. B., and Ginsburg, S. (1955) A powerful reactivator of alkylphosphate-inhibited acetylcholinesterase, *Biochim. Biophys. Acta* 18, 168–170.
- Froede, H. C., and Wilson, I. B. (1971) Acetylcholinesterase, in *The Enzymes* (Boyer, P. D., Ed.) 3rd ed., Vol. 5, pp 87–114, Academic Press, New York and London.
- Flanagan, J., and Jones, A. L. (2001) *Antidotes*, pp 245–267, Taylor and Francis, London and New York.
- Sussman, J. L., Harel, M., Frolow, F., Oefner, C., Goldman, A., Toker, L., and Silman, I. (1991) Atomic structure of acetylcholinesterase from *Torpedo californica*: A prototypic acetylcholine-binding protein, *Science* 253, 872–897.
- Bourne, Y., Taylor, P., and Marchot, P. (1995) Acetylcholinesterase inhibition by fasciculin: crystal structure of the complex, *Cell* 83, 503–512.
- Kryger, G., Harel, M., Giles, K., Toker, L., Velan, B., Lazar, A., Kronman, C., Barak, D., Ariel, N., Shafferman, A., Silman, I., and Sussman, J. L. (2000) Three-dimensional structure of a complex of E2020 with acetylcholinesterase from *Torpedo californica*, *Acta Crystallogr., Sect. D* 56, 1385–1394.
- Berman, H. A., and Leonard, K. (1989) Chiral reactions of acetylcholinesterase probed with enantiomeric methylphosphonothioates, *J. Biol. Chem.* 264, 3942–3950.
- Hosea, N. A., Berman, H. A., and Taylor, P. (1995) Specificity and orientation of trigonal carboxylesters and tetrahedral phosphonylesters in cholinesterase, *Biochemistry* 34, 11528–11536.
- Hosea, N. A., Radić, Z., Tsigelny, I., Berman, H. A., Quinn, D. M., and Taylor, P. (1996) Aspartate 74 as a primary determinant in acetylcholinesterase governing specificity to cationic organophosphates, *Biochemistry* 35, 10995–11004.
- Taylor, P., Hosea, N. A., Tsigelny, I., Radić, Z., and Berman, H. A. (1997) Determining ligand orientation and transphosphorylation mechanism on acetylcholinesterase by R_P, S_P enantiomer selectivity and site-specific mutagenesis, *Enantiomer* 2, 249–260.
- Ordentlich, A., Barak, D., Kronman, C., Benschop, H. P., De Jong, L. P. A., Ariel, N., Barak, R., Segall, Y., Velan, B., and Shafferman, A. (1999) Dissection of the human acetylcholinesterase active center determinants of substrate specificity—Identification of residues constituting the anionic site, the hydrophobic site, and the acyl pocket, *Biochemistry* 38, 3055–3066.
- Kovarik, Z., Radić, Z., Berman, H. A., Simeon-Rudolf, V., Reiner, E., and Taylor, P. (2003) Acetylcholinesterase active centre and gorge conformations analysed by combinatorial mutations and enantiomeric phosphonates, *Biochem. J.* 373, 33–40.
- Ashani, Y., Radić, Z., Tsigelny, I., Vellom, D. C., Pickering, N., Quinn, D. M., Doctor, B. P., and Taylor, P. (1995) Amino acid residues controlling reactivation of organophosphoryl conjugates of acetylcholinesterase by mono- and bisquaternary oximes, *J. Biol. Chem.* 270, 6370–6380.
- Grosfeld, H., Barak, D., Ordentlich, A., Velan, B., and Shafferman, A. (1996) Interactions of oxime reactivators with diethylphosphoryl adducts of human acetylcholinesterase and its mutant derivatives, *Mol. Pharmacol.* 50, 639–649.
- Masson, P., Froment, M.-T., Bartels, C. F., and Lockridge, O. (1997) Importance of aspartate-70 in organophosphate inhibition, oxime re-activation and aging of human butyrylcholinesterase, *Biochem. J.* 325, 53–61.
- Lockridge, O., Blong, R. M., Masson, P., Froment, M.-T., Millard, C. B., and Broomfield, C. A. (1997) A single amino acid substitution, Gly117His, confers phosphotriesterase (organophosphorus acid anhydride hydrolase) activity on human butyrylcholinesterase, *Biochemistry* 36, 786–795.
- Wong, L., Radić, Z., Brüggemann, R. J. M., Hosea, N., Berman, H. A., and Taylor, P. (2000) Mechanism of oxime reactivation of acetylcholinesterase analyzed by chirality and mutagenesis, *Biochemistry* 39, 5750–5757.
- Radić, Z., Pickering, N. A., Vellom, D. C., Camp, S., and Taylor, P. (1993) Three distinct domains in the cholinesterase molecule confer selectivity for acetylcholinesterase and butyrylcholinesterase inhibitors, *Biochemistry* 32, 12074–12084.
- Ordentlich, A., Barak, D., Kronman, C., Flashner, Y., Leitner, M., Segall, Y., Ariel, N., Cohen, S., Velan, B., and Shafferman, A. (1993) Dissection of the human acetylcholinesterase active center determinants of substrate specificity—Identification of residues constituting the anionic site, the hydrophobic site, and the acyl pocket, *J. Biol. Chem.* 268, 17083–17095.
- Marchot, P., Ravelli, R. B. G., Raves, M. L., Bourne, Y., Vellom, D. C., Kanter, J., Camp, S., Sussman, J. L., and Taylor, P. (1996) Soluble monomeric acetylcholinesterase from mouse—expression, purification, and crystallization in complex with fasciculin, *Protein Sci.* 5, 672–679.
- Ellman, G. L., Courtney, K. D., Andres, V., Jr., and Featherstone, R. M. (1961) A new and rapid colorimetric determination of acetylcholinesterase activity, *Biochem. Pharmacol.* 7, 88–95.
- Berman, H. A. (1998) A view from the gorge. Reactivation and importance of water, in *Structure and Function of Cholinesterases and Related Proteins* (Doctor, B. P., Taylor, P., Quinn, D. M., Rotundo, R. L., and Gentry, M. K., Eds.) pp 413–417, Plenum Press, New York and London.
- Jennings, L. L., Malecki, M., Komives, E. A., and Taylor, P. (2003) Direct analysis of the kinetic profiles of organophosphate-acetylcholinesterase adducts by MALDI-TOF mass spectrometry, *Biochemistry* 42, 11083–11091.
- Luo, C., Saxena, A., Smith, M., Garcia, G., Radić, Z., Taylor, P., and Doctor, B. P. (1999) Phosphoryl oxime inhibition of acetylcholinesterase during oxime reactivation is prevented by edrophonium, *Biochemistry* 38, 9937–9947.
- Ashani, Y., Bhattacharjee, A. K., Leader, H., Saxena, A., and Doctor, B. P. (2003) Inhibition of cholinesterase with cationic phosphonyl oximes highlights distinctive properties of the charged pyridine groups of quaternary oxime reactivators, *Biochem. Pharmacol.* 33, 191–202.
- Pang, Y.-P., Kollmeyer, T. M., Hong, F., Lee, J.-C., Hammond, P. I., Haugabouk, S. P., and Brimijoin, S. (2003) Rational design of alkylene-linked bis-pyridiniumaldoximes as improved acetylcholinesterase reactivators, *Chem. Biol.* 10, 491–502.
- Luo, C., Leader, H., Radić, Z., Maxwell, D. M., Taylor, P., Doctor, B. P., and Saxena, A. (2003) Two possible orientations of the HI-6 molecule in the reactivation of organophosphate-inhibited acetylcholinesterase, *Biochem. Pharmacol.* 66, 387–392.

BI036191A

Inhibitors of Different Structure Induce Distinguishing Conformations in the Omega Loop, Cys⁶⁹–Cys⁹⁶, of Mouse Acetylcholinesterase*

Received for publication, May 6, 2002, and in revised form, August 9, 2002
Published, JBC Papers in Press, August 24, 2002, DOI 10.1074/jbc.M204391200

Jianxin Shi, Zoran Radić, and Palmer Taylor‡

From the Department of Pharmacology, University of California, San Diego, La Jolla, California 92093

We have shown previously that association of reversible active site ligands induces a conformational change in an omega loop (Ω loop), Cys⁶⁹–Cys⁹⁶, of acetylcholinesterase. The fluorophore acrylodan, site-specifically incorporated at positions 76, 81, and 84, on the external portion of the loop not lining the active site gorge, shows changes in its fluorescence spectrum that reflect the fluorescent side chain moving from a hydrophobic environment to become more solvent-exposed. This appears to result from a movement of the Ω loop accompanying ligand binding. We show here that the loop is indeed flexible and responds to conformational changes induced by both active center and peripheral site inhibitors (gallamine and fasciculins). Moreover, phosphorylation and carbamoylation of the active center serine shows distinctive changes in acrylodan fluorescence spectra at the Ω loop sites, depending on the chirality and steric dimensions of the covalently conjugated ligand. Capping of the gorge with fasciculins, although it does not displace the bound ligand, dominates in inducing a conformational change in the loop. Hence, the ligand-induced conformational changes are distinctive and suggest multiple loop conformations accompany conjugation at the active center serine. The fluorescence changes induced by the modified enzyme may prove useful in the detection of organophosphates or exposure to cholinesterase inhibitors.

Acetylcholinesterase (AChE)¹ plays a pivotal role in neurotransmission by terminating the action of neurotransmitter, acetylcholine, at neuromuscular junction and other cholinergic synapses (1–3). AChE is one of most efficient enzymes known with hydrolysis of its natural substrate reaching diffusion-controlled limits. Inhibitors of AChE target two sites in the active site gorge: an active center at the base of a narrow gorge 20 Å in depth and a peripheral site at the gorge rim (4). At the active center, a residue triad (Ser²⁰³–

Glu³³⁴–His⁴⁴⁷) promotes acyl transfer and hydrolysis of the substrate, whereas Trp⁸⁶ at the gorge base primarily stabilizes choline moiety of the substrate through a cation– π interaction. Active site inhibitors block substrate binding either by associating with the tryptophan in the choline binding site (tacrine and edrophonium) or by reacting irreversibly with catalytic serine (carbamates and organophosphates). Peripheral site inhibitors, such as propidium and gallamine, inhibit catalytic activity through both steric blockade and allosterically altering catalytic efficiency of the active center residues (4–8).

To elucidate the conformational changes associated with mechanistically distinctive inhibitors, we developed a means for physically monitoring the conformation of purified mouse AChE by site-directed labeling with an environmentally sensitive fluorophore, acrylodan. Six single cysteine mutants were prepared for acrylodan conjugation (Fig. 1). Three were on the Cys⁶⁹–Cys⁹⁶ omega loop (Ω loop) flanking the active site gorge: L76C near the tip of the loop, and E81C and E84C on the outer surface not lining the gorge. Two residues on the opposing face of the gorge, H287C and Y124C, were selected, solvent exposure of which would be expected to be occluded by bound ligands that extend to the outer reaches of the gorge. A final residue, A262C, on a distal disulfide loop and whose temperature coefficient (B factor) would indicate flexible loop movement (9, 10), was selected as a control region. This residue is not anticipated to be influenced by ligand-induced changes in conformation. Our previous study showed a bathochromic emission shift of acrylodan conjugated at Ω loop residues 76, 81, and 84 upon binding of inhibitors, such as tacrine, edrophonium, huperzine A, and *m*-(*N,N,N*-trimethylammonio)trifluoromethyl acetophenone, that interact with Trp 86 in the choline binding site (11). Acrylodan fluorescence is exquisitely sensitive to dipole moment of the surrounding solvent or macromolecular milieu (12–14). A bathochromic shift reflects exposure to solvent around the fluorophore. This pattern likely results from a concerted movement in the Cys⁶⁹–Cys⁹⁶ Ω loop upon binding of reversible inhibitors.

Because a conformational change in the Ω loop induced by ligand is not reflected in the crystal structures of the AChEs studied to date (9–10, 15–18), and steady state catalysis by Ω loop mutant AChEs yielded minimal evidence for the loop being involved in the catalytic cycle (19, 20), we developed a means to measure directly conformation and solvent exposure in and around the active center gorge. In this study, we investigate the conformational changes reflected in acrylodan fluorescence for peripheral site inhibitors and for a congeneric series of carbamates and organophosphates that react covalently with the active center serine. Fluorescence measurements, combined with kinetics of inhibitor association, reveal a linkage

* This work was supported by United States Public Health Service Grants GM-R37-18360 and ES10337 and Department of Army Medical Defense Grant 17-1-8014 (to P. T.), and by National Institutes of Health Training Grant GM07752 (to J. S.). The costs of publication of this article were defrayed in part by the payment of page charges. This article must therefore be hereby marked "advertisement" in accordance with 18 U.S.C. Section 1734 solely to indicate this fact.

‡ To whom correspondence should be addressed. Tel.: 858-534-1366; Fax: 858-534-8248; E-mail: pwtaylor@ucsd.edu.

¹ The abbreviations used are: AChE, acetylcholinesterase; mAChE, mouse acetylcholinesterase; MEPQ, 7-[(methylethoxy)phosphinyl]-oxyl]-1-methylquinolinium iodide; DDVP, *O,O*-dimethyl *O*-(2,2-dichlorovinyl)phosphate; DFP, diisopropyl fluorophosphate; DMBMP, 3,3-dimethylbutyl methylphosphonyl; TCh, thiocholine; acrylodan, 6-acryloyl-2-dimethylaminonaphthalene; M7C, *N,N*-dimethylcarbamoyl *N*-methyl-7-hydroxyquinolinium.

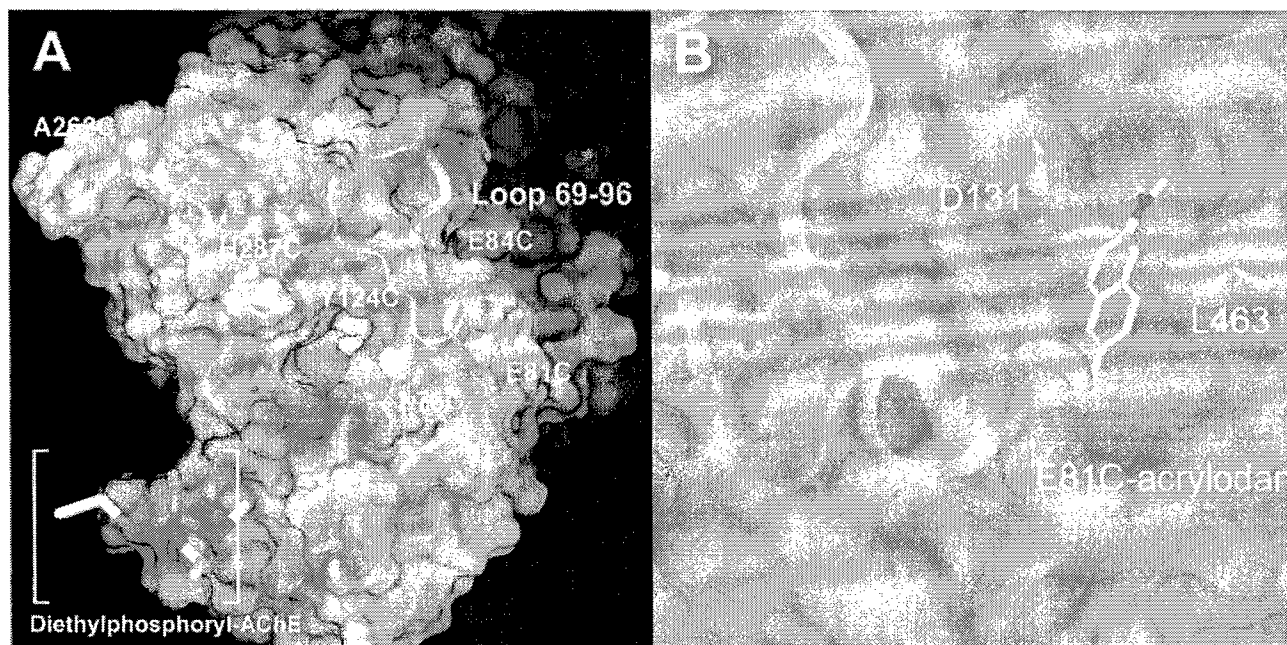


FIG. 1. *Panel A*, locations of introduced cysteines for fluorophore modification of mouse AChE. Residues 76, 81, and 84 are at the tip (residue 76) and outer portion (residues 81 and 84) of the Ω loop. Residues 124 and 287 are on an opposing face of the gorge and make up part of the peripheral anionic site. Residue 262 is on a small distal disulfide loop showing a large thermal factor in the crystal structure. White surface at the base of active site gorge shows the ethyl moiety of diethylphosphoryl-AChE when conjugated to serine 203 at the base of the active center gorge. *Panel B*, expanded view of the acrylodan side chain at the 81-position determined from an energy-minimized structure of mouse AChE (43). The aminonaphthalene moiety of acrylodan resides between the side chains of Asp¹³¹ and Leu⁴⁶³.

between inhibition and a conformational change in the Ω loop. Ligand conjugation at the active center and association at the peripheral site induce distinctive conformational changes in the loop. Because the character of the spectral changes is dependent on chirality and dimensions of the ligand as well as its site of association, the Ω loop exhibits considerable flexibility in the solution conformations of AChE.

MATERIALS AND METHODS

Inhibitors and Substrates—Acetylthiocholine iodide, 5,5'-dithiobis(2-nitrobenzoic acid), DFP, dithiothreitol, physostigmine, gallamine, neostigmine, and paraoxon were purchased from Sigma-Aldrich. Acrylodan was obtained from Molecular Probes (Eugene, OR), echothiophate was obtained from Ayerst Laboratories (Philadelphia, PA), and DDVP was obtained from Bayer Inc. (West Haven, CT). Rivastigmine was obtained as the commercial product (Exelon) from Novartis. Fasciculin 2 (purified from the venom of *Dendroaspis angusticeps*) was a gift of Dr. Pascale Marchot (University of Marseille, Marseille, France). Drs. Yacov Ashani and Bhupendra P. Doctor (Walter Reed Army Research Center, Washington, DC) kindly provided 7-[(methylethoxy)phosphinyl]oxyl-1-methylquinolinium iodide (MEPQ) and procainamide-linked Sepharose CL-4B resin. The chiral organophosphonate enantiomers, (*S*_p)-dimethylbutyl methylphosphonothiocholine ((*S*_p)-DMBMP-TCh), (*S*_p)-cycloheptyl methylphosphonothiocholine, (*S*_p)-isopropyl methylphosphonothiocholine, and (*R*_p)-dimethylbutyl methylphosphonothiocholine ((*R*_p)-DMBMP-TCh) were kindly provided by Dr. Harvey Berman (State University of New York, Buffalo, NY).

Expression, Mutagenesis, and Purification of mAChE—Mouse AChE was produced by transfection of expression plasmid (pCDNA3, Invitrogen, San Diego, CA) containing an encoding cDNA where the AChE sequence was terminated at position 548. The plasmid was transfected into human embryonic kidney (HEK293) cells. Cells were selected with G418 to obtain stable producing cell lines, and AChE was expressed as a secreted soluble enzyme in serum-free media (21). Mutant enzymes were generated by standard mutagenesis procedures, and cassettes containing the mutation were subcloned into pCDNA3 (21). Nucleotide sequences of the cassettes were confirmed by double-stranded sequencing to ensure that spurious mutations were not introduced. Affinity chromatography permitted one-step purification of AChE. From 4–6 liters of media, mutant and wild type enzyme were purified in quantities ranging between 5 and 25 mg, as previously described (22–24).

Purity was ascertained by SDS-PAGE and by specific activity determination. The cysteine-substituted enzymes show kinetics of acetylcholine hydrolysis similar to wild type enzyme (11).

Acrylodan Labeling—Mutant enzymes were pretreated with 0.25 mM dithiothreitol for 30 min at room temperature to ensure reduction of the introduced cysteine. Excess dithiothreitol was removed by use of a G-50 Sephadex spin column (Roche Molecular Biochemicals) equilibrated in 10 mM Tris-HCl, 100 mM NaCl, 40 mM MgCl₂, pH 8.0. Conditions for acrylodan labeling and stoichiometry estimates have been described previously (11). Stoichiometry of labeling of the various preparations, estimated from a comparison of enzyme concentration by protein (280 nm) to acrylodan (360–380 nm) absorbance, ranged as follows: L76C, 0.7–1.0; E81C, 0.77–1.0; E84C, 0.77–1.0; Y124C, 0.78–1.0; A262C, 0.69–0.92; and H287C, 0.78–1.0. Specificity of labeling was assessed by comparison of areas under the fluorescence emission curves for acrylodan-treated mutant and wild type enzymes. Specific labeling for each mutant was: L76C, 72–85%; E81C, 81–92%; E84C, 85–93%; Y124C, 83–92%; A262C, 77–93%; H287C, 70–82%.

Enzyme Inhibition—Picomolar concentrations of enzyme in 0.01% bovine serum albumin and 0.1 M sodium phosphate buffer, pH 7.0, were reacted with covalent inhibitor in the absence of substrate at 25 °C. Typically, four inhibitor concentrations were used. Inhibition was monitored by measuring residual enzyme activity by removal of aliquots during the course of the reaction. Bimolecular rate constants (*k*_i) were determined by the plot of pseudo first order rate constant (*k*_{obs}) against inhibitor concentration (25).

Spectrofluorometric Assays—Steady state emission spectra were measured at room temperature using a Jobin Yvon/Spex FluoroMax II spectrofluorometer (Instrument S.A., Inc., Edison, NJ) with the excitation and emission bandwidths set at 5 nm. The excitation wavelength for acrylodan was set at 359 nm, and emission was monitored between 420 and 600 nm. Spectral changes in the presence of irreversible inhibitors were determined by allowing the reaction of the acrylodan-labeled enzymes to proceed until ≥99% inhibition was achieved. In the case of inhibitors with chromogenic leaving groups, the inhibited enzyme was passed through a G-50 Sephadex spin column (Roche Molecular Biochemicals) to remove the leaving group. Quantum yield changes in presence of MEPQ and paraoxon were determined by measuring the concentration of labeled enzyme by tryptophan emission and area of acrylodan fluorescence emission curve before and after organophosphate conjugation. Association of echothiophate and neostigmine with acrylodan-labeled E81C and E84C was assessed from the kinetics of

TABLE I
Bimolecular rate constants for reaction of wild type and mutated AChE with echothiophate, neostigmine, and rivastigmine in the presence and absence of fluorescent (acrylodan) labeling

Data shown as means \pm standard deviation typically from three experiments. WT, wild type.

Enzyme	Echothiophate		Neostigmine		Rivastigmine	
	k_i $10^4 \text{ M}^{-1} \text{ min}^{-1}$	$k_{i,WT}/k_{i, \text{mutant}}$	k_i $10^4 \text{ M}^{-1} \text{ min}^{-1}$	$k_{i,WT}/k_{i, \text{mutant}}$	k_i $10^4 \text{ M}^{-1} \text{ min}^{-1}$	$k_{i,WT}/k_{i, \text{mutant}}$
Wild type ^a	235 \pm 17		571 \pm 7		372 \pm 8	
E81C ^a	199 \pm 14	1.2	566 \pm 8	1	372 \pm 2	1
E81C-acrylodan ^b	71 \pm 10	3.3	134 \pm 19	4.3	98 \pm 8	3.8
E84C ^a	86 \pm 4	2.7	175 \pm 3	3.3	95 \pm 6	3.9
E84C-acrylodan ^b	4.8 \pm 0.2	50	15 \pm 0.4	39	9 \pm 0.4	41

^a Kinetic constants derived from measurements of inhibition of acetylthiocholine catalysis.

^b Kinetic constants derived from intensity of the fluorescence signals.

change in fluorescence at 470 and 477 nm, respectively, following addition of a stoichiometric excess of inhibitor at several concentrations. Data were fitted to a single exponential approach to equilibrium. Bimolecular rate constants (k_i) were determined by the plot of pseudo first order rate constant (k_{obs}) against inhibitor concentration (25). Association of rivastigmine with acrylodan-labeled E81C was monitored from the kinetics of the increase in fluorescence at 460 nm. To ensure the observed change in fluorescence upon rivastigmine association was caused by carbamoylation and not reversible binding of rivastigmine, the enzyme was reacted with the fluorescent carbamoylating agent, M7C, to ascertain the concentration of residual reactive serines (26).

RESULTS

Kinetics of Organophosphate and Carbamate Inhibition—We determined the bimolecular rate constants (k_i) for echothiophate, neostigmine, and rivastigmine with unmodified and modified AChE (Table I). For the wild type, E81C, and E84C mutant enzymes, the constants (k_i) were obtained from measurements of enzyme activity, whereas changes in fluorescent signal were used to monitor reaction with the acrylodan-modified enzyme. A typical example of monitoring of the fluorescence change is shown in Fig. 2. The data in Table I show that substitution of cysteine at the 81-position does not affect the carbamoylation and phosphorylation rates, whereas the modification at the 84-position causes a 3–4-fold reduction in rate. Upon modification of the introduced cysteine with acrylodan, reaction rates are reduced 3–4-fold compared with wild type following conjugation at the 81-position, whereas the reduction is 40–50-fold upon conjugation at the 84-position. It is important to note that the magnitude of these reductions in carbamoylation or phosphorylation rates by mutation and conjugation at each position is nearly the same, despite the inhibitors differing in their reactivity by a few orders of magnitude. In the case of rivastigmine, we measured the reaction rates by competition with excess M7C (26) and achieved similar kinetics of inhibition. This indicates that the spectral shift produced by rivastigmine likely reflects a conformational change induced by progressive carbamoylation rather than formation of a reversible complex.

Effect of Achiral Organophosphates on Acrylodan Emission Spectra—Organophosphates readily phosphorylate the active site serine (27), presumably generating a pentavalent trigonal bipyramidal intermediate before dissociation of leaving group. The resulting phosphorylated complex resembles the tetrahedral transition states of acylation and deacylation of the trigonal esters. The diethylphosphoryl conjugate at the active site serine formed by reaction with echothiophate produces very little perturbation at positions 76, 262, and 287, consistent with their positions being well removed from the phosphorylation site (Table II). A bathochromic emission shift is observed at position 84, although of smaller magnitude when compared with the shift induced by other ligands (Tables II–V). Interestingly, large hypsochromic shifts and enhancements of quantum

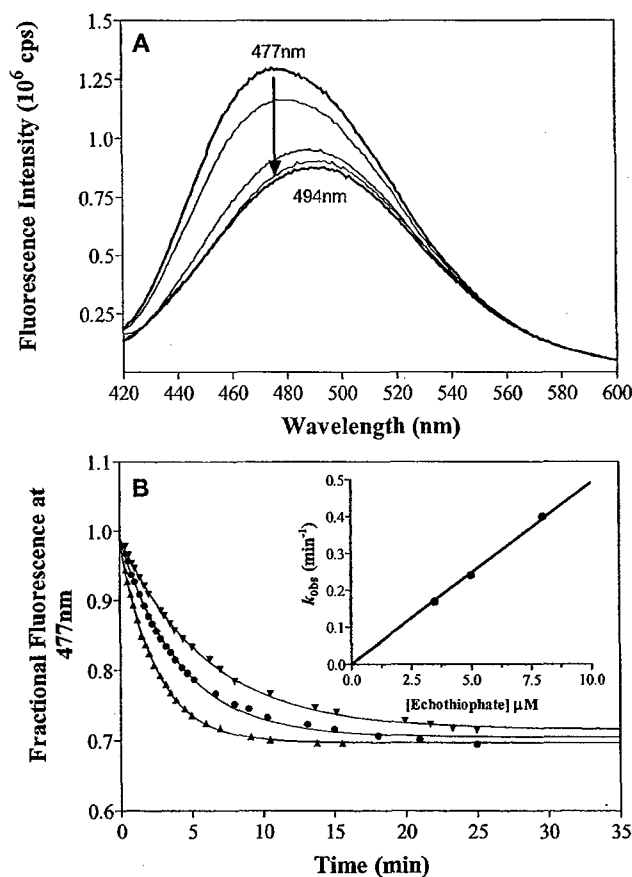


FIG. 2. Association of echothiophate with E84C acrylodan-modified AChE. Panel A, fluorescence emission spectra of acrylodan-labeled E84C AChE following addition of excess echothiophate. Echothiophate forms the diethylphosphoryl enzyme leading to a bathochromic shift and reduction of fluorescence quantum yield. Excess echothiophate (2 μM) was added to 94 nM AChE, and fluorescence spectra were taken at following time points: 0, 1, 11, 26, and 43 min. Panel B, time course of the fluorescence changes. Initial E84C acrylodan-modified AChE concentration was 190 nM. Excess echothiophate was added, and decrease in fluorescence signal at 477 nm was monitored using an ISA Jobin Yvon-Spex Fluoromax fluorometer. The three echothiophate concentrations were 3.5 (∇), 5.0 (\bullet), and 8.0 (\blacktriangle) μM . Control enzyme samples, to which buffer rather than echothiophate was added, did not show decreases in fluorescence emission over the time intervals measured.

yield are observed at positions 81 and 124. This pattern appears to be unusual, because the reversible active center ligands studied previously (11) and the dimethylphosphoryl conjugate formed from DDVP, which yields a phosphoryl serine with one methylene group shorter than echothiophate, confer little shift at position 124 and a large bathochromic shift at position 81.

with the active site serine, paraoxon produces the same diethylphosphoryl conjugate as echothiophate. However, its leaving group is a neutral aromatic moiety rather than the cationic moiety of echothiophate. Because a similar spectral

TABLE V
Fluorescence emission parameters of mouse AChE mutants labeled with acrylodan

Data are shown as mean values of at least three determinations. Chromic shifts were determined by comparison of fluorescence emission maximum between control and covalently modified AChE.

Enzyme	Acrylodan Chromic Shift (nm)					
	Acrylodan Emission Maxima	Ethylmethyl Carbamoyl Conjugate	Ethylmethyl Carbamoyl Conjugate + Fasciculin	Diethyl Phosphoryl Conjugate + Fasciculin	Diisopropyl Phosphoryl Conjugate + Fasciculin	Saturating Fasciculin Alone ^a
L76C	505	0	0	0	0	0
E81C	489	-30	21	21	21	21
E84C	477	20	35	35	35	35
Y124C	500	-4	-27	-33	-33	-23
A262C	517	0	0	0	0	0
H287C	524	0	-17	-17	-17	-17

^a Data from Ref. 11.

shift follows paraoxon conjugation, the conformational change is induced by the conjugated phosphate, rather than being influenced by binding of residual leaving group.

If we extend additional methylene units to the diisopropyl phosphoryl conjugate formed by DFP, we observe a chromic shifts at the 81- and 84-positions similar to the diethylphosphoryl conjugate. However, the hypsochromic shift at the 124-position becomes slightly smaller for the diisopropyl phosphoryl conjugate. Measurements were made immediately after reaction to preclude aging (*i.e.* spontaneous loss of an alkoxy moiety rendering an anionic conjugate) of the diisopropyl phosphoryl moiety (28).

Effect of Chiral Organophosphonates on Acrylodan Emission Spectra—To compare phosphoryl and phosphonyl conjugates of similar dimensions, racemic MEPQ was used to generate an ethyl methylphosphonyl conjugate. Kinetic studies show an enantiomeric preference of MEPQ, where presumably the *S_p* enantiomer reacts ~10-fold faster than the *R_p* enantiomer.² Hence, reaction with a stoichiometric excess of MEPQ should ensure one enantiomer covalently reacts preferentially with the enzyme. No discernable emission changes are observed at residues 262 and 287. Similar to DDVP, a bathochromic shift is observed for acrylodan at both positions 81 and 84. A moderate hypsochromic shift is observed at the 124-position, and very small change at the 76-position.

Table III also shows the changes in acrylodan emission for a series of *S_p* methylphosphonates with increasing alkoxy substituent dimensions. Because the absolute stereochemistry of the methylphosphonates is known (29), the chiral *S_p* methylphosphonates will direct their phosphoryl oxygen toward the oxyanion hole, the small methylphosphonyl moiety will be directed to the acyl pocket, and the more bulky alkoxy group directed to choline binding site (30). For the three *S_p* enantiomers, very little or no change in emission maxima for acrylodan at positions 124, 262, and 287 is discerned. Similar to reversible active site ligands that interact with choline binding site (11), bathochromic shifts are observed at the Ω loop positions with the largest shift at E84C, an intermediate value at E81C, and only small change at L76C. The ethyl methylphosphonyl conjugate, which contains the smallest alkoxy moiety among *S_p* conjugates, induces the smallest bathochromic shift at the 81- and 84-positions.

R_p alkyl methylphosphonates react far more slowly with the enzyme than the *S_p* enantiomers (30), and we use formation of the (*R_p*)-3,3-dimethylbutyl methylphosphonyl enzyme as an example. Formation of initial reversible complex can be detected by an immediate reduction in quantum yield of acrylo-

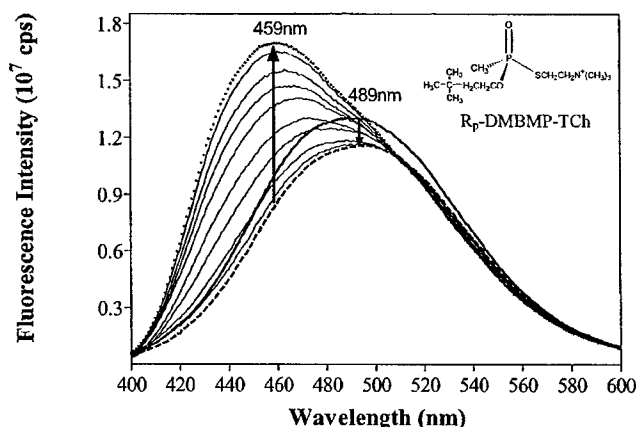


FIG. 3. Fluorescence emission spectra of acrylodan-labeled E81C AChE following addition of (*R_p*)-dimethylbutyl methylphosphonothiocholine (*R_p*-DMBMP-TCh). We observed a reduction in quantum yield immediately following addition of (*R_p*)-DMBMP-TCh, followed by a progressive hypsochromic shift and enhancement in quantum yield. Equivalent concentrations of enzyme (300 nM) were present for all measurements. A stoichiometric amount of (*R_p*)-DMBMP-TCh (340 nM) was added, and fluorescence spectrum was taken at following time points: 0, 1, 2, 8, 20, 53, 74, 89, 100, 115, and 150 min. The large shift for E81C reveals an isoemissive point at 510 nm, indicative of two (reversible DMBMP-TCh... AChE complex and conjugated DMBMP-AChE) discrete species in the progressive reaction. Acrylodan-labeled E81C AChE free in solution (*solid line*), reversibly bound with (*R_p*)-DMBMP-TCh (*dashed line*), and covalently conjugated DMBMP-AChE (*dotted line*). (*R_p*)-DMBMP-AChE yields an emission maximum of 459 nm, a difference of 51 nm from the (*S_p*)-DMBMP-AChE (Table III).

dan at 81 with little change in emission maximum (Fig. 3). This is followed by a progressive hypsochromic shift that reflects the covalent reaction with the active center serine. The isoemissive point at 510 nm, evident through the course of the slow reaction, likely reflects the presence of two species (*i.e.* the reversible DMBMP-TCh... AChE complex and the conjugated DMBMP-AChE being the dominant species in the progressive reaction). The resulting hypsochromic shift of conjugated acrylodan to 459 nm markedly contrasts with the *S_p* enantiomer with its bathochromic shift in emission spectrum. These two enantiomers provide the critical clue for linking fluorescence emission maxima at the 81-position to the characteristics of structural perturbations of the Ω loop.

Effect of Carbamates on Acrylodan Emission Spectra—Formation of a carbamoyl serine conjugate of AChE affords an alternative means for forming a relatively stable modified enzyme conjugate (27). Kinetic studies and crystallographic evidence show the carbamoyl oxygen of the covalent conjugate

² Z. Radić, unpublished observation.

directed toward the oxyanion hole, and the alkyl carbamoyl group pointing toward the acyl pocket (25, 31, 32). Similar to the tetrahedral phosphoryl and phosphonyl conjugates, the trigonal carbamoylated enzymes produce very little perturbation at positions 76, 262, and 287 (Table IV). The monomethyl (physostigmine), dimethyl (neostigmine), and ethylmethyl (rivastigmine) carbamoyl conjugates all produce a small hypsochromic shift and enhancement in acrylodan quantum yield at residue 124. All carbamates, similar to the organophosphates, produce 18–23-nm bathochromic shifts and decreases in quantum yield at position 84. Consistent with the organophosphate series, dimethylcarbamoyl AChE formed from neostigmine and ethylmethylcarbamoyl AChE formed from rivastigmine both produce significant hypsochromic shifts of acrylodan conjugated at position 81. The smaller methylcarbamoyl modification produces little change in E81C spectrum.

Influence of Fasciculin Capping on the Spectrum of Phosphorylated and Carbamoylated AChEs—Because fasciculin is known to interact at the rim of the active center gorge of AChE (33–35) and can cap the gorge with a conjugated ligand at the base of the gorge (26, 36), we examined the acrylodan spectra of the conjugated enzymes after fasciculin addition. Here again, the most informative position to analyze is 81. Irrespective of whether conjugation at the active center causes a hypsochromic or bathochromic shift, the fasciculin complex yields an emission maximum of 510 nm (Table V, Fig. 4). Thus, fasciculin association dominates over the conformational changes induced by the phosphorylating or carbamoylating agents at the active center of AChE.

Effect of the Peripheral Site Inhibitor, Gallamine, on Acrylodan Emission—Similar to fasciculin (11), addition of gallamine produces substantial hypsochromic shifts and enhancements in quantum yield with acrylodan conjugated at both the 124- and 287-positions, and a change of smaller magnitude at 76-position (Tables V and VI). This reflects an increase in hydrophobicity experienced by the conjugated fluorophores at the gorge entry upon gallamine binding. Addition of gallamine produces bathochromic shifts of 9 nm at position 84 and 14 nm at position 81. Compared with other AChE inhibitors, whether reversible or covalent, gallamine produces the smallest bathochromic shift seen at residue 84 (Tables II–VI).

DISCUSSION

We have used a structure-based approach to design a biosensor that responds to phosphorylation and carbamoylation of mAChE. Site-directed placement of an environmentally sensitive fluorophore, acrylodan, offers a sensor that not only responds to covalent conjugation of AChE, but also distinguishes AChE inhibitors based on chirality and molecular dimensions. Because the crystallographic structures (15–18) and the steady state kinetic studies (19, 20) have not revealed conformational changes in the Ω loop, studies that employ physical parameters to measure conformation in solution take on increased significance.

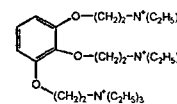
Acrylodan is known to show large Stokes shifts with differences in dielectric constant of the solvent. This presumably results from its excited state exhibiting an increased dipole moment that, in turn, is stabilized by solvents of higher dielectric constant (12–14). The increase in the emission maxima (bathochromic shift) likely reflects the acrylodan side chain becoming exposed to the solvent.

Ω Loop Substitutions at 81 and 84—We previously showed large bathochromic shifts for acrylodan side chains at 81 and 84 upon association of reversible active site ligands. Both of these residues are well removed from the active center serine (Fig. 1) and should be influenced only allosterically by the bound or conjugated ligand at the active center. We have at-

TABLE VI
Effect of gallamine on fluorescence emission parameters of mouse AChE mutants labeled with acrylodan

Data are shown as mean values of at least three determinations. Relative quantum yields were determined by comparison of areas of the fluorescence emission curves.

Enzyme	Acrylodan Emission Maxima (nm)			
	No Gallamine	Saturating Gallamine	Chromic Shift	Relative Quantum Yield
L76C	505	501	-4	1.20
E81C	489	503	14	0.78
E84C	477	486	9	0.69
Y124C	500	475	-25	1.19
A262C	517	517	0	0.98
H287C	524	510	-14	1.77



tributed the enhanced solvent exposure to increased strain on the Ω loop resulting from ligand-induced closure of the gorge (11). However, the differences we see here between acrylodan labeling at the 84- and 81-positions suggest a greater degree of conformational flexibility in the Ω loop than can be ascribed simply to two conformational states.

Catalytic and inhibition parameters are differentially affected by cysteine substitution and acrylodan modification at the 81- and 84-positions. Our previous studies showed that substitution of cysteine at 84 had a greater effect on steady state catalytic parameters than the substitution at 81. Nevertheless, considering that AChE is highly refined for catalytic efficiency and the catalytic enhancement over H_2O catalysis of the ester is $\sim 10^{14}$ -fold (3), the acrylodan-substituted enzymes remain highly efficient. Moreover, the magnitude of the reduction in phosphorylation or carbamoylation rate resulting from acrylodan conjugation appears to be independent of the reactivity of the carbamoylating or phosphorylating agent (Table I).

The analysis of the changes in emission maxima at the 84-position show that all conjugating ligands and peripheral site ligands (Tables II–VI) induce a bathochromic shift in emission similar to ligands that bind reversibly at the choline subsite of the active center. Hence, all ligands appear to enhance solvent exposure of the acrylodan side chain at the 84-position. An ordering of the emission maxima at the 84-position for the S_p methylphosphonyl enzymes shows the greatest shift with the larger ligands. This trend is also evident for S_p methylphosphonyl conjugates at the 81-position. Thus, if the magnitude of the shift reflects fractional gorge opening and closing, then the larger ligands promote gorge closure or shift the equilibrium of conformations toward a closed gorge state.

The spectral changes seen at the 81-position appear to be the most discriminating with respect to the conjugated ligand, and here our structure-activity analysis reveals a clear trend. Ligands that conjugate to the active center serine and have the appropriate dimensions or chirality so as to fit into and not perturb the acyl pocket all cause bathochromic shifts in emission spectrum. This applies to the dimethylphosphoryl conjugate, all of the S_p methylphosphonyl conjugates and perhaps to the methylcarbamoyl conjugate. It should be noted that all of these compounds would allow for insertion of the phosphoryl and carbamoyl oxygen in the oxyanion hole formed by hydrogen bonds donors from amide backbone hydrogens at Gly¹²¹, Gly¹²², and Ala²⁰⁴ without deforming the acyl pocket (31).

By contrast, the diethyl and diisopropyl phosphoryl conjugates and the corresponding R_p phosphonyl-AChE derivatives cannot stabilize their phosphoryl or phosphonyl oxygen in the

oxyanion hole unless the alkoxy moiety perturbs or moves out of the acyl pocket. Direct evidence for this comes from the crystallographic structure of the DFP-AChE that reveals significant perturbation of the two phenylalanines in the acyl pocket (18).

Additionally, long-standing prior investigations of substrate and inhibitor specificity permit a similar deduction. Over 50 years ago, Augustinsson (36) found that propionylcholine is an effective substrate for AChE, whereas butyrylcholine is not. This finding, when viewed with contemporary structures, suggests that the limits of acyl pocket tolerance occur at the propionyl to butyryl juncture. Thus, a dimethylphosphoryl conjugate would extend linearly from the serine hydroxyl a similar distance to the transition state for formation of propionyl serine. A diethylphosphoryl conjugate would have dimensions similar to the transition state for butyryl serine. A methylcarbamoyl chain would also be similar to the propionyl fits, whereas the dimethyl or ethylmethyl amino substitutions would impart additional steric constraints (32). Likewise, other early studies showed that associations of reversible inhibitors to AChE conjugated with phosphorylating or sulfonylating agents were unimpeded with smaller modifying groups, but sterically hindered with larger modifying groups (37, 38).

The limitations on acyl pocket dimensions position the conjugated ligand to alter potentially both the acyl pocket loop defined by residues Trp²⁸⁶-Ser²⁹⁸ (39) and the neighboring Ω loop Cys⁶⁹-Cys⁹⁶. Constraints on acyl pocket dimensions appear to affect conformation of both loops. Direct perturbation of the acyl pocket side-chain positions have been observed with DFP conjugation and the formation of its aged product (18). Additionally, by not fitting in the acyl pocket, the conjugated alkyl groups will reside elsewhere in the gorge, therein influencing Ω loop conformation and the extent of gorge closure as we observed for the side-chain 81-position. Morel and collaborators (39) have proposed various cross-gorge interconnectivities of side chains based on mutagenesis and thermal denaturation experiments.

Residues in the Active Center Gorge in Apposition to the Ω Loop—Residues 124 and 287 lie across the gorge from the Ω loop with H287C at the rim of the gorge and Y124C, residing below the rim and within the gorge interior (Fig. 1). We previously showed a lack of spectral shift at 124 and 287 sites with binding of reversible active site inhibitors (11). Residue 287 is also not affected by any of the conjugating inhibitors. Similar to these reversible active site inhibitors, the larger chiral S_p organophosphonates produce little change in acrylodan emission maxima at the 124-position. By contrast, echothiophate, paraoxon, DFP, and MEPQ all cause a substantial hypsochromic shift and enhancement in quantum yield. Because of the small size of these alkyl moieties in phosphoryl or phosphonyl derivatives, they are unlikely to interact directly with 124, although they may affect solvent structure in the gorge. An increase of one methylene unit in phosphoryl conjugate from dimethylphosphoryl (DDVP) to diethylphosphoryl (echothiophate and paraoxon) gives a spectral change suggestive of solvent exclusion around the 124-position. A much smaller but clear hypsochromic shift is observed for carbamates, perhaps reflecting the different geometry in which the carbamoyl moieties position themselves in the gorge.

Interpretation of the basis of the changes in emission for acrylodan at the 124-position is likely to be complicated by three imposing factors. First, acrylodan at the 124-position can be expected to reside well within the gorge and ligands affecting H₂O structure in the gorge may affect its environment. Second, this side chain could be influenced by ligands occupying the oxyanion hole formed in part by amide hydrogen donors from Gly¹²¹ and Gly¹²². Third, perturbation of the acyl

pocket may indirectly influence the position of the position 124 residue. The crystallographic structure of aged DFP conjugate reveals that the isopropyl group of DFP causes a displacement of acyl pocket loop that includes peripheral site residue Trp²⁸⁶ (18). Although Tyr¹²⁴ is not an acyl pocket loop residue, it is in close apposition with Trp²⁸⁶. Similar to DFP, the ethyl group of echothiophate and paraoxon could also cause a movement in the acyl pocket loop (Trp²⁸⁶-Ser²⁹⁸). This conformational change coupled with solvent exclusion upon ligand binding may lead to the substantial hypsochromic shift and enhancement of quantum yield at the 124-position.

Allosteric Effect of Peripheral Site Inhibitors—Gallamine, a tris-quaternary ligand that binds at the peripheral site, induces a distinctive hypsochromic shift at the 124- and 287-positions. This pattern correlates remarkably with the first series of peripheral site ligand complexed mAChE solved recently (40). The crystallographic structure shows the aromatic pyrogallol moiety of gallamine in π - π stacking interaction with Trp²⁸⁶, and van der Waals contact with Tyr¹²⁴. Furthermore, bathochromic shifts observed at the 81- and 84-positions reflect a linkage between the binding at the peripheral site and allosteric conformational change in the Ω loop.

The marked decrease in fluorescence intensity and bathochromic shifts at the position 81 and 84 residues seen with fasciculin capping of covalently modified enzymes reveal a distinct conformation that the Ω loop adopts in fasciculin-AChE complex when compared with the various serine-modified enzymes. The dominance of conformation change induced by fasciculin binding likely reflects the large molecular dimensions of the peptidic toxin. When bound, ~30% of the fasciculin molecule is buried in the complex, giving rise to a van der Waals contact area of 1100 Å² (9).

Acrylodan-conjugated Enzyme as a Biosensor for Inactivation of Acetylcholinesterase—The surprisingly large and discriminating spectral shifts produced by close congeners of the organophosphates offer an opportunity for detection of organophosphate or carbamate exposure. With the fluorophore intrinsically conjugated to the protein target, reagent addition is not required for detection. Remote sensing of organophosphate exposure would be particularly valuable for oxon forms of the organophosphate insecticides (malathion, parathion, diazinon, and chlorpyrifos) that react directly with AChE as well as the more insidious nerve agents (sarin, soman, VX, cyclosarin, and tabun), where cumulative conjugation could be monitored (2, 41, 42). Moreover, by using multiple wavelength detection, the individual inhibitors can be distinguished. For example, maloxon and methylparaoxon forming the dimethylphosphoryl enzyme can be distinguished from paraoxon and chlorpyrifos oxon using dual detection at 510 and 477 nm for acrylodan conjugated at the 81-position. Inhibitions by R_p and S_p dimethylbutyl methylphosphonates yield conjugates that show emission maxima at 459 and 510 nm, respectively. The S_p methylphosphonates show smaller differences in fluorescence emission between them, but monitoring a combination of site-directed acrylodan-modified AChEs may distinguish individual methylphosphonate conjugates.

REFERENCES

1. Rosenberry, T. L. (1975) *Adv. Enzymol. Relat. Areas Mol. Biol.* **43**, 103-218
2. Taylor, P. (2001) in *Goodman & Gilman's The Pharmacological Basis of Therapeutics* (Hardman, J. G., and Limbird, L. E., eds) pp. 161-1176, 10th Ed., McGraw-Hill Medical Publishing Division, New York
3. Quinn, D. M. (1987) *Chem. Rev.* **87**, 955-979
4. Taylor, P., and Lappi, S. (1975) *Biochemistry* **14**, 1989-1997
5. Changeux, J. P. (1966) *Mol. Pharmacol.* **2**, 369-392
6. Berman, H. A., and Taylor, P. (1978) *Biochemistry* **17**, 1704-1713
7. Szegletes, T., Mallender, W. D., and Rosenberry, T. L. (1998) *Biochemistry* **37**, 4206-4216
8. Szegletes, T., Mallender, W. D., Thomas, P. J., and Rosenberry, T. L. (1999)

- Biochemistry* **38**, 122–133
9. Bourne, Y., Taylor, P., and Marchot, P. (1995) *Cell* **83**, 503–512
 10. Bourne, Y., Taylor, P., Bougis, P. E., and Marchot, P. (1999) *J. Biol. Chem.* **274**, 2963–2970
 11. Shi, J., Boyd, A. E., Radic, Z., and Taylor, P. (2001) *J. Biol. Chem.* **276**, 42196–42204
 12. Lakowicz, J. R. (1999) *Principles of Fluorescence Spectroscopy*, 2nd Ed., Kluwer Academic and Plenum Publishers, New York
 13. Lew, J., Coruh, N., Tsigelny, I., Garrod, S., and Taylor, S. S. (1997) *J. Biol. Chem.* **272**, 1507–1513
 14. Prendergast, F. G., Meyer, M., Carlson, G. L., Iida, S., and Potter, J. D. (1983) *J. Biol. Chem.* **258**, 7541–7544
 15. Sussman, J. L., Harel, M., Frolow, F., Oefner, C., Goldman, A., Tokar, L., and Silman, I. (1991) *Science* **253**, 872–879
 16. Harel, M., Schalk, I., Ehretsabatier, L., Bouet, F., Goeldner, M., Hirth, C., Axelsen, P. H., Silman, I., and Sussman, J. L. (1993) *Proc. Natl. Acad. Sci. U. S. A.* **90**, 9031–9035
 17. Raves, M. L., Harel, M., Pang, Y. P., Silman, I., Kozikowski, A. P., and Sussman, J. L. (1997) *Nat. Struct. Biol.* **4**, 57–63
 18. Millard, C. B., Kryger, G., Ordentlich, A., Greenblatt, H. M., Harel, M., Raves, M. L., Segall, Y., Barak, D., Shafferman, A., Silman, I., and Sussman, J. L. (1999) *Biochemistry* **38**, 7032–7039
 19. Velan, B., Barak, D., Ariel, N., Leitner, M., Bino, T., Ordentlich, A., and Shafferman, A. (1996) *FEBS Lett.* **395**, 22–28
 20. Faerman, C., Ripoll, D., Bon, S., Lefeuvre, Y., Morel, N., Massoulie, J., Sussman, J., and Silman, I. (1996) *FEBS Lett.* **386**, 65–71
 21. Boyd, A. E., Marnett, A. B., Wong, L., and Taylor, P. (2000) *J. Biol. Chem.* **275**, 22401–22408
 22. Marchot, P., Ravelli, R. B., Raves, M. L., Bourne, Y., Vellom, D. C., Kanter, J., Camp, S., Sussman, J. L., and Taylor, P. (1996) *Protein Sci.* **5**, 672–679
 23. Berman, J. D., and Young, M. (1971) *Proc. Natl. Acad. Sci. U. S. A.* **68**, 395–398
 24. De la Hoz, D., Doctor, B. P., Ralston, J. S., Rush, R. S., and Wolfe, A. D. (1986) *Life Sci.* **39**, 195–199
 25. Radic, Z., Gibney, G., Kawamoto, S., MacPhee-Quigley, K., Bongiorno, C., and Taylor, P. (1992) *Biochemistry* **31**, 9760–9767
 26. Radic, Z., and Taylor, P. (2001) *J. Biol. Chem.* **276**, 4622–4633
 27. Wilson, I. B. (1960) in *The Enzymes* (Boyer, P. D., Lardy, H., and Myrback, K., eds) Vol. 4, 2nd Ed., pp. 501–520, Academic Press, New York
 28. Aldridge, W. N., and Reiner, E. (1972) *Enzyme Inhibitors as Substrates: Interactions of Esterases with Esters of Organophosphorus and Carbamic Acids*, North-Holland Publishing Co., Amsterdam
 29. Berman, H. A., and Leonard, K. (1989) *J. Biol. Chem.* **264**, 3942–3950
 30. Hosea, N. A., Berman, H. A., and Taylor, P. (1995) *Biochemistry* **34**, 11528–11536
 31. Ariel, N., Ordentlich, A., Barak, D., Bino, T., Velan, B., and Shafferman, A. (1998) *Biochem. J.* **335**, 95–102
 32. Bar-On, P., Millard, C. B., Harel, M., Dvir, H., Enz, A., Sussman, J. L., and Silman, I. (2002) *Biochemistry* **41**, 3555–3564
 33. Taylor, P., and Radic, Z. (1994) *Annu. Rev. Pharmacol. Toxicol.* **34**, 281–320
 34. Marchot, P., Khelif, A., Ji, Y. H., Mansuelle, P., and Bougis, P. E. (1993) *J. Biol. Chem.* **268**, 12458–12467
 35. Mallender, W. D., Szegetes, T., and Rosenberry, T. L. (1999) *J. Biol. Chem.* **274**, 8491–8499
 36. Augustinsson, K. B. (1948) *Acta Physiol. Scand. Suppl.* **52**, 1–182
 37. Belleau B., and DiTullio V. (1970) *J. Am. Chem. Soc.* **92**, 6320–6325
 38. Taylor, P., and Jacobs, N. M. (1974) *Mol. Pharmacol.* **10**, 93–107
 39. Morel, N., Bon, S., Greenblatt, H. M., Van Belle, D., Wodak, S. J., Sussman, J. L., Massoulie, J., and Silman, I. (1999) *Mol. Pharmacol.* **55**, 982–992
 40. Bourne, Y., Taylor, P., Berman, H. A., Radic, Z., and Marchot, P. (2002) *Xlth International Symposium on Cholinergic Mechanisms*, St. Moritz, Switzerland, May 4–9, 2002, p. 39
 41. Millard, C. B., and Broomfield, C. A. (1995) *J. Neurochem.* **64**, 1909–1918
 42. Koelle, G. B. (1994) *J. Appl. Toxicol.* **14**, 105–109
 43. Wong, L., Radic, Z., Bruggemann, R. J., Hosea, N., Berman, H. A., and Taylor, P. (2000) *Biochemistry* **39**, 5750–5757

Reversibly Bound and Covalently Attached Ligands Induce Conformational Changes in the Omega Loop, Cys⁶⁹–Cys⁹⁶, of Mouse Acetylcholinesterase*

Received for publication, July 20, 2001, and in revised form, August 20, 2001
Published, JBC Papers in Press, August 21, 2001, DOI 10.1074/jbc.M106896200

Jianxin Shi, Aileen E. Boyd‡, Zoran Radic, and Palmer Taylor§

From the Department of Pharmacology, University of California, San Diego, La Jolla, California 92093

We have used a combination of cysteine substitution mutagenesis and site-specific labeling to characterize the structural dynamics of mouse acetylcholinesterase (mAChE). Six cysteine-substituted sites of mAChE (Leu⁷⁶, Glu⁸¹, Glu⁸⁴, Tyr¹²⁴, Ala²⁶², and His²⁸⁷) were labeled with the environmentally sensitive fluorophore, acrylodan, and the kinetics of substrate hydrolysis and inhibitor association were examined along with spectroscopic characteristics of the acrylodan-conjugated, cysteine-substituted enzymes. Residue 262, being well removed from the active center, appears unaffected by inhibitor binding. Following the binding of ligand, hypsochromic shifts in emission of acrylodan at residues 124 and 287, located near the perimeter of the gorge, reflect the exclusion of solvent and a hydrophobic environment created by the associated ligand. By contrast, the bathochromic shifts upon inhibitor binding seen for acrylodan conjugated to three omega loop (Ω loop) residues 76, 81, and 84 reveal that the acrylodan side chains at these positions are displaced from a hydrophobic environment and become exposed to solvent. The magnitude of fluorescence emission shift is largest at position 84 and smallest at position 76, indicating that a concerted movement of residues on the Ω loop accompanies gorge closure upon ligand binding. Acrylodan modification of substituted cysteine at position 84 reduces ligand binding and steady-state kinetic parameters between 1 and 2 orders of magnitude, but a similar substitution at position 81 only minimally alters the kinetics. Thus, combined kinetic and spectroscopic analyses provide strong evidence that conformational changes of the Ω loop accompany ligand binding.

Acetylcholinesterase (AChE),¹ a serine hydrolase in the α/β -fold hydrolase protein superfamily (1), terminates nerve sig-

nals by catalyzing hydrolysis of the neurotransmitter acetylcholine at a diffusion limited rate (2, 3). The crystallographic structure of mouse AChE reveals a catalytic triad (Ser²⁰³, Glu³³⁴, and His⁴⁴⁷) located at the bottom of a narrow active site gorge 20 Å in depth (4–6). Because the cross-section of the physiological substrate acetylcholine is larger than the narrowest part of the gorge, the remarkably high turnover rate of AChE raises questions regarding substrate access to the catalytic site.

Molecular dynamic simulations suggest that rapid fluctuations of gorge width combined with diffusion facilitated by electrostatic forces could enhance substrate accessibility (7–10). In addition, the high affinity and slowly dissociating complex of fasciculin and AChE retains slight residual catalytic activity (11, 12), despite the occlusion of the active site gorge by fasciculin as shown in the crystal structures (5, 13, 14). Rapid fluctuations in residues lining the gorge walls may leave transient gaps at the fasciculin-AChE interface and may account for residual activity.

The large omega loop (Ω loop), Cys⁶⁹–Cys⁹⁶, flanking the active site gorge in mouse AChE corresponds to the activation loop of Cys⁶⁰–Cys⁹⁷ in *Candida rugosa* lipase, a related α/β -fold hydrolase protein (15–17). Crystallographic studies of the lipase revealed that the activation loop occludes the active center in the absence of substrate but folds back in the presence of lipid substrate allowing its access. Although kinetic and structural studies of AChE have not revealed evidence for such large substrate, induced lid-like movements (18, 19), high catalytic turnover rates for the cholinesterases might indicate that small amplitude motions along the Ω loop allow rapid access of incoming substrate and release of reaction product (19). To elucidate the nature of the ligand-dependent conformational changes of AChE, we have employed cysteine substitution mutagenesis and site-directed labeling with an environmentally sensitive fluorophore, acrylodan. The emission spectrum and quantum yield of the fluorophore are dependent on the effective dielectric constant and thus reflect the degree of solvent exposure and the local polarity experienced by the fluorophore (20). For example, when acrylodan is conjugated to a cysteine lining the gorge, upon fasciculin binding, it becomes sandwiched between the fasciculin loop and wall of the gorge, thereby becoming protected from solvent (20).

To examine further the role of the Ω loop in ligand binding, we have conjugated cysteines at various positions on the Ω loop and opposing gorge wall. Six single cysteine mutants were prepared for acrylodan conjugation (Fig. 1). Three were on the Ω loop as follows: L76C near the tip of the loop and E81C and E84C on their outer surface not lining the gorge. Two residues on the opposing face of the gorge H287C and Y124C were selected, along with a distal residue A262C whose temperature coefficient (B factor) would indicate flexible movement of an-

* This work was supported by United States Public Health Service (USPHS) Grant GM18360, Department of Army Medical Defense Grant 17-1-8014 (to P. T.), USPHS Training Support Grant GM07752 (to J. S.), and an ASERT fellowship (to A. E. B.). The costs of publication of this article were defrayed in part by the payment of page charges. This article must therefore be hereby marked "advertisement" in accordance with 18 U.S.C. Section 1734 solely to indicate this fact.

‡ Present address: Dept. of Oral and Maxillofacial Surgery, University of California, San Francisco, CA 94153-0440.

§ To whom correspondence should be addressed: Dept. of Pharmacology, University of California, San Diego, La Jolla, CA 92093. Tel.: 858-534-1366; Fax: 858-534-8248; E-mail: pwtaylor@ucsd.edu.

¹ The abbreviations used are: AChE, acetylcholinesterase; mAChE, mouse acetylcholinesterase; DTNB, 5,5'-dithio-bis(2-nitrobenzoic acid); MEPQ, 7-[[[(methylethoxy)phosphoryl]-oxyl]-1-methylquinolinium iodide; TFK⁺, *m*-(*N,N,N*-trimethylammonio)trifluoromethyl acetophenone; TFK^o, *m*-*tert*-butyl trifluoromethylacetophenone; acrylodan, 6-acryloyl-2-dimethylaminonaphthalene.

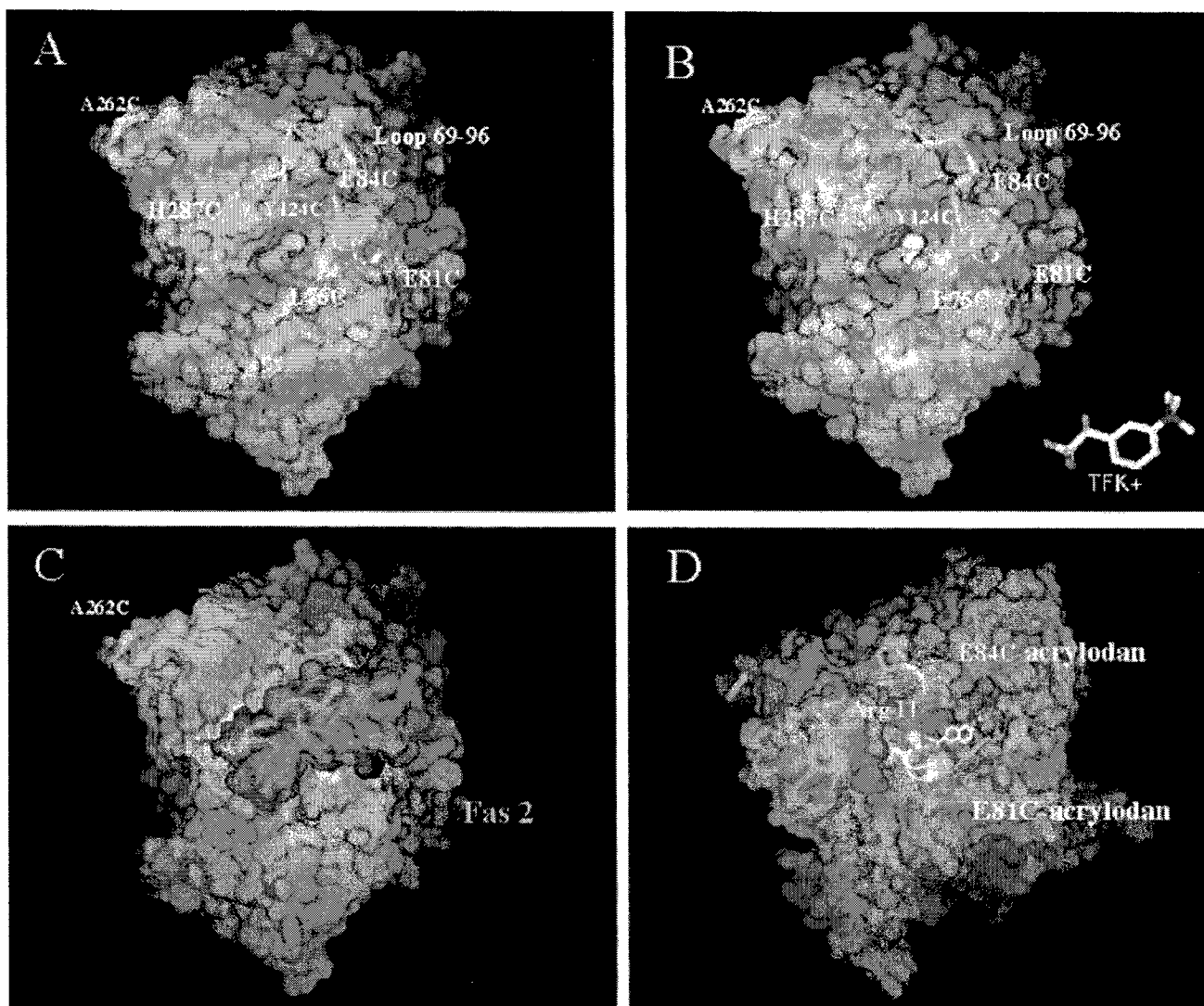


FIG. 1. Locations of introduced cysteines for fluorophore modification. Residues 76, 81, and 84 are at the tip (76) and outer portion (81, 84) of the Ω loop. Residues 124 and 287 are on an opposing face of the gorge and make up part of the peripheral anionic site. Residue 262 is on a peripheral disulfide loop and in the crystal has a large thermal factor. *A–D*, Connolly surface representations of structure. *A*, unliganded AChE (6); *B*, TFK⁺ conjugated with AChE; note partial exposure of the *white* molecule, TFK⁺, at the base of the gorge (33); *C*, fasciculin 2 bound AChE at the mouth of the gorge (5); *D*, fasciculin 2 complex with AChE, rotated 90°. Acrylodan conjugated to E84C is shown in *yellow*; and acrylodan conjugated to E81C is shown in *green*. (Note in *D* the proximity between arginine 11 on Fas 2 and the acrylodan side chain at position 84).

other disulfide loop on which it resides (5, 6). We examined the kinetics of substrate catalysis and inhibitor association with the modified enzymes, and we correlate these kinetic parameters with the spectroscopic changes in the conjugated acrylodan upon ligand association. Fluorescence measurements reveal changes in conformation reflected in the substituted side chains well removed from the active center gorge. The results suggest that ligand binding at the catalytic site allosterically alters the conformation of a specific segment of the Ω loop whereby gorge closure occurs and residue side chain positions distal to the binding site are affected.

EXPERIMENTAL PROCEDURES

Inhibitors and Substrates—Acetylthiocholine iodide, 5,5'-dithiobis(2-nitrobenzoic acid) (Ellman's reagent), dithiothreitol, tacrine (9-amino-1,2,3,4-tetrahydroacridine hydrochloride hydrate), BW286c51, decamethonium, and edrophonium were purchased from Sigma. *m*-(*N,N,N*-trimethylammonio)trifluoromethylacetophenone (TFK⁺) and (–)-huperzine A were purchased from Calbiochem. Acrylodan was obtained from Molecular Probes (Eugene, OR). Fasciculin 2 (purified from the venom of *Dendroaspis angusticeps*) was a gift of Dr. Pascale Marchot (University of Marseille, France). Drs. Yacov Ashani and Bhupendra P.

Doctor (Walter Reed Army Research Center, Washington, D. C.) kindly provided 7-[[methylethoxy]phosphinyl]-oxyl]-1-methylquinolinium iodide (MEPQ) and procainamide-linked Sepharose CL-4B resin. *m*-tert-Butyl trifluoromethylacetophenone (TFK⁰) was synthesized as described (21) and kindly provided by Dr. Daniel Quinn, University of Iowa, Iowa City, IA. All other chemicals were of the highest grade commercially available.

Expression, Mutagenesis, and Purification of mAChE—Mouse AChE was produced by transfection of expression plasmid (pCDNA3, Invitrogen, San Diego, CA) containing an encoding cDNA where the AChE sequence was terminated at position 548. The plasmid was transfected into HEK293 cells. Cells were selected with G418 to obtain stable producing cell lines, and AChE was expressed as a secreted soluble enzyme in serum-free media (20). Mutant enzymes were generated by standard mutagenesis procedures, and cassettes containing the mutation were subcloned into pCDNA 3 (20). Nucleotide sequences of the cassettes were confirmed by double-stranded sequencing to ensure that spurious mutations were not introduced into the coding sequence. Affinity chromatography using (*m*-aminophenyl)trimethylammonium linked through a long chain to Sepharose CL-4B resin (Sigma) permitted one-step purification of AChE. From 4 to 6 liters of media, mutant and wild type enzyme were purified in quantities ranging between 5 and 25 mg, as described previously (22–24). Purity was ascertained by SDS-PAGE and by measurements of specific activity.

TABLE I
Constants for acetylthiocholine hydrolysis by wild type and mutant mouse AChEs

Data shown as means \pm S.D. typically from three measurements. Data were fit to the Equation, $v = (1 + b[S]/K_{SS})V_{max}/(1 + [S]/K_{SS})(1 + K_m/[S])$, where $[S]$ is substrate concentration, K_{SS} is the substrate inhibition or activation constant, and b is the relative catalytic turnover of the ternary complex (12).

Enzyme	K_m μM	K_{SS} mM	b	k_{cat} $10^5/min$	k_{cat}/K_m $10^9/M \cdot min$
WT ^a	54 ± 16	14 ± 5	0.2 ± 0.07	1.6 ± 0.4	3.0
Y124C ^a	65 ± 17	20 ± 14	0.2 ± 0.09	1.4 ± 0.3	2.2
H287C ^a	58 ± 7	12 ± 6	0.2 ± 0.06	1.8 ± 0.2	3.1
A262C ^a	59 ± 4	11 ± 3	0.2 ± 0.04	1.6 ± 0.1	2.7
L76C	97 ± 19	17 ± 1	0.2 ± 0.03	1.8 ± 0.1	1.9
E81C	57 ± 6	11 ± 1	0.2 ± 0.03	1.6 ± 0.1	2.9
E84C	190 ± 9	26 ± 2	0.2 ± 0.05	1.9 ± 0.4	1.0

^a Data are from Ref. 20.

Assay of Catalytic Activity—The spectrophotometric method of Ellman was used (25), and kinetic constants for acetylthiocholine hydrolysis were determined by fitting the observed rates as described (26). Titration of active sites with known concentrations of the irreversible phosphorylating agent, MEPQ, was accomplished by the method of Levy and Ashani (27).

Acrylodan Labeling—Mutant enzymes were pretreated with 0.25 mM dithiothreitol for 30 min at room temperature to ensure reduction of the introduced cysteine. Excess dithiothreitol was removed by use of a G-50 Sephadex spin column (Roche Molecular Biochemicals) equilibrated in 10 mM Tris, 100 mM NaCl, 40 mM MgCl₂, pH 8.0. A volume of 1 μ l of acrylodan at 100 times the enzyme concentration was slowly mixed with the enzyme to achieve an \sim 5-fold molar excess of acrylodan to mutant enzyme. Labeling was allowed to proceed for at least 12 h at 4 $^{\circ}$ C, and unreacted acrylodan was removed by size exclusion chromatography using Sephadex G-25 (Amersham Pharmacia Biotech) in 0.1 M sodium phosphate buffer, pH 7. Concentrations of acrylodan-labeled enzyme were determined from the maximal acrylodan absorbance found between 360 and 380 nm ($\epsilon \sim 16,400 M^{-1} cm^{-1}$). Stoichiometry of labeling of the various preparations, estimated from a comparison of enzyme concentration by protein (280 nm) to acrylodan (360–380 nm) absorbance, ranged as follows: L76C, 0.7–0.8; E81C, 0.79–1.0; E84C, 0.77–1.0; Y124C, 0.79–1.0; A262C, 0.69–0.85; and H287C, 0.82–0.88. Specificity of labeling was assessed by comparison of areas under the fluorescence emission curves for acrylodan-treated mutant and wild type enzymes. Specific labeling for each mutant was as follows: L76C, 70–85%; E81C, 81–91%; E84C, 85–93%; Y124C, 83–90%; A262C, 80–90%; H287C, 70–76%.

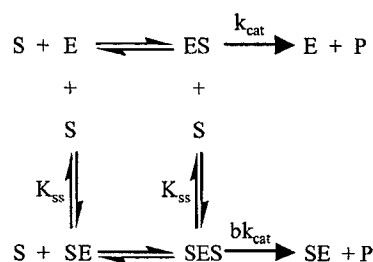
Trifluoroacetophenone Inhibition—Picomolar amounts of enzyme in 0.01% bovine serum albumin in 0.1 M sodium phosphate buffer, pH 7.0, were reacted with TFK⁺ in the absence of substrate. Inhibition was monitored by measuring residual enzyme activity by removal of aliquots during the course of the reaction. Bimolecular rate constants of inhibition were determined by nonlinear fits of the data (28).

Spectrofluorometric Assays—Steady-state emission spectra were measured at room temperature using a Jobin Yvon/Spex FluoroMax II spectrofluorometer (Instrument S.A., Inc., Edison, NJ) with the excitation and emission bandwidths set at 5 nm. The excitation wavelength for acrylodan was set at 359 nm, and emission was monitored between 420 and 600 nm. Equilibrium dissociation constants, K_d , for BW286c51 and edrophonium with the acrylodan-labeled enzyme were obtained by titration of a fixed quantity of labeled enzyme (54–120 nM) with various concentrations of indicated inhibitors. K_d values were obtained by monitoring the fractional decrease in the total area under the fluorescence emission curves from 420 to 600 nm for the acrylodan-labeled E84C or a limited segment of the emission between 450 and 485 nm for the acrylodan-labeled E81C. For ligands of high affinity such as BW286c51, where binding is nearly stoichiometric, data were fitted to Equation 1.

$$\Delta F = \Delta F_{max} (E_t + I_t + K_d - (E_t + I_t + K_d)^2 - 4 E_t I_t)^{0.5} (2E_t)^{-1} \quad (\text{Eq. 1})$$

ΔF and ΔF_{max} are the change and maximum change in fluorescence, respectively; E_t is the total enzyme concentration, and I_t is the total inhibitor concentration. Association of TFK⁺ with acrylodan-labeled E81C and E84C was assessed from the kinetics of decrease in fluorescence at 470 and 477 nm respectively, following addition of a stoichiometric excess TFK⁺ at several concentrations. Data were fitted to a single exponential approach to equilibrium.

Association and dissociation rate constants of edrophonium and BW286c51 with E81C and E84C AChEs were determined from changes in the tryptophan fluorescence using a stopped-flow spectrophotometer



SCHEME 1. In this scheme substrate can combine at two discrete sites to form two binary complexes, ES and SE (where S is substrate; E is enzyme; and P is product). Only ES results in substrate hydrolysis. For simplicity, S is assumed to combine equally well with E and ES . The efficiency of substrate hydrolysis of the ternary complex SES , as compared with ES , is reflected in the value of the parameter, b , the relative catalytic turnover of the ternary complex (26).

as described previously (29). Time-dependent decreases in tryptophan fluorescence were observed upon excitation at 276 nm by means of a 305-nm emission cut-off filter.

RESULTS

Characterization of Substrate Hydrolysis and Fasciculin 2 Inhibition—The cysteine-substituted enzymes show kinetics of acetylthiocholine hydrolysis similar to wild type enzyme (Table I and Scheme 1) suggesting that all mutant enzymes fold correctly despite the presence of the newly introduced cysteine. The K_m value of E84C shows slightly less than a 4-fold increase, whereas the change in turnover rate, k_{cat} , is minimal. Similar changes in kinetic constants were observed previously for E84Q mAChE (28). Since K_m , in diffusion limited catalysis, depicts the initial encounter between substrate and enzyme, an increase in K_m likely arises from the reduction of negative charge that electrostatically steers the cationic substrate into the active center gorge. Interestingly, a similar E81C mutation has little or no effect on substrate hydrolysis. Not all negatively charged residues around the active center appear to be involved equivalently in electrostatic steering.

Association and dissociation rates of fasciculin with A262C, H287C, and Y124C mutant enzymes were also found to be close to the rates with wild type enzyme (20). Fasciculin, at low concentrations, is also capable of associating with the mutant enzymes after acrylodan conjugation (Fig. 2). In addition, enzyme activity measurements of fasciculin-bound acrylodan conjugates show greater than 99% inhibition (data not shown).

Influence of Residue Modification on Inhibition by *m*-Tri-methylammoniotrifluoromethylacetophenone—TFK⁺ binding to cysteine-substituted enzymes, both free and modified with acrylodan, was also examined (Table II). For E81C and E84C, the association rate constants (k_{on}) for TFK⁺ were obtained from measurements of enzyme activity. Although positions 81 and 84 are both spatially removed from TFK⁺-binding site, k_{on}

for E84C is slightly slower than that for wild type enzyme. By contrast, E81C shows no difference in the kinetic constants. Conjugation of acrylodan, a neutral naphthalene derivative, with E84C reduces k_{on} of TFK⁺ 7-fold compared with unconjugated E84C, whereas conjugation of E81C with acrylodan only reduces k_{on} of TFK⁺ slightly. For acrylodan-labeled mutants, k_{on} was measured from the time-dependent decrease of fluorescence signal (Fig. 3).

Influence of Residue Modification on Inhibition by Noncovalent Active Site Inhibitors—A similar trend in inhibition kinetics was seen with noncovalent active site inhibitors such as edrophonium and BW286c51 (Table II). An increase over wild type K_d of 2-fold occurs for edrophonium binding to E84C, and

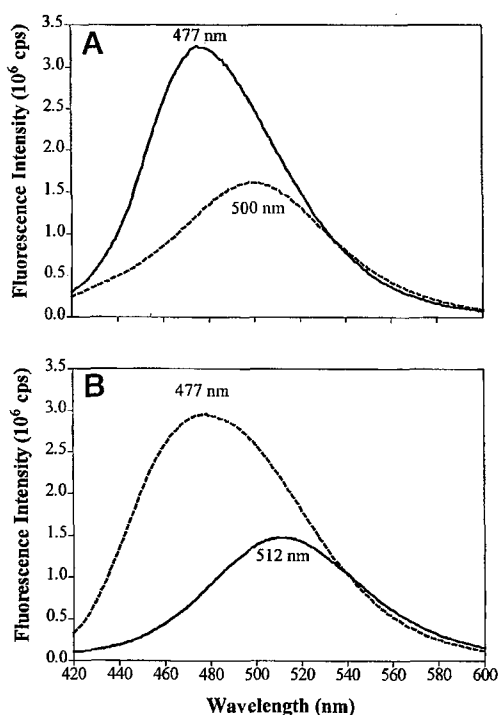


FIG. 2. Fluorescence emission spectra of acrylodan-labeled Y124C (A) and E84C (B) AChE free in solution (dashed line) and complexed with fasciculin (solid line). A, for acrylodan-labeled Y124C, fasciculin produces a hypsochromic shift and enhancement of fluorescence quantum yield. The large shift for Y124C reveals a clear isoemissive point indicative of the two (free and fasciculin bound) species. Equivalent concentrations of enzyme (215 nM) were present for all conditions. The concentration of fasciculin was 215 nM. B, for acrylodan-labeled E84C fasciculin produces a bathochromic shift and reduction of fluorescence quantum yield. Equivalent concentrations of enzyme (270 nM) were present for all conditions. The concentration of fasciculin was 800 nM.

an 18-fold increase in K_d is observed for BW286c51 binding. Similar increases in K_d of edrophonium and BW286c51 were seen for E84Q human AChE (18). By comparison, E81C showed no alterations in ligand binding constants. For acrylodan-labeled mutants, K_d was measured from the fluorescence signals of an equilibrium titration (Fig. 4). Acrylodan-labeled E84C shows K_d increases of 10-fold for edrophonium and 3-fold for BW286c51 compared with unreacted E84C. For acrylodan-labeled E81C, only a slight increase in K_d is seen for both ligands. The high concentration of acrylodan-labeled E81C required for equilibrium titrations precludes an accurate estimate of K_d for high affinity ligands such as BW286c51.

Effect of Fasciculin on Acrylodan Fluorescence Emission—The peptide toxin, fasciculin, inhibits AChE by tightly capping the mouth of active center gorge (Fig. 1) (11, 30–32). Table III shows changes in emission maxima of acrylodan-labeled AChE mutants in the presence of fasciculin. There is no discernible change in fluorescence emission of acrylodan-conjugated A262C (20), consistent with the position 262 being distal to the fasciculin-binding site. The large hypsochromic shifts seen at both the 124 and 287 positions reflect solvent exclusion and an increase in hydrophobicity experienced by the fluorophores in the gorge upon fasciculin binding (20). For the Ω loop mutant, L76C, fasciculin binding produces a 40% increase in quantum yield but no change in emission maximum. Bathochromic shifts are found at both the 81 and 84 positions, with position 84 producing a shift of larger magnitude (Fig. 2 and Table III).

Effect of Covalently Conjugated Active Site Inhibitors on Acrylodan Fluorescence Emission—Changes in emission maxima of acrylodan-labeled AChE mutants in the presence of conjugating trifluoroacetophenones are shown in Table IV. The trifluoroacetophenones inhibit the enzyme by conjugating to form a hemiketal at active site serine without dissociation of leaving group (33). Both the isosteric neutral and cationic trifluoroketones (TFK⁰ and TFK⁺) produced no discernible changes in emission spectra of acrylodan conjugated at H287C and A262C, consistent with a fluorophore position distant from gorge base and hence not in direct contact with ligand. Remarkably, both TFK⁰ and TFK⁺ produce a substantial bathochromic shift (at least 30 nm) with acrylodan-E84C. The trifluoroketones also produce spectral shift of intermediate value (20 nm) for E81C and a much smaller change (4–6 nm) for L76C. Interestingly, neutral TFK⁰ produces a large 22 nm of hypsochromic shift with the Y124C acrylodan conjugate.

O,O-Dimethyl-*O*-(2,2-dichlorovinyl)phosphate, a small achiral organophosphonate, phosphorylates the active site serine of mAChE, with subsequent departure of the dichlorovinyl group (34, 35). The small and symmetrical dimethyl phosphoryl conjugate remaining at the active site serine might lead one to suspect very little perturbation, if any at all, in fluorescence

TABLE II
Kinetic and equilibrium constants for reaction of enzymes with TFK⁺, edrophonium, and BW284c51 in the presence and absence of fluorescent (acrylodan) cysteine labeling compound

Data are shown as means from two to three measurements. Individual determinations are within 33% of the mean. Rates for TFK⁺ are calculated based on ratios of the hydrated and unhydrated ketone (21).

Enzyme	TFK ⁺		Edrophonium		BW284c51	
	k_{on}	$\frac{k_{on} \text{ WT}}{k_{on} \text{ mutant}}$	K_d	$\frac{K_d \text{ mutant}}{K_d \text{ WT}}$	K_d	$\frac{K_d \text{ mutant}}{K_d \text{ WT}}$
	$10^9 \text{ M}^{-1} \text{ min}^{-1}$		nM		nM	
Wild type	150		250 ^a		2.0 ^a	
E81C	150	1	260 ^b	1	2.6 ^b	1.3
E81C-acrylodan	94	1.6	640	2.6	6.9	3.5
E84C	93	1.6	550 ^b	2.2	35 ^b	18
E84C-acrylodan	13	11	6300	25	130	65

^a Data are from Ref. 29.

^b Equilibrium dissociation constants are derived from the ratio of k_{off}/k_{on} using stopped-flow measurement of tryptophan fluorescence quenching.

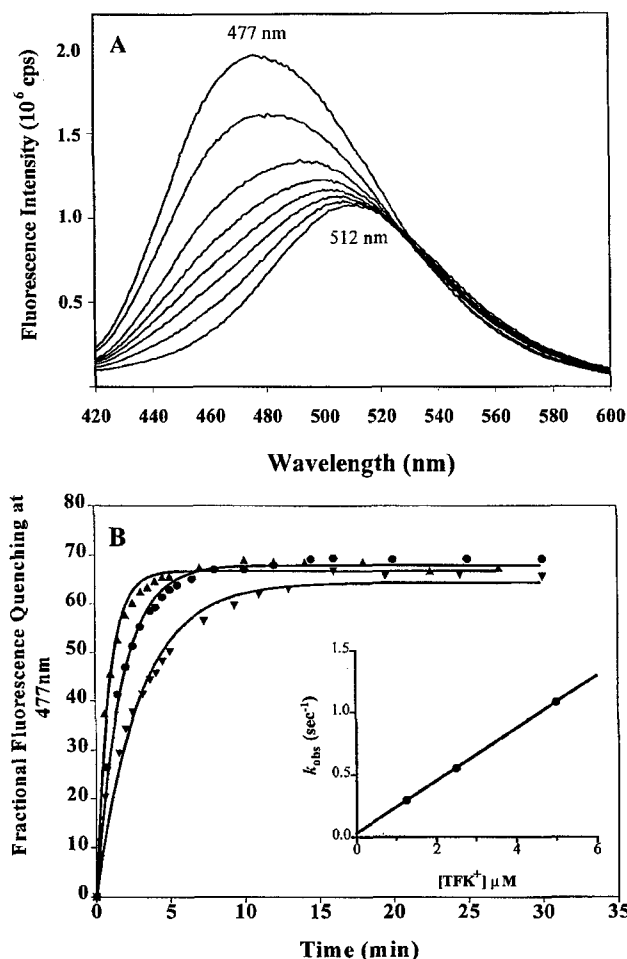


FIG. 3. Association of TFK⁺ with E84C acrylodan-modified AChE. A, fluorescence emission spectra of acrylodan-labeled E84C AChE following addition of excess TFK⁺. TFK⁺ produces a bathochromic shift and reduction of fluorescence quantum yield. The large chromic shift reveals a clear isoemissive point indicative of the two (free and TFK⁺ bound) species. Initial enzyme concentration was 130 nM. Excess TFK⁺ (1.25 μM) was added, and fluorescence spectra were recorded at the following times: 0, 1, 2.5, 4.3, 5.8, 7.4, 10.6, and 22 min. B, time course of the fluorescence changes. Initial E84C acrylodan-modified AChE concentration was 150 nM. Excess TFK⁺ was added, and decrease in fluorescence signal at 477 nm was monitored using an ISA Jobin Yvon-Spex Fluoromax fluorometer. The three TFK⁺ concentrations were 1.25 (▼), 2.5 (●), and 5.0 (▲) μM. Control enzyme samples, to which buffer rather than TFK⁺ was added, did not show decreases in fluorescence signals over the time intervals measured. The inset shows rates plotted as a function of TFK⁺ concentration. k_{on} for TFK⁺ is calculated based on ratios of the hydrated and unhydrated ketone (21).

spectra. Indeed, acrylodan conjugated at positions 124, 262, and 287 showed very little or no change in spectrum. However, bathochromic shifts at positions 81 and 84 were observed, although of smaller magnitude for E84C when compared with other ligands (Table IV).

Effect of Noncovalent Active Site Inhibitors on Acrylodan Fluorescence Emission—Noncovalent active site inhibitors, such as edrophonium, tacrine, and huperzine, associate primarily with the choline subsite at the base of active site gorge. Crystal structures of inhibitors bound to *Torpedo californica* AChE revealed that these ligands should have no direct contact with the conjugated fluorophore at all six cysteine-substituted sites (36, 37). Upon edrophonium, tacrine, or huperzine association, alteration of acrylodan emission maxima is undetectable for positions 124, 287, and 262 (Table V). However, as seen for other ligands, acrylodan conjugated at E84C surprisingly

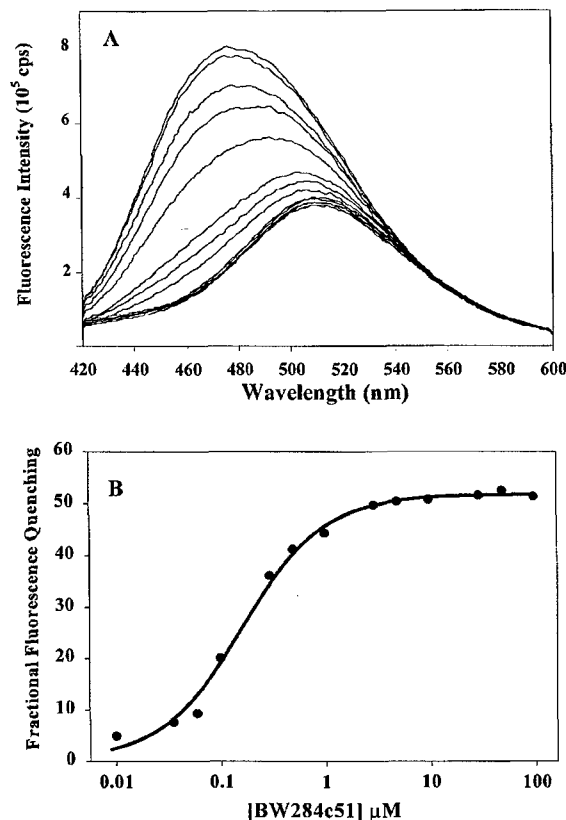


FIG. 4. Association of BW284c51 with the E84C acrylodan-modified AChE. A, fluorescence emission spectra of acrylodan-labeled E84C AChE following titration with BW284c51. BW284c51 produces a bathochromic shift and reduction of fluorescence quantum yield. Initial enzyme concentration was 70 nM. BW284c51 concentrations were 0, 0.01, 0.035, 0.06, 0.1, 0.3, 0.5, 1, 3, 5, 10, 30, 50, and 100 μM. B, the decrease in fluorescence measured by areas under the respective fluorescence emission curves is plotted as a function of BW284c51 concentration. K_d is determined by fitting the data with Equation 1 as outlined under "Materials and Methods."

TABLE III

Fluorescence emission parameters of mouse AChE mutants labeled with acrylodan in the presence of fasciculin

Data are shown as mean values of at least three determinations. Relative quantum yields were determined by comparison of areas of the fluorescence emission curves.

Enzyme	Acrylodan Emission Maxima (nm)			Relative Quantum Yield
	No Fasciculin	Saturating Fasciculin	Chromic Shift (nm)	
L76C	505	505	0	1.40
E81C	489	510	21	1.16
E84C	477	512	35	0.47
*Y124C	500	477	-23	1.78
*A262C	517	517	0	0.97
*H287C	524	507	-17	5.0

^a Data are from Ref. 20.

shows a bathochromic shift of 33 nm (from 477 to 510 nm) upon inhibitor binding. A change of smaller magnitude is seen in the case of acrylodan-L76C (from 505 to 509 nm) and acrylodan-E81C (from 480 to 510 nm) with noncovalent active site inhibitors. Ligand binding results in a common emission maximum ($\lambda_{max} \sim 510$ nm) for acrylodan at the three Ω loop positions.

Effect of Bisquaternary Inhibitors on Acrylodan Emission Spectrum—Extended bisquaternary inhibitors, such as BW286c51 and decamethonium, belong to a class of inhibitors

TABLE IV

Fluorescence emission parameters of mouse AChE mutants labeled with acrylodan in the presence of covalent active site inhibitors

Data are shown as mean values of at least three determinations. Relative quantum yields were determined by comparison of areas of the fluorescence emission curves. Data for the unconjugated enzymes are found in Table III.

Acrylodan Emission Maxima (nm)			
Enzyme	Conjugated TFK ⁰	Chromic Shift (nm)	Relative Quantum Yield
L76C	509	4	0.87
E81C	510	21	0.89
E84C	507	30	0.59
Y124C	478	-22	1.15
A262C	517	0	0.97
H287C	524	0	0.90



Acrylodan Emission Maxima (nm)			
Enzyme	Conjugated TFK ⁺	Chromic Shift (nm)	Relative Quantum Yield
L76C	511	6	0.92
E81C	510	21	0.89
E84C	512	35	0.52
Y124C	503	3	0.70
A262C	517	0	0.97
H287C	524	0	1.07



Acrylodan Emission Maxima (nm)			
Enzyme	Conjugated DDVP	Chromic Shift (nm)	Relative Quantum Yield
L76C	503	-2	1.27
E81C	510	21	0.19
E84C	496	19	0.39
Y124C	496	-4	1.27
A262C	517	0	0.97
H287C	524	0	1.03

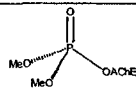
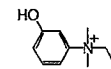


TABLE V

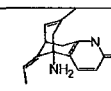
Fluorescence emission parameters of acrylodan-labeled mouse AChE mutants in the presence of reversible active site inhibitors

Data are shown as mean values of at least three determinations. Relative quantum yields were determined by comparison of areas of the fluorescence emission curves. Data for the unliganded enzymes are found in Table III.

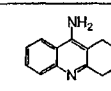
Acrylodan Emission Maxima (nm)			
Enzyme	Saturating Edrophonium	Chromic Shift (nm)	Relative Quantum Yield
L76C	509	4	0.92
E81C	510	21	0.91
E84C	510	33	0.60
Y124C	500	0	0.79
A262C	517	0	0.97
H287C	524	0	1.13



Acrylodan Emission Maxima (nm)			
Enzyme	Saturating Huperzine A	Chromic Shift (nm)	Relative Quantum Yield
L76C	511	6	0.86
E81C	510	21	0.88
E84C	510	33	0.55
Y124C	500	0	0.63
A262C	517	0	0.97
H287C	524	0	1.13



Acrylodan Emission Maxima (nm)			
Enzyme	Saturating Tacrine	Chromic Shift (nm)	Relative Quantum Yield
L76C	509	4	0.87
E81C	510	21	0.91
E84C	510	33	0.45
Y124C	497	-3	0.51
A262C	517	0	0.97
H287C	524	0	1.13



that interact with two binding sites of AChE simultaneously (32, 38–39). The quaternary ammonium moiety on one end of the molecule associates with the Trp⁸⁶ residue that characterized the choline-binding site, whereas the other end resides near Trp²⁸⁶ at the active site gorge rim. Table VI shows changes in emission maxima of acrylodan-labeled AChE mutants in the presence of bisquaternary inhibitors. No changes are observed at position 262. By contrast, both decamethonium and BW284c51 caused a pronounced hypsochromic shift and increase in quantum yields with acrylodan conjugated at Y124C and H287C. Addition of decamethonium produced a hypsochromic shift of 35 nm at position 124, and a modest 7 nm shift at position 287. BW284c51 has a similar effect; for the Ω loop mutants, L76C, E81C, and E84C, bathochromic shifts of similar magnitude to the monoquaternary ligands were observed (Tables V and VI).

DISCUSSION

Characteristics of Fluorescence from Acrylodan-conjugated Cysteine Residues—Fluorescence emission of acrylodan is exquisitely sensitive to the dielectric constant of the solvent. In general, the fluorescence emission spectrum of acrylodan shifts

toward the red (bathochromic) shift, and the quantum yield decreases as the polarity of solvent increases (20, 40–42). This sensitivity to solvent polarity arises from the interaction of the excited state of acrylodan with its surrounding solvent. The excited state is more polar than the ground state and, as such, will interact with a polar solvent so as to align solvent dipoles. This alignment lowers the energy of the excited state and causes the red shift of the emission spectrum. Hence, an acrylodan-labeled enzyme with an emission maximum of 510–525 nm likely reflects exposure of the side chain to solvent (20, 42). On the other hand, acrylodan emission maxima in the range of 475–500 nm likely reflect solvent exclusion and a more hydrophobic environment surrounding the fluorophore. The time course of TFK⁺ reaction with acrylodan-E84C (Fig. 3) reveals a large spectral shift from 477 to 512 nm, indicating acrylodan conjugated at this position has moved to a more hydrophilic environment with TFK⁺ bound. The large spectral shift yields a clear isomissive point, which arises when only two distinct emitting species are present, in this case the free enzyme and the TFK⁺ conjugate.

Influence of Residue Modification on Ligand Binding—The changes in emission spectra of acrylodan-labeled Ω loop residues 81 and 84 have been exploited to monitor ligand binding

TABLE VI
Fluorescence emission parameters of acrylodan-labeled mouse AChE mutants in the presence of bisquaternary ligands

Data are shown as mean values of at least three determinations. Relative quantum yields were determined by comparison of areas of the fluorescence emission curves. Data for the unliganded enzymes are found in Table III.

Acrylodan Emission Maxima (nm)			
Enzyme	Saturating BW284c51	Chromic Shift (nm)	Relative Quantum Yield
L76C	508	3	1.13
E81C	510	21	0.98
E84C	512	35	0.47
Y124C	487	-13	1.05
A262C	517	0	0.97
H287C	510	-14	2.73

Acrylodan Emission Maxima (nm)			
Enzyme	Saturating Decamethonium	Chromic Shift (nm)	Relative Quantum Yield
L76C	508	3	1.05
E81C	510	21	0.94
E84C	505	28	0.59
Y124C	465	-35	1.85
A262C	517	0	0.97
H287C	517	-7	1.76

(Table II). We observe that cysteine substitution and acrylodan conjugation at position 84 affect ligand binding kinetics but not at position 81. Cysteine substitution at position 84 has little influence on catalytic parameters derived from steady-state catalysis (Table I). The K_m of E84C increases less than 4-fold compared with the wild type enzyme. By contrast, a similar substitution at position 81 has no effect on ACh steady-state catalysis. Precise quantitation of these catalytic parameters for the acrylodan-conjugated enzyme is complicated by incomplete modification by acrylodan. However, inhibitor association can be measured using the change in fluorescence signal (Table II). Here we observe reductions in binding kinetics for several ligands (Table II) ranging between 1 or 2 orders of magnitude at position 84 but very little change at position 81. Although a portion of the reduction at position 84 is due to the cysteine substitution, acrylodan conjugation has a small, but significant (3–10-fold), influence on ligand binding. Even though both the 81 and 84 residues reside on the enzyme surface removed from the active center gorge, modification only at position 84 appreciably affects the energetics of ligand binding. The acrylodan moiety, whose dimension is slightly larger than the indole moiety of tryptophan, may impart steric restrictions to the region around the 84 site contributing to the energy cost in ligand binding. A small alteration in ligand binding energy (1.5–3.0 kcal/mol) is not unexpected if the conformation of Ω loop plays a role in ligand binding.

Velan *et al.* (18) have examined steady-state kinetics for a large number of Ω loop substitutions and truncations. Modification of Glu⁸⁴ and its neighboring residues were found to have limited effect on steady-state kinetics. Faerman *et al.* (19) inserted a cysteine at position 82 to pair with a second cysteine residing proximally in the body of the enzyme. Although it could not be firmly established that a disulfide bond formed,

little change in kinetic parameters (K_m and k_{cat}) was observed. Because of compensating contributions of the component primary constants, it is often difficult to correlate changes in steady-state kinetic parameters with structural perturbations. Our site-directed fluorophore labeling provides a physical assessment of the localized conformational change in the Ω loop. In cases where the fluorophore makes direct contact with the ligand, as for acrylodan-labeled Y124C and H287C with fasciculin, the energetic perturbations from substitution are larger, since complementarity of the binding site may be altered through the insertion of acrylodan side chain at the interface between the ligand and its binding site (20).

Acrylodan Modification at a Site Distal to the Active Center Core—We chose the A262C modification as a positional reference for a site distal to the active center. This residue is also located at the tip of a disulfide loop but is located ~30 Å away from the rim of the active center gorge. Crystallographic studies show this region to have a high temperature coefficient (B factor), indicative of substantial molecular motion of this surface residue. In fact, the position of this residue and its immediate neighbors is only secured in crystal forms where proximity of the symmetry-related AChE molecule limits its movement in the crystal structure (6).

Acrylodan substitutions at this position show a long wavelength emission ($\lambda_{max} = 517$ nm) indicative of exposure to a hydrophilic environment (Table III). Moreover, none of the ligands studied, whether they are covalently attached to the active center (TFK or alkylphosphates), reversibly bound to the active center (edrophonium), span between the active center and peripheral site (decamethonium and BW286c51), or bind only to peripheral site (fasciculin), affect the spectroscopic properties of acrylodan conjugated at site 262 (Tables III–VI). This pattern indicates a lack of global conformational change affecting residue environments in a disulfide loops well removed from the active center (Fig. 1).

Residues Residing on the Active Center Gorge in Apposition with the Ω Loop—Residues 124 and 287 lie in close proximity to the Ω loop with H287C at the rim of the gorge and Y124C, residing just below the rim in the gorge interior (Fig. 1). The crystal structure of the complex shows fasciculin to “cap” these residues, and our previous studies show hypsochromic shifts of acrylodan upon fasciculin binding (20). None of the reversibly bound active center ligands (edrophonium, huperzine, and tacrine) induce a spectral shift at position 124 or 287. However, modest quenching is observed at position 124 upon binding of these active center ligands. The bisquaternary ligands, which should approach or come in close apposition with these residues, cause significant hypsochromic shifts. The large shift for decamethonium at position 124 may reflect the ability of the cluster of aromatic residues to collapse around the methylene chain of decamethonium enlodged within the active center gorge. Crystallographic studies show one quaternary ammonium of decamethonium to be consistently positioned in the vicinity of Trp⁸⁴; however, both the flexible side chain and the outermost quaternary group are found to assume multiple positions in the decamethonium-AChE complexes studied to date (6, 29).

The distinct spectra observed for the two isosteric trifluoroacetophenone conjugates is surprising (Table IV). Covalent inhibition of cationic trifluoroacetophenone (TFK⁺) produces very little spectral shift of acrylodan at either position 124 or 287. This is consistent with the crystal structures where the trimethyl ammonio moiety of TFK⁺ forms a cation- π interaction with Trp⁸⁶, and the trifluoroacetophenone moiety forms a hemiketal bond with the active center serine 203 (33). However, the isosteric *t*-butyl congener (TFK⁰) shifts the environ-

ment of residue 124 to that resembling a hydrophobic state. This difference suggests that the orientation of this hemiketal conjugate differs where the *t*-butyl group extends toward the gorge exit. TFK⁰ inhibits the wild type enzyme 70-fold slower than TFK⁺, presumably due to lack of cation- π interaction and slightly different ligand orientation (21). Alkyl phosphorylation with small alkyl groups also has little influence on the environment at position 124 (Table IV).

Ω Loop Substitutions—Our greatest surprise emerged from studies on the outer portion of the Ω loop, defined by residues between Cys⁶⁹ and Cys⁹⁶, where we have examined three positions extending from the near tip of the loop (Leu⁷⁶) at the gorge rim descending toward the active center (Glu⁸¹ and Glu⁸⁴). The residues modified are all on the outer surface and do not form the inner gorge wall. Since residues 81 and 84 carry acidic side chains, they might be expected to show solvent exposure in the native enzyme and not be involved in the internal stabilization of the loop, as is evident in the crystal structure of the mouse enzyme (5, 6). In the absence of ligand, the spectra of the conjugated acrylodan moiety reveal different degrees of solvent exposure with the acrylodan at position 84 being the most protected in an hydrophobic environment, acrylodan at 81 being intermediate, and acrylodan at 76 being most exposed. Examination of crystal structures of mouse enzyme revealed a surface cavity near the side chain of the 84 site (5, 6). The observed λ_{\max} likely reflects acrylodan buried in this surface cavity when conjugated to the 84 site (Fig. 1).

The presence of fasciculin causes a large bathochromic shift of acrylodan fluorescence at both the 81 and 84 positions, as well as increase in quantum yield of acrylodan at 76. The lack of a shift in emission seen for acrylodan at the 76 position may simply reflect a balance between a small environmental change at 76 upon ligand binding in general and partial solvent occlusion at this position by fasciculin. In the case of Glu⁸⁴, the bathochromic shift likely reflects Arg¹¹ of fasciculin loop I coming in van der Waals contact with the 84 side chain and displacing acrylodan into a more polar environment. However, an explanation of the bathochromic shift at position 81 requires a more involved analysis. Although 81 is removed from the fasciculin-binding site, fasciculin has a sufficient molecular dimension to restrict the Ω loop so that the entire loop freezes or closes upon fasciculin binding. Thus, fasciculin binding may confer strain on the α -carbon backbone structure of the Ω loop such that the acrylodan side chain at positions 81 and 84 becomes exposed to the hydrophilic environment. The fact that substitutions at both positions yielded acrylodan spectra with equivalent emission maxima after ligand binding suggests a conformational involvement of the entire loop.

Similar to fasciculin, small ligands that bind to the active center produce a similar strain. All of the small ligands, whether reversibly bound or covalently attached, elicit marked changes in acrylodan emission with the largest spectral shift seen for E84C, an intermediate value seen for E81C, and only small change observed for L76C. In each case the conformational change induced by the ligand causes the acrylodan to move into a region of higher dielectric constant, presumably being more solvent-exposed. The pattern is remarkably consistent among the ligands, and only the small organophosphate when conjugated induces a shift of smaller magnitude. A likely explanation for the observed conformational changes is that ligand binding to the active center induces gorge closure, which is mediated throughout the Ω loop. The strain placed on the α -carbon backbone upon gorge closure causes the side chains to shift positions and become exposed to hydrophilic environment.

DeFarri *et al.* (43) have noted that the peripheral site inhibitor, thioflavin T, when bound to AChE, shows a large enhance-

ment of fluorescence. Simultaneous binding of an active center ligand and thioflavin partially quenches the enhanced fluorescence of bound thioflavin. Radic and Taylor (29) have observed that bound active center ligands cause a partial quenching of the native tryptophan fluorescence in AChE. Since these ligands lack the spectral overlap for fluorescence resonance energy transfer, the bound ligand is likely to influence the connectivity between aromatic residues present in the gorge, thereby influencing fluorescence quantum yields. Taken together, these studies suggest that ligands induce conformational changes in AChE giving rise to a gorge conformation collapsed around the bound ligand. Our site-directed cysteine mutagenesis and fluorescence labeling studies allow one to delineate the involvement of particular residues on the Ω loop in this conformational change.

Crystallographic Structures and Solution Dynamics of the Acetylcholinesterase Complex—In the several crystal structures of AChE with conjugated or reversibly bound ligand that have been studied, little evidence for change in enzyme conformation has been detected with a difference of less than a root mean square of 1 Å² for the α -carbon backbone between the apoenzyme and the various complexes (4–6, 13, 14, 33–35, 44). Changes in side chain orientation occur most notably in the phenyl ring at position 337 for certain reversible complexes (34) and phenylalanine 297, when bulky organophosphates are conjugated to the active site serine (44). However, based on the multiple positions of the outer trimethylammonio moiety in decamethonium for mouse (6) and *Torpedo* crystal structures (34), some flexibility may exist particularly within the gorge itself. Brownian dynamics often require reducing the radii of the attacking ligand or the residues lining the gorge in order to simulate the kinetics of diffusion-limited substrate access observed experimentally (45). Thus, all of crystal structures reported to date reveal a closed gorge with constrained dimensions. Our solution-based fluorescence studies provide the first physical evidence for localizing the ligand-induced conformational change to residues in the Cys⁶⁹–Cys⁹⁶ Ω loop. These findings raise an interesting possibility that the unliganded enzyme exists in a rapidly converting conformational equilibrium between open and closed states, and both ligand binding and conditions of crystallization favor formation of a closed gorge state. In fact, analysis of the molecular dynamics of a solvated mouse AChE shows fluctuations yielding an average widening of the gorge over a 10-ns interval (46). Such opening and closing motions of the gorge may also be integral to the catalytic cycle of transacylation and deacylation during ester hydrolysis.

REFERENCES

1. Cygler, M., Schrag, J. D., Sussman, J. L., Harel, M., Silman, I., Gentry, M. K., and Doctor, B. P. (1993) *Protein Sci.* **2**, 366–382
2. Rosenberry, T. L. (1975) *Adv. Enzymol. Relat. Areas Mol. Biol.* **43**, 103–218
3. Quinn, D. M. (1987) *Chem. Rev.* **87**, 955–979
4. Sussman, J. L., Harel, M., Frolow, F., Oefner, C., Goldman, A., Tokar, L., and Silman, I. (1991) *Science* **253**, 872–879
5. Bourne, Y., Taylor, P., and Marchot, P. (1995) *Cell* **83**, 503–512
6. Bourne, Y., Taylor, P., Bougis, P. E., and Marchot, P. (1999) *J. Biol. Chem.* **274**, 2963–2970
7. Ripoll, D. R., Faerman, C. H., Axelsen, P. H., Silman, I., and Sussman, J. L. (1993) *Proc. Natl. Acad. Sci. U. S. A.* **90**, 5128–5132
8. Tan, R. C., Truong, T. N., McCammon, J. A., and Sussman, J. L. (1993) *Biochemistry* **32**, 401–403
9. Wlodek, S. T., Shen, T., and McCammon, J. A. (2000) *Biopolymers* **53**, 265–271
10. Zhou, H. X., Wlodek, S. T., and McCammon, J. A. (1998) *Proc. Natl. Acad. Sci. U. S. A.* **95**, 9280–9283
11. Eastman, J., Wilson, E. J., Cervejansky, C., and Rosenberry, T. L. (1995) *J. Biol. Chem.* **270**, 19694–19701
12. Radic, Z., Quinn, D. M., Vellom, D. C., Camp, S., and Taylor, P. (1995) *J. Biol. Chem.* **270**, 20391–20399
13. Harel, M., Kleywegt, G. J., Ravelli, R. B., Silman, I., and Sussman, J. L. (1995) *Structure* **3**, 1355–1366
14. Kryger, G., Harel, M., Giles, K., Tokar, L., Velan, B., Lazar, A., Kronman, C., Barak, D., Ariel, N., Shafferman, A., Silman, I., and Sussman, J. L. (2000) *Acta Crystallogr. Sec. D Biol. Crystallogr.* **56**, 1385–1394

15. Schrag, J. D., and Cygler, M. (1993) *J. Mol. Biol.* **230**, 575-591
16. Grochulski, P., Li, Y., Schrag, J. D., Bouthillier, F., Smith, P., Harrison, P., Rubin, B., and Cygler, M. (1993) *J. Biol. Chem.* **268**, 72843-72847
17. Grochulski, P., Li, Y., Schrag, J. D., and Cygler, M. (1993) *Protein Sci.* **3**, 82-91
18. Velan, B., Barak, D., Ariel, N., Leitner, M., Bino, T., Ordentlich, A., and Shafferman, A. (1996) *FEBS Lett.* **395**, 22-28
19. Faerman, C., Ripoll, D., Bon, S., Lefevre, Y., Morel, N., Massoulie, J., Sussman, J., and Silman, I. (1996) *FEBS Lett.* **386**, 65-71
20. Boyd, A. E., Marnett, A. B., Wong, L., and Taylor, P. (2000) *J. Biol. Chem.* **275**, 22401-22408
21. Nair, H. K., Seravalli, J., Arbuckle, T., and Quinn, D. M. (1994) *Biochemistry* **33**, 8566-8576
22. Marchot, P., Ravelli, R. B., Raves, M. L., Bourne, Y., Vellom, D. C., Kanter, J., Camp, S., Sussman, J. L., and Taylor, P. (1996) *Protein Sci.* **5**, 672-679
23. Berman, J. D., and Young, M. (1971) *Proc. Natl. Acad. Sci. U. S. A.* **68**, 395-398
24. De la Hoz, D., Doctor, B. P., Ralston, J. S., Rush, R. S., and Wolfe, A. D. (1986) *Life Sci.* **39**, 195-199
25. Ellman, G. L., Courtney, K. D., Andres, V. J., and Featherstone, R. M. (1961) *Biochem. Pharmacol.* **7**, 88-95
26. Radic, Z., Pickering, N. A., Vellom, D. C., Camp, S., and Taylor, P. (1993) *Biochemistry* **32**, 12074-12084
27. Levy, D., and Ashani, Y. (1986) *Biochem. Pharmacol.* **35**, 1079-1085
28. Radic, Z., Kirchhoff, P. D., Quinn, D. M., McCammon, J. A., and Taylor, P. (1997) *J. Biol. Chem.* **272**, 23265-23277
29. Radic, Z., and Taylor, P. (2001) *J. Biol. Chem.* **276**, 4622-4633
30. Radic, Z., Duran, R., Vellom, D. C., Li, Y., Cervenansky, C., and Taylor, P. (1994) *J. Biol. Chem.* **269**, 11233-11239
31. Taylor, P., and Radic, Z. (1994) *Annu. Rev. Pharmacol. Toxicol.* **34**, 281-320
32. Marchot, P., Khelif, A., Ji, Y. H., Mansuelle, P., and Bougis, P. E. (1993) *J. Biol. Chem.* **268**, 12458-12467
33. Harel, M., Quinn, D. M., Nair, H. K., Silman, I., and Sussman, J. L. (1996) *J. Am. Chem. Soc.* **118**, 2340-2346
34. Wilson, I. B. (1960) in *The Enzymes* (Boyer, P. D., Lardy, H., and Myrback, K., eds) Vol. 4, 2nd Ed., pp. 501-520, Academic Press, New York
35. Wong, L., Radic, Z., Brüggemann, R. J., Hosea, N., Berman, H. A., and Taylor, P. (2000) *Biochemistry* **39**, 5750-5757
36. Harel, M., Schalk, I., Ehretsabatier, L., Bouet, F., Goeldner, M., Hirth, C., Axelsen, P. H., Silman, I., and Sussman, J. L. (1993) *Proc. Natl. Acad. Sci. U. S. A.* **90**, 9031-9035
37. Raves, M. L., Harel, M., Pang, Y. P., Silman, I., Kozikowski, A. P., and Sussman, J. L. (1997) *Nat. Struct. Biol.* **4**, 57-63
38. Taylor, P., and Lappi, S. (1975) *Biochemistry* **14**, 1989-1997
39. Taylor, P., and Jacobs, N. M. (1974) *Mol. Pharmacol.* **10**, 93-107
40. Lakowicz, J. R. (1999) *Principles of Fluorescence Spectroscopy*, 2nd Ed., pp. 185-210, Kluwer Academic Publishers and Plenum Publishing Corp., New York
41. Lew, J., Coruh, N., Tsigelny, I., Garrod, S., and Taylor, S. S. (1997) *J. Biol. Chem.* **272**, 1507-1513
42. Prendergast, F. G., Meyer, M., Carlson, G. L., Iida, S., and Potter, J. D. (1983) *J. Biol. Chem.* **258**, 7541-7544
43. De Ferrari, G. V., Mallender, W. D., Inestrosa, N. C., and Rosenberry, T. L. (2001) *J. Biol. Chem.* **276**, 23282-23287
44. Millard, C. B., Kryger, G., Ordentlich, A., Greenblatt, H. M., Harel, M., Raves, M. L., Segall, Y., Barak, D., Shafferman, A., Silman, I., and Sussman, J. L. (1999) *Biochemistry* **38**, 7032-7039
45. Tara, S., Elcock, A. H., Kirchhoff, P. D., Briggs, J. M., Radic, Z., Taylor, P., and McCammon, J. A. (1998) *Biopolymers* **46**, 465-474
46. Tai, K., Shen, T., Börjesson, U., Philippopoulos, M., and McCammon, J. A. (2001) *Biophys. J.* **81**, 715-724

Nanosecond Dynamics of the Mouse Acetylcholinesterase Cys⁶⁹–Cys⁹⁶ Omega Loop*

Received for publication, April 9, 2003, and in revised form, May 16, 2003
Published, JBC Papers in Press, May 19, 2003, DOI 10.1074/jbc.M303730200

Jianxin Shi‡§, Kaihsu Tai¶, J. Andrew McCammon¶, Palmer Taylor‡**, and David A. Johnson‡†

From the ‡Department of Pharmacology, University of California, San Diego, La Jolla, California 92093-0636, ¶Howard Hughes Medical Institute and Departments of Pharmacology and of Chemistry and Biochemistry, University of California, San Diego, La Jolla, California 92093-0365, and §§Division of Biomedical Sciences, University of California, Riverside, California 92521-0121

The paradox of high substrate turnover occurring within the confines of a deep, narrow gorge through which acetylcholine must traverse to reach the catalytic site of acetylcholinesterase has suggested the existence of transient gorge enlargements that would enhance substrate accessibility. To establish a foundation for the experimental study of transient fluctuations in structure, site-directed labeling in conjunction with time-resolved fluorescence anisotropy were utilized to assess the possible involvement of the omega loop (Ω loop), a segment that forms the outer wall of the gorge. Specifically, the flexibility of three residues (L76C, E81C, and E84C) in the Cys⁶⁹–Cys⁹⁶ Ω loop and one residue (Y124C) across the gorge from the Ω loop were studied in the absence and presence of two inhibitors of different size, fasciculin and huperzine. Additionally, to validate the approach molecular dynamics was employed to simulate anisotropy decay of the side chains. The results show that the Ω loop residues are significantly more mobile than the non-loop residue facing the interior of the gorge. Moreover, fasciculin, which binds at the mouth of the gorge, well removed from the active site, decreases the mobility of 5-(((2-acetyl)amino)ethyl)amino)naphthalene-1-sulfonic acid reporter groups attached to L76C and Y124C but increases the mobility of the reporter groups attached to E81C and E84C. Huperzine, which binds at the base of active-site gorge, has no effect on the mobility of reporter groups attached to L76C and Y124C but increases the mobility of the reporter groups attached to E81C and E84C. Besides showing that fluctuations of the Ω loop residues are not tightly coupled, the results indicate that residues in the Ω loop exhibit distinctive conformational fluctuations and therefore are likely to contribute to transient gorge enlargements in the non-liganded enzyme.

Acetylcholinesterase (AChE),¹ ranking among the most catalytically efficient enzymes known, catalyzes the hydrolysis of the neurotransmitter acetylcholine with a turnover number of 10^4 s^{-1} (1, 2). Curiously, catalysis shows high efficiency despite the cross-sectional dimension of acetylcholine is nearly equal to the width of the narrowest portion of the 20-Å-long and tortuous gorge leading to the catalytic center (Fig. 1A) (3–7). This paradox suggests the existence of an enlarged solution conformational state(s) of the active-center gorge. Molecular dynamics simulations support the existence of breathing or gating motions that could enhance substrate accessibility to the active site (8–10).

One segment of the gorge that may play a major role in gorge enlargement is the large Ω loop (defined by the Cys⁶⁹–Cys⁹⁶ disulfide bond) that corresponds to the activation loop (Cys⁶⁰–Cys⁹⁷) of *Candida rugosa* lipase, a related carboxyl esterase with an α , β -hydrolase fold (11, 12). X-ray crystallographic analysis of the apo form of this lipase shows the activation loop occluding the active site in the absence of substrate and folding backward allowing substrate access when lipid is bound. We previously demonstrated by examining the steady-state emission from selective acrylodan-labeled side chains that AChE-inhibitor binding induces distinctive conformational changes in certain regions of the mouse AChE Cys⁶⁹–Cys⁹⁶ Ω loop (13).

To determine whether the Cys⁶⁹–Cys⁹⁶ Ω loop could contribute to gorge enlargement, we used site-directed labeling with IAEDANS at various positions in conjunction with time-resolved fluorescence anisotropy to compare the backbone flexibility of three residues in the Ω loop (L76C, E81C, and E84C) with the flexibility of a residue in the active-site gorge, but not part of the Ω loop (Y124C). We also examined the influence of two inhibitors on conformational flexibility, one of which interacts directly with the Ω loop at the gorge entry (fasciculin), whereas the other (huperzine) associates with side chains of the loop near the gorge base. IAEDANS replaced acrylodan in this study, because it is conjugated more readily to active-site gorge residues than thioreactive fluorescein derivatives, and because its relatively long emission lifetime allows better resolution of whole body from local depolarization processes. Additionally, molecular dynamics simulations of side chain motions of the four individual residues where cysteine was substituted showed agreement with anisotropy decay parameters of the wild type (wt) enzyme. We found that the conjugated Ω loop residues were significantly more flexible than the non-

* This work was supported in part by the United States Public Health Service Grants R37-GM18360 and P42-ES10337, by Department of Army Medical Defense Grant 17C-1-8014 (to P. T.), by the National Science Foundation, the National Institutes of Health, San Diego Supercomputer Center and National Biomedical Computational Resource, the W. M. Keck Foundation, and Accelrys Inc. (to J. A. McC.). The costs of publication of this article were defrayed in part by the payment of page charges. This article must therefore be hereby marked "advertisement" in accordance with 18 U.S.C. Section 1734 solely to indicate this fact.

§ Predoctoral fellow supported by National Institutes of Health Grant T32-GM07752.

¶ Predoctoral fellow of the La Jolla Interfaces in Science Training Program and supported by the Burroughs Wellcome Fund.

** To whom correspondence should be addressed: Dept. of Pharmacology, University of California, San Diego, La Jolla, CA 92093-0636. E-mail: pwtaylor@ucsd.edu.

¹ The abbreviations used are: AChE, acetylcholinesterase; mAChE, mouse acetylcholinesterase; acrylodan, 6-acryloyl-2-dimethylaminonaphthalene; IAEDANS, 5-(((2-iodoacetyl)amino)ethyl)amino)naphthalene-1-sulfonic acid; AEDANS, 5-(((acetyl)amino)ethyl)amino)naphthalene-1-sulfonic acid; wt, wild type; PDB, protein data bank; wt, wild type.

TABLE I
Effect of huperzine and fasciculin on steady-state emission parameters of IAEDANS-labeled mouse AChE

Data are shown as mean values of at least three determinations.

Mutant	Emission maxima (nm) ^a			Relative quantum yield ^b	
	Control	Huperzine	Fasciculin	Huperzine	Fasciculin
L76C	485	485	478	1.0	1.11
E81C	489	494	492	0.82	0.90
E84C	484	491	486	0.77	0.97
Y124C	482	482	469	1.0	1.55

^a The excitation wavelength was 340 nm.

^b Relative quantum yields were determined by comparison of areas under the emission spectra of each labeled mutant in the absence of ligand with its spectra in the presence of the indicated ligand. Concentrations of fasciculin and huperzine were 1.3 and 4 μ M, respectively.

loop residue. Also, the effects of the inhibitors were consistent with the flexibility of the Ω loop contributing to transient gorge enlargement that could enhance substrate accessibility and product egress.

EXPERIMENTAL PROCEDURES

Materials—Acetylthiocholine iodide, 5,5'-dithiobis(2-nitrobenzoic acid) (Ellman's reagent), and dithiothreitol were purchased from Sigma. (–)-Huperzine A was purchased from Calbiochem. 5-(((2-Iodoacetyl)amino)ethyl)amino)naphthalene-1-sulfonic acid (IAEDANS) was obtained from Molecular Probes (Eugene OR). Fasciculin 2 (purified from the venom of *Dendroaspis angusticeps*) was a gift of Dr. Pascale Marchot (University of Marseille, France). Drs. Yacov Ashani and Bhupendra P. Doctor (Walter Reed Army Research Center, Washington, D. C.) kindly provided procainamide-linked Sepharose CL-4B resin. All other chemicals were of the highest grade commercially available.

Expression, Mutagenesis, and Purification of mAChE—Mouse AChE was produced by transfection of expression plasmid (pcDNA3, Invitrogen) containing an encoding cDNA where the AChE sequence was terminated at position 548. The plasmid was transfected into human embryonic kidney (HEK293) cells. Cells were selected with G418 to obtain stable producing cell lines, and AChE was expressed as a secreted soluble enzyme in serum-free media. Mutant enzymes were generated by standard mutagenesis procedures, and cassettes containing the mutation were subcloned into pcDNA3. Nucleotide sequences of the cassettes were confirmed by double-stranded sequencing to ensure that spurious mutations were not introduced into the coding sequence. Affinity chromatography using (*m*-aminophenyl) trimethyl ammonium linked through a long chain to Sepharose CL-4B resin (Sigma) permitted one-step purification of L76C, E81C, and E84C mAChE. Procainamide-linked Sepharose CL-4B resin was utilized in the purification of Y124C mAChE. From 4 to 6 liters of media, mutant and wild type enzyme were purified in quantities ranging between 5 and 25 mg (14). Purity was ascertained by SDS-PAGE and by measurements of specific activity.

IAEDANS Labeling—Mutant and wt enzymes were pretreated with 0.25 mM dithiothreitol for 30 min at room temperature to ensure the introduced cysteine was in a reduced state. Dithiothreitol was removed by use of a G-50 Sephadex spin column (Roche Applied Science) equilibrated in 10 mM Tris, 100 mM NaCl, 40 mM MgCl₂, pH 8.0. IAEDANS (1 μ l) at 100 times the enzyme concentration was slowly mixed with the enzyme to achieve approximately a 10-fold molar excess of IAEDANS to enzyme. Labeling was allowed to proceed for 12–16 h at 4 °C, and excess reagent was removed by fractionation on a Sephadex G-25 (Amersham Biosciences) column equilibrated with 0.1 M sodium phosphate buffer, pH 7. Enzyme concentrations were determined from absorbance at 280 nm, $\epsilon = 1.14 \times 10^5 \text{ M}^{-1} \text{ cm}^{-1}$ (14). Labeling stoichiometries were determined to be close to 1.0 from the ratio of absorption at 340 to 280 nm for the labeled enzymes. Because the absorption peak wavelength of IAEDANS at 340 nm, $\epsilon = 5.7 \times 10^3 \text{ M}^{-1} \text{ cm}^{-1}$, is close to that for the protein, these ratios only provide rough estimates of labeling. Specificity of labeling was assessed by comparison of areas under the fluorescence emission curves for IAEDANS-treated mutant with wild type enzymes.

Steady-state Emission Spectra—Steady-state emission spectra were measured at room temperature using a Jobin Yvon/Spex FluoroMax II spectrofluorometer (Instrument S.A., Inc., Edison, NJ) with the excitation and emission bandwidths set at 5 nm.

Time-resolved Fluorescence Anisotropy—Time-resolved emission anisotropy was monitored on time-correlated single photon-counting instrument. Its custom-built fabrication included an IBH (Edinburgh,

UK) UV-NanoLED™ flash lamp run at 1 MHz and an IBH model TBX-04 photon detector. Vertically ($I_v(t)$) and orthogonally ($I_o(t)$) polarized emission components were collected by exciting samples with vertically polarized light while orienting the emission polarizer (Polaroid HNP'B dichroic film) in either a vertical or orthogonal direction. Excitation and emission bands were selected with a Corning 7-60 interference filter and a Schott KV-450 nm cut-on filter, respectively. Typically, 2×10^4 peak counts were collected in 1–2 min when the emission polarizer was vertically oriented. The orthogonal emission decay profile was generated over the same time interval used to generate the vertical emission decay profile. Samples were held at 22 °C. To minimize convolution artifacts, flash lamp profiles were recorded by removing the emission filter and monitoring light scatter from a suspension of latex beads. The data analysis software corrected the wavelength-dependent temporal dispersion of the photoelectrons by the photomultiplier. The polarization bias (G) of the detection instrumentation was determined by measuring the integrated photon counts/ 6×10^6 lamp flashes that were detected while the samples were excited with orthogonally polarized light and the mission monitored with a polarizer oriented in the vertical and orthogonal direction ($G = 0.9936$).

Emission anisotropy, $r(t)$, is given by the expression shown in Equation 1,

$$r(t) = \frac{I_v(t) - G \cdot I_o(t)}{I_v(t) + 2G \cdot I_o(t)} \quad (\text{Eq. 1})$$

From this and the expression for the total emission, $S(t)$, for a macroscopically isotropic sample,

$$S(t) = I_v(t) + 2G \cdot I_o(t) \quad (\text{Eq. 2})$$

was deconvolved simultaneously from the individual polarized emission components expressed as shown in Equations 3 and 4,

$$I_v(t) = \frac{S(t)}{3} (1 + 2r(t)) \quad (\text{Eq. 3})$$

and

$$I_o(t) = \frac{S(t)}{3} (1 - r(t)) \quad (\text{Eq. 4})$$

Thus, both $I_v(t)$ and $I_o(t)$ were determined by the same fitting functions, $S(t)$ and $r(t)$, and fitting parameters.

Fluorescence lifetimes were determined by initially generating a total emission profile from $I_v(t)$ and $I_o(t)$ with Equation 2, and then fitting this decay profile to a biexponential decay expression with the Globals Unlimited™ (Laboratory for Fluorescence Dynamics, Urbana, IL) software package. The resulting lifetimes were entered and fixed in the second step of the analysis process where $I_v(t)$ and $I_o(t)$ were simultaneously analyzed for the parameters of $S(t)$ and $r(t)$ with the Globals Unlimited™ program. Here $r(t)$ is a nonassociative anisotropy decay function as shown in Equation 5.

$$r(t) = r_0 f_{sb} \exp(-t/\phi_{fast}) + r_0(1 - f_{sb}) \exp(-t/\phi_{slow}) \quad (\text{Eq. 5})$$

where r_0 is the amplitude of the anisotropy at time 0; f_{sb} is the fraction of the anisotropy decay associated with the fast decay processes, and ϕ is rotational correlation time of the anisotropy decay. Rotational correlation times are measured for the two (fast and slow) processes. This nonassociative model assumes that the rotational correlation times are common to each of the emission relaxation times. Goodness of fit was evaluated from the value of χ^2 and visual inspection of the difference between the experimental data and the empirical anisotropy decay

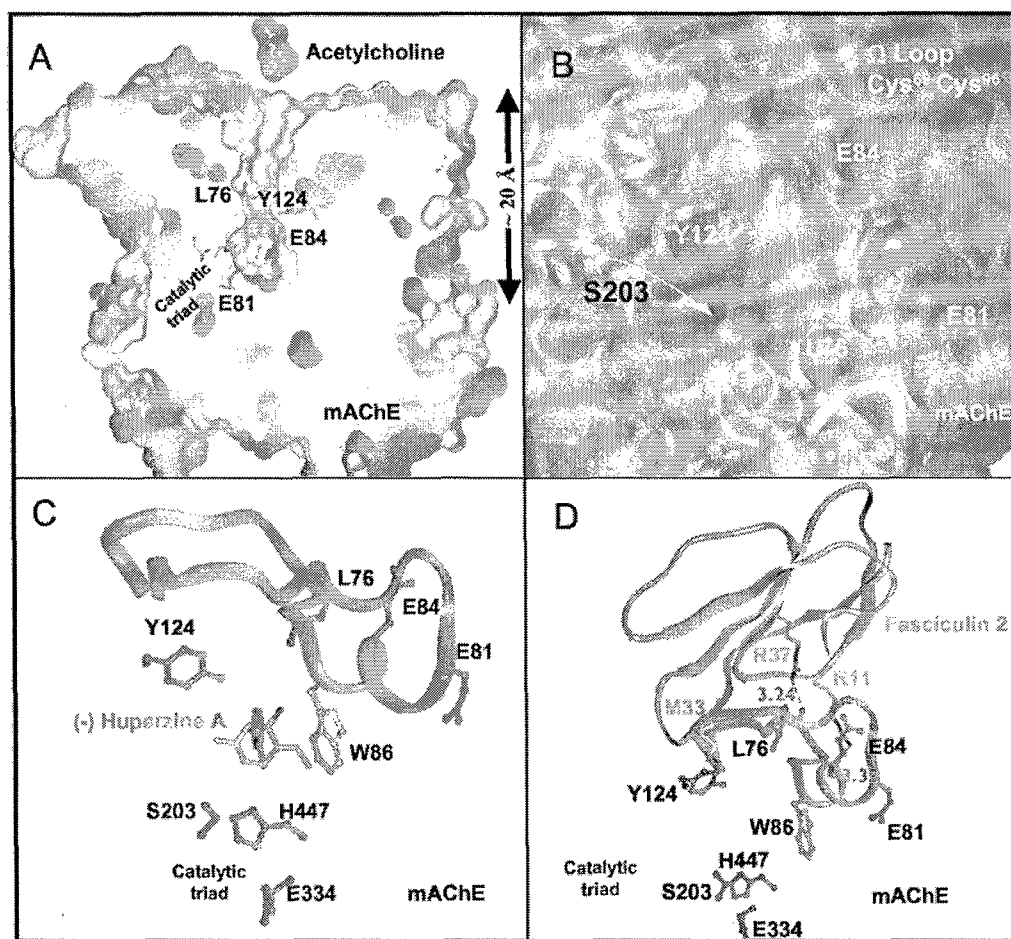


FIG. 1. Locations of substituted cysteines for fluorophore conjugation. **A**, cutaway view of mAChE crystallographic structure showing an active-site gorge 20 Å in depth (PDB code 1MAA). The view is taken from the side with catalytic triad (Ser²⁰³, Glu³³⁴, and His⁴⁴⁷) on the *bottom left*. **B**, Connolly surface presentation of mAChE looking into the gorge entry with catalytic serine highlighted in *red* at its base. Residues 76, 81, and 84 displayed in *blue* are at the tip (76) and outer portion (81, 84) of the Cys⁶⁹-Cys⁹⁶ loop. Residue 124 displayed in *green* is on an opposing face of the gorge and makes up part of the peripheral anionic site. **C**, model of mAChE in complex with huperzine based on crystal structure of huperzine: *Torpedo californica* AChE (PDB code 1VOT). Huperzine binds at the bottom of active-site gorge and makes surprisingly few specific contacts in the active-site gorge. **D**, fasciculin 2 complexed to mAChE adapted from PDB code 1KU6. Note: hydrogen bonding between the guanidino nitrogen moieties of Arg¹¹ and Arg³⁷ in fasciculin and carbonyl oxygen moieties of Glu⁸⁴ (3.33 Å) and Leu⁷⁶ (3.24 Å) on mAChE, respectively.

model. (It is worth noting that the observed τ_0 values typically are less than the fundamental anisotropy of the reporter group (0.33). This most probably reflects the fact that the very fast depolarizing motions produced by tether arm movements are not resolvable by commercial instruments.)

Molecular Dynamics Simulation of Anisotropy Decay—The decay of anisotropy because of side chain and segmental motions was simulated utilizing the approach developed by Ichiye and Karplus (15). Specifically, the anisotropy decay of a fluorophore conjugated to a protein side chain was represented as the decay in the time correlation function shown in Equation 6,

$$\rho(\tau) = \langle P_2[\hat{\mu}(t) \cdot \hat{\mu}(t - \tau)] \rangle_t \quad (\text{Eq. 6})$$

where $\hat{\mu}$ is a normalized vector properly chosen to represent the local motion being reported by the fluorophore. In our calculations, $\hat{\mu}$ was chosen to be a normalized vector representing the direction that goes from the α -carbon to an atom near the tip of the wild type residue. To wit, for the glutamate residue, we used the average of the two normalized C_α -O_γ vectors; for leucine, the normalized C_α -H_γ vector; and for tyrosine, the normalized C_α -O_H vector.

For this study, the previously reported 10-ns molecular dynamics simulation of the unliganded wt mAChE (16) was extended to afford a 15-ns trajectory. Frames (snapshots of the trajectory containing the coordinates of all the atoms) were calculated at 1-ps time intervals, and the rotational degrees of freedom were removed by superimposing all frames into a reference frame, minimizing the root mean squared deviations. With these trajectories on a nanosecond time scale, it was

possible to simulate anisotropy decay due to just the combination of side chain and segmental motions; deconstruction of the vectors to resolve the side chain and the segmental motions was not attempted.

RESULTS AND DISCUSSION

Characterization of Labeled Mutants—Acetylthiocholine hydrolysis kinetics of the cysteine-substituted mutants were shown previously to be similar to the wt enzyme suggesting that all mutant enzymes fold correctly despite the presence of the substituted cysteines (13). Moreover, the specific labeling for each mutant was estimated to be 71–80%, 89–93%, 79–80%, and 74–84% for L76C, E81C, E84C, and Y124C, respectively. Substrate and inhibitor recognition by the IAEDANS-labeled mutants is evident from both fasciculin (1.3 μ M) and huperzine (4 μ M) producing greater than 95% inhibition of the rate of acetylthiocholine hydrolysis (data not shown). This is not surprising, because previous kinetic studies showed that k_{on} and k_{off} of fasciculin were unaltered in the cysteine mutants (17).

In the absence of ligand, the emission maxima of the four IAEDANS-labeled mutants were similar ranging between 482 and 489 nm (Table I). The active-site ligand, (–)-huperzine A, a herbal alkaloid used in Chinese traditional medicine, binds at the base of active-site gorge and should have no direct interac-

tion with all cysteine-conjugated sites based on the x-ray crystal structure of the huperzine-AChE complex (Fig. 1C) (18). Huperzine only affected the steady-state emission properties of the E81C- and E84C-labeled mutants, red shifting the emission maxima 5 and 7 nm and decreasing the relative quantum yields by 18 and 23%, respectively (Table I). This pattern suggests that the huperzine increases the polarity of the microenvironment around the Glu⁸¹ and Glu⁸⁴ but not around the Leu⁷⁶ and Tyr¹²⁴ side chains.

Fasciculin, a peptidic peripheral site inhibitor that caps the mouth of the active-site gorge, influences the microenvironment of the substituted positions in a complex manner. The crystal structure of fasciculin-mAChE complex shows hydrogen bonding between the guanidino moieties of Arg¹¹ and Arg³⁷ in fasciculin and the carbonyl oxygens of Glu⁸⁴ and Leu⁷⁶ on the AChE, respectively (Fig. 1D) (4). Met³³ of fasciculin also is in close proximity but not "in van der Waals contact" with Tyr¹²⁴ in the AChE. The largest spectral changes were observed with the labeled Y124C mutant where fasciculin blue-shifted the emission maxima 13 nm and increased the relative quantum yield by 55% (Table I). A similar pattern was seen with the L76C conjugate, but the blue shift was 7 nm, and the relative quantum yield enhancement was 11%. The emission properties of E81C- and E84C-labeled mutants were much less affected by fasciculin binding; the emission maxima were red-shifted 3 and 2 nm, and the relative intensities were decreased by 10 and 3%, respectively (Table I). These results indicate that fasciculin dramatically decreased the polarity around the reporter groups attached to Y124C and to a lesser extent around L76C. Also, fasciculin slightly increased the polarity around the reporter groups attached to E81C and E84C, which is qualitatively the result found using acrylodan instead of IAEDANS (13).

Emission and Anisotropy Decay—For brevity, just the parallel and perpendicular emission decay profiles of one labeled mutant (E84C) along with the corresponding anisotropy decay profile are illustrated in Fig. 2. The total emission decay profiles ($S(t)$, Equation 2) of all the mutants were best fit to a three-exponential decay function whose geometric averaged lifetimes are summarized in Table II and ranged from 10.0 to 14.6 ns. The ranges of values of the short, intermediate, and long lifetimes of the various conjugates studied were 1.1–3.4, 9.3–16.0, and 18.2–27.9 ns, respectively (data not shown).

Anisotropy decay profiles for the IAEDANS conjugates, with the exception of the labeled Y124C mutant complexed to fasciculin, were well fit by a nonassociative biexponential model (Equation 5). These profiles are illustrated in Fig. 3, and the best fit parameters are summarized in Table II. Except for the huperzine-bound E84C mutant, the processes associated with the "slow" rotational correlation times accounted for 60–80% of the total resolvable anisotropy decay, and the values of these rotational correlation times ranged between 69 and 132 ns (Table II). This range of values is greater than what might be predicted from a protein with 547 amino acids and three *N*-linked oligosaccharides of average mass determined by matrix-assisted laser desorption/ionization-mass spectrometry. However, sedimentation equilibrium measurements for this protein correlate best with a molecular mass of 122,000 Da, suggesting that at higher concentrations the molecule may form a reversibly associating dimer.² The longest emission lifetimes (18.2–27.9 ns) are long enough to allow estimation of a global rotational correlation time. The crystal structure shows mAChE to have limited dimensional asymmetry so only a single rotational correlation would be resolvable. Because faster emission decay step(s) are also present, deconvolution of components of the

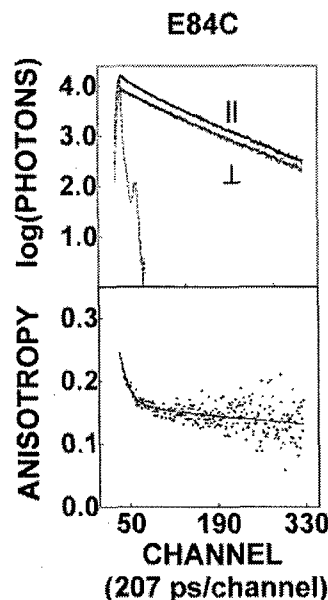


FIG. 2. Emission and anisotropy decay of IAEDANS-E84C mAChE. The upper panel illustrates the parallel (\parallel) and perpendicular (\perp) emission decays (single data points). A smooth line through these points was generated with the best fit parameters for a double exponential decay equation. The flash lamp profile is shown as a dotted line. The lower panel shows the time-resolved anisotropy decay (single data points), and a smooth line through these points was generated with the best fit parameters (Table II) for a double exponential nonassociative model (Equation 5). The concentration of the labeled mutants was 1.68 μ M.

intermediate and slow phase is subject to uncertainty. Consequently, slow internal fluctuations contributing to the decay rate cannot be ruled out. For the case of huperzine-bound E84C mutant, the ϕ_{slow} values ranged between 80 and 260 ns. This broader range of values probably reflects a greater uncertainty in ϕ_{slow} measurements when the slow decay processes represent a small fraction of the total resolvable anisotropy decay, as was the case for the huperzine-bound E84C mutant (31%; Table II).

Comparison of the fast anisotropy decay components of the apo form of the labeled mutants show two features. First, reporter groups attached to substituted cysteines whose native side chains in the crystal structure project into the active-site gorge (L76C and Y124C) are less mobile than reporter groups attached to Ω loop-substituted cysteines located on the outer surface of the enzyme (E81C and E84C). This conclusion is seen in the time 0 anisotropy and $f_{\text{xb}}/\phi_{\text{fast}}$ values (Table II). The time 0 anisotropy values (r_0), which likely reflect very fast and unresolvable tether-arm motions (19–21), are higher for the L76C (0.27) and Y124C (0.28) than the E81C (0.25) and E84C (0.25) labeled mutants (Table II). This would suggest, not surprisingly, greater hindrance to the tether-arm movements of the gorge-residing residues. The $f_{\text{xb}}/\phi_{\text{fast}}$ values of reporter groups attached to the residues that project into the gorge are smaller (L76C, 0.07 and Y124C, 0.05) than the $f_{\text{xb}}/\phi_{\text{fast}}$ values of reporter groups that are on the outer surface of the enzyme (E81C, 0.13 and E84C, 0.15; Table II). Because the $f_{\text{xb}}/\phi_{\text{fast}}$ ratio is on the time scale of backbone motions and can be analyzed in terms of the diffusion rate in a "diffusion-in-a-cone model" (22), these results indicate that the ranking of segmental mobility of the residues examined is as follows: E84C > E81C >> L76C > Y124C. The second feature that emerges from a comparison of the fast anisotropy decay parameters, r_0 and $f_{\text{xb}}/\phi_{\text{fast}}$, is that the reporter groups attached to the substituted cysteines in the Cys⁶⁹–Cys⁹⁶ Ω loop (L76C, E81C, and E84C)

² D. Comoletti, unpublished observations.

TABLE II

Effect of huperzine and fasciculin on the anisotropy decay parameters of mouse AChE-labeled with IAEDANS

Data are shown as means (\pm S.D.) from at least three determinations. The vertically and orthogonally polarized emission decays were initially analyzed for the $S(t)$ parameter (Equation 2), and then for the $r(t)$ parameter (Equation 5) with the Globals Unlimited™ computer program. The experimental details are described under "Experimental Procedures." The mutants were present at the following concentrations: AEDANS-L76C, 1.63 μ M; AEDANS-E81C, 1.69 μ M; AEDANS-E84C, 1.68 μ M; and AEDANS-Y124C, 2.75 μ M. To ensure saturation of enzyme with inhibitors, concentrations of huperzine (4 μ M) and fasciculin (3.17 μ M) were added to AEDANS-L76C, AEDANS-E81C, and AEDANS-E84C; huperzine (4.8 μ M) and fasciculin (4 μ M) were added to AEDANS-Y124C.

Mutant	Inhibitor	r_0^a	f_{xb}^b	ϕ_{fast}^c	f_{xb}/ϕ_{fast}	ϕ_{slow}^d	ϕ_r^{2e}	τ^f
L76C	None	0.27 \pm 0.01	0.26 \pm 0.01	ns	0.07 \pm 0.01	ns	1.2	10.0 \pm 0.1
	Huperzine	0.28 \pm 0.02	0.26 \pm 0.01	3.5 \pm 0.3	0.07 \pm 0.01	84–111	1.3	9.7 \pm 0.1
	Fasciculin	0.27 \pm 0.01	0.22 \pm 0.01	4.8 \pm 0.3	0.05 \pm 0.01	92–118	1.2	10.2 \pm 0.2
E81C	None	0.25 \pm 0.01	0.29 \pm 0.01	2.3 \pm 0.2	0.13 \pm 0.01	76–105	1.3	14.6 \pm 0.1
	Huperzine	0.26 \pm 0.01	0.40 \pm 0.01	2.3 \pm 0.1	0.18 \pm 0.01	84–118	1.2	13.6 \pm 0.1
	Fasciculin	0.26 \pm 0.01	0.34 \pm 0.02	2.2 \pm 0.1	0.16 \pm 0.01	77–100	1.3	13.6 \pm 0.1
E84C	None	0.25 \pm 0.01	0.42 \pm 0.02	2.9 \pm 0.1	0.15 \pm 0.01	90–132	1.3	12.6 \pm 0.2
	Huperzine	0.22 \pm 0.02	0.69 \pm 0.02	2.8 \pm 0.2	0.25 \pm 0.03	80–260	1.2	10.2 \pm 0.2
	Fasciculin	0.26 \pm 0.01	0.24 \pm 0.02	4.6 \pm 0.8	0.05 \pm 0.01	69–87	1.1	11.3 \pm 0.7
Y124C	None	0.28 \pm 0.01	0.16 \pm 0.01	3.6 \pm 0.6	0.05 \pm 0.01	75–89	1.2	14.5 \pm 0.2
	Huperzine	0.29 \pm 0.02	0.18 \pm 0.01	4.0 \pm 0.7	0.04 \pm 0.01	74–91	1.4	13.8 \pm 0.4
	Fasciculin	ND ^g	ND	ND	ND	ND	ND	18.2 \pm 0.1

^a The time 0 anisotropy.^b The fraction of the observed anisotropy decay associated with the "fast" depolarization processes.^c Fast rotational correlation time.^d The range of the "slow" rotational correlation times that yield χ_r^2 values 5% above the minimum.^e The reduced χ^2 .^f Geometric averaged lifetimes ($\Sigma\alpha_i\tau_i$, where $\Sigma\alpha_i = 1$).^g ND, not determined.

are more mobile than the reporter group attached to the non- Ω loop residue (Y124C) (Table II).

Ligand Binding and Anisotropy Decay—The influence of huperzine and fasciculin on the anisotropy decay parameters of the labeled mutants studied is complex and ligand-dependent.

Huperzine, which should not interact with the modified Ω loop residues (Fig. 1C), selectively increased the mobility of just the labeled E81C and E84C residues without affecting the mobility of the labeled L76C or Y124C residues. This is evidenced in the f_{xb}/ϕ_{fast} values of the labeled-E81C and E84C mutants that increased upon huperzine binding from 0.13 to 0.18 and from 0.15 to 0.25, respectively (Table II; Fig. 3). The fact that the fluctuations of just the E81C and E84C were perturbed, and not L76C in the Ω loop, is indicative of a lack of conformational coupling between Leu⁷⁶ and Glu⁸¹/Glu⁸⁴ positions in the Ω loop. Hence, the Ω loop does not behave as a rigid flap.

Consistent with the crystal structure showing fasciculin hydrogen bonding (from the guanidino moiety of Arg³⁷) to the carbonyl oxygen of Leu⁷⁶ (2.83 Å; Fig. 1), the f_{xb}/ϕ_{fast} value of the labeled L76C mutant decreases upon fasciculin binding from 0.07 to 0.05 (Table II) suggesting decreased segmental mobility around L76C. For the E81C mutant, where the wild type crystal structure does not predict any direct interaction with fasciculin, the f_{xb}/ϕ_{fast} value increased from 0.13 to 0.16 (Table II), indicating a modest increase in segmental mobility of the E81C residue, a behavior similar to that seen for huperzine. Combining hydrophobic and electrostatic interactions, the fasciculin-mAChE complex encompasses an interface of 1100 Å. It is surprising that, despite strong suppression of mobility throughout, we observed enhanced dynamic motion around E81C.

For the E84C mutant, whose side chain may come in closer contact with fasciculin than E81C, fasciculin binding may introduce multiple factors that control decay of anisotropy. Fasciculin slowed the fast anisotropy decay processes suggesting a reduced segmental mobility (f_{xb}/ϕ_{fast} decreases from 0.15 to 0.05) and accelerated the slow anisotropy decay processes (the range of ϕ_{slow} values decreased from 90–132 to 69–87 ns; Table II). These seemingly complex decay profile emerges without

direct occlusion between the fluorophore and toxin as evidenced by the fact that fasciculin binding produced no significant change in r_0 and only a minimal change in the steady-state and emission lifetime parameters (Tables I and II). However, the fasciculin molecule should stabilize the Ω loop near the rim of the gorge, and Arg¹¹ on fasciculin may electrostatically interact with the sulfonic acid moiety of the conjugated AEDANS. A possible explanation for the complex decay profile at Glu⁸⁴ is that fasciculin induced large amplitude, slow backbone fluctuations around E84C that both slowed the segmental fluctuation rate and increased its amplitude. Such internal fluctuations might occur if the C-terminal half of the Ω loop starting at about Glu⁸¹ became less tethered to the core of the molecule and underwent larger angular excursions on a time scale between ~10 and ~50 ns. Such conformational fluctuations would accelerate the observed slow rotational correlation time. From this perspective, fasciculin has a disordering effect at both E81C and E84C. Clearly, additional studies are required to establish the mechanistic basis for these increased fluctuations.

For the labeled Y124C mutant, the anisotropy decay could not be reasonably fit to a simple decay model. Instead of continuously decreasing from time 0, the anisotropy increased very slightly for a few nanoseconds and then decreased. Moreover, the total depolarization process was much slower than any other decay profiles examined (Fig. 3). This pattern of decay probably results from a complex association of emission lifetimes with specific rotary diffusional processes (23). Combined with the very substantial (55%) increase in the total emission described above and the close proximity of Tyr¹²⁴ to fasciculin in the crystal structure of mAChE (PDB code 1KU6), which would presumably be closer in the 5(((acetyl)amino)ethyl)amino)naphthalene-1-sulfonic acid (AEDANS)-labeled mutant, the complex anisotropy decay of the fasciculin-bound and labeled Y124C mutant strongly suggests a direct reporter group-fasciculin interaction and subsequent reduction in the mobility of Y124C. This direct interaction makes problematic an assessment of the effect of fasciculin on the segmental motion around the Tyr¹²⁴ residue in the wild type enzyme.

FIG. 3. Effect of huperzine and fasciculin on the anisotropy decay of the IAEDANS-labeled mAChE mutants. The time-resolved anisotropy decay (single data points) and a smooth line through these points were generated with the best fit parameters (Table II) for a double exponential nonassociative decay model (Equation 5). Data points represent enzymes without inhibitors (\bullet), with huperzine ($+$), or with fasciculin (\blacktriangle). The peak of the flash lamp profile arbitrarily defined the zero time point. To ensure saturation of enzyme with inhibitors, concentrations of huperzine ($4\ \mu\text{M}$) and fasciculin ($3.17\ \mu\text{M}$) were added to IAEDANS-E81C (A), IAEDANS-E84C (B), and IAEDANS-L76C (C); huperzine ($4.8\ \mu\text{M}$) and fasciculin ($4\ \mu\text{M}$) were added to IAEDANS-Y124C (D). The concentrations of IAEDANS-L76C, IAEDANS-E81C, IAEDANS-E84C, and IAEDANS-Y124C were 1.63, 1.69, 1.68, and $2.75\ \mu\text{M}$, respectively.

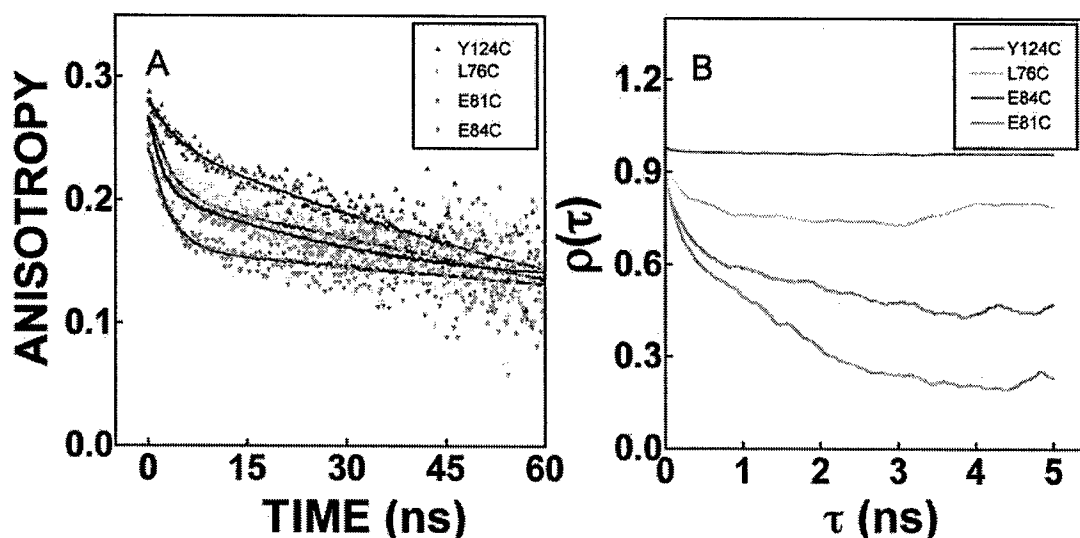
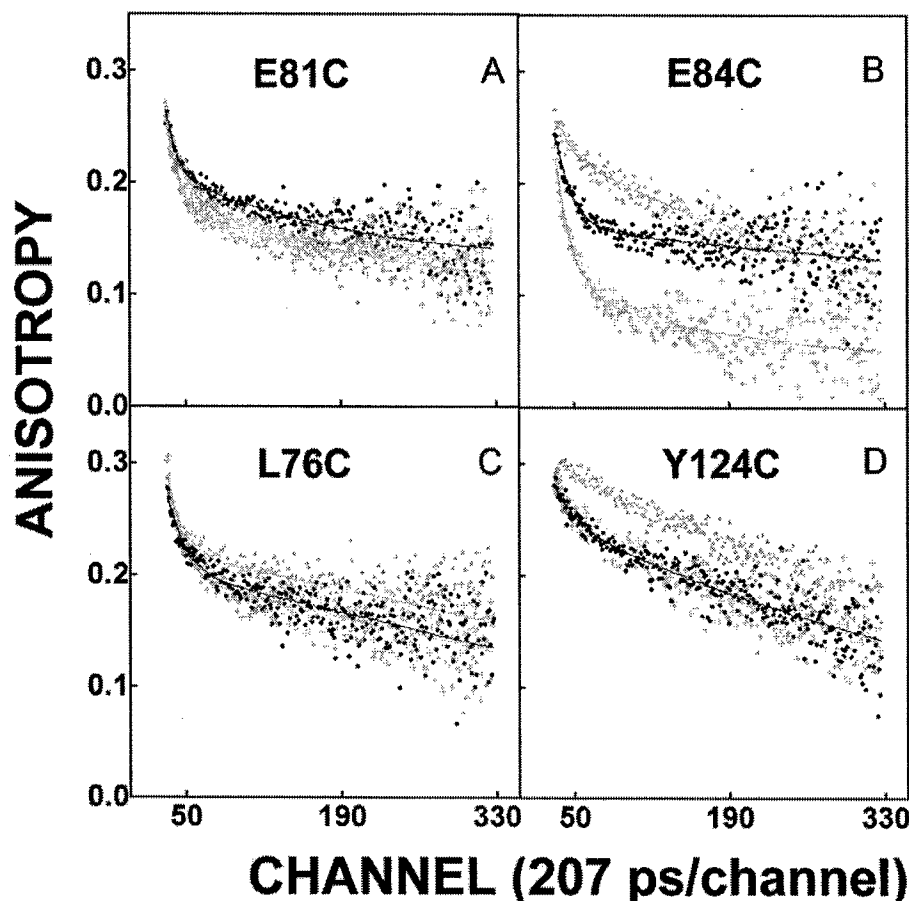


FIG. 4. Comparison of the experimental and simulated anisotropy decay. A, overlay of experimental anisotropy decays of unliganded AEDANS-L76C ($+$) (green), AEDANS-E81C (\bullet) (orange), AEDANS-E84C (\blacktriangledown) (red), and AEDANS-Y124C (\blacktriangle) (blue) mAChE. B, the time correlation function $\rho(\tau)$ from the 15-ns mAChE molecular dynamics simulation based on PDB code 1MAH.

Comparison of Experimental and Simulated Anisotropy Decay—To validate further fluorescence anisotropy decay to measure segmental mobility, the anisotropy parameters were compared with the calculated decay in the time correlation function $\rho(\tau)$ (where $\rho(\tau)$ is time correlation function of a vector representing the direction that goes from the α -carbon to an atom near the tip of the wt side chain) for each mutated site. The results of this comparison for the apoenzyme are illustrated in Fig. 4. Because $\rho(\tau)$ has the characteristics of a time

correlation function, it becomes less trustworthy as τ increases and the number of samples diminishes. Therefore, only the first one-third of the 15-ns $\rho(\tau)$ profile is shown (Fig. 4B). For the unliganded mAChE, the simulated mobility ranking for the four sites of interest was E81C > E84C > L76C > Y124C. This is similar, but not identical, to the experimental anisotropy measures of segmental mobility, $f_{\text{sb}}/\phi_{\text{fast}}$, whose mobility ranking was E84C > E81C > L76C > Y124C.

Why the theoretical calculations show the motions of residue

81 randomizing more rapidly than residue 84, whereas the experimental data show the opposite, is unclear. However, there are several explanations to be considered. First, experimental anisotropy decay is dependent upon the orientation of the emission transition dipole relative to the major directions of the movement of the reporter group, and the correlation function is not. Second, cysteine substitutions and fluorophore conjugation could have perturbed the local environment differentially affecting the mobilities of the substituted side chains. Finally, the experimental $f_{\text{sb}}/\phi_{\text{fast}}$ ratio is not measuring the same motions as $\rho(\tau)$. $\rho(\tau)$ reflects both side chain and segmental motions of the studied residue, whereas $f_{\text{sb}}/\phi_{\text{fast}}$ is more reflective of ensemble averaged segmental motions of the fluorophore conjugated and adjacent amino acid residues (20).

General Conclusions—As discussed above, several lines of evidence point toward the existence of transient gorge enlargements that would facilitate substrate binding and product egress. These include molecular dynamics simulations that predict breathing or gating movements (8–10) and the paradoxically high substrate turnover number in relation to the small diameter of the active-site gorge when compared with the cross-sectional size of acetylcholine. This report adds further credence to the existence of transient gorge enlargements by experimentally demonstrating that the outer wall of the active-site gorge, the Cys⁶⁹–Cys⁹⁶ Ω loop, is conformationally flexible and capable of undergoing residue-specific and ligand-dependent changes in backbone motions. The fact that all published AChE crystal structures depict only a narrow active-site gorge does not provide conclusive evidence for a static, narrow active-site gorge in solution (5–7). A growing body of evidence suggests that the conditions of AChE crystallization simply favor a narrow gorge conformational state (13).

Although we only have a fragmentary experimental picture of the conformational dynamics of the mAChE, this report and an ongoing study using site-directed labeling with fluorescein maleimide of three additional sites near the gorge shows only a partial degree of coupling of the fluctuations between residues. If this reflects a general feature of AChE conformational dynamics, then it would suggest that the transient gorge enlargements result from random or near random (non-concerted) fluctuations that periodically result in gorge enlargement. These near random fluctuations leading to periodic gorge enlargements would presumably occur in a time frame of nanoseconds or subnanoseconds (24). Despite the high catalytic efficiency of AChE with a turnover number of 10^4 s^{-1} , this time interval for gorge fluctuations is short in relation to the time required for individual catalytic steps or appreciable diffusion of substrate.

In summary, we examined the possibility that the Cys⁶⁹–Cys⁹⁶ Ω loop, which forms the outer wall of the active-site gorge of mAChE, plays a role in transient gorge enlargement by using site-directed labeling in conjunction with time-resolved fluorescence anisotropy. A molecular dynamics simulation of the side chain and segmental motions of the mutated residues was also performed to further validate this approach. The results indi-

cate the Ω loop residues examined show torsional motion and segmental fluctuations and therefore could contribute to transient gorge enlargements. In turn, these rapid fluctuations occur in a time frame that is short with respect to diffusional translation of substrate (24) and could be expected to enhance substrate accessibility and product egress. Examination of the effects of two inhibitors, one of which interacts directly with the outer portion of the Ω loop (fasciculin) and one of which does not (huperzine), also reveals internal loop flexibility and that the backbone movements are not all tightly coupled. This later observation suggests the possibility that transient gorge enlargements result from random or near random (non-concerted) fluctuations that periodically widen the gorge. Systematic mapping of other positions on the AChE surface should be able to further delineate regions involved and ultimately reveal solution conformations of AChE not discernible in a static crystal structure.

Acknowledgments—We thank Dr. Zoran Radic for advice and many valuable discussions related to this study, Dr. Davide Comolletti for analytical ultracentrifugation, and Dr. Lori Jennings for matrix-assisted laser desorption/ionization time-of-flight-mass spectrometric analysis of mAChE.

REFERENCES

- Rosenberry, T. L. (1975) *Adv. Enzymol. Relat. Areas Mol. Biol.* **43**, 103–218
- Quinn, D. M. (1987) *Chem. Rev.* **87**, 955–979
- Sussman, J. L., Harel, M., Frolow, F., Oefner, C., Goldman, A., Tokor, L., and Silman, I. (1991) *Science* **253**, 872–879
- Bourne, Y., Taylor, P., and Marchot, P. (1995) *Cell* **83**, 503–512
- Harel, M., Schalk, I., Ehretsabatie, L., Bouet, F., Goeldner, M., Hirth, C., Axelsen, P. H., Silman, I., and Sussman, J. L. (1993) *Proc. Natl. Acad. Sci. U. S. A.* **90**, 9031–9035
- Harel, M., Quinn, D. M., Nair, H. K., Silman, I., and Sussman, J. L. (1996) *J. Am. Chem. Soc.* **118**, 2340–2346
- Bourne, Y., Taylor, P., Bougis, P. E., and Marchot, P. (1999) *J. Biol. Chem.* **274**, 2963–2970
- Gilson, M. K., Straatsma, T. P., McCammon, J. A., Ripoll, D. R., Faerman, C. H., Axelsen, P. H., Silman, I., and Sussman, J. L. (1994) *Science* **263**, 1276–1278
- Wlodek, S. T., Clark, T. W., Scott, L. R., and McCammon, J. A. (1997) *J. Am. Chem. Soc.* **119**, 9513–9522
- Shen, T., Tai, K., Henchman, R. H., and McCammon, J. A. (2002) *Acc. Chem. Res.* **35**, 332–340
- Grochulski, P., Li, Y., Schrag, J. D., Bouthillier, F., Smith, P., Harrison, D., Rubin, B., and Cygler, M. (1993) *J. Biol. Chem.* **268**, 12843–12847
- Grochulski, P., Li, Y., Schrag, J. D., and Cygler, M. (1994) *Protein Sci.* **3**, 82–91
- Shi, J., Boyd, A. E., Radic, Z., and Taylor, P. (2001) *J. Biol. Chem.* **276**, 42196–42204
- Marchot, P., Ravelli, R. B., Raves, M. L., Bourne, Y., Vellom, D. C., Kanter, J., Camp, S., Sussman, J. L., and Taylor, P. (1996) *Protein Sci.* **5**, 672–679
- Ichiiye, T., and Karplus, M. (1983) *Biochemistry* **22**, 2884–2893
- Tai, K., Shen, T., Borjesson, U., Philippopoulos, M., and McCammon, J. A. (2001) *Biophys. J.* **81**, 715–724
- Boyd, A. E., Marnett, A. B., Wong, L., and Taylor, P. (2000) *J. Biol. Chem.* **275**, 22401–22408
- Raves, M. L., Harel, M., Pang, Y. P., Silman, I., Kozikowski, A. P., and Sussman, J. L. (1997) *Nat. Struct. Biol.* **4**, 57–63
- Lakowicz, J. R. (1999) *Principles of Fluorescence Spectroscopy*, 2nd Ed., pp. 321–345, Kluwer Academic and Plenum Publishers, New York
- Gangal, M., Cox, S., Lew, J., Clifford, T., Garrod, S. M., Aschbacher, M., Taylor, S. S., and Johnson, D. A. (1998) *Biochemistry* **37**, 13728–13735
- Gangal, M., Clifford, T., Deich, J., Cheng, X., Taylor, S. S., and Johnson, D. A. (1999) *Proc. Natl. Acad. Sci. U. S. A.* **96**, 12394–12399
- Kinosita, K., Jr., Kawato, S., and Ikegami, A. (1977) *Biophys. J.* **20**, 289–305
- Steiner, R. F. (1991) in *Topics in Fluorescence Spectroscopy* (Lakowicz, J. R., ed) pp. 13–14, Plenum Press, New York
- Zhou, H. X., Wlodek, S. T., and McCammon, J. A. (1998) *Proc. Natl. Acad. Sci. U. S. A.* **95**, 9280–9283

Nanosecond Dynamics of Acetylcholinesterase Near the Active Center Gorge*

Received for publication, February 10, 2004
Published, JBC Papers in Press, April 12, 2004, DOI 10.1074/jbc.M401482200

Aileen E. Boyd^{‡§}, Cristina S. Dunlop^{‡¶}, Lilly Wong[‡], Zoran Radić[‡], Palmer Taylor^{‡||},
and David A. Johnson^{**}

From the [‡]Department of Pharmacology, University of California, La Jolla, California 92093-0636 and the

^{**}Division of Biomedical Sciences, University of California, Riverside, California 92521-0121

To delineate the role of peptide backbone flexibility and rapid molecular motion in acetylcholinesterase catalysis and inhibitor association, we investigated the decay of fluorescence anisotropy at three sites of fluorescein conjugation to cysteine-substitution mutants of the enzyme. One cysteine was placed in a loop at the peripheral site near the rim of the active center gorge (H287C); a second was in a helical region outside of the active center gorge (T249C); a third was at the tip of a small, flexible Ω loop well separated from the gorge (A262C). Mutation and fluorophore conjugation did not appreciably alter catalytic or inhibitor binding parameters of the enzyme. The results show that each site examined was associated with a high degree of segmental motion; however, the A262C and H287C sites were significantly more flexible than the T249C site. Association of the active center inhibitor, tacrine, and the peripheral site peptide inhibitor, fasciculin, had no effect on the anisotropy decay of fluorophores at positions 249 and 262. Fasciculin, but not tacrine, on the other hand, dramatically altered the decay profile of the fluorophore at the 287 position, in a manner consistent with fasciculin reducing the segmental motion of the peptide chain in this local region. The results suggest that the motions of residues near the active center gorge and across from the Cys⁶⁹–Cys⁹⁶ Ω loop are uncoupled and that ligand binding at the active center or the peripheral site does not influence acetylcholinesterase conformational dynamics globally, but induces primarily domain localized decreases in flexibility proximal to the bound ligand.

Catalysis of the hydrolysis of acetylcholine by the serine hydrolase, acetylcholinesterase (AChE),¹ occurs at or near the diffusion limit (1, 2). The crystal structure of AChE reveals the enzyme active center to be at the base of a narrow, aromatic side chain lined gorge, some 18–20 Å in depth (3–5). How the

substrate can rapidly traverse this tortuous route, acylate the active center serine with concomitant choline departure, and then deacylate with acetate departure in each catalytic cycle of ~100 μ s has been a source of puzzlement. A large dipole moment aligned with the gorge entry portal enhances diffusional ingress (6–8). Alternative portals have been proposed as routes for access or removal of H₂O, H⁺, or products (9–11); however, the finding that mutations in the vicinity of the proposed alternative portals do not alter steady-state catalytic parameters argues against a second access route being a rate-limiting step (12, 13).

Molecular dynamic simulations have pointed to flexibility and/or fluctuations in gating that may enhance accessibility to the active center (14, 15). A 10-ns molecular dynamic simulation of mouse AChE analyzed in terms of projections on the principal components suggests that collective motions on many time scales contribute to the opening of the gorge (16). Residues at the gorge opening and constriction point generally have larger correlation vectors pointing away from the gorge than do residues located peripheral to the gorge, suggesting large amplitude gorge opening motions.

Although molecular dynamic simulations support the existence of a conformationally active gorge, little experimental support exists. Analysis of the various published crystal structures of the apo and ligand-bound enzyme from various sources yield no indication that the gorge exists in “open” and “closed” states. On the other hand, Laue crystallography, with its diminished exposure time of x-ray radiation, has the potential to detect short lifetime intermediates in formation of AChE complexes (17). Also, we have reported that both active center and peripheral site inhibitors alter dramatically the emission maxima of acrylodan conjugated to mouse AChE cysteine mutants (18). Because many of the affected residues do not directly contact the bound ligand, the findings reveal ligand-dependent conformational changes in the Cys⁶⁹–Cys⁹⁶ Ω -loop, which forms one of the walls of the active center gorge (18, 19). Additionally, we have found substantial internal flexibility at this Ω -loop as well as changes in flexibility induced by ligand binding (20).

To extend our observations on the AChE conformational dynamics to additional areas around the active center gorge, we measured the effects of two inhibitors on the backbone flexibility of three surface sites across the active center gorge from the Cys⁶⁹–Cys⁹⁶ Ω -loop using site-directed labeling in combination with time-resolved fluorescence anisotropy. Specifically, we chose three aligned sites for cysteine substitution and fluorescein conjugation, starting at the rim of the gorge (H287C), extending radially to an adjacent surface α -helix (T249C), and then to the tip of a small and mobile Ω -loop (A262C), some 20 Å away from the gorge rim (Fig. 1). Time-

*This work was supported in part by United States Public Health Services Grants R37-GM18360 and P42-E10337, Department of Army Medical Defense Grant 17C-951-5027, and a University of California Intercampus Grant. The costs of publication of this article were defrayed in part by the payment of page charges. This article must therefore be hereby marked “advertisement” in accordance with 18 U.S.C. Section 1734 solely to indicate this fact.

§ Supported by National Institutes of Health Training Grant GM07752.

¶ Present address: Wayne State University School of Medicine, Detroit, MI 48201.

|| To whom correspondence should be addressed: Dept. of Pharmacology, University of California, La Jolla, CA 92093-0636. Tel.: 858-534-4028; Fax: 858-534-8248; E-mail: pwtaylor@ucsd.edu.

¹ The abbreviations used are: AChE, acetylcholinesterase; FM, fluorescein 5-maleimide; IAF, 5-iodoacetamidofluorescein.

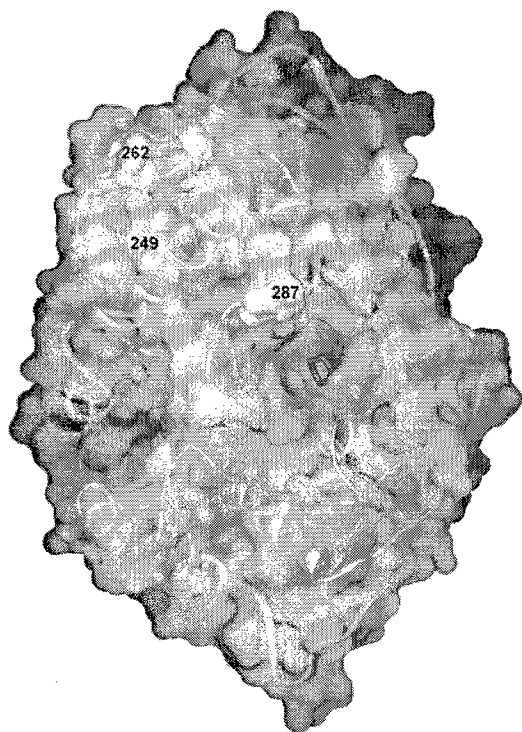


Fig. 1. Locations of the sites of cysteine substitution and fluorescein conjugation. Illustrated is a surface presentation of mouse AChE looking into the active center gorge (Protein Data Bank code 1KU6) with the Cys⁶⁹-Cys⁹⁶ Ω -loop, highlighted in green, and the three sites of cysteine substitution and fluorescein conjugation (Thr²⁴⁹, Ala²⁶², and His²⁸⁷), highlighted in yellow. The position of bound tacrine, shown in red, was derived from the crystallographic coordinates of the *Torpedo californica* AChE-tacrine complex (Protein Data Bank code 1ACJ) and overlaid into the mouse AChE structure.

resolved fluorescence anisotropy yields information on the excited state of the fluorophore in the picosecond to nanosecond time frame (21), a time domain much shorter than the AChE catalytic cycle. With this approach we hoped to assess the basic characteristics of the motion at sites near the gorge but across from the Cys⁶⁹-Cys⁹⁶ Ω -loop. We reasoned that if the opening motions were conformationally linked, ligand association, which would influence peptidyl backbone flexibility adjacent to the bound ligand, should also affect motion and flexibility parameters at more distal loci. The results reveal distinct modes of molecular motion in the individual regions examined. Also, the very limited effects of ligand binding upon anisotropy decay suggest uncoupled movements of the regions examined, a finding consistent with a model for transient gorge openings that is dominated by random segmental movements.

EXPERIMENTAL PROCEDURES

Materials—Acetylthiocholine iodide, 5,5'-dithio-bis(2-nitrobenzoic acid) (Ellman's reagent), dithiothreitol, and tacrine (9-amino-1,2,3,4-tetrahydroacridine hydrochloride hydrate) were purchased from Sigma. Fluorescein 5-maleimide (FM) and 5-iodoacetaminofluorescein (IAF) were obtained from Molecular Probes. Fasciculin 2 (purified from the venom of *Dendroaspis angusticeps*) was a gift of Dr. Pascale Marchot (University of Marseille, France). Drs. Yacov Ashani and Bhupendra P. Doctor (Walter Reed Army Research Center, Washington, D. C.) kindly provided 7-[[methylethoxyphosphinyl]-oxyl]-1-methylquinolinium iodide. All other chemicals came from commercial sources and were, at least, reagent grade.

Enzyme Preparation—Mutagenesis procedures to generate the cysteine-substituted mutants are described elsewhere (22). Briefly, cDNAs encoding a monomeric form of the mouse enzyme truncated at position 548 were placed in the mammalian expression vector, pcDNA3 (Invitrogen), and were subjected to PCR-mediated (QuikChangeTM, Stratagene) mutagenesis. Restriction enzyme analyses allowed detection of the mu-

tations. To ensure the absence of spurious mutations, cassettes encompassing the mutated site were subcloned into pcDNA3 vectors that had not been exposed to the mutagenesis procedure, and their nucleotide sequences were verified by double stranded sequencing.

Human embryonic kidney (HEK 293) cells, purchased from American Type Culture Collection (Manassas, VA), were plated in Dulbecco's modified Eagle's medium supplemented with 10% fetal bovine serum at a density of 1.5×10^6 cells per 10-cm dish, 24 h prior to transfection. Standard HEPES/calcium phosphate precipitation methods were used to apply 10 μ g of plasmid DNA per plate to the cell monolayers. The next day, cells were rinsed with phosphate-buffered saline and supplied with serum-free media for continued growth (Ultraculture, Bio-Whittaker, Walkersville, MD). Large scale productions of mutant enzymes entailed creation of stable cell lines that exhibited G418 (Gemini Bio-Products, Woodland, CA) resistance following cotransfection with a neomycin resistance gene as described elsewhere (22, 23). Harvests of mutant AChE in serum-free media from confluent cells in three-liter flasks (Nalge Nunc Int., Rochester, NY) typically continued for several weeks after which expression levels began to decline.

Affinity chromatography with trimethyl (*m*-aminophenyl)ammonium linked through a long tether arm to Sepharose CL-4B resin (Sigma) permitted one-step purification of AChE, both mutant and wild-type in amounts between 5 and 25 mg, as previously described (24–26). Purity was assessed by SDS-PAGE and by comparisons of specific activity with absorbance at 280 nm to measure protein concentration ($\epsilon_{280} = 1.14 \times 10^5 \text{ M}^{-1} \text{ cm}^{-1}$ (27)).

Catalytic Activity—The catalytic activity of each unlabeled and labeled mutant was measured with the Ellman assay (28). K_m and K_{ss} (the dissociation constant of a ternary complex resulting in substrate inhibition or activation) were evaluated as described in previous kinetic schemes (23). The x intercept of a plot of the residual catalytic activity versus the concentration of the irreversible inhibitor 7-[[methylethoxy]-phosphinyl]-oxyl]-1-methylquinolinium iodide yielded the enzyme concentration, and, in turn, k_{cat} (29).

Fluorescein Labeling—The mutant enzymes were pretreated with 0.25 mM dithiothreitol for 30 min at room temperature to ensure that all of the free cysteines were reduced, and free dithiothreitol was removed with a G-50 Sephadex spin column (Roche Diagnostics) equilibrated in 0.1 M sodium phosphate buffer, pH 7. FM and IAF were dissolved in dimethylformamide to make stock concentrations between 6 and 15 mM. The thioactive probes, FM and IAF, at 100 times the enzyme concentration, were added to the enzyme solutions to achieve either a 3-fold molar excess in the case of the A262C mutant or a 20-fold molar excess in the case of the T249C and H287C mutants. Labeling was allowed to proceed for 12 h at 4 °C for the A262C mutant and for 2 h at 37 °C for the T249C and H287C mutants.

Unconjugated fluorescein derivatives were removed by gel-filtration with G-25 Sephadex (Amersham Biosciences), equilibrated with 0.1 M sodium phosphate buffer, pH 7. Parallel labeling reactions with wild-type mouse AChE were performed to assess nonspecific labeling. Stoichiometries of fluorescein-labeled mutants were estimated spectrophotometrically by substitution of the measured absorbance values at 280 nm (A_{280}) and 495 nm (A_{495}) into the following expression.

$$\frac{[\text{Fluorescein}]}{[\text{AChE}]} = \frac{A_{495}/83,000}{(A_{280} - 0.18A_{495})/114,000} \quad (\text{Eq. 1})$$

Steady-state Emission—Steady-state emission spectra were measured at room temperature using a FluoroMax II spectrofluorometer (Jobin Yvon Inc., Edison, NJ).

Time-resolved Fluorescence Anisotropy—Emission anisotropy was determined by time-correlated single photon-counting measurements (30) with an IBH (Edinburgh, UK) 480-nm NanoLEDTM flash lamp run at 1 MHz and IBH model TBX-04 photon detector. The vertically $[I_v(t)]$ and orthogonally $[I_o(t)]$ polarized emission components were collected by exciting samples with vertically polarized light while orienting the emission polarizer (Polaroid HNPB dichroic film) in either a vertical or orthogonal direction. Excitation and emission bands were selected with an Oriel 500-nm short-pass interference filter (catalog number 59876) and a Corning 3-68 cut on filter with a half-maximum transmission of 540 nm, respectively. Typically, 2×10^4 peak counts were collected (in 1–2 min) when the emission polarizer was vertically oriented. The orthogonal emission decay profile was generated over the same time interval that was used to generate the vertical emission decay profile. Samples were held at 22 °C. To minimize convolution artifacts, flash lamp profiles were recorded by removing the emission filter and monitoring light scatter from a suspension of latex beads. The data analysis software corrected the wavelength-dependent temporal

dispersion of the photoelectrons by the photomultiplier. The polarization bias (G) of the detection instrumentation was determined by measuring the integrated photon counts/ 6×10^6 lamp flashes while the samples were excited with orthogonally polarized light and the emission was monitored with a polarizer oriented in the vertical and orthogonal directions ($G = 1.028$).

The emission anisotropy decay, $r(t)$, given by the expression,

$$r(t) = \frac{I_{\parallel}(t) - G I_{\perp}(t)}{I_{\parallel}(t) + 2G I_{\perp}(t)} \quad (\text{Eq. 2})$$

and total emission decay, $S(t)$, for a macroscopically isotropic sample,

$$S(t) = I_{\parallel}(t) + 2G I_{\perp}(t) \quad (\text{Eq. 3})$$

were deconvolved simultaneously from the individual polarized emission components expressed as,

$$I_{\parallel} = \frac{S(t)}{3} [1 + 2r(t)] \quad (\text{Eq. 4})$$

and the following.

$$I_{\perp}(t) = \frac{S(t)}{3} [1 - r(t)] \quad (\text{Eq. 5})$$

Thus, both $I_{\parallel}(t)$ and $I_{\perp}(t)$ are determined by the same fitting functions, $S(t)$ and $r(t)$, and fitting parameters.

The fluorescence lifetimes for each sample were determined by initially generating a total emission decay profile from $I_{\parallel}(t)$ and $I_{\perp}(t)$ with Equation 3 and then globally fitting $I_{\parallel}(t)$ and $I_{\perp}(t)$ decay profiles to Equations 4 and 5 with the lifetime parameters fixed and with the following anisotropy decay expression.

$$r(t) = r_0 f_{\text{sb}} \exp(-t/\phi_{\text{fast}}) + r_0(1 - f_{\text{sb}}) \exp(-t/\phi_{\text{slow}}) \quad (\text{Eq. 6})$$

Here, r_0 is the amplitude of the anisotropy at time 0, f_{sb} is the fraction of the anisotropy decay associated with the fast decay processes, and ϕ is the rotational correlation time of the anisotropy decay. The subscripts *fast* and *slow* denote the fast and slow decay processes, respectively. A nonassociative model was assumed, indicating that the emission relaxation times are common to all the rotational correlation times. The fluorescence data were analyzed using the Globals software package developed at the Laboratory for Fluorescence Dynamics at the University of Illinois, Urbana-Champaign. Goodness of fit was evaluated from the values of the reduced χ^2 and by visual inspection of the weighted-residual plots.

To better define the uncertainty of the measured slow, presumably whole body, rotational correlation times, a range (not a mean \pm S.D.) of ϕ_{slow} values was determined for each data set that produced a reasonably acceptable fit to the anisotropy decay. Specifically, a unidimensional search procedure was performed that involved directed searches along the ϕ_{slow} parameter axis, not allowing other fitting parameters to vary, to find the minimum and maximum ϕ_{slow} values that raised the χ^2 values by 5%.

Estimation of Stokes' Radius—The Stokes' radius of wild-type AChE was estimated by gel filtration with a Superdex 200 HR 10/30 column (Amersham Biosciences) equilibrated with 0.1 M ammonium acetate buffer, pH 7.2. The elution volumes of wild-type AChE and proteins with known Stokes' radii were measured. The estimated value of the wild-type AChE Stokes' radius of wild-type AChE was read from a curve derived using the known Stokes' radii and the elution parameters of the standards, following the equation of Porath (31).

Molecular Dynamic Simulations of FM-H287C Mutant—A series of short, 3-ps molecular dynamic simulations were performed on the mouse AChE-fasciculin complex coordinates (Protein Data Bank code 1KU6) with FM attached to Cys²⁸⁷ to assess the effects of bound fasciculin on the torsional rotation of the succinimidythioether (maleimide) tether arm connecting the fluorescein reporter group to the α -carbonyl backbone. The hydrogens were added in InsightII prior to calculations, and the pH was set to 7.0. Sets of 21 molecular dynamic simulations were run with an SGI Octane computer (SiliconGraphics, Inc., Mountain View, CA) using the Discover 2.9 module within the InsightII 2000.1 computer program (Accelrys, San Diego, CA), both in the presence and absence of fasciculin. With the exception of the 19 AChE residues (from Gln²⁷⁹ to Phe²⁹⁷) forming a surface loop, including FM attached to Cys²⁸⁷, all the atoms of mouse AChE and fasciculin were "frozen" during simulation. No water was present, the dielectric constant was set to 80, and the structure was not minimized prior to the

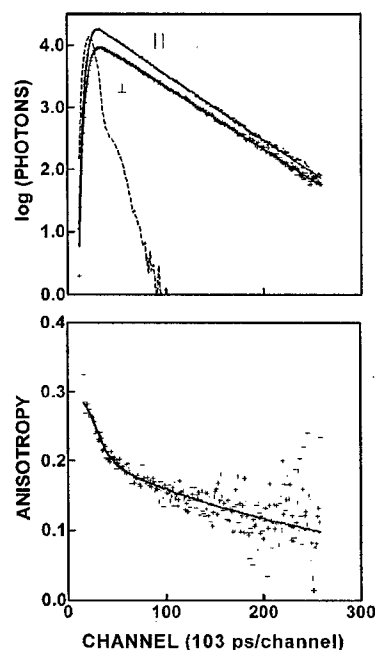


FIG. 2. Emission and anisotropy decay of the FM-T249C mouse AChE mutant. The upper panel shows the parallel (●) and perpendicular (+) emission decays (single data points), the fit of these data points to a single exponential decay equation (smooth lines), and the flash lamp profile (dashed line). The lower panel shows the time-resolved anisotropy decay (+), and a solid line through these points that was generated with the best-fit parameters (Table I) for a double exponential nonassociative decay model (Equation 6). The concentration of the labeled mutant was 150 nM.

subsequent molecular dynamic simulations. The protocol included initial equilibration of the system at 300 K, heating to 700 K, then slow cooling in 50-K increments back to 300 K, followed by minimization of the system.

RESULTS

Characterization of Unlabeled and Labeled Mutants—SDS-PAGE analysis of the labeled and unlabeled mutants revealed a single, wide band of silver staining migrating with the variably glycosylated wild-type mouse AChE. Comparison of the steady-state emission from labeled mutants and parallel, wild-type AChE showed 6–7% nonspecific labeling. Based upon spectrophotometric ratios, stoichiometries of labeling for the labeled mutants were: T249C, 0.2 ± 0.04 ; A262C, 0.4 ± 0.1 ; and H287C, 0.3 ± 0.06 . The K_m , K_{ss} , and k_{cat} values for the cysteine mutants, the conjugated cysteine mutants, and wild-type AChE preparations were within experimental error of each other (data not shown). Because labeling was not stoichiometric, we also looked for a fractional component in the substrate concentration dependence curves that showed a different K_m , but were unable to detect two components in the curves. Moreover, titration with both tacrine and fasciculin produced virtually complete inhibition of catalytic activity of the labeled mutants with similar K_I values as observed for the wild-type AChE. Together, these findings indicate that labeled mutants fold correctly despite cysteine substitution and reporter group conjugation at these positions.

Fluorescence Emission—The uncorrected emission (517 ± 1 nm) and excitation (494 ± 1 nm) maxima for the conjugated enzymes are typical of fluorescein in an aqueous environment. Neither fasciculin nor tacrine had a significant effect upon the excitation or emission spectra of either the T249C or A262C conjugates; however, fasciculin red shifted slightly (2–3 nm) the emission spectrum and enhanced the apparent quantum yield by ~12% of the IAF-labeled H287C mutant, indicating a

TABLE I
Effect of fasciculin and tacrine on the anisotropy decay parameters of FM-labeled mouse AChE mutants

Data are shown as mean (\pm S.D.) from at least three determinations. The vertically and orthogonally polarized emission decays were initially analyzed for the $S(t)$ parameter (Equation 3), and then for the $r(t)$ parameter (Equation 6) with the Globals Unlimited™ computer program. The experimental details are described under "Experimental Procedures." The mutants were present at the following concentrations: FM-T249C, 150 nM; FM-A262C, 190 nM; FM-H287C, 135 nM. To ensure saturation of enzyme with inhibitors, concentrations of fasciculin (4.7 to 5.7 μ M) and tacrine (40 μ M) were 10-fold over the total enzyme concentration and at least 100-fold over the K_i of tacrine or fasciculin for wild-type mouse AChE.

Mutant	Inhibitor	r_0^a	f_{sb}^b	ϕ_{fast}^c	ϕ_{slow}^d	ψ_r^{2e}	τ^f
				ns	ns		ns
T249C	None	0.30 \pm 0.01	0.32 \pm 0.01	1.2 \pm 0.2	34–49	1.3	4.25 \pm 0.01
	Fasciculin	0.30 \pm 0.01	0.33 \pm 0.01	1.3 \pm 0.3	35–49	1.3	4.16 \pm 0.01
	Tacrine	0.31 \pm 0.03	0.33 \pm 0.01	1.0 \pm 0.4	33–48	1.2	4.26 \pm 0.01
A262C	None	0.29 \pm 0.03	0.47 \pm 0.01	0.8 \pm 0.2	41–72	1.5	4.26 \pm 0.01
	Fasciculin	0.29 \pm 0.02	0.47 \pm 0.01	0.8 \pm 0.2	43–71	1.4	4.27 \pm 0.01
	Tacrine	0.28 \pm 0.02	0.46 \pm 0.01	0.8 \pm 0.2	40–63	1.5	4.27 \pm 0.01
H287C	None	0.30 \pm 0.01	0.50 \pm 0.01	0.9 \pm 0.1	31–44	1.3	4.11 \pm 0.01
	Fasciculin	0.30 \pm 0.01	0.34 \pm 0.01	1.8 \pm 0.1	36–49	1.2	4.28 \pm 0.02
	Tacrine	0.32 \pm 0.03	0.49 \pm 0.01	0.9 \pm 0.2	29–41	1.4	4.10 \pm 0.01

^a The time 0 anisotropy.

^b The fraction of the observed anisotropy decay associated with the fast depolarization processes.

^c Fast rotational correlation time.

^d The range of the slow rotational correlation times that yield χ_r values 5% above the minimum.

^e The reduced χ^2 .

^f Geometric averaged lifetimes ($\Sigma\alpha_i\tau_i$, where $\Sigma\alpha_i = 1$).

ligand-induced change of the microenvironment around the reporter group attached to the H287C site of conjugation (data not shown).

Estimation of Rotational Correlation Times—From the gel filtration measurements, wild-type AChE was estimated to have a Stokes' radius of 51 Å. Substituting this value into the Stokes-Einstein equation yielded a rotational correlation time of 128 ns.

Time-resolved Fluorescence Anisotropy of FM Conjugates—For brevity, the emission and the anisotropy decay profiles of only the FM-T249C conjugate are illustrated (Fig. 2). The time course of emission decay of each mutant examined was well fit to a biexponential decay model. For simplicity, only the geometric averaged excited state lifetimes are summarized (Table I) and ranged between 4.11 and 4.26 ns. The actual range of short and long wavelength emission lifetimes for the various nonliganded mutants were 4.26–4.82 and 2.98–4.01 ns, respectively. The amplitudes of the longer lifetime components ranged between 31 and 87% of the total decay amplitude (data not shown).

Time-resolved fluorescence anisotropy directly monitors the reorientation of the emission transition dipole moment of a fluorescent reporter group in the picosecond/nanosecond time domain. When conjugated to a specific protein side chain, the $I_{\parallel}(t)$ and $I_{\perp}(t)$ emission profiles are usually well fit to a model-free nonassociative biexponential equation (Equation 6). Under conditions where the protein-conjugated reporter group diffuses relatively freely at the end of its tether arm and where there are no significant internal motions in the time domain between the whole body diffusion and local backbone movements, the main types of motions (tether arm, local backbone, and whole body) should be resolvable from each other and are represented in the basic elements of the biexponential equation (time 0 amplitude, r_0), the rotational correlation time, and fractional amplitude of the fast components (ϕ_{fast} and f_{sb}) and slow rotational correlation time (ϕ_{slow}) processes (32). In the present case, the whole body rotational correlation time predicted by the Stokes-Einstein equation (128 ns) is slower than the observed ϕ_{slow} values, which ranged between 31 and 72 ns (Table I). This disparity may reflect the existence of internal motions of intermediate decay rates that obscure the depolarization from whole body rotational diffusion or arise from the inherent limitation of quantifying rotational diffusion times that are more than 10 times slower than the emission lifetime of the reporter group.

Visual comparison of the time-resolved anisotropy decays of the three mutants (Fig. 3) shows that the fluorescein attached to A262C and H287C mutants reorients (depolarizes) more rapidly than the fluorescein attached to the T249C mutant, but with similar time 0 anisotropy values. Quantitatively, these similarities and differences were primarily observed in the fractional amplitude of the measurable fast decay processes (f_{sb}). The f_{sb} values for the FM-A262C and FM-H287C conjugates represent about half of the resolvable anisotropy decay (0.47 and 0.50, respectively), but only a third (0.32) of the FM-T249C mutant. The values for the time 0 anisotropy (r_0 ; range 0.29–0.30) and the fast rotational correlation time (ϕ_{fast} ; range 0.8–1.2 ns) were essentially the same for all the mutants studied. Taken together, these results indicate a high level of α -carbon flexibility around each residue examined, although the Thr²⁴⁹ residue is significantly less flexible than the Ala²⁶² and His²⁸⁷ residues.

Influence of Ligand Binding on Anisotropy Decay of FM Conjugates—Active and peripheral site inhibitors, tacrine and fasciculin, respectively, were bound to AChE at a concentration of at least 100 times their dissociation constants to ensure >99% occupation (23, 33). Alteration in the decay of anisotropy was observed only upon binding of fasciculin to FM-H287C mutant (Table I and Fig. 4). Specifically, fasciculin reduced the amplitude of the fast decay process by 32% and doubled the fast decay time without significantly affecting either the time 0 anisotropy or the slow decay, presumably reflecting whole body rotational diffusion (Table I). Additionally, some fasciculin-induced change in the microenvironment of the fluorophore is evident, because fasciculin increased slightly the emission lifetime (from 4.11 to 4.28 ns, Table I) and caused a 2–3-nm red shift in the emission maximum of the fluorescein (data not shown). These results suggest that, whereas the microenvironment around the reporter group changed slightly, the tether arm motions of the reporter group were not significantly hindered by a direct interaction with bound fasciculin. The fasciculin-induced alterations in anisotropy decay, therefore, result from reduced segmental flexibility around H287C at the edge or rim of the active site gorge.

This interpretation is supported by molecular dynamic simulations of the mouse AChE coordinates with FM attached to H287C in both the presence and absence of fasciculin. Visual examination of the pattern of positions of FM at the end of these simulations (Fig. 5) shows only a small difference pro-

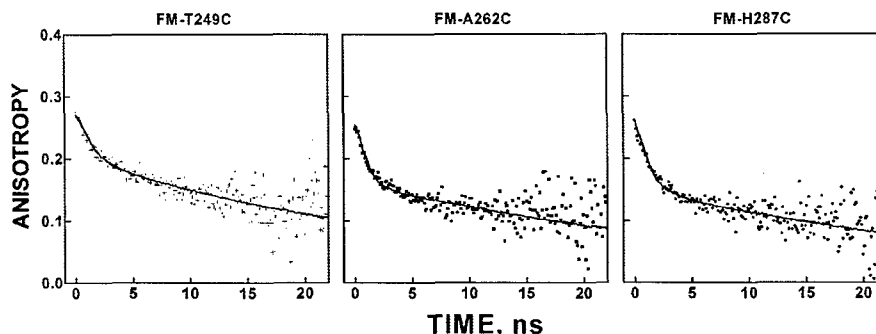


FIG. 3. Anisotropy decays of FM-T249C, FM-A262C, and FM-H287C mouse AChE mutants. Shown are the time-resolved anisotropy decays (single data points), and the solid lines through these points that were generated with the best-fit parameters (Table I) for a double exponential nonassociative decay model (Equation 6). The peak of the flash lamp profile arbitrarily defined the zero time point. The concentrations of FM-T249C (+), FM-A262C (■), and FM-H287C (●) were 150, 190, and 135 nM, respectively.

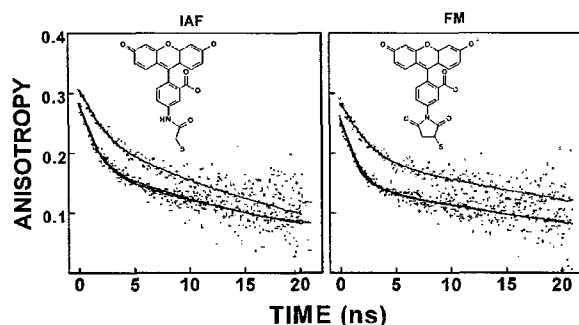


FIG. 4. Effect of fasciculin and tacrine on the anisotropy decay of the FM- and IAF-labeled H287C mutants. The time-resolved anisotropy decay (single data points) and the solid lines through these points were generated with the best-fit parameters (Table II) for a double exponential nonassociative decay model (Equation 6). Data points represent enzyme without inhibitors (●), with tacrine (+), or with fasciculin (□). The peak of the flash lamp profile arbitrarily defined the zero time point. The concentrations of FM-H287C, IAF-H287C, fasciculin, and tacrine were 135 nM, 145 nM, 4.7 μ M, and 40 μ M, respectively.

duced by the presence of fasciculin. The pattern of final positions of FM appears slightly more spherical in the absence of fasciculin. Quantitatively, the mean distance in movements of the C_{α} of Cys²⁸⁷ from its initial position was 2.6 ± 1.9 Å (for FM-mouse AChE alone) and 0.96 ± 0.59 Å for FM-mouse AChE complexed to fasciculin. These findings support the experimental results that fasciculin significantly lowers flexibility of the C_{α} at position 287.

Anisotropy Decay with IAF—To confirm that the changes in anisotropy decay induced by fasciculin were not unique to the tether arm, we also examined the influence of fasciculin and tacrine on the anisotropy decay parameters of an IAF-H287C mutant conjugate. The anisotropy decay profile of this conjugate was very similar to the FM conjugated to the same position, where fasciculin, but not tacrine, reduced the amplitude and slowed the rate of the fast depolarization processes (Fig. 4 and Table II). Thus, the influence of fasciculin on the decay parameters appears independent of the tether arm joining fluorescein to the cysteine side chain. Here, the length of the tether arms of both conjugates are the same, but the FM derivative with its succinimidylthioether linkage should have less torsional freedom than the acetamidothioether linkage of the IAF conjugate.

DISCUSSION

The apparent paradox of diffusion-limited catalysis of esters occurring within the confines of a narrow gorge in AChE has prompted computational and mutational investigations into

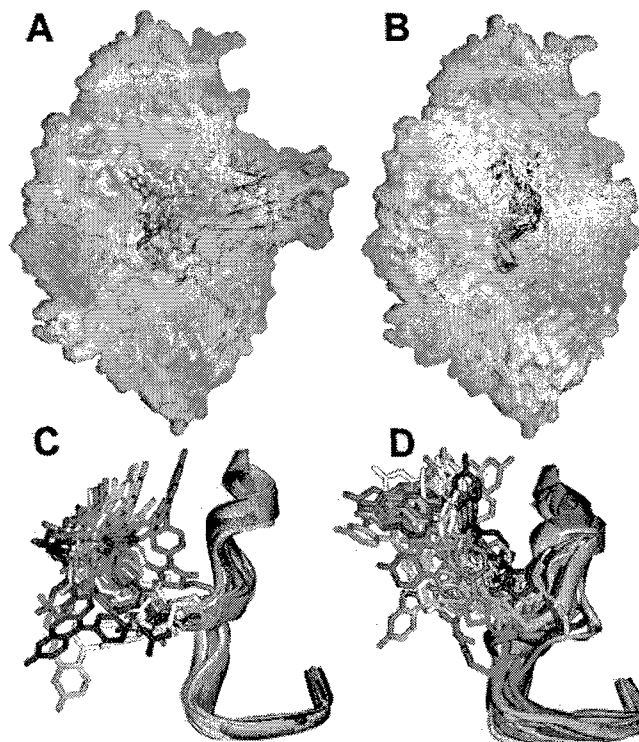


FIG. 5. Molecular dynamic simulations of the effect of fasciculin binding on the torsional movements of Cys²⁸⁷ and attached FM. Twenty-one 3-ps simulations were performed on the x-ray coordinates of the mouse AChE-fasciculin complex with FM attached to Cys²⁸⁷ in the presence (A and C) and absence (B and D) of fasciculin as described under "Experimental Procedures." Only the residues between Gln²⁷⁹ and Phe²⁹⁷ and attached FM were allowed to move; the rest of mouse AChE and fasciculin atoms were "frozen" for the simulations. The positions of the FM bonds and the Gln²⁷⁹ to Phe²⁹⁷ backbone are shown in a different color for each simulation. Transparent Connolly surfaces of mouse AChE and fasciculin are shown in gray and brown, respectively. In panels C and D, the views of the positions of the FM bonds and the Gln²⁷⁹ to Phe²⁹⁷ backbone are rotated by $\sim 60^\circ$ around the vertical axis and enlarged from the panel (A and B) above.

the dynamics of substrate entry and product egress from the active center. Although alternative entry routes have been suggested from molecular dynamic calculations (9–11), mutational studies have not supported additional entry or exit portals for the charged substrate or product (12, 13). Accordingly, more recent computational studies have been directed to analyzing how conformational flexibility within AChE may give rise to greater access to the active center than is evident in the static crystal structure (16). The current investigation of decay of anisotropy of site-directed fluorophores presents an ap-

TABLE II

Effect of fasciculin and tacrine on the anisotropy decay parameters of IAF-labeled H287C mouse AChE mutant

Data are shown as mean (\pm S.D.) from at least three determinations. The mutant was present at a concentration of 145 nM. To ensure saturation of enzyme with inhibitors, concentrations of fasciculin (4.7 μ M) and tacrine (40 μ M) were 10-fold over the total enzyme concentration and at least 100-fold over the K_i of tacrine or fasciculin for wild-type mouse AChE.

Condition	r_0^a	f_{xb}^b	ϕ_{fast}^c	ϕ_{slow}^d	ψ_r^{2e}	τ^f
None	0.32 \pm 0.02	0.42 \pm 0.01	ns	ns	1.3	ns
Fasciculin	0.34 \pm 0.01	0.29 \pm 0.01	1.1 \pm 0.2	22–29	1.3	3.83 \pm 0.02
Tacrine	0.30 \pm 0.02	0.44 \pm 0.01	1.5 \pm 0.3	23–29	1.3	4.04 \pm 0.03
			1.3 \pm 0.2	23–30	1.4	3.80 \pm 0.01

^a The time zero anisotropy.^b The fraction of the observed anisotropy decay associated with the fast depolarization processes.^c Fast rotational correlation time.^d The range of the slow rotational correlation times that yield ψ_r^2 values 5% above the minimum.^e The reduced ψ_r^2 .^f Geometric averaged lifetimes ($\Sigma\alpha_i\tau_i$, where $\Sigma\alpha_i = 1$).

proach to extending analysis of conformation from static equilibrium measurements of fluorescence to time-resolved analysis in the picosecond to nanosecond time frame.

Time-resolved fluorescence anisotropy enables one to monitor directly reorientation of a fluorophore in the time frame of several excited state lifetimes. When a fluorophore is tethered to the macromolecule, depolarization is achieved by multiple relaxation modes that most likely occur in distinct time frames. Torsional motion around the tether arm, if unhindered, will occur in a subnanosecond time frame, not resolvable with commercial instruments. Restriction of motion around the tether will diminish the amplitude and slow the decay rate of this phase. Segmental motion of a domain within the molecule containing the fluorophore will give rise to a fast, but usually measurable depolarization; the rate and amplitude of which will depend upon the mass of the domain, the extent of the angular excursion, and the orientation of the absorbance/emission transition moments relative to the diffusion cone angle. Finally, global motion of the entire protein where the fluorophore is affixed to the macromolecule will in most cases produce the slowest rate of anisotropy decay. The latter will be governed by the multiple rotational correlation times of the macromolecule, which are not resolvable unless the molecule is highly dimensionally asymmetric.

Decay of Anisotropy of the FM Conjugates—The structure of the small Ω -loop bounded by the disulfide bond at Cys²⁵⁷ and Cys²⁷² is not well resolved in AChE crystal structures unless the loop is stabilized by interaction with the symmetry related molecule (34). The large thermal or B factors for this region in the crystal structures suggest that the tip of this disulfide loop is either highly flexible or experiences static disorder in the crystal (35). Indeed, when FM is conjugated to A262C, the amplitudes of the very fast ($r_i - r_0$) and fast (r_0f_{xb}) decay phases represent \sim 17 and 39% of the total anisotropy decay, where r_i is the fundamental anisotropy of the fluorophore. Hence, independent motions of the fluorescein tether arm through torsional motion ($r_i - r_0$) and flexible domain motion ($r_0 - f_{xb}$) in the AChE molecule are the dominant modes of anisotropy decay at the 262 position.

When fluorescein is attached to the H287C mutant, we note similar amplitudes for the very rapid and rapid decay phases, 14 and 43%. Again, the major mode of depolarization of the fluorescein conjugated at position 287 occurs by modes other than the global rotation of the molecule. The average crystallographic B factors for the α -carbon chain atoms of residue His²⁸⁷ are far smaller than that seen for residue 262 (Table III). The disparity between B factors at the 287 and 262 positions, in the face of similar large components of rapid depolarization of the attached fluorescein, suggests either that His²⁸⁷ is stabilized in the crystalline state or that the large average B factors associated with Ala²⁶² arise from a equilibrium (*i.e.* static dis-

TABLE III
Comparison of the average main chain atom crystallographic B factors for residues Thr²⁴⁹, Ala²⁶², and His²⁸⁷

Residue	B factor ^a	Normalized B factor ^b
Thr ²⁴⁹	19.6	-1.74
Ala ²⁶²	79.2	1.83
His ²⁸⁷	33.9	-0.88

^a The B factors listed here are the average main chain atom values (amino nitrogen, carboxy carbon, and α carbon) of the indicated residue for chain A of the tetrameric crystal structure of mouse AChE (Protein Data Bank code 1MAA (34)).

^b Calculated by subtracting the average main-chain atom B factors of all residues forming chain A (average equals 48.59) from the average main chain atoms of the indicated residue and then dividing by the standard deviation of the B factors of all residues forming chain A (standard deviation equals 16.67).

order) between multiple positions of the small Ω -loop in the crystal structure. Stabilization of His²⁸⁷ by crystallization forces could be part of the process that favors a closed gorge state in the crystal and explains why no open gorge crystal structures of AChE have been observed.

By contrast, when fluorescein is conjugated at T249C, a smaller fraction of the anisotropy decay occurs by the rapid modes, 14 and 27%. This difference most likely arises from a more structured α -carbon backbone in the vicinity of Thr²⁴⁹, a region shown to be helical in the crystal structure (Ala²⁴¹-Val²⁵⁵) (34).

Influence of Ligand Binding on the Anisotropy Decay Parameters—To examine whether ligand binding influences anisotropy decay and hence dynamic parameters at various locations near the active center gorge, we initially selected two ligands whose complexes with AChE have been determined crystallographically. Tacrine binds at the active center at the base of the gorge with its aromatic ring system stacked between the indole moiety of Trp⁸⁴ and the phenyl ring of Phe³³⁰ in Torpedo AChE (36) corresponding to Trp 86 and Tyr 337 of mouse AChE. In fact, the latter residue shows a conformational movement associated with tacrine binding causing a parallel stacking of the tacrine ring between the two aromatic side chains. By contrast, fasciculin, a peptide of 61 amino acids, associates at the mouth of the gorge greatly limiting ligand access to the catalytic center (4, 37). The AChE crystal structure shows that His²⁸⁷ approaches a van der Waals distance to the bound fasciculin residues.

The binding of tacrine, despite it being inhibitory to all of the conjugated enzymes, has no effect on the lifetime or anisotropy decay parameters for fluorescein conjugated at positions 249, 262, and 287. Hence, this result would indicate that ligand binding does not cause a global conformation change that would be evident at these three disparate locations on the macromolecule. However, this finding does not preclude li-

gands inducing changes in conformation and side chain mobility in regions of the AChE molecule that are not reflected in our three labeling positions (11, 18, 19, 38).

Fasciculin, which binds with a K_d for the wild-type enzyme in the range of 4 pM (33) and whose crystal structure shows a van der Waals peptide to protein contact area of 1100 Å² (4), also does not affect the anisotropy decay parameters at positions 262 and 249. However, conjugated fluorescein at position 287 shows a small change in the Stokes' shift and emission lifetime, and a major change in the decay of anisotropy. The reduction of the amplitudes of the rapid decay phases and the slowing of the rapid decay phase likely reflect a small torsional restraint on the tethered fluorescein and a stabilization of movement of the loop encompassing residue 287 produced by the bound fasciculin.

The differential influence of fasciculin on the anisotropy decay of three fluorophores positioned in distinct locations on the AChE molecule, again, indicates that this ligand does not induce global changes in the conformational dynamics of the enzyme. Based on the limited number of sites examined, fasciculin appears to have stabilized a local domain of the molecule reducing the intrinsic flexibility in the region around His²⁸⁷ and probably in neighboring areas of direct contact.

Implications—These results combined with our previous analysis of the segmental dynamics of three sites on the Cys⁶⁹–Cys⁹⁶ Ω-loop (20) paint a consistent picture of AChE with conformationally active surface backbone elements whose movements are poorly coupled to one another. Such a conformationally dynamic structure supports a model for transient gorge openings that is dominated by random segmental movements.

Also, the above studies further demonstrate the potential of time-resolved studies of fluorescence anisotropy to examine molecular motion in distinct regions of a molecule and its ligand-associated complexes whose overall structural template has been delineated through x-ray crystallography. The principal advantages of the technique stem from measurements conducted in solution and under conditions simulating ligand binding *in situ*. Cysteine substitution mutagenesis enables one to select individual side chains in strategic regions of the molecule and examine each locus in a systematic fashion with multiple fluorophores. The individual fluorophores selected for conjugation can differ in lifetime, spectroscopic parameters, and capacity to modify the substituted cysteines. Hence, a comprehensive analysis of time-resolved fluorescence typically requires analysis of a variety of residue positions often with more than a single probe. This presents a particular challenge for larger extracellular proteins because their production usually requires eukaryotic expression systems that typically yield limited quantities of protein. Also, glycosylation and intrinsic disulfide bonds characteristic of extracellular proteins may add further complexity to achieving appropriate expression. Our study establishes that the residue-directed fluorophore approach to labeling can yield valuable information even when the macromolecule is a large glycosylated protein.

In summary, we have extended our previous study of the conformational dynamics of the AChE Cys⁶⁹–Cys⁹⁶ Ω-loop, a segment that forms the outer wall of the active center gorge, to include three additional sites positioned roughly in a line that starts at the rim of the gorge across from the Ω-loop and projecting radially ~20 Å away from the gorge. Similar to our previous study, site-directed labeling in conjunction with time-resolved fluorescence anisotropy was utilized. The results reveal both distinct modes of molecular motion as well as a high

degree of backbone flexibility. Additionally, there appears to be limited coupling of the conformational fluctuations between the sites examined, because ligand binding only affected the one site that was in close proximity to the bound inhibitor. This indicates that ligand association did not produce global changes in the conformational flexibility of the enzyme. Moreover, these results combined with our previous analysis of the conformational dynamics of the Cys⁶⁹–Cys⁹⁶ Ω-loop add support to the view that the area around the active center gorge rim is conformationally active and is consistent with a model for transient gorge openings that are dominated by random segmental movements.

REFERENCES

- Rosenberry, T. L. (1975) *Adv. Enzymol. Relat. Areas Mol. Biol.* **43**, 103–218
- Quinn, D. M. (1987) *Chem. Rev.* **253**, 955–979
- Sussman, J. L., Harel, M., Frolow, F., Oefner, C., Goldman, A., Tokar, L., and Silman, I. (1991) *Science* **253**, 872–879
- Bourne, Y., Taylor, P., and Marchot, P. (1995) *Cell* **83**, 503–512
- Kryger, G., Harel, M., Giles, K., Tokar, L., Velan, B., Lazar, A., Kronman, C., Barak, D., Ariel, N., Shafferman, A., Silman, I., and Sussman, J. L. (2000) *Acta Crystallogr. Sect. D* **56**, 1385–1394
- Ripoll, D. R., Faerman, C. H., Axelsen, P. H., Silman, I., and Sussman, J. L. (1993) *Proc. Natl. Acad. Sci. U. S. A.* **90**, 5128–5132
- Radić, Z., Kirchhoff, P. D., Quinn, D. M., McCammon, J. A., and Taylor, P. (1997) *J. Biol. Chem.* **272**, 23265–23277
- Wlodek, S. T., Shen, T., and McCammon, J. A. (2000) *Biopolymers* **53**, 265–271
- Gilson, M. K., Straatsma, T. P., McCammon, J. A., Ripoll, D. R., Faerman, C. H., Axelsen, P. H., Silman, I., and Sussman, J. L. (1994) *Science* **263**, 1276–1278
- Wlodek, S. T., Clark, T. W., Scott, L. R., and McCammon, J. A. (1997) *J. Am. Chem. Soc.* **119**, 9513–9522
- Tara, S., Straatsma, T. P., and McCammon, J. A. (1999) *Biopolymers* **50**, 35–43
- Kronman, C., Ordentlich, A., Barak, D., Velan, B., and Shafferman, A. (1994) *J. Biol. Chem.* **269**, 27819–27822
- Faerman, C., Ripoll, D., Bon, S., Le Feuvre, Y., Morel, N., Massoulie, J., Sussman, J. L., and Silman, I. (1996) *FEBS Lett.* **386**, 65–71
- Zhou, H. X., Wlodek, S. T., and McCammon, J. A. (1998) *Proc. Natl. Acad. Sci. U. S. A.* **95**, 9280–9283
- Shen, T. Y., Tai, K., and McCammon, J. A. (2001) *Phys. Rev. E Stat. Nonlin. Soft Matter Phys.* **63**, 041902
- Tai, K., Shen, T., Borjesson, U., Philippopoulos, M., and McCammon, J. A. (2001) *Biophys. J.* **81**, 715–724
- Ravelli, R. B., Ravess, M. L., Ren, Z., Bourgeois, D., Roth, M., Kroon, J., Silman, I., and Sussman, J. L. (1998) *Acta Crystallogr. Sect. D* **54**, 1359–1366
- Shi, J., Boyd, A. E., Radić, Z., and Taylor, P. (2001) *J. Biol. Chem.* **276**, 42196–42204
- Shi, J., Radić, Z., and Taylor, P. (2002) *J. Biol. Chem.* **277**, 43301–43308
- Shi, J., Tai, K., McCammon, J. A., Taylor, P., and Johnson, D. A. (2003) *J. Biol. Chem.* **278**, 30905–30911
- Steiner, R. F. (1991) in *Topics in Fluorescence Spectroscopy* (Lakowicz, J. R., ed) Vol. 2, Plenum Press, New York
- Boyd, A. E., Marnett, A. B., Wong, L., and Taylor, P. (2000) *J. Biol. Chem.* **275**, 22401–22408
- Radić, Z., Pickering, N. A., Vellom, D. C., Camp, S., and Taylor, P. (1993) *Biochemistry* **32**, 12074–12084
- Berman, J. D., and Young, M. (1971) *Proc. Natl. Acad. Sci. U. S. A.* **68**, 395–398
- De la Hoz, D., Doctor, B. P., Ralston, J. S., Rush, R. S., and Wolfe, A. D. (1986) *Life Sci.* **39**, 195–199
- Marchot, P., Ravelli, R. B., Ravess, M. L., Bourne, Y., Vellom, D. C., Kanter, J., Camp, S., Sussman, J. L., and Taylor, P. (1996) *Protein Sci.* **5**, 672–679
- Taylor, P., Jones, J. W., and Jacobs, N. M. (1974) *Mol. Pharmacol.* **10**, 78–92
- Ellman, G. L., Courtney, K. D., Andres, V. J., and Featherstone, R. M. (1961) *Biochem. Pharmacol.* **7**, 88–95
- Levy, D., and Ashani, Y. (1986) *Biochem. Pharmacol.* **35**, 1079–1085
- Yguerabide, J. (1972) *Methods Enzymol.* **26**, 498–578
- Siegel, L. M., and Monty, K. J. (1966) *Biochim. Biophys. Acta* **112**, 346–362
- Gangal, M., Cox, S., Lew, J., Clifford, T., Garrod, S. M., Aschbahr, M., Taylor, S. S., and Johnson, D. A. (1998) *Biochemistry* **37**, 13728–13735
- Radić, Z., Duran, R., Vellom, D. C., Li, Y., Cervenansky, C., and Taylor, P. (1994) *J. Biol. Chem.* **269**, 11233–11239
- Bourne, Y., Taylor, P., Bougis, P. E., and Marchot, P. (1999) *J. Biol. Chem.* **274**, 2963–2970
- Glusker, J. P., and Trueblood, K. N. (1985) *Crystal Structure Analysis: A Primer*, 2nd Ed., Oxford University Press, New York
- Harel, M., Schalk, I., Ehret-Sabatier, L., Bouet, F., Goeldner, M., Hirth, C., Axelsen, P. H., Silman, I., and Sussman, J. L. (1993) *Proc. Natl. Acad. Sci. U. S. A.* **90**, 9031–9035
- Harel, M., Kleywegt, G. J., Ravelli, R. B., Silman, I., and Sussman, J. L. (1995) *Structure* **3**, 1355–1366
- Tara, S., Helms, V., Straatsma, T. P., and McCammon, J. A. (1999) *Biopolymers* **50**, 347–359

Direct Analysis of the Kinetic Profiles of Organophosphate–Acetylcholinesterase Adducts by MALDI-TOF Mass Spectrometry[†]

Lori L. Jennings,^{*,‡} Michael Malecki,^{§,||} Elizabeth A. Komives,[§] and Palmer Taylor[‡]

Departments of Pharmacology and Chemistry and Biochemistry, Howard Hughes Medical Institute Mass Spectrometry Facility, University of California, San Diego, La Jolla, California 92093

Received May 9, 2003; Revised Manuscript Received July 18, 2003

ABSTRACT: A sensitive matrix-assisted laser desorption/ionization time-of-flight (MALDI-TOF) mass spectrometry procedure has been established for the detection and quantitation of acetylcholinesterase (AChE) inhibition by organophosphate (OP) compounds. Tryptic digests of purified recombinant mouse AChE (mAChE) were fractionally inhibited by paraoxon to form diethyl phosphoryl enzyme. The tryptic peptide of mAChE that contains the active center serine residue resolves to a molecular mass of 4331.0 Da. Phosphorylation of the enzyme by paraoxon results in covalent modification of the active center serine and a corresponding increase in molecular mass of the tryptic peptide by 136 Da. The relative abundance of AChE peptides containing a modified active center serine strongly correlates with the fractional inhibition of the enzyme, achieving a detection range of phosphorylated to nonphosphorylated enzyme of 5–95%. Modifications of AChE by OP compounds resulting in dimethyl, diethyl, and diisopropyl phosphoryl adducts have been monitored with subpicomole amounts of enzyme. The individual phosphorylated adducts of AChE that result from loss of one alkyl group from the inhibited enzyme (the aging reaction) and the reappearance of unmodified AChE (spontaneous reactivation) have been resolved by the kinetic profiles and relative abundance of species. Further, the tryptic peptide containing the active center serine of AChE, isolated from mouse brain by anion-exchange and affinity chromatography, has been monitored by mass spectrometry. Native brain AChE, purified from mice treated with sublethal doses of metrifonate, has demonstrated that enzyme modifications resulting from OP exposure can be detected in a single mouse brain. For dimethyl phosphorylated AChE, OP exposure has been monitored by the ratio of tryptic peptide peaks that correspond to unmodified (uninhibited and/or reactivated), inhibited, and aged enzyme.

Acetylcholinesterase (AChE;¹ EC 3.1.1.7) is a serine hydrolase that regulates cholinergic neurotransmission in the peripheral and central nervous systems by hydrolyzing acetylcholine with a remarkably high catalytic efficiency. Mammalian AChE is encoded by a single gene that is alternatively spliced to yield molecular isoforms that differ in tissue-specific expression, solubility, and mode of membrane attachment (1, 2). The catalytic triad of AChE contains aligned serine, histidine, and glutamate residues. It is well established that the catalytic activity of AChE is inhibited by organophosphates (OPs), a diverse group of compounds

commonly used as pesticides as well as chemical warfare agents. The inhibition of AChE by OP compounds involves phosphorylation of the active site serine residue and the formation of stable phosphoryl AChE adducts (3). Subsequent reactions that occur spontaneously with OP–AChE conjugates include dephosphorylation of AChE to generate reactivated enzyme and dealkylation of phosphorylated AChE, by a unimolecular process referred to as aging (4, 5), to result in enzyme that is irreversibly inactivated.

Mechanisms of phosphorylation, reactivation, and aging of AChE by OP compounds have been extensively studied. Site-directed mutagenesis, molecular modeling, and kinetic studies have been used to determine reaction rate constants and elucidate important structural determinants for the interaction of OPs with AChE (references cited in ref 6). Aged phosphoryl enzyme conjugates have been directly observed of AChE inhibited by soman, sarin, methyl phosphonofluoridate, and DFP using NMR studies (7) and X-ray crystallography (8). Mass spectrometric approaches have been used to investigate the reaction pathways for OP-mediated AChE inhibition. The reaction products of AChE phosphorylation and aging of the OP–AChE conjugates with tabun and analogues, methamidophos, and other methyl phosphonofluoridates have been resolved (9–11). The mechanism of AChE inhibition by (1*S*,3*S*)-isomalathion (12) and

[†] This work was supported by NIEHS Grant P42-ES10337.

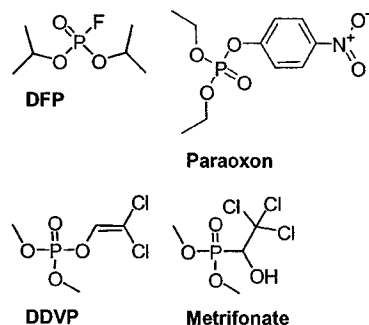
^{*} To whom correspondence should be addressed. Telephone: 858-534-1366. Fax: 858-534-8248. E-mail: ljennings@ucsd.edu.

[‡] Department of Pharmacology, University of California, San Diego.

[§] Department of Chemistry and Biochemistry, University of California, San Diego, and Howard Hughes Medical Institute Mass Spectrometry Facility.

^{||} Present address: Division of Medical Sciences, Harvard Medical School, Boston, MA 02115.

¹ Abbreviations: AChE, acetylcholinesterase; mAChE, mouse acetylcholinesterase; ACP, active center peptide of acetylcholinesterase; ATCh, acetylthiocholine; MALDI-TOF MS, matrix-assisted laser desorption/ionization time-of-flight mass spectrometry; OPs, organophosphates; DFP, diisopropyl fluorophosphate; paraoxon, diethyl *p*-nitrophenyl phosphate; DDVP, *O,O*-dimethyl *O*-(2,2-dichlorovinyl) phosphate; metrifonate, (2,2,2-trichloro-1-hydroxyethyl)phosphonic acid dimethyl ester; BSA, bovine serum albumin.

Chart 1: Structures of Organophosphates^a

^a Chemical formulas of the organophosphate AChE inhibitors: DFP, diisopropyl fluorophosphate; paraoxon, diethyl *p*-nitrophenyl phosphate; DDVP, *O,O*-dimethyl *O*-(2,2-dichlorovinyl) phosphate; metrifonate, (2,2,2-trichloro-1-hydroxyethyl)phosphonic acid dimethyl ester.

products of aged soman-inhibited AChE (13) have also been reported.

In the current work, a MALDI-TOF mass spectrometric procedure has been established for the sensitive detection and quantitation of AChE inhibition by DDVP, paraoxon, and DFP (Chart 1). The quantitation of analytes by MALDI-TOF MS has been reported for proteins and peptides (14–16) as well as low molecular mass species as substrates and products of biocatalytic reactions (17). In this study, the relative signal intensities for the tryptic peptides of AChE that contain the active center serine residue, unmodified or phosphorylated by OP treatment, have been monitored kinetically, quantitated, and compared to activity measurements as determined by standard methods (18). Modifications of the active center serine of AChE by OPs have been observed with subpicomole amounts of enzyme, and the analysis has proved a reliable means to determine the fractional inhibition of enzyme activity. It is demonstrated that AChE modifications by OPs can be quantified by MALDI-TOF MS. Moreover, the relative abundance of OP-inhibited AChE that has spontaneously reactivated and phosphoryl conjugates that have undergone aging have been resolved at specific time intervals.

The study of OP–AChE conjugates has been extended to an *in vivo* system, where endogenous AChE isolated from mouse brain tissue has been analyzed by mass spectrometry to detect phosphoryl enzyme adducts that result from exposure of mice to OPs. In previous studies, endogenous AChE has been purified from vertebrate brain tissue of human and calf (19), rabbit (20), rat (21), pig (22), quail (23), and chicken (24) to investigate structure–activity relationships for the enzyme with substrates and inhibitors and establish the distribution of AChE molecular isoforms. The significant advance reported here is that native and modified AChE from a single mouse brain has been isolated and characterized. The detection sensitivity of MALDI-TOF MS analysis is sufficient to resolve discrete modifications of AChE and has facilitated the analysis of brain enzyme isolated by a strategy that does not require pooling of tissue or purification of enzyme from multiple animals.

MATERIALS AND METHODS

Chemicals and Reagents. ATCh, DTNB, DFP, paraoxon, metrifonate, and DEAE-Tris-acryl resin were purchased from Sigma (St. Louis, MO). DDVP was purchased from ICN

Biomedical Inc. (Irvine, CA). Sequence-grade modified trypsin was purchased from Promega (Madison, WI). Acridinium-conjugated affinity resin was synthesized as previously described (19, 25, 26). CHCA matrix (α -cyano-4-hydroxycinnamic acid) was purchased from Agilent Technologies (Palo Alto, CA).

Hazardous Procedures. OPs are highly toxic and should be handled with caution by trained personnel in a well-ventilated hood. OP chemicals are hydrolyzed by dilution into 4 M NaOH to render them inactive as cholinesterase inhibitors.

Recombinant Mouse Acetylcholinesterase (mAChE). Recombinant AChE was produced by transfection of an expression plasmid encoding the 547 N-terminal amino acid residues of mouse AChE into human embryonic kidney cells (HEK-293). Soluble monomeric mAChE, secreted in the culture medium of stable cell clones expressing high levels of recombinant enzyme, was purified by affinity chromatography and characterized as previously described (2, 27). The purity of recombinant mAChE used in experiments was confirmed by SDS–polyacrylamide gel electrophoresis and silver stain of native protein and protein that had been enzymatically deglycosylated with peptide–*N*-glycosidase F (PNGase F). The specific activity of recombinant mAChE preparations was calculated from AChE activity measurements and protein content, as determined by the methods of Ellman (18) and Bradford (28), respectively.

Organophosphate Treatment of Mouse Acetylcholinesterase (in Vitro). To achieve fractional inhibition of recombinant mAChE by OP treatment, samples were prepared by adding paraoxon to mAChE at various enzyme-to-inhibitor molar ratios. At an initial concentration of 10 μ M enzyme in 100 mM sodium phosphate buffer, pH 7.0, mAChE was treated with freshly prepared substocks of paraoxon at various concentrations from 0 to 12 μ M. Following incubation at room temperature for 45 min, an aliquot was removed to measure the fractional activity by Ellman assay. Activity measurements were performed in the presence of 100 mM sodium phosphate buffer, pH 7.0, 0.1 mg/mL BSA, 0.3 mM DTNB, and 0.5 mM ATCh. Residual OP and other reaction byproducts were removed from the incubation mixture, and the buffer was exchanged to 50 mM ammonium bicarbonate, pH 7.4, by spin filtering using Microcon-30 devices (Millipore, Bedford, MA). Samples were evaporated to dryness by vacuum centrifugation and redissolved in 50 mM ammonium bicarbonate buffer to a protein concentration of 0.7 mg/mL (Bradford assay) for subsequent digestion by trypsin.

To resolve modifications of mAChE that result from extended exposure to OP compounds, time course experiments were conducted with DFP, paraoxon, and DDVP. A 1.5-fold molar excess of OP was added to mAChE (10 μ M enzyme in 100 mM sodium phosphate, pH 7.0, buffer) and incubated at room temperature. At various time intervals, an aliquot was removed to measure AChE activity, then frozen, and stored at -80°C . The OP-inhibited mAChE samples were thawed and prepared in parallel for mass spectrometric analysis, in the same manner as that described for fractional inhibition studies.

Trypsin Proteolysis of mAChE. mAChE (5–15 μ g) was subjected to proteolytic digestion by incubation with sequence-grade modified trypsin (1:50 protein ratio of trypsin:mAChE) at 37°C for 3 h. The tryptic peptides from mAChE

fractionally inhibited by paraoxon were lyophilized and dissolved in 0.1% (v/v) trifluoroacetic acid (TFA) for analysis by mass spectrometry. In other instances, the total peptides from tryptic digests of mAChE were fractionated prior to mass spectrometric analysis. Trypsinized mAChE was adsorbed to reverse-phase resin using a ZipTip-C4 (Millipore) and eluted with solutions containing 0.1% (v/v) TFA and increasing concentrations of acetonitrile in a step-increment gradient of 20%, 25%, 30%, 35%, 40%, and 60% (v/v) acetonitrile, as previously described (11).

Purification of Acetylcholinesterase from Mouse Brain. Mice (male, 7–8 weeks old, 20–25 g) were treated with saline or acute sublethal doses of metrifonate (200 or 400 mg/kg) by ip injection. The animals were sacrificed 45 min after treatment, and the brains were removed, frozen on liquid nitrogen, and stored at -80°C . The purification procedure was performed at 4°C , and all buffer solutions were ice cold. Unless indicated otherwise, buffer solutions contained 0.02% (w/v) NaN_3 as a preservative and the following protease inhibitors, added immediately prior to use: 5 mg/L leupeptin, 5 mg/L aprotinin, 5 mg/L pepstatin A, 10 mg/L bacitracin, 15 mg/L benzamidin, and 40 mg/L soybean trypsin inhibitor. Aliquots were taken at each stage of the purification procedure to measure AChE activity and protein content.

Enriched membrane extracts were prepared from brain tissue that was partially thawed and homogenized by Polytron (Brinkmann Instruments, Westbury, NJ) in a hypotonic buffer solution of 10 mM Tris-HCl, pH 7.4, and 1 mM EDTA. The homogenate was centrifuged at 150000g in a Beckman 60 Ti rotor (40000 rpm) for 1 h at 4°C . The pellet was resuspended in an extraction buffer of 20 mM sodium phosphate, pH 7.0, 0.15 M NaCl, 1 mM EDTA, and 0.5% (v/v) Triton X-100 and ultracentrifuged (60 Ti rotor, 40000 rpm, 2 h, 4°C). The supernatant, containing detergent-solubilized membranes, was removed, frozen on liquid nitrogen, and stored at -80°C .

The solubilized membrane fraction was further enriched by anion-exchange chromatography on DEAE-Tris-acryl resin. The extract from a mouse brain was diluted into binding buffer [20 mM bis-Tris propane hydrochloride, pH 7.0, 0.05% (v/v) Triton X-100] and adsorbed to a 10 mL DEAE-Tris-acryl gel bed previously equilibrated with binding buffer. Following a wash with two bed volumes of binding buffer, a protein fraction containing the majority of AChE activity (about 80%) was eluted with 20 mM piperazine hydrochloride, pH 5.0, 0.2 M NaCl, and 0.05% (v/v) Triton X-100.

Endogenous AChE was purified from the enriched protein fraction by affinity chromatography on *N*-methylacridinium-conjugated Sepharose 4B resin, with modifications to procedures previously reported (19). A 25:75 slurry of acridinium resin in buffer was added to the DEAE-Tris-acryl eluate (1 mL of slurry per 10 mL of eluate) and incubated in batch with gentle mixing at 4°C for 2–3 h. The mixture was poured into a small column, and the resin was washed with 20 bed volumes of buffer A [10 mM sodium bicarbonate, pH 8.0, 0.1 M NaCl, 40 mM MgCl_2 , 0.05% (v/v) Triton X-100], followed by a second wash with buffer A containing an additional 0.1 M NaCl. AChE was eluted from the acridinium resin by incubation with 5 mM decamethonium hydrochloride in buffer A, without protease inhibitors, for 1

h with gentle mixing. The eluate was diluted with 50 mM ammonium bicarbonate, pH 7.4, buffer, to reduce the concentration of Triton X-100 to 0.005% (v/v; below the CMC value), prior to being concentrated and buffer exchanged by spin-filtering using a Centricon-30 device (Millipore). Preparation of endogenous mAChE for analysis by mass spectrometry was performed in a manner similar to that described for recombinant mAChE samples.

Mass Spectrometry. Matrix-assisted laser desorption/ionization time-of-flight mass spectrometry (MALDI-TOF MS) was performed on a PE Biosystems Voyager DE-STR Biospectrometry workstation (Framingham, MA). Mass spectra were acquired in positive-ion linear mode under delayed extraction conditions, using an acceleration voltage of 25 kV and laser intensity of 2000–2400 V with a 337 nm pulsed nitrogen laser. External calibration was performed using ACTH peptide (amino acid residues 7–38) and bovine insulin, with average masses of 3657.93 and 5734.59 Da, respectively. Trypsinized mAChE or tryptic peptides of mAChE that were fractionated by adsorption to C4 reverse-phase resin were mixed with a matrix of 5 mg/mL α -cyano-4-hydroxycinnamic acid (CHCA) in 50% (v/v) acetonitrile and 0.3% (v/v) TFA, pH 2.2. A 1 μL aliquot of the peptide-matrix mixture was spotted, in duplicate, on a polished MALDI-TOF MS target plate and dried by semifast evaporation at 50°C . Analyte-matrix cocrystals appeared homogeneous in nature. The mass spectra shown are the average of 256 laser scans collected from multiple locations on the target spot and monitored by a digital oscilloscope during acquisition. Laser intensity was adjusted such that ion intensity did not exceed 60–70% of the maximum threshold value. The data were processed and quantified with the PE Biosystems Grams 3.0 software program.

Analytical Procedures. SDS-polyacrylamide gel electrophoresis, silver stain, and immunoblotting techniques were performed by standard procedures. Affinity-purified polyclonal antibodies to mAChE were produced by Bethyl Laboratories (Montgomery, TX) by immunization of rabbits with purified recombinant mAChE protein in soluble monomeric form. The antibodies were characterized in our laboratory, based on strict criteria, and shown to react with high avidity and specificity for mAChE protein in immunoblotting and immunoprecipitation procedures.

RESULTS

Fractional Inhibition of mAChE by Paraoxon: Detection and Quantitation by MALDI-TOF MS. The catalytic triad of mAChE contains the active center serine at position 203. Proteolytic digestion of mAChE with trypsin generates a 42 amino acid peptide extending from Leu 178 to Arg 219 that contains the active center serine residue. The tryptic peptide, subsequently referred to as active center peptide (ACP), has a theoretical average mass of 4331.0 Da. MALDI-TOF mass spectra acquired in positive-ion linear mode from trypsinized recombinant mAChE resolve the ACP with an observed average mass of 4331.0 (± 0.5) Da.

Paraoxon-mediated inhibition of mAChE results in diethyl phosphorylated enzyme. Complete AChE inhibition is associated with loss of unmodified ACP (4331.0 Da) and the appearance of modified peptide (4467.0 Da), corresponding to the expected mass increase of 136 Da from the diethyl

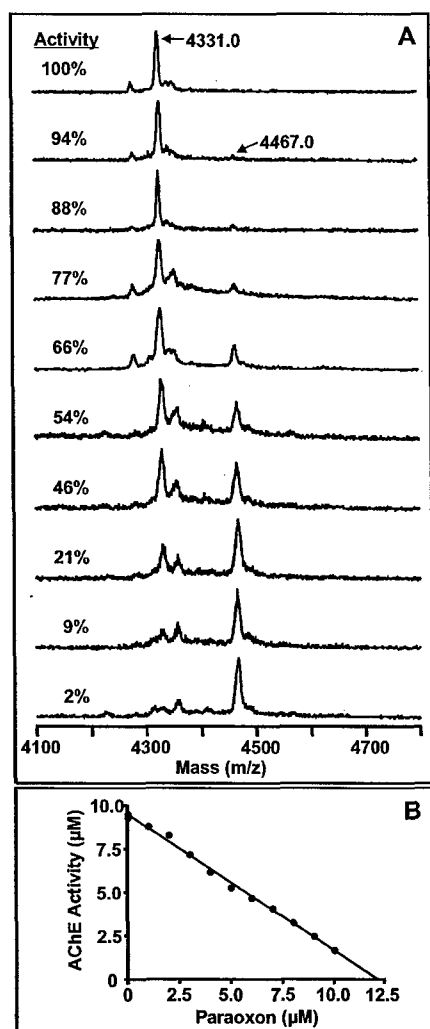


FIGURE 1: Fractional inhibition of mAChE by paraoxon. (A) Representative MALDI-TOF mass spectra acquired from total peptides of mAChE tryptic digests fractionally inhibited by paraoxon (0–12 μ M). Residual enzyme activity for each sample, as determined by Ellman assay, is indicated. Paraoxon-mediated inhibition of mAChE results in the diethyl phosphoryl enzyme adduct and a corresponding increase of 136 Da in the molecular mass of the active center peptide (ACP), from 4331.0 to 4467.0 Da. AChE inhibition is associated with a reduction in the signal intensity of unmodified ACP and a corresponding increase in diethyl phosphorylated ACP. (B) Activity measurements following treatment of mAChE by various concentrations of paraoxon, demonstrating that a stoichiometric ratio of OP is required to achieve fractional inhibition of AChE activity.

phosphorylated ACP adduct. Mass spectra acquired from tryptic digests of mAChE, incubated with 0–12 μ M concentrations of paraoxon to achieve a range of fractionally inhibited enzyme, are shown in Figure 1, panel A. Residual enzyme activity was determined by Ellman assay, and the data shown in Figure 1, panel B, confirm that a stoichiometric ratio of paraoxon was required to achieve fractional inhibition of enzyme activity. As the amount of inhibited mAChE enzyme increases in each sample, the signal intensity for unmodified ACP in mass spectra is reduced in a manner that parallels a larger signal intensity for the diethyl phosphoryl ACP adduct.

The relative amount of unmodified ACP and the diethyl phosphorylated ACP conjugate was determined, in multiple

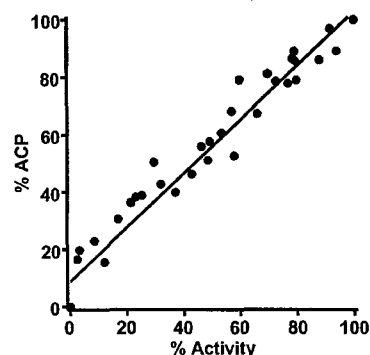


FIGURE 2: The relative abundance of unmodified ACP, determined by ion intensity from MALDI-TOF mass spectra, strongly correlates ($r^2 = 0.96$) with the residual activity of mAChE following paraoxon treatment. The relative abundance of unmodified ACP (4331.0 Da), referred to as % ACP, was calculated by the fraction of unmodified ACP compared to total ion intensity of the unmodified and diethyl phosphoryl ACP adduct (4467.0 Da) acquired from tryptic digests of paraoxon-inhibited mAChE. Representative mass spectra are shown in Figure 1. Data are compiled from six independent experiments.

trials, from ion intensity in mass spectra acquired from trypsinized, paraoxon-inhibited enzyme (Figure 2). The phosphorylation stoichiometry (percent ACP) was calculated from peak ion intensity by dividing unmodified ACP by the total of unmodified ACP and the diethyl phosphoryl ACP adduct. The percent ACP and residual enzyme activity measurements are both normalized to 100%. The relative abundances of unmodified ACP strongly correlate with the residual activities of mAChE following paraoxon inhibition. Therefore, the relative signal intensity of unmodified and phosphorylated ACP is directly related to the abundance of the OP–mAChE conjugate. The fractional inhibition studies demonstrate that MALDI-TOF mass spectrometry can be used as a quantitative measure to determine the degree of enzyme modification by OP compounds. It is evident that, in some samples where no residual AChE activity was measured, a minor fraction of unmodified ACP was resolved. It is likely that a small amount (less than 10%) of inactive enzyme is present in some preparations of recombinant mAChE and may account for the minor deviation seen in the correlation plot of activity versus ACP abundance.

Time-Resolved Organophosphate Modifications of Recombinant mAChE. Inhibition of mAChE by the OP compounds, paraoxon, DDVP, and DFP, resulting in diethyl, dimethyl, and diisopropyl phosphorylation of the enzyme, respectively, has been monitored with subpicomole amounts of enzyme. The relative abundance of phosphoryl ACP adducts that result from enzyme inhibition, loss of one alkyl group from the inhibited enzyme (the aging reaction), and dephosphorylation to give unmodified mAChE (reactivation) has been resolved at various time intervals. For each of the OPs, the expected mass increase for the ACP upon phosphorylation of mAChE and mass reduction for ACP phosphoryl adducts upon aging are given in Table 1.

Treatment of mAChE with paraoxon results in enzyme inhibition via diethyl phosphorylation of the active center serine. The inhibited enzyme can reactivate or undergo aging, whereby loss of one ethyl group renders the enzyme nonreactivable. At various times after the addition of a molar excess of paraoxon to mAChE, aliquots of treated enzyme were removed for tryptic digestion and mass

Table 1: Theoretical Masses for mAChE Active Center Peptides following Modification with Organophosphates^a

organo-phosphate	phosphoryl adduct	ACP (unmodified)	Δ mass from inhibition	inhibited ACP adduct	Δ mass from aging	aged ACP adduct
DFP	diisopropyl	4331.0	+164	4495.0	-42	4453.0
paraoxon	diethyl	4331.0	+136	4467.0	-28	4439.0
DDVP	dimethyl	4331.0	+108	4439.0	-14	4425.0

^a The average theoretical mass for unmodified active center peptide (ACP) from trypsinized mAChE is 4331.0 Da. The phosphoryl ACP adducts of mAChE that result from treatment by the OP compounds, DFP, paraoxon, and DDVP, reflect dialkylphosphoryl adducts and are given as average mass (Da). The "aged" phosphoryl ACP adducts are calculated to reflect the loss of one alkyl group from the inhibited enzyme-OP conjugate. Mass values reflect the loss of hydrogen from the Ser residue upon inhibition by the OP compound and addition of hydrogen to the oxyanion following the aging reaction.

spectrometric analysis. The reactions of inhibition, aging, and reactivation of AChE require a conformationally stable enzyme and the unique configuration of the active center, comprised of several subsites (29). Therefore, the relative amounts of mAChE phosphoryl species resulting from OP-mediated inhibition for specific time intervals will not vary following tryptic digestion of intact enzyme. mAChE tryptic peptides were fractionated by adsorption to C4 reverse-phase resin, with the ACP and phosphoryl ACP adducts isolated by elution in 60% (v/v) acetonitrile and 0.1% (v/v) TFA solution. In control experiments, where mAChE was labeled by [³H]DFP and monitored by scintillation counting, greater than 95% of the ACP from trypsinized mAChE eluted from the C4 reverse-phase resin in the fraction containing 60% (v/v) acetonitrile.

The relative abundance of ACP phosphoryl species was determined from ion intensity in acquired mass spectra (Figure 3) and shown, with comparison to enzyme activity measurements, in Figure 4. Since paraoxon treatment of mAChE results in complete and rapid enzyme inhibition, diethyl phosphorylated ACP (4467.0 Da) is predominant at early time points. A small fraction of aged enzyme is indicated by the monoethyl phosphoryl ACP adduct (4439.0 Da) at 8 h. The relative abundance of aged enzyme increases with time, as evident by the larger peak intensity of the aged ACP adduct. With extended incubation, some unmodified ACP reappears (48 h) and is indicative of hydrolysis of the phosphoryl serine bond and enzyme reactivation. This was confirmed by activity measurements. The abundance of the diethyl phosphorylated enzyme decreases in a manner that parallels the reactivation and aging time course. The fraction of mAChE that has aged is stable and does not reactivate. A minor amount of mAChE in this preparation is presumed to be catalytically inactive, since unmodified ACP (less than 12%) is evident in samples that have no detectable activity by Ellman assay.

The relative abundance of phosphoryl species can be fit to a scheme of parallel first-order reactions, allowing for some residual reinhibition that may occur at early time points due to an initial excess of OP inhibitor. The rate constant for diethyl phosphoryl adducts (k_{overall}) would represent the sum of the rate constants for formation of monoethyl phosphoryl adducts (k_{aging}) and unmodified ACP ($k_{\text{reactivation}}$). Rate constants of $k_{\text{overall}} = 0.0161 \text{ h}^{-1}$ ($t_{1/2} \sim 43 \text{ h}$), determined by the disappearance of the diethyl phosphoryl adduct, $k_{\text{aging}} = 0.0099 \text{ h}^{-1}$ ($t_{1/2} \sim 70 \text{ h}$), determined by the formation of the monoethyl phosphoryl adduct, and $k_{\text{reactivation}} = 0.0070 \text{ h}^{-1}$ ($t_{1/2} \sim 99 \text{ h}$), determined by the regeneration of the free serine, were estimated from the profiles in Figure 4.

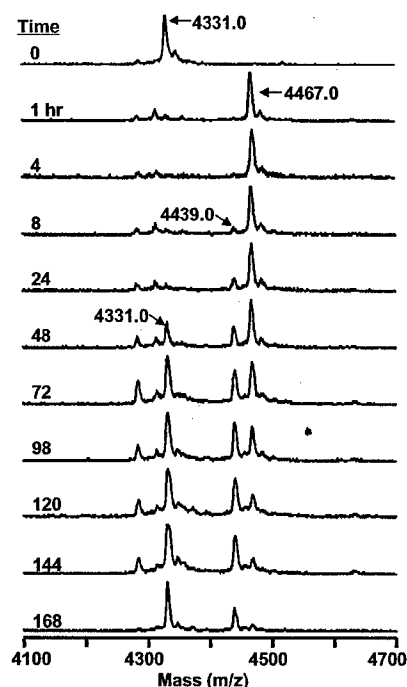


FIGURE 3: ACP conjugates of mAChE, resolved by time, following enzyme inhibition with paraoxon in molar excess. At various time intervals, an aliquot of paraoxon-treated mAChE was taken for mass spectrometric analysis. Samples were trypsinized, and the peptides were fractionated by reverse-phase chromatography to enrich for ACP adducts, as described in the text. Enzyme inhibition results in the diethyl phosphoryl ACP adduct (4467.0 Da). The aging reaction, which is defined as the loss of one ethyl group from the OP-enzyme conjugate, is represented by the monoethyl phosphoryl ACP adduct (4439.0 Da). The reappearance of unmodified ACP (4331.0 Da) is indicative of enzyme reactivation. MALDI-TOF mass spectra are representative of three experiments. In this and subsequent figures, a small shoulder on peak is observed of approximately 16 mass units above the parent peak. We presume this represents oxidation of a methionine in the ACP to a sulfoxide.

In a similar time course study, mAChE was inhibited by DDVP, where loss of enzyme activity is associated with dimethyl phosphorylation of the active center serine. As shown in Figure 5, the inhibited enzyme and aged conjugate are resolved from the unmodified and reactivated enzyme as dimethyl and monomethyl phosphoryl ACP adducts of 4439.0 and 4425.0 Da, respectively. Enzyme reactivation is evident at 4 h by the reappearance of unmodified ACP (4331.0 Da). In comparison to that observed with paraoxon, the aged conjugate appears more rapidly with DDVP-inhibited mAChE. The aging half-time of dimethyl phosphoryl AChE is significantly shorter than for diethyl phosphoryl AChE; dimethyl phosphorylated AChE has an

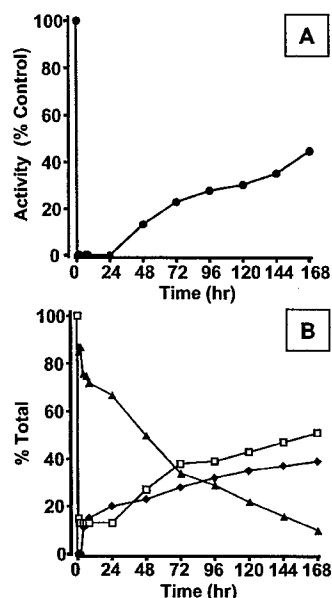


FIGURE 4: Relative abundance of ACP and phosphoryl adducts in mass spectra acquired from mAChE at various times following paraoxon inhibition of mAChE. (A) mAChE activity (●) was measured by Ellman assay at various time periods after the addition of a molar excess of paraoxon to the enzyme. (B) The ratio of ACP adducts at each time point was calculated from the signal intensity in mass spectra acquired from fractionated tryptic digests of paraoxon-inhibited mAChE samples. Unmodified ACP (□), diethyl phosphoryl ACP adduct (▲), and monoethyl phosphoryl ACP adduct (◆) represent control/reactivated, inhibited, and aged AChE enzyme, respectively.

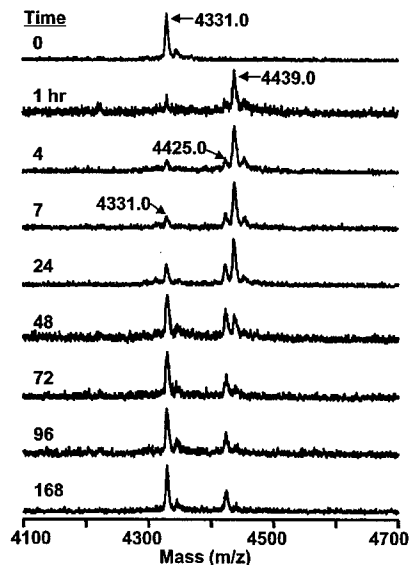


FIGURE 5: OP conjugates of mAChE following inhibition with a molar excess of DDVP, monitored by MALDI-TOF MS. Mass spectra were acquired from samples taken at various times, as indicated, and prepared for analysis by tryptic digestion and reverse-phase fractionation. Inhibition of mAChE by DDVP results in dimethyl phosphorylated enzyme and an increase in molecular mass of the ACP to 4439.0 Da. Aging of the OP-enzyme conjugate is demonstrated by the appearance of the monomethyl phosphoryl ACP adduct (4425.0 Da). Reactivation of the dimethyl phosphoryl mAChE conjugate is evident by the reappearance of unmodified ACP (4331.0 Da).

aging half-time of about 4 h (30, 31). Moreover, spontaneous reactivation of dimethyl phosphoryl enzyme proceeds more

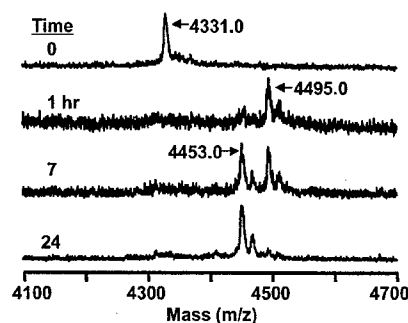


FIGURE 6: ACP and OP adducts of mAChE resulting from treatment with DFP in molar excess. MALDI-TOF mass spectra were acquired from fractionated tryptic peptides prepared from samples taken at time intervals as indicated. DFP-inhibited mAChE and the aged OP-enzyme conjugate are represented by diisopropyl (4495.0 Da) and monoisopropyl (4425.0 Da) phosphoryl-ACP adducts, respectively. mAChE reactivation (unmodified ACP) is not evident, as treatment with a molar excess of DFP results in nearly complete aging of the inhibited enzyme in a 24 h period.

rapidly than aging, and the reappearance of unmodified ACP is evident at early time intervals.

Inhibition of mAChE by DFP leads to the formation of a diisopropyl phosphoryl conjugate with the active center serine and a corresponding ACP adduct with mass of 4495.0 Da (Figure 6). DFP-modified enzyme readily undergoes the aging reaction, as demonstrated by the substantial abundance of the ACP adduct at 7 h with mass of 4453.0 Da, representing the loss of one isopropyl group from the complex. The propensity of the diisopropyl phosphoryl conjugate of mAChE to undergo the aging reaction results in complete monoisopropyl phosphorylated ACP within 24 h, indicating virtually no spontaneous reactivation occurs.

Endogenous mAChE Purified from Brain. Endogenous AChE, purified from the brain tissue of a single mouse, has been resolved by SDS-PAGE (Figure 7, panel A). A protein with an apparent mass of about 68 kDa is evident, with a diffuse banding pattern suggesting that AChE is heterogeneously glycosylated. It migrates with a similar electrophoretic mobility to recombinant mAChE. In crude homogenate from a single mouse brain, on average, the specific abundance (molar ratio) of AChE is 0.5 pmol/mg of total protein, and the total abundance of AChE is about 15 pmol or 1 μ g of protein. Since the molecular mass of mAChE is about 65 kDa, pure enzyme would have a specific abundance of 15 nmol/mg of protein. Therefore, a purification of AChE from mouse brain to near homogeneity would represent an approximate 30000-fold enrichment. The immunoblot in Figure 7 (panel B) shows endogenous AChE samples purified from the brain of a mouse treated with saline or different doses of metrifonate. It is evident that the relative yields of protein from the control and metrifonate-treated mice are similar, indicating that unmodified and phosphorylated AChE purifies with equal efficiency by acridinium affinity chromatography.

Recombinant mAChE was used in control experiments to determine the relative yields of acridinium affinity purification for unmodified AChE and enzyme fully inhibited by OPs. Dimethyl phosphorylated mAChE purified with efficiency similar to that of the unmodified enzyme, while the diethyl phosphorylated enzyme gave a significantly reduced yield. Given that acridinium interacts near the acyl pocket

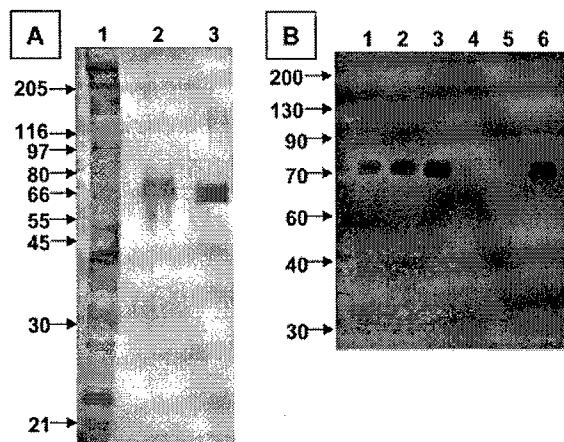


FIGURE 7: Endogenous AChE purified from mouse brain. (A) Silver stain of SDS-polyacrylamide gel electrophoresis. Lanes: 1, enriched membrane extract from mouse brain; 2, endogenous AChE purified from mouse brain as described in the text (the AChE from mouse brain migrates with an apparent molecular mass of approximately 68 kDa); 3, recombinant soluble monomeric mAChE (50 ng). (B) Immunoblot with rabbit anti-mAChE affinity-purified polyclonal antibodies of endogenous AChE purified from the brain of (lane 1) control mouse, (2, 3) mice treated with metrifonate (200 and 400 mg/kg ip), respectively, (4) total AChE knockout mouse, (5) blank, and (6) recombinant mAChE protein (20 pg). The migration of molecular mass markers is indicated by arrows and mass given in kDa.

of the AChE active site, the size of the alkyl group at the phosphorylated serine appears to be a crucial determinant for purification efficiency. The larger diethyl phosphoryl modification likely interferes, by steric hindrance, with acridinium-AChE interactions, where the smaller dimethyl phosphorylated adduct does not. Further, using recombinant mAChE inhibited by DDVP, it was determined that the relative abundances of inhibited, aged, and reactivated species did not progress during the procedures required for purification of endogenous enzyme.

No reactive protein is evident in samples prepared from brain tissue of mouse that is a total knockout for AChE (32), demonstrating high specificity of the purification procedure. Some proteolytic products are seen in AChE from control animals but not in AChE isolated from mice that were treated with OP, a likely indication of proteolysis mediated by serine proteases consequentially inhibited by OP.

Endogenous AChE isolated from mouse brain was trypsinized, fractionated by reverse-phase resin, and resolved by MALDI-TOF mass spectrometry to elucidate the peptide containing the active center serine (Figure 8). Metrifonate spontaneously hydrolyses *in vivo* to DDVP and thereby inhibits AChE through modification of the active center serine to a dimethyl phosphoryl adduct. For control mice, the active center peptides from endogenous brain AChE resolve to the expected mass for unmodified ACP, 4331.0 Da. In mice treated with acute doses of metrifonate, AChE modifications are indicated by the dimethyl and monomethyl phosphoryl ACP adducts, with masses of 4439.0 and 4425.0 Da, respectively. In both the 200 and 400 mg/kg metrifonate treatments, a significant fraction of the phosphorylated AChE enzyme has undergone the aging reaction and is thereby predicted to be irreversibly inhibited. Further, a larger fraction of unmodified ACP is evident in the animal exposed to a lower dose of metrifonate, representing enzyme that may be

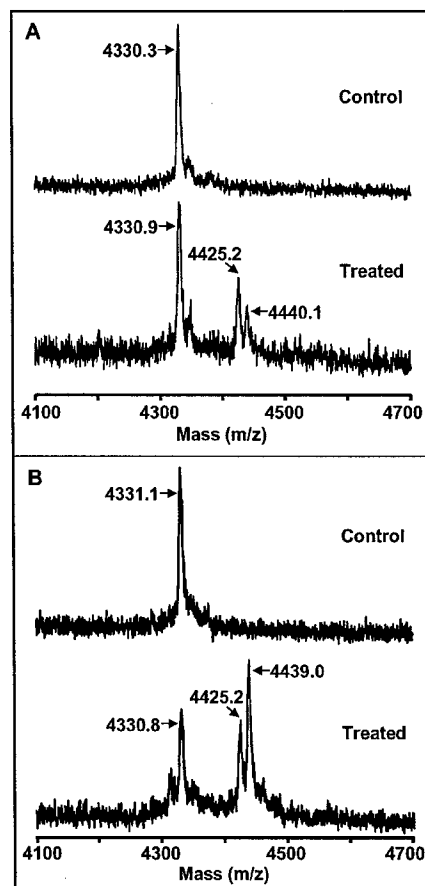


FIGURE 8: Endogenous mouse brain AChE. Mass spectra were acquired from AChE purified from mouse brain, digested with trypsin, and fractionated by reverse-phase resin. (A) Saline-injected control and mouse treated with 200 mg/kg metrifonate. (B) Control and 400 mg/kg metrifonate-treated mouse. Animals were sacrificed 45 min after ip injection. Unmodified ACP (4331.0 Da) of endogenous AChE from control and OP exposed mice is observed. OP-AChE conjugates are observed in metrifonate-treated animals that correspond to inhibited and aged enzyme, dimethyl and monomethyl phosphoryl ACP adducts (4439.0 and 4425.0 Da), respectively. Representative mass spectra from three independent experiments are shown.

uninhibited, spontaneously reactivated, or catalytically inactive.

DISCUSSION

The analysis of trypsinized AChE by MALDI-TOF MS has shown that specific chemical modifications that result from enzyme inhibition mediated by OP compounds can be detected with exquisite sensitivity and their relative abundance determined. It has been generally believed that quantitation of proteins and peptides from ion intensity on mass spectra acquired by MALDI-TOF MS is limited by variability due to sample preparation, inhomogeneous crystallization methods, and a phenomenon referred to as ion suppression (33). We have overcome such limitations by establishing a procedure to acquire mass spectra of the tryptic peptide of AChE containing the active center serine that has proved to be robust and highly reproducible. In multiple experiments conducted with mAChE inhibited by paraoxon, the relative abundances of AChE peptides containing a modified active center serine strongly correlate with the

fractional inhibition of the enzyme, achieving a wide detection range of phosphorylated to nonphosphorylated enzyme.

A comprehensive analysis by mass spectrometry has elucidated distinct chemical modifications of AChE inhibited by OPs that form diisopropyl, diethyl, and dimethyl phosphoryl AChE adducts. A simple fractionation of trypsinized AChE by reverse-phase chromatography gives an enrichment of the peptide containing the active center serine that enhanced the detection sensitivity of the MALDI-TOF MS procedure to subpicomole levels. The relative abundance of phosphoryl AChE conjugates that occur with time following inhibition by OPs has been observed and gives a measure of the propensity of the inhibited enzyme to spontaneously reactivate or undergo the aging process. Mass spectrometric analysis of AChE, as described in this report, allows for the direct observation of the abundance of reactivated enzyme and aged conjugate following inhibition by OPs. This approach offers advantages compared to classical methods that have relied on indirect measures of catalytic activity determined by nucleophilic reactivation of OP-inhibited AChE (30, 31, 34).

The abundance of aged enzyme for DFP-treated mAChE monitored by monoisopropyl phosphoryl adducts at 7 h following inhibition is about 50%, consistent with the aging half-time ($t_{1/2}$) of 6.7 h reported by others for AChE inhibited by DFP (34). For paraoxon-mediated inhibition of AChE, a reactivation $t_{1/2}$ of 83 h (34) and aging $t_{1/2}$ of 31–60 h have been observed (30, 34). In this study, the fractions of reactivated and aged species of mAChE that resolve following treatment with paraoxon are about equal and similarly increase in abundance with time. Since the presence of excess OP and reinhibition would initially suppress observation of reactivated enzyme, and giving consideration to the reported rate constants for the diethyl phosphorylated enzyme, the fraction of aged species should exceed that of reactivated enzyme. Our results suggest that diethyl phosphoryl AChE conjugates may undergo aging at a rate slower than previously determined by nucleophile reactivation studies. The rates of reactivation and aging for dimethyl phosphoryl enzyme conjugates that result from OP-inhibited AChE were recently studied by measuring activity and susceptibility to oxime nucleophiles (31). Spontaneous hydrolysis of the phosphoryl serine bond occurred with a $t_{1/2}$ of 0.7 h. In the presence of excess inhibitor, the $t_{1/2}$ of aging was 4.2 h (31). The relative amounts of reactivated and aged enzyme determined here by mass spectrometric analysis are consistent with these rate constants. The aged enzyme adduct appears early in the time course, when reactivation is masked by reinhibition. As excess inhibitor is depleted, spontaneous hydrolysis predominates, and a large abundance of reactivated enzyme is observed. Concomitantly, a plateau is observed for the fraction of aged enzyme conjugate. The ability to quantitate the complement of OP-AChE adducts and hydrolytic products by MALDI-TOF MS has enabled us to resolve kinetic profiles for the separate processes of inactivation, aging, and reactivation of AChE as an isolated enzyme and demonstrate its potential for exposure detection in intact tissue.

Native AChE purified from brain tissue of mice treated with an acute dose of metrifonate has shown that phosphorylation of endogenous enzyme resulting from OP exposure

can be detected in a single mouse brain. Moreover, the relative abundance of the unmodified enzyme and phosphoryl AChE conjugates evident after treatment with different doses of metrifonate confirms that subtle differences in AChE modifications can be detected. The amount of phosphorylated AChE in the animal exposed to 200 mg/kg (ip) metrifonate is clearly less than for the 400 mg/kg treated mouse. In fact, it is noteworthy that a significant fraction of OP-inhibited AChE in the metrifonate-treated animals is observed as the monomethyl phosphoryl conjugate, corresponding to aged enzyme. The half-time of reactivation and aging for dimethyl phosphorylated human AChE, as determined by *in vitro* studies, is reported as 0.7 and 4.2 h, respectively (31). The relative abundance of aged AChE conjugates within the 45 min time interval of OP exposure in these animals would not have been predicted to occur for the dimethyl phosphorylated enzyme. However, with *in vivo* treatment regimens of OP exposure, it is difficult to estimate the amount of inhibitor available to interact with brain AChE in the treated mice. The presence of excess inhibitor, perhaps sequestered in tissue, would suppress observation of spontaneous reactivation and thereby lead to a progressive accumulation of aged enzyme.

Most of the OP insecticides in current worldwide use form either the dimethyl or diethyl phosphoryl conjugates with AChE. We show here that these conjugates exhibit progressive spontaneous hydrolysis and aging, but at different rates. Since the aged species can no longer be reactivated, either by oxime or spontaneously, and the nonaged species will be susceptible to hydrolysis and subsequent reinhibition, aged species should accumulate with the multiple inactivation–reactivation events occurring upon chronic exposure. Accordingly, the simultaneous measurement of the complement of the three species should provide an indication of the duration of exposure to the OP.

Substantial variability of AChE activity levels in the various tissues of animal species within defined populations has been reported, even among litter mate siblings from inbred mouse colonies (32). With the aim to develop a technology to correlate endogenous AChE inactivation with biological end points, the sensitive detection of the phosphoryl AChE by MALDI-TOF MS provides a direct measure of the covalent modification of enzyme in animals exposed to OPs. This approach of measuring the conjugate directly thereby circumvents the limitations of biological variation when reductions in AChE activity from a range of standard values determined from control animals are monitored.

ACKNOWLEDGMENT

The authors thank Shelley Camp and Dr. Zoran Radić for helpful scientific discussions, Limin Zhang, Michael Marquez, and Brian dela Torre for maintenance of mouse colonies, Limin Zhang for expert assistance with mice OP treatments and tissue dissection, Melissa Zhang, Esther Kim, Cindy Garcia, Sventja von Daake, Annie Li, and Joannie Ho for preparation of purified recombinant mAChE, and Melissa Passino for technical support with some fractional inhibition studies. Dr. Oksana Lockridge of the University of Nebraska Medical Center (Omaha, NE) kindly supplied breeding pairs for the total AChE knockout mice.

REFERENCES

1. Li, Y., Camp, S., Rachinsky, T. L., Getman, D., and Taylor, P. (1991) *J. Biol. Chem.* 266, 23083-23990.
2. Rachinsky, T. L., Camp, S., Li, Y., Ekstrom, T. J., Newton, M., and Taylor, P. (1990) *Neuron* 5, 317-327.
3. Taylor, P. (2001) in *Goodman and Gilman's, the Pharmacological Basis of Therapeutics* (Limbird, L. E., Ed.) pp 175-192, McGraw-Hill, New York.
4. Michel, H. O., Hackley, B. E., Jr., Berkowitz, L., List, G., Hackley, E. B., Gillilan, W., and Pankau, M. (1967) *Arch. Biochem. Biophys.* 121, 29-34.
5. Benschop, H. P., and Keijzer, J. H. (1966) *Biochim. Biophys. Acta* 128, 586.
6. Ordentlich, A., Barak, D., Kronman, C., Benschop, H. P., De Jong, L. P., Ariel, N., Barak, R., Segall, Y., Velan, B., and Shafferman, A. (1999) *Biochemistry* 38, 3055-3066.
7. Segall, Y., Waysbort, D., Barak, D., Ariel, N., Doctor, B. P., Grunwald, J., and Ashani, Y. (1993) *Biochemistry* 32, 13441-13450.
8. Millard, C. B., Kryger, G., Ordentlich, A., Greenblatt, H. M., Harel, M., Raves, M. L., Segall, Y., Barak, D., Shafferman, A., Silman, I., and Sussman, J. L. (1999) *Biochemistry* 38, 7032-7039.
9. Barak, D., Ordentlich, A., Kaplan, D., Barak, R., Mizrahi, D., Kronman, C., Segall, Y., Velan, B., and Shafferman, A. (2000) *Biochemistry* 39, 1156-1161.
10. Barak, R., Ordentlich, A., Barak, D., Fischer, M., Benschop, H. P., De Jong, L. P., Segall, Y., Velan, B., and Shafferman, A. (1997) *FEBS Lett.* 407, 347-352.
11. Elhanany, E., Ordentlich, A., Dgany, O., Kaplan, D., Segall, Y., Barak, R., Velan, B., and Shafferman, A. (2001) *Chem. Res. Toxicol.* 14, 912-918.
12. Doorn, J. A., Gage, D. A., Schall, M., Talley, T. T., Thompson, C. M., and Richardson, R. J. (2000) *Chem. Res. Toxicol.* 13, 1313-1320.
13. Viragh, C., Kovach, I. M., and Pannell, L. (1999) *Biochemistry* 38, 9557-9561.
14. Desiderio, D. M., Wirth, U., Lovelace, J. L., Fridland, G., Umstot, E. S., Nguyen, T. M., Schiller, P. W., Szeto, H. S., and Clapp, J. F. (2000) *J. Mass Spectrom.* 35, 725-733.
15. Hensel, R. R., King, R. C., and Owens, K. G. (1997) *Rapid Commun. Mass Spectrom.* 11, 1785-1793.
16. Tang, X., Sadeghi, M., Olumee, Z., Vertes, A., Braatz, J. A., McIlwain, L. K., and Dreifuss, P. A. (1996) *Anal. Chem.* 68, 3740-3745.
17. Kang, M. J., Tholey, A., and Heinzle, E. (2000) *Rapid Commun. Mass Spectrom.* 14, 1972-1978.
18. Ellman, G. L., Courtney, D., Valentino, A. J., and Featherstone, R. M. (1961) *Biochem. Pharmacol.* 7, 88-95.
19. Vallette, F. M., Marsh, D. J., Muller, F., Massoulie, J., Marcot, B., and Viel, C. (1983) *J. Chromatogr.* 257, 285-296.
20. Mintz, K. P., and Brimijoin, S. (1985) *J. Neurochem.* 44, 225-232.
21. Rakonczay, Z., Mallol, J., Schenk, H., Vincendon, G., and Zanetta, J. P. (1981) *Biochim. Biophys. Acta* 657, 243-256.
22. Reavill, C. A., and Plummer, D. T. (1978) *J. Chromatogr.* 157, 141-151.
23. Son, J. Y., Shin, S., Choi, K. H., and Park, I. K. (2002) *Int. J. Biochem. Cell Biol.* 34, 204-210.
24. Rotundo, R. L. (1984) *J. Biol. Chem.* 259, 13186-13194.
25. Rosenberry, T. L., and Richardson, J. M. (1977) *Biochemistry* 16, 3550-3558.
26. Webb, G., and Clark, D. G. (1978) *Arch. Biochem. Biophys.* 191, 278-288.
27. Marchot, P., Ravelli, R. B., Raves, M. L., Bourne, Y., Vellom, D. C., Kanter, J., Camp, S., Sussman, J. L., and Taylor, P. (1996) *Protein Sci.* 5, 672-679.
28. Bradford, M. M. (1976) *Anal. Biochem.* 72, 248-254.
29. Ordentlich, A., Barak, D., Kronman, C., Ariel, N., Segall, Y., Velan, B., and Shafferman, A. (1996) *J. Biol. Chem.* 271, 11953-11962.
30. Worek, F., Backer, M., Thiermann, H., Szinicz, L., Mast, U., Klimmek, R., and Eyer, P. (1997) *Hum. Exp. Toxicol.* 16, 466-472.
31. Worek, F., Diepold, C., and Eyer, P. (1999) *Arch. Toxicol.* 73, 7-14.
32. Xie, W., Stribley, J. A., Chatonnet, A., Wilder, P. J., Rizzino, A., McComb, R. D., Taylor, P., Hinrichs, S. H., and Lockridge, O. (2000) *J. Pharmacol. Exp. Ther.* 293, 896-902.
33. Sechi, S., and Oda, Y. (2003) *Curr. Opin. Chem. Biol.* 7, 70-77.
34. Aldridge, W. N., and Reiner, E. (1972) *Enzyme inhibitors as substrates. Interactions of esterases with esters of organophosphorus and carbamic acids*, American Elsevier, New York.

BI034756X



Acetylcholinesterase (AChE) gene modification in transgenic animals: Functional consequences of selected exon and regulatory region deletion

Shelley Camp^{a,*}, Limin Zhang^a, Michael Marquez^a, Brian de la Torre^a,
Jeffery M. Long^{a,b}, Goran Bucht^{a,1}, Palmer Taylor^a

^a University of California, San Diego, 9500 Gilman Dr. Department of Pharmacology, La Jolla, CA 92093-0636, USA

^b Department of Pediatrics, University of California, SD 92093-0627, USA

Abstract

AChE is an alternatively spliced gene. Exons 2, 3 and 4 are invariantly spliced, and this sequence is responsible for catalytic function. The 3' alternatively spliced exons, 5 and 6, are responsible for AChE disposition in tissue [J. Massoulie, The origin of the molecular diversity and functional anchoring of cholinesterases. *Neurosignals* 11 (3) (2002) 130–143; Y. Li, S. Camp, P. Taylor, Tissue-specific expression and alternative mRNA processing of the mammalian acetylcholinesterase gene. *J. Biol. Chem.* 268 (8) (1993) 5790–5797]. The splice to exon 5 produces the GPI anchored form of AChE found in the hematopoietic system, whereas the splice to exon 6 produces a sequence that binds to the structural subunits PRiMA and ColQ, producing AChE expression in brain and muscle. A third alternative RNA species is present that is not spliced at the 3' end; the intron 3' of exon 4 is used as coding sequence and produces the read-through, unanchored form of AChE.

In order to further understand the role of alternative splicing in the expression of the AChE gene, we have used homologous recombination in stem cells to produce gene specific deletions in mice. Alternatively and together exon 5 and exon 6 were deleted. A cassette containing the neomycin gene flanked by loxP sites was used to replace the exon(s) of interest. Tissue analysis of mice with exon 5 deleted and the neomycin cassette retained showed very low levels of AChE expression, far less than would have been anticipated. Only the read-through species of the enzyme was produced; clearly the inclusion of the selection cassette disrupted splicing of exon 4 to exon 6. The selection cassette was then deleted in exon 5, exon 6 and exons 5 + 6 deleted mice by breeding to Ella-cre transgenic mice. AChE expression in serum, brain and muscle has been analyzed.

Another AChE gene targeted mouse strain involving a region in the first intron, found to be critical for AChE expression in muscle cells [S. Camp, L. Zhang, M. Marquez, B. delaTorre, P. Taylor, Knockout mice with deletions of alternatively spliced exons of Acetylcholinesterase, in: N.C. Inestrosa, E.O. Campus (Eds.), VII International Meeting on Cholinesterases, Pucon-Chile Cholinesterases in the Second Millennium: Biomolecular and Pathological Aspects. P. Universidad Catolica de Chile-FONDAP Biomedicina, 2004, pp. 43–48; R.Y.Y. Chan, C. Boudreau-Larivière, L.A. Angus, F. Mankal, B.J. Jasmin, An intronic enhancer containing an N-box motif is required for synapse- and tissue-specific expression of the acetylcholinesterase gene in skeletal muscle fibers. *Proc. Natl. Acad. Sci. USA* 96 (1999) 4627–4632], is also presented. The intronic region was floxed and then deleted by mating with Ella-cre transgenic mice. The deletion of this region produced a dramatic phenotype; a mouse with near normal AChE expression in brain and other CNS tissues, but no AChE expression in muscle. Phenotype and AChE tissue activities are compared with the total AChE knockout mouse [W. Xie, J.A. Chatonnet, P.J. Wilder, A. Rizzino, R.D. McComb, P. Taylor,

* Corresponding author. Tel.: +1 858 534 1367; fax: +1 858 534 8248.

E-mail address: scamp@ucsd.edu (S. Camp).

¹ Present address: Department of Medical Countermeasures, Division on NBC Defence, Swedish Defence Research Agency, S-901 82 Umeå Sweden.

S.H. Hinrichs, O. Lockridge, Postnatal developmental delay and supersensitivity to organophosphate in gene-targeted mice lacking acetylcholinesterase. *J. Pharmacol. Exp. Ther.* 293 (3) (2000) 896–902].
© 2005 Elsevier Ireland Ltd. All rights reserved.

Keywords: AChE gene; Alternative splicing; Intron; Regulatory region; Knockout mouse

1. Introduction

The AChE gene, while quite compact in length (the coding region of the mouse gene is covered in 8.5 kb of genomic sequence) encodes multiple gene products through alternative splicing. The catalytic domain, produced by the invariantly spliced exons 2, 3, and 4 is expressed in specific locations throughout the body as dictated by alternative splicing. The use of exon 5 produces a glycosylphosphatidylinositol (GPI) anchor that is used in the hematopoietic system, expressing AChE activity on platelets and erythrocytes. Splicing to exon 6 produces an AChE C-terminal or “T” sequence that yields AChE that is widely distributed, notably in brain and muscle, but also in other tissues. This C-terminal sequence gives rise to the expression of amphiphilic monomers, dimers and tetramers (G1a, G2a, G4a); soluble tetramers (G4na); as well as asymmetric monomers, dimers and tetramers that attach to collagen subunits via the ColQ subunit. The third alternative at the 3′ end of the AChE gene is actually not a splice but the production of an RNA species that retains the intron found 3′ of exon 4. Expression of this form of AChE *in vivo* and its presence in tissue is not well characterized.

Although there are alternative acceptors in the 3′ end of the AChE gene, the only documented donor site is defined by the 3′ end of exon 4. The exon 4/5 spliced message includes exon 6 as 3′ UTR [2]; similarly the retained intron message most likely includes exons 5 and 6 as UTR, but due to the rare expression of this form of RNA, the message has not been completely defined.

Our purpose in the production of these knockout mice is to establish the functional importance of the various spliced AChE forms in the intact animal; this begins with determining the severity of a phenotype produced by the deletion of a selected exon or pair of exons. Such deletions would reveal the consequences of altered disposition or the absence of AChE in particular tissues.

Many studies of the regulation of AChE production have been done in mouse muscle cell lines where myoblasts that do not produce AChE activity or message can be compared with differentiated myotubes in which both protein and RNA are found [4]. Following

transfection of the whole AChE gene into myoblasts and subsequent differentiation, the enhanced AChE activity from the transfected gene is found to mirror endogenous activity. When introns are deleted from the gene, differentiated activity is altered; the most severe reduction is seen with the deletion of the intron between exons 1 and 2. In fact the deletion of a 255 bp region ablates AChE activity (and message) in differentiated C2C12 cells [6]. Since the intron between exons 1 and 2 appears to control expression in C2C12 cells, we questioned whether the regulatory region is required in generalized AChE expression or only selectively in muscle expression. We have developed a mouse in which this essential region of the gene is flanked by loxP sites, and can therefore be deleted from the genome in a tissue or developmental stage specific manner.

2. Materials and methods

2.1. Basic molecular biology techniques

Basic molecular biology techniques were used in the construction of plasmids for gene targeting. Constructs and screening for the exon deletions, Del E5, Del E5 + 6 and Del E6 have been described [3]. Most importantly, all mouse genomic DNA used was from the strain 129 SvJ to ensure identity with the stem cells to be transfected. DNA used in constructs either came from a 129 SvJ library (Incyte Genomics, clone address 341/C04, BAC Mouse ES Rel II) or was amplified by PCR from 129SvJ stem cells. The selection cassette (loxP/neomycin/loxP) used in the exon specific deletions came from Dr. Goran Bucht, that used in the intron regulatory region deletion (loxP/neomycin, thymidine kinase /loxP) came from a pFlox vector provided by Dr. Marth [7]. In all constructs pBluescript (KS and SK from Stratagene) served as the vector backbone and provided the means for bacterial amplification. Site directed mutagenesis used to alter the mouse gene employed QuikChange® II Site-Directed Mutagenesis from Stratagene.

2.2. Location of sequences in the AChE gene

Numbering used to locate sequences in the AChE gene is that of Wilson et al. [8] in GenBank accession

number AF312033. AChE exon 1 begins at 7511 and the second poly-adenylation signal used in the AChE message is at 14909.

2.3. Principles of gene targeting

The basic concepts of gene targeting, including the use of site-specific recombination systems, are well described in [9].

2.4. AChE knockout nomenclature

AChE del E5 (or E5+6)/Neo: The named exon is deleted, the neomycin selection cassette is retained. AChE del E5 (or E6, or E5+6): The named exon is deleted, the neomycin cassette is deleted through the expression of Cre-recombinase. AChE-RR refers to the intron regulatory region. Floxed denotes that the 255 bp region of the intron has been flanked by loxP sites (AChE-RR (floxed)). The floxed intron regulatory region was then deleted by mating to an Ella-cre transgenic mouse, producing an independent mouse colony, AChE-RR (deleted). Floxed and deleted null (–/–) mice are compared independently with their wild-type and heterozygous littermates for the purpose of this study.

All mice are currently of a mixed background (129, C57Bl/6, Black Swiss and FVB strains). We continue breeding toward pure-strain C57Bl/6 for more accurate comparisons.

2.5. Tissue AChE activity

All tissue activities are expressed as Units AChE activity/gram of tissue. AChE was extracted from tissue by powdering the tissue in a stainless steel mortar and pestle at liquid nitrogen temperatures and then homogenizing the powder, on ice, in [0.01 M sodium phosphate buffer, pH 7.0, with 1.1 M NaCl, 0.1 M EGTA, and 0.5% Tween 20]. 5 µg/ml Pepstatin A, 5 µg/ml Leupeptin, 5 µg/ml Aprotinin, 10 µg/ml Bacitracin, 0.1 mM Benzamidase were added to prevent proteolysis. Muscle was homogenized in 25 volumes of buffer, brain in 10 volumes. Homogenates were spun at 12 k × g for 10 min and the supernatant was assayed for activity. Serum activity was determined by collecting blood and allowing it to clot at room temperature. The clot was then left to contract overnight at 4 °C producing a serum layer. Serum activity is expressed as Units/ml serum. AChE activity was determined according to Ellman [10] with acetylthiocholine iodide at 0.5 mM. Ethopropazine (10 µM) was used to inhibit butyrylcholinesterase (BuChE) in all assays.

2.6. Behavioral analysis

The behavioral test battery described in [11,12] was modified to account for the muscle tremors displayed by the exon 5+6 deleted mice. Many standard tests were impossible to interpret reliably because of these tremors. All statistical analyses of behavioral data were performed using a Student's *t*-test.

2.7. Statistics

Calculation of standard deviation and *t*-tests used to assess significant differences were performed using GraphPad Prism version 3.0 for Windows, GraphPad Software, San Diego California USA, www.graphpad.com.

2.8. Production of the mice

2.8.1. Exon deleted mice

The knockout mice were made using targeted homologous recombination. The knockout regions are shown in Fig. 1. Panel A represents the wild-type gene. In all knockouts the in-frame stop codon, located in the intron between exons 4 and 5, was left intact to allow expression of read-through AChE. Hence, AChE lacking the capacity to oligomerize and associate with membranes should be expressed. We have developed three independent knockout mouse strains with deletions in the alternatively spliced 3' end of the AChE gene (1B, 1C, and 1D); all were developed as shown in Fig. 2.

The wild-type gene (Fig. 2A) was modified by site directed mutagenesis (Fig. 2B) to include Cla I restriction enzyme sites flanking the region to be deleted. (The same 5' sites were used to make the exon 5 and exons 5+6 deletions whereas the same 3' sites were used to make the exon 6 and exons 5+6 deletions). The deleted region was replaced by a cassette, 2.1 kb in length, that included the neomycin gene flanked by loxP sites (Fig. 2C). This altered AChE gene containing wild-type AChE gene sequence of 4 kb on the 5' end and 6 kb on the 3' end was propagated in pBluescript.

The exon deletion constructs were linearized at a unique restriction site in the vector and electroporated into 129SvJ stem cells. Stem cells were exposed to G418 and the surviving colonies were screened for homologous recombination by Southern blotting using a probe from a region outside the homologous arms of the transfected construct. The selected cells were then injected into blastocysts (C57Bl/6) and implanted in a foster

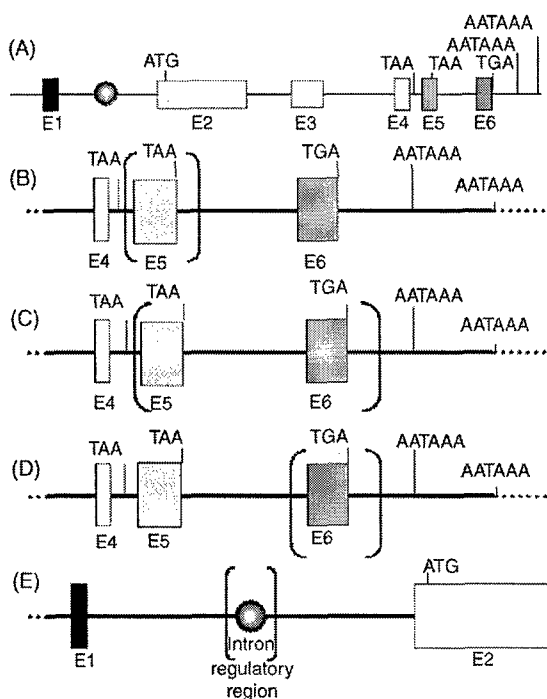


Fig. 1. Location of deletions in the AChE gene. Rectangles represent exons, a circle represents the intron regulatory region, and brackets mark deletions. (A) Wild-type AChE gene, showing introns, translational stop signals, polyadenylation signals and exons 1–6. (B) Delete exon 5, 153 bp deletion (12710–12863). (C) Delete exons 5 and 6, 853 bp deletion (12710–13562). (D) Delete exon 6, 255 bp deletion (13307–13562). (E) Flox or delete intron regulatory region, 255 bp floxed or deleted, (8181–8438).

mouse mother. Chimeric pups were bred to black mice at maturity and agouti pups from the resulting litters were screened by PCR for the presence of the altered AChE gene. Heterozygous mice were then bred to produce homozygotes.

To eliminate the possible influence of the neomycin gene insert on overall expression and splicing, heterozygous animals were bred with transgenic Ella-cre mice (a kind gift from Anthony Wynshaw-Boris, [13]). Ella-cre mice carry the bacterial Cre-recombinase gene driven by the viral Ella promoter. Production of Cre-recombinase is turned on at fertilization, and the loxP flanked sequence is thus permanently deleted during very early embryogenesis. Pups from matings of AChE del E5/Neo \times Ella-cre, AChE del E5+6/Neo \times Ella-cre and AChE del E6 \times Ella-cre were screened by PCR for the presence and absence of wild-type, exon deleted/Neo containing, exon deleted/Neo deleted, and Cre-recombinase sequences. Mouse strains AChE del E5, AChE del E6, and AChE del E5+6 were then established by inbreeding the heterozygous exon deleted, Neo deleted mice.

2.8.2. Intron regulatory region floxed and deleted mice

The steps to the construction of the mouse with a floxed (flanked by loxP sites) intron regulatory region (bp 8183–8438 [8]) in the AChE intron between exons 1 and 2 are shown in Fig. 3. The construct that was transfected into the mouse stem cells contained 3 loxP sites. The floxed regulatory region and the floxed selection cassette shared a common central loxP site. The construct shown in Fig. 3B was electroporated into stem cells and those cells that survived exposure to G418 were screened for homologous recombination of the gene construct in place of the wild-type gene. This screening employed a Southern blot probe outside of the region included in the construct. Selected cells showed an equal intensity of wild-type and altered alleles. After karyotyping to insure chromosomal integrity, stem cells were electroporated with a plasmid that expressed Cre-recombinase and selected using the negative selectable marker thymidine kinase. Colonies surviving exposure to gancyclovir were analyzed by PCR, sequencing, and Southern blotting to find cells that retained the floxed regulatory region while having the selection cassette deleted. The steps from blastocyst implantation to the birth of chimeric mice paralleled that of the mice with exon deletions.

AChE expression in serum, brain, and muscle from the floxed intron regulatory region mice when compared with that from wild-type littermates was not significantly different by unpaired *t*-test (data not shown). The first test of the floxed intron regulatory mouse was mating with an Ella-cre mouse to see the effect of the deletion of the regulatory region from conception.

3. Results

3.1. Phenotype

Null mice (AChE del E5/Neo and AChE del E5+6/Neo) with a retained neomycin gene, when compared with their wild-type littermates, revealed several obvious differences. The homozygous knockout mice are smaller and weaker than their littermates. They also vocalize with audible chirping where their wild-type littermates do not. The AChE del E5+6/Neo deleted mice were tested extensively and found to be severely impaired in four measures of muscle strength (wire hang, cage top hang, grip strength and pole test), and did not perform well in two measures of balance and coordination (rotorod and balance beam). These mice also performed poorly in a test of physical exertion (tread mill). The exon deleted, neomycin gene retained animals also seem to be

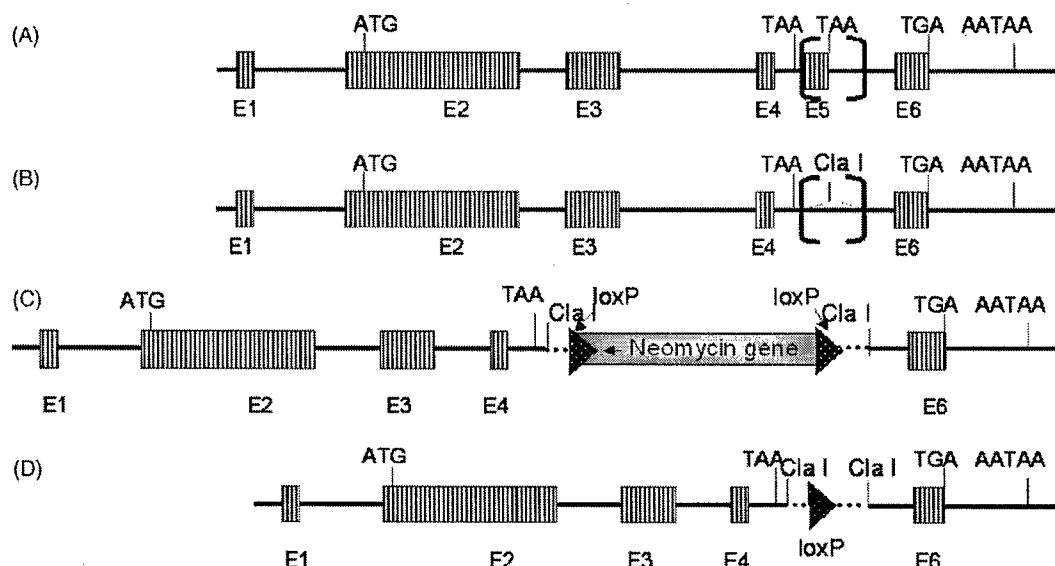


Fig. 2. Construction of alternatively spliced exon deletions. Boxes represent exons, triangles are loxP sites, and brackets mark the deletion. The deletion of exon 5 is used as an example. (A) Wild-type gene with region to be deleted in brackets. (B) Exon 5 deleted, replaced by a single, unique Cla I site. (C) Neomycin gene used for selection of transfected stem cells, flanked by loxP sites, is inserted in the introduced Cla I site. (D) Through the action of Cre-recombinase the neomycin gene can be removed, the disruption of the AChE gene is reduced to a single loxP site and the surrounding sequences used in cloning.

more prone to seizures than their wild-type or heterozygous littermates (unpublished observations). Mice with the retained neomycin gene do not seem to be able to raise viable pups.

The phenotype of the AChE del E5 + 6, neomycin deleted mouse shows some physical improvement over the neomycin gene retained animals. Although the mice still perform poorly in feats of strength (wire hang, cage-

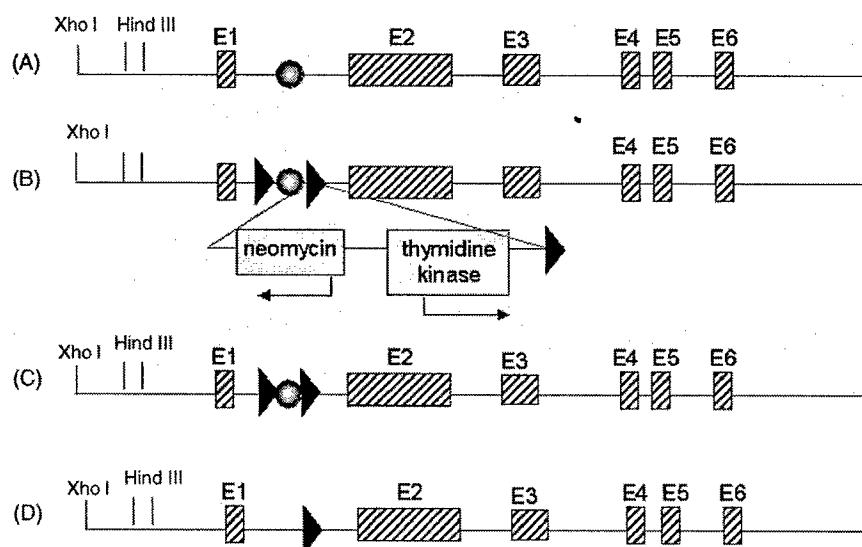


Fig. 3. Steps to a floxed and deleted intron regulatory region. Approximately 9 kb of genomic sequence is shown. AChE exons are shown as diagonally striped boxes, the critical 255 bp intron regulatory region is shown as a circle, loxP sites are represented by triangles. (A) The wild-type AChE gene. (B) Stem cell DNA after homologous recombination. The regulatory region is now flanked by loxP sites as is the neomycin/thymidine kinase selection cassette. (C) Stem cell DNA after Cre-recombinase transfection and southern blot selection for partial deletion by Cre-recombinase. Deletion of the selection cassette with retention of the floxed AChE regulatory region is shown. Stem cells were used for injection into blastocysts at this stage, and chimeric mice were screened for germline transmission of the altered allele. Heterozygous floxed mice, AChE-RR (floxed), were then bred to homozygosity. (D) The regulatory region is deleted by mating AChE-RR (floxed) mice with Ella-cre mice to delete the intron regulatory region at fertilization.

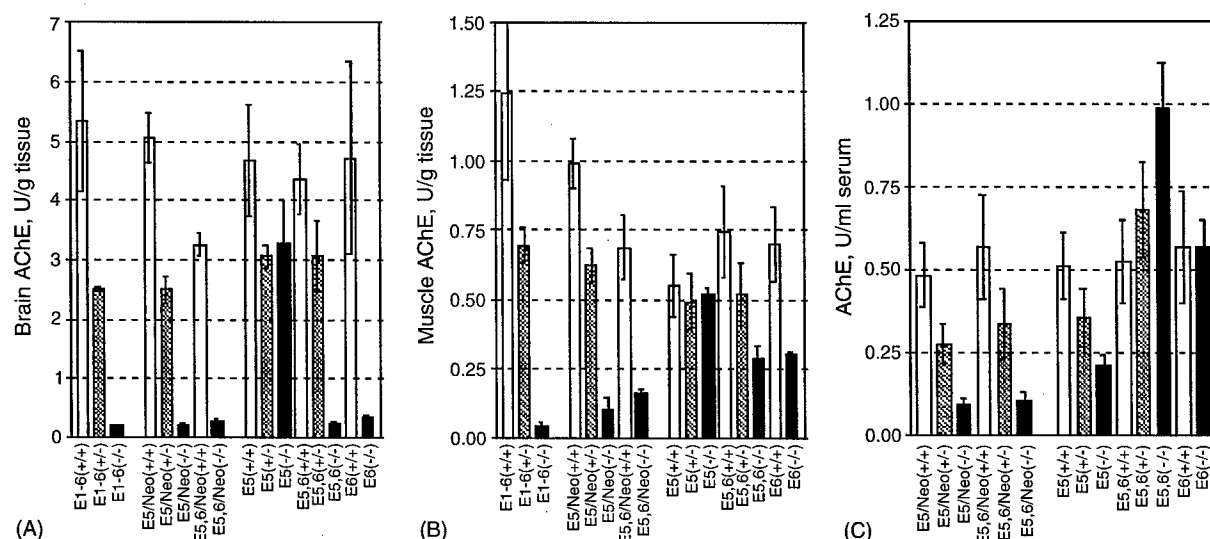


Fig. 4. Knockout mouse AChE activity in serum, brain and muscle. AChE activity in wild-type (open bars), heterozygous (striped bars) and homozygous (black bars) knockout mice from each colony. (E1–6) is the total AChE knockout from O. Lockridge [5]. (E5/Neo) and (E5, 6/Neo): exon deleted, neomycin cassette retained colonies. (E5), (E5, 6) and (E6): exon and neomycin deleted colonies. Bars represent the average AChE activity from at least three mice; error bars are standard deviations. Values from wild-type mice are included to emphasize the variation between inbred, mixed strain mice. (A) Brain. (B) Muscle. (C) Serum.

top hang, grip strength and pole test), their performance on the tread mill and rotorod was not detectably impaired when compared with wild-type littermates.

3.2. Distribution of AChE activity

Initial results showing AChE activity from the Neo retained and Cre deleted altered AChE mouse genes are shown in Fig. 4. Brain (Fig. 4A) and muscle (Fig. 4B) AChE activities are compared with the total AChE knockout. The charts show comparisons between wild-type, heterozygous and homozygous animals from the same colony. Large variations in AChE activity from animal to animal exist even in the wild-type controls, likely due to the mixed genetic background of the mice.

An outstanding feature in all three tissues is the extremely low amounts of AChE produced by animals with the retained neomycin insert. AChE values are much lower than one would have anticipated, especially with the AChE del E5/Neo animal. Because exon 6 and its splice acceptor were left intact, we anticipated splicing of exons 1, 2, 3, 4 and 6 to give activity in brain and muscle. There is little difference, in fact, between the AChE values for the AChE del E5/Neo and AChE del E5 + 6/Neo animals.

When the inserted neomycin gene is deleted from the genome of the knockout animal, a return of AChE activity is seen. This is quite dramatic with the exon 5 deleted animal. AChE in brain and muscle is now not significantly different from that of wild-type littermates.

Serum AChE (Fig. 4C) stays depressed although the exon 5 spliced GPI anchored AChE forms are thought to be associated with the hematopoietic system [1]. If one looks at serum AChE on sucrose density gradients in both Triton X-100 and Brij-96 (summary in Table 1) one sees two peaks, the major peak is a monomer that runs at 3S and the minor peak runs at 11S. Neither peak shifts to a lower S value in Brij-96 indicating that neither species has an exposed region of hydrophobic residues that could associate with the detergent.

Serum from the exon 5 + 6 deleted mouse without the neomycin insert is interesting in that the amount of AChE activity nearly doubles over that of the wild-type mouse. This AChE runs as a single peak at 3S, characteristic of a monomer (Table 1). One expects to see monomeric, read through AChE as no other splice options are available.

The deletion of the intron regulatory region produced most intriguing results. We first tested tissue and blood

Table 1
Sucrose density gradient analysis of serum AChE

	Triton X-100	Brij-96
Wild-type	3.5S, 11S	4S, 10.5S
Delete Exon 5	3S, 11S	4S, 11S
Delete Exons 5 + 6	4S	4.5S

Sedimentation coefficients of major peaks are shown. Serum samples were run on 3–20% sucrose density gradients (in the buffer described under ‘tissue activity’ in the methods section) in the presence of either Triton X-100 or Brij-96. Gradients were spun for 18–20 h at 40,000 rpm in an SW 41-Ti rotor (Beckman Coulter) at 4 °C.

from the floxed (AChE-RR(floxed)) mouse and found AChE levels to be not significantly different from those of wild-type littermates. When the intron region was deleted from the genome (AChE-RR (del)), results are quite dramatic; AChE activity in muscle is drastically reduced, but brain activity is near normal. Serum AChE is also severely reduced in the intron deleted mice. When this serum is run on a sucrose density gradient and AChE activity is measured, there is a very small peak at 3S (data not shown).

4. Discussion

The construction and analysis of a complement of knockout mouse strains have added a new dimension to the analysis of gene deletions in cultured cells. Some of the findings are predictable, while others reveal new complexities that surround the regulation of AChE gene expression.

The most prevalent spliced form of the AChE message is the joining of exons 1, 2, 3, 4, and 6. The protein encoded by this message is found predominantly in brain and muscle. It seems that the deletion of exon 6 ablates activity in brain, but muscle retains about 40% of normal activity. The deletion of both exons 5 and 6 together causes an identical reduction, so it is probable that there is default production of read-through AChE in the absence of exon 6 rather than production of the GPI anchored form. Sedimentation analysis of AChE from muscle extracts should confirm the splice choice. The phenomenon of altering the default splice in muscle has been studied extensively in C2C12 cells [14] and it is possible to change the absolute splice to exon 6. The AChE activity differences between brain and muscle are also interesting in terms of AChE regulation. It will be important to look at relative message levels in both tissues to determine whether this muscle/brain difference comes at the level of translation, message production, or protein turnover in different tissues.

One would have expected that AChE in the brain and muscle of the AChE del E5/Neo knockout would be near normal, as it is the exon 6 spliced sequence that is primarily expressed in these tissues [15]. The consequences of the inclusion of the 2.1 kb neomycin cassette are dramatic; although alternatively spliced exon 6 with all its cis-acting splice consensus sequences intact is available and the tissue is producing the correct trans-acting factors, the architectural modification of the unspliced message prevents the splice to exon 6.

If the neomycin insert replaces the deletion of exons 5 and 6, AChE expression in brain, muscle and serum is virtually abolished. When the neomycin sequence is

deleted, AChE levels in muscle increase very slightly and serum levels increase more markedly; the animals, although they are still weak, show improved physical performance on the rotorod and treadmill. A small increase in AChE production helps mitigate the severely compromised phenotype.

Preliminary studies of RNA in muscle and brain by RT-PCR show that the Neo retained knockouts are making message that includes the neomycin gene and that this RNA is stable (data not shown). In contrast to the intron deletion knockout where no RNA is found [6], the loss of AChE expression in the neomycin gene containing AChE exon deleted knockouts is likely not a consequence of diminished transcription or altered RNA stability.

Examination of serum from the knockout animals has provided some surprising results. Knockout mice with exon 5 deleted have ~40% of the wild-type level of AChE, exon 6 deleted animals produce normal levels of AChE, but when both exons 5 and 6 are deleted the knockout homozygote produces double the normal amount of serum AChE. Sucrose density gradient analysis of serum from these animals shows that except for the small amount of soluble tetramer seen in wild-type and exon 5 deleted animals, the major AChE species is a monomer. This monomer does not shift in the presence of Brij 96; it does not bind detergent, and appears to be identical in knockout and in wild-type mice. Indeed it seems that the read-through species of AChE is expressed in the wild-type mouse and it can be found in serum. It will be interesting to search for the origin of its production and synthesis. Why the exon 5 + 6 deleted animal produces twice as much AChE in serum as the wild-type animal is a phenomenon that bears further investigation. Perhaps this up-regulation of AChE will help elucidate control or feedback mechanisms found in the intact animal.

The 11S peak is missing in serum from the exon 5 + 6 deleted mouse. This allows us to assign the 11S species the title of soluble tetramer, (G4na) a gene product of the splice to exon 6, confirming the structures shown by Massoulie et al. [16].

Acknowledgements

This work was supported by research grants to P.T. from the NIH (GM18360-33), NIEHS (ES10337-04), and the US Army Medical Defense Command (DAMD17-02-2-0025). We thank Dr. J. Marth for supplying the plasmid used in the construction of the intron regulatory region mouse. We very much appreciate the support of Drs. Anthony Wynshaw-Boris and Oksana Lockridge, their advice and encouragement

throughout this project has been invaluable. Thanks and kudos to Ella Kothari and the UCSD Transgenic Core (<http://cancer.ucsd.edu/tgm>) who electroporated and maintained the embryonic stem cells as well as successfully conducting the blastocyst injections and implantations that resulted in the birth of the knockout chimera.

References

- [1] J. Massoulie, The origin of the molecular diversity and functional anchoring of cholinesterases, *Neurosignals* 11 (3) (2002) 130–143.
- [2] Y. Li, S. Camp, P. Taylor, Tissue-specific expression and alternative mRNA processing of the mammalian acetylcholinesterase gene, *J. Biol. Chem.* 268 (8) (1993) 5790–5797.
- [3] S. Camp, L. Zhang, M. Marquez, B. delaTorre, P. Taylor, Knockout mice with deletions of alternatively spliced exons of Acetylcholinesterase, in: N.C. Inestrosa, E.O. Campus (Eds.), VII International Meeting on Cholinesterases, Pucon-Chile Cholinesterases in the Second Millennium: Biomolecular and Pathological Aspects, P. Universidad Catolica de Chile-FONDAP Biomedicina, 2004, pp. 43–48.
- [4] R.Y.Y. Chan, C. Boudreau-Larivière, L.A. Angus, F. Mankal, B.J. Jasmin, An intronic enhancer containing an N-box motif is required for synapse- and tissue-specific expression of the acetylcholinesterase gene in skeletal muscle fibers, *Proc. Natl. Acad. Sci. USA* 96 (1999) 4627–4632.
- [5] W. Xie, J.A. Chatonnet, P.J. Wilder, A. Rizzino, R.D. McComb, P. Taylor, S.H. Hinrichs, O. Lockridge, Postnatal developmental delay and supersensitivity to organophosphate in gene-targeted mice lacking acetylcholinesterase, *J. Pharmacol. Exp. Ther.* 293 (3) (2000) 896–902.
- [6] S. Camp, P. Taylor, Intronic elements appear essential for the differentiation-specific expression of acetylcholinesterase in C2C12 myotubes, in: B.P. Doctor, P. Taylor, D.M. Quinn, R.L. Rotundo, M.K. Gentry (Eds.), *Structure and Function of Cholinesterases and Related Proteins*, Plenum Press, New York, 1998, pp. 51–55.
- [7] D. Chui, M. Oh-Eda, Y.F. Liao, K. Panneerselvam, A. Lal, K.W. Marek, H.H. Freeze, K.W. Moremen, M.N. Fukuda, J.D. Marth, Alpha-mannosidase-II deficiency results in dyserythropoiesis and unveils an alternate pathway in oligosaccharide biosynthesis, *Cell* 90 (1997) 157–167.
- [8] M.D. Wilson, C. Riemer, D.W. Martindale, P. Schnupf, A.P. Boright, T.L. Cheung, D.M. Hardy, S. Schwartz, S.W. Scherer, L.C. Tsui, W. Miller, B.F. Koop, Comparative analysis of the gene-dense ACHE/TFR2 region on human chromosome 7q22 with the orthologous region on mouse chromosome 5, *Nucleic. Acids Res.* 29 (6) (2001) 1352–1365.
- [9] A.L. Joyner (Ed.), *Gene Targeting A Practical Approach*, second ed., Oxford University Press Inc, New York, 2000.
- [10] G.L. Ellman, K.D. Courtney, V. Andres Jr., R.M. Featherstone, A new and rapid colorimetric determination of acetylcholinesterase activity, *Biochem. Pharmacol.* 7 (1961) 88–95.
- [11] J.C. Corbo, T.A. Deuel, J.M. Long, P. LaPorte, E. Tsai, A. Wynshaw-Boris, C.A. Walsh, Doublecortin is required in mice for lamination of the hippocampus but not the neocortex, *J. Neurosci.* 22 (17) (2002) 7548–7557.
- [12] K.L. McIlwain, M.Y. Merriweather, L.A. Yuva-Paylor, R. Paylor, The use of behavioral test batteries: effects of training history, *Physiol. Behav.* 73 (5) (2001) 705–717.
- [13] X. Xu, C. Li, L. Garrett-Beal, D. Larson, A. Wynshaw-Boris, C.X. Deng, Direct removal in the mouse of a floxed neo gene from a three-loxP conditional knockout allele by two novel approaches, *Genesis* 30 (2001) 1–6.
- [14] Z.D. Luo, S. Camp, A. Muter, P. Taylor, Splicing of 5' introns dictates alternative splice selection of acetylcholinesterase pre-mRNA and specific expression during myogenesis, *J. Biol. Chem.* 273 (43) (1998) 28486–28495.
- [15] C. Legay, Why so many forms of acetylcholinesterase? *Microsc. Res. Tech.* 49 (1) (2000) 56–72.
- [16] J. Massoulie, S. Belbeoch, N. Perrier, S. Bon, Molecular organization and functional localization of acetylcholinesterase, in: N.C. Inestrosa, E.O. Campus (Eds.), VII International Meeting on Cholinesterases, Pucon-Chile Cholinesterases in the Second Millennium: Biomolecular and Pathological Aspects, P. Universidad Catolica de Chile-FONDAP Biomedicina, 2004, pp. 1–5.

Click Chemistry In Situ: Acetylcholinesterase as a Reaction Vessel for the Selective Assembly of a Femtomolar Inhibitor from an Array of Building Blocks**

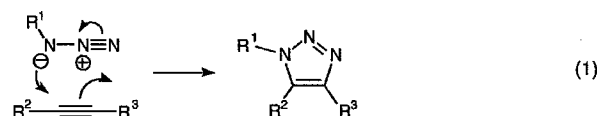
Warren G. Lewis, Luke G. Green, Flavio Grynszpan, Zoran Radić, Paul R. Carlier, Palmer Taylor, M. G. Finn,* and K. Barry Sharpless*

The generation and/or optimization of lead compounds by combinatorial methods has become widely accepted in medicinal chemistry, and is the subject of continued improvement.^[1–3] However, most combinatorial strategies remain dependent upon iterative cycles of synthesis and screening. The direct involvement of the target, usually a receptor or enzyme, in the selection, evolution, and screening of drug candidates can accelerate the discovery process by short-circuiting its traditionally stepwise nature.^[4–11]

The use of an enzyme target to select building blocks and synthesize its own inhibitor is a relatively unexplored option. This approach depends on the simultaneous binding of two ligands, decorated with complementary reactive groups, to adjacent sites on the protein; their co-localization is then likely to accelerate the reaction that connects them.^[12] When the catalysis of such bond formation is blocked by product inhibition, the higher affinity products^[12–14] then serve as lead compounds. This and similar approaches that have been adopted by a number of investigators employ one of five types

of connecting reactions: formation of hydrazone or Schiff base adducts, disulfide bond formation, alkylation of free thiols or amines, epoxide ring-opening, or olefin metathesis.^[5, 6, 8, 11, 15–19] Most closely related to the work described herein is the generation of carbonic anhydrase inhibitors by using the S_N2 reaction of a thiol with an α -chloroketone in the presence of the enzyme target.^[16]

Most of the above strategies share the limitation that the reactive groups on the ligand probes (building blocks), being either electrophiles or nucleophiles, are likely to react in undesired ways within biochemical systems. An alternative is offered by the “cream of the crop” among “click reactions”^[20]—the Huisgen 1,3-dipolar cycloaddition of azides and acetylenes to give 1,2,3-triazoles [Eq. (1)].^[21–23] This water-



tolerant reaction employs functional groups that are generally compatible with enzymes under physiological conditions^[24, 25] and are readily incorporated into diverse organic building blocks. Its dependence on the enforced propinquity and proper alignment of the reactants, which gives rise to large negative values of ΔS^\ddagger , makes it ideal for the purpose at hand. Mock and co-workers established that the rate and regioselectivity of the azide–alkyne cycloaddition can be dramatically enhanced by sequestering the two components inside a host structure.^[26–29] Their results with cucurbituril ($M_w = 997$ Da) as the catalyst in water bear an uncanny resemblance to those reported here for reaction inside a protein host.

We selected the enzyme acetylcholinesterase (AChE), which plays a key role in neurotransmitter hydrolysis in the central and peripheral nervous systems,^[30, 31] as the target. AChE contains a narrow gorge approximately 20 Å in depth, lined with aromatic side chains.^[32, 33] The active center, comprised of the acylation and choline-binding sites, is located at the gorge base; a “peripheral” site is found at its rim. Small-molecule ligands for each of these sites are known, and inhibitors that span the active center and the peripheral site have also been shown to exhibit tighter binding than the individual components.^[34–39]

As a proof of principle AChE was used to select and synthesize a triazole-linked bivalent inhibitor by using known site-specific ligands as building blocks. A selection of site-specific inhibitors based on tacrine^[38, 40] and phenanthridinium^[38, 41] motifs decorated with alkyl azides and alkyl acetylenes of varying chain lengths (Scheme 1) was prepared by variations of known methods.^[40, 42, 43] Although reversible AChE inhibitors are used clinically to treat Alzheimer's dementia,^[44] these compounds should be handled with care, since high-affinity inhibitors are potentially neurotoxic. The building blocks shown in Scheme 1 allow for the presentation of 98 potential bivalent inhibitors to AChE: 34 regioisomeric pairs (*syn* and *anti* triazoles) of mixed tacrine/phenanthridinium adducts (TZ2–6/PA2–6 and TA1–3/PZ6–8) and 15


[*] Prof. M. G. Finn, Prof. K. B. Sharpless, W. G. Lewis, Dr. L. G. Green
Department of Chemistry
The Scripps Research Institute
10550 North Torrey Pines Road
La Jolla, CA 92037 (USA)
Fax: (+1)858-784-7562
E-mail: mgfinn@scripps.edu, sharpless@scripps.edu

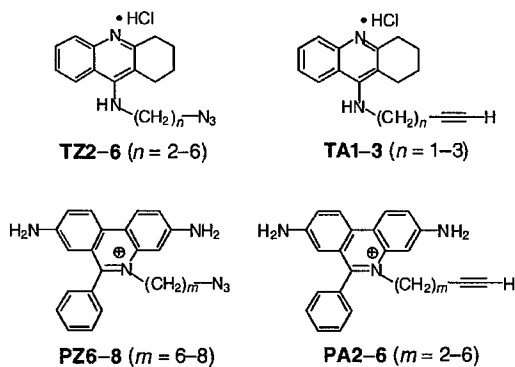
Prof. F. Grynszpan
Department of Molecular Biology
The Scripps Research Institute
10550 North Torrey Pines Road
La Jolla, CA 92037 (USA)

Dr. Z. Radić, Prof. P. Taylor
Department of Pharmacology
University of California San Diego
La Jolla, CA 92093-0636 (USA)

Prof. P. R. Carlier
Department of Chemistry
Virginia Polytechnic Institute and State University
Blacksburg, VA 24061 (USA)

[**] We thank the National Institute of General Medical Sciences, National Institutes of Health (GM-28384, K.B.S.; R-37 GM 18360, P.T.), the National Science Foundation (CHE-9985553, K.B.S.), The Skaggs Institute for Chemical Biology (K.B.S., M.G.F.; W.G.L. is a Skaggs Predoctoral Fellow), the W. M. Keck Foundation (K.B.S.), and the J. S. Guggenheim Memorial Foundation (F.G.) for financial support. We are grateful to Dr. Pascale Marchot (University of Marseille, France) for providing us with a purified preparation of *Electrophorus electricus* AChE for kinetic measurements. We also thank Prof. D. W. Armstrong, C. Mitchell, Dr. G. M. Morris, Dr. X. Wu, Dr. Z. Shen, and Prof. G. Siuzdak for assistance in the execution of this project, and Professors V. V. Fokin and R. Ghadiri for valuable discussions. W.G.L. and L.G.G. contributed equally to this work.

 Supporting information for this article is available on the WWW under <http://www.angewandte.com> or from the author.



Scheme 1. Azide and acetylene building blocks. Key: T = tacrine, P = phenanthridinium, A = alkyne terminus, Z = azide terminus, n , m = number of CH_2 units in the chain connecting the binding and reactive moieties.

regioisomeric pairs of tacrine/tacrine triazoles (**TA1-3**/**TZ2-6**).^[45] Each of the possible binary mixtures was incubated in the presence of *Electrophorus* AChE at room temperature.^[46] The rate of reaction under these conditions in the absence of enzyme is negligible,^[47] so detectable amounts of triazole products should form only when the azide and alkyne are brought together by the enzyme. Therefore, product formation is a direct indication of a potential "hit".

Examination of the 49 reactions by DIOS mass spectrometry^[48, 49] showed only one combination, **TZ2** + **PA6**, in which a detectable amount of the corresponding triazole (compound **1**) was produced, an observation confirmed for a subset of reactions by more cumbersome HPLC-MS methods.^[39] Control experiments established that blocking of the enzyme active center in either covalent or noncovalent fashion inhibits the formation of triazole **1**^[39] which demonstrates that the binding cleft of AChE serves as a template for the 1,3-dipolar cycloaddition reaction. Furthermore, it was found that 2 ± 1 equivalents of triazole were made per equivalent of active enzyme^[39] which suggests that the adduct was bound tightly by AChE.

Authentic samples of triazoles from seventeen of the possible azide-alkyne combinations were prepared by heating the components together at 80°C in the absence of solvent for six days. The products were obtained in high yield, typically as equimolar mixtures of the *syn* (1,5-triazole) and *anti* (1,4-triazole) regioisomers. When desired, the regioisomers were separated by HPLC and independently characterized by MS and $^1\text{H-NMR}$ (nOe). Comparison of the HPLC traces of the enzyme-templated product and the authentic mixture of *syn*- and *anti*-**1** (from thermal cycloaddition between **TZ2** and **PA6** in the absence of enzyme) revealed that the in situ reaction generates predominantly the *syn* isomer (Figure 1).

Detailed kinetic analyses of the binding and inhibitory properties of *syn*- and *anti*-**1** against *Electrophorus Torpedo*, and mouse AChE were performed by using both stopped-flow^[50] and conventional (Ellman assay^[51]) techniques (Table 1).^[39, 52] Dissociation constants (K_d) of *syn*-**1** of 77 to 410 femtomolar (fM) were found, depending on the species, which makes it the most potent noncovalent AChE inhibitor known to date by approximately two orders of magnitude.^[53, 54] The *anti*-**1** isomer exhibited K_d between 720 fM and 14 pM, a value as much as 140 times larger than that of the *syn* compound. Thus, the more active *syn*-triazole regioisomer is the same structure that is preferentially assembled by the enzyme.

The dissociation constants for both *syn*- and *anti*-**1** are substantially lower (i.e. higher affinity) than their components (10–100 nM for tacrine and low μM for propidium). We find that both isomers access the enzyme at rates similar to each other and to tacrine, but differ in their rates of dissociation (off-rates), with that for *syn*-**1** being extremely slow. In addition to the entropic benefits expected from tethering two binding elements to each other, the linker assembly, which

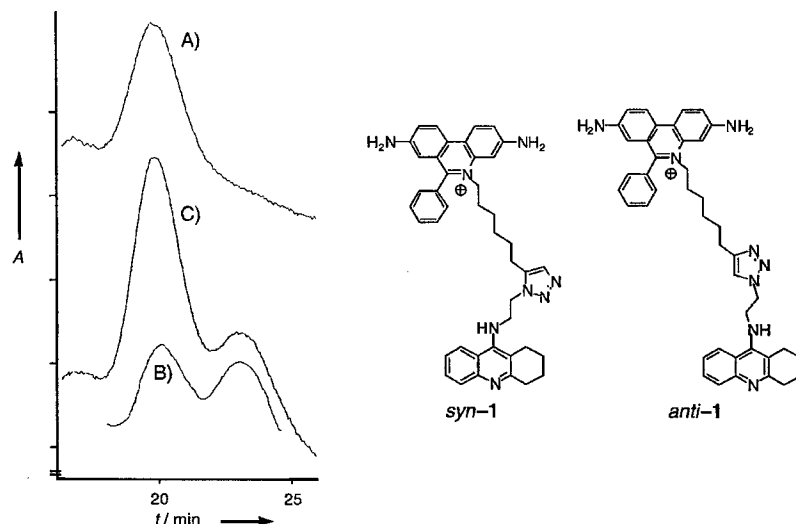


Figure 1. Left: HPLC analysis of thermal and AChE-templated assembly of **TZ2** and **PA6**. A) Product from in situ assembly in the presence of AChE. B) Triazole **1** prepared by thermal reaction; equal amounts of *syn* and *anti* isomers were isolated. C) Solution (A) plus a small amount of solution (B). Right: *syn*- and *anti*-isomers of **1**.

Table 1. Kinetic parameters derived for binding of **1**, and literature data for related noncovalent inhibitors of AChE from various species.

Inhibitor	k_{on} [$10^{10} \text{ M}^{-1} \text{ min}^{-1}$]	k_{off} [min^{-1}]	K_d	AChE source
<i>syn</i> - 1	1.5	0.0015	99 fM	<i>E. electricus</i>
	1.3	0.0011	77 fM	<i>T. californica</i>
	1.3	0.0079	410 fM	mouse
<i>anti</i> - 1	1.8	0.25	14000 fM	<i>E. electricus</i>
	3.2	0.026	720 fM	<i>T. californica</i>
	2.4	0.30	8900 fM	mouse
tacrine ^[38]	0.78	138	18 nM	mouse
propidium ^[38]	1.4	15000	1100 nM	mouse
huprine X ^[55]	0.044	0.009	26 pM	human
ambenonium ^[35]	0.31	0.78	250 pM	human

consists of the two methylene chains and the triazole, may also interact favorably with the enzyme.

Docking of *anti* and *syn-1* in AChE from *Torpedo californica* (PDC code 1ACJ with Trp279 adopting the conformation found in 1ACL) with the program AutoDock v.3.05^[56] shows that the tacrine portion of the inhibitor can be accommodated at the bottom of the active center gorge (practically superimposed on tacrine in the crystal structure), while the phenanthridinium piece is likely to be located in the peripheral site at the rim of the gorge (Figure 2). Interestingly, the triazole moiety is predicted to lie below (deeper than) the narrowest point of the gorge (defined by Phe330, Tyr334, Phe331, Phe288, Trp233, Phe290, and Tyr121).^[57]

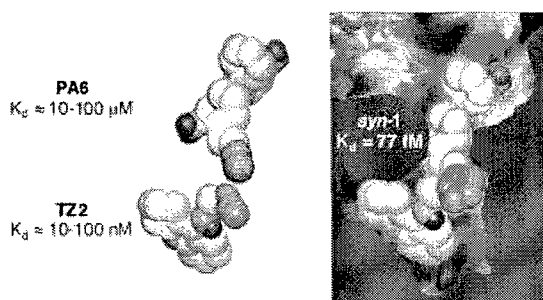


Figure 2. Left: **TZ2** and **PA6** components used for in situ assembly of **1**. The estimated binding constants to AChE shown are those of the tacrine and propidium, respectively, which lack azide or alkyne functional groups. Right: Clipping plane (blue) revealing the *T. californica* AChE active center gorge. The lowest-energy docked conformer of *syn-1* is shown. Alkyne and triazole carbon atoms appear in pink, nitrogen atoms in blue, and nitrogen-bound H atoms in black; all other H atoms are omitted for clarity.

It is apparent that the narrow confines of the AChE gorge impart high selectivity to the assembly reaction. For example, a preliminary survey of the relative potency of a selection of adducts made by thermal 1,3-dipolar cycloaddition as described above shows that the connectivity of the triazole does not seem to be as important as its position (both **TZ2/PA6** (**1**) and **TA2/PZ6** are highly potent, but **TZ6/PA2** is not). While we suspect that the unique adduct preferentially assembled by the enzyme (i.e., *syn-1*) is also likely to be the strongest inhibitor among the 98 triazoles which could have been synthesized, further measurements are in progress to confirm or refute this hypothesis.

We have shown that an enzyme can select and synthesize an extremely potent inhibitor from a parallel array of building blocks by using 1,3-dipolar cycloaddition reactions. This process, which is distinguished by its slow background rate and biocompatibility, provides an excellent probe of the AChE binding landscape. Function can be developed in situ as the individual blocks explore the biomolecular target for recognition elements. A permanent nexus in the form of the robust triazole linkage is made only when two cross-reactive blocks find themselves temporarily moored at adjacent sites, locking in topological and/or dynamic information about the biostructure which recruited them.

We anticipate that “false positives” will be relatively rare in the “in situ” approach. Assuming that the enzyme active site

or an important allosteric site is the template, and that the background rate of the reaction that connects the blocks is low, the formation of a bond between two blocks in situ virtually guarantees that the resulting adduct will be a valuable hit or lead compound for enzyme inhibition. A potential disadvantage of the application of “in situ” click chemistry to inhibitor discovery is the possibility of “false negatives” (effective inhibitors that are not assembled in the enzyme). Improvements in analytical methods and adjustments in the background rate of reaction of the components will help alleviate this problem.

In principle, target-directed assembly of inhibitors could be monitored by assays of enzyme activity instead of detection of the linked inhibitor molecule. In our view, such screening for function, when feasible, is almost always preferred. However, when function is difficult to measure in high-throughput fashion, the detection of potential inhibitors formed by the target is an attractive alternative, as demonstrated here. This latter approach should also facilitate true combinatorial experiments, in which multiple candidate blocks are incubated with the target.

In general, the in situ and traditional (screening of prefabricated candidates) methods of discovery are complementary, and tend to merge with the use of increasingly reliable synthetic transformations. That such a potent inhibitor as *syn-1* was found directly by using the azide–alkyne cycloaddition to unite the probe molecules is interesting, but its broad utility as a search tool remains to be established. Nevertheless, the special qualities of this reaction bode well for its use in creating or amplifying function.

Received: January 21, 2001 [Z18552]

- [1] See the following special issues of *Curr. Opin. Chem. Biol.* devoted to combinatorial chemistry *Curr. Opin. Chem. Biol.* **2001**, *5*(3), 229–336 (Eds.: T. Caulfield, K. Burgess); *Curr. Opin. Chem. Biol.* **2000**, *4*(3), 243–355 (Eds.: M. Bradley, L. Weber); *Curr. Opin. Chem. Biol.* **1999**, *3*(3), 241–356 (Eds.: P. A. Bartlett, G. F. Joyce).
- [2] B. A. Bunin, J. M. Dener, D. A. Livingston, *Annu. Rep. Med. Chem.* **1999**, *34*, 267–286.
- [3] S. R. Wilson, A. W. Czarnik, *Combinatorial Chemistry*, Wiley, New York, **1997**.
- [4] a) A. V. Eliseev, *Curr. Opin. Drug Discovery Dev.* **1998**, *1*, 106–115; b) O. Ramström, J.-M. Lehn, *Nat. Rev. Drug Disc.* **2002**, *1*, 26–36.
- [5] J.-M. Lehn, A. V. Eliseev, *Science* **2001**, *291*, 2331–2332.
- [6] T. Bunyapaiboonsri, O. Ramström, S. Lohmann, J.-M. Lehn, L. Peng, M. Goeldner, *ChemBioChem* **2001**, *2*, 438–444.
- [7] D. J. Maly, I. C. Choong, J. A. Ellman, *Proc. Natl. Acad. Sci. USA* **2000**, *97*, 2419–2424.
- [8] K. C. Nicolaou, R. Hughes, S. Y. Cho, N. Winssinger, C. Smethurst, H. Labischinski, R. Endermann, *Angew. Chem.* **2000**, *112*, 3981–3986; *Angew. Chem. Int. Ed.* **2000**, *39*, 3823–3828.
- [9] S. B. Shuker, P. J. Hajduk, R. P. Meadows, S. W. Fesik, *Science* **1996**, *274*, 1531–1534.
- [10] X. Cheng, R. Chen, J. E. Bruce, B. L. Schwartz, G. A. Anderson, S. A. Hofstadler, D. C. Gale, R. D. Smith, J. Gao, G. B. Sigal, M. Mammen, G. M. Whitesides, *J. Am. Chem. Soc.* **1995**, *117*, 8859–8860.
- [11] D. C. Rideout, T. Calogeropoulou, in *Synergism and Antagonism in Chemotherapy*, Academic Press, Orlando, **1991**, chap. 14, pp. 507–535.
- [12] A. J. Kirby, *Adv. Phys. Org. Chem.* **1980**, *17*, 183–278.
- [13] W. P. Jencks, *Proc. Natl. Acad. Sci. USA* **1981**, *78*, 4046–4050.
- [14] M. Mammen, S.-K. Choi, G. M. Whitesides, *Angew. Chem.* **1998**, *110*, 2908–2953; *Angew. Chem. Int. Ed.* **1998**, *37*, 2755–2794.
- [15] J. F. A. Chase, P. K. Tubbs, *Biochem. J.* **1969**, *111*, 225–235.

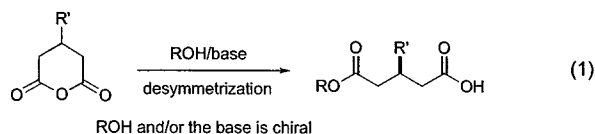
- [16] R. Nguyen, I. Huc, *Angew. Chem.* **2001**, *113*, 1824–1826; *Angew. Chem. Int. Ed.* **2001**, *40*, 1774–1776.
- [17] J. Inglese, S. J. Benkovic, *Tetrahedron* **1991**, *47*, 2351–2364.
- [18] S. E. Greasley, T. H. Marsilje, H. Cai, S. Baker, S. J. Benkovic, D. L. Boger, I. A. Wilson, *Biochemistry* **2001**, *40*, 13538–13547.
- [19] K. C. Nicolaou, R. Hughes, S. Y. Cho, N. Winssinger, H. Labischinski, R. Endermann, *Chem. Eur. J.* **2001**, *7*, 3824–3843.
- [20] H. C. Kolb, M. G. Finn, K. B. Sharpless, *Angew. Chem.* **2001**, *113*, 2056–2075; *Angew. Chem. Int. Ed.* **2001**, *40*, 2004–2021.
- [21] A. Michael, *J. Prakt. Chem.* **1893**, *48*, 94.
- [22] R. Huisgen in *Profiles, Pathways, and Dreams* (Ed.: J. I. Seeman), American Chemical Society, Washington, DC, **1994**.
- [23] In the description of “click chemistry,” (ref. [20]) we inadvertently omitted mention of the powerful block cycloaddition-connection strategies pioneered by Warrener and co-workers (see, for example, R. N. Warrener, D. N. Butler, *Aldrichimica Acta* **1997**, *30*, 119–129; R. N. Warrener, D. N. Butler, D. Margetic, F. M. Pfeffer, R. A. Russel, *Tetrahedron Lett.* **2000**, *41*, 4671–4675). This body of work offers many beautiful examples of modular synthetic sequences for the construction of polycyclic skeletons and other interesting structures. Its success relies, both in design and execution, on a handful of concerted cycloaddition reactions—pure “fusion” events that are premier examples of click chemistry.
- [24] E. Saxon, C. R. Bertozzi, *Science* **2000**, *287*, 2007–2010.
- [25] K. L. Kiick, E. Saxon, D. A. Tirrell, C. R. Bertozzi, *Proc. Natl. Acad. Sci. USA* **2002**, *99*, 19–24.
- [26] W. L. Mock, T. A. Irra, J. P. Wepsiec, T. L. Manimaran, *J. Org. Chem.* **1983**, *48*, 3619–3620.
- [27] W. L. Mock, T. A. Irra, J. P. Wepsiec, M. Adhya, *J. Org. Chem.* **1989**, *54*, 5302–5308.
- [28] W. L. Mock, *Top. Curr. Chem.* **1995**, *175*, 1–24.
- [29] See also: J. Chen, J. Rebek, Jr., *Org. Lett.* **2002**, *4*, 327–329; C. A. Booth, D. Philp, *Tetrahedron Lett.* **1998**, *39*, 6987–6990; S. J. Howell, N. Spencer, D. Philp, *Tetrahedron* **2001**, *57*, 4945–4954.
- [30] D. M. Quinn, *Chem. Rev.* **1987**, *87*, 955–979.
- [31] P. Taylor, Z. Radić, *Annu. Rev. Pharmacol. Toxicol.* **1994**, *34*, 281–320.
- [32] J. L. Sussman, I. Silman, P. H. Axelsen, C. Hirth, M. Goeldner, F. Bouet, L. Ehret-Sabatier, I. Schalk, M. Harel, *Proc. Natl. Acad. Sci. USA* **1993**, *90*, 9031–9035.
- [33] J. L. Sussman, M. Harel, F. Frolow, C. Oefner, A. Goldman, L. Toker, I. Silman, *Science* **1991**, *253*, 872–879.
- [34] H. A. Berman, M. Baker, M. McCauley, K. J. Leonard, M. W. Nowak, M. M. Decker, P. Taylor, *Mol. Pharmacol.* **1987**, *31*, 610–616.
- [35] A. S. Hodge, D. R. Humphrey, T. L. Rosenberry, *Mol. Pharmacol.* **1992**, *41*, 937–942.
- [36] Y.-P. Pang, P. Quiram, T. Jelacic, F. Hong, S. Brimjoin, *J. Biol. Chem.* **1996**, *271*, 23646–23649.
- [37] P. R. Carlier, D.-M. Du, Y.-F. Han, J. Liu, E. Perola, I. D. Williams, Y.-P. Pang, *Angew. Chem.* **2000**, *112*, 1845–1847; *Angew. Chem. Int. Ed.* **2000**, *39*, 1775–1777.
- [38] Z. Radić, P. Taylor, *J. Biol. Chem.* **2001**, *276*, 4622–4633.
- [39] See Supporting Information for details.
- [40] P. R. Carlier, Y. F. Han, E. S.-H. Chow, C. P.-L. Li, H.-S. Wang, T. X. Lieu, H. S. Wong, Y.-P. Pang, *Bioorg. Med. Chem.* **1999**, *7*, 351–357.
- [41] S. Lappi, P. Taylor, *Biochemistry* **1975**, *14*, 1989–1997.
- [42] S. A. Ross, M. Pitié, B. Meunier, *J. Chem. Soc. Perkin Trans. 1* **2000**, 571–574.
- [43] The proposed structures were first examined computationally against AChE from electric ray *Torpedo californica* (PDB codes 1ACJ and 1ACL) with AutoDock 3.05^[56] to ensure that tethers likely to be optimal would not be omitted. These calculations predicted that a chain length of 2–3 methylenes on the tacrine moiety and 5–6 on the phenanthridinium moiety would present favorable conformations to allow the cycloaddition reaction to occur in the enzyme.
- [44] E. Albert, F. Phillip in *Alzheimer Disease: From Molecular Biology to Therapy* (Eds.: R. Berker, E. Giacobini), Birkhauser, Boston, **1996**, pp. 211–215.
- [45] Phenanthridinium/phenanthridinium combinations were not explored as they would not be expected to provide a dual-site inhibitor, the phenanthridinium moiety being too large to function as an active center ligand.
- [46] The tacrine components in water were each added to solutions of *Electrophorus* AChE (Sigma) in 2 mM ammonium citrate buffer (pH 7.3–7.5) and allowed to stand for 90 minutes at room temperature. The corresponding coupling partner was then added and the solutions were thoroughly mixed. The final concentrations were: AChE, 1.0 mg mL⁻¹ of the commercial material (titrated concentration of functioning active centers = 1 μM); tacrine component, 30 μM; phenanthridinium component, 66 μM.
- [47] A second-order rate constant of $1.9 \pm 0.7 \times 10^{-5} \text{ M}^{-1} \text{ min}^{-1}$ was determined for the uncatalyzed reaction of **TZ2** and **PA6** over 9 days at 18 °C in 1-butanol. This is comparable to $7.0 \times 10^{-5} \text{ M}^{-1} \text{ min}^{-1}$ obtained by Mock et al. at 40 °C.^[26,27] Under these conditions, the reaction would take approximately 40 years to reach 80% completion.
- [48] DIOS = Desorption/Ionization on Silicon.
- [49] DIOS-MS is uniquely tolerant of macromolecular impurities and buffer salts which allows convenient analysis of the crude reaction mixtures. J. Wei, J. Buriak, G. Siuzdak, *Nature* **1999**, *401*, 243–246; J. J. Thomas, Z. Shen, J. E. Crowell, M. G. Finn, G. Siuzdak, *Proc. Natl. Acad. Sci. USA* **2001**, *98*, 4932–4937; Z. Shen, J. J. Thomas, C. Averbuj, K. M. Broo, M. Engelhard, J. E. Crowell, M. G. Finn, G. Siuzdak, *Anal. Chem.* **2001**, *73*, 612–619.
- [50] Z. Radić, P. D. Kirchhoff, D. M. Quinn, J. A. McCammon, P. Taylor, *J. Biol. Chem.* **1997**, *272*, 23265–23277.
- [51] L. G. Ellman, K. D. Courtney, V. J. Andres, R. M. Featherstone, *Biochem. Pharmacol.* **1961**, *7*, 88–95.
- [52] The association rate constants (k_{on}) were determined by both direct measurements of inhibitor binding to AChE and by measurements of time-dependent loss of AChE activity in reaction with inhibitor. The stopped-flow technique was used to measure rates of quenching of intrinsic AChE tryptophan fluorescence upon binding of inhibitor at micromolar concentrations as previously described.^[38] The time-dependent loss of AChE activity was measured upon mixing AChE with picomolar concentrations of inhibitor in ten-fold excess. The AChE activity in aliquots of the reaction mixture was determined by Ellman assay^[51] at intervals of several minutes to an hour. The second-order rate constants of inhibitor association were obtained by linear fit of first-order decay rates of either AChE fluorescence or its activity, at several inhibitor concentrations. The first-order dissociation constants (k_{off}) were determined by measurements of the return of AChE activity by Ellman assay upon 5000-fold dilution of 50–100 nM concentrations of AChE·1 complex into 250 μg mL⁻¹ solution of herring sperm DNA (Boehringer) in buffer (thereby the reassociation of the inhibitor to AChE by virtue of the affinity of the phenanthridinium part of the molecule for duplex DNA is competitively suppressed). The dissociation constant was determined by nonlinear fit of first-order increase in enzyme activity up to 70–80% of the AChE control activity in a mixture containing no inhibitor. All experiments were performed in at least triplicate with the standard error of determination equal to or smaller than 20% of the mean value. The measurements were performed in 0.1 M phosphate buffer pH 7.0 at 22 °C on a SX.18 MV stopped-flow instrument (Applied Photophysics) or Cary 1E UV/Vis spectrophotometer (Varian).
- [53] The trifluoroketone of Quinn and co-workers forms a hemiketal with the serine residue of the active center and exhibits a K_i value based on the total concentration of inhibitor of 80 pM. Most of this species exists in the inactive hydrated form. When one factors in the equilibrium concentration of the active carbonyl species, the inhibitor constant reaches low femtomolar levels [H. K. Nair, K. Lee, D. M. Quinn, *J. Am. Chem. Soc.* **1993**, *115*, 9939–9941; M. Harel, D. M. Quinn, H. K. Nair, *J. Am. Chem. Soc.* **1996**, *118*, 2340–2346]. Triazole syn-1 suffers no such equilibrium deactivation.
- [54] The inhibitory power of **1** exceeds even that of the fasciculins family of snake venom toxins, which occlude the mouth of the AChE gorge with binding constants of 0.44–40 pM, depending on the fasciculins and the source of the enzyme: P. Marchot, A. Khelif, Y. H. Ji, P. Mansuelle, P. E. Bougis, *J. Biol. Chem.* **1993**, *268*, 12458–12467; R. Duran, C. Cerveñansky, F. Dajas, K. F. Tipton, *Biochim. Biophys. Acta* **1994**, *1201*, 381–388; Z. Radić, R. Duran, D. C. Vellom, Y. Li, C. Cerveñansky, P. Taylor, *J. Biol. Chem.* **1994**, *269*, 11233–11239; J. Eastman, E. J. Wilson, C. Cerveñansky, T. L. Rosenberry, *J. Biol. Chem.* **1995**, *270*, 19696–19701; G. Puu, M. Koch, *Biochem. Pharmacol.* **1990**, *40*, 2209–2214.

- [55] P. Camps, B. Cusack, W. D. Mallender, R. El Achab, J. Morral, D. Muñoz-Torrero, T. L. Rosenberry, *Mol. Pharmacol.* **2000**, *57*, 409–417.
- [56] G. M. Morris, D. S. Goodsell, R. S. Halliday, R. Huey, W. E. Hart, R. K. Belew, A. J. Olson, *J. Comput. Chem.* **1998**, *19*, 1639–1662.
- [57] Although the lead inhibitor **1** was assembled by *Electrophorus electricus* AChE, it has a similarly high affinity for the *Torpedo californica* enzyme. This observation suggests a high degree of functional similarity with respect to binding in the active center gorge for these two enzymes (see: S. Simon, J. Massoulié, *J. Biol. Chem.* **1997**, *272*, 33045–33055), and justifies our use of the crystallographically well-characterized (2.8 Å resolution) *Torpedo* enzyme for modeling studies. At the present time *Electrophorus* AChE has only been characterized to 4.2 Å resolution (Y. Bourne, J. Grassi, P. E. Bourgis, P. Marchot, *J. Biol. Chem.* **1999**, *274*, 30370–30376).

Highly Enantioselective Desymmetrization of Anhydrides by Carbon Nucleophiles: Reactions of Grignard Reagents in the Presence of (–)-Sparteine**

Ryo Shintani and Gregory C. Fu*

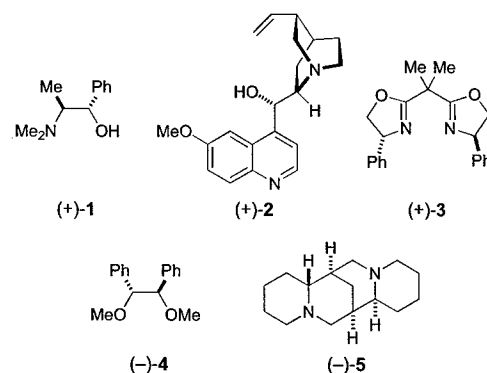
The desymmetrization of *meso* and other prochiral compounds represents a powerful approach to asymmetric synthesis,^[1] and a number of enantioselective total syntheses have been based on this strategy.^[2] The desymmetrization of anhydrides has been a particular focus of interest. Most investigations of this family of substrates have employed an alcohol as the nucleophile^[3] [for example, a chiral alcohol^[4] or an achiral alcohol in combination with a chiral catalyst^[5] Eq. (1)]. In addition, success has been reported for reactions with a stoichiometric quantity of an enantiopure reducing agent^[6] or amine.^[7]



On the other hand, very little progress has been described for the desymmetrization of anhydrides with carbon-based nucleophiles. In fact, to the best of our knowledge, only one report has begun to successfully address this challenge, a study by Real and co-workers that focused on the reaction of a

single substrate, a bicyclic anhydride, with Grignard reagents bearing chiral oxazolidine auxiliaries.^[8] In an attempt to remedy this methodological deficiency, we have recently initiated an investigation of the desymmetrization of anhydrides by carbon nucleophiles. Rather than covalently attaching a chiral auxiliary to the nucleophile and then releasing it, we chose to concentrate our efforts on the use of chiral ligands as the source of asymmetry. Here we report that (–)-sparteine-bound Grignard reagents effectively desymmetrize an array of cyclic anhydrides to furnish ketoacids in very good enantiomeric excess.

In our initial work, we decided to explore the ring-opening of 3-phenylglutaric anhydride by phenylmagnesium chloride. We examined a structurally diverse set of chiral ligands (Scheme 1) that have proved useful in a number of other



Scheme 1. Ligands used in preliminary experiments.

enantioselective processes, including a simple aminoalcohol (Table 1, entry 1), a cinchona alkaloid (entry 2), a bisoxazoline (entry 3), and a dimethyl ether (entry 4). Disappointingly, all were rather ineffective at desymmetrizing the anhydride (<40% *ee*). Fortunately, however, we discovered that readily available (–)-sparteine accomplishes the ring opening with high enantioselectivity (88% *ee*; entry 5).

Of course, we are not the first to document the remarkable capacity of (–)-sparteine to control enantioselection. Pioneering observations by Nozaki et al. in the 1960's^[9] have been followed by fascinating studies by a number of groups, including those of Hoppe and Beak.^[10, 11] The large majority

Table 1. Desymmetrization of 3-phenylglutaric anhydride by PhMgCl: a survey of chiral ligands.^[a]

Entry	Ligand	<i>ee</i> [%]	Yield [%]
1 ^[b]	(+)- 1	1	76
2 ^[b]	(+)- 2	12	76
3	(+)- 3	32	66
4	(–)- 4	39	77
5	(–)- 5	88	63

[a] All data are the average of two runs. [b] 2.0 equiv of PhMgCl was used.

[*] Prof. Dr. G. C. Fu, R. Shintani
Department of Chemistry
Massachusetts Institute of Technology
Cambridge, MA 02139 (USA)
Fax: (+1) 617-258-7500
E-mail: gcf@mit.edu

[**] We thank Ivory D. Hills for X-ray crystallographic work. Support has been provided by Bristol-Myers Squibb, Novartis, Pfizer, and Pharmacia. Funding for the MIT Department of Chemistry Instrumentation Facility has been furnished in part by NSF CHE-9808061 and NSF DBI-9729592.

Supporting information for this article is available on the WWW under <http://www.angewandte.com> or from the author.

Freeze-frame inhibitor captures acetylcholinesterase in a unique conformation

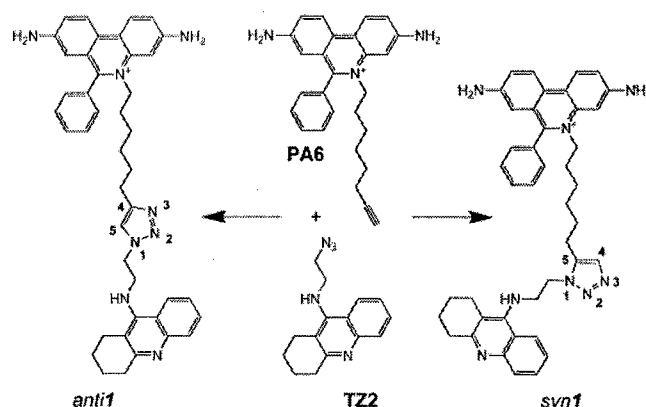
Yves Bourne^{*†}, Hartmuth C. Kolb[‡], Zoran Radić[§], K. Barry Sharpless^{*†¶}, Palmer Taylor[§], and Pascale Marchot^{*†¶}

[¶]Ingénierie des Protéines, Centre National de la Recherche Scientifique Unité Mixte de Recherche–6560, Institut Fédératif de Recherche Jean Roche, Université de la Méditerranée, Faculté de Médecine Secteur Nord, F-13916 Marseille Cedex 20, France; ^{*}Architecture et Fonction des Macromolécules Biologiques, Centre National de la Recherche Scientifique Unité Mixte de Recherche–6098, 31 Chemin Joseph Aiguier, F-13402 Marseille Cedex 20, France; [‡]Department of Chemistry, [¶]The Skaggs Institute for Chemical Biology, The Scripps Research Institute, La Jolla, CA 92037; and [§]Department of Pharmacology, University of California at San Diego, La Jolla, CA 92093-0636

Contributed by K. Barry Sharpless, December 10, 2003

The 1,3-dipolar cycloaddition reaction between unactivated azides and acetylenes proceeds exceedingly slowly at room temperature. However, considerable rate acceleration is observed when this reaction occurs inside the active center gorge of acetylcholinesterase (AChE) between certain azide and acetylene reactants, attached via methylene chains to specific inhibitor moieties selective for the active center and peripheral site of the enzyme. AChE catalyzes the formation of its own inhibitor in a highly selective fashion: only a single *syn1*-triazole regioisomer with defined substitution positions and linker distances is generated from a series of reagent combinations. Inhibition measurements revealed this *syn1*-triazole isomer to be the highest affinity reversible organic inhibitor of AChE with association rate constants near the diffusion limit. The corresponding *anti1* isomer, not formed by the enzyme, proved to be a respectable but weaker inhibitor. The crystal structures of the *syn1*- and *anti1*-mouse AChE complexes at 2.45- to 2.65-Å resolution reveal not only substantial binding contributions from the triazole moieties, but also that binding of the *syn1* isomer induces large and unprecedented enzyme conformational changes not observed in the *anti1* complex nor predicted from structures of the apoenzyme and complexes with the precursor reactants. Hence, the freeze-frame reaction offers both a strategically original approach for drug discovery and a means for kinetically controlled capture, as a high-affinity complex between the enzyme and its self-created inhibitor, of a highly reactive minor abundance conformer of a fluctuating protein template.

Acetylcholinesterase (AChE) rapidly terminates cholinergic neurotransmission by catalyzing the hydrolysis of the neurotransmitter, acetylcholine, and inhibitors of AChE have been used for over a century in various therapeutic regimens (1, 2). The structure of the target enzyme reveals a narrow gorge ≈ 20 Å in depth with the catalytic triad of the active center at its base (3). Distinctive inhibitors bind to the active center or to a peripheral anionic site (PAS) located at the rim of the gorge near the enzyme surface (4–6). Previously, we generated a library of active site and PAS inhibitors with respective tacrine and phenanthridinium nuclei, each equipped with an azide or acetylene group at the end of a flexible methylene chain, to enable the reporting 1,3-dipolar cycloaddition to occur (Scheme 1) (7). AChE itself served as the reaction vessel, synthesizing its own inhibitor from these building blocks, in effect, by equilibrium-controlled sampling of various possible pairs of reactants in its active center gorge until irreversible cycloaddition between azide and acetylene ensued at an intersecting point within the gorge, between the two anchoring positions. From 49 building block combinations, the enzyme selected the TZ2/PA6 pair to form, with an enhanced reaction rate, a highly regioselective *syn1* triazole as the sole product (Scheme 1). In contrast, chemical synthesis by thermal reaction in the absence of enzyme proceeds very slowly and provides an $\approx 1:1$ mixture of *syn1* and *anti1* regioisomers, which differ in the nitrogen substitution positions on the 1,2,3-triazole. Although both are high-affinity inhibitors, the *syn1* isomer, with a 100-fold greater affinity and a subpico-



Scheme 1. Structures of the *anti1* and *syn1* TZ2PA6 regioisomers formed by 1,3-dipolar cycloaddition (7). The phenanthridinium, triazole, and tacrine moieties are shown from top to bottom.

molar dissociation constant for certain AChEs (7), has a potency greater than all known noncovalent organic AChE inhibitors and high selectivity for individual cholinesterases.

The discovery that enzymes can serve as atomic-scale reaction templates for creating their own inhibitors offers an original approach to drug discovery. In this light, we have solved the crystal structures of complexes of mouse AChE (mAChE) (8, 9) with the TZ2PA6 *anti1* and *syn1* regioisomers at 2.45- and 2.65-Å resolution (Table 1 and Fig. 1) and have analyzed further their respective binding kinetics and affinities (Table 2). We show that the distinctive binding properties of the two isomers in solution are related to discrete rearrangements in both the ligand and enzyme conformations. Indeed, the active center gorge and PAS conformations for the two crystalline complexes differ greatly, where binding of the higher affinity *syn1* isomer unveils a unique enzyme conformation not predicted from the structures of either the apo form or the complexes with the precursor reactants (10, 11). Hence these structures reveal that the *syn1* compound specifically formed on the enzyme effectively freezes in frame a highly reactive AChE conformer, and that the two TZ2PA6 regioisomers select distinct conformations from an unliganded enzyme that is presumably fluctuating between multiple conformational states. Because the unique structural features seen for the *syn1*-mAChE complex likely reflect the unique proximity

Abbreviations: AChE, acetylcholinesterase; mAChE, mouse AChE; PAS, peripheral anionic site.

Data deposition: The atomic coordinates and structure factors of the *anti1*- and *syn1*-mAChE complex structures have been deposited in the Protein Data Bank, www.rcsb.org (PDB ID codes 1Q84 and 1Q83, respectively).

[†]To whom correspondence may be addressed. E-mail: marchot.p@jean-roche.univ-mrs.fr or yves@afmb.cnrs-mrs.fr.

© 2004 by The National Academy of Sciences of the USA

Table 1. Data collection and refinement statistics

	TZ2PA6 isomer complexed to mAChE	
	<i>anti1</i>	<i>syn1</i>
Data collection*		
Beamline (European Synchrotron Radiation Facility)	ID14-EH1	ID14-EH2
Wavelength, Å	0.933	0.933
Resolution range, Å	25–2.45	25–2.65
Total observations	549,476	513,851
Unique reflections	74,834	59,650
Multiplicity	3.9	3.6
Completeness, %	99.8 (99.7)	99.8 (99.9)
$I/\sigma(I)$	9.3 (1.8)	8.2 (1.8)
R_{sym}^{\dagger}	5.7 (43.5)	6.5 (42.0)
Refinement*		
R factor/ R_{free} , %	18.4/21.4	18.1/22.0
rms deviation [§]		
Bonds, Å/angles, °	0.015/1.5	0.015/1.5
Chiral volume, Å ³	0.085	0.084
Mean B factors, Å		
Main/side chains	53.4/55.2	49.7/51.6
Solvent/carbohydrate	50.8/91.5	46.7/95.2
Ligand/polyethylene glycol	63.5/72.2	57.2/66.3
rms deviation on B factors, Å ²		
Main/side chains	0.9/1.6	0.9/1.6

*Values in parentheses are those for the last shell.

[†] $R_{\text{sym}} = \sum |I - \langle I \rangle| / \sum I$, where I is an individual reflection measurement and $\langle I \rangle$ is the mean intensity for symmetry-related reflections.

[‡]R factor = $\sum ||F_o| - |F_c|| / \sum |F_o|$, where F_o and F_c are observed and calculated structure factors, respectively. R_{free} is calculated for 2% of randomly selected reflections excluded from refinement.

[§]rms deviation from ideal values.

of reactants causing the higher affinity *syn1* isomer to be the sole reaction product *in situ*, these structures also provide insights on the cycloaddition reaction occurring on a flexible protein template and at a locus remote from the anchoring binding sites of the precursors. Thus, the unique structure of the complex captured by click chemistry leads to an unusual strategy for drug design where the most selective agents induce distinctive conformational states of the target.

Experimental Procedures

Preparation and Analysis of the Complexes. The TZ2PA6 *anti1* and *syn1* isomers were synthesized as described (7). Monomeric mAChE expressed from human embryonic kidney-293 cells (9) was purified by affinity chromatography by using propidium elution (10). The *anti1*- and *syn1*-mAChE complexes were prepared by using a 2-fold molar excess of the inhibitors and concentrations well above their K_{ds} ($\approx 135 \mu\text{M}$ i.e., $15 \cdot 10^6 \times K_{\text{i(anti)}}$ and $330 \cdot 10^6 \times K_{\text{i(syn)}}$; Table 2) (7, 10). Titration of the isomer stock solutions ($\epsilon_{490\text{nm}} = 6,000 \text{ M}^{-1}\cdot\text{cm}^{-1}$) and analysis of the complex solutions were carried out spectrophotometrically (10).

Crystallization and Data Collection. Crystallization was achieved at 4°C by vapor diffusion by using hanging drops (1–2 μl) and a protein-to-well solution ratio of 1:1 with polyethylene glycol-600 25–32% (vol/vol) in 20–100 mM Hepes, pH 6.0–7.5, as the well solution. The crystals were directly flash-cooled in the nitrogen gas stream (100 K); optimal occupancies of the crystalline PASs were controlled by spectrophotometry before data collection (10). The crystals belonged to the orthorhombic space group $P2_12_12_1$ with unit cell dimensions $a = 79.7 \text{ Å}$, $b = 111.9 \text{ Å}$, and $c = 226.5 \text{ Å}$.

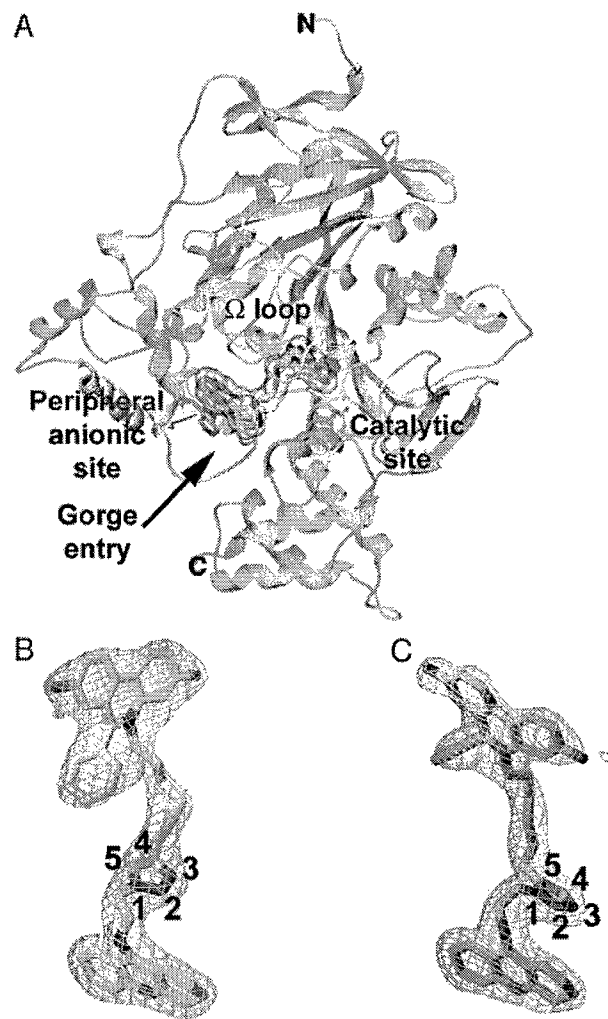


Fig. 1. Overall fold and structural quality of the TZ2PA6–mAChE complexes. (A) Overall view of the mAChE molecule (cyan ribbon) showing the *syn1* isomer (orange bonds; transparent molecular surface) bound within the enzyme active-site gorge; the long Ω loop Cys-69–Cys-96 is displayed in yellow. (B and C) Determined structures of the bound *anti1* and *syn1* isomers (yellow and orange bonds, respectively; blue nitrogens; numbered triazole atoms; same orientation as in Scheme 1), with the respective 2.45- and 2.65-Å resolution final $2F_o - F_c$ electron density maps contoured at 1σ (cyan).

Oscillation images were integrated with DENZO (12), and data were scaled and merged with SCALA (13).

Structure Determination and Refinement. Coordinates of the *anti1* and *syn1* molecules were obtained from docked simulations of TZ2PA6–TcAChE complexes (7). The apo-mAChE structure (Protein Data Bank ID code 1J06) (10) without solvent was used as a starting model to refine the *anti1*- and *syn1*-mAChE complex structures with CNS (14) and REFMAC (15) (Table 1). Rigid-body refinements on each of the two subunits in the crystalline mAChE dimer (10) gave R factor values of 25.2% and 24.8% (R_{free} values of 25.8% and 25.3%) for the *anti1* and *syn1* complexes, respectively, by using all data in the 25- to 2.45/2.65-Å resolution range. The resulting $2F_o - F_c$ and $F_o - F_c$ electron density maps were used to position the inhibitors and correct the protein model with the graphics program TURBO-FRODO (16).

The final two TZ2PA6–mAChE structures comprise residues Glu-1–Ala-541 and Glu-4–Thr-540 for the two mAChE mole-

Table 2. Kinetic parameters for inhibition of various cholinesterases by the TZ2PA6 isomers

Enzyme	<i>syn1</i>			<i>anti1</i>		
	k_{on} , $10^{10} \text{ M}^{-1} \cdot \text{min}^{-1}$	k_{off} , 10^{-3} min^{-1}	K_i , fM	k_{on} , $10^{10} \text{ M}^{-1} \cdot \text{min}^{-1}$	k_{off} , 10^{-3} min^{-1}	K_i , fM
mAChE*	1.7	7.1	410	2.5	220	8,900
mAChE mutant Trp286Ala	0.94	19	2,000	0.87	1,800	210,000
AChE, <i>Electrophorus electricus</i> *	1.5	1.5	99	1.8	250	14,000
AChE, <i>Torpedo californica</i> *	1.4	1.1	77	3.2	23	720
AChE, <i>Drosophila melanogaster</i>	2.0	72	3,600	3.4	58	1,700
Butyrylcholinesterase, mouse	0.36	2.6	720	0.69	3.2	460

Parameters are means of $n \geq 3$ individual values with SD $\leq 20\%$.

*Modified from ref. 7.

cules in the asymmetric unit (10). High-temperature factors and weak electron densities are associated with residues Cys-257, Pro-258, and Asp-265 in the short Ω loop Cys-257-Cys-272 and with the surface loop region Asp-491-Pro-498. The average rms deviation (rmsd) between the *anti1* and *syn1* complex structures is 0.24 Å for 535 C α atoms. Between the *anti1* and *syn1* complexes and the apo form, the rmsds are 0.19 and 0.23 Å for 534 and 533 C α atoms, respectively. The stereochemistries of the bound isomers were checked by using the MM2 force field as implemented in MACROMODEL (17). Those of the structures were analyzed with PROCHECK (18); with the exception of the catalytic Ser-203, no residues were found in the disallowed regions of the Ramachandran plot. Figs. 1–3 were generated with SPOCK (19) and RASTER3D (20).

Inhibition Studies. Inhibition constants were measured from the ratio of dissociation and association rates ascertained by conventional mixing and stopped-flow instrumentation (7). The mAChE Trp286Ala mutant was expressed, sequence verified, and concentrated from the expression medium as described (21). Purified AChE from *D. melanogaster* was a gift from D. Fournier (Institut de Pharmacologie et de Biologie Structurale, Toulouse, France).

Results and Discussion

Overall View of the TZ2PA6–mAChE Complexes. The structures of mAChE in complexes with the *anti1* and *syn1* regioisomers (Fig. 1) show the canonical catalytic subunit, made up of a 12-stranded central β -sheet surrounded by 14 α -helices (10, 22, 23), and well-ordered bound inhibitor molecules. The isomer-binding site may be deconstructed into three discrete loci: (i) the active center at the base of the gorge that binds the tacrine moiety; (ii) an intervening site in the constricted region within the gorge that associates with the triazole moiety and adjacent methylene groups; and (iii) the PAS at the rim of the gorge that binds the phenylphenanthridinium moiety.

The *anti1*–mAChE Complex. In the *anti1* complex, the tacrine moiety is positioned at the base of the mAChE gorge similar to the *T. californica* AChE–tacrine complex (11) (Fig. 2A). However, the density maps clearly reveal a slight bend in the moiety that may enhance π – π stacking of the tetrahydroaminoacridine ring inserted between the Trp-86 and Tyr-337 aromatic side chains. At the region of constriction formed by the side chains of Tyr-124, Phe-297, Tyr-337, and Phe-338, ≈ 5 –8 Å into the gorge, the triazole establishes van der Waals contacts with the Phe-297 and Tyr-341 side chains. The hydroxyl groups of Tyr-337 and Tyr-124, on opposite sides of the gorge, are hydrogen-bonded to the triazole N2 and N3 atoms and may interact with the heteroaromatic π -system. The dimethylene linker connecting the tacrine and triazole is well ordered within the gorge and in van der Waals contact with the side chains of the conserved residues Asp-74, Tyr-124, and Tyr-341.

At the PAS, the phenylphenanthridinium moiety is positioned by the hexamethylene chain that links it to the triazole. Major interactions include a near-parallel stacking of the planar phenanthridinium with the Trp-286 indole, an edge-to-face arrangement with the Tyr-72 ring, and stabilizing interactions with the Ser-293 hydroxyl and Gln-291 carbonyl (Figs. 2A and 3A). The *anti1* exocyclic phenyl moiety, nearly buried at the gorge entrance and in a T shaped arrangement with the Tyr-72 and Trp-286 side chains, orients to establish van der Waals contacts with the Asp-74, Tyr-124, and Tyr-341 side chains and hydrogen bonds with the Tyr-72 hydroxyl and Ser-293 N, O, and O γ atoms. Partial delocalization of electrons between the Trp-286 indole and the phenanthridinium observed in the density maps suggests formation of a charge–transfer complex, similar to that observed in the decidium–mAChE complex (10) (Fig. 2D).

The architecture of the PAS region in the *anti1*–mAChE complex (Figs. 2A and 3A) is virtually identical to that seen in the decidium– and propidium–mAChE complexes (10), and the major interactions involved in the phenanthridinium–Trp-286 stacking are retained (Fig. 2D). Yet the phenylphenanthridinium adopts distinctive orientations in the PAS in the three complexes. In the *anti1* complex, the phenanthridinium is rotated by $\approx 180^\circ$ around its centroid axis, whereas this centroid is translated by 1.5 Å from its position in the other two complexes. This positioning leads to stabilizing interactions of the *anti1* phenanthridinium with the Gln-291 and Ser-293 side chains, instead of the His-287 imidazole located across the gorge opening, and to a distinct environment for the exocyclic phenyl group. This versatility in the rotational and translational orientations of the bound phenylphenanthridinium relative to the Trp-286 side chain adds a new dimension to the design of molecules that associate with the PAS region.

The *syn1*–mAChE Complex. The structure of the *syn1*–mAChE complex differs considerably from that of the *anti1*–mAChE complex, due to the respective 1,5- and 1,4-disubstitution of the *syn1* and *anti1* 1,2,3-triazole rings (Scheme 1, Fig. 1). The *anti1* isomer adopts an elongated flat shape, whereas the *syn1* isomer presents a corkscrew-like topology that provides greater surface complementarity with the gorge walls, resulting in fewer solvent-filled voids around the bound *syn1* (Figs. 2B and C and 3B). Whereas the tacrine moiety in both complexes is positioned similarly within the active site, the triazole in the *syn1* complex is shifted 2 Å deeper into the gorge, where it is held in place by the tacrine ring and the Phe-297 and Phe-338 side chains. Consequently, a single π –aromatic interaction may exist between the *syn1* triazole and Tyr-124 hydroxyl, and a water-bridged hydrogen bond is created between the triazole N3 and the catalytic Ser-203 O γ and Gly-121 amide backbone. Additional van der Waals contacts occur between the triazole and the Gly-121–Gly-122 dipeptide backbone and Tyr-124 side chain. The shifted *syn1* triazole occludes the Tyr-337 ring, which sweeps

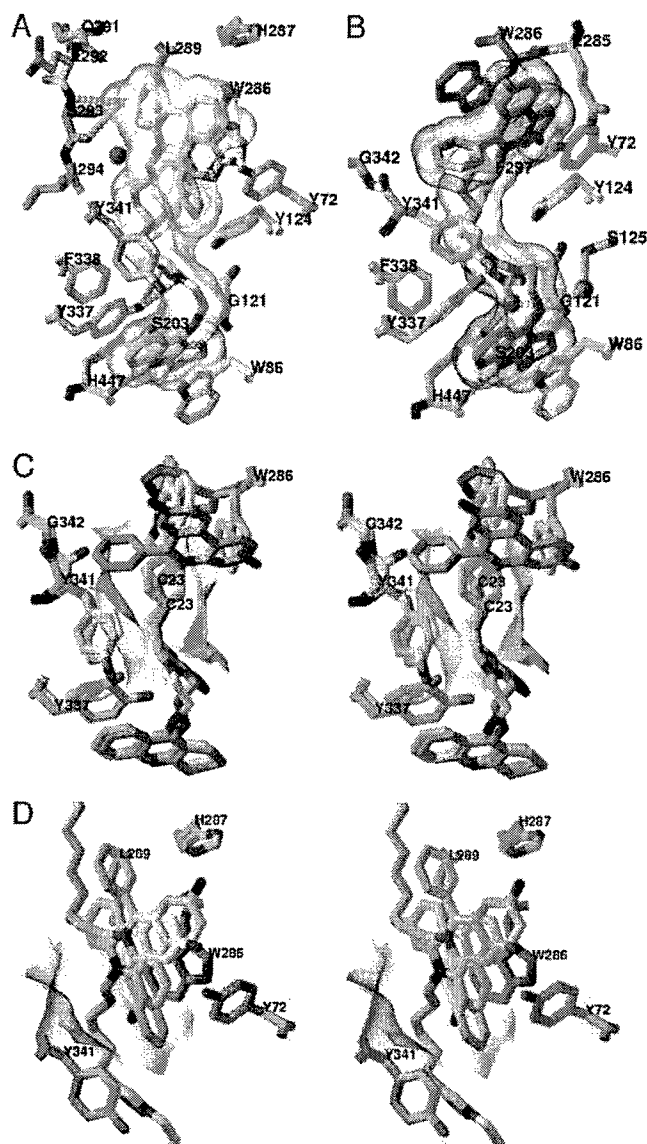


Fig. 2. Close-up views of the TZ2PA6–mAChE complexes. (A and B) Bound *anti1* and *syn1* isomers (colored as in Fig. 1) with interacting mAChE side chains colored white, yellow, and green/magenta (blue, nitrogens; red, oxygens) for those that respectively interact with the tacrine, triazolo, and phenanthridinium moieties of the isomers. The isomer molecular surfaces are displayed in transparency. The side chains of the catalytic residues Ser-203, Glu-334, and His-447 are shown as white bonds, and hydrogen bonds between mAChE residues and the isomers are shown as white dotted lines. (C) Stereo superimposition of the *anti1* and *syn1* complexes (colored as in A and B) according to all C α atoms of mAChE. The side chains of residues Trp-286 and Tyr-337 and of dipeptide Tyr-341–Gly-342, which adopt distinctive positions in the complexes, are shown in magenta and green, respectively. The χ values for the Trp-286 side chain are (*anti* $\chi_1 = -73^\circ$, $\chi_2 = 100^\circ$; *syn* $\chi_1 = -158^\circ$, $\chi_2 = 50^\circ$). (D) Stereo superimposition of the *anti1* complex with the decidium–mAChE complex (Protein Data Bank ID code 1J07; ref. 10) according to all C α atoms of mAChE in the two complexes. The *anti1* and decidium phenylphenanthridinium moieties (yellow and white bonds, respectively; blue, nitrogens) adopt distinct positions and orientations relative to Trp-286 in the PAS, whereas their alkyl chains diverge. The side chains of the PAS residues are highlighted in green (blue, nitrogens; red, oxygens). The mAChE molecular surface buried at the *anti1* complex interface is displayed in transparency.

out in a 60° arc, resulting in a hydroxyl group displacement of 4.5 Å and in new interactions with the Tyr-341 ring near the gorge entry.

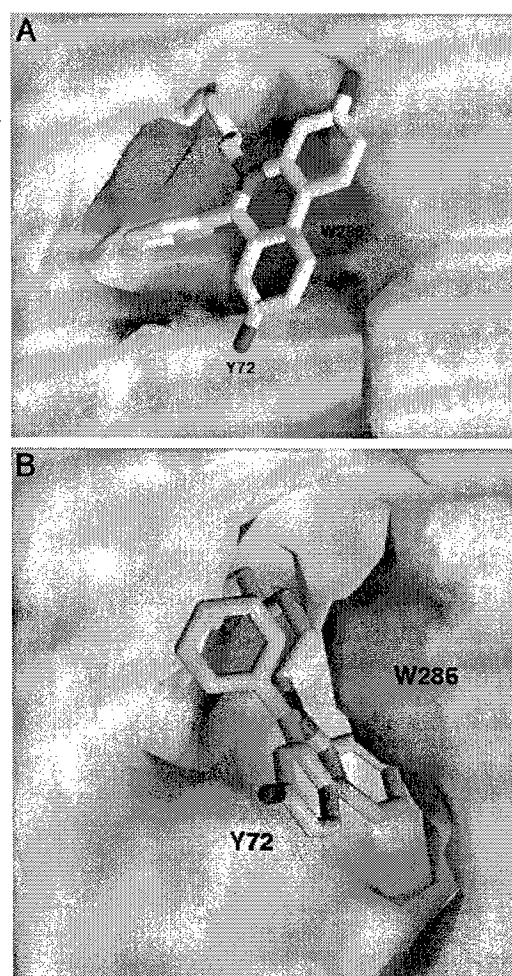


Fig. 3. Distinctive topographies of the PAS regions in the *anti1* and *syn1* complexes. Views of the PAS region of mAChE bound to the phenanthridinium moiety present in the *anti1* (A) and *syn1* (B) isomers (colored as in Figs. 1 and 2). The mAChE molecular surfaces buried at the complex interfaces are shown in yellow, with the Tyr-72 and Trp-286 side chains highlighted in green and magenta, respectively. The mAChE surface areas (Connolly's surfaces) buried to a 1.6-Å radius probe at the *anti1* and *syn1* complex interfaces by the phenylphenanthridinium and linker first carbon are 256 and 313 Å² (the double-face burying of the *syn1* phenanthridinium being counterbalanced by the deeper burying of the *anti1* phenyl). The gorge mouth openings (Richards' surface) for the *anti1* and *syn1* complexes are 14 and 29 Å², respectively.

The position and orientation of the *syn1* triazole at the gorge constriction influence the phenylphenanthridinium position at the PAS (Figs. 2 *B* and *C* and 3*B*). Compared to the *anti1* complex, the overall span of the linker is shortened by 1.5 Å in the more compact *syn1* triazole, a value close to the length of a C–C bond (Fig. 1 *B* and *C*). As a result of the reduced linking distance, the *syn1* phenanthridinium moiety is constrained to a narrow region deep within the gorge where it would sterically clash with the Trp-286 indole. This causes the Trp-286 side chain to be dislodged from the PAS surface and to swing into the solvent, with differences of 85° and 50° in the χ_1 and χ_2 values, respectively. This distinct side chain conformation enlarges the opening at the gorge rim 2-fold, creating a 10 × 9 Å groove delimited by the Tyr-72 and uniquely positioned Trp-286 side chains on each side and by Glu-285 at its base, wherein the phenanthridinium tightly intercalates (Figs. 2 *B* and *C* and 3*B*). Hence, the aromatic plate of the *syn1* phenanthridinium, oriented 90° from its position in the *anti1* complex, is wedged

neatly between the two aromatic side chains where it is stabilized by π - π interactions with centroids separated by 3.6–3.8 Å. This causes the phenyl group to become solvent exposed and establish discrete van der Waals contacts with residues Leu-76, Tyr-341, and Gly-342 at the gorge rim.

Kinetic Analysis of *syn1* and *anti1* Isomer Binding. Comparison of the relative rates of association and dissociation shows that the enhanced affinity of the *syn1* isomer for mAChE largely results from a slower dissociation rate (Table 2). The small differences seen in the association rates would be anticipated in view of the rates being at or near the diffusion rate limit. Hence the enhanced affinity of the *syn1* isomer is reflected in a greater activation barrier for dissociation of the complex. Several conformational changes and positional rearrangements of side chains observed within the PAS and active-site gorge correlate with the *syn1* isomer being more tightly sequestered in the active site gorge.

The *syn1* isomer displays up to 5-fold greater affinity for *E. electricus* and *T. californica* AChEs than for mAChE, and the selectivity of *E. electricus* AChE for the *syn1* isomer is as much as 300-fold higher than that of any other AChE species assayed (Table 2). Only low-resolution structures of *E. electricus* AChE are available (24), but the limited sequence differences found at the PAS and within the gorge do not reveal particular determinants responsible for the higher selectivity. In contrast, *D. melanogaster* AChE, with its Glu, Tyr, and Met substitutions for mAChE residues Tyr-72, Asp-74, and Tyr-124, and mouse butyrylcholinesterase, with its Arg and Asn substitutions for Trp-286 and Tyr-72 (see <http://bioweb.enscm.inra.fr/ESTHER/general?what=index>), show an inverted but small selectivity for the *anti1* isomer, consistent with a more open gorge and fewer aromatic side chains at the PAS in these enzymes. Moreover, removal of the indole ring at the rim of the mAChE gorge by a Trp286Ala mutation results in higher dissociation rates and up to 20-fold reduction in affinity for the *syn1* and *anti1* complexes. These results further emphasize the importance of the peripheral aromatic side chains in trapping the *syn1* phenanthridinium and of Trp-286 in stabilizing both complexes despite the distinctive orientations of the indole side chain.

Functional Role of the Central Triazole Moiety. The triazole moieties of the *syn1*- and *anti1*-mAChE complexes are both tightly bound within the gorge, due to rearrangements in both ligand position and mAChE conformation (Fig. 2). Hence, the triazoles actively contribute to the binding interactions in the respective complexes instead of acting as passive linkers. The high affinities of the complexes (Table 2) arise not only from proximity reducing entropic contributions for a “divalent” ligand with separate binding groups but also from interactions along the gorge wall. The observation that the alternate synthesis product TZ6PA2 with inverted dimethylene and hexamethylene linkers is a weak AChE inhibitor (7) provides additional evidence for specific position-sensitive triazole contributions to the overall binding energy. The formative adaptability of this five-membered heterocycle is reflected in *syn1* cycloaddition occurring with the azide and acetylene extended in a parallel orientation, effectively shortening the intervening linker through the triazole by one bond length, whereas they would lie antiparallel in formation of the *anti1* triazole product (7). The triazole’s large dipole (>5 Debye), which bisects the ring plane near atoms N3 and C5 (Scheme 1, Fig. 1 B and C), and the capacity of the N2 and N3 electron lone pairs to serve as hydrogen bond acceptors not only enhance binding affinity but also contribute to the efficiency of the 1,3-dipolar-coupling reaction. The conformation of the *syn1* complex is congruent with *syn1*’s shorter linker, compared to the *anti1* complex. This is evident from the positioning of the phenanthridinium at the PAS, where it resides closer to

the tetrahydroaminoacridine in the *syn1* than in the *anti1* complex (Fig. 1 B and C, Fig. 2C). To achieve this disposition of proximal reactants, a substantial conformational change occurs at the rim of the gorge with a secondary change evident in the vicinity of the triazole formed by the cycloaddition (Figs. 2C and 3). Hence, the reactivity of the azide and acetylene precursors in the gorge and the resulting affinity of the triazole formed could not have been predicted from structures of apo-AChE (10) or of complexes with close congeners to the precursors (10, 11). To date, inhibitors containing substituted 1,2,3-triazoles have been observed only in plant glycolate oxidase inhibitors (25) and β -lactam antimicrobials (26).

Functional Role of the Trp-286 Indole. Most AChE crystal structures show the Trp-286 side chain centered in the PAS with one face of the indole buried at the rim of the gorge and the other occluded by either a symmetry-related AChE molecule or a bound PAS ligand (ref. 3, and subsequent structures derived from the same TcAChE crystal form; refs. 10, 11, 22, 23, 27, and 28). Only the apo-mAChE structure (10), solved from the crystal form used here, shows the Trp-286 external face fully accessible to solvent, providing it with potential mobility. Indeed, binding of the *syn1* isomer displaces the Trp-286 side chain from the AChE hydrophobic core toward the solvent, with one face of the indole now stacked with the phenanthridinium and the other face still exposed to the solvent and in van der Waals contact with Leu-289 (Figs. 2C and 3). One of the phenanthridinium rings is buried in a near-parallel stacking interaction with the Tyr-124 ring at the bottom of the groove, whereas the other two rings insert into the Trp-286-Tyr-72 parallel sandwich. The buried phenanthridinium amino group is hydrogen bonded to Glu-285. Whereas the phenanthridinium ring system in the bound *anti1* isomer is virtually planar, the *syn1* system adopts a slightly curved shape conforming to the induced groove where it intercalates.

Indirect evidence suggests that the PAS region, with its surface-exposed aromatic groups, may be responsible for the adhesion properties of AChE (29). Recognition and adhesion play important roles in synapse maintenance, as seen with the structurally related neurexins (30). They may also play a role for the AChE-promoted nucleation of amyloid peptides in the Alzheimer’s disease pathogenesis (31). The flip in the Trp-286 indole and the newfound π - π and cation- π interactions seen in the *syn* complex raise the possibility that an open conformation of AChE with distinctive exposure of aromatic groups is involved in these adhesion functions. π -orbital stacking mediated by aromatic side chains is instrumental in other molecular recognition and cell adhesion processes (32). Other intercalations of polycyclic aromatic compounds between protein aromatic side chains or nucleotide bases involve the isoalloxazine moiety of the flavin cofactor and flavodoxin (33); ethidium derivatives and the multidrug-resistant-binding protein QacR (34) and adjacent base pairs (see Nucleic Acid Database, code 1JTY); the benzothiazole moiety of thioflavin and DNA (35) and β -sheet amyloid structures (36); and perhaps thioflavin and the PAS of AChE (37).

Role of the AChE Gorge Flexibility in Catalysis and Inhibitor Binding. Controversy surrounds how AChE, with its catalytic triad at the base of a narrow gorge, sustains high catalytic efficiency. Alternate portals for substrate and product access have been proposed (38); however, catalytic and inhibitor-binding parameters are influenced only by mutations in the gorge (21) and not in the vicinity of the putative additional portals (39). Rapid fluctuations giving rise to transient enlargements of the gorge appear critical (40). Ligand binding evidently induces a closed gorge state, whereas the unliganded enzyme seems to fluctuate rapidly between multiple states with varying degrees of gorge openness (41, 42).

Previous structural analysis of PAS ligands associated with

mAChE showed that the tips of the long Ω loop Cys-69-Cys-96 and loop Val-340-Gly-342 bordering on the gorge (Fig. 1A) possessed sufficient mobility to enlarge the gorge entry, thereby facilitating access to and from the active center (10). In fact, only the *syn1*-mAChE complex exhibits an increase of up to 12 Å in the mean temperature factors for residues at the loop tips where movement of 1.2 Å of Leu-76 and an inversion of the Gly-342 carbonyl carbon occur; the weak electron densities for the Leu-76 and Tyr-341 side chains are also consistent with substantial localized fluctuations. Hence, the flexibility of the AChE long Ω loop differs from the hinge-like motion of a homologous loop that, in the structurally related lipases, forms a rigid flap and opens only in the presence of the lipid substrate (43, 44). Moreover, ligand binding to AChE may cause the gorge to collapse around the ligand, minimizing internal dimensions (41, 42). This notion is supported by the observed repositioning of the Tyr-337 side chain and associated perturbation of Tyr-341, which not only alter the gorge shape but also enlarge its width at the position of constriction to accommodate the *syn1* triazole (Fig. 2C). Such large conformational changes involving these residues were not observed for the PAS or active center complexes from which the precursor reactants were designed (10, 11). These computational and experimental results point to concerted fluctuations all along the gorge, which may facilitate access of incoming substrate to the active site at the gorge base and presumably occur in short time frames relative to diffusional translation of substrate (40).

In summary, the use of the enzyme active-site gorge as an atomic-scale template for inhibitor synthesis (7) and of structural

analyses of the *anti1*- and *syn1*-mAChE complexes has revealed (i) an *in situ* phenomenon (7) that bears an uncanny resemblance to pioneering studies begun in 1983 by W. L. Mock (45); (ii) inherent flexibility and conformational fluctuations in the AChE molecule; and (iii) a most stable and selective complex that could not have been predicted from the apo-enzyme structure (10). The highly exergonic nature of the 1,3-dipolar-[2 + 3]-cycloaddition ($\Delta H > 50$ kcal/mol) has allowed us to immobilize and then identify by structural means an otherwise minor abundance conformation of the enzyme. Because only the higher-affinity *syn1*-triazole regioisomer is associated with major changes in enzyme conformation, the crystalline *syn1*-mAChE complex becomes the lead template in the design of selective pharmacologic agents directed toward the catalytic or noncatalytic functions of AChE. If, in fact, AChE through its PAS plays a role in synaptic adhesion processes and in nucleating plaque formation associated with dementia (29), then AChE inhibitors that also influence surface conformation may offer a means of enhancing therapeutic efficacy.

We are grateful to D. Fournier for providing the *D. melanogaster* enzyme, L. Green for synthesis of the regioisomers; F. Grynspan, M. G. Finn, and W. G. Lewis for discussion; M. Juin for assistance in crystallogensis; and G. Sulzenbacher, M. Czjzek, and the ID14 staff of the European Synchrotron Radiation Facility for expert assistance in data collection. This work was supported by grants from the Association Française contre les Myopathies (to P.M.); U.S. Public Health Service (R37-GM18360) and Department of Army Medical Defense (17-1-8014) (to P.T.); and National Institutes of Health (GM 28384), National Science Foundation (CHE-9985553), National Institute of General Medical Sciences, and the W. M. Keck Foundation (to K.B.S.).

- Argyl-Robertson, D. (1863) *Edinb. Med. J.* **8**, 815–820.
- Dale, H. H. (1914) *J. Pharmacol. Exp. Ther.* **6**, 147–190.
- Sussman, J. L., Harel, M., Frolow, F., Oefner, C., Goldman, A., Toker, L., & Silman, I. (1991) *Science* **253**, 872–879.
- Changeux, J.-P. (1966) *Mol. Pharmacol.* **2**, 369–392.
- Taylor, P. & Lappi, S. (1975) *Biochemistry* **14**, 1989–1997.
- Taylor, P. (2001) in *Goodman and Gilman's Pharmacological Basis of Therapeutics* (eds. Hardman, J. G. & Limbird, L. E.), 10th Ed., pp. 175–192.
- Lewis, W. G., Green, L. G., Grynspan, F., Radić, Z., Carlier, P. R., Taylor, P., Finn, M. G., & Sharpless, K. B. (2002) *Angew. Chem. Int. Ed.* **41**, 1053–1057.
- Rachinsky, T. L., Camp, S., Li, Y., Ekström, J., Newton, M., & Taylor, P. (1990) *Neuron* **5**, 317–327.
- Marchot, P., Ravelli, R. B. G., Raves, M. L., Bourne, Y., Vellom, D. C., Kanter, J., Camp, S., Sussman, J. L., & Taylor, P. (1996) *Protein Sci.* **5**, 672–679.
- Bourne, Y., Taylor, P., Radić, Z., & Marchot, P. (2003) *EMBO J.* **22**, 1–12.
- Harel, M., Schalk, I., Ehret-Sabatier, L., Bouet, F., Goeldner, M., Hirth, C., Axelsen, P. H., Silman, I., & Sussman, J. L. (1993) *Proc. Natl. Acad. Sci. USA* **90**, 9031–9035.
- Otwinowski, Z. & Minor, W. (1997) *Methods Enzymol.* **276**, 307–326.
- Collaborative Computational Project Number 4 (1994) *Acta Crystallogr. D* **50**, 760–763.
- Brünger, A. T., Adams, P. D., Marius Clore, G., DeLano, W. L., Gros, P., Grosse-Kunstleve, R. W., Jiang, J.-S., Kuszewski, J., Nilges, M., Pannu, N. S., et al. (1998) *Acta Crystallogr. D* **54**, 905–909.
- Murshudov, G., Vagin, A., & Dodson, E. J. (1997) *Acta Crystallogr. D* **53**, 240–255.
- Roussel, A. & Cambillau, C. (1989) in *Silicon Graphics Geometry Partners Directory*, eds. Silicon Graphics Committee (Silicon Graphics, Mountain View, CA), pp. 77–78.
- Mohamadi, F., Richards, N. G. J., Guida, W. C., Liskamp, R., Lipton, M., Caufield, C., Chang, G., Hendrickson, T., & Still, W. C. (1990) *J. Comput. Chem.* **11**, 440–467.
- Laskowski, R. A., MacArthur, M. W., Moss, D. S., & Thornton, J. M. (1993) *J. Appl. Crystallogr.* **26**, 283–291.
- Christopher, J. A. (1998) SPOCK (Center for Macromolecular Design, Texas A&M University, College Station, TX).
- Merritt, E. A. & Bacon, D. J. (1997) *Methods Enzymol.* **277**, 505–524.
- Radić, Z., Pickering, N. A., Vellom, D. C., Camp, S., & Taylor, P. (1993) *Biochemistry* **32**, 12074–12084.
- Bourne, Y., Taylor, P., & Marchot, P. (1995) *Cell* **83**, 503–512.
- Bourne, Y., Taylor, P., Bougis, P. E., & Marchot, P. (1999) *J. Biol. Chem.* **274**, 2963–2970.
- Bourne, Y., Grassi, J., Bougis, P. E., & Marchot, P. (1999) *J. Biol. Chem.* **274**, 30370–30376.
- Stenberg, K. & Lindqvist, Y. (1997) *Protein Sci.* **6**, 1009–1015.
- Kuzin, A. P., Nukaga, M., Nukaga, Y., Hujer, A. M., Bonomo, R. A., & Knox, J. R. (2001) *Biochemistry* **40**, 1861–1866.
- Harel, M., Kleywegt, G. J., Ravelli, R. B., Silman, I., & Sussman, J. L. (1995) *Structure (London)* **3**, 1355–1366.
- Kryger, G., Silman, I., & Sussman, J. L. (1999) *Acta Crystallogr. D* **56**, 1385–1394.
- Soreq, H. & Seidman, S. (2001) *Nat. Rev. Neurosci.* **2**, 294–302.
- Ichchenko, K., Nguyen, T., & Sudhof, T. C. (1996) *J. Biol. Chem.* **271**, 2676–2682.
- Inestrosa, N. C., Alvarez, A., Perez, C. A., Moreno, R. D., Vicente, M., Linker, C., Casanueva, O. I., Soto, C., & Garrido, J. (1996) *Neuron* **16**, 881–891.
- Zacharias, N. & Dougherty, D. A. (2002) *Trends Pharmacol. Sci.* **23**, 281–287.
- Genzor, C. G., Perales-Alcon, A., Sancho, J., & Romero, A. (1996) *Nat. Struct. Biol.* **3**, 329–332.
- Schumacher, M. A., Miller, M. C., Grkovic, S., Brown, M. H., Skurray, R. A., & Brennan, R. G. (2001) *Science* **294**, 2158–2163.
- Canete, M., Villanueva, A., Juarranz, A., & Stockert, J. C. (1987) *Cell. Mol. Biol.* **33**, 191–199.
- LeVine, H., III (1999) *Methods Enzymol.* **309**, 274–284.
- De Ferrari, G. V., Mallender, W. D., Inestrosa, N. C., & Rosenberry, T. L. (2001) *J. Biol. Chem.* **276**, 23282–23287.
- Gilson, M. K., Straatsma, T. P., McCammon, J. A., Ripoll, D. R., Faerman, C. H., Axelsen, P. H., Silman, I., & Sussman, J. L. (1994) *Science* **263**, 1276–1278.
- Kronman, C., Ordentlich, A., Barak, D., Velan, B., & Shafferman, A. (1994) *J. Biol. Chem.* **269**, 27819–27822.
- Shen, T., Tai, K., Henschman, R. H., & McCammon, J. A. (2002) *Acc. Chem. Res.* **35**, 332–340.
- Shi, J., Radić, Z., & Taylor, P. (2002) *J. Biol. Chem.* **277**, 43301–43308.
- Shi, J., Tai, K., McCammon, A. J., Taylor, P., & Johnson, D. A. (2003) *J. Biol. Chem.* **278**, 30905–30911.
- Cyglar, M., Schrag, J., Sussman, J. L., Harel, M., Silman, I., Gentry, M. K., & Doctor, B. P. (1993) *Protein Sci.* **2**, 366–382.
- Grochulski, P., Li, Y., Schrag, J. D., & Cyglar, M. (1994) *Protein Sci.* **3**, 82–91.
- Mock, W. L. (1995) *Top. Curr. Chem.* **175**, 1–24.

In Situ Click Chemistry: Enzyme Inhibitors Made to Their Own Specifications

Roman Manetsch,[†] Antoni Krasinski,[†] Zoran Radić,[‡] Jessica Raushel,[†]
Palmer Taylor,[‡] K. Barry Sharpless,[†] and Hartmuth C. Kolb^{*†}

Contribution from the Department of Chemistry and the Skaggs Institute for Chemical Biology, The Scripps Research Institute, 10550 North Torrey Pines Road, La Jolla, California 92037, and the Department of Pharmacology, University of California, San Diego, 9500 Gilman Drive, La Jolla, California 92093

Received June 18, 2004; E-mail: hckolb@scripps.edu

Abstract: The in situ click chemistry approach to lead discovery employs the biological target itself for assembling inhibitors from complementary building block reagents via irreversible connection chemistry. The present publication discusses the optimization of this target-guided strategy using acetylcholinesterase (AChE) as a test system. The application of liquid chromatography with mass spectroscopic detection in the selected ion mode for product identification greatly enhanced the sensitivity and reliability of this method. It enabled the testing of multicomponent mixtures, which may dramatically increase the in situ screening throughput. In addition to the previously reported in situ product *syn-TZ2PA6*, we discovered three new inhibitors, *syn-TZ2PA5*, *syn-TA2PZ6*, and *syn-TA2PZ5*, derived from tacrine and phenylphenanthridinium azides and acetylenes, in the reactions with *Electrophorus electricus* and mouse AChE. All in situ-generated compounds were extremely potent AChE inhibitors, because of the presence of multiple sites of interaction, which include the newly formed triazole nexus as a significant pharmacophore.

Introduction

The past decade has seen a paradigm shift in drug discovery from testing small numbers of "handcrafted" compounds and natural products to high-throughput screening of large combinatorial libraries.¹ These developments have gone hand in hand with dramatic improvements in methods for producing, handling, and screening large numbers of compounds.^{2–5} Despite these achievements, challenges related to the synthesis, purification, and diversity of compound libraries and the pharmacological properties of their members still exist,^{6,7} and combinatorial chemistry has not yet achieved its full potential.^{8,9} Since typically more than 99% of all compounds in a library are inactive in a given screen, methods for producing just the active compounds are highly desirable. Target-guided synthesis (TGS) seeks to address this challenge by using the target enzyme for assembling its own inhibitors from a collection of building block reagents.

Only building blocks that adhere to the protein's binding sites react with each other to form highly potent inhibitors that simultaneously access multiple binding pockets within the protein. These target-guided approaches avoid the classical screening of large compound libraries altogether, and hit identification can be as simple as determining whether a given combination of building blocks has resulted in a product. Follow-up tests for determining the inhibitory potency, bioavailability, toxicity, and the development of structure–activity relationships (SAR) can then be limited to a small number of target-generated compounds, which may dramatically improve the efficiency of the discovery process.

The concept of target-guided synthesis was pioneered almost 20 years ago by Rideout et al., who observed a marked synergism between the cytotoxic effects of decanal and *N*-amino-guanidines, which was proposed to be due to the self-assembly of cytotoxic hydrazones inside cells.^{10,11} Since then, several approaches to target-guided synthesis have been explored: (1) dynamic combinatorial chemistry,^{12–21} (2) stepwise target-guided synthesis,^{22,23} and (3) kinetically controlled target-

[†] The Scripps Research Institute.

[‡] University of California, San Diego.

- (1) Nicolaou, K. C.; Hanko, R.; Hartwig, W. In *Handbook of Combinatorial Chemistry*; Nicolaou, K. C., Hanko, R., Hartwig, W., Eds.; Wiley-VCH: Weinheim, Germany, 2002; Vol. 1, pp 3–9.
- (2) Kolb, H. C.; Sharpless, K. B. *Drug Discovery Today* **2003**, *8*, 1128–1137.
- (3) Terrett, N. *Combinatorial Chemistry*; Oxford University Press: Oxford, U.K., 1998.
- (4) Nicolaou, K. C.; Hanko, R.; Hartwig, W. *Handbook of Combinatorial Chemistry*; Wiley-VCH: Weinheim, Germany, 2002; Vol. 1.
- (5) Nicolaou, K. C.; Hanko, R.; Hartwig, W. *Handbook of Combinatorial Chemistry*; Wiley-VCH: Weinheim, Germany, 2002; Vol. 2.
- (6) Kassel, D. B.; Myers, P. L. *Pharm. News* **2002**, *9*, 171–177.
- (7) Geysen, H. M.; Schoenen, F.; Wagner, D.; Wagner, R. *Nat. Rev. Drug Discovery* **2003**, *2*, 222–230.
- (8) Fixing the drugs pipeline. *The Economist*, March 11, 2004; available online at http://www.economist.com/printedition/displayStory.cfm?Story_ID=2477075.
- (9) Kubinyi, H. *Nat. Rev. Drug Discovery* **2003**, *2*, 665–668.

- (10) Rideout, D. *Science* **1986**, *233*, 561–563.
- (11) Rideout, D.; Calogeropoulou, T.; Jaworski, J.; McCarthy, M. *Biopolymers* **1990**, *29*, 247–262.
- (12) Huc, I.; Lehn, J.-M. *Proc. Natl. Acad. Sci. U.S.A.* **1997**, *94*, 2106–2110.
- (13) Ramstrom, O.; Lehn, J.-M. *ChemBioChem* **2000**, *1*, 41–48.
- (14) Lehn, J.-M.; Eliseev, A. V. *Science* **2001**, *291*, 2331–2332.
- (15) Bunyapiboonsri, T.; Ramstrom, O.; Lohmann, S.; Lehn, J.-M.; Peng, L.; Goeldner, M. *ChemBioChem* **2001**, *2*, 438–444.
- (16) Eliseev, A. V. *Pharm. News* **2002**, *9*, 207–215.
- (17) Ramstrom, O.; Lehn, J.-M. *Nat. Rev. Drug Discovery* **2002**, *1*, 26–36.
- (18) Otto, S. *Curr. Opin. Drug Discovery Dev.* **2003**, *6*, 509–520.
- (19) Erlanson, D. A.; Braisted, A. C.; Raphael, D. R.; Randal, M.; Stroud, R. M.; Gordon, E. M.; Wells, J. A. *Proc. Natl. Acad. Sci. U.S.A.* **2000**, *97*, 9367–9372.

guided synthesis.^{24–31} The dynamic combinatorial chemistry approach introduced by Lehn et al.¹² relies on building blocks bearing complementary functional groups that react reversibly with each other to form a thermodynamically controlled mixture of products. In the presence of the enzyme, the equilibrium is skewed toward the compounds that show the highest affinity toward the enzyme. Their identification requires the equilibrium to be “frozen” (e.g., by hydride reduction or by lowering the pH) before analysis by HPLC or MS can be performed. The multistep variant of TGS makes only indirect use of the enzyme for inhibitor synthesis.^{22,23} In the first step, a library of building blocks is screened to identify candidates that bind to the enzyme. In the second step, the building blocks with the highest affinity are linked together using conventional combinatorial chemistry approaches. The library of “divalent” molecules is then screened for high affinity inhibitors using traditional assays. The kinetically controlled approach uses the enzyme target itself for the synthesis of inhibitors by equilibrium controlled sampling of various possible pairs of reactants until an irreversible reaction induced by the enzyme essentially connects the pair that best fits its binding pockets.^{24–31}

Recently, several successful applications of the kinetically controlled approach to TGS have been reported. For example, Benkovic and Boger have developed multisubstrate adduct inhibitors (MAI) of the enzyme glycylamide ribonucleotide transformylase (GAR Tfase) by enzyme-templated alkylation of one of its substrates with a folate-derived electrophile.^{26–28} More recently, Huc described a similar approach, in which inhibitors of carbonic anhydrase were generated by alkylation of a thiol with α -chloroketones in the presence of the Zn(II) enzyme.²⁹ Competition experiments revealed that the enzyme-templated reaction had produced mainly the alkylation product with the highest affinity for the target. Nicolaou and co-workers have utilized a target-accelerated combinatorial synthesis approach to develop dimeric derivatives of vancomycin.^{30,31} Appropriately functionalized monomeric vancomycin derivatives were subjected to olefin metathesis or disulfide formation in the presence of vancomycin's target, Ac-D-Ala-D-Ala or Ac₂-L-Lys-D-Ala-D-Ala, resulting in the formation of highly potent dimers.

The scope of most TGS methods is limited because of their use of highly reactive reagents (strong electrophiles or nucleo-

philes, metathesis catalysts etc.), which can react in many “unproductive” pathways, including ones that destroy the enzyme target. In contrast, the recently developed in situ click chemistry approach to kinetically controlled TGS²⁴ uses bio-orthogonal reactions and reagents, for example, the [1,3]-dipolar cycloaddition reaction³² between azides and acetylenes. This system is especially well-suited for TGS, since (a) the reaction is extremely slow at room temperature, despite the very high driving force that makes it irreversible, (b) it does not involve components that might disturb the binding sites (external reagents, catalysts, byproducts), and (c) the reactants are inert to biological molecules. Mock et al. had previously provided proof-of-concept by demonstrating that the azide/acetylene [1,3]-dipolar cycloaddition is accelerated by 4 to 5 orders of magnitude by the synthetic receptor cucurbituril to give exclusively the *anti*-triazole regioisomer.^{33–35}

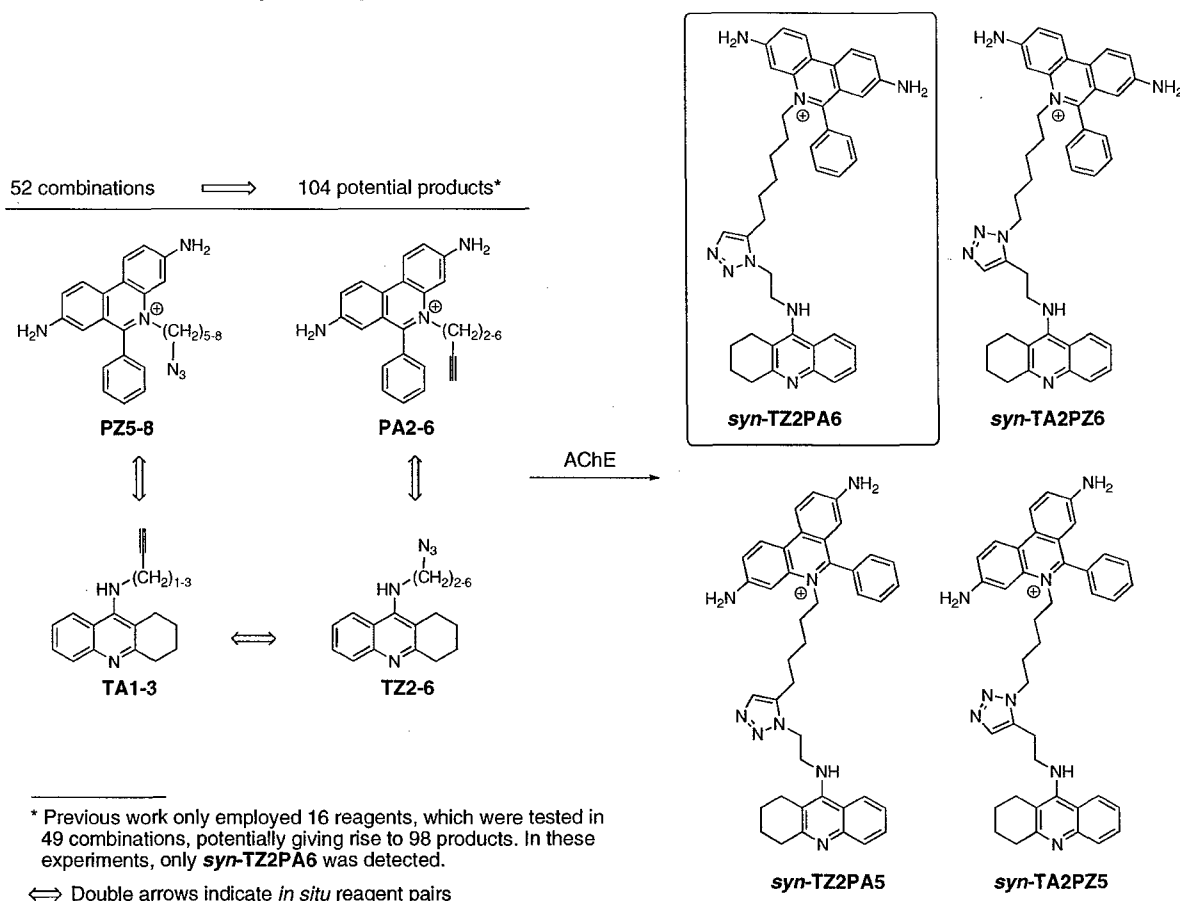
The biological target for the initial in situ click chemistry study, acetylcholinesterase (AChE), catalyzes the hydrolysis of the neurotransmitter acetylcholine and thus plays a key role in the central and peripheral nervous system.³⁶ Its inhibitors have been employed for over a century in various therapeutic regimens and to investigate the role of acetylcholine in neurotransmission.^{37,38} The catalytic site of the enzyme is located at the bottom of a 20 Å deep narrow gorge. A second, peripheral binding site is positioned at the other end of this gorge, near the protein surface.^{39,40} A building block library of azides and acetylenes based on the known site-specific inhibitors tacrine (active site ligand) and phenylphenanthridinium (peripheral site ligand) was developed to probe whether the enzyme would combine selected pairs of complementary reagents to synthesize its “divalent” inhibitors (cf. Scheme 1).²⁴

A series of 49 binary mixtures of these reagents was incubated with *Electrophorus electricus* AChE (electric eel AChE) at room temperature for 6 days, potentially giving rise to 98 products. Analysis of the crude reaction mixtures by desorption/ionization on silicon mass spectrometry⁴¹ (DIOS-MS) revealed only one product, **TZ2PA6**, which was shown by HPLC to be only the 1,5-disubstituted triazole (“*syn*-triazole”) (Scheme 1). This compound, formed by the enzyme, turned out to be the most potent noncovalent AChE inhibitor known to date, with K_d values between 77 fM (*Torpedo californica*) and 410 fM (murine AChE). In contrast, the *anti*-**TZ2PA6** isomer, not formed by the enzyme, is less active by 2 orders of magnitude.

Recent X-ray structures of both the *syn*- and *anti*-**TZ2PA6** mouse AChE complexes confirmed the multivalent nature of the protein ligand interactions, with the tacrine moiety accessing the active center of the enzyme and the phenylphenanthridinium group the peripheral site (Figure 1).²⁵ Interestingly, these studies

- (20) Erlanson, D. A.; Lam, J. W.; Wiesmann, C.; Luong, T. N.; Simmons, R. L.; DeLano, W. L.; Choong, I. C.; Burdett, M. T.; Flanagan, W. M.; Lee, D.; Gordon, E. M.; O'Brien, T. *Nat. Biotechnol.* **2003**, *21*, 308–314.
- (21) Ramström, O.; Lohmann, S.; Bunyapiboonkiet, T.; Lehn, J.-M. *Chem.-Eur. J.* **2004**, *10*, 1711–1715.
- (22) Maly, D. J.; Choong, I. C.; Ellman, J. A. *Proc. Natl. Acad. Sci. U.S.A.* **2000**, *97*, 2419–2424.
- (23) Kehoe, J. W.; Maly, D. J.; Verdugo, D. E.; Armstrong, J. I.; Cook, B. N.; Ouyang, Y.-B.; Moore, K. L.; Ellman, J. A.; Bertozzi, C. R. *Bioorg. Med. Chem. Lett.* **2002**, *12*, 329–332.
- (24) Lewis, W. G.; Green, L. G.; Grynszpan, F.; Radic, Z.; Carlier, P. R.; Taylor, P.; Finn, M. G.; Sharpless, K. B. *Angew. Chem., Int. Ed.* **2002**, *41*, 1053–1057.
- (25) Bourne, Y.; Kolb, H. C.; Radic, Z.; Sharpless, K. B.; Taylor, P.; Marchot, P. *Proc. Natl. Acad. Sci. U.S.A.* **2004**, *101*, 1449–1454.
- (26) Inglesc, J.; Benkovic, S. J. *Tetrahedron* **1991**, *47*, 2351–2364.
- (27) Boger, D. L.; Haynes, N.-E.; Kito, P. A.; Warren, M. S.; Ramcharan, J.; Marolewski, A. E.; Benkovic, S. J. *Bioorgan. Med. Chem.* **1997**, *5*, 1817–1830.
- (28) Greasley, S. E.; Marsilje, T. H.; Cai, H.; Baker, S.; Benkovic, S. J.; Boger, D. L.; Wilson, I. A. *Biochemistry* **2001**, *40*, 13538–13547.
- (29) Nguyen, R.; Huc, I. *Angew. Chem., Int. Ed.* **2001**, *40*, 1774–1776.
- (30) Nicolaou, K. C.; Hughes, R.; Cho, S. Y.; Winssinger, N.; Smethurst, C.; Labischinski, H.; Endermann, R. *Angew. Chem., Int. Ed.* **2000**, *39*, 3823–3828.
- (31) Nicolaou, K. C.; Hughes, R.; Cho, S. Y.; Winssinger, N.; Labischinski, H.; Endermann, R. *Chem.-Eur. J.* **2001**, *7*, 3824–3843.

- (32) Huisgen, R. In *1,3-Dipolar Cycloaddition Chemistry*; Padwa, A., Ed.; Wiley: New York, 1984; Vol. 1, pp 1–176.
- (33) Mock, W. L.; Irra, T. A.; Wepsiec, J. P.; Manimaran, T. L. *J. Org. Chem.* **1983**, *48*, 3619–3620.
- (34) Mock, W. L.; Irra, T. A.; Wepsiec, J. P.; Adhya, M. *J. Org. Chem.* **1989**, *54*, 5302–5308.
- (35) Mock, W. L. *Top. Curr. Chem.* **1995**, *175*, 1–24.
- (36) Taylor, P.; Radic, Z. *Annu. Rev. Pharmacol. Toxicol.* **1994**, *34*, 281–320.
- (37) Argyl-Robertson, D. *Edinburgh Med. J.* **1863**, *8*, 815–820.
- (38) Dale, H. H. *J. Pharmacol. Exp. Ther.* **1914**, *6*, 147–190.
- (39) Sussman, J. L.; Harel, M.; Frolow, F.; Oefner, C.; Goldman, A.; Tokar, L.; Silman, I. *Science* **1991**, *253*, 872–879.
- (40) Harel, M.; Schalk, I.; Ehret-Sabatier, L.; Bouct, F.; Goeldner, M.; Hirth, C.; Axelsen, P. H.; Silman, I.; Sussman, J. L. *Proc. Natl. Acad. Sci. U.S.A.* **1993**, *90*, 9031–9035.
- (41) Wei, J.; Buriak, J. M.; Siuzdak, G. *Nature* **1999**, *399*, 243–246.

Scheme 1. In Situ Click Chemistry Screening^a

^a Fifty-two binary mixtures of azide and alkyne building blocks were incubated with eel AChE, as indicated by the double arrows, potentially giving rise to 104 products. Previous work was done without **PZ5**, potentially giving rise to 98 products from 49 reagent combinations, and providing **syn-TZ2PA6** as the sole product of the *in situ* reaction with the enzyme.²⁴

revealed that the triazole unit, created by the azide/alkyne cycloaddition, engages in hydrogen bonding and stacking interactions with amino acid residues in the wall of the gorge. Several important conclusions can be drawn from this observation. First, triazoles are not just passive linkers, but rather active pharmacophores that may contribute significantly to protein binding, as in the case of the *in situ*-generated product, **syn-TZ2PA6**. Second, the tremendous rate acceleration by AChE⁴² is due not only to entropic effects, but also to an enthalpic stabilization of the triazole-like transition state, leading to the observed product. In a more general sense, it appears likely that an “*in situ* hit” is a good binder, because the same entropic and enthalpic factors that cause the observed rate acceleration may also stabilize the newly formed triazole in the complex and thus add to the overall binding interactions, which also involve the two residues that are held together by the triazole linker.

The higher potency of **syn-TZ2PA6** compared to the anti-isomer manifests itself in a strikingly different binding mode at the peripheral site. The phenylphenanthridinium moiety of the tightly bound *syn*-product inserts itself between tryptophan-286 and tyrosine-72 residues near the gorge rim (Figure 1),

causing the enzyme to adopt a minor abundance conformation in which the tryptophan residue swings out into the solvent to make room for the ligand. This conformation has never been seen before in AChE X-ray structures of the free enzyme or its inhibitor complexes. Thus, the *in situ* click chemistry approach allows one to identify conformations that associate with high affinity inhibitors and that would not be detected by conventional structural methods. These findings have interesting implications for drug discovery, as it is possible to trap a flexible enzyme in a minor abundance conformation by an inhibitor, which is formed inside its binding pockets through the irreversible reaction of complementary building blocks.

The goal of this study was to optimize the *in situ* approach to drug discovery and to investigate its scope. We started by optimizing the mass spectroscopy-based analysis method, since a highly sensitive and reliable method was deemed crucial for success. We then revisited the AChE system to search for additional *in situ* hits from binary azide/acetylene mixtures and from multireagent mixtures (combinatorial screening), to study the species dependence of product formation, and to determine *syn/anti* ratios and binding affinities for all products.

Results and Discussion

Optimization of the Analysis Method. Poor and variable levels of purity of the acetylcholinesterase enzyme make great demands on the analytical techniques used to detect the

(42) The enzyme-free reaction under these conditions ($[TZ2] = 4.6 \mu M$; $[PA6] = 24 \mu M$) is extremely slow, taking several thousand years to reach 50% conversion at 18 °C (second-order rate constant at 18 °C in 1-BuOH, $K = 1.9 \times 10^{-5} M^{-1} min^{-1}$).²⁴ Apart from the expected entropic stabilization, the transition state may also experience stabilization through hydrogen bonding and stacking interactions with the protein.²⁵

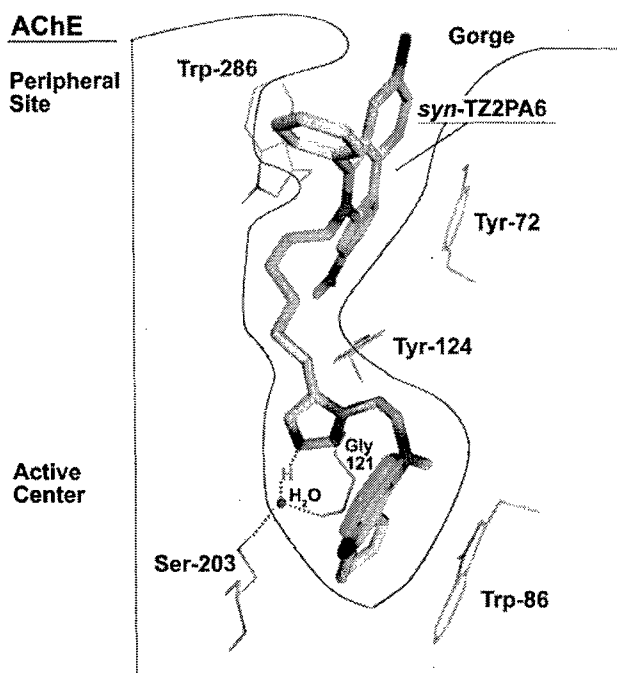


Figure 1. Schematic representation of the binding interactions between *syn*-TZ2PA6 and mouse AChE.²⁵

formation of templated inhibitors, especially when they are tightly bound. In previous experiments, the DIOS-MS method was found to be capable of detecting small quantities of new molecules in the presence of large amounts of protein, but signal-to-noise ratios were still very low. This issue has now been resolved by purifying the samples before MS analysis using standard LC/MS techniques with selected ion monitoring to increase sensitivity even further. *The analysis is extremely easy to perform, allowing crude reaction mixtures to be screened and products to be unambiguously identified by their molecular weights and retention times.*

The new analytical method was validated on the known in situ hit TZ2PA6. After incubating the building blocks TZ2 and PA6 with eel AChE for 6 h, analysis by LC/MS–SIM gave a distinct product signal with a characteristic molecular weight and retention time (Figure 2). Thus, the high sensitivity of this analysis method allowed us to reduce the incubation time from 6 days to as little as 6 h, thereby significantly enhancing the efficiency of lead discovery by in situ click chemistry.⁴³ Control experiments, in which mixtures of the same building blocks were incubated in the presence of bovine serum albumin (BSA) instead of AChE, or in the absence of any protein, failed to give detectable amounts of triazole.

In Situ Lead Discovery. Encouraged by these results, we decided to revisit the AChE system using a library of tacrine and phenylphenanthridinium building blocks (“T-P library”), which contained one additional member, PZ5, compared to previous work, and to screen for additional in situ hits with the

(43) The in situ screening experiments were generally performed with the following concentrations: 1 μ M for the enzyme, 4.6 μ M for tacrine components, and 24 μ M for phenylphenanthridinium components. Because of the sensitive nature of the analysis method, the building block concentrations can be reduced to as low as 1 μ M for tacrine reagents and 6 μ M for phenylphenanthridinium reagents, without a significant loss of intensity of the product peak. However, lowering the phenylphenanthridinium component concentration to 1 μ M dramatically decreased the reaction rate and makes the intensity of the product signal prohibitively small.

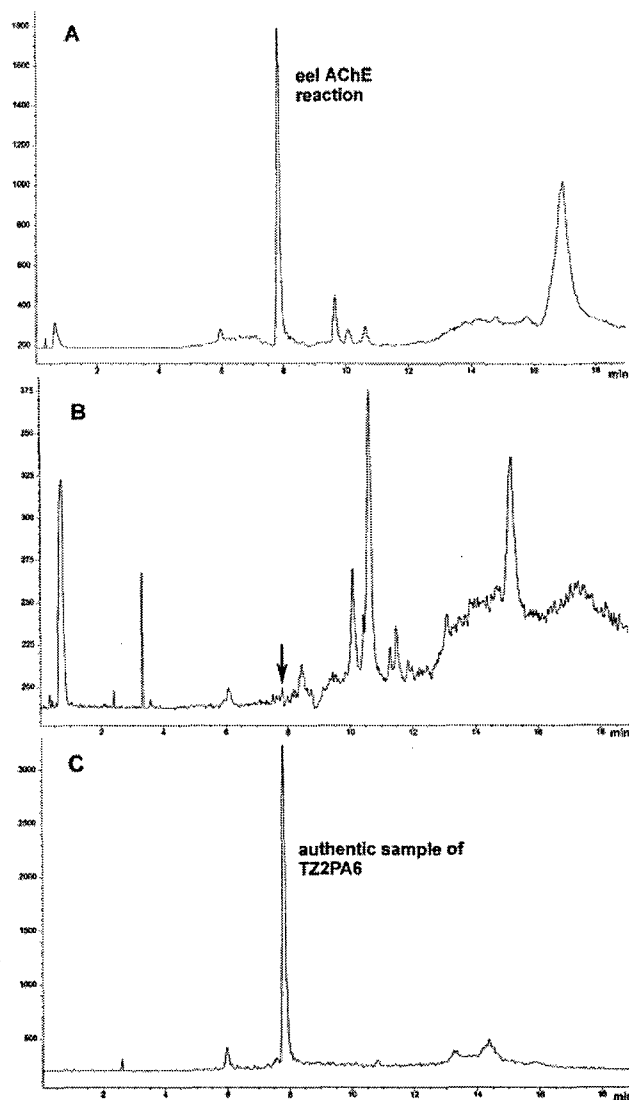


Figure 2. In situ hit identification by LC/MS–SIM, exemplified by the TZ2/PA6 pair. (A) TZ2 (4.6 μ M) and PA6 (24 μ M) after incubation with eel AChE (1.04 μ M) at pH 7.5 for 6 h. (B) TZ2 and PA6 incubated in the presence of BSA (3 mg/mL) instead of AChE. The same trace is obtained in the absence of any protein (note that the Y-scale of the BSA trace is expanded 8.5 times compared to the eel AChE trace to clearly demonstrate the absence of any product in this sample). (C) Authentic sample of TZ2PA6.

more sensitive LC/MS–SIM method. In the “in situ screening mode”, potential hits are identified by looking for significant differences between the chromatograms of the enzyme reactions and the control reactions (BSA in place of AChE, absence of any protein). The potential hits are then validated by additional control experiments (e.g., performing the enzyme reaction in the presence of a known active site inhibitor) and eventually by comparing retention times with synthetic samples (cf. Table 3). This screening procedure led to the identification of three new hit compounds—TZ2PA5, TA2PZ6, and TA2PZ5—in addition to the known hit, TZ2PA6, by incubating 52 binary tacrine- and phenanthridinium-based azide/acetylene mixtures as illustrated in Scheme 1 (i.e., PZ5–8/TA1–3, PA2–6/TZ2–6, and TA1–3/TZ2–6) with eel AChE for 1 day. All hits were validated as described and by MALDI mass spectroscopy, which revealed distinct molecular ions for the respective products in

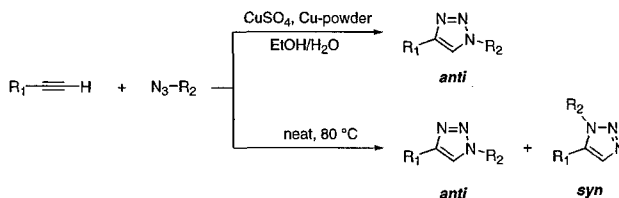
all four in situ reaction mixtures. Thus, only **TZ/PA** and **TA/PZ** combinations, not **TZ/TA** combinations, provided in situ hits.

Interestingly, all four hit compounds have the newly formed triazole moieties separated by two methylene units from the tacrine core. Other compounds with the same overall spacing between tacrine and phenanthridinium moieties, but a different location of the triazole (e.g., **TZ6PA2**), are not formed, suggesting that the triazole-genesis event is critically linked to a specific location in the protein's gorge. This notion is supported by the X-ray crystal structures of **TZ2PA6**/mouse AChE complexes,²⁵ which reveal that the triazole units are tightly bound inside the gorge through hydrogen bonding and stacking interactions (Figure 1). It is reasonable to assume that these product-stabilizing interactions in that location also favor the transition state leading to the product. Such active participation by the protein, in addition to entropic factors, would explain the dramatic rate acceleration observed in this system, over that for the uncatalyzed cycloaddition reaction.⁴²

Species Dependence. We decided to investigate the species dependence of product formation, since the X-ray studies were performed with mouse AChE, while eel enzyme was used for the in situ screen (58% sequence identity and 70% residue homology by NCBI Blast2).^{44,45} Incubation of binary azide/acetylene mixtures from the **T-P** building block library with mouse AChE and analysis by LC/MS–SIM provided the same four hit compounds—**TZ2PA6**, **TZ2PA5**, **TA2PZ6**, and **TA2PZ5**—as before. Thus, not only is mouse AChE able to make its inhibitors, it does so with the same building block preferences as the eel enzyme.

Combinatorial in Situ Screening. In situ click chemistry promises a big boost for lead discovery above all because it eliminates the need for high-throughput screening of large compound libraries, since the biological target itself has been forced to generate its inhibitors, which can readily be identified. Moreover, while previous experiments had used only binary azide/acetylene mixtures,²⁴ we have now found that the enzyme is able to select and assemble the best inhibitors from more complex mixtures of azide and acetylene building blocks. This not only reduces the amount of enzyme per reagent combination, but also increases the screening throughput. Multicomponent in situ click chemistry screening was made possible by the new LC/MS–SIM method, because of its higher sensitivity and greater reliability of product identification through chromatographic separation of the reaction components. In a proof-of-concept experiment, the azide **TZ2** and a mixture of four phenylphenanthridinium building blocks, **PA2–PA5**, were incubated with eel AChE under standard conditions at 37 °C overnight. LC/MS–SIM analysis of the reaction mixture showed the expected compound **TZ2PA5** to be the sole product. Encouraged by this success, we expanded this multicomponent approach to the entire tacrine azide/phenylphenanthridinium acetylene library. To avoid combinations with degenerate molecular weights (e.g., **TZ3PA5** has the same molecular weight as **TZ2PA6**), which would complicate product identification,

Scheme 2. Synthesis of Triazoles as Reference Compounds for the Determination of the *syn/anti* Ratio of in Situ Hits by HPLC^a



^a Equimolar *syn*- and *anti*-triazole mixtures were prepared by heating neat mixtures of the corresponding azides and alkynes at 80 °C for 6 days. The pure *anti*-regioisomers were readily prepared by the copper(I)-catalyzed reaction between the azide and alkyne reagents.^{46,47}

especially in view of the similar chromatographic behavior of the **TZ-PA** compounds, we decided to conduct the experiment in five batches: Mixtures of all five phenanthridinium acetylenes, **PA2–PA6**, were incubated with one tacrine azide at a time in the presence of mouse or eel AChE. Analysis by LC/MS–SIM revealed the expected hits, **TZ2PA5** and **TZ2PA6** (cf. Supporting Information). These experiments demonstrate that multicomponent screening is feasible, albeit at the cost of a slightly reduced sensitivity.

Determination of the *syn/anti* Selectivity. The X-ray cocrystal structures revealed that the more weakly bound *anti*-**TZ2PA6** has little effect on the enzyme conformation, whereas the higher affinity *syn*-**TZ2PA6** isomer, with its shorter spacer length between the tacrine and phenanthridinium moieties (the distance between the aromatic ring atoms of the tacrine and phenanthridinium moieties that are connected to the linker is 1.52 Å shorter in the *syn*-isomer, which is equivalent to about one C–C bond), forces the enzyme into a very different, and unprecedented conformation. This prompted the question of whether AChE would compensate for the deletion of one methylene unit in **TZ2PA5** by forming the “longer” *anti*-triazole instead of the “shorter” *syn*-isomer. Hence, we set out to study the *syn/anti* selectivity for the formation of **TZ2PA5** and the other new in situ hits by LC/MS–SIM. These efforts greatly benefited from the recently discovered Cu(I)-catalyzed process, which provides pure *anti*-triazoles from azides and terminal alkynes.^{46,47} Thus, **TZ2PA5**, **TA2PZ6**, and **TA2PZ5** were synthesized each as a mixture of *syn*- and *anti*-triazoles by the thermal cycloaddition reaction and as isomerically pure *anti*-triazoles by Cu(I) catalysis (Scheme 2).

Regioisomer assignment for the triazoles generated by AChE was accomplished by comparing the HPLC traces from the in situ reactions with authentic samples from the thermal and Cu(I)-catalyzed reactions (cf. Table 3).^{46,47} The new LC/MS–SIM system allowed us to obtain reliable results with single injections using only one-third of the amount of enzyme, compared to the previously used and much less sensitive HPLC–UV method. We were able to confirm the original assignment of the *syn*-geometry for enzyme-generated **TZ2PA6**,²⁴ and we found all the other products, **TZ2PA5**, **TA2PZ6**, and **TA2PZ5**, from both the eel and mouse AChE reactions to also contain almost exclusively *syn*-triazoles. Figure 3 exemplifies the results for the **TA2/PZ6** pair. While this is not surprising in the case of **TA2PZ6** in view of its similarity to **TZ2PA6**, we had expected

(44) The computation was performed at the Swiss Institute of Bioinformatics (SIB) using the BLAST network service. The SIB BLAST network service uses a server developed at SIB and the National Center for Biotechnology Information (NCBI) BLAST 2 software.

(45) Altschul, S. F.; Madden, T. L.; Schäffer, A. A.; Zhang, J.; Zhang, Z.; Miller, W.; Lipman, D. J. *Nucleic Acids Res.* **1997**, *25*, 3389–3402.

(46) Rostovtsev, V. V.; Green, L. G.; Fokin, V. V.; Sharpless, K. B. *Angew. Chem., Int. Ed.* **2002**, *41*, 2596–2599.

(47) Tormøe, C. W.; Christensen, C.; Meldal, M. *J. Org. Chem.* **2002**, *67*, 3057–3064.

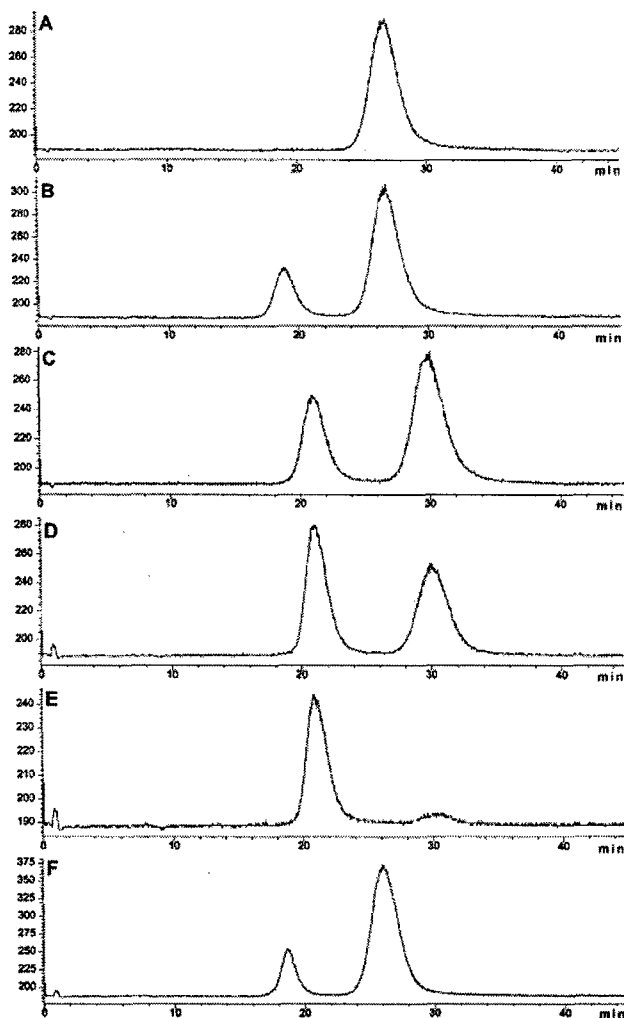


Figure 3. Regioisomer determination for mouse AChE-derived in situ hits. The in situ product, **TA2PZ6**, was compared by LC/MS-SIM to authentic samples from the thermal and the Cu(I)-catalyzed reactions.⁴⁸ (A) *anti*-**TA2PZ6** prepared by the Cu(I)-catalyzed reaction. (B) Co-injection of *anti*-**TA2PZ6** prepared by the Cu(I) catalysis and a mixture of *syn*- and *anti*-**TA2PZ6** prepared by the thermal reaction. (C) Mixture of *syn*- and *anti*-**TA2PZ6** prepared by the thermal reaction. (D) Co-injection of **TA2PZ6** prepared by the in situ click reaction and a mixture of *syn*- and *anti*-**TA2PZ6** prepared by the thermal reaction. (E) In situ click chemistry reaction. (F) Co-injection of the in situ click chemistry reaction and *anti*-**TA2PZ6**, prepared by the Cu(I)-catalyzed reaction.

the shorter linker in **TZ2PA5** and **TA2PZ5** to cause a switch into the “anti-mode”, which would have extended the linker by approximately 1.5 Å. These results suggest that the stereoelectronic requirements for effective catalysis of the cycloaddition inside the enzyme gorge are very strict. We are in the process of investigating this further by X-ray crystallography.

Binding Measurements. The equilibrium dissociation constants for the *syn*- and *anti*- **TA2PZ6**, **TA2PZ5**, **TZ2PA5**, and **TZ2PA6**²⁴ isomers, calculated as the ratios of their first-order dissociation and second-order association rate constants, are listed in Table 1, along with the corresponding free energy of binding values. All eight compounds were respectable inhibitors of both mouse and eel AChE, with dissociation constants in the femtomolar and picomolar range. Even though the femtomolar potency of the original in situ-generated inhibitor, *syn*-**TZ2PA6**, remains unsurpassed for both enzymes, the new in

situ hits, *syn*-**TZ2PA5**, *syn*-**TA2PZ6**, and *syn*-**TA2PZ5** are close. K_d values span 3 orders of magnitude, which is mainly due to an 1800-fold variability of dissociation rate constants k_{off} in the case of the eel enzyme, and 90-fold variability in the case of mouse AChE. In contrast, the on-rates k_{on} vary only by a factor of 3.

The range in dissociation constants is largest for the eel enzyme, where the free binding energy changes by 4.3 kcal/mol (295 K) from the tightest binder, *syn*-**TZ2PA6** (99 fM), to the weakest compound, *anti*-**TA2PZ5** (140 000 fM). In the case of the mouse enzyme, the free energy difference between the best binder, *syn*-**TZ2PA6** (410 fM), and the weakest inhibitor, *anti*-**TA2PZ5** (44 000 fM), is only 2.7 kcal/mol. We were able to derive a linear free energy relationship from the binding data, which allows us to calculate binding energy changes upon modifying the ligand structure, for example, from *syn*-**TZ2PA6** to *anti*-**TA2PZ5**. The mean values for the energy increments for each structural modification are summarized in Table 2. Further details are provided in the Supporting Information.

The energy differences derived from the linear free energy relationship closely match the experimental values. For example, *syn*-**TZ2PA6** was calculated to be 4.3 kcal/mol more tightly bound than *anti*-**TA2PZ5** in the eel AChE case (3.1 kcal/mol for *syn*-to-*anti* isomerization, plus 0.15 kcal/mol for linker shortening, plus 1.0 kcal/mol for inversion of triazole orientation), whereas the difference is only 3.0 kcal/mol in the mouse enzyme case (1.9 kcal/mol for *syn*-to-*anti* isomerization, plus 0.7 kcal/mol for linker shortening, plus 0.4 kcal/mol for inversion of triazole orientation). The fact that a linear free energy relationship can be successfully applied suggests that the inhibitors are stabilized by largely independent multipoint interactions with the protein, and the data indicate that not only the tacrine and phenanthridinium moieties but also the triazole ring are involved in binding. Consequently, the triazole apparently functions as an independent pharmacophore.

Many of the structure–activity trends revealed in Table 1 are species-dependent. In general, eel AChE rate constants are more dependent on the triazole substitution pattern, while mouse AChE is more sensitive to changes in linker length. For example, the *syn*/*anti* preference is much greater for eel AChE (average preference: 3.1 kcal/mol \pm 0.3 kcal/mol, 200-fold) than for mouse AChE (average preference: 1.9 kcal/mol \pm 0.4 kcal/mol, 26-fold). Also, the inversion of triazole ring orientation (**TZ2PA6** \rightarrow **TA2PZ6**, **TZ2PA5** \rightarrow **TA2PZ5**) leads to a marked increase of the dissociation rate in the case of the eel enzyme (1.0 \pm 0.2 kcal/mol, 5.5-fold), while the effects for the mouse enzyme were less pronounced (0.4 \pm 0.4 kcal/mol, 2-fold). For the *syn*-triazole inhibitors, which are the products of the in situ click reactions, the shortening of the linker between the triazole and phenanthridinium moieties from six (*syn*-**TZ2PA6**, *syn*-**TA2PZ6**) to five methylene groups (*syn*-**TZ2PA5**, *syn*-**TA2PZ5**) has only a very small effect on the dissociation constants K_d for the eel enzyme (−0.12 kcal/mol, 0.8-fold), while it leads to a 5-fold increase in the case of mouse AChE (0.97 kcal/mol). In contrast, for the *anti*-triazoles, the shortening of the linker reduces the binding affinity for both the mouse and eel enzymes.

The observed species-specific differences of rate and binding trends indicate that the two enzymes interact differently with

Table 1. Interaction Constants and Free Energies of Binding ($-RT \ln K_d$ at $T = 295$ K) of Triazole Inhibitors with Acetylcholinesterases

inhibitor		k_{cat} ($10^{10} \text{ M}^{-1} \text{ min}^{-1}$)	k_{off} (min^{-1})	K_d (fM)	$-RT \ln K_d$ (kcal mol^{-1})	AChE source
TA2PZ5	<i>syn</i>	1.5	0.0081	540	16.6	<i>Electrophorus</i>
		1.5	0.045	3 000	15.6	mouse
	<i>anti</i>	0.98	1.4	140 000	13.3	<i>Electrophorus</i>
		1.1	0.50	44 000	14.0	mouse
TZ2PA5	<i>syn</i>	0.76	0.00077	100	17.5	<i>Electrophorus</i>
		1.2	0.028	2300	15.7	mouse
	<i>anti</i>	0.90	0.38	42 000	14.0	<i>Electrophorus</i>
		1.3	0.43	33 000	14.1	mouse
TA2PZ6	<i>syn</i>	1.2	0.010	830	16.3	<i>Electrophorus</i>
		1.4	0.0086	610	16.5	mouse
	<i>anti</i>	1.4	1.4	100 000	13.5	<i>Electrophorus</i>
		1.7	0.71	42 000	14.0	mouse
TZ2PA6	<i>syn</i>	1.5	0.0015	99	17.6	<i>Electrophorus</i>
		1.7	0.0071	410	16.7	mouse
	<i>anti</i>	1.8	0.25	14 000	14.7	<i>Electrophorus</i>
		2.5	0.22	8900	14.9	mouse

Table 2. Energy Increments for Structural Changes

structural change	mean $\Delta(-RT \ln K_d)$ (kcal mol^{-1})	AChE source
<i>syn</i> \rightarrow <i>anti</i>	3.1 ± 0.3	<i>Electrophorus</i>
	1.9 ± 0.4	mouse
P6 \rightarrow P5	0.15 ± 0.38	<i>Electrophorus</i>
	0.69 ± 0.45	mouse
TZ \rightarrow TA	1.0 ± 0.2	<i>Electrophorus</i>
	0.37 ± 0.36	mouse
$\Sigma(\text{syn} \rightarrow \text{anti} + \text{P6} \rightarrow \text{P5} + \text{TZ} \rightarrow \text{TA})$	$\Sigma \Delta(-RT \ln K_d)^a$ $4.3 (4.3)$ $3.0 (2.7)$	<i>Electrophorus</i> mouse

^a Energy difference values calculated from increments are shown in bold typeface; experimental values are in parentheses.

Table 3. Analytical HPLC Conditions for Selected Compounds

compound		elution solvent mixture				retention time (min)
		A (%)	B (%)	C (%)	D (%)	
TZ2PA6 ^a	<i>syn</i>			56	44	28.4
	<i>anti</i>			56	44	34.6
TZ2PA5 ^a	<i>syn</i>			56	44	19.2
	<i>anti</i>			56	44	25.2
TA2PZ6 ^a	<i>syn</i>			54	46	20.8
	<i>anti</i>			54	46	29.9
TA2PZ5 ^a	<i>syn</i>			56	44	20.6
	<i>anti</i>			56	44	24.7
TZ2PA6 ^{b,c}	gradient	gradient				7.8
TZ2PA5 ^{b,c}	gradient	gradient				7.6
TA2PZ6 ^{b,c}	gradient	gradient				7.7
TA2PZ5 ^{b,c}	gradient	gradient				7.6
TA2 ^c	gradient	gradient				7.2
TZ2 ^c	gradient	gradient				7.3
PA5 ^c	gradient	gradient				8.6
PA6 ^c	gradient	gradient				8.4
PZ5 ^c	gradient	gradient				8.5
PZ6 ^c	gradient	gradient				8.7

^a Analytical HPLC column Cyclobond I 2000 DMP (10×4.6 mm) preceded by a Phenomenex C18 ODS guard column. Isocratic elution at $0.5 \text{ mL} \cdot \text{min}^{-1}$. ^b Mixture of *syn*- and *anti*-triazoles. ^c Analytical column Zorbax SB-C8 (2.1×50 mm) preceded by a Phenomenex C18 ODS guard column. Flow rate $0.3 \text{ mL} \cdot \text{min}^{-1}$. At 0 min, elution solvent mixture A/B = 100/0, at 10 min, elution solvent mixture A/B = 0/100, at 18 min, elution solvent mixture A/B = 0/100.

the products of the in situ reactions and their anti-congeners. While this may not be seen as surprising in view of the relatively low sequence identity (58%) between the two enzymes, detailed analysis of the primary structures reveals a fully conserved interior of the active center gorge starting from Trp286 of the

peripheral site and ending with Trp86 at the bottom of the gorge. Thus, more global properties of the gorge, such as its overall shape or flexibility, not directly and exclusively determined by conserved interior residues, may be responsible for the observed trends.

Experimental Section

General. Reactions requiring anhydrous conditions were run under nitrogen in glassware flame dried under vacuum. Reagents were purchased from Acros or Aldrich and were used as received. Reaction progress was monitored by TLC using Merck silica gel 60 F-254 with detection by UV. Silica gel 60 (Merck 40–63 μm) was used for column chromatography. The preparation of the library of tacrine and phenylphenanthridinium building blocks was published in a previous article.²⁴

Instrumentation. ¹H NMR and ¹³C NMR spectra were recorded with Bruker DRX-600, Bruker DRX-500, or Varian Inova-400 spectrometers. Proton magnetic resonance (¹H NMR) spectra were recorded at 600, 500, or 400 MHz. Data are presented as follows: chemical shift (ppm), multiplicity (*s* = singlet, *d* = doublet, *t* = triplet, *q* = quartet, *quin* = quintet, *m* = multiplet), coupling constant (Hz), and integration. Carbon magnetic resonance (¹³C NMR) spectra were recorded at 150, 125, or 100 MHz. Data for ¹³C NMR are reported in terms of chemical shifts (ppm). Infrared spectra were recorded on an Avatar 370 Fourier transform spectrometer (IR) and are reported as follows: wavenumbers (cm^{-1}), description (*w* = weak, *m* = medium, *s* = strong, *b* = broad). High-resolution mass spectra (HRMS) were recorded at the mass spectrometry facility at The Scripps Research Institute, La Jolla, CA. HPLC was performed on an Agilent 1100 LC/MSD with an Agilent 1100 SL mass spectrometer, using four different elution solvents: elution solvent A (0.05% TFA in H₂O), elution solvent B (0.05% TFA in CH₃CN), elution solvent C (1% Me₃N/formic acid in H₂O, pH = 7.5), and elution solvent D (MeOH).

General Procedures for in Situ Click Chemistry Experiments. **Determination of Acetylcholinesterase Concentrations.** The concentrations of the eel and mouse enzymes were calculated in terms of molarity of active sites based on quantitative measurements of enzyme activity. Commercially available preparations of *Electrophorus* AChE were found to contain approximately 10% active enzyme. The concentration was determined by quantitative measurement of AChE activity using the Ellman assay as previously described.²⁴ Concentrations of highly purified preparations of mouse AChE, prepared from expression in HEK cells using a recombinant cDNA,^{49,50} containing

(48) All samples were analyzed by LC/MS–SIM with electrospray detection on a Cyclobond I 2000 DMP column (4.6×100 mm, preceded by a Phenomenex C18 ODS guard column) using isocratic elution conditions.

practically homogeneous enzyme, were determined by quantitative measurement of AChE activity using the Ellman assay and comparing that activity to previously determined values⁴⁹ of k_{cat} in quantitative agreement with band intensities in gels of polyacrylamide gel electrophoresis.

In Situ Click Chemistry Screening Procedure for Binary Reagent Mixtures. The tacrine component (i.e., **TZ2** through **TZ6** or **TA1** through **TA3** dissolved in MeOH) was added to $\sim 1 \mu\text{M}$ solutions of *Electrophorus* AChE (type V-S, Sigma) or mouse AChE^{49,50} in buffer (2 mM ammonium citrate, 100 mM NaCl, pH = 7.3–7.5) followed immediately by one of the phenylphenanthridinium components (i.e., **PA2** through **PA6** and **PZ5** through **PZ8**, respectively) and mixed. The final concentrations were as follows: eel or mouse AChE: $1 \mu\text{M}$; tacrine component: $4.6 \mu\text{M}$; phenylphenanthridinium component: $24 \mu\text{M}$; MeOH: 1.5%. Under these conditions, approximately 99.5% of the active sites are in complex with the tacrine component ($K_d(\text{tacrine}) = 18 \text{ nM}$ for mAChE²⁴), and 95% of the peripheral binding sites are in complex with the phenanthridinium reagent ($K_d(\text{propidium}) = 1100 \text{ nM}$ ²⁴). Each reaction mixture was incubated at 37°C for at least 6 h. Samples of the reactions were injected directly ($15 \mu\text{L}$) into the LC/MSD instrument to perform LC/MS–SIM analysis (Zorbax SB-C8 reverse-phase column, preceded by a Phenomenex C18 guard column, electrospray ionization and mass spectroscopic detection in the positive selected-ion mode, tuned to the expected molecular mass of the product). The cycloaddition products were identified by their retention times and molecular weights. Control experiments in the absence of enzyme or in the presence of BSA instead of enzyme failed to produce product signals. For the BSA experiments, AChE was substituted for bovine serum albumin (3 mg/mL). Methanol (1:1 dilution) was added to the reaction mixture prior to LC/MS–SIM analysis to prevent precipitation of the expected **TZ-PA** triazole product.

In Situ Click Chemistry Screening Procedure for Multicomponent Incubations. A methanolic solution ($11.0 \mu\text{L}$) of phenylphenanthridinium building blocks **PA2**–**PA6** (stock solution contains $400 \mu\text{M}$ of each building block) was added to a solution of mouse AChE (1.1 mL of $1 \mu\text{M}$ AChE, 2 mM ammonium citrate, 100 mM NaCl, pH = 7.3–7.5). This mixture was then distributed into five different Eppendorf vials ($198 \mu\text{L}$ per vial), and each sample was mixed with one of the tacrine building blocks (**TZ2**–**TZ6**; $2.0 \mu\text{L}$ of a 1.92 mM methanolic stock solution). The final concentrations were as follows: mouse AChE: $1 \mu\text{M}$; tacrine component: $19.2 \mu\text{M}$; phenylphenanthridinium component: $4.0 \mu\text{M}$; MeOH: 2%. Each reaction mixture was incubated at 37°C for at least 24 h. Samples of the reactions were injected directly ($15 \mu\text{L}$) into the LC/MSD instrument to perform LC/MS–SIM analysis. The cycloaddition products were identified by their retention times and molecular weights.

LC–MS Analysis. Although the analysis by DIOS–MS, as described previously,²⁴ required only submicroliter amounts for a single measurement, the results suffered from poor signal/noise ratios. In contrast, the LC/MS method with selected ion monitoring is considerably more sensitive, with detection limits in the nanomolar range. The eluent contains 0.05% TFA, which results in fast denaturation of the enzyme and release of product on the column (we have obtained a linear correlation between the concentration of *syn*-**TZ2PA6** and its LC/MS–SIM signal in the presence of an excess of mAChE, cf. Supporting Information, section 2). This allows the compound, e.g., **TZ2PA6**, to be readily detected in the presence of the enzyme at concentrations as low as 4 nM , which corresponds to 0.4% of the used enzyme active site concentration. The analyses were performed on an Agilent 1100 LC/MSD instrument by reverse-phase HPLC using a $30 \times 2.1 \text{ mm}$ Zorbax SB-C8 column, preceded by a Phenomenex C18 ODS guard

column. The injection volume was $15\text{--}30 \mu\text{L}$, and the components were eluted using a gradient (flow rate at $0.3 \text{ mL}\cdot\text{min}^{-1}$; at 0 min elution solvent mixture A/B = 100/0; at 10 min elution solvent mixture A/B = 0/100; at 18 min elution solvent mixture A/B = 0/100). The mass spectrometer was set to the positive ion mode with selected ion monitoring of only the expected m/z . Under these conditions, in situ click chemistry products derived from binary building block mixtures are readily detectable after 6 h of incubation in the presence of enzyme.

Regioisomer Determination. The sensitive LC/MS–SIM method was employed for determining the regioisomer distribution of the in situ click chemistry products **TZ2PA6**, **TZ2PA5**, **TA2PZ5**, and **TA2PZ6**. The assignment was accomplished by comparing the retention times of the in situ products with authentic samples, prepared by thermal cycloaddition (yielding an approximately 1:1 mixture of regioisomers) and copper-catalyzed azide/alkyne reaction (yielding pure anti-regioisomers). The in situ reaction mixtures were injected directly ($15\text{--}80 \mu\text{L}$) into the LC/MS as well as co-injected with the reference compounds. Comparison of all traces revealed that the syn-isomers were formed preferentially in situ. The chromatography was performed on a $100 \times 4.6 \text{ mm}$ Cyclobond I 2000 DMP column, preceded by a Phenomenex C18 ODS guard column. The MS detector settings used were the same as those for the screening of reactions.

Synthesis of Building Blocks and Reference Compounds.

CAUTION! All of the compounds described here (and especially the most potent polyvalent inhibitors) are potentially neurotoxic. They must be handled with extreme care by trained personnel.

Tacrine Building Block TA2. A mixture of 9-chloro-1,2,3,4-tetrahydroacridine (1.0 g, 4.61 mmol), but-3-ynylammonium chloride (0.54 g, 5.05 mmol), and triethylamine (0.93 g, 9.2 mmol) in pentanol (3 mL) was heated at reflux for 16 h. The reaction mixture was diluted with CH_2Cl_2 , washed with saturated NaHCO_3 solution, dried over MgSO_4 , and concentrated. The residue was purified by chromatography ($\text{EtOAc}/\text{MeOH} = 9/1$) to give pure alkyne **TA2** (1.06 g, 4.23 mmol, 92%). ^1H NMR (400 MHz, CD_3OD): δ 8.44 (*d*, $J = 8.6 \text{ Hz}$, 1H), 8.04 (*d*, $J = 8.1 \text{ Hz}$, 1H), 7.95 (*t*, $J = 6.4 \text{ Hz}$, 1H), 7.84 (*t*, $J = 7.5 \text{ Hz}$, 1H), 7.56 (*t*, $J = 7.5 \text{ Hz}$, 1H), 3.92 (*m*, 2H), 3.04 (*m*, 2H), 2.76–2.60 (*m*, 4H), 2.51 (*t*, $J = 2.1 \text{ Hz}$, 1H), 1.81 (*m*, 4H) ppm; ^{13}C NMR (400 MHz, CD_3OD): δ 156.8, 152.0, 138.6, 133.4, 126.1, 125.8, 120.0, 116.7, 112.5, 82.1, 74.1, 46.8, 28.8, 25.06, 22.3, 21.1, 20.6 ppm; UV–vis ($\text{H}_2\text{O}/\text{CH}_3\text{CN}/\text{TFA} = 40/60/0.05$): λ_{max} (relative intensities) 248 (100%), 346 (43%) nm; IR: ν 3340 (br), 3220 (s), 2940 (m), 2860 (m), 1620 (s), 1580 (w), 1560 (w), 1500 (m), 1470 (m), 1400 (w), 1350 (w), 1260 (m), 1120 (w), 1080 (w), 1030 (m), 950 (w), 830 (m) cm^{-1} ; HRMS (ESI-TOF) calcd for $\text{C}_{17}\text{H}_{19}\text{N}_2$ (MH^+), 251.1543; found, 251.1547.

Phenylphenanthridinium Building Blocks. Building blocks **PA5**, **PZ6**, and **PZ5** were prepared according to previously reported methods.²⁴

PA5: ^1H NMR (500 MHz, CD_3OD): δ 8.64 (*d*, $J = 9.1 \text{ Hz}$, 1H), 8.54 (*d*, $J = 9.2 \text{ Hz}$, 1H), 7.88–7.76 (*m*, 3H), 7.64–7.52 (*m*, 3H), 7.40–7.34 (*m*, 2H), 6.46 (*d*, $J = 2.2 \text{ Hz}$, 1H), 4.52 (*t*, $J = 7.9 \text{ Hz}$, 2H), 2.22 (*t*, $J = 2.5 \text{ Hz}$, 1H), 2.16–2.12 (*m*, 4H), 1.44–1.32 (*m*, 4H) ppm; ^{13}C NMR (500 MHz, CD_3OD): δ 160.2, 153.1, 149.7, 136.5, 133.7, 132.3, 130.8, 130.1, 129.9, 129.6, 126.8, 126.0, 123.9, 121.5, 119.7, 110.4, 99.8, 84.5, 70.1, 54.9, 29.4, 28.7, 26.5, 18.2 ppm; UV–vis ($\text{H}_2\text{O}/\text{CH}_3\text{CN}/\text{TFA} = 40/60/0.05$): λ_{max} (relative intensities) 293 (100%), 324 (30%) nm; IR: ν 3360 (m), 3240 (m), 2960 (s), 2930 (s), 2870 (m), 1730 (s), 1620 (s), 1580 (w), 1490 (m), 1470 (m), 1260 (s), 1160 (m), 1080 (m), 1030 (s), 830 (w) cm^{-1} ; HRMS (ESI-TOF) calcd for $\text{C}_{26}\text{H}_{26}\text{N}_3$ (M^+), 380.2127; found, 321.2126.

PZ5: ^1H NMR (500 MHz, CD_3OD): δ 8.62 (*d*, $J = 9.1 \text{ Hz}$, 1H), 8.59 (*d*, $J = 9.2 \text{ Hz}$, 1H), 7.83–7.72 (*m*, 3H), 7.68–7.54 (*m*, 3H), 7.38–7.32 (*m*, 2H), 6.46 (*d*, $J = 2.4 \text{ Hz}$, 1H), 4.52 (*t*, $J = 8.1 \text{ Hz}$, 2H), 2.06–1.88 (*m*, 2H), 1.78–1.26 (*m*, 6H) ppm; ^{13}C NMR (500 MHz, CD_3OD): δ 159.9, 152.7, 149.5, 136.4, 133.8, 132.3, 130.8, 130.1, 129.8, 129.4, 126.7, 126.1, 123.8, 121.2, 119.8, 110.4, 99.8, 52.1, 31.0,

(49) Radic, Z.; Pickering, N. A.; Vellom, D. C.; Camp, S.; Taylor, P. *Biochemistry* **1993**, *32*, 12074–12084.

(50) Marchot, P.; Ravelli, R. B. G.; Ravet, M. L.; Bourne, Y.; Vellom, D. C.; Kanter, J.; Camp, S.; Sussman, J. L.; Taylor, P. *Protein Sci.* **1996**, *5*, 672–679.

29.4, 29.1, 24.8 ppm; UV-vis ($\text{H}_2\text{O}/\text{CH}_3\text{CN}/\text{TFA} = 40/60/0.05$): λ_{max} (relative intensities) 292 (100%), 324 (30%) nm; IR: ν 3440 (w), 3360 (m), 3240 (m), 2930 (s), 2860 (s), 2090 (s), 1640 (s), 1630 (s), 1500 (m), 1470 (w), 1260 (s), 1160 (s), 1030 (s), 830 (w) cm^{-1} ; HRMS (ESI-TOF) calcd for $\text{C}_{24}\text{H}_{25}\text{N}_6$ (M^+), 397.2141; found, 397.2130.

PZ6: ^1H NMR (600 MHz, CD_3OD): δ 8.63 (d , $J = 9.1$ Hz, 1H), 8.56 (d , $J = 9.2$ Hz, 1H), 7.82–7.76 (m , 3H), 7.64–7.54 (m , 3H), 7.39–7.33 (m , 2H), 6.48 (d , $J = 2.4$ Hz, 1H), 3.46–3.29 (m , 2H), 2.06–1.88 (m , 2H), 1.80–1.62 (m , 4H) 1.22–1.58 (m , 4H) ppm; ^{13}C NMR (600 MHz, CD_3OD): δ 160.3, 153.0, 149.7, 136.5, 133.8, 132.3, 130.9, 130.1, 129.9, 129.6, 126.8, 126.0, 123.8, 121.6, 119.7, 110.4, 99.8, 52.4, 30.9, 29.7, 27.5, 27.1, 26.9 ppm; UV-vis ($\text{H}_2\text{O}/\text{CH}_3\text{CN}/\text{TFA} = 40/60/0.05$): λ_{max} (relative intensities) 292 (100%), 324 (28%) nm; IR: ν 3450 (w), 3360 (m), 3240 (m), 2930 (s), 2860 (m), 2100 (s), 1640 (m), 1630 (m), 1500 (m), 1460 (w), 1260 (s), 1160 (s), 1030 (s), 830 (w) cm^{-1} ; HRMS (ESI-TOF) calcd for $\text{C}_{25}\text{H}_{27}\text{N}_6$ (M^+), 411.2297; found, 411.2292.

General Procedure for the Preparation of Regioisomerically Pure *syn*-Triazoles. Azide (50 μmol) and alkyne (50 μmol) were dissolved in methanol (1 mL), and the solvent was subsequently removed under reduced pressure. The residue was heated in an oven at 80–120 $^{\circ}\text{C}$ for 4–7 days, affording the corresponding triazole as a *syn*/*anti* mixture of approximately 1:1. The regioisomers were separated by semipreparative HPLC (Cyclobond I 2000 DMP, 250 \times 10 mm) to yield regioisomerically pure triazoles.

***syn*-TZ2PA5:** ^1H NMR (600 MHz, CD_3OD): δ 8.62 (d , $J = 9.1$ Hz, 1H), 8.56 (d , $J = 9.2$ Hz, 1H), 8.24 (d , $J = 8.2$ Hz, 2H), 7.74–7.16 (m , 11 H), 6.45 (d , $J = 2.0$ Hz, 1H), 4.66 (t , $J = 7.3$ Hz, 2H), 4.37 (m , 2H), 4.18 (t , $J = 7.2$ Hz, 2H), 2.97 (s , 2H), 2.57 (t , $J = 6.9$ Hz, 2H), 1.93–1.76 (m , 6H), 1.41–1.12 (m , 6H) ppm; UV-vis ($\text{H}_2\text{O}/\text{CH}_3\text{CN}/\text{TFA} = 40/60/0.05$): λ_{max} (relative intensities) 248 (98%), 292 (100%), 333 (52%) nm; IR: ν 3340 (br), 2950 (m), 2840 (m), 1640 (w), 1620 (w), 1580 (m), 1520 (w), 1500 (w), 1450 (w), 1410 (w), 1320 (w), 1260 (w), 1230 (w), 1110 (w), 1020 (s) cm^{-1} ; HRMS (ESI-TOF) calcd for $\text{C}_{41}\text{H}_{43}\text{N}_8$ (M^+), 647.3611; found, 647.3595.

***syn*-TA2PZ6:** ^1H NMR (500 MHz, CD_3OD): δ 8.62 (d , $J = 9.1$ Hz, 1H), 8.57 (d , $J = 9.2$ Hz, 1H), 8.24 (d , $J = 8.2$ Hz, 2H), 7.72–7.12 (m , 11 H), 6.41 (d , $J = 2.2$ Hz, 1H), 4.70–4.37 (m , 4H), 4.30–4.13 (m , 2H), 2.83 (s , 2H), 2.78–2.60 (m , 4H), 1.93–1.76 (m , 6H), 1.41–1.12 (m , 6H) ppm; UV-vis ($\text{H}_2\text{O}/\text{CH}_3\text{CN}/\text{TFA} = 40/60/0.05$): λ_{max} (relative intensities) 248 (97%), 293 (100%), 334 (55%) nm; IR: ν 3310 (br), 2930 (m), 2860 (m), 1690 (w), 1620 (m), 1590 (m), 1520 (w), 1490 (w), 1450 (m), 1410 (w), 1340 (m), 1260 (m), 1180 (w), 1150 (w), 1050 (s), 950 (w), 830 (w) cm^{-1} ; HRMS (ESI-TOF) calcd for $\text{C}_{42}\text{H}_{45}\text{N}_8$ (M^+), 661.3767; found, 661.3753.

***syn*-TA2PZ5:** ^1H NMR (400 MHz, CD_3OD): δ 8.68–8.23 (m , 4H), 7.77–7.10 (m , 11 H), 6.45 (d , $J = 2.3$ Hz, 1H), 4.56–4.17 (m , 6H), 3.01 (s , 2H), 2.62 (t , $J = 7.48$ Hz, 2H), 1.93–1.79 (m , 6H), 1.38–1.15 (m , 6H) ppm; UV-vis ($\text{H}_2\text{O}/\text{CH}_3\text{CN}/\text{TFA} = 40/60/0.05$): λ_{max} (relative intensities) 247 (97%), 293 (100%), 334 (53%) nm; IR: ν 3350 (br), 2940 (m), 2850 (w), 1620 (w), 1590 (m), 1520 (w), 1480 (w), 1460 (m), 1410 (m), 1350 (m), 1250 (m), 1180 (w), 1160 (w), 1080 (w), 1020 (s), 950 (w), 830 (w) cm^{-1} ; HRMS (ESI-TOF) calcd for $\text{C}_{41}\text{H}_{43}\text{N}_8$ (M^+), 647.3611; found, 647.3596.

General Procedure for the Synthesis of Isomerically Pure *anti*-Triazoles. An aqueous CuSO_4 solution (100 mM, 25 μL) and copper powder (2 mg) were added to a solution of azide (50 μmol) and alkyne (50 μmol) in ethanol (200 μL). The reaction mixture was stirred at room temperature for 2–4 days. The *anti*-triazole was purified by semipreparative HPLC.

***anti*-TZ2PA5:** ^1H NMR (600 MHz, CD_3OD): δ 8.62 (d , $J = 9.1$ Hz, 1H), 8.56 (d , $J = 9.2$ Hz, 1H), 7.96 (d , $J = 8.6$ Hz, 2H), 7.72–7.24 (m , 11 H), 6.38 (d , $J = 2.3$ Hz, 1H), 4.70 (t , $J = 7.8$ Hz, 2H), 4.37 (m , 2H), 4.21 (t , $J = 6.1$ Hz, 2H), 2.91 (s , 2H), 2.53 (t , $J = 7.4$ Hz, 2H), 1.88–1.72 (m , 6H), 1.41–1.16 (m , 6H) ppm; UV-vis ($\text{H}_2\text{O}/\text{CH}_3\text{CN}/\text{TFA} = 40/60/0.05$): λ_{max} (relative intensities) 248 (96%), 292

(100%), 334 (51%) nm; IR: ν 3340 (br), 2930 (m), 2870 (w), 2100 (s), 1730 (w), 1700 (w), 1590 (s), 1520 (w), 1490 (w), 1450 (m), 1370 (m), 1350 (m), 1230 (m), 1180 (m), 1160 (m), 1040 (w), 950 (m), 840 (m) cm^{-1} ; HRMS (ESI-TOF) calcd for $\text{C}_{41}\text{H}_{43}\text{N}_8$ (M^+), 647.3611; found, 647.3597.

***anti*-TA2PZ6:** ^1H NMR (500 MHz, CD_3OD): δ 8.64 (d , $J = 9.2$ Hz, 1H), 8.60 (d , $J = 9.2$ Hz, 1H), 8.03 (d , $J = 8.4$ Hz, 2H), 7.82–7.34 (m , 11 H), 6.48 (d , $J = 2.2$ Hz, 1H), 4.70–4.37 (m , 4H), 4.30–4.13 (m , 2H), 2.88 (s , 2H), 2.78–2.67 (m , 4H), 1.88–1.72 (m , 6H), 1.41–1.16 (m , 6H) ppm; UV-vis ($\text{H}_2\text{O}/\text{CH}_3\text{CN}/\text{TFA} = 40/60/0.05$): λ_{max} (relative intensities) 248 (86%), 292 (100%), 334 (48%) nm; IR: ν 3330 (br), 3360 (m), 2940 (m), 2870 (w), 2100 (s), 1730 (w), 1700 (w), 1590 (s), 1520 (w), 1490 (w), 1450 (m), 1370 (m), 1230 (m), 1160 (m), 1120 (w), 1060 (s), 950 (m), 830 (m) cm^{-1} ; HRMS (ESI-TOF) calcd for $\text{C}_{42}\text{H}_{45}\text{N}_8$ (M^+), 661.3767; found, 661.3756.

***anti*-TA2PZ5:** ^1H NMR (400 MHz, CD_3OD): δ 8.71–8.23 (m , 4H), 7.67–7.12 (m , 11 H), 6.45 (d , $J = 2.2$ Hz, 1H), 4.40–4.2 (m , 6H), 3.01 (s , 2H), 2.62 (t , $J = 7.42$ Hz, 2H), 1.95–1.72 (m , 6H), 1.38–1.20 (m , 6H) ppm; UV-vis ($\text{H}_2\text{O}/\text{CH}_3\text{CN}/\text{TFA} = 40/60/0.05$): λ_{max} (relative intensities) 248 (95%), 292 (100%), 334 (51%) nm; IR: ν 3340 (br), 2940 (m), 2840 (w), 2100 (s), 1690 (w), 1590 (s), 1520 (w), 1480 (w), 1450 (m), 1350 (m), 1250 (m), 1180 (m), 1160 (m), 1040 (s), 950 (m), 830 (m) cm^{-1} ; HRMS (ESI-TOF) calcd for $\text{C}_{41}\text{H}_{43}\text{N}_8$ (M^+), 647.3611; found, 647.3596. Table 3 shows analytical HPLC conditions for selected compounds.

Determination of AChE–Inhibitor Association and Dissociation Rate Constants. The association rate constants (k_{on}) were determined by following the rate of quenching of the intrinsic AChE tryptophan fluorescence upon inhibitor binding using the stopped-flow technique.⁵¹ For femtomolar and low picomolar inhibitors, we determined the first-order dissociation rate constants (k_{off}) by measuring the return of AChE activity upon 5000-fold dilution of 50–100 nM concentrations of AChE–inhibitor complex into 250 $\mu\text{g}/\text{mL}$ solution of calf thymus DNA (USB Corp., Cleveland, OH) using the Ellman assay.⁵² The DNA sequesters the free phenanthridinium ion upon its release from the AChE complex through intercalation, thus preventing its reassociation with AChE when inhibitor concentrations in the reactivation medium are above their K_d . High picomolar inhibitors dissociated faster, and the reactivation medium contained no DNA, but substrate acetylthiocholine and thiol reagent DTNB were added to the reactivation medium for continuous monitoring of enzyme activity immediately upon dilution of AChE–inhibitor complex. The dissociation constants were determined by nonlinear fitting of the first-order increase in enzyme activity up to 100% of the AChE control activity in mixture containing no inhibitor. Alternatively, k_{off} values of fast dissociating inhibitors were determined using stopped-flow techniques, by following the partial return of intrinsic tryptophan fluorescence caused by dissociation of the AChE–inhibitor complex upon mixing with high concentration (100 μM) of competing ligand (amibenonium or other tight binding ligand) to prevent inhibitor reassociation.

All experiments were performed in at least triplicate with the standard error of determination smaller than 20% of the mean value. The measurements were performed in 0.1 M phosphate buffer pH 7.0 at 22 $^{\circ}\text{C}$ on a SX.18 MV stopped-flow instrument (Applied Photophysics) or Cary 1E UV–vis spectrophotometer (Varian).

The equilibrium dissociation constants for the *syn*- and *anti*-TA2PZ6, TA2PZ5, and TZ2PA5 isomers, calculated as the ratios of their first-order dissociation and second-order association rate constants, are listed in Table 1, along with the dissociation constants for the TZ2PA6 isomers obtained previously.²⁴

(51) Radic, Z.; Taylor, P. J. *Biol. Chem.* **2001**, *276*, 4622–4633.

(52) Ellman, G. L.; Courtney, K. D.; Valentino Andres, J.; Featherstone, R. M. *Biochem. Pharmacol.* **1961**, *7*, 88–95.

Conclusions

We have optimized the in situ click chemistry approach to lead discovery and increased its scope using acetylcholinesterase as the target. The application of LC/MS–SIM for product identification greatly enhanced the sensitivity and reliability of the method and allowed the incubation times to be decreased from 6 days to as little as 6 h. Three new AChE inhibitors, in addition to the known compound, **TZ2PA6**, were identified from a library of tacrine and phenanthridinium azide and acetylene reagents, which contained the building blocks from previous work and the new **PZ5**.²⁴ All inhibitors, **TZ2PA6**, **TZ2PA5**, **TA2PZ6**, and **TA2PZ5**, were produced with almost complete selectivity for the *syn*-triazole isomer by both eel and mouse enzymes. This is a surprising discovery for **TZ2PA5** and **TA2PZ5**, in view of their reduced linker lengths. The *syn*-triazoles, formed by the enzyme, are more than 100 times more potent than the corresponding anti-isomers. Detailed binding studies revealed all in situ hit compounds to be extremely potent AChE inhibitors, with dissociation constants in the femtomolar range, due to the multivalent nature of the binding interactions, which also involve the newly formed *syn*-triazole heterocycle as an active pharmacophore.²⁵ The LC/MS–SIM technique enables the testing of multicomponent mixtures, thereby dramatically increasing the efficiency of the method and setting

the stage for medium- or even high-throughput screening. We are currently completing a search for novel and druglike AChE inhibitors based on this method and are investigating other enzyme and receptor targets, such as HIV protease, carbonic anhydrase, and nicotinic acetylcholine receptors.

Acknowledgment. We thank Professors M. G. Finn, V. V. Fokin, and Mr. W. G. Lewis for advice and helpful discussions. We are grateful to Professor G. Siuzdak and Mr. J. Apon for MALDI mass spectroscopy support. We also thank Dr. Luke Green for providing samples of azides and acetylenes used in initial experiments. This work was supported by the Swiss National Science Foundation and the Novartis Research Foundation (R.M.), by the Skaggs Foundation (H.C.K., A.K., R.M.), and the NIH (K.B.S. and P.T., Grants No. R-37GM18360 and DAMDC17C-02-2-0025 to P.T.).

Supporting Information Available: LC/MS–SIM traces for in situ click chemistry and control experiments, experimental details, LC/MS–SIM traces for regioisomer determination, and tables with free energy increments for structural modifications. This material is available free of charge via the Internet at <http://pubs.acs.org>.

JA046382G

In Situ Selection of Lead Compounds by Click Chemistry: Target-Guided Optimization of Acetylcholinesterase Inhibitors

Antoni Krasiński,[†] Zoran Radić,[‡] Roman Manetsch,[†] Jessica Raushel,[†]
Palmer Taylor,[‡] K. Barry Sharpless,^{†,§} and Hartmuth C. Kolb^{*,†,§}

Contribution from the Department of Chemistry and the Skaggs Institute for Chemical Biology,
The Scripps Research Institute, 10550 North Torrey Pines Road, La Jolla, California 92037, and
the Department of Pharmacology, #0636, University of California, San Diego,
9500 Gilman Drive, La Jolla, California 92093

Received November 18, 2004; E-mail: hckolb@scripps.edu

Abstract: The target-guided, in situ click chemistry approach to lead discovery has been successfully employed for discovering acetylcholinesterase (AChE) inhibitors by incubating a selected enzyme/tacrine azide combination with a variety of acetylene reagents that were not previously known to interact with the enzyme's peripheral binding site. The triazole products, formed by the enzyme, were identified by HPLC-mass spectrometry analysis of the crude reaction mixtures. The target-guided lead discovery search was also successful when performed with reagent mixtures containing up to 10 components. From 23 acetylene reagents, the enzyme selected two phenyltetrahydroisoquinoline (PIQ) building blocks that combined with the tacrine azide within the active center gorge to form multivalent inhibitors that simultaneously associate with the active and peripheral binding sites. These new inhibitors are up to 3 times as potent as our previous phenylphenanthridinium-derived compounds, and with dissociation constants as low as 33 femtomolar, they are the most potent noncovalent AChE inhibitors known. In addition, the new compounds lack a permanent positive charge and aniline groups and possess fewer fused aromatic rings. Remarkably, despite the high binding affinity, the enzyme displayed a surprisingly low preference for one PIQ enantiomer over the other.

Introduction

By employing the biological targets themselves for assembling inhibitors within the confines of their binding sites, target-guided synthesis (TGS) promises to revolutionize lead discovery. The newly formed inhibitors usually display much higher binding affinities for their biological targets than the individual components, since they simultaneously engage in multiple binding interactions.^{1,2} In principle, lead discovery by TGS is independent of the function of the target, since it relies solely on its ability to hold the reagents in close proximity until they become connected via the "arranged" chemical reaction. As long as 20 years ago, Rideout et al. reported a marked synergism between the cytotoxic effects of decanal and *N*-amino-guanidines, which they suggested to result from the self-assembly of cytotoxic hydrazones inside cells.^{3,4} Since then, several approaches to target-guided synthesis have been developed: dynamic combinatorial chemistry,^{5–14} stepwise target-

guided synthesis,^{15,16} and kinetically controlled target-guided synthesis.^{17–25} The latter approach uses irreversible reactions to unite reagents inside the protein's binding pockets. Most

- [†] Department of Chemistry, The Scripps Research Institute.
[§] The Skaggs Institute for Chemical Biology, The Scripps Research Institute.
[‡] University of California, San Diego.
- (1) Jain, A.; Huang, S. G.; Whitesides, G. M. *J. Am. Chem. Soc.* **1994**, *116*, 5057–5062.
 - (2) Mammen, M.; Chio, S.-K.; Whitesides, G. M. *Angew. Chem., Int. Ed.* **1998**, *37*, 2755–2794.
 - (3) Rideout, D. *Science* **1986**, *233*, 561–563.
 - (4) Rideout, D.; Calogeropoulos, T.; Jaworski, J.; McCarthy, M. *Biopolymers* **1990**, *29*, 247–262.
 - (5) Huc, I.; Lehn, J.-M. *Proc. Natl. Acad. Sci. U.S.A.* **1997**, *94*, 2106–2110.

- (6) Ramström, O.; Lehn, J.-M. *ChemBioChem* **2000**, *1*, 41–48.
- (7) Lehn, J.-M.; Eliseev, A. V. *Science* **2001**, *291*, 2331–2332.
- (8) Bunyapaiboonsri, T.; Ramström, O.; Lohmann, S.; Lehn, J.-M.; Peng, L.; Goeldner, M. *ChemBioChem* **2001**, *2*, 438–444.
- (9) Eliseev, A. V. *Pharm. News* **2002**, *9*, 207–215.
- (10) Ramström, O.; Lehn, J.-M. *Nat. Rev. Drug Discovery* **2002**, *1*, 26–36.
- (11) Otto, S. *Curr. Opin. Drug Discovery Dev.* **2003**, *6*, 509–520.
- (12) Erlanson, D. A.; Braisted, A. C.; Raphael, D. R.; Randal, M.; Stroud, R. M.; Gordon, E. M.; Wells, J. A. *Proc. Natl. Acad. Sci. U.S.A.* **2000**, *97*, 9367–9372.
- (13) Erlanson, D. A.; Lam, J. W.; Wicsmann, C.; Luong, T. N.; Simmons, R. L.; DeLano, W. L.; Choong, I. C.; Burdett, M. T.; Flanagan, W. M.; Lee, D.; Gordon, E. M.; O'Brien, T. *Nat. Biotechnol.* **2003**, *21*, 308–314.
- (14) Ramström, O.; Lohmann, S.; Bunyapaiboonsri, T.; Lehn, J.-M. *Chem.–Eur. J.* **2004**, *10*, 1711–1715.
- (15) Maly, D. J.; Choong, I. C.; Ellman, J. A. *Proc. Natl. Acad. Sci. U.S.A.* **2000**, *97*, 2419–2424.
- (16) Kehoe, J. W.; Maly, D. J.; Verdugo, D. E.; Armstrong, J. I.; Cook, B. N.; Ouyang, Y.-B.; Moore, K. L.; Ellman, J. A.; Bertozzi, C. R. *Bioorg. Med. Chem. Lett.* **2002**, *12*, 329–332.
- (17) Lewis, W. G.; Green, L. G.; Grynszpan, F.; Radić, Z.; Carlier, P. R.; Taylor, P.; Finn, M. G.; Sharpless, K. B. *Angew. Chem., Int. Ed.* **2002**, *41*, 1053–1057.
- (18) Bourne, Y.; Kolb, H. C.; Radić, Z.; Sharpless, K. B.; Taylor, P.; Marchot, P. *Proc. Natl. Acad. Sci. U.S.A.* **2004**, *101*, 1449–1454.
- (19) Ingles, J.; Benkovic, S. J. *Tetrahedron* **1991**, *47*, 2351–2364.
- (20) Boger, D. L.; Haynes, N.-E.; Kito, P. A.; Warren, M. S.; Ramcharan, J.; Marolewski, A. E.; Benkovic, S. J. *Bioorg. Med. Chem.* **1997**, *5*, 1817–1830.
- (21) Greasley, S. E.; Marsilje, T. H.; Cai, H.; Baker, S.; Benkovic, S. J.; Boger, D. L.; Wilson, I. A. *Biochemistry* **2001**, *40*, 13538–13547.
- (22) Nguyen, R.; Huc, I. *Angew. Chem., Int. Ed.* **2001**, *40*, 1774–1776.
- (23) Nicolaou, K. C.; Hughes, R.; Cho, S. Y.; Winssinger, N.; Smethurst, C.; Labischinski, H.; Endermann, R. *Angew. Chem., Int. Ed.* **2000**, *39*, 3823–3828.

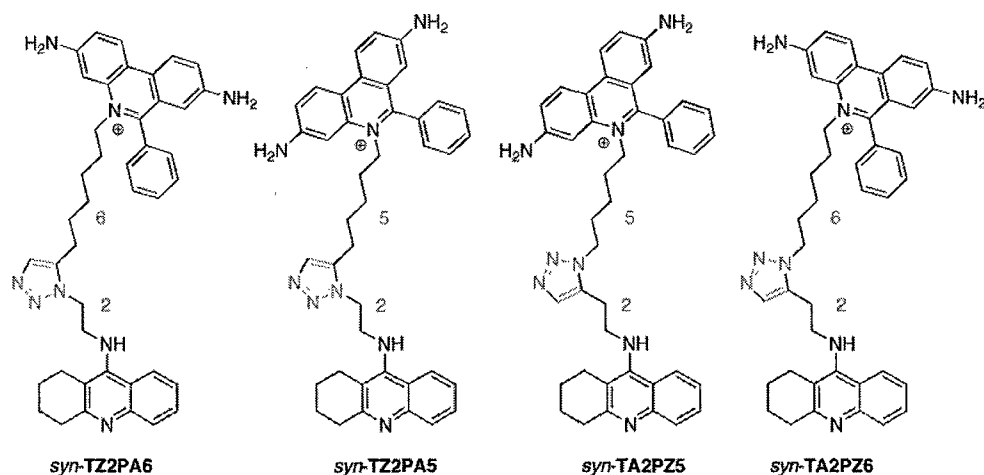


Figure 1. Four in situ click chemistry hit compounds based on tacrine and phenylphenanthridinium reagents.

approaches to TGS employ highly reactive reagents (strong electrophiles or nucleophiles, metathesis catalysts, etc.), which can cause side reactions and even destroy the biological target. To avoid such complications, we have developed an extremely reliable approach to kinetically controlled TGS, called in situ click chemistry,^{17,26} which employs the completely bio-orthogonal [1,3]-dipolar cycloaddition reaction²⁷ between azides and acetylenes. This process is self-contained, hence no external reagents, catalysts, or byproducts that might interfere, and the "reactants" themselves are largely "invisible" in a biological milieu. Most importantly, despite its high driving force (> 50 kcal/mol) the uncatalyzed reaction has a surprisingly high activation barrier of approximately 25 kcal/mol, causing it to be extremely slow at room temperature and its rate to be highly dependent on parameters that stabilize the transition state.²⁸ This was first exploited by Mock et al., who observed a 10⁵-fold increase of the cycloaddition reaction rate when azide and acetylene groups are held together in close proximity inside the synthetic receptor, cucurbituril, leading to irreversible formation of a triazole.^{29–31} In previous work we have shown that acetylcholinesterase (AChE) is able to assemble extremely potent inhibitors, which simultaneously access the enzyme's active and peripheral binding sites,^{32–35} from azide and acetylene reagents, each linked to known active and peripheral site inhibitors, tacrine and phenylphenanthridinium, respectively.^{17,26} Later we found that carbonic anhydrase is also capable of assembling its own inhibitors within the confines of its active

center region, suggesting the in situ click chemistry technique is applicable to a broad range of targets.³⁶ Indeed, the scope of the method is not limited to proteins, as demonstrated by Dervan et al., who have used the azide/acetylene cycloaddition to explore the double-stranded DNA-templated interconnection of hairpin polyamides in the minor groove to produce tandem hairpin dimers in site-specific fashion, which are capable of targeting longer sequences.²⁵

Recent key breakthroughs in our labs were made possible by an improved method for analyzing the in situ click chemistry reaction mixtures.²⁶ Instead of using MALDI/DIOS (desorption/ionization on silicon) mass spectrometry,^{37,38} as done previously,¹⁷ we now use HPLC with compound detection through electrospray mass spectrometry in the positive selected ion mode (LC/MS-SIM). For our purpose this method is more reliable, enabling identification of the product triazoles by both retention time and molecular weight. Additionally, chromatographic removal of the molecules that might otherwise obscure the mass spectrum of the product allows us to reduce the reaction time from 6 days to 6 hours and lower the reagent concentrations considerably. The following results were obtained under these conditions.

(1) From 52 combinations of azide- and acetylene-bearing tacrine and phenylphenanthridinium reagents, potentially giving rise to 104 products, only four were assembled inside mouse or eel acetylcholinesterase to form, with high selectivity, 1,5-disubstituted ("syn") triazoles (Figure 1). These enzyme-generated compounds are femtomolar inhibitors, whereas the corresponding 1,4-disubstituted ("anti") triazole derivatives are much less active.

(2) The triazole units of all enzyme-generated inhibitors were two methylene units away from the tacrine moiety, even though the enzyme had the opportunity to assemble products with different linker spacings. Recent X-ray crystallographic studies of complexes of *anti*- and *syn*-TZ2PA6 and mouse AChE revealed that the formed triazole moieties are optimally positioned to contribute to protein binding through hydrogen bonding and stacking interactions.¹⁸ This implies not only that triazoles

- (24) Nicolaou, K. C.; Hughes, R.; Cho, S. Y.; Winssinger, N.; Labischinski, H.; Endermann, R. *Chem.-Eur. J.* **2001**, *7*, 3824–3843.
- (25) Poulin-Kerstien, A. T.; Dervan, P. B. *J. Am. Chem. Soc.* **2003**, *125*, 15811–15821.
- (26) Manetsch, R.; Krasinski, A.; Radić, Z.; Raushel, J.; Taylor, P.; Sharpless, K. B.; Kolb, H. C. *J. Am. Chem. Soc.* **2004**, *126*, 12809–12818.
- (27) Huisgen, R. In *1,3-Dipolar Cycloaddition Chemistry*; Padwa, A., Ed.; Wiley: New York, 1984; Vol. 1, pp 1–176.
- (28) Himo, F.; Lovell, T.; Hilgraf, R.; Rostovtsev, V. V.; Noodleman, L.; Sharpless, K. B.; Fokin, V. V. *J. Am. Chem. Soc.* **2005**, *127*, 210–216.
- (29) Mock, W. L.; Irra, T. A.; Wepsiec, J. P.; Manimaran, T. L. *J. Org. Chem.* **1983**, *48*, 3619–3620.
- (30) Mock, W. L.; Irra, T. A.; Wepsiec, J. P.; Adhya, M. *J. Org. Chem.* **1989**, *54*, 5302–5308.
- (31) Mock, W. L. *Top. Curr. Chem.* **1995**, *175*, 1–24.
- (32) Du, D.-M.; Carlier, P. R. *Curr. Pharm. Des.* **2004**, *10*, 3141–3156.
- (33) Han, Y. F.; Li, C. P.-L.; Chow, E.; Wang, H.; Pang, Y.-P.; Carlier, P. R. *Bioorg. Med. Chem.* **1999**, *7*, 2569–2575.
- (34) Carlier, P. R.; Han, Y. F.; Chow, E. S.-H.; Li, C. P.-L.; Wang, H.; Lieu, T. X.; Wong, H. S.; Pang, Y.-P. *Bioorg. Med. Chem.* **1999**, *7*, 351–357.
- (35) Pang, Y.-P.; Quiram, P.; Jelacic, T.; Hong, F.; Brimijoin, S. *J. Biol. Chem.* **1996**, *271*, 23646–23649.

- (36) Mocharla, V. P.; Colasson, B.; Lee, L.; Roeper, S.; Sharpless, K. B.; Wong, C.-H.; Kolb, H. C. *Angew. Chem., Int. Ed.* **2005**, *44*, 116–120.
- (37) Wei, J.; Buriak, J. M.; Siuzdak, G. *Nature* **1999**, *399*, 243–246.
- (38) Thomas, J. J.; Shen, Z.; Crowell, J. E.; Finn, M. G.; Siuzdak, G. *Proc. Natl. Acad. Sci. U.S.A.* **2001**, *98*, 4932–4937.

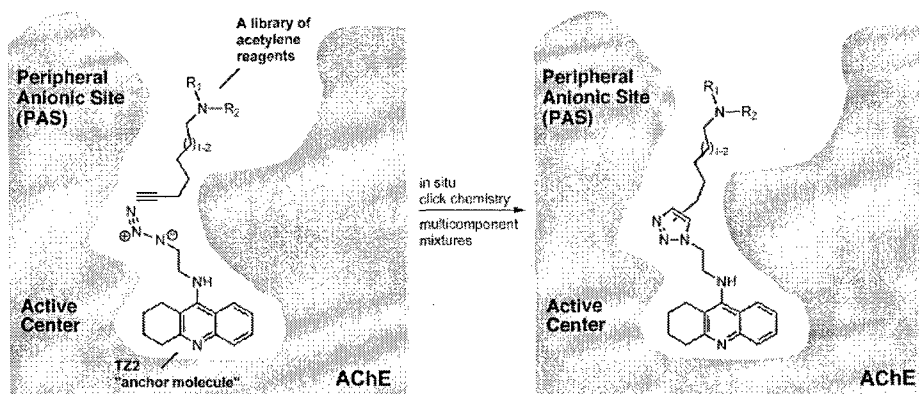


Figure 2. In situ click chemistry screening for AChE inhibitors, containing novel peripheral site ligands.

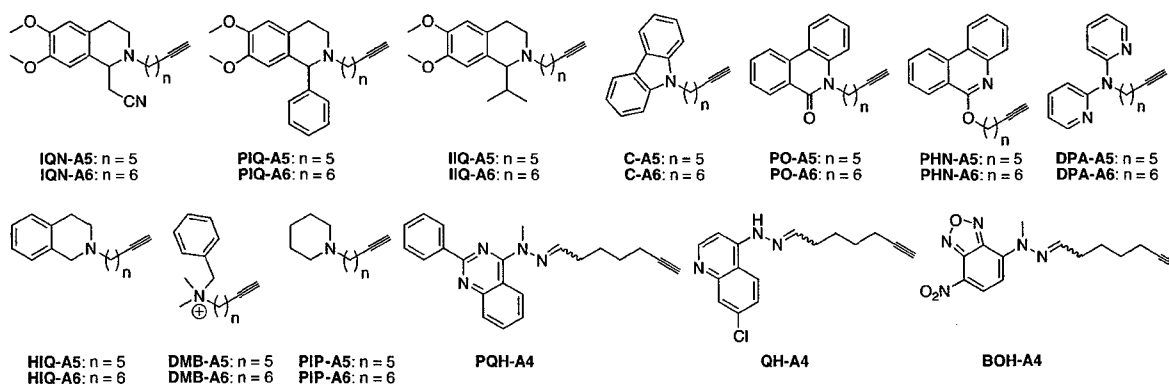


Figure 3. A library of 23 acetylene reagents for in situ click chemistry screening. All chiral compounds are racemic.

are valuable pharmacophoric units but also that the enzyme may have actively accelerated their formation by lowering the transition state energies of their formation through favorable binding interactions.

(3) Due to the chromatographic separation and greater reliability, the new LC/MS-SIM based analysis method enabled us to increase screening throughput by using multicomponent mixtures of building blocks. Thus, medium- or high-throughput in situ click chemistry screening for lead discovery is now within reach.

Results and Discussion

These results have set the stage for performing the first ever search for AChE inhibitors through in situ click chemistry based on building blocks that were not previously known to interact with the target. All previous experiments had employed known active site and peripheral binding site ligands. To minimize the number of variables, we decided to continue to use the tacrine building block **TZ2** as an "anchor molecule" that, in complex with the enzyme, would recruit and irreversibly link together novel peripheral site binders to form multivalent AChE inhibitors that simultaneously access multiple binding sites within the enzyme (Figure 2). A two-methylene spacer between tacrine and the azide was chosen, since previous experiments had proven this distance to be optimal.²⁶ On the basis of analogous considerations, we designed a library of complementary acetylene reagents carrying aromatic heterocyclic phenylphenanthridinium mimics with a spacing of five or six methylene units. To increase the screening throughput, we planned to test multireagent mixtures containing up to 10 acetylene reagents at a time. This multicomponent in situ click chemistry screening

approach is conceptually interesting, as it addresses the question of whether an enzyme complex of one reaction partner, capable of triazole genesis (e.g., the tacrine azide **TZ2**), can find and select its "best" triazole-forming partner(s) when presented with mixtures of candidates with unknown binding affinities and so discover its own potent biligand inhibitors. In the case at hand, the goal was to replace the phenylphenanthridinium component of our previous "in situ-made" AChE inhibitors with a moiety conferring greater pharmacologic potential.

The acetylenic building blocks were readily synthesized by alkylating commercially available amines with the appropriate iodoalkynes or by forming hydrazones from 7-heptynal (cf. Supporting Information). The complete acetylene reagent library is shown in Figure 3. The heterocycles were chosen to simplify the structure and eliminate the permanent positive charge, yet retain many of the features of the phenanthridinium moiety.

For concept validation, initial in situ click chemistry screens were performed by incubating binary **TZ2**/acetylene mixtures with eel or mouse AChE at pH 7.4 for at least 6 h and analyzing each reaction mixture by LC/MS-SIM.²⁶ Most alkynes gave no detectable product, except for the phenyltetrahydroisoquinolines **PIQ-A5** and **PIQ-A6**, which formed significant amounts of triazoles. Their identity was confirmed by chromatographic comparison of the in situ click chemistry reaction mixtures with authentic samples of **TZ2PIQ-A5** and **TZ2PIQ-A6**, which were synthesized by a thermal cycloaddition reaction. Thus, two new in situ hits have been found, composed of the tacrine active site ligand and the phenyltetrahydroisoquinoline peripheral site ligands. The latter were not previously known to bind to the peripheral binding site of AChE, and they may have better

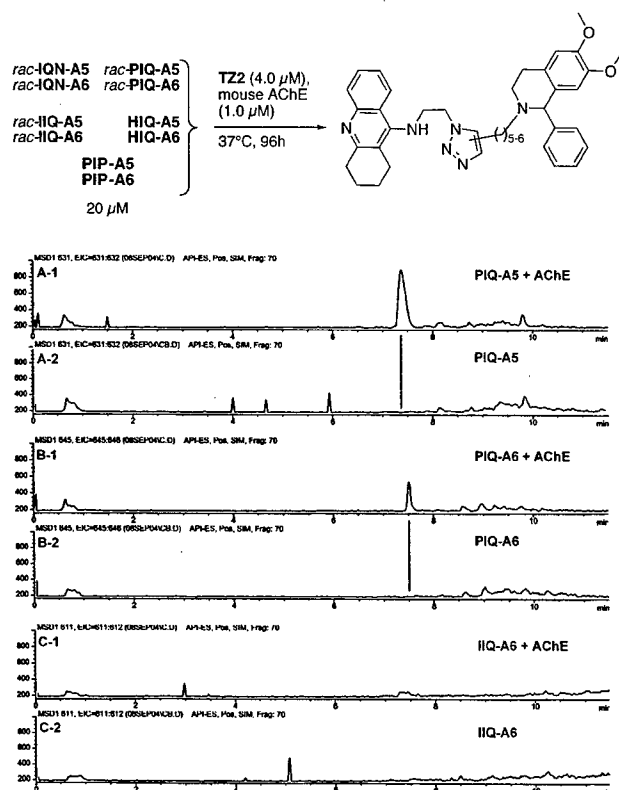


Figure 4. Multicomponent in situ click chemistry screen. Extracted ion LC/MS-SIM chromatograms for the multicomponent in situ reaction (traces A-1, B-1, C-1) and for the background reaction containing all reagents, but no enzyme (traces A-2, B-2, C-2). Traces A-1 and -2: Extracted ion chromatograms for **TZZPIQ-A5**; note the presence of product in the enzyme reaction, while no product is formed in the absence of AChE. Traces B-1 and -2: Extracted ion chromatograms for **TZZPIQ-A6**. Again, product is present only in the enzyme reaction. Traces C-1 and -2: Extracted ion chromatograms for **TZZIIQ-A6**. No product is formed in either the enzyme or the control reactions. The extracted ion traces for the remaining building blocks are similar to this trace, demonstrating that the corresponding triazoles are below the detection limit in the in situ reaction mixture.

pharmacological properties than the previous phenylphenanthridinium-derived inhibitors, due to the lack of a positive charge, the absence of aniline groups, and the presence of fewer fused aromatic rings. The new hits were validated by demonstrating that no triazole was formed in the absence of AChE, or when the enzyme was replaced by bovine serum albumin (BSA) (cf. Figure 4 for results from a multicomponent screen).

After successful completion of in situ click chemistry experiments with binary **TZZ**/acetylene mixtures, we turned our attention to multicomponent screens. Incubation of a mixture of 10 structurally related alkynes (16 compounds, if all enantiomers are counted, cf. Figure 4) with **TZZ** and the enzyme gave only the expected triazole products **TZZPIQ-A5** and **TZZPIQ-A6**; that is, none of the other acetylenes that were present in the mixture were converted into triazoles. Thus, the **TZZ**/enzyme complex (over 99% active site saturation by **TZZ** under the reaction conditions³⁹) was able to recognize subtle differences in alkyne structure (compare **IQN**, **PIQ**, and **IIQ**) and form triazole products exclusively with its preferred reagents, **PIQ-A5** and **PIQ-A6**. These results demonstrate that highly efficient multicomponent screens are practical and that

Table 1. Inhibition Constants of Acetylene Reagents for Eel and Mouse AChE^{a,b}

entry	compound	K_i (μ M)	
		mouse AChE	eel AChE
1	IQN-A5	77	60
2	IQN-A6	210	74
3	PIQ-A5	34	18
4	PIQ-A6	21	7.8
5	IIQ-A5	>400	100
6	IIQ-A6	>400	67
7	C-A5	>400	>400
8	C-A6	>400	>400
9	PO-A5	>400	>400
10	PO-A6	>400	>400
11	PHN-A5	n.d. ^c	n.d. ^c
12	PHN-A6	n.d. ^c	n.d. ^c
13	DPA-A5	42	84
14	DPA-A6	83	110
15	HIQ-A5	99	46
16	HIQ-A6	190	43
17	DMB-A5	14	20
18	DMB-A6	14	20
19	PIP-A5	>400	320
20	PIP-A6	>400	170
21	PQH-A4	38	5.8
22	QH-A4	>400	>400
23	BOH-A4	4.1	0.50
24	PA6	0.36	n.d.

^a The measurements were performed in 100 mM phosphate buffer pH 7.0 (+0.01% BSA to stabilize the enzyme) at 22 °C. Constants were determined in duplicate experiments using Hunter and Downs plots.⁴⁰ ^b For comparison, the dissociation constant K_d of **TZZ** for mouse AChE is 0.023 μ M. ^c Not determined due to low solubility of the compound.

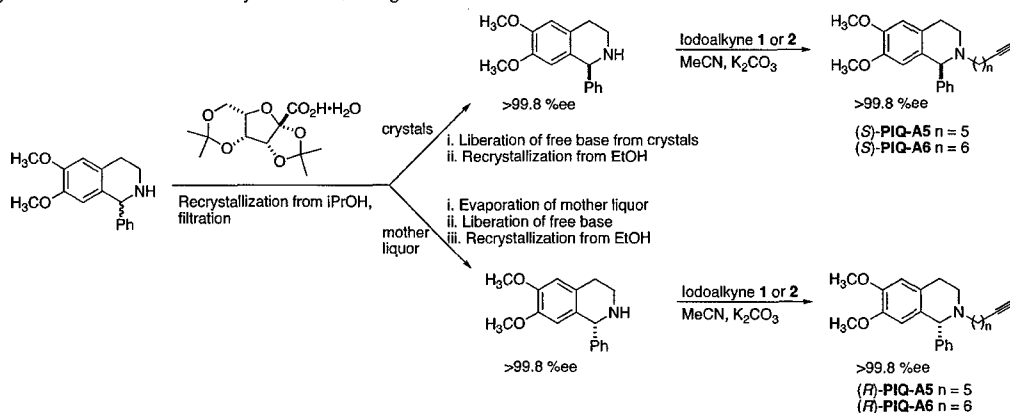
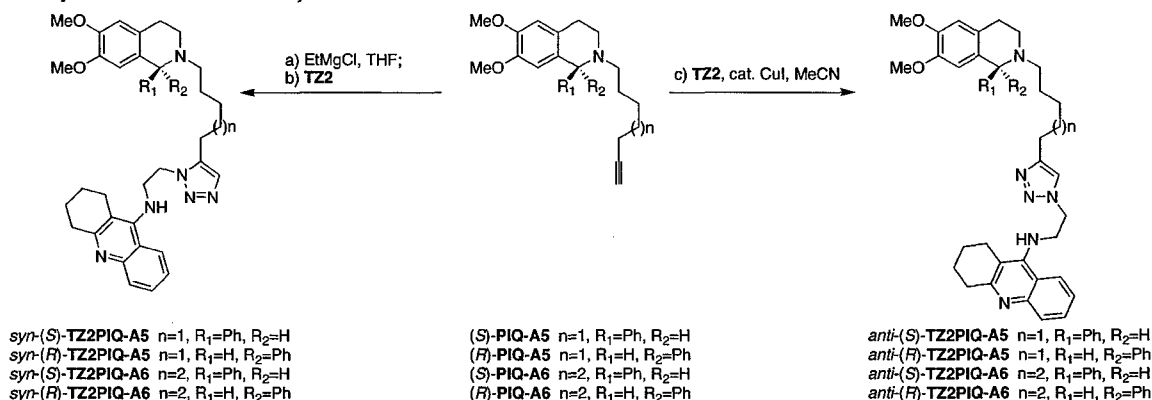
in situ click chemistry products are formed even when competing reagents (here **PIQ-A5** and **PIQ-A6**) are present.

Determination of Dissociation Constants for Acetylene Reagents. The inhibition of AChE by the acetylene reagents was measured at 22 °C and pH 7.0 (Table 1). With inhibition constants in the micromolar range (8–34 μ M), the phenyltetrahydroisoquinoline derivatives **PIQ-A5** and **PIQ-A6** are about 1 to 2 orders of magnitude less potent than the phenylphenanthridinium acetylenes used previously (K_d of **PA6** for mouse AChE: 0.36 μ M), demonstrating that even this relatively low level of affinity is sufficient for the target-templated reaction to take place. While the **PIQ** compounds are among the higher affinity in the set, there are five other compounds (entries 13, 17, 18, 21, and 23) with an approximately equal or higher potency. Surprisingly, these compounds did not form in situ products, despite their high binding affinity to the protein and the presence of identical linker moieties, revealing a lack of correlation between a reagent's binding affinity and its ability to undergo target-templated cycloaddition. It is possible that these compounds are not peripheral site ligands, but rather active site binders, thereby preventing the in situ reaction from occurring, or that the spatial orientation of the acetylene group of the enzyme-bound reagent is suboptimal. The fact that these compounds do not show substrate-competitive inhibition expected of association with the active center appears to rule out the former possibility, and stereoelectronic factors seem to be decisive.

Enantioselectivity. Initially, all reagents were either achiral or racemic, prompting the question whether AChE would prefer one enantiomer over the other for the in situ reaction in the case of **PIQ-A5** and **PIQ-A6**. To study the relative in situ click chemistry rates, we prepared each reagent in its pure enantiomeric forms through the synthesis and optical resolution of the

(39) AChE concentration: 1 μ M; **TZZ** concentration: 4–5 μ M; dissociation constant of **TZZ** for mouse AChE: K_d = 23 nM.

Scheme 1. Synthesis of Enantiomerically Pure PIQ Reagents

Scheme 2. Synthesis of TZ2-Derived *syn*- and *anti*-Triazoles from PIQ-A5 and PIQ-A6^a

^a Reagents and conditions: (a) EtMgCl (1.0 equiv), THF, rt to 60 °C, 30 min; (b) TZ2 (0.5 equiv), rt to 60 °C, 4 h, 65–85% yield over 2 steps; (c) TZ2 (1.0 equiv), CuI (5 mol %), MeCN, rt, 12 h, 80–90% yield.

precursor *rac*-6,7-dimethoxy-1-phenyl-1,2,3,4-tetrahydroisoquinoline,^{41,42} followed by alkylation with 7-iodohept-1-yne (**1**) or 8-iodooct-1-yne (**2**) (cf. Scheme 1). The enantiopure alkynes were also needed for kinetic and structural studies of enzyme–inhibitor complexes (vide infra).

Interestingly, the in situ click chemistry reaction rates for the enantiomers of each acetylene component are quite similar (cf. Supporting Information). In case of the mouse enzyme, the *R* isomers react slightly faster than the *S* enantiomers, whereas the opposite is true for the eel enzyme. We are in the process of investigating the molecular origin of the lack of selectivity through X-ray crystallography.

Determination of the Regioselectivity. We synthesized all regioisomers and enantiomers of the TZ2-derived PIQ-A5 and PIQ-A6 triazoles to elucidate the regioselectivity of the enzyme reaction and to develop a deeper understanding of the structure–activity relationship (Scheme 2). For the preparation of *anti*-triazoles, the recently discovered copper(I)-catalyzed process was employed,^{43,44} whereas *syn*-isomers were synthesized by way of magnesium acetylides.^{45–48}

The comparison of LC/MS-SIM traces of enzyme-produced triazoles and the reference compounds revealed a striking

similarity to the tacrine/phenylphenanthridinium system in that all in situ reaction products are 1,5-disubstituted (*syn*) triazoles (Figure 5). The *syn* selectivity was independent of the linker length, the source of the enzyme (eel or mouse AChE), and the absolute configuration of the PIQ component (cf. Supporting Information for LC/MS-SIM traces).

Determination of AChE-Inhibitor Association and Dissociation Rate Constants. All kinetic parameters of inhibitor binding to and dissociation from eel and mouse AChE were measured as described previously,²⁶ except for one modification. For determining the first-order dissociation rate constants by measuring the return of AChE activity upon 5000-fold dilution of 50–100 nM concentrations of AChE–inhibitor complex, we employed purified inactive mouse AChE mutant Ser203Ala (20–70 nM), instead of DNA, for sequestering the inhibitors upon their release from the complex with the active wild-type AChE to prevent their reassociation at concentrations approaching or higher than their *K*_d. This modification was necessary, since the current set of inhibitors did not intercalate with DNA as efficiently as the phenylphenanthridinium derivatives used previously. The equilibrium dissociation constants for the *syn*- and *anti*-isomers, calculated as the ratios of their first-order

(40) Hunter, A.; Downs, C. D. *J. Biol. Chem.* **1945**, *87*, 427–446.

(41) Kumar, P.; Dhawan, K. N.; Kishor, K.; Bhargava, K. P.; Satsangi, R. K. *J. Heterocycl. Chem.* **1982**, *19*, 677–679.

(42) Lee, D. U.; Wiegand, W. *Bull. Korean Chem. Soc.* **1991**, *12*, 373–376.

(43) Rostovtsev, V. V.; Green, L. G.; Fokin, V. V.; Sharpless, K. B. *Angew. Chem., Int. Ed.* **2002**, *41*, 2596–2599.

(44) Tornøe, C. W.; Christensen, C.; Meldal, M. *J. Org. Chem.* **2002**, *67*, 3057–3064.

(45) Krasinski, A.; Fokin, V. V.; Sharpless, K. B. *Org. Lett.* **2004**, *6*, 1237–1240.

(46) Akimova, G. S.; Chistokletov, V. N.; Petrov, A. A. *Zh. Org. Khim.* **1967**, *3*, 968–974.

(47) Akimova, G. S.; Chistokletov, V. N.; Petrov, A. A. *Zh. Org. Khim.* **1967**, *3*, 2241–2247.

(48) Akimova, G. S.; Chistokletov, V. N.; Petrov, A. A. *Zh. Org. Khim.* **1968**, *4*, 389–394.

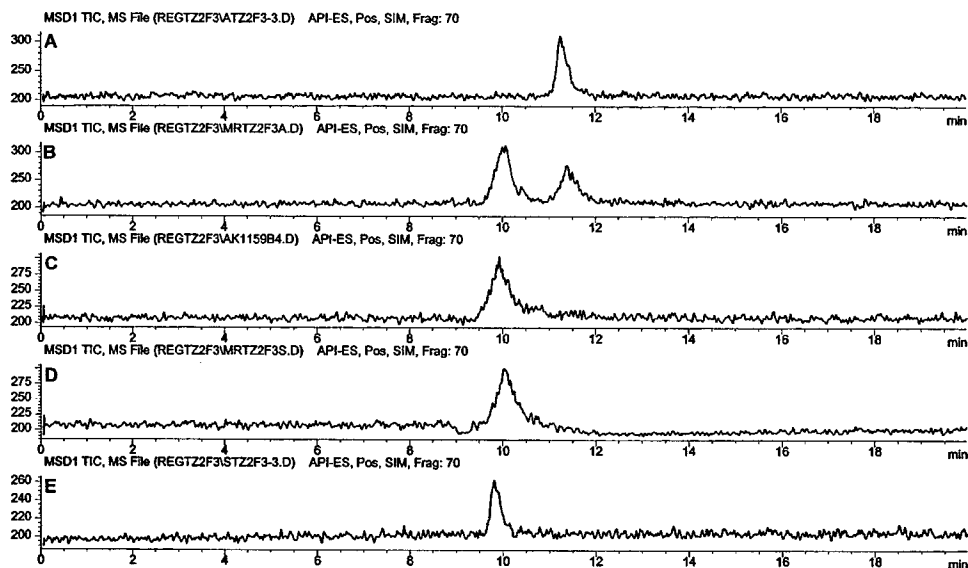


Figure 5. Regioisomer (*syn/anti*) determination for mouse AChE-derived in situ hits. The in situ product, (*R*)-**TZ2PIQ-A5**, was compared by LC/MS-SIM to authentic samples from the Cu(I)-catalyzed and Mg-mediated reactions. (A) *anti*-(*R*)-**TZ2PIQ-A5** prepared by the Cu(I)-catalyzed reaction; (B) co-injection of (*R*)-**TZ2PIQ-A5**, formed by AChE, and *anti*-(*R*)-**TZ2PIQ-A5**, prepared by the Cu(I)-catalyzed reaction; (C) in situ click reaction; (D) co-injection of the in situ click reaction and *syn*-(*R*)-**TZ2PIQ-A5** prepared by the Mg-mediated reaction; (E) *syn*-(*R*)-**TZ2PIQ-A5** prepared by the Mg-mediated reaction.

Table 2. Kinetic Parameters and Dissociation Constants for in Situ-Generated Inhibitors and Related Compounds

inhibitor		k_{on} ($10^{10} \text{ M}^{-1} \text{ min}^{-1}$)	k_{off} (min^{-1})	K_{d} (fM)	AChE source
(S)- TZ2PIQ-A5	<i>syn</i> -	0.70	0.00023	33	eel
		0.77	0.0038	500	mouse
	<i>anti</i> -	0.52	1.10	210 000	eel
(R)- TZ2PIQ-A5		0.72	6.2	870 000	mouse
	<i>syn</i> -	0.67	0.00024	36	eel
		0.84	0.00088	100	mouse
(S)- TZ2PIQ-A6	<i>anti</i> -	0.40	0.77	190 000	eel
		0.58	1.0	180 000	mouse
	<i>syn</i> -	0.90	0.00087	96	eel
(R)- TZ2PIQ-A6		0.97	0.0110	1100	mouse
	<i>anti</i> -	0.41	0.83	200 000	eel
		0.67	2.8	420 000	mouse
TZ2HIQ-A6	<i>syn</i> -	0.67	0.0024	360	eel
		0.73	0.012	1700	mouse
	<i>anti</i> -	0.50	0.82	170 000	eel
TZ2PA6		0.64	1.4	220 000	mouse
	<i>syn</i> -	1.0	0.012	1200	eel
		1.5	0.081	5400	mouse
	<i>anti</i> -	0.47	10	2 100 000	eel
		0.58	11	1 900 000	mouse
	<i>syn</i> -	1.5	0.0015	99	eel
		1.7	0.0071	410	mouse
	<i>anti</i> -	1.8	0.25	14 000	eel
		2.5	0.22	8900	mouse

dissociation and second-order association rate constants, are listed in Table 2, along with the dissociation constants for the **TZ2PA6** isomers reported previously.²⁶

Interestingly, despite their higher binding affinities, the **PIQ**-derived inhibitors display 2 to 3 times lower on-rates than the original **PA**-derived inhibitors. Nevertheless, the on-rates k_{on} are all very large, close to diffusion controlled, and the observed binding affinity trends are due mainly to variations in off-rates k_{off} , which are extremely slow for the tightest binding compounds.

The best inhibitors proved to be the enzyme-generated phenyltetrahydroisoquinoline derivatives (*S*)- and (*R*)-**TZ2PIQ**-

A5, which do not carry a permanent positive charge and aniline groups as did the previous champion, **TZ2PA6**, while being 3 times as potent in the case of eel AChE. In fact, with a dissociation constant of less than 40 fM (eel AChE), these compounds are the most potent noncovalent AChE inhibitors known to date. As a general observation, all in situ-generated compounds tested here show a greater affinity for the eel enzyme (33–360 fM) than for mouse AChE (100–1700 fM).

Despite the tight binding of the **TZ2PIQ** triazoles, there is no clear enantiomeric preference. This observation is in line with the lack of selectivity for either one of the two enantiomeric reactants in the in situ click chemistry reaction (vide supra). Thus, in the case of **TZ2PIQ-A5**, having a 5-methylene linker between the triazole ring and the tetrahydroisoquinoline moiety, the *R* isomer is bound about 5 times more tightly than the *S* enantiomer in the case of mouse AChE, while there is no difference between the enantiomers in case of eel enzyme. The reverse trend is observed in the case of the **TZ2PIQ-A6** triazoles, having a 6-methylene linker, where the *S* isomer has a higher binding affinity for either enzyme.

As before, the in situ-generated *syn*-triazoles are several orders of magnitude more potent inhibitors than the corresponding *anti*-isomers, not formed by the enzyme. However, the extent of the difference is more than an order of magnitude larger than for phenylphenanthridinium triazoles, ranging from 600- to 5600-fold preference for the *syn*-triazoles (the average difference in the free energy of binding is about 4 kcal/mol, cf. Supporting Information for additional free energy data). In the case of the phenylphenanthridinium triazoles, the *syn*-preference was only 14- to 420-fold. In general, our data suggest that compounds that are *not* formed by the enzyme, e.g., *anti*-triazoles and **TZ2HIQ-A6**, bind more weakly than the in situ-generated triazoles.

Experimental Section

CAUTION! All of the compounds described here (and especially the most potent polyvalent inhibitors) are potentially neurotoxic. They

must be handled with extreme care by trained personnel. Azide-containing compounds, particularly those lower in saturated carbon and oxygen content, are potentially explosive and must be handled with care.

General Procedures for in Situ Click Chemistry Experiments. Determination of Acetylcholinesterase and Stock Concentrations.

The enzyme concentrations were determined by quantitative measurement of AChE activity using the Ellman assay as described previously.^{17,26} All in situ click chemistry reactions were performed at an active site concentration of 1 μ M. The stock concentrations for all triazole compounds were determined in duplicate by titration of the inhibitor solutions with two different AChE preparations of known concentration.

In Situ Click Chemistry Screening Procedure for Binary Reagent Mixtures. The tacrine azide **TZ2** was dissolved in MeOH and added to \sim 1 μ M solutions of eel AChE (Type V-S, Sigma) or mouse AChE^{49,50} in buffer (2 mM ammonium citrate, 100 mM NaCl, pH = 7.3–7.5) followed immediately by one of the acetylene components and mixed. The final concentrations were as follows: eel or mouse AChE, 1 μ M; tacrine azide (**TZ2**), 4.6 μ M, acetylene component, 24 μ M; MeOH, 1.5%. Each reaction mixture was incubated at 37 °C for at least 6 h. Samples of the reactions were injected directly (15 μ L) into the LC/MSD instrument to perform LC/MS-SIM analysis (Zorbax SB-C8 reverse-phase column, preceded by a Phenomenex C18 guard column, electrospray ionization, and mass spectroscopic detection in the positive selected ion mode, tuned to the expected molecular weight of the product). The cycloaddition products were identified by their retention times and molecular weights. Control experiments in the absence of enzyme or in the presence of bovine serum albumin (BSA, 3 mg/mL) instead of enzyme failed to produce product signals. For these control experiments, methanol (1:1 dilution) was added to the reaction mixtures prior to LC/MS-SIM analysis, to prevent possible precipitation of the expected triazole product.

In Situ Click Chemistry Screening Procedure for Multicomponent Incubations. A methanolic solution (1.0 μ L) of acetylene building blocks (10 reagents at 2 mM concentration each) was added to a solution of **TZ2** and mouse AChE (99 μ L of 1 μ M AChE, 4.2 μ M **TZ2**, 2 mM ammonium citrate, 100 mM NaCl, pH = 7.3–7.5). The final concentrations were as follows: mouse AChE, 1 μ M; tacrine component (**TZ2**), 4.2 μ M; acetylene component, 20 μ M; MeOH, 1%. Each reaction mixture was incubated at 37 °C for at least 24 h. Samples of the reactions were injected directly (15 μ L) into the LC/MSD instrument to perform LC/MS-SIM analysis, as described previously.²⁶ The chromatograms were analyzed for the presence of in situ reaction products by extracting single ion traces for all expected molecular weights (cf. Figure 4).

Conclusions

This study reveals that the in situ click chemistry approach has great potential for lead discovery and optimization. As established here, suitable reagents for the generation of potent inhibitors within the enzyme's binding sites can be found without prior knowledge of their affinities for the protein, provided that one of the two components has sufficient affinity

to serve as an "anchor molecule". In the present study, the anchor is the azide **TZ2**, which is present at a concentration sufficient to saturate the enzyme active site. We have discovered two new potent in situ hit compounds through screening of reagent mixtures using the reliable LC/MS-SIM method for analyzing in situ click chemistry mixtures. The hit compounds **TZ2PIQ-A5** and **TZ2PIQ-A6** were made by both eel and mouse AChE with high regioselectivity for the *syn*-triazole product. With low-femtomolar dissociation constants, these compounds are the most potent noncovalent AChE inhibitors known. They lack a permanent positive charge and aniline groups and possess fewer fused aromatic rings than the original inhibitors. The corresponding *anti*-isomers, not made by the enzymes, were 2–4 orders of magnitude less potent. The affinities of the offered building block components do not always correlate well with the propensity for formation of hit compounds. The unique synergism found for formation of these hit compounds within the enzyme likely results from the proximity of the reactant moieties and their ability to adopt the appropriate orientation. In addition, the enzyme-templated cycloaddition is most likely promoted by an enthalpic stabilization of the transition state, probably through compensation of the strong dipole moment that is developed during triazole genesis. Previous crystallographic studies have revealed the unusual positioning of a tryptophan and a tyrosine at the peripheral binding site pointing toward a potential ability of the reactive building blocks to induce or stabilize a unique enzyme conformation that allows the reaction to take place. Currently, we are focusing our research on the mechanism of the in situ click chemistry involving a combination of kinetic studies and structural biology.

Acknowledgment. We are grateful to Prof. G. Siuzdak and Mr. J. Apon for MALDI mass spectrometry support. We also thank Prof. Pascale Marchot (Laboratoire de Biochimie, Institut Fédératif de Recherche Jean Roche, Université de la Méditerranée, Marseille, France) for providing samples of purified eel AChE. This work was supported by the Swiss National Science Foundation (R.M.); the Novartis Research Foundation (R.M.); the Skaggs Institute for Research (A.K., J.R., H.C.K.); the National Institute of General Medical Sciences, National Institutes of Health, GM28384 (K.B.S.) and GM R37-18360 (P.T.); DAMDC17C-02-2-0025 (P.T.); and the W. M. Keck Foundation (K.B.S.).

Supporting Information Available: LC/MS-SIM traces for in situ click chemistry and control experiments, experimental details and LC/MS-SIM traces for regioisomer determination, comparison of reaction rates between the **PIQ** acetylene enantiomers, experimental procedures for reagent and triazole synthesis, and their characterization, and tables with free energy increments for structural modifications. This material is available free of charge via the Internet at <http://pubs.acs.org>.

JA043031T

- (49) Radić, Z.; Pickering, N. A.; Vellom, D. C.; Camp, S.; Taylor, P. *Biochemistry* **1993**, *32*, 12074–12084.
(50) Marchot, P.; Ravelli, R. B. G.; Raves, M. L.; Bourne, Y.; Vellom, D. C.; Kanter, J.; Camp, S.; Sussman, J. L.; Taylor, P. *Protein Sci.* **1996**, *5*, 672–679.



Two possible orientations of the HI-6 molecule in the reactivation of organophosphate-inhibited acetylcholinesterase

Chunyuan Luo^{a,*}, Haim Leader^a, Zoran Radic^b, Donald M. Maxwell^c, Palmer Taylor^b,
Bhupendra P. Doctor^a, Ashima Saxena^a

^a*Division of Biochemistry, Walter Reed Army Institute of Research, Silver Spring, MD 20910-7500, USA*

^b*Department of Pharmacology, University of California at San Diego, La Jolla, CA 92093-0636, USA*

^c*US Army Medical Research Institute of Chemical Defense, Aberdeen Proving Ground, Aberdeen, MD 21010, USA*

Received 18 November 2002; accepted 21 March 2003

Abstract

The inhibition of acetylcholinesterase (AChE) by organophosphorus compounds (OPs) causes acute toxicity or death of the intoxicated individual. One group of these compounds, the OP nerve agents, pose an increasing threat in the world due to their possible use in the battlefield or terrorist acts. Antidotes containing oxime compounds to reactivate the inhibited enzyme are highly valued for treatment against OP poisoning. One of these reactivators, HI-6, was shown to be significantly more effective in treating soman toxicity than other oximes, such as 2-PAM, TMB4, and obidoxime. However, HI-6 was less effective in reactivating AChE inhibited by the OP pesticide, paraoxon. In this study, the mechanism for HI-6-induced reactivation of OP–AChE conjugates was investigated using mouse mutant AChEs inhibited with different OPs including organophosphate paraoxon, and several methylphosphonates. Results indicate that the HI-6 molecule may assume two different orientations in the reactivation of AChE inhibited by organophosphate and Sp methylphosphonates. These conclusions were further corroborated by reactivation studies using an analog of HI-6 in which the bispiridinium moieties are linked by a methylene bridge rather than an ether oxygen.

© 2003 Elsevier Science Inc. All rights reserved.

Keywords: Acetylcholinesterase; Reactivation; Organophosphates; HI-6; Oxime

The inhibition of acetylcholinesterase (AChE; E 3.1.1.7) by organophosphorus compounds (OPs) causes acute intoxication. Chemical nerve agents pose an increasing threat in the world due to their possible use in battlefield or terrorist acts. At the same time, OP pesticides, such as paraoxon and its analogs, are being used throughout the world in agriculture causing hundreds of thousands of

intoxication cases each year. At the present time, available antidotes against OP poisoning use oximes, such as 2-PAM, obidoxime, TMB4, and HI-6, to reactivate the inhibited enzyme. Of the nerve agents, soman is the greatest challenge since both the rapid aging of the soman-inhibited enzyme (de-alkylation) and the bulkiness of the pinacolyl residue prevent efficient reactivation of the inhibited enzyme by most oximes. HI-6, an oxime first synthesized in the early 1970s, was shown to be a very effective antidote in reactivating soman-inhibited AChE. But compared with other oximes, HI-6 was much less effective in reactivating paraoxon- or methylparaoxon-inhibited AChE, making it unsuitable for the treatment of OP pesticide poisoning [1,2]. The mechanism for the selectivity of HI-6 in reactivating soman-inhibited enzyme over paraoxon-inhibited enzyme is not yet known.

Several recent studies have demonstrated the successful use of site-directed mutagenesis to explore the interactions between OP-conjugated AChE and oxime reactivators

* Corresponding author. Tel.: +1-301-319-9089; fax: +1-301-319-9150.

E-mail address: chunyuan.luo@na.amedd.army.mil (C. Luo).

Abbreviations: AChE, acetylcholinesterase; MoAChE, recombinant mouse wild-type acetylcholinesterase; OPs, organophosphorus compounds; POX, phosphonyl or phosphoryl oximes; DEPQ, 7-(*O,O*-diethylphosphinyloxy)-1-methylquinolinium methyl sulfate; MEPQ, 7-(*O*-ethyl methylphosphinyloxy)-1-methylquinolinium iodide; iPrMP, isopropyl methyl phosphonothiocholine; 2-PAM, 2-[hydroxyimino methyl]-1-methylpyridinium chloride; TMB4, 1,1'-trimethylene bis(4-hydroxyimino methyl) pyridinium dichloride; obidoxime (toxogonin), 1,1'-(oxybis-methylene)bis[4-(hydroxyimino)methyl] pyridinium dichloride; HI-6, 1-(2-hydroxyiminomethyl-1-pyridinium)-1-(4-carboxy-aminopyridinium)-dimethyl ether hydrochloride.

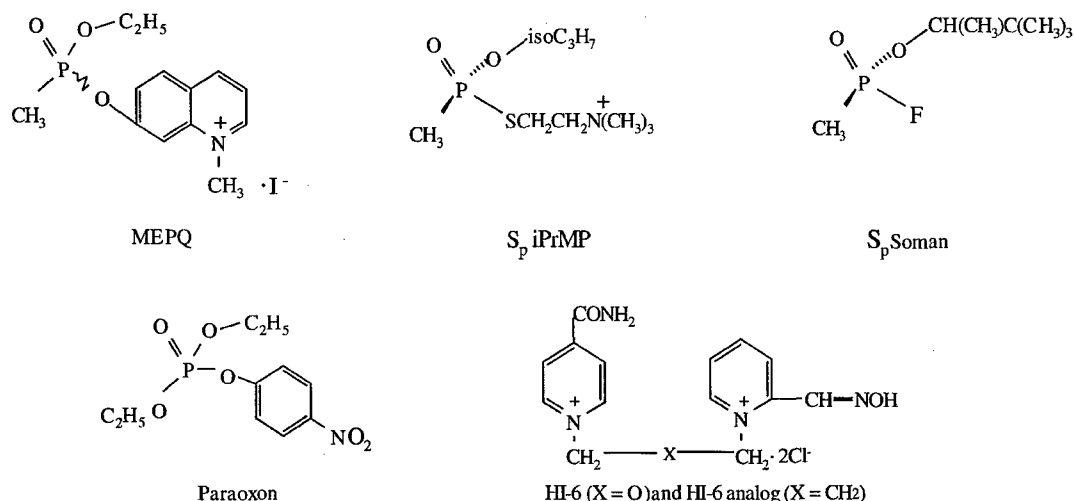


Fig. 1. Structures of organophosphate, organophosphonates, and oximes used in the study.

[3–6]. However, an important issue in the study of reactivation kinetics is the possibility of phosphoryl oxime (POX) inhibition of the reactivated enzyme during the reactivation process that may prevent the accurate determination of reactivation rate constants [6–8]. In our previous studies, we demonstrated that of the four oximes, 2-PAM, TMB4, obidoxime, and HI-6, HI-6 was the only one that did not show any complications due to POX inhibition during the reactivation of AChE inhibited by either organophosphonate (MEPQ) or organophosphate (DEPQ). Therefore, we conducted reactivation kinetic studies with HI-6 using mouse wild-type and mutant AChEs inhibited by different OP compounds, including organophosphate paraoxon, racemic methylphosphonate MEPQ, Sp enantiomeric iPrMP, and SpSc soman (Fig. 1). The results of our study highlight some significant differences between the interactions of HI-6 with organophosphate- and methylphosphonate-inhibited AChEs during reactivation, which are also supported by reactivation studies using an analog of HI-6 that is devoid of the ether chain oxygen.

1. Materials and methods

1.1. Materials

MEPQ and Sp iPrMP were prepared by the method reported previously [9,10]. HI-6 was obtained from the Division of Experimental Therapeutics, Walter Reed Army Institute of Research. HI-6 analog was synthesized by method deployed in oxime synthesis and the structure confirmed by proton NMR. Recombinant mouse wild-type AChE (MoAChE) and mutant enzymes were prepared by the method previously reported [11,12]. Organophosphate paraoxon was purchased from Sigma Chemical Co. Bio-Spin 6 chromatography columns were purchased from Bio-Rad Laboratories. Other chemicals were from commercial resources.

1.2. AChE assay

AChE activity was determined spectrophotometrically by the method of Ellman *et al.* [13]. The assay mixture contained 1 mM acetylthiocholine (ATC; or 30 mM ATC in the case of W86A mutant AChE) as the substrate and 0.5 mM 5,5-dithiobis-(2-nitrobenzoic acid) (DTNB) in 50 mM sodium phosphate buffer, pH 8.0. All measurements were performed at 25°.

1.3. Determination of the reactivation rate constants of OP-inhibited enzyme by oximes

AChE–OP complexes were prepared by adding greater than the stoichiometric amount of OP to wild-type or mutant MoAChEs in a total volume of 100 μ L and incubating for 20 min at 25°. Excess OP was removed from the complex using a Bio-Spin column 6. The enzyme conjugate was then diluted 10-fold with 0.05% BSA in 50 mM phosphate buffer, pH 8.0, containing the oxime. The final oxime concentration in the reactivation mixture ranged from 50 μ M to 3 mM. At specified time intervals, 5–10 μ L of reactivation mixture was withdrawn and diluted into the assay mixture to monitor change in enzyme activity. The first-order reactivation rate constant, k_{obs} , was determined by fitting the experimental data to equation for one-phase exponential association:

$$\% (E_{\text{react}})_t = A(1 - e^{-k_{\text{obs}} \times t})$$

A plot of k_{obs} vs. [oxime] was used to obtain the second-order reactivation rate constant as described by Ashani *et al.* [3]. Due to the chirality of the phosphorus in MEPQ, the phosphoryl conjugate enzyme consists of two enantiomers that are reactivated at different rates. The reactivation rate constants of the two species were calculated using a two-phase exponential association equation, assuming an equal distribution of the two species under the condition that a stoichiometric amount of MEPQ was used for the inhibition of AChE.

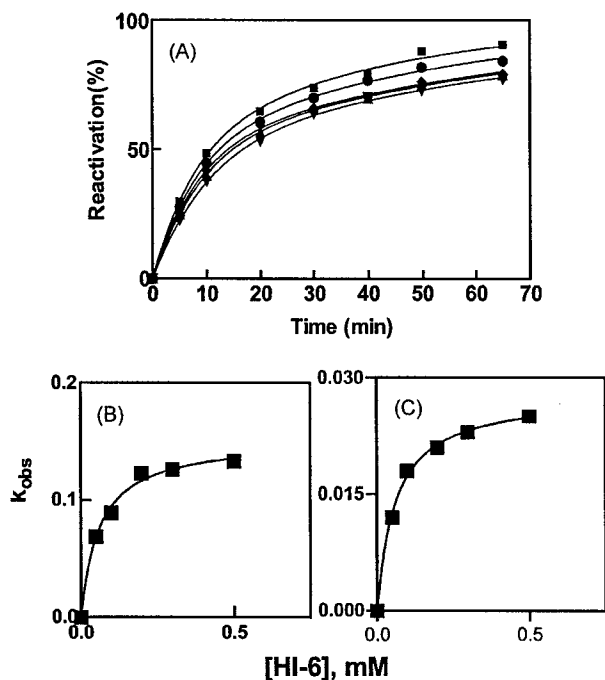


Fig. 2. Reactivation kinetics of MEPQ-inhibited wild-type MoAChE by HI-6. (A) Reactivation kinetics of one representative experimental data of MEPQ-inhibited wild-type MoAChE by HI-6 (0.05 to 0.5 mM); symbols represent the following concentrations of HI-6: (▼) 0.05 mM; (▲) 0.1 mM; (◆) 0.2 mM; (●) 0.3 mM; (■) 0.5 mM. (B) Secondary plot of the k_{obs} for the fast-reactivation species vs. [HI-6] for the second-order kinetic constants. (C) Secondary plot of the k_{obs} for the slow-reactivation species vs. [HI-6].

2. Results

2.1. Reactivation rate constants of OP-inhibited MoAChE by HI-6

As shown in Fig. 2, the reactivation data for MEPQ-inhibited wild-type MoAChE using five different HI-6 concentrations fit to the two-phase exponential association equation well. The secondary plot of k_{obs} vs. [HI-6] yields values of the second-order reactivation rate constants of 2700 and 462 $M^{-1} min^{-1}$ for the fast- and slow-reactivation species, respectively. The second-order reactivation rate constants of wild-type MoAChE inhibited with other OPs determined using this method showed that these constants varied considerably depending on the structure of OP (Table 1). Sp iPrMP- and SpSc soman-inhibited AChEs, as well as the fast-reactivation species of MEPQ-inhibited AChE were reactivated several fold faster than paraoxon-inhibited AChE and the slow-reactivation species of MEPQ-inhibited AChE.

2.2. Effect of mutations on the reactivation of OP-inhibited MoAChE by HI-6

Mutations of F295 to Leu or F297 to Ile reduced the reactivation rate of the fast-reactivation species of MEPQ-

Table 1

Second-order rate constants (k , $M^{-1} min^{-1}$) for the reactivation of OP-inhibited mouse wild-type and mutant AChEs by HI-6

Enzyme	MEPQ ^a	Sp iPrMP	SpSc soman ^b	Paraoxon
Wild-type	2700 (fast); 462 (slow)	2650	1751	590
F295L	1263 (fast); NA (slow)	3320 ^c	5420	2.15
F297I	1325 (fast); 1.3 (slow)	2400 ^c	3460	1.47
W86A ^d	947 (fast); 84 (slow)	3606	5245	22.6
W286A	673 (fast); 105 (slow)	913	732	151
Y124Q	31 (fast); 19 (slow)	74	11.3 ^c	103

Data are mean values of two to four experiments with all reactivation experiments carried out at 25° in 50 mM PO₄ buffer, pH 8.0, except where indicated.

^a The reactivation rate constants of MEPQ-inhibited enzymes were obtained by fitting the kinetic data to the two-component equation [3], and the maximal reactivation was more than 92% except with F295L, where only 55–62% reactivation was observed after 50 hr.

^b Reactivation was carried out at 25° in 50 mM PO₄ buffer, pH 8.0, after inhibition in 50 mM Tris buffer, pH 9.5; maximal reactivation is from 86 to 95% except where indicated.

^c Data cited from Wong *et al.* [5] where the reactivation rate constants were determined in 50 mM Tris–HCl buffer, pH 8.0.

^d The activity assay for W86A was performed using 30 mM ATC instead of 1 mM.

^e Data estimated from k_{obs} of a single concentration of HI-6 assuming that it is in the linear range of the saturation curve, maximal reactivation was 31%.

inhibited enzyme about 2-fold, but the reactivation rates for the slow-reactivation species were reduced >300-fold for F297I AChE or to a negligible reactivation rate for F295L AChE. The reactivations of both the active anionic site mutant, W86A, and the peripheral anionic site mutant, W286A, were only reduced by a factor of 3–5 for the fast- and slow-reactivation species of MEPQ-inhibited enzyme. However, the mutation of another peripheral anionic site residue, Y124 to Gln, reduced the reactivation rate constant of the fast-reactivation species by 87-fold, and the slow-reactivation species by 24-fold. This mutation significantly reduced the HI-6-induced reactivation rate constants for both Sp iPrMP-inhibited enzyme (36-fold) and SpSc soman-inhibited enzyme (155-fold). Also, 1.4- to 3-fold increases in HI-6-induced reactivations were observed with Sp iPrMP and SpSc soman-inhibited F295L, F297I, and W86A with the exception of iPrMP-inhibited F297I, whose reactivation rate constant decreased slightly compared with wild-type enzyme.

The effects of these mutations on the reactivation rate constants of paraoxon-inhibited mouse AChEs were quite different from those inhibited by all the methylphosphonates studied. First, the reactivation rate of paraoxon-inhibited wild-type enzyme by HI-6 was 3- to 5-fold slower compared with Sp iPrMP- and Sp soman-inhibited AChEs or the fast-reactivation species of MEPQ-inhibited AChE, despite the fact that paraoxon-inhibited enzyme could be reactivated very easily by other bispyridinium oximes such as LüH6 [1,2]. Second, the reactivation rate constants of paraoxon-inhibited F295L and F297I AChEs displayed

Table 2

Comparison of the second-order rate constants for the reactivation of OP-inhibited mouse wild-type AChE by HI-6 and its analog

OPs	k_r ($M^{-1} \text{ min}^{-1}$)	
	HI-6	HI-6 analog
MEPQ		
Fast-reactivation species	2700	544
Slow-reactivation species	462	291
Paraoxon	690	668

The second-order reactivation rate constants were determined as described in Table 1. Data were in k_r ($M^{-1} \text{ min}^{-1}$).

drastic reductions (275- to 400-fold) compared with the wild-type enzyme, while this was not observed with most of the methylphosphonate-inhibited AChEs. Third, the reactivation rate constant of paraoxon-inhibited W86A AChE by HI-6 was 26-fold lower compared to wild-type AChE, a phenomenon not observed with any of the methylphosphonate-enzyme conjugates. Finally, the reactivation rate of paraoxon-inhibited Y124Q AChE by HI-6 showed only a 5-fold reduction instead of the 36- to 155-fold reductions observed with the Sp methylphosphonate-enzyme conjugates.

2.3. Comparison of the reactivation kinetics of MEPQ- and paraoxon-inhibited wild-type mouse AChEs by HI-6 and its analog

Reactivation studies with mutant enzymes showed that the HI-6-induced reactivation of AChEs inhibited by Sp methylphosphonate, but not by organophosphate paraoxon, displayed a significant dependence on the peripheral

anionic site amino acid, Y124. Computer modeling by Ashani *et al.* [3] previously indicated that Y124 might interact with the ether oxygen through a hydrogen bond to facilitate the orientation of HI-6 during reactivation of MEPQ-inhibited AChE. Therefore, we conducted reactivation studies with an HI-6 analog to determine if the substitution of the ether oxygen by methylene group has any effect on the reactivation of different AChE-OP conjugates. Results in Table 2 show that absence of that oxygen significantly reduced the reactivation potency of the oxime for the fast-reactivation species of MEPQ-inhibited enzyme by 5-fold, but not the slow-reactivation species or paraoxon-inhibited enzyme.

3. Discussion

Studies on the reactivation of OP-inhibited AChE will not only enhance our understanding of the reactivation mechanism, but also help the design for better and more effective reactivators. Reactivation by oxime compounds is a process of nucleophilic reaction involving the deprotonized negative oxygen of the oxime group to attack the phosphorus atom of OP moiety in the active center of AChE, resulting in the departure of AChE from OP-enzyme conjugate (Fig. 3 depicted the binding relationship of MEPQ-conjugated AChE and HI-6 molecule). The search for better reactivator is important for improving the efficacy of antidotes against OP toxicity. HI-6, a bispyridinium oxime containing the structural features of 2-PAM, is a very powerful reactivator of nonaged soman-inhibited AChE [14]. Results of reactivation studies using AChE inhibited by MEPQ, a methylphosphonate,

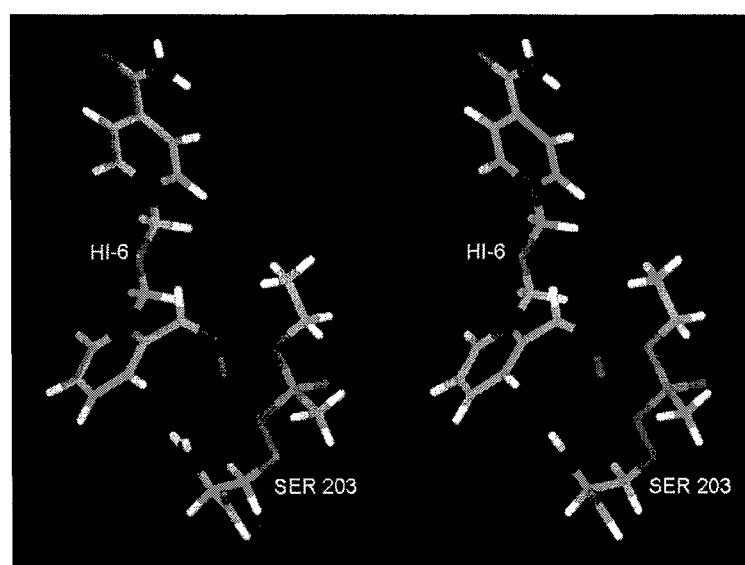


Fig. 3. Stereoview of relationship between MEPQ-inhibited AChE and oxime reactivator HI-6. The stereoview was made using Insight II (version 2000); the phosphorus atom of MEPQ is marked in pink, the methyl and ethoxyl groups are marked in green, and the oxygen of the oxime group of HI-6 is marked in red. The deprotonized negative oxygen of the oxime group approaches the phosphorus atom of Sp MEPQ residue in the active center of AChE to initiate nucleophilic attack, resulting in the departure of OP residue and generation of free enzyme.

suggested that the enhanced reactivation potency of HI-6 is due to the interaction of the second pyridinium ring with the peripheral anionic site of AChE which facilitates the orientation of HI-6 during reactivation [3]. However, other oximes containing the second pyridinium structure, such as obidoxime and TMB4, display very poor reactivation potencies for AChE inhibited by soman, also a methylphosphonate. Therefore, the mechanism for increased activity of HI-6 in reactivating soman-inhibited AChE is unclear.

In this study, we used three methylphosphonates with increasing size of the alkoxy groups, i.e. ethyl, isopropyl, and pinacolyl, and an organophosphate paraoxon, to form enzyme–OP conjugates for reactivation by HI-6. Two of these three methylphosphonates (Sp iPrMP and SpSc soman) were pure Sp enantiomers and expected to yield a single enzyme–OP species. Since MEPQ is a racemic compound, it produced equal amounts of two enzyme–OP species that exhibited different rates of reactivation in the presence of oximes. According to Ashani *et al.* [3], the fast-reactivation species is the one that is formed by the Sp enantiomer of MEPQ with enzyme, while the slow-reactivation species is the one formed by the Rp enantiomer. Our studies using Sp iPrMP and SpSc soman support this contention, since considerably fast rates of reactivation were observed for AChE inhibited by these two bulkier Sp enantiomers. It is also interesting to note that increasing the size of the alkoxy group from ethyl or isopropyl to pinacolyl only slightly reduced the rate of reactivation by HI-6. This indicates that steric hindrance caused by the SpSc soman moiety does not play a significant role in HI-6-induced reactivation. The W86 located at the choline-binding site may be used by HI-6 in orienting the oxime to attack the OP moiety. However, Sp iPrMP- and SpSc soman-inhibited W86A AChE promoted HI-6 reactivation at a rate comparable to that of wild-type enzyme, indicating that HI-6 does not need the facilitation of choline-binding site W86 for the nucleophilic attack by the oxime molecule.

W286 is regarded as the core component of the peripheral anionic site of AChE and only moderate reductions in the second-order rate constants were demonstrated in HI-6-induced reactivations of W286A AChE conjugated with all Sp methylphosphonates. However, another peripheral site mutant, Y124Q, produced 36- to 155-fold reductions in the reactivation rate constants with these three methylphosphonates, indicating that Y124 is the residue at the peripheral site that plays an important role in facilitating HI-6-induced reactivation of the Sp methylphosphonate–enzyme conjugates.

The 5- and 3-fold lower second-order reactivation rate constants of paraoxon-inhibited AChE compared to those of Sp iPrMP- and SpSc soman-inhibited AChE, respectively, are difficult to reconcile on the basis of steric rationale that AChE inhibited by a small organophosphate, paraoxon, is more refractory to HI-6 reactivation than that inhibited by the bulkier methylphosphonates. Since 2-PAM, TMB4, and obidoxime are more efficient reactivators of diethylphosphorylated AChE than HI-6 [5,14,15], it is likely that a factor, other than steric hindrance, is responsible for the refractoriness of this conjugate towards HI-6 reactivation.

Molecular modeling studies suggest that the orientation of the OP moiety in the active center is crucial for achieving fast oxime-induced reactivation of AChE conjugates with the Sp enantiomers, but not with the Rp enantiomers of methylphosphonates [5]. Since the structures of both MEPQ and paraoxon share a common ethoxy group, if the other ethoxy group of paraoxon can assume an orientation in the acyl pocket, the reactivation of paraoxon-inhibited mutant enzymes should follow a pattern similar to that of AChE inhibited by the Sp enantiomer of MEPQ. However, the reactivation study with HI-6 showed that the pattern of the reactivation of different mutant enzymes inhibited with paraoxon is different from all Sp methylphosphonate-inhibited enzymes. This indicates that the slower HI-6 reactivation rate observed with paraoxon-inhibited enzyme is due to a different orientation of the OP residue in the active site gorge compared with the Sp methylphosphonates. This is also supported by the study with mutant Y124Q, which demonstrated ≥ 36 -fold decrease in the reactivation rate constants with all Sp methylphosphonate–enzyme conjugates. Reactivation of paraoxon-inhibited Y124Q resulted in a 6-fold decrease in the second-order rate constant, suggesting that the peripheral site of the enzyme is not as important in the reactivation of paraoxon-inhibited AChE as it is in the reactivation of methylphosphonate–enzyme conjugates. At the same time, the choline-binding site mutant, W86A, reduced the reactivation rate constant of paraoxon-inhibited enzyme much more significantly than it did with all the Sp methylphosphonates. This indicates that, unlike the reactivation of Sp methylphosphonate-inhibited AChEs, HI-6 may use the choline-binding site to orient the oxime molecule for nucleophilic attack in the reactivation of paraoxon-inhibited AChE. Therefore, the results of site-directed mutagenesis studies suggest that HI-6 may take two different orientations in the reactivation of AChE inhibited by the Sp methylphosphonates and organophosphate, paraoxon.

Reactivation of wild-type AChE by HI-6 analog showed that deletion of the ether oxygen only reduced the reactivation potency for the fast-reactivation species of MEPQ-inhibited enzyme, which is the conjugate formed by the Sp enantiomer of MEPQ. For the slow-reactivation species and paraoxon-inhibited enzyme, deletion of the ether oxygen had negligible effect on the reactivation potency of the oxime. This also supports the hypothesis that HI-6 assumes different orientations during the reactivation of AChE inhibited by organophosphate paraoxon and Sp methylphosphonates.

Acknowledgments

We thank Dr. Cholanayakanahalli R. Vinayaka for preparing the three dimensional picture in this paper.

References

- [1] Worek F, Kirchner T, Backer M, Szinicz L. Reactivation by various oximes of human erythrocyte acetylcholinesterase inhibited by different organophosphorus compounds. *Arch Toxicol* 1996;70: 497–503.
- [2] Worek F, Diepold C, Eyer P. Dimethylphosphoryl-inhibited human cholinesterases: inhibition, reactivation, and aging kinetics. *Arch Toxicol* 1999;73:7–14.
- [3] Ashani Y, Radic Z, Tsigelny I, Vellom DC, Pickering NA, Quinn DM, Doctor BP, Taylor P. Amino acid residues controlling reactivation of organophosphonyl conjugates of acetylcholinesterase by mono- and bisquaternary oximes. *J Biol Chem* 1995;270:6370–80.
- [4] Grosfeld H, Barak D, Ordentlich A, Velan B, Shafferman A. Interactions of oxime reactivators with diethylphosphoryl adducts of human acetylcholinesterases and its mutant derivatives. *Mol Pharmacol* 1996;50:639–49.
- [5] Wong L, Radic Z, Bruggemann RJM, Hosea N, Berman H, Taylor P. Mechanism of oxime reactivation of acetylcholinesterase analyzed by chirality and mutagenesis. *Biochemistry* 2000;39:5750–7.
- [6] Luo C, Saxena A, Smith M, Garcia G, Radic Z, Taylor P, Doctor BP. Phosphoryl oxime inhibition of acetylcholinesterase during oxime reactivation is prevented by edrophonium. *Biochemistry* 1999;38: 9937–47.
- [7] Luo C, Ashani Y, Doctor BP. Acceleration of oxime-induced reactivation of organophosphate-inhibited fetal bovine serum acetylcholinesterase by monoquaternary and bisquaternary ligands. *Mol Pharmacol* 1998;53:718–26.
- [8] Leader H, Vincze A, Manisterski B, Rothschild N, Dosoretz C, Ashani Y. Characterization of *O,O*-diethylphosphoryl oxime as inhibitors of cholinesterases and substrates of phosphotriesterases. *Biochem Pharmacol* 1999;58:503–15.
- [9] Levy D, Ashani Y. Synthesis and *in vitro* properties of a powerful quaternary methylphosphonate inhibitor of acetylcholinesterase: a new marker in the blood-brain barrier research. *Biochem Pharmacol* 1986;35:1079–85.
- [10] Berman HA, Decker MM. Kinetic, equilibrium, and spectroscopic studies on dealkylation (“aging”) of alkyl organophosphonyl acetylcholinesterase: electrostatic control of enzyme topography. *J Biol Chem* 1986;261:10646–106652.
- [11] Radic Z, Pickering NA, Vellom DC, Camp S, Taylor P. Three distinct domains in the cholinesterase molecule confer selectivity for acetyl- and butyrylcholinesterase inhibitors. *Biochemistry* 1993;32:12074–84.
- [12] Vellom DC, Radić Z, Li Y, Pickering NA, Camp S, Taylor P. Amino acid residues controlling acetylcholinesterase and butyrylcholinesterase specificity. *Biochemistry* 1993;32:12–7.
- [13] Ellman GL, Courtney KD, Andres V, Featherstone RM. A new and rapid colorimetric determination of acetylcholinesterase activity. *Biochem Pharmacol* 1961;7:88–95.
- [14] Puu G, Artursson E, Bucht G. Reactivation of nerve agent inhibited human acetylcholinesterases by HI-6 and obidoxime. *Biochem Pharmacol* 1986;35:1505–10.
- [15] Ashani Y, Leader H, Rothschild N, Dosoretz C. Combined effect of organophosphorus hydrolase and oxime on the reactivation rate of diethylphosphoryl-acetylcholinesterase conjugates. *Biochem Pharmacol* 1998;55:159–68.

Aromatic amino-acid residues at the active and peripheral anionic sites control the binding of E2020 (Aricept®) to cholinesterases

Ashima Saxena¹, James M. Fedorko¹, C. R. Vinayaka¹, Rohit Medhekar², Zoran Radić³, Palmer Taylor³, Oksana Lockridge⁴ and Bhupendra P. Doctor¹

¹Division of Biochemistry, Walter Reed Army Institute of Research, Silver Spring, MD, USA; ²Department of Chemistry, University of California Davis, CA, USA; ³University of California San Diego, La Jolla, CA, USA; ⁴Eppley Cancer Institute, University of Nebraska Medical Center, Omaha, NE, USA

E2020 (*R,S*)-1-benzyl-4-[(5,6-dimethoxy-1-indanon)-2-yl]-methylpiperidine hydrochloride is a piperidine-based acetylcholinesterase (AChE) inhibitor that was approved for the treatment of Alzheimer's disease in the United States. Structure-activity studies of this class of inhibitors have indicated that both the benzoyl containing functionality and the *N*-benzylpiperidine moiety are the key features for binding and inhibition of AChE. In the present study, the interaction of E2020 with cholinesterases (ChEs) with known sequence differences, was examined in more detail by measuring the inhibition constants with *Torpedo* AChE, fetal bovine serum AChE, human butyrylcholinesterase (BChE), and equine BChE. The basis for particular residues conferring selectivity was then confirmed by using site-specific mutants of the implicated residue in two template enzymes. Differences in the reactivity of E2020 toward AChE and BChE (200- to 400-fold) show that residues at

the peripheral anionic site such as Asp74(72), Tyr72(70), Tyr124(121), and Trp286(279) in mammalian AChE may be important in the binding of E2020 to AChE. Site-directed mutagenesis studies using mouse AChE showed that these residues contribute to the stabilization energy for the AChE–E2020 complex. However, replacement of Ala277(Trp279) with Trp in human BChE does not affect the binding of E2020 to BChE. Molecular modeling studies suggest that E2020 interacts with the active-site and the peripheral anionic site in AChE, but in the case of BChE, as the gorge is larger, E2020 cannot simultaneously interact at both sites. The observation that the K_i value for mutant AChE in which Ala replaced Trp286 is similar to that for wild-type BChE, further confirms our hypothesis.

Keywords: acetylcholinesterase; butyrylcholinesterase; E2020; site-directed mutagenesis; molecular modeling.

Alzheimer's disease (AD) affects approximately 5–15% of the population of the US over age 65. According to the cholinergic hypothesis, memory impairments in patients with this senile dementia disease are due to a selective and irreversible deficiency in the cholinergic functions in the brain [1]. There is a selective loss of neurons containing choline acetyltransferase, the enzyme responsible for the synthesis of acetylcholine (ACh), resulting in decreased

levels of ACh in the cortical tissue [2,3]. In a recent study, Winkler *et al.* demonstrated that the presence of cerebral ACh is necessary for cognitive behavior and it can improve learning deficits and memory loss in rats that have incurred severe damage to the nucleus basalis of Meynert [4]. One approach to improving memory and cognition in patients with AD has been to increase ACh levels through the use of cholinesterase (ChE) inhibitors [5]. These agents enhance cholinergic neurotransmission by inhibiting acetylcholinesterase [AChE (EC 3.1.1.7)], the enzyme responsible for the breakdown of ACh. In fact, clinical studies with reversible ChE inhibitors such as tacrine, the first available agent for the treatment of AD in the US and physostigmine, a carbamate-type inhibitor, suggest that these agents may be able to enhance memory in patients with AD [6,7], but their clinical value is limited due to their acute hepatotoxicity, adverse peripheral side-effects, and short duration of action [5].

In November 1996, E2020 [(*R,S*)-1-benzyl-4-[(5,6-dimethoxy-1-indanon)-2-yl]methyl]piperidine hydrochloride], a novel AChE inhibitor which is also known as donepezil and is marketed as Aricept® by Eisai Inc., (Teaneck, NJ, USA) was approved by the US Food and Drug Administration for the treatment of mild-to-moderate AD in the US [8]. E2020 belongs to the new class of synthetic AChE inhibitors, which contain an

Correspondence to A. Saxena, Division of Biochemistry, Walter Reed Army Institute of Research, 503 Robert Grant Avenue, Silver Spring, MD 20910–7500, USA.

Fax: +1 301 319 9150, Tel.: +1 301 319 9406,

E-mail: ashima.saxena@na.amedd.army.mil

Abbreviations: AD, Alzheimer's disease; ChE, cholinesterase; AChE, acetylcholinesterase; BChE, butyrylcholinesterase; Mo, mouse; Hu, human; ACh, acetylcholine; ATC, acetylthiocholine iodide; BTC, butyrylthiocholine iodide; DTNB, 5,5'-dithiobis(2-nitrobenzoic acid); E2020, (*R,S*)-1-benzyl-4-[(5,6-dimethoxy-1-indanon)-2-yl]methylpiperidine hydrochloride.

Note: the dual numbering system gives the residue number in the species designated followed by the corresponding residue in *Torpedo* AChE [23].

(Received 19 May 2003, revised 26 August 2003, accepted 17 September 2003)

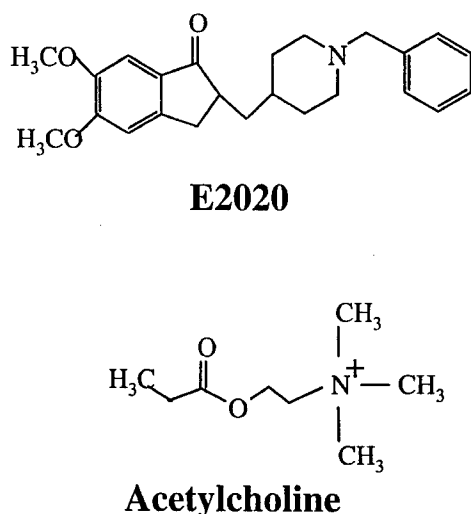


Fig. 1. Structures of E2020 and acetylcholine.

N-benzylpiperidine and an indanone moiety and is structurally distinct from other compounds in use or under study for the treatment of AD. These unique structural features make E2020 a potent and selective inhibitor of AChE [9]. Due to the structural similarity between E2020 and acetylcholine (Fig. 1), it was expected to be a competitive inhibitor of AChE [10]. However, inhibition studies of electric eel AChE with E2020 showed that it is a mixed competitive inhibitor of AChE with a K_i value of 4.27 nM [11]. The presence of an asymmetric carbon atom at the 2-position of the indanone ring yields two enantiomers of E2020 of which the (*R*)-form inhibited AChE sixfold more potently than the (*S*)-form [12]. As both enantiomers of E2020 display similar pharmacokinetic profiles in dogs, racemic E2020 was developed as a potential therapeutic for the palliative treatment of AD [13]. E2020 is 360- to 1200-fold less effective as an inhibitor of butyrylcholinesterase [BChE (EC 3.1.1.8)] compared to AChE, depending on the source of enzyme [14,15]. On the other hand, inhibitors such as tacrine and physostigmine, show poor selectivity between AChE and BChE. Clinical studies have indicated that inhibition of plasma BChE may result in potentiating peripheral side-effects [16]. Indeed, in clinical trials, 5 and 10 mg of donepezil hydrochloride administered once daily was effective for the treatment of mild-to-moderate AD without causing peripheral adverse effects, laboratory test abnormalities, or hepatotoxicity [17,18].

Due to the lack of an X-ray crystal structure of AChE during the design and development of E2020, extensive quantitative structure-activity relationship (QSAR) and molecular modeling studies were performed on a series of indanone-benzylpiperidines synthesized by Eisai. These studies elucidated the effect of substitutions on the benzyl and indanone rings of this class of inhibitors on their inhibition potency [19]. A distinct active molecular shape for E2020 and its analogs was postulated based on the X-ray crystal structure, conformational analysis, and molecular shape comparisons of these molecules [20]. These studies suggested that the similar inhibition potency of the two enantiomers of E2020 is due to the high degree

of shape similarity between the two isomers. When the X-ray crystal structure of *Torpedo californica* AChE became available, the binding sites of E2020 in AChE were predicted by docking studies [12,21]. The results of these studies suggest that both enantiomers of E2020 span the entire AChE gorge with the possibility of multiple binding sites for each form. However, in all these models, the benzyl group interacts with Trp84 at the bottom of the gorge, the piperidine ring interacts with Tyr70, Asp72, Tyr121 and Tyr334 in the middle of the gorge, and the indanone ring interacts with Trp279 at the lip of the gorge. The calculated modes of binding of E2020 to acylated AChE are similar to those observed for free enzyme which is consistent with the observation that E2020 and its analogs can inhibit acylation as well as deacylation steps in the enzymatic reaction [12]. The orientation of E2020 in the active-site gorge of AChE proposed by molecular modeling studies was also observed in the three-dimensional structure of the *Torpedo* AChE-(*R*)-E2020 complex reported later [22]. The authors concluded that the aromatic residues at positions 330 and 279 were responsible for the binding and selectivity of E2020 to AChE.

In the present study, the interaction of E2020 with mammalian AChE was examined in more detail with three distinct ChEs with known sequence differences. The basis for particular residues conferring selectivity was then confirmed by using site-specific mutants of the implicated residue in two template enzymes. Differences in the reactivity of E2020 toward AChE and BChE and a comparison of K_i values of E2020 for mouse (Mo) AChE mutants of Trp86(84), Asp74(72), and Trp286(279) [23] revealed that these residues contribute the most to the stabilization energy for the AChE-E2020 complex. However, when the effect of these mutations on the binding of E2020 were examined using the human (Hu) BChE template, replacement of Ala277(*Trp*279) with Trp did not affect the binding of E2020 to BChE, suggesting that the orientation of E2020 in the BChE gorge may be different from that in the AChE gorge. These findings were confirmed by molecular modeling studies, which enabled us to propose an orientation for E2020 in the active-site gorge of AChE and BChE.

Materials and methods

Materials

Acetylthiocholine iodide (ATC), butyrylthiocholine iodide (BTC), and 5,5'-dithiobis(2-nitrobenzoic acid) (DTNB) were obtained from Sigma Chemical Co. Racemic E2020 obtained from Eisai Co., Tsukuba-shi, Ibaraki, Japan, was a gift from A. P. Kozikowski (Georgetown University, Washington, DC, USA). Electrophoretically pure AChE from FBS was purified as described [24], and BChE from horse serum was purified by affinity chromatography using the procedure similar to the one described for FBS AChE. AChE from *Torpedo californica* was a gift from I. Silman (Weizmann Institute, Rehovot, Israel). One milligram of pure native AChE or BChE contained approximately 14 and 11 nmol of active sites, respectively.

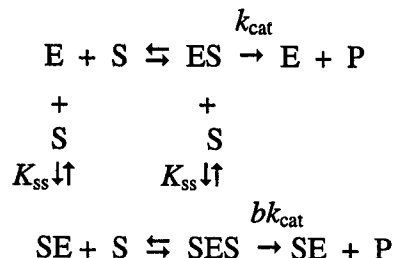
Recombinant wild-type and mutants of Mo AChE were expressed, purified and characterized with respect to catalytic parameters as described [25]. Recombinant wild-type and mutants of Hu BChE were expressed in CHO K1 cells in serum free medium and partially purified on procaine-amide-Sepharose affinity gel as described [26].

Measurement of cholinesterase activity and inhibition

AChE and BChE activities were measured in 50 mM sodium phosphate, pH 8.0, at 25 °C as described [27] using ATC and BTC as substrates, respectively. Inhibition of enzyme activity was measured in 50 mM sodium phosphate, pH 8.0, over a substrate concentration range of 0.01–30 mM and at least six inhibitor concentrations to determine the components of competitive and noncompetitive inhibition. For each enzyme, the measurements were repeated at least three times to obtain the values of the inhibition constants.

Analysis of catalytic parameters

The catalytic parameters of wild-type and mutant AChE and BChE were compared by measuring catalysis as a function of ATC or BTC concentration. The interaction of substrate (S) with enzyme (E) can be described more appropriately by the following general scheme, where the substrate binds to two discrete sites on the enzyme molecule forming two binary complexes, ES and SE [28]:



Scheme I

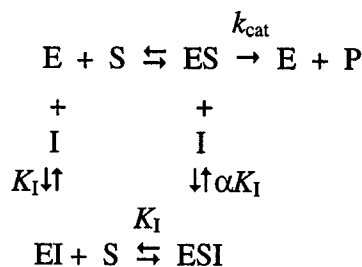
In this scheme, K_{ss} represents the binding of a second substrate molecule to the binary enzyme-substrate complexes and b reflects the efficiency of hydrolysis of the ternary complex, SES, as compared to the binary complex, ES. Scheme I is described by the following equation:

$$v = \left(\frac{1 + b[S]/K_{\text{ss}}}{1 + [S]/K_{\text{ss}}} \right) \left(\frac{V_{\text{max}}}{1 + K_{\text{m}}/[S]} \right) \quad (1)$$

where, K_{m} is the Michaelis-Menten constant, v is the initial velocity, and V_{max} is the maximal velocity. The values for K_{m} , V_{max} , K_{ss} and b were determined by nonlinear least square analysis of the data.

Analysis of inhibition data

The interaction of an inhibitor (I) with an enzyme (E) can be described by the following scheme:



Scheme II

where ES is the enzyme-substrate complex and P is the product. K_{I} and αK_{I} are the inhibition constants reflecting the interaction of inhibitor with the free enzyme and the enzyme-substrate complex, respectively. Plots of initial velocities vs. substrate concentrations at a series of inhibitor concentrations were analyzed by nonlinear least squares methods to determine the values of K_{m} and V_{max} as described above (Fig. 2). The dependence of $V_{\text{max}}/K_{\text{m}}$ and V_{max} on $[I]$ is given by:

$$V_{\text{max}}/K_{\text{m}} = \left(\frac{(V_{\text{max}}/K_{\text{m}})K_{\text{I}}}{K_{\text{I}} + [I]} \right) \quad (2)$$

Non-linear regression analysis of the plots of $V_{\text{max}}/K_{\text{m}}$ and V_{max} values vs. E2020 concentrations were used for the determination of K_{I} and αK_{I} values, respectively [29].

Molecular modeling

Molecular modeling was carried out on a Silicon Graphics Octane workstation using the molecular simulation software INSIGHT II. The coordinates of Mo AChE–(R)-E2020 complex were generated using the crystal structure coordinates from the Protein Data Bank. The X-ray crystal structure of *Torpedo californica* AChE–E2020 complex (PDB code 1eve [22]); was superimposed on the X-ray crystal structure of Mo AChE (PDB code 1mah [30]). The root-mean-square deviation (rmsd) between the C_{α} atoms of the two structures is 0.87 Å. The coordinates of the ligand, E2020, were transferred to Mo AChE to form the initial model of the Mo AChE–E2020 complex. Visual inspection of this model showed that Tyr337 was making unfavorable van der Waals contacts with E2020. The side chain torsion angles of Tyr337 were rotated to relieve the unfavorable contacts. Energy minimization was performed on this complex using the DISCOVER cff91 force field (Accelrys, Inc., San Diego, CA, USA) with a distance dependent dielectric constant for the electrostatic interactions. Molecular dynamics simulation (at 300 K) was performed on the minimum energy complex for 20 ps and the resulting complex was energy minimized to obtain the final Mo AChE–E2020 complex. In all our calculations, the coordinates of the residues of the protein lying outside a sphere of 25 Å diameter centered around E2020 were kept fixed.

The coordinates of the Hu BChE–E2020 complex were generated using the reported homology model (PDB code 1eho [31]), and the crystal structure of *Torpedo californica* AChE–E2020 complex (PDB code 1eve [22]). The rms deviation between the C_{α} atoms of the homology model of

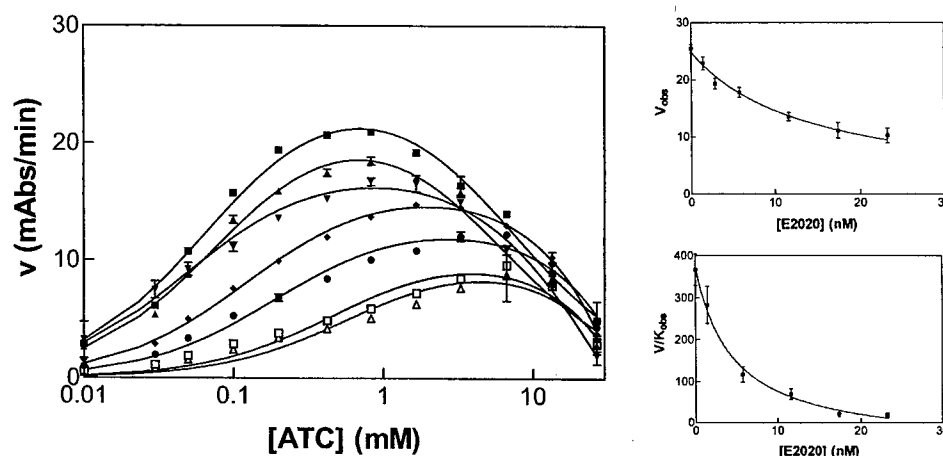


Fig. 2. Representative analysis of the inhibition of recombinant mouse acetylcholinesterase by E2020. The inhibition of wild-type Mo AChE is shown. Plots of initial velocities vs. substrate concentrations at a series of E2020 concentrations were analyzed by nonlinear least squares methods to determine the values of K_m and V_{max} as described in Materials and methods. To the right are plots showing V_{max}/K_m and V_{max} values as a function of E2020 concentration. Non-linear regression analyses of the plots were used for the determination of K_I and αK_I values, respectively [29]. (■), Enzyme control; (▲), 0.29 nM E2020; (▼), 0.58 nM E2020; (◆), 1 nM E2020; (●), 2.32 nM E2020; (□), 5.28 nM E2020; (△), 28 nM E2020.

Hu BChE and the X-ray crystal structure of AChE–E2020 is 0.96 Å. After visual inspection of the complex, the side chain torsion angles of Tyr332 were rotated to relieve the unfavorable van der Waals contacts with E2020. Energy minimization and molecular dynamics simulation (at 300 K) for 20 ps followed by a final energy minimization were performed as described for the Mo AChE–E2020 complex.

The models for the single mutant Y337A and the triple mutant Y72(70)N/Y124(121)Q/W286(279)R of Mo AChE–E2020 were generated using the final energy minimized structure of Mo AChE–E2020 complex. The conformations of the side chains of the mutated residues were generated using the Biopolymer module in INSIGHT II. The mutant complexes were subjected to energy minimization, molecular dynamics simulation for 20 ps, and energy minimization as before. The lowest energy structures were examined to elucidate the effect of mutations in the active-site residues on the binding of E2020 to AChE. The model for the triple mutant N68(Y70)Y/Q119(Y121)Y/A277(W279)W of Hu BChE–E2020 complex was generated as described above. The coordinates for the various molecular models of Mo AChE–E2020 and Hu BChE–E2020 complexes can be requested from the Correspondence.

Results

Inhibition of cholinesterases by E2020

Inhibition studies with FBS AChE, Mo AChE, and *Torpedo* AChE showed that E2020 is a potent inhibitor of AChE with K_I values of ≈ 3 nM (Table 1). These values are consistent with a K_I value of 4.27 nM reported for electric eel AChE [11], and IC_{50} values of 5.7 nM and 8 nM for AChEs from rat brain [15] and human erythrocytes [14], respectively. The K_I values reported in Table 1 also show that E2020 is a 200- to 400-fold less potent inhibitor of equine and Hu BChE with K_I values of 0.64 μ M and 1.11 μ M, respectively. Previous studies reported IC_{50} values of

Table 1. Dissociation constants for the inhibition of cholinesterases by E2020.

Enzyme	K_I^a (μ M)	αK_I (μ M)	$\Delta\Delta G^b$
Mo AChE	0.0022 ± 0.0007	0.023 ± 0.008	0
FBS AChE	0.0029 ± 0.0002	0.017 ± 0.003	0
<i>Torpedo</i> AChE	0.0031 ± 0.001	0.004 ± 0.001	0
Hu BChE	1.11 ± 0.29	3.33 ± 0.66	3.5
Equine BChE	0.64 ± 0.28	1.97 ± 0.51	3.2

^a K_I values determined from nonlinear regression analysis of V vs. $[S]$ plots at various E2020 concentrations [29]. The values are average of at least three determinations. ^b Calculated according to the formula $\Delta\Delta G_{BChE-AChE} = RT \ln K'_I/K_I$, where K'_I and K_I are the dissociation constants for BChE and AChE, respectively [28].

0.29 μ M and 7.1 μ M for BChEs from equine [14] and rat plasma [15], respectively. Differences in the reactivity of E2020 toward AChE and BChE suggest that the aromatic residues lining the AChE gorge are responsible for the binding and selectivity of E2020 to AChE.

Inhibition of mouse acetylcholinesterase mutants by E2020

Six of 14 bulky aromatic residues at positions 72(70), 124(121), 286(279), 295(288), 297(290) and 337(330) in AChE are replaced by nonaromatic residues in BChE [32]. To delineate the relative contributions of these residues to the binding of E2020, we analyzed single and triple mutants of Mo AChE for their activity toward E2020, and estimated the binding forces by partitioning the free energy of binding (Table 2). As shown in Table 2 and consistent with previous studies with electric eel AChE [11], E2020 is a mixed-type of inhibitor of wild-type Mo AChE, with a K_I value of 2.2 nM. The inhibitory activity of E2020 toward Mo AChE was affected predominantly by replacement of the anionic subsite residue Trp86, and the peripheral anionic site residues, Asp74 and Trp286. Trp86 (Trp82 in BChE) and

Table 2. Dissociation constants and free energy differences for the inhibition of mutant mouse acetylcholinesterases by E2020.

Enzyme	K_i^a (μM)	αK_i (μM)	$\Delta\Delta G^b$
Wild-type	0.0022 ± 0.0007	0.023 ± 0.008	0
Hydrophobic pocket			
W86A	0.69 ± 0.11	1.4 ± 0.5	3.4
Y337F	0.0005 ± 0.00003	0.0004 ± 0.0001	−0.9
Y337A	0.0004 ± 0.00005	0.003 ± 0.0002	−1.0
Acyl pocket			
F295L	0.027 ± 0.005	0.04 ± 0.009	1.5
F297I	0.07 ± 0.02	—	2.1
Peripheral anionic site			
Y72N	0.02 ± 0.002	0.05 ± 0.008	1.3
D74N	5.1 ± 0.7	15.7 ± 7.5	4.6
Y124Q	0.02 ± 0.004	0.05 ± 0.007	1.3
W286A	3.2 ± 0.5	4.8 ± 0.3	4.4
Y72N/Y124N/ W286R	8.7 ± 0.3	15.0 ± 1.4	4.8

^a K_i values determined by nonlinear regression analysis of V vs. [S] plots at various E2020 concentrations [29]. The values are average of at least three determinations. ^b Calculated according to the formula $\Delta\Delta G = RT \ln K'_1/K_1$, where K'_1 and K_1 are the dissociation constants for mutant and wild-type Mo AChE, respectively [28].

Asp74 (Asp70 in BChE) are present in both AChE and BChE and Trp286 is replaced by Ala277 in BChE.

The two aromatic residues that are part of the choline binding pocket of mammalian AChE are Trp86(84) and Tyr337(*Phe330*). Substitution of Trp86 by Ala resulted in a 300-fold increase in K_i value compared to wild-type AChE corresponding to a loss of 3.4 kcal of stabilization energy (Table 1). This finding is consistent with a π – π interaction between the phenyl ring of E2020 and Trp86 of AChE observed in the X-ray crystal structure of the *Torpedo* AChE–E2020 complex [22]. However, the effect of Tyr337 mutation on the binding of E2020 to Mo AChE was different from that predicted by these studies. The mutation of Tyr337 to Phe or Ala in Mo AChE resulted in a gain of binding energy suggesting that the bulky Tyr residue was sterically hindering the binding of E2020 to AChE.

The two Phe residues at positions 295(288) and 297(290), which define the dimensions of the acyl pocket of mammalian AChE also appear to interact with E2020. Although replacement of Phe at either position by a nonaromatic residue reduced the binding of E2020 to mutant enzymes, a larger effect was observed for the F297I mutant AChE (Table 2). These data suggest that the two aromatic residues might act as primers in positioning the substituted aromatic ring of E2020. Also, E2020 is a competitive inhibitor of F297I Mo AChE, suggesting that the mutation of F297I completely destroys the interaction of E2020 at the peripheral anionic site of mutant AChE.

A comparison of K_i values of E2020 for mutants of Asp74, Tyr72, Tyr124, and Trp286, located in the peripheral anionic site of AChE show that these residues contribute to the stabilization energy for the AChE–E2020 complex. The elimination of charge in D74N and replacement of the aromatic amino-acid residue by a nonaromatic residue in W286A caused 2300-fold and 1400-fold increases in K_i

values of E2020 for mutant AChEs, respectively. As the individual contributions of Tyr72, Tyr124, and Trp286 to the binding energy do not add up, these residues probably cooperate with each other in the stabilization of the E2020–AChE complex, i.e. they are not independent. The mutation of Tyr72 to Asn or Tyr124 to Gln eliminates 1.3 kcal of stabilization energy while the mutation of Trp286 to Ala removes 4.4 kcal. These results are consistent with the observed interaction of the indanone ring of E2020 with the residues at the peripheral anionic site in the X-ray crystal structure of the *Torpedo* AChE–E2020 complex [22]. Mutation of all three residues yields an enzyme with a greater difference in E2020 affinity than that observed between AChE and BChE. These results suggest that the orientation of E2020 in the BChE gorge may be different from that in the AChE gorge and different residues may be contributing to the stabilization energy of the BChE–E2020 complex.

Inhibition of Human butyrylcholinesterase mutants by E2020

To ascertain the role of aromatic residues in the peripheral anionic site of BChE in the binding of E2020, we conducted site-directed mutagenesis studies with Hu BChE mutants in which the nonaromatic residues were replaced with aromatic residues at these positions. Consistent with observations made with equine and Hu BChE, E2020 showed mixed-type of inhibition with recombinant wild-type Hu BChE with a K_i value of $\approx 2 \mu\text{M}$ (Table 3). Unlike the choline binding pocket of AChE which is defined by aromatic residues at positions 84 and 330, the choline binding pocket of mammalian BChE has Trp82(84) and Ala328(*Phe330*). As in AChE, substitution of Trp82 by Ala also resulted in a 50-fold increase in K_i value of E2020 compared to wild-type BChE. Although this effect is less dramatic than the 300-fold increase observed in Mo AChE, it is consistent with a π – π interaction between the phenyl ring of E2020

Table 3. Dissociation constants for the inhibition of mutant human butyrylcholinesterases by E2020.

Enzyme	K_i (μM)	αK_i (μM)
Wild-type	2.3 ± 1.0	2.0 ± 0.6
Hydrophobic pocket		
W82A	$> 120^b$	— ^b
A328F	22.8 ± 7.8	25.9 ± 12.3
A328Y	3.9 ± 0.9	45.3 ± 10.3
Acyl pocket		
V288F	3.5 ± 0.7	6.6 ± 0.3
Peripheral anionic site		
D70G	$> 30^c$	— ^c
Q119Y	12.9 ± 0.5	—
A277W	2.4 ± 0.5	0.7 ± 0.3
Q119Y/V288F/A328Y	0.8 ± 0.3	—
N68Y/Q119Y/A277W	—	1.2 ± 0.4

^a K_i values determined by nonlinear regression analysis of V vs. [S] plots at various E2020 concentrations [29]. The values are average of at least three determinations. ^b No inhibition at up to $120 \mu\text{M}$. ^c No inhibition at up to $30 \mu\text{M}$.

and Trp82 of BChE proposed for AChE. The mutation of Ala328 to an aromatic residue has either a minor decrease or no effect on the binding of E2020 to mutant BChE. This result is different from that obtained with Mo AChE mutants, which showed that the bulky Tyr337 residue sterically hindered the binding of E2020 to AChE, and suggests that the orientation of E2020 in the AChE gorge is different from that in the BChE gorge. The replacement of Val288(*Phe290*) in the acyl pocket of Hu BChE by Phe had no effect on the binding of E2020 to mutant enzyme.

The residues, Asp70(72), Asn68(*Tyr70*), Gln119(*Tyr121*), and Ala277(*Trp279*) in BChE, correspond to the residues in the peripheral anionic site of AChE. As the residues at positions 68, 119 and 277 are nonaromatic, Asp70 is the main component of the peripheral anionic site of BChE [33]. These residues have been implicated in the binding of E2020 to AChE. If the decreased binding of E2020 to BChE is due to the absence of aromatic residues at positions 68, 119, and 277, then replacement of these residues by aromatic residues should improve the binding of E2020 to mutant BChEs. The elimination of charge in D70G caused a greater than 15-fold increase in the K_i value of E2020 for mutant BChE, suggesting that, as in AChE, this residue is involved in the binding of E2020 to BChE. Replacement of nonaromatic residues at positions 119 or 277 by Tyr and Trp, respectively, did not improve the binding of E2020 to BChE. The Hu BChE analog of wild-type Mo AChE is the triple mutant N68Y/Q119Y/A277W and E2020 is an uncompetitive inhibitor of this mutant BChE, with an αK_i value of 1.2 μM (Table 3). These results are consistent with the observed interaction of the indanone ring of E2020 with the residues at the peripheral anionic site of AChE. However it appears that for this interaction at the peripheral site to occur in BChE, the interaction of the phenyl ring of E2020 at the active-site has to be compromised. These results suggest that the larger dimension of the BChE gorge and the lack of aromatic residues in the peripheral anionic site of BChE may be contributing to the poor binding of E2020 to BChE. To further support the results of kinetic studies, molecular modeling experiments were performed on the AChE/BChE-E2020 complexes.

Energy-minimized structures of E2020 bound to cholinesterases

The X-ray crystal structures of Mo AChE [30] and *Torpedo californica* AChE-E2020 complex [22] and the homology

based model for Hu BChE [31] were used to generate models of ChE-E2020 complexes to interpret our kinetic data. As shown in Table 4, the rmsd for the C_α atoms of various ChEs in the native state and as E2020 complexes range from 0.25 to 0.96, suggesting that the enzyme backbone does not undergo significant conformational changes upon complex formation. Figure 3A shows the interaction of E2020 with various amino-acid residues at the active and the peripheral anionic sites of Mo AChE. Consistent with site-directed mutagenesis data, the following energetically favorable interactions of E2020 with the enzyme molecule were identified: (a) a strong π - π interaction between the phenyl group of E2020 and Trp86 of AChE, which are parallel to each other; (b) an electrostatic interaction between the positively charged ammonium group of E2020 and the γ -oxygen of Asp74 which are separated by a distance of 5.4 Å; (c) a π - π interaction between the indanone ring of E2020 and Trp286 in the peripheral anionic site of AChE; (d) Tyr72 and Tyr124 may be hydrogen bonding with the methoxy oxygen of E2020 or they might be responsible for sterically positioning the substituted phenyl ring of E2020 for optimum π - π interaction with Trp286 and (e) Phe295 and Phe297 are in close proximity of the substituted aromatic ring of E2020 and might act as primers in positioning the ring for maximum interaction with Trp86.

Site-directed mutagenesis studies with Y337F and Y337A Mo AChE indicate that this Tyr destabilizes the binding of E2020 to AChE. A close examination of the Mo AChE-E2020 structure shown in Fig. 3A indicates that Tyr337, Tyr341 and Asp74 are involved in a network of hydrogen bonds, which undermines the electrostatic interaction between Asp74 and the ammonium group of E2020. Consequently, the mutation of Tyr337 to Phe or Ala (Fig. 3B), obviates the hydrogen bond between Asp74 and Tyr341, strengthening the ionic interaction between Asp74 of AChE and the ammonium group of E2020. Investigation of the Y337A Mo AChE-E2020 complex also reveals that the 10% increase in size of the active-site gorge caused by this mutation [34] allows a more favorable π - π interaction in which the indanone ring of E2020 is sandwiched between Trp286 and Tyr341 of AChE.

To further confirm the role played by the peripheral anionic site in stabilizing the E2020-AChE complex, the three peripheral anionic site residues in the enzyme were mutated to yield a triple mutant of Mo AChE Y72N/Y124Q/W286R, which is homologous to wild-type Mo

Table 4. Root mean square deviations (in Å) in the C_α positions of various cholinesterase structures.

	Torpedo AChE-E2020 ^a	Mo AChE-fasciculin ^a	Fig. 3A ^b	Fig. 3B ^b	Fig. 3C ^b	Hu BChE ^c	Fig. 4A ^b
Mo AChE-fasciculin	0.87						
Fig. 3A	0.89	0.42					
Fig. 3B	0.91	0.44	0.45				
Fig. 3C	0.91	0.45	0.26	0.38			
Hu BChE	0.96	0.89	0.64	0.71	0.61		
Fig. 4A	0.93	0.81	0.57	0.59	0.54	0.51	
Fig. 4B	0.95	0.82	0.69	0.72	0.44	0.53	0.25

^a The crystal structures were obtained from Protein Data Bank [22,30]. ^b Mo AChE-E2020 and Hu BChE-E2020 models described in this study. ^c Homology based model [31].

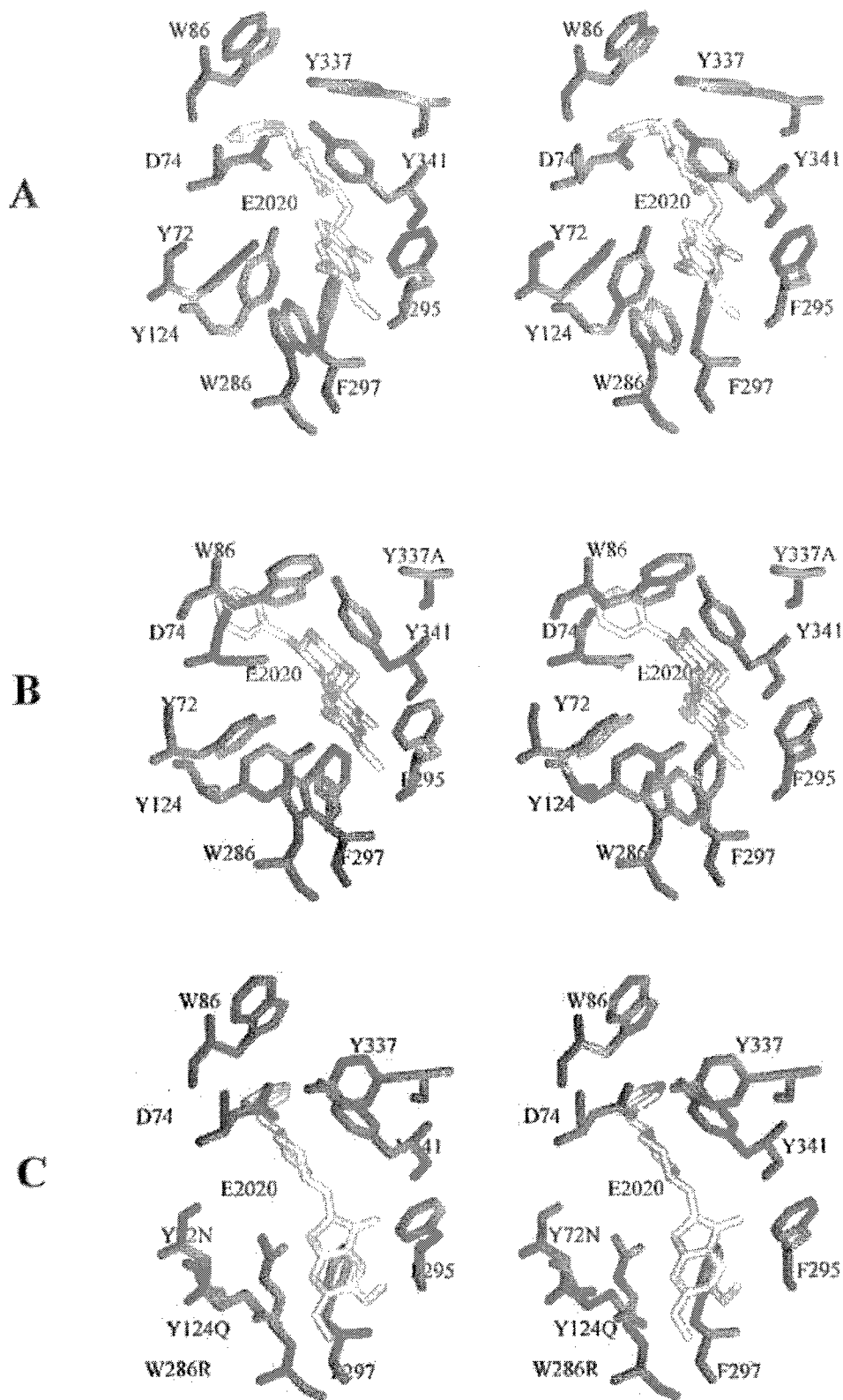


Fig. 3. Stereoview of E2020 modeled into the active-site gorge of Mouse AChE. Amino-acid residues within 5 Å of the E2020 molecule in the active-site gorge of (A) wild-type Mo AChE; (B) Y337A Mo AChE; and (C) Y72N/Y124Q/W286R Mo AChE are shown.

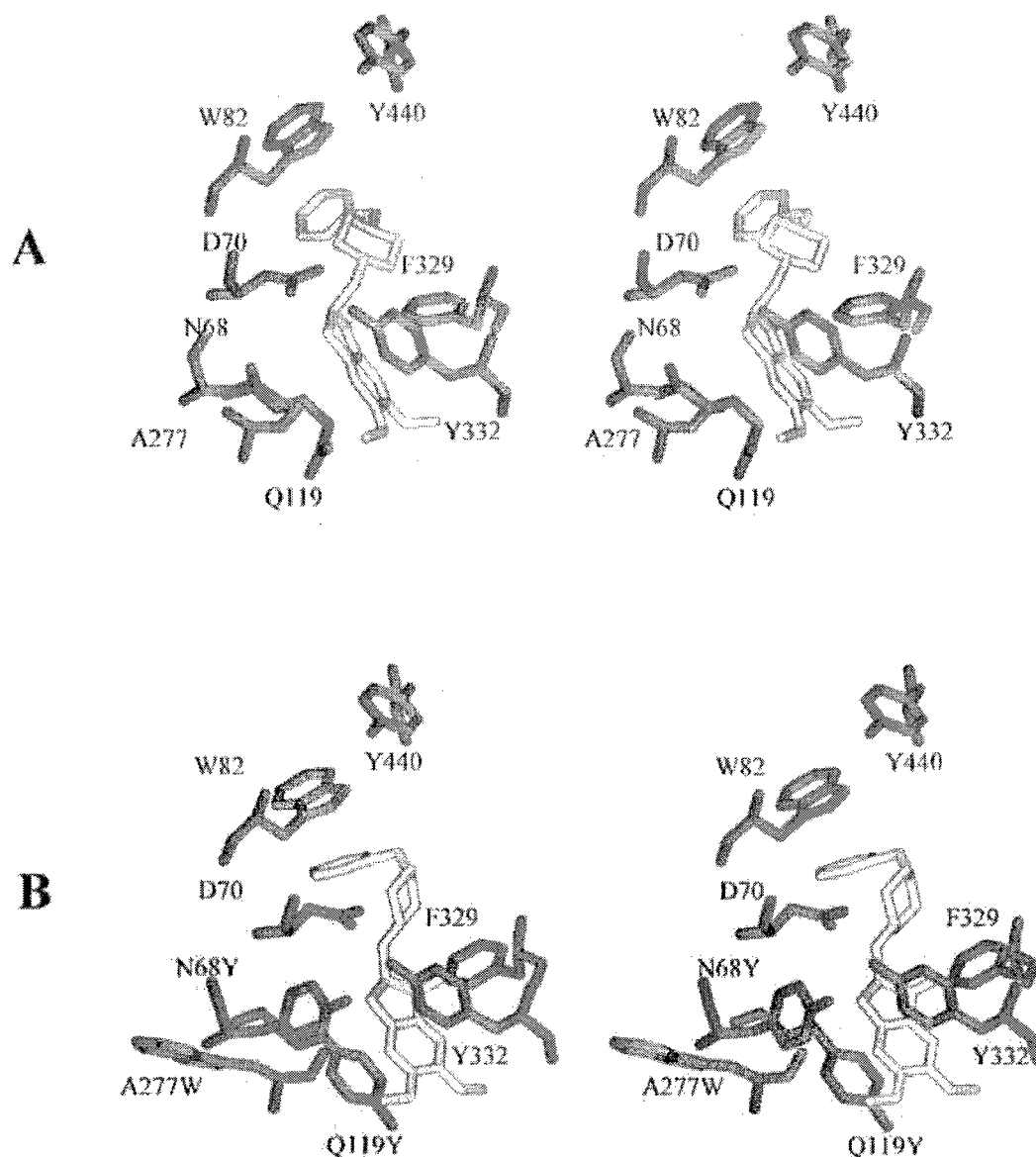


Fig. 4. Stereoview of E2020 modeled into the active-site gorge of Human BChE. Amino-acid residues within 5 Å of the E2020 molecule in the active-site gorge of (A) wild-type Hu BChE and (B) N68Y/Q119Y/A277W Hu BChE are shown. The complex of E2020 with Hu BChE (A) shows the following major interactions which are supported by site-directed mutagenesis studies: (a) the π - π interaction of the phenyl ring of E2020 with W82 of BChE; (b) a strong electrostatic interaction between the charged ammonium nitrogen of E2020 and the γ -oxygen of D70(72) of BChE. These two interactions were also observed in the Mo AChE-E2020 complex. The structure of triple mutant Hu BChE-E2020 complex (Panel B) shows that because the BChE gorge is significantly larger than the AChE gorge, E2020 cannot simultaneously interact with W82 in the active-site and W277 in the peripheral anionic site of mutant BChE.

BChE. The resulting complex was minimized and molecular dynamic calculations were performed to optimize the interactions in the complex. As shown in Fig. 3C, this complex has no obvious interactions with the indanone ring of E2020.

Figure 4A shows the complex of E2020 with Hu BChE. The following major interactions supported by site-directed mutagenesis studies were noted in this structure: (a) the π - π interaction of the phenyl ring of E2020 with Trp82 of BChE; (b) a strong electrostatic interaction between the charged ammonium nitrogen of E2020 and the γ -oxygen of Asp70 of

BChE which are separated by a distance of 5.6 Å. These two interactions were also observed in the AChE-E2020 complex. However, there were no interactions of E2020 at the peripheral anionic site of BChE, as the aromatic residues Tyr72(70), Tyr124(121) and Trp286(279) present in AChE are replaced by nonaromatic residues in BChE.

The N68(70)Y/Q119(121)Y/A277(279)W triple mutant was constructed in an effort to build a peripheral anionic site in BChE similar to AChE. Figure 4B shows the structure of the triple mutant Hu BChE-E2020 complex. As the BChE gorge is significantly larger than the AChE gorge, E2020

cannot simultaneously interact with Trp82 in the active-site and Trp277 in the peripheral anionic site of mutant BChE. Thus, in the triple mutant, E2020 can involve in a π - π interaction either with Trp82 in the active site or with Trp277 in the peripheral anionic site.

Discussion

E2020 is a potent and selective inhibitor of AChE whose superior inhibition characteristics, minimal side-effects, and fast pharmacokinetics, may prove useful not only for the treatment of AD and other nervous system related dementias, but also for prophylaxis against organophosphate toxicity. Efforts aimed at understanding the interaction of E2020 with AChE include docking of E2020 into the active-site gorge of *Torpedo* AChE [12] and determination of the X-ray crystal structure of the *Torpedo* AChE–E2020 complex [22]. Previous studies suggest that the rigid solid state structures of enzyme-inhibitor complexes revealed by X-ray crystallography may not always reflect the dynamics of enzyme-inhibitor interactions in solution [34–36]. Therefore, we conducted site-directed mutagenesis and molecular modeling studies simultaneously with Mo AChE and Hu BChE, to get more insight into the binding specificity of E2020 for AChE and its decreased activity toward BChE.

Site-directed mutagenesis and molecular modeling studies with Mo AChE demonstrated that residues at the anionic subsite such as Trp86(84) and Tyr337(*Phe330*), the acyl pocket such as Phe295(288) and Phe297(290), and the peripheral anionic site such as Asp74(72), Tyr72(70), Tyr124(121), and Trp286(279) contribute to the binding of E2020 to AChE. Asp74 and Trp86 are present in both AChE and BChE, and the mutation of Trp86 (Trp82 in BChE) to a nonaromatic residue has a dramatic effect on the binding of E2020 to AChE and BChE. This is due to the elimination of a strong π - π interaction between the phenyl group of E2020 and the indole ring of Trp86. The strong electrostatic interaction between the positively charged piperidine of E2020 and the negatively charged carboxylate of Asp74 is also important for the stability of the AChE–E2020 complex. Most surprising was the effect of mutation of Tyr337 to Phe or Ala in Mo AChE, which results in a gain of binding energy suggesting that the bulky Tyr residue sterically hinders the binding of E2020 to AChE. This is also evident in the molecular model of Y337A Mo AChE–E2020 complex, which shows that there are two reasons for the increase in binding of E2020 to mutant AChE: (a) the mutation of Tyr337 to Ala weakens the hydrogen bond between Tyr341 and Asp74, making the electrostatic interaction between Asp74 and E2020 stronger; (b) the mutation increases the dimensions of the active-site gorge, allowing a more favorable π - π interaction between the indanone ring of E2020 with Tyr341. Previous studies indicated that Tyr337 is the most flexible residue in the active-site gorge of AChE [34]. It appears to stabilize the binding of ligands such as huperzine A, edrophonium, acridines and one end of bisquaternary compounds such as BW284C51 and decamethonium [28,34,35] and destabilizes the binding of phenothiazines such as ethopropazine due to steric hindrance between the diethylamino-2-isopropyl moiety with the aromatic side chain of Y337 [28].

The roles of the two aromatic residues in the acyl pocket, Phe295 and Phe297 in the binding of E2020 are not immediately apparent. These two residues are in close proximity to the substituted aromatic ring of E2020 and might act as primers in positioning the ring for maximum interaction of the indanone ring with Trp286. The F297I Mo AChE–E2020 complex shows that there is enough room for the indanone ring to move, which can weaken its interaction with Trp286 of AChE. The role of Phe297 in promoting the binding of E2020 to the peripheral anionic site can be validated by the observation that the mutation of Phe297 to Ile completely destroys the interaction of E2020 at the peripheral anionic site making it a competitive inhibitor of AChE.

The contributions of the three aromatic residues Tyr72(70), Tyr124(121) and Trp286(279), located at the peripheral anionic site to the stabilization of the E2020–AChE complex, were also confirmed by site-directed mutagenesis studies. These residues are conserved in AChEs and have been shown to contribute to the stabilization of 'peripheral' site inhibitor complexes [28,37]. Mutation of Trp286 to a nonaromatic amino-acid residue as in BChE, results in a dramatic decrease in the affinity of E2020 for the mutant enzyme. This is due to the loss of the π - π interaction between the indanone ring of E2020 and the indole ring of Trp286. Similarly, Y72N and Y124Q mutant Mo AChEs had lower affinities for E2020 compared to wild-type enzyme. Replacement of all three aromatic residues in the peripheral anionic site with nonaromatic residues (as in BChE) resulted in the triple mutant Y72N/Y124Q/W286R AChE, which shows a much reduced affinity for E2020. This result is supported by the molecular model of triple mutant–E2020 complex, which does not show any interactions with the indanone ring of E2020.

The results of site-directed mutagenesis and molecular modeling studies with Mo AChE were further confirmed by conducting similar studies with Hu BChE. The π - π interaction of the phenyl ring of E2020 with Trp82 and a strong electrostatic interaction between the positively charged ammonium nitrogen of E2020 and the γ -oxygen of Asp70 were preserved in the model of Hu BChE–E2020 complex and confirmed by site-specific mutagenesis studies. However, there were no interactions of the indanone ring of E2020 at the peripheral anionic site of BChE. This is because the aromatic residues in the peripheral anionic site of AChE, which stabilize the E2020–AChE complex through π - π interactions, are replaced by nonaromatic residues, Asn68(Tyr70), Gln119(Tyr121), and Ala277(Trp279) in BChE. Replacement of nonaromatic residues at positions 119 or 277 by Tyr and Trp in Hu BChE, respectively, does not improve the binding of E2020. In fact, E2020 is an uncompetitive inhibitor of the triple mutant, N68Y/Q119Y/A277W of Hu BChE. This result is supported by the model of N68Y/Q119Y/A277W Hu BChE–E2020, which shows that E2020 cannot simultaneously interact with Trp82 in the active-site and Trp277 in the peripheral anionic site.

To further examine the role of the dimension and the microenvironment of the gorge in determining the selectivity of E2020 for ChEs, the molecular models of Mo AChE–E2020 and Hu BChE–E2020 complexes were overlaid according to their C $_{\alpha}$ positions (Fig. 5). The deviation in the C $_{\alpha}$ rmsd values for these complexes is 0.89, suggesting a

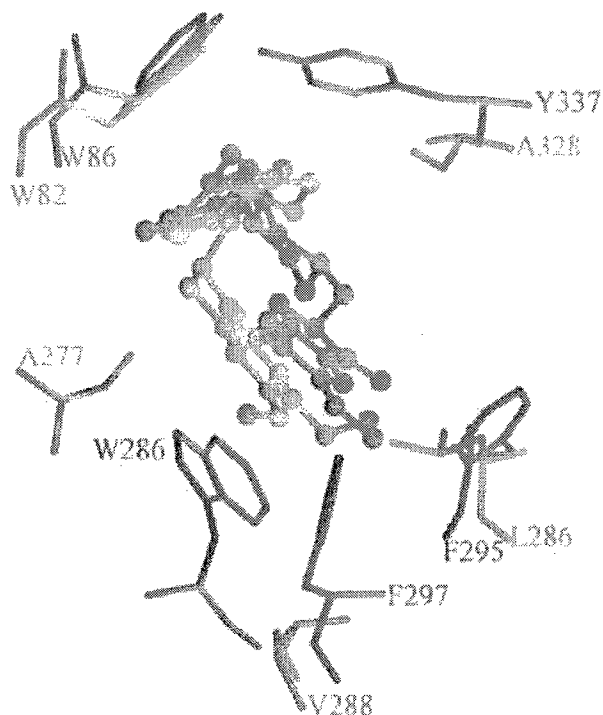


Fig. 5. Overlay of Mo AChE-E2020 and Hu BChE-E2020 complexes. The orientations of E2020 (ball-and-stick representation) in the active-site gorge of Mo AChE (magenta) and Hu BChE (green) are shown.

close resemblance between the two complexes. Inspection of this figure allows the comparison of the orientation of E2020 in the two gorges and also shows that the poor binding of E2020 to Hu BChE is due to the absence of aromatic residues at the peripheral anionic site and the larger dimensions of the gorge. These results are in agreement with a previous study which showed that the volume of the BChE gorge is $\approx 200 \text{ \AA}^3$ larger than that of the AChE gorge which may allow the positioning of inhibitors in alternate configurations [34]. The importance of gorge dimensions in accommodating bulky inhibitors was also seen in the binding of propidium, decamethonium, tacrine and ethopropazine. The phenyl and the indanone rings in E2020 are ideally spaced to allow their simultaneous interaction with the active-site and the peripheral anionic site in the narrow gorge of AChE, respectively. The weaker binding of E2020 to BChE is due to the lack of an aromatic residue at position 277, which corresponds to Trp286 in Mo AChE as well as the larger dimension of the BChE gorge. This conclusion is supported by two observations: (a) the K_i value for wild-type Hu BChE is close to the K_i value for the W286A Mo AChE and (b) the K_i value of E2020 for the peripheral anionic site construct of Hu BChE is similar to that for wild-type Hu BChE. Although this mutant BChE is analogous to AChE, inhibition was uncompetitive suggesting that E2020 was interacting only at the peripheral anionic site of the mutant enzyme. As the active-site gorge of BChE is larger than that of AChE, and the distance between the indanone and the phenyl ring of E2020 is shorter than the distance between the active-site and the peripheral anionic site, E2020 can either bind at the active site or at the

peripheral anionic site. The observed dependence of the inhibitory potency of a series of *N*-benzylpiperidine benzisoxazoles on the length of the spacer that connects the piperidine to the benzisoxazole group [15] further supports our conclusion.

The results presented here are for the most part in agreement with docking studies [12] and the X-ray crystal structure of the *Torpedo* AChE-E2020 complex [22], which show major π - π interactions between the indanone ring of E2020 and Trp279 of AChE at the peripheral anionic-site and between the benzyl ring of E2020 and Trp84 of AChE at the bottom of the gorge. However, two of the conclusions drawn from the crystallographic studies cannot be reconciled with kinetic studies conducted in solution. First, although racemic E2020 was used for soaking *Torpedo* AChE crystals, only (*R*)-E2020 was detected in the X-ray crystal structure of *Torpedo* AChE-E2020 complex. This result is in disagreement with pharmacological studies with the (*R*) and (*S*) enantiomers of E2020 which show that both forms display similar binding affinities toward AChE [12]. The authors explained this result on the basis of AChE-induced *S*-to-*R* tautomerization of E2020, which appears less likely in view of the fact that the half-life of racemization in solution is 77.7 h at 37 °C [13]. A more plausible explanation for this observation is that a high degree of shape similarity suggested by the X-ray crystal structure, conformational analysis, and molecular shape comparisons of the two enantiomers of E2020 [10], may have precluded a distinction between the crystal structures of *Torpedo* AChE-(*R*) E2020 and *Torpedo* AChE-(*S*) E2020 complexes. Second, based on the X-ray crystal structure of the *Torpedo* AChE-(*R*) E2020 complex, the authors concluded that interactions of E2020 with the aromatic residues at positions 330 and 279 were responsible for the binding and selectivity of E2020 for AChE. However, our pharmacokinetic data with Mo AChE Tyr337 mutants and Hu BChE Ala328 mutants show that the residue at position 330 destabilizes the binding of E2020 to AChE. This discrepancy in the results of kinetic studies and the X-ray crystal structure regarding the role of Phe330 in the binding and selectivity of inhibitors to AChE, is not unique to E2020 and was noted for huperzine A and tacrine also [34]. These studies suggest that the rigid solid state structures of enzyme-inhibitor complexes may not always reflect the dynamics of enzyme-inhibitor interactions in solution.

Acknowledgements

We thank Prof. Alan P. Kozikowski (Georgetown University Medical Center, Washington, DC, USA) for the generous gift of E2020. We would also like to thank Dr N. Pattabiraman (Lombardi Cancer Center, Georgetown University, Washington, DC, USA) for help with molecular modeling studies.

References

- Perry, E.K. (1986) The cholinergic hypothesis - ten years on. *Br. Med. Bull.* **42**, 63-69.
- Davies, P. (1979) Neurotransmitter-related enzyme in senile dementia of the Alzheimer type. *Brain Res.* **171**, 319-327.

3. Richter, J.A., Perry, E.K. & Tomlinson, B.E. (1980) Acetylcholine and choline levels in post-mortem human brain tissue: preliminary observations in Alzheimer's disease. *Life Sci.* **26**, 1683–1689.
4. Winkler, J., Suhr, S.T., Gage, F.H., Thal, L.J. & Fisher, L.J. (1995) Essential role of neocortical acetylcholine in spatial memory. *Nature* **375**, 484–487.
5. Becker, R.E. & Giacobini, E. (1988) Mechanisms of cholinesterase inhibition in senile dementia of the Alzheimer type: Clinical, pharmacological, and therapeutic aspects. *Drug Dev. Res.* **12**, 163–195.
6. Schwartz, A.S. & Kohlsaedt, E.V. (1986) Physostigmine effects in Alzheimer's disease: relationship to dementia severity. *Life Sci.* **38**, 1021–1028.
7. Summers, W.K., Majovski, L.V., Marsh, G.M., Tachiki, K. & Kling, A. (1986) Oral tetrahydroaminoacridine in long-term treatment of senile dementia, Alzheimer type. *N. Engl. J. Med.* **315**, 1241–1245.
8. Barner, E.L. & Gray, S.L. (1998) Donepezil use in Alzheimer disease. *Ann. Pharmacother.* **32**, 70–77.
9. Sugimoto, H., Tsuchiya, Y., Sugumi, H., Higurashi, K., Karibe, N., Iimura, Y., Sasaki, A., Kawakami, Y., Nakamura, T., Araki, S., Yamanishi, Y. & Yamatsu, K. (1990) Novel piperidine derivatives. Synthesis and anti-acetylcholinesterase activity of 1-benzyl-4-[2-(N-benzoylamino) ethyl]piperidine derivatives. *J. Med. Chem.* **33**, 1880–1887.
10. Kawakami, Y., Inoue, A., Kawai, T., Wakita, M., Sugimoto, H. & Hopfinger, A.J. (1996) The rationale for E2020 as a potent acetylcholinesterase inhibitor. *Bioorg. Med. Chem.* **4**, 1429–1446.
11. Nochi, S., Asakawa, N. & Sato, T. (1995) Kinetic study on the inhibition of acetylcholinesterase by 1-benzyl-4-[(5,6-dimethoxy-1-indanon)-2-yl]methylpiperidine hydrochloride (E2020). *Biol. Pharm. Bull.* **18**, 1145–1147.
12. Inoue, A., Kawai, T., Wakita, M., Iimura, Y., Sugimoto, H. & Kawakami, Y. (1996) The simulated binding of (+)-2,3-dihydro-5,6-dimethoxy-2-[[1-phenylmethyl]-4-piperidinyl]methyl]-1H-inden-1-one hydrochloride (E2020) and related inhibitors to free and acylated acetylcholinesterases and corresponding structure-activity analyses. *J. Med. Chem.* **39**, 4460–4470.
13. Matsui, K., Oda, Y., Ohe, H., Tanaka, S. & Asakawa, N. (1995) Direct determination of E2020 enantiomers in plasma by liquid chromatography-mass spectrometry and column-switching techniques. *J. Chromatogr.* **694**, 209–218.
14. Villalobos, A., Blake, J.F., Biggers, C.K., Butler, T.W., Chapin, D.S., Chen, Y.L., Ives, J.L., Jones, S.B., Liston, D.R., Nagel, A.A., Nason, D.M., Nielson, J.A., Shalaby, I.A. & White, W.F. (1994) Novel benzisoxazole derivatives as potent and selective inhibitors of acetylcholinesterase. *J. Med. Chem.* **37**, 2721–2734.
15. Sugimoto, H., Iimura, Y., Yamanishi, Y. & Yamatsu, K. (1995) Synthesis and structure-activity relationships of acetylcholinesterase inhibitors: 1-benzyl-4-[(5,6-dimethoxy-1-indanon)-2-yl]methylpiperidine hydrochloride and related compounds. *J. Med. Chem.* **38**, 4821–4829.
16. Hulme, E.C., Birdsall, N.J.M. & Buckley, N.J. (1990) Muscarinic receptor subtypes. *Ann. Rev. Pharmacol. Toxicol.* **30**, 633–673.
17. Rogers, S.L. & Friedhoff, L.T. and the Donepezil Study Group. (1996) The efficacy and safety of donepezil in patients with Alzheimer's disease: results of a US multicenter, randomized, double-blind, placebo-controlled trial. *Dementia* **7**, 293–303.
18. Rogers, S.L., Doody, R.S., Mohs, R.C. & Friedhoff, L.T. and the Donepezil Study Group. (1998) Donepezil improves cognition and global function in Alzheimer disease. *Arch. Inter. Med.* **158**, 1021–1031.
19. Cardozo, M.G., Iimura, Y., Sugimoto, H., Yamanishi, Y. & Hopfinger, A.J. (1992) QSAR analysis of the substituted indanone and benzylpiperidine rings of a series of indanone-benzylpiperidine inhibitors of acetylcholinesterase. *J. Med. Chem.* **35**, 584–589.
20. Cardozo, M.G., Kawai, T., Iimura, Y., Sugimoto, H., Yamanishi, Y. & Hopfinger, A.J. (1992) Conformational analyses and molecular shape comparisons of a series of indanone-benzylpiperidine inhibitors of acetylcholinesterase. *J. Med. Chem.* **35**, 590–601.
21. Pang, Y.-P. & Kozikowski, A.P. (1994) Prediction of the binding site of 1-benzyl-4-[(5,6-dimethoxy-1-indanon)-2-yl]methyl]piperidine in acetylcholinesterase by docking studies with the SYSDOC program. *J. Comp. Aid. Mol. Des.* **8**, 683–693.
22. Kryger, G., Silman, I. & Sussman, J.L. (1999) Structure of acetylcholinesterase complexed with E2020 (Aricept): implications for the design of new anti-Alzheimer drugs. *Structure* **7**, 297–307.
23. Massoulie, J., Sussman, J.L., Doctor, B.P., Soreq, H., Velan, B., Cygler, M., Rotundo, R., Shafferman, A., Silman, I. & Taylor, P. (1992) Recommendations for nomenclature in cholinesterases. In *Multidisciplinary Approaches to Cholinesterase Functions* (Shafferman, A. & Velan, B., eds), pp. 285–288. Plenum Press, New York.
24. De La Hoz, D., Doctor, B.P., Ralston, J.S., Rush, R.S. & Wolfe, A.D. (1986) A simplified procedure for the purification of large quantities of mammalian acetylcholinesterase. *Life Sci.* **39**, 195–199.
25. Hosea, N.A., Radic, Z., Tsigelny, I., Berman, H.A., Quinn, D.M. & Taylor, P. (1996) Aspartate 74 as a primary determinant in acetylcholinesterase governing specificity to cationic organophosphonates. *Biochemistry* **35**, 10995–11004.
26. Millard, C.B., Lockridge, O. & Broomfield, C.A. (1998) Organophosphorus acid anhydride hydrolase activity in human butyrylcholinesterase: synergy results in a somanase. *Biochemistry* **37**, 237–247.
27. Ellman, G.L., Courtney, D., Andres, V. & Featherstone, R.M. (1961) A new and rapid colorimetric determination of acetylcholinesterase activity. *Biochem. Pharmacol.* **1**, 88–95.
28. Radi, Z., Pickering, N., Vellom, D.C., Camp, S. & Taylor, P. (1993) Three distinct domains in the cholinesterase molecule confer selectivity for acetyl- and butyrylcholinesterase inhibitors. *Biochemistry* **32**, 12074–12084.
29. Nair, H.K., Seravalli, J., Arbuckle, T. & Quinn, D.M. (1994) Molecular recognition in acetylcholinesterase catalysis: free-energy correlations for substrate turnover and inhibition by trifluoro ketone transition-state analogs. *Biochemistry* **33**, 8566–8576.
30. Bourne, Y., Taylor, P. & Marchot, P. (1995) Acetylcholinesterase inhibition by fasciculins: crystal structure of the complex. *Cell* **83**, 503–512.
31. Harel, M., Sussman, J.L., Krejci, E., Bon, S., Chanal, P., Massoulie, J. & Silman, I. (1992) Conversion of acetylcholinesterase to butyrylcholinesterase: modeling and mutagenesis. *Proc. Natl Acad. Sci. USA* **89**, 10827–10831.
32. Gentry, M.K. & Doctor, B.P. (1991) Alignment of amino acid sequences of acetylcholinesterases and butyrylcholinesterases. In *Cholinesterases: Structure, Function, Mechanism, Genetics and Cell Biology* (Massoulie, J., Bacou, F., Barnard, E.A., Chatonnet, A., Doctor, B.P. & Quinn, D.M., eds), pp. 394–398. American Chemical Society, Washington DC.
33. Masson, P., Froment, M.-T., Bartels, C. & Lockridge, O. (1996) Asp70 in the peripheral anionic site of human butyrylcholinesterase. *Eur. J. Biochem.* **235**, 36–48.
34. Saxena, A., Redman, A.M.G., Jiang, X., Lockridge, O. & Doctor, B.P. (1997) Differences in active site gorge dimensions of cholinesterases revealed by binding of inhibitors to human butyrylcholinesterase. *Biochemistry* **36**, 14642–14651.

35. Saxena, A., Qian, N., Kovach, I.M., Kozikowski, A.P., Pang, Y.-P., Vellom, D.C., Radi, Z., Quinn, D., Taylor, P. & Doctor, B.P. (1994) Identification of amino acid residues involved in the binding of Huperzine A to cholinesterases. *Protein Sci.* **3**, 1770–1778.
36. Raves, M.L., Harel, M., Pang, Y.-P., Silman, I., Kozikowski, A.P. & Sussman, J.L. (1997) Structure of acetylcholinesterase complexed with the nootropic alkaloid, (-)-huperzine A. *Nat. Struct. Biol.* **4**, 57–63.
37. Vellom, D.C., Radić, Z., Ying, L., Pickering, N.A., Camp, S. & Taylor, P. (1993) Amino acid residues controlling acetylcholinesterase and butyrylcholinesterase specificity. *Biochemistry* **32**, 12–17.



Molecular basis of interactions of cholinesterases with tight binding inhibitors

Zoran Radić^{a,*}, Roman Manetsch^b, Antoni Krasiński^b, Jessica Raushel^b,
John Yamauchi^a, Cindy Garcia^a, Hartmuth Kolb^b,
K. Barry Sharpless^b, Palmer Taylor^a

^a Department of Pharmacology 0636, University of California at San Diego, La Jolla, CA 92093, USA

^b Department of Chemistry, The Scripps Research Institute, La Jolla, CA 92037, USA

Abstract

Among the large variety of reversible inhibitors that bind to cholinesterases (ChE), only a few exhibit exquisitely strong binding reflected in low femtomolar to picomolar equilibrium dissociation constants. These tight binding inhibitors owe their high affinity to distinctive modes of interaction with the enzyme: naturally occurring snake toxins, the fasciculins, share a large 1000 Å² complementary surface for its complex with acetylcholinesterases (AChE; EC 3.1.1.7); transition state analogs trifluoroacetophenones form a covalent bond with the active serine; disubstituted 1,2,3-triazole inhibitors formed in situ are selected by AChE for optimal interaction surface over the length of the active center gorge. All these inhibitors bind with higher affinity to AChEs than to the closely related butyrylcholinesterases (BuChE; EC 3.1.1.8). Selectivity of individual inhibitors towards BuChE increases with increasing their molecular size. Interaction kinetics for all three classes of compounds reveal very slow rates of dissociation of the AChE-inhibitor complexes or conjugates combined with very fast association rates. The influence of conformational flexibility of the active center gorge on the affinity of inhibitor binding was demonstrated by comparing binding properties of a series of disubstituted 1,2,3-triazoles having systematically varied structures. Analysis of the linear free energy relationships of binding to both mouse and *Electrophorus* AChE reveals independent contributions of individual structural elements of inhibitors to their binding with the triazole ring emerging as an independently contributing pharmacophore. These tight binding inhibitor interactions reveal useful information not only on the conformational flexibility of ChEs, but also on the diversity of modes of interaction that achieve inhibition.

© 2005 Elsevier Ireland Ltd. All rights reserved.

Keywords: Acetylcholinesterase; Click chemistry; Conformational flexibility; Fasciculin; Femtomolar inhibitors; Interaction kinetics; Reversible inhibition; Tight binding; Triazole inhibitors; Trifluoroacetophenone

1. Introduction

AChE and the similar yet distinct enzyme from the ChE family, BuChE, catalyze acetylcholine hydrolysis comparably well, only differing in their ability to catalyze hydrolysis of carboxylic acid esters of larger acyl

group size such as butyrylcholine or benzoylcholine. Discrete structural differences allow BuChE to accommodate bulky ligands, including the covalent inhibitors isoOMPA and bambuterol, and the reversible inhibitor ethopropazine, all often studied inhibitors of ChEs [1,2]. The site of catalysis in both ChEs is buried ~20 Å deep in the center of a globular catalytic subunit of similar fold. The deviation (RMSD: root mean squared deviation) in protein backbone conformations of AChEs from

* Corresponding author.

E-mail address: zradic@ucsd.edu (Z. Radić).

Torpedo californica (TAcHE), mouse (mAChE), human (hAChE) and *Drosophila melanogaster* (DAChE) and of human BuChE shows a modest 0.93 Å (0.88–1.1 Å), only slightly higher than the average RMSD of 0.70 Å (range 0.55–0.87 Å), found for conformational variability between mAChE, hAChE and TAcHE and lower than 1.2 Å (range 1.1–1.2 Å) determined for the structurally divergent DAChE in comparison to other three AChEs.

The most potent, reversible ChE inhibitors associate with AChE at low picomolar and femtomolar concentrations. With these low dissociation constants even the rapidly associating ligands, limited only by the rate of diffusion, form inhibitory complexes that dissociate very slowly, with half-lives measured in days and months [3,4].

Three structurally diverse groups of reversible inhibitors show the highest affinity with the ChEs. These are the 61 amino acid large snake venom toxins, fasciculins; the low molecular weight transition state analogues trifluoroacetophenones; and the somewhat larger disubstituted 1,2,3-triazoles.

2. Fasciculins

The fasciculin (Fas) family of toxins consists of three very similar three-fingered toxins isolated from venoms of *Dendroaspis* snakes (Fig. 1). Fas2 found in *Dendroaspis angusticeps* is the most extensively studied and has picomolar inhibitory potency, similar to Fas1 which differs by only one amino acid and is found in the same venom. Fas3 found in *Dendroaspis viridis* differs by three amino acids from Fas2 and is an order of magnitude more potent inhibitor [5]. Fas2 and Fas3 associate with AChE at $2\text{--}6 \times 10^8 \text{ M}^{-1} \text{ min}^{-1}$, about two orders of magnitude slower than diffusion limited

reaction rates. It is thus possible that only a small fraction of enzyme and/or toxin conformations existing in solution can form an AChE*Fas2 complex seen in crystallized state [6–8]. Crystal structures of Fas2 bound to mAChE [6], TAcHE [7], and hAChE [8] show similar Fas2 conformations with the average backbone RMSD of $0.63 \pm 0.16 \text{ Å}$ ($n = 10$). This deviation in Fas2 structure is slightly, but consistently, smaller than the differences between the five AChE-bound structures and the structure of a free Fas2 with a RMSD of $0.81 \pm 0.07 \text{ Å}$ ($n = 5$) (Table 1).

On the other hand, conformations of both mAChE and TAcHE in complex with Fas2 differ from conformations of unliganded AChEs more than other crystallized AChE*ligand complexes. For 28 TAcHE*ligand crystal structures, the average difference in α conformation in comparison to unliganded TAcHE structure (PDB code 1ea5) is $0.27 \pm 0.09 \text{ Å}$, while for the TAcHE*Fas2 complex (PDB code 1fss) that difference is 0.54 Å. For 12 complexes of mAChE the average α difference is $0.29 \pm 0.11 \text{ Å}$, while two mAChE*Fas2 complexes (PDB codes 1mah and 1ku6) show an average RMSD of $0.55 \pm 0.10 \text{ Å}$. Formation of a tight AChE*Fas2 complex, is thus restricted to only a fraction of conformational states of both partners, particularly the enzyme, resulting in submaximal association rates. The high degree of complementarity of the more than 1000 Å^2 interaction surface of the resulting intermolecular fit in the complex [6–8] ensures very slow rates for its dissociation and low pM inhibition constants.

The much larger size of the active center gorge opening of BuChE does not allow for such a tight and complementary fit between Fas and the enzyme resulting in nearly millimolar inhibition constant for BuChE*Fas2 interaction [10].

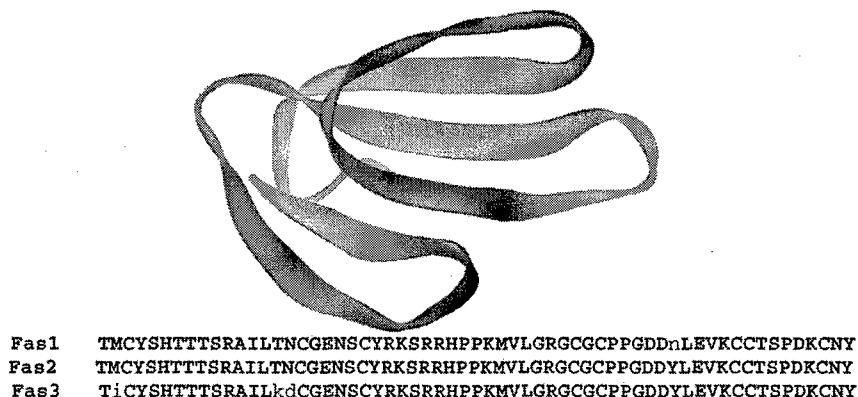


Fig. 1. Protein backbone fold for 61 amino acid long Fas2 represented by gray ribbon and alignment of sequences of three fasciculins. Nonconserved residues are printed in lowercase type.

Table 1

Structural pairwise overlays of Fas molecule found in seven different crystal structures

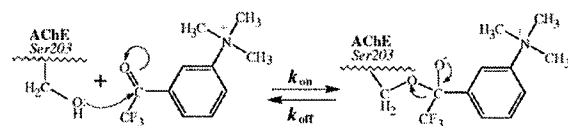
Structure	PDB id#	RMSD (C α backbone) (Å)						
		1b4l	1f8u	1fss	1ku6	1mah	1fsc	1fas
hAChE*Fas2	1b4l	0	0.23	0.75	0.69	0.66	0.89	2.61
hAChE*Fas2	1f8u	0.23	0	0.72	0.68	0.65	0.87	2.62
TACHe*Fas2	1fss	0.75	0.72	0	0.72	0.67	0.82	2.54
mAChE*Fas2	1ku6	0.69	0.68	0.72	0	0.50	0.75	2.50
mAChE*Fas2	1mah	0.66	0.65	0.67	0.50	0	0.74	2.50
Fas2	1fsc	0.89	0.87	0.82	0.75	0.74	0	2.52
Fas1	1fas	2.61	2.62	2.54	2.50	2.50	2.52	0

Only backbone atoms of Fas were used in pairwise alignments. Sequences were overlaid and RMSD calculated using SwissPDBViewer version 3.7 software interface and VMD program [9].

3. Trifluoroacetophenones

Unlike interactions between Fas and AChE that rely on high degree of complementarity of large interacting intermolecular surfaces, the tight interaction of trifluoroacetophenones (TFKs) with AChE is in large part a consequence of covalent bond formation and a pronounced three point interaction, between the two molecules. The structure of trimethylammonio trifluoroacetophenone (TFK⁺), when bound to AChE, mimics tetrahedral transition state in hydrolysis of acetylcholine in an all *trans* conformation [11,12] (Scheme 1).

The crystal structure of TFK⁺ covalently attached to TACHe reveals, in addition to the covalent bond between O γ of TACHe Ser200 and the carbonyl carbon of TFK⁺, close cation– π interactions between the qua-



Scheme 1. Mechanism of interaction of TFK⁺ with AChEs. Formation and breakdown of covalent bond with the active serine 203 of mammalian AChEs.

ternary nitrogen of TFK⁺ and 4–5 Å distant aromatic side chains of Trp84 and Phe330 (Fig. 2). At about 2 Å away the carbonyl oxygen of TFK⁺ forms three hydrogen bonds to the enzyme amide backbone, and three fluorines are surrounded by the acyl pocket phenylalanines some 3 Å distant. TFK⁺ associates with AChE at diffusion limited rates ($k_{on} = 2.2\text{--}4.8 \times 10^{11} \text{ M}^{-1} \text{ min}^{-1}$),

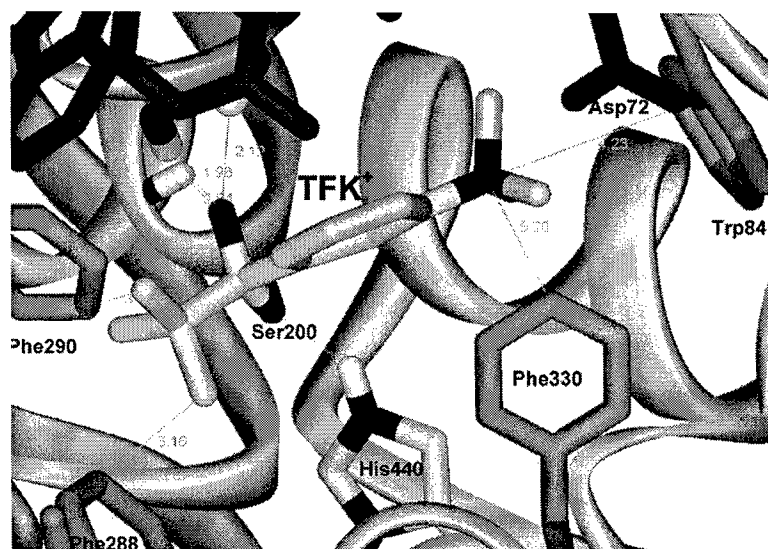
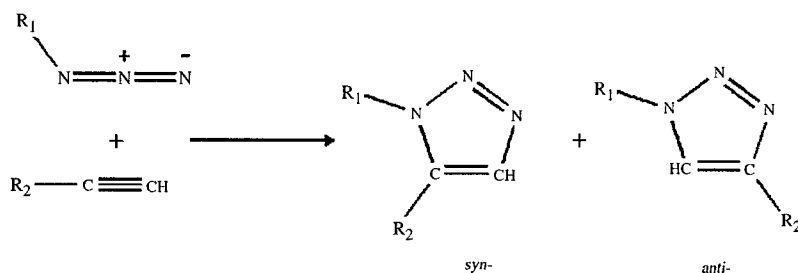


Fig. 2. Crystal structure of TFK⁺ covalently bound to the active serine 200 of the *Torpedo californica* AChE. Distances between TFK⁺ and choline binding site residues (Trp84 and Phe330), acyl pocket residues (Phe288 and Phe290), peripheral site Asp72 and the oxyanion hole (PDB code 1amn, [13]).



Scheme 2. Formation of disubstituted 1,2,3-triazoles by the [3+2]-Huisgen cycloaddition reaction between azides and alkynes.

but dissociation is very slow consistent with breaking of the hemiketal bond with the serine hydroxyl and additional strong interaction points between the two molecules ($k_{\text{off}} = 0.0006\text{--}0.006\text{ min}^{-1}$, depending on AChE species). This results in very high inhibitory potency with K_i in the low fM range (1.3–16 fM).

Substituting the active Ser203 of mAChE with Ala eliminates evidence for tight TFK⁺ binding to mAChE, but substituting catalytic triad His 447 with Ile has only a small effect on TFK⁺ binding rates, even though both Ser203Ala and His447Ile mutants appear catalytically inactive for acetylthiocholine hydrolysis and organophosphate conjugation. These observations suggest that, while Ser203 is required for tight binding interaction with TFK⁺, its ionization state or nucleophilicity is not as critical for formation of AChE-TFK⁺ adduct as for an ester bond formation. The role of catalytic triad His447 in AChE in addition to potentiating nucleophilicity of the active Ser203, is suggested to be in stabilizing the tetrahedral transition state in substrate hydrolysis and recruiting the water molecule required for its breakdown.

4. Disubstituted 1,2,3-triazoles

The tightest binding reversible, non-covalent inhibitors of AChE are not natural products, but 1,2,3-triazole derivatives [3]. The unique strategy used to design these inhibitors was to allow biological target, in this case the AChE molecule, to serve as a template for synthesis of its own inhibitor out of two building blocks. The library of building blocks structurally related to known AChE inhibitors tacrine and propidium was decorated with reactive acetylene and azide functionalities and presented to AChE. Tacrine and propidium selectively bind to the AChE peripheral binding site and to the AChE active center, respectively. The alkynes and azides, highly bioorthogonal reagents, in the absence of a catalyst very slowly form a pair of disubstituted 1,2,3-triazoles in the [3+2]cycloaddition reaction. The two products are regioisomers, *syn*- and *anti*-triazole (Scheme 2). Incubation of seventeen alkyne and azide building blocks (Fig. 3) in fifty two pairwise combinations with a micromolar concentration of either *Electrophorus electricus* AChE (EAChE) or mAChE,

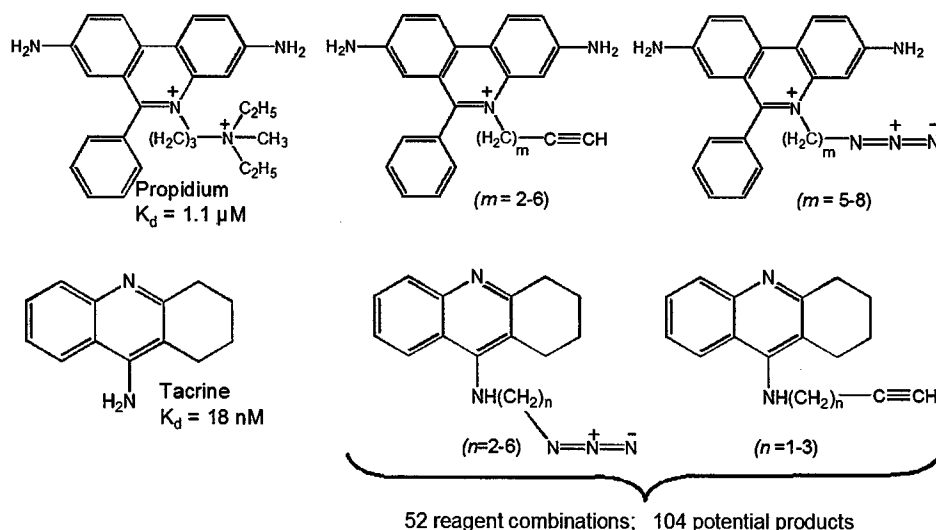


Fig. 3. Acetylene and azide building blocks of the P library in comparison with active center (tacrine), and peripheral site inhibitors (propidium).

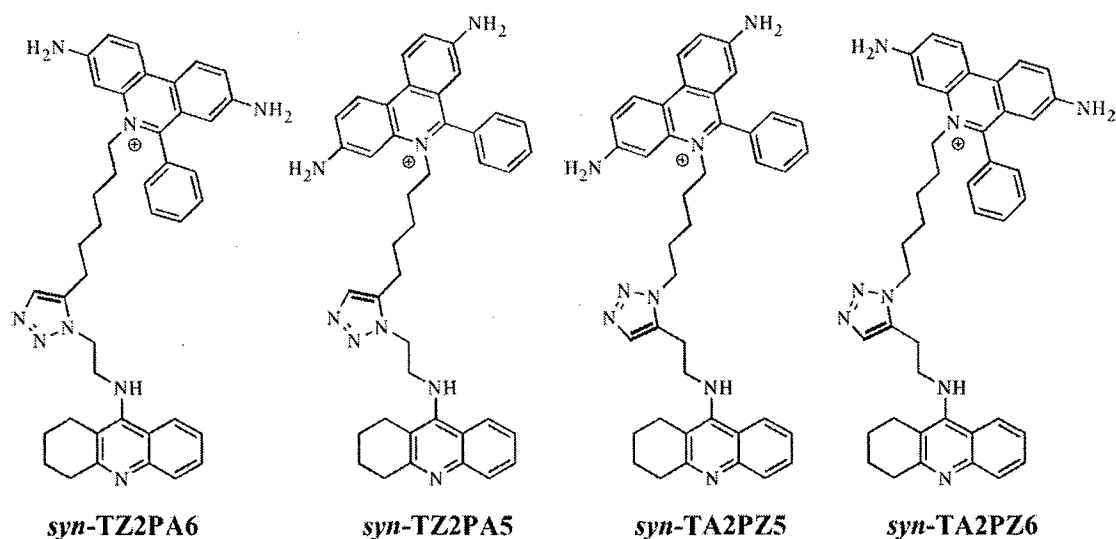


Fig. 4. Four disubstituted 1,2,3-triazoles formed in situ, in the AChE molecule, from building blocks of the phenylphenanthridinium based (P library) shown in Fig. 3.

yielded only four (Fig. 4) out of 104 possible different disubstituted 1,2,3-triazole products. All four in situ formed triazoles were *syn*-isomers. In the presence of enzyme, the cycloaddition reaction was accelerated by about four orders of magnitude yielding nanomolar concentrations of disubstituted 1,2,3-triazoles following 6 h of reaction. Effectively, one triazole molecule was formed every minute for about every 36,000 molecules

of AChE, thus the reaction is catalyzed 9–10 orders of magnitude slower than hydrolysis of acetylcholine.

The inhibitory potency of the four in situ formed disubstituted 1,2,3-triazoles was extremely high, in the femtomolar range, requiring that their inhibition constants for the EAcHE and mAChE (Table 2) be determined as a ratio of independently determined dissociation and association rate constants [14].

Table 2

Interaction constants and free energies of binding ($-RT \ln K_d$ at $T=295$ K) of disubstituted 1,2,3-triazole inhibitors of the P library with AChEs

Inhibitor	k_{on} ($10^{10} \text{ M}^{-1} \text{ min}^{-1}$)	k_{off} (min^{-1})	K_d (fM)	$-RT \ln K_d$ (kcal mol^{-1})	AChE
TA2PZ5					
<i>syn</i> -	1.5	0.0081	540	16.6	EAcHE
	1.5	0.045	3,000	15.6	mAChE
<i>anti</i> -	0.98	1.4	140,000	13.3	EAcHE
	1.1	0.50	44,000	14.0	mAChE
TZ2PA5					
<i>syn</i> -	0.76	0.00077	100	17.5	EAcHE
	1.2	0.028	2,300	15.7	mAChE
<i>anti</i> -	0.90	0.38	42,000	14.0	EAcHE
	1.3	0.43	33,000	14.1	mAChE
TA2PZ6					
<i>syn</i> -	1.2	0.010	830	16.3	EAcHE
	1.4	0.0086	610	16.5	mAChE
<i>anti</i> -	1.4	1.4	100,000	13.5	EAcHE
	1.7	0.71	42,000	14.0	mAChE
TZ2PA6					
<i>syn</i> -	1.5	0.0015	99	17.6	EAcHE
	1.7	0.0071	410	16.7	mAChE
<i>anti</i> -	1.8	0.25	14,000	14.7	EAcHE
	2.5	0.22	8,900	14.9	mAChE

For the purpose of this kinetic characterization triazoles were synthesized by conventional methods [14].

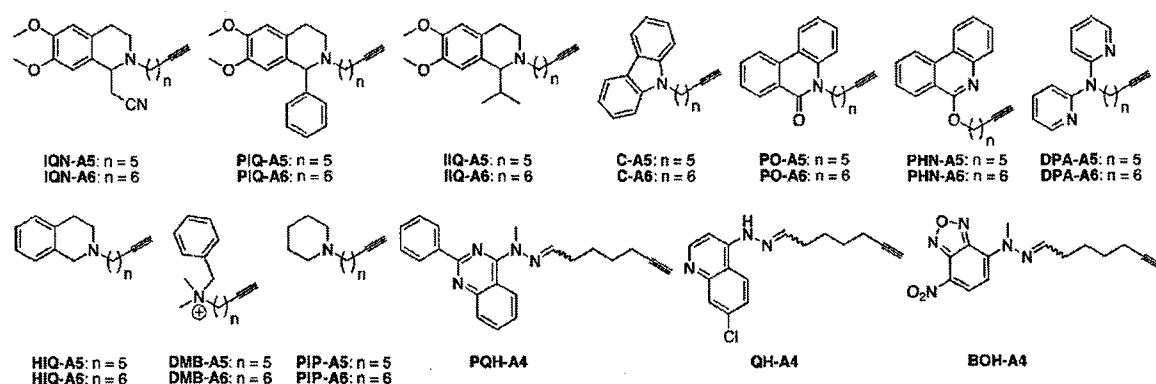


Fig. 5. HET library of acetylene reagents. This library was incubated with the azide **TZ2** in presence of mAChE or EAcHE.

Anti-isomers, that do not form by the in situ reaction, were one to two orders of magnitude poorer inhibitors of both EAcHE and mAChE than the corresponding *syn*-isomers. All eight compounds, however, were respectable inhibitors, with dissociation constants in the femtomolar to low picomolar range. The femtomolar potency of *syn*-**TZ2PA6**, appears unsurpassed for both enzymes, while *syn*-**TZ2PA5** and *syn*-**TA2PZ6**, are a close second. K_d values span three orders of magnitude, which is mainly due to the striking 1800-fold differences in the slow dissociation rates constants, k_{off} , in the case of the *Electrophorus* enzyme, and 90-fold difference for mAChE. In contrast, the fast, diffusion limited association rates k_{on} vary only by a factor of two. Thus, all eight triazoles owe their high inhibitory potencies to rapid rates of complex formation, occurring in milliseconds and very slow dissociation with half-lives of up to several days. Rapid transitions between conformations of the gorge enabling transient widenings may account for the near diffusion controlled rates into a geometrically restricted gorge.

Recently, disubstituted 1,2,3-triazoles of even higher potency have been discovered by an in situ click chemistry approach, in which twenty-three acetylene building blocks were incubated with the tacrine azide **TZ2** in presence of mAChE or EAcHE [15]. The aromatic heterocycles of acetylene reagents of this library (HET library) lack a permanent positive charge (Fig. 5).

Four chiral disubstituted 1,2,3-triazoles, *syn*-(*S*)-**TZ2PIQ-A5**, *syn*-(*S*)-**TZ2PIQ-A6**, *syn*-(*R*)-**TZ2PIQ-A5**, and *syn*-(*R*)-**TZ2PIQ-A6** formed in situ in both mAChE and in EAcHE when chiral building blocks **PIQ-A5** and **PIQ-A6** were combined with **TZ2** (Fig. 6). Their inhibitory potencies in addition to the potencies of their corresponding *anti*-isomers are listed in Table 3.

Constants for the HET library derived triazoles in Table 3 follow general trends observed for con-

stants of P library derived triazoles in Table 2. In both tables, comparison of the inhibitors extending from the strongest to the weakest revealed contributions of three discrete structural components. For the P library derived inhibitors those are *syn*- versus *anti*-regioisomeric configuration, linker length between phenylphenanthridinium and triazole of six versus five methylenes (A6 \rightarrow A5 or Z6 \rightarrow Z5), and inversion of the in situ formed triazole ring orientation (TZPA \rightarrow TAPZ), as reflected in comparison of the strongest inhibitor *syn*-**TZ2PA6** to the two to three orders of magnitude weaker inhibitor *anti*-**TA2PZ5**, the weakest in Table 2. For the HET library derived inhibitors the difference between the

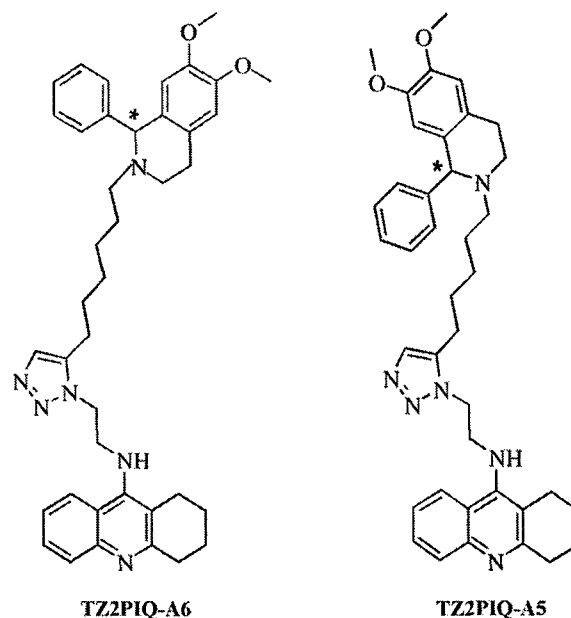


Fig. 6. Chiral disubstituted 1,2,3-triazoles formed in situ from building blocks of the HET library (Fig. 5), in combination with the tacrine azide **TZ2**.

Table 3

Interaction constants and free energies of binding ($-RT \ln K_d$ at $T=295\text{ K}$) of disubstituted 1,2,3-triazole inhibitors of the HET library with acetylcholinesterases

Inhibitor	k_{on} ($10^{10} \text{ M}^{-1} \text{ min}^{-1}$)	k_{off} (min^{-1})	K_d (fM)	$-RT \ln K_d$ (kcal mol $^{-1}$)	AChE
(S)-TZ2PIQ-A5					
<i>syn</i> -	0.70	0.00023	33	18.2	EACHE
	0.77	0.0038	500	16.6	mACHE
<i>anti</i> -	0.52	1.10	210,000	13.1	EACHE
	0.72	6.2	870,000	12.2	mACHE
(R)-TZ2PIQ-A5					
<i>syn</i> -	0.67	0.00024	36	18.2	EACHE
	0.84	0.00088	100	17.6	mACHE
<i>anti</i> -	0.40	0.77	190,000	13.1	EACHE
	0.58	1.0	180,000	13.2	mACHE
(S)-TZ2PIQ-A6					
<i>syn</i> -	0.90	0.00087	96	17.6	EACHE
	0.97	0.0110	1,100	16.1	mACHE
<i>anti</i> -	0.41	0.83	200,000	13.1	EACHE
	0.67	2.8	420,000	12.7	mACHE
(R)-TZ2PIQ-A6					
<i>syn</i> -	0.67	0.0024	360	16.8	EACHE
	0.73	0.012	1,700	15.9	mACHE
<i>anti</i> -	0.50	0.82	170,000	13.2	EACHE
	0.64	1.4	220,000	13.0	mACHE

strongest (S)-TZ2PIQ-A5 to the weakest (R)-TZ2PIQ-A6 inhibitor similarly included six to five methylene linker size reduction in addition to *S* to *R* inverted chiral preference. *Syn*- versus *anti*-regioisomeric configuration had so pronounced an effect in the HET library set of triazoles that it masked effects of other structural modifications, thus resulting in more than three orders of

magnitude reduction in binding for every *syn*- versus *anti*-triazole pair.

The average energy differences per individual structural change listed for the two libraries in Table 4 further emphasize that for the optimal fit in the inhibitory complex the elongated slender triazole molecules need to be tilted in order to follow the curvature of the AChE active

Table 4

Energy increments for structural changes in in situ formed disubstituted 1,2,3-triazoles of P and HET libraries (Tables 2 and 3)

Structural change	Mean $\Delta (-RT \ln K_d)$ (kcal mol $^{-1}$)		AChE
	P library	HET library	
<i>syn</i> \rightarrow <i>anti</i>	3.1 ± 0.3	4.5 ± 0.5	EACHE
	1.9 ± 0.4	3.7 ± 0.6	mACHE
A6 \rightarrow A5 (or Z6 \rightarrow Z5)	0.15 ± 0.38	-0.52 ± 0.64	EACHE
	0.69 ± 0.45	-0.51 ± 0.87	mACHE
TZPA \rightarrow TAPZ	1.0 ± 0.2	N/A	EACHE
	0.37 ± 0.36		mACHE
<i>S</i> \rightarrow <i>R</i>	N/A	0.18 ± 0.36	EACHE
		-0.48 ± 0.59	mACHE
$\sum(\textit{syn} \rightarrow \textit{anti}) + (\text{A6} \rightarrow \text{A5}) + (\text{TZPA} \rightarrow \text{TAPZ})$ (P library) or $\sum(\textit{syn} \rightarrow \textit{anti}) + (\text{A5} \rightarrow \text{A6}) + (\text{S} \rightarrow \text{R})$ (HET library)	4.3 (4.3)	5.2 (5.1)	EACHE
	3.0 (2.7)	3.7 (3.7)	mACHE

Energy difference values calculated from increments are shown in bold typeface; experimental values are in parentheses.

center gorge as found for *syn*-isomers. That is particularly manifested in the HET library derived compounds whose smaller peripheral site group allows them to bind deeper into the enzyme active center gorge. Apart from the *syn*-*anti*-difference in regioisomeric configuration the inversion of the triazole ring orientation, as shown for the P library, affected inhibitory binding the most. Thus interactions of the ring, bearing a strong dipole moment, with the active center gorge residues contribute significantly to the overall energy of binding. The triazole moiety is thus an active pharmacophore in the inhibitory interaction with AChE. This interaction is significantly more pronounced for EAcChE than for mAChE prompting questions on the molecular basis for the interspecies difference. The two enzymes, however, share very high degree of similarity in the active center gorge, from the peripheral site Trp286 to the Trp86 at the gorge base indicating that the difference in triazole (and thus the dipole orientations) inversion influence might come from interaction of an inhibitor with more global properties of the enzyme molecule, such as positioning and magnitude of its overall dipole moment that might differ in AChEs of the two species.

Inhibition of BuChE with selected triazoles, as shown for the P library derived triazoles [16], is generally very strong with constants in high femtomolar range, however, a looser or less tailored inhibitor fit in the large active center gorge of BuChE may account for the diminished energy of interaction.

5. Conclusions

The tightest inhibitory interactions with ChEs are not confined to a specific region of enzyme molecule but occur in three different structural domains. Fasciculins bind to the peripheral binding site, TFKs to the active serine of the catalytic site, and in situ generated disubstituted 1,2,3-triazoles occupy the active center gorge between the two sites. In their inhibitory interaction, TFKs exploit structural features of enzyme highly evolved for the efficient substrate hydrolysis and large fasciculins interact with the outer available AChE surface, while disubstituted 1,2,3-triazoles are synthesized within the AChE template to fit optimally the active center gorge ensuring not only high affinity but also specificity of the interaction. Steric and functional complementarity between inhibitor and enzyme molecules ensure high stabilization energies of all corresponding complexes. The narrow and hydrophobic active center gorge of AChE appears better suited for tight binding interactions of that type, as compared to BuChE, resulting in low femtomolar inhibition constants for the

tightest binding *syn*-triazoles. While slow dissociation rates of inhibitory complexes appear decisive for the high affinity interaction, the association rates approaching the diffusion limitation additionally contribute to the overall stability of the inhibitory complexes. Conformational flexibility within the long, narrow, and hydrophobic active center gorge of AChE, presumably accounting for transient opening states, likely facilitates accessibility in diffusion limited association.

Acknowledgements

This work was supported by the Swiss National Science Foundation (R.M.); the Novartis Research Foundation (R.M.); the Skaggs Institute for Research (A.K., J.R., H.C.K.); the National Institute of General Medical Sciences, National Institutes of Health, GM28384 (K.B.S.) and GM R37-18360 (P.T.); DAMDC17C-02-2-0025 (P.T.); and the W.M. Keck Foundation (K.B.S.).

References

- [1] D.C. Vellom, Z. Radić, Y. Li, N.A. Pickering, S. Camp, P. Taylor, Amino acid residues controlling acetylcholinesterase and butyrylcholinesterase specificity, *Biochemistry* 32 (1993) 12–17.
- [2] Z. Radić, N.A. Pickering, D.C. Vellom, S. Camp, P. Taylor, Three distinct domains in the cholinesterase molecule confer selectivity for acetyl- and butyrylcholinesterase inhibitors, *Biochemistry* 32 (1993) 12074–12084.
- [3] W.G. Lewis, L.G. Green, F. Grynszpan, Z. Radić, P.R. Carlier, P. Taylor, M.G. Finn, K.B. Sharpless, Click chemistry in situ: acetylcholinesterase as a reaction vessel for the selective assembly of a femtomolar inhibitor from an array of building blocks, *Angew. Chem. Int. Ed. Engl.* 41 (2002) 1053–1057.
- [4] Y. Bourne, Z. Radić, H.C. Kolb, K.B. Sharpless, P. Taylor, P. Marchot, Structural insights into conformational flexibility at the AChE peripheral site and active center gorge, *Chem.-Biol. Interact.* (this issue).
- [5] P. Marchot, A. Khelif, Y.H. Ji, P. Mansuelle, P.E. Bougis, Binding of 125I-fasciculin to rat brain acetylcholinesterase. The complex still binds diisopropyl fluorophosphate, *J. Biol. Chem.* 268 (1993) 12458–12467.
- [6] Y. Bourne, P. Taylor, P. Marchot, Acetylcholinesterase inhibition by fasciculin: crystal structure of the complex, *Cell* 83 (1995) 503–512.
- [7] M. Harel, G.J. Kleywegt, R.B. Ravelli, I. Silman, J.L. Sussman, Crystal structure of an acetylcholinesterase-fasciculin complex: interaction of a three-fingered toxin from snake venom with its target, *Structure* 3 (1995) 1355–1366.
- [8] G. Kryger, M. Harel, K. Giles, L. Toker, B. Velan, A. Lazar, C. Kronman, D. Barak, N. Ariel, A. Shafferman, I. Silman, J.L. Sussman, Structures of recombinant native and E202Q mutant human acetylcholinesterase complexed with the snake-venom toxin fasciculin-II, *Acta Crystallogr. D Biol. Crystallogr.* 56 (2000) 1385–1394.
- [9] W. Humphrey, A. Dalke, K. Schulten, VMD—visual molecular dynamics, *J. Mol. Graphics* 14 (1996) 33–38.

- [10] Z. Radić, R. Duran, D.C. Vellom, Y. Li, C. Cervenansky, P. Taylor, Site of fasciculin interaction with acetylcholinesterase, *J. Biol. Chem.* 269 (1994) 11233–11239.
- [11] S. Malany, M. Sawai, S.M. Sikorski, J. Seravalli, D.M. Quinn, Z. Radić, P. Taylor, C. Kronman, B. Velan, A. Shafferman, Transition state structure and rate determination for the acylation stage of acetylcholinesterase catalyzed hydrolysis of (acetylthio)choline, *J. Am. Chem. Soc.* 122 (2000) 2981–2987.
- [12] H.K. Nair, J. Seravalli, T. Arbuckle, D.M. Quinn, Molecular recognition in acetylcholinesterase catalysis: free-energy correlations for substrate turnover and inhibition by trifluoro ketone transition-state analogs, *Biochemistry* 33 (1994) 8566–8576.
- [13] M. Harel, D.M. Quinn, H.K. Nair, I. Silman, J.L. Sussman, The X-ray structure of a transition state analog complex reveals the molecular origins of the catalytic power and substrate specificity of acetylcholinesterase, *J. Am. Chem. Soc.* 118 (1996) 2340–2346.
- [14] R. Manetsch, A. Krasinski, Z. Radić, J. Raushel, P. Taylor, K.B. Sharpless, H.C. Kolb, In situ click chemistry: enzyme inhibitors made to their own specifications, *J. Am. Chem. Soc.* 126 (2004) 12018–12809.
- [15] A. Krasinski, Z. Radić, R. Manetsch, J. Raushel, P. Taylor, K.B. Sharpless, H.C. Kolb, In situ selection of lead compounds by click chemistry: target-guided optimization of acetylcholinesterase inhibitors, *J. Am. Chem. Soc.* 127 (2005) 6686–6692.
- [16] Y. Bourne, H.C. Kolb, Z. Radić, K.B. Sharpless, P. Taylor, P. Marchot, Freeze-frame inhibitor captures acetylcholinesterase in a unique conformation, *Proc. Natl. Acad. Sci. U.S.A.* 101 (2004) 1449–1454.

CHAPTER 12

Structure and Function of Cholinesterases

ZORAN RADIĆ AND PALMER TAYLOR

University of California at San Diego, La Jolla, California

I. INTRODUCTION

From the beginning of the past century until the early 1970s, assay of the cholinesterases was based mainly on their capacity to catalyze the hydrolysis of acetylcholine and on the selectivity of compounds that interfere with the catalytic reaction (Dale, 1914). In the late 1960s and early 1970s, inhibitors and substrates were found to bind to a remote site(s), thereby allosterically interfering with the catalytic reaction (Changeux, 1966; Aldridge and Reiner, 1969; Taylor and Lappi, 1975). Improvements in protein purification techniques identified the active center and sufficient sequence to clone the gene encoding the enzyme (Schumacher *et al.*, 1986). Five years later, the first three-dimensional structure of a cholinesterase was solved (Sussman *et al.*, 1991). Those events led to rapid accumulation of structural information on cholinesterases in the years to come, resulting in the determination of at least 125 primary structures and 61 three-dimensional structures of cholinesterases available today. In this chapter, we summarize the available structural information in the context of the evolutionary and functional relationships of the cholinesterases and related α/β hydrolase fold proteins.

II. CHOLINESTERASE FAMILY OF ENZYMES

Two structurally and functionally very similar, yet distinct enzymes form the family of cholinesterases (ChEs). Acetylcholinesterase (AChE; EC 3.1.1.7) and butyrylcholinesterase (BuChE; EC 3.1.1.8) both catalyze acetylcholine (ACh) hydrolysis with similarly high efficiency and only differ in efficiency to catalyze the hydrolysis carboxylic acid esters of larger acyl group size, such as butyrylcholine or benzoylcholine. Larger substrates are hydrolyzed much better by BuChE due to small but significant differences in their structure that also allows BuChE to

much better bind generally bulky ligands, including covalent inhibitors *iso*OMPA and bambuterol and reversible inhibitor ethopropazine, all well-known specific inhibitors of ChEs (Vellom *et al.*, 1993; Radić *et al.*, 1993). The site of catalysis in both enzymes is buried ~20 Å deep in the center of the globular catalytic subunit. Tissue distributions and physiological functions of the two enzymes in higher organisms are different. AChE is mainly found in the central nervous systems, neuromuscular junctions, and the hematopoietic system of vertebrates, and it plays a key role in cholinergic neurotransmission. BuChE is found in liver, blood serum, and kidney. Its primary physiological role is not completely clear, but it may be involved in hydrolysis of dietary esters. Mice lacking the AChE gene and activity have normal BuChE activities and can survive more than 1 year but are more sensitive to organophosphate (OP) inhibitors, suggesting that BuChE activity may substitute at least in part for AChE activity (Adler *et al.*, 2004). The mammalian cholinesterase profile contrasts with that of *Drosophila*, which acts BuChE and in which AChE knockout results in embryonic lethality (Greenspan *et al.*, 1980). In humans and most other vertebral species, only one gene encodes AChE. Insects and worms can have multiple genes encoding up to two (insects) or four (worms) AChEs.

A. Primary Structure

Catalytic subunits of both AChE and BuChE consist of a single 500- to 600-amino acid-long peptide. The first amino acid sequence of an AChE was determined by Schumacher and colleagues in 1986 by cloning cDNA for the enzyme from fish *Torpedo californica*, whereas the first BuChE sequence was determined by sequencing purified enzyme protein isolated from human serum (Lockridge *et al.*, 1987). A search of the SwissProt database revealed approximately 125 full-length or nearly full-length cholinesterase sequences, including approximately 108 AChE and 17 BuChE sequences. More than half of these refer to proteins

whose function was not established directly but was inferred from sequence comparisons. The largest numbers of deposited sequences are of insect cholinesterases (51 sequences), including aphids (16 sequences), flies (15 sequences), and mosquitoes (10 sequences), followed by 19 entries of mammalian sequences. Also numerous are parasite (17 sequences) and worm (16 sequences) entries. The distribution of species with known cholinesterase sequences reflects an interest in studying enzymes targeted by OP and carbamate (CM) pesticides. Some deposited AChE sequences originate from species that developed resistance to pesticides used to eradicate them, most notably insects such as, mosquitoes, and flies. Cholinesterase activities have been documented in a number of plants and algae (Gupta and Gupta, 1997; Gupta *et al.*, 1998; Fletcher *et al.*, 2004), but their sequences are not known. Among the simpler life-forms, recently resolved genomic sequences of fungus *Neurospora crassa* (Galagan *et al.*, 2003) and virus Mimivirus (Raoult *et al.*, 2004) revealed cholinesterase-like sequences, suggesting utilization of cholinesterase activity in simple life cycles of primitive organisms. Table 1 summarizes full-length amino acid sequences of fish (ACES_TORCA; i.e., *T. californica*), insect (ACES_DROME; i.e., *Drosophila melanogaster*, 36% identify with *Torpedo*), human (ACES_HUMAN, 55% identify with *Torpedo* AChE), and mouse (ACES_MOUSE, 56% identify with *Torpedo* AChE) AChEs; human and mouse BuChEs; as well as four cholinesterases of very simple organisms — fungi (Q6MGI2 and Q872U5, 21 and 20% identify with *Torpedo* AChE, respectively), tunicata *Oikopleura dioica* (Q675X9, 14% identify with *Torpedo* AChE), and virus (Q5UR02, 21% identify with *Torpedo* AChE).

Out of approximately 50 serine residues found in cholinesterase sequences, only one is directly involved and essential in catalysis, Ser200, as confirmed by site-directed mutagenesis (Gibney *et al.*, 1990). It is found in all sequences in Table 1, including viral and fungal proteins. A detailed comparison shown in Table 2 includes all 125 currently available cholinesterase sequences. The active Ser200 is conserved in 124 sequences and shifted by one residue c-terminal only in human hookworm *Necator Americanus* AChE (Q8IT86). It is not clear whether this protein is catalytically active, but similar one-position shifts in the active serine, although N-terminal, are found in sequences of structurally related, but catalytically inactive, neuroligins, a family of neuroadhesive proteins from human, mouse, and rat sharing approximately 30% amino acid identity with AChE. Besides Ser200, five more serines are very well conserved throughout the family: Ser91, Ser205, Ser212, Ser226, and Ser428. The amino acid fragment (195–205) around the active Ser200 is well conserved in most cholinesterases. Of the 11 residues of the fragment, Gly202 appears to be strictly conserved in all 125 sequences, whereas the pattern Gly-X-Ser200-X-Gly-X-X-Ser

can be found in 123 sequences; exceptions are the simple marine organism *Oikopleura dioica* (Q675X9) and worm *N. Americanus* AChE. Interestingly, 13 of 15 deposited fly AChE sequences have, starting with Ser200, the conserved pattern Ser-x-x-Ser-Ser-Ser, and one of the sequences (Q8MXC9) has a Ser-Ser-Gly-Ser-Ser-Ser pattern. Residues His440 and Glu327 were identified as the remaining two elements of the catalytic triad. Site-directed mutagenesis showed that substitution of His440Gln in *T. californica* AChE yielded inactive protein (Gibney *et al.*, 1990), and Glu327 was identified as part of the catalytic triad only upon resolution of the first three-dimensional structure of an AChE (Sussman *et al.*, 1991). The two residues are conserved in 123 (Glu327) and 124 (His440) sequences, suggesting that *Oikopleura* and one of two fungal proteins (Q6MGI2) in which residues other than Glu and His are found may not be catalytically active. Several other glutamates and histidines are well conserved in the cholinesterase family. Glu92 is conserved in all 125 sequences, and Glu199, Glu443, and His209 are conserved in almost all of them, whereas positions 172, 297, and 397 have either Asp or Glu always conserved.

Besides the catalytic triad, additional residues are known to be critical for maintaining the catalytic activity of cholinesterases. The oxyanion hole stabilizes carbonyl oxygen of ACh during hydrolysis. It is formed by protein backbone amide nitrogen protons of residues Gly118, Gly119, and Ala201, as suggested by the positioning of trifluoroacetophenone, an ACh transition state analogue, in the three-dimensional structure of *Torpedo* AChE (PDB code 1AMN; Harel *et al.*, 1996). Two of three residues are likely sufficient to form a functional oxyanion hole entity, and all 125 sequences in Table 2 have at least two of three oxyanion hole residues conserved. The most conserved is Gly118 (in 124 sequences), followed by Ala201 (in 120 sequences). The Ala201 is substituted with serine in 5 sequences. Gly119, is conserved in 115 sequences with serine substitution in 6 of the remaining 10 sequences.

Two additional sequence fragments exceptionally well conserved throughout the cholinesterase family are required for catalytic activity, although their involvement in the catalytic process is not fully understood. Residues 91–95 with sequence SEDCL (Ser-Glu-Asp-Cys-Leu) are conserved in 115 of 122 residues, motif xEDCL is conserved in 120 of 122 sequences, and motif xExxL is conserved in all 122 sequences. Two anionic residues in that fragment, Glu92 and Asp93, are involved in a salt bridge and a hydrogen bond formation with Arg44 and Tyr96, respectively. Both are conserved in number of cholinesterases, particularly Arg44, which is absent only in viral and *O. dioica* AChEs out of 125 sequences. Substitutions of Glu92Gln, Glu92Leu, Glu93Val, and Arg44Glu in single-site *Torpedo* AChE mutants resulted in the complete loss of catalytic activity, indicating their important role in folding and maintaining the three-dimensional structure of a disulfide loop

(Q6MGI2 and Q872U5) from *Neurospora crassa*^a

(continues)

TABLE 1. (continued)

ACES_TORCA	PHANDLGDAVTLQYTDWMDNNGIKNRDGLDDIVGDHNVICPLMHFNKNTKFGNGTVLYFFNHRASNLVPEWGMGVHGYEIEFVFGPLVKELNYTAEEALSRRIIMHYWATFAKTG	480
ACES_DROME	GK--QAEEAIIFOYTSWE--NPGYQOQOIGRAVGDHFTCTNEIAQAALAEERG--VHYFFTHRTSTSLGEMWGVULHGEIEYFFGQPLNNS--RPVERELGKRMLSAVIEFAKTG	470
ACES_HUMAN	PQVSLAAEAVALVHTDMLHEPDPARLREALSDVGDHNVCPVQAOLAGLAAQG--VYAVVEHRASTLSWPLMGMVPHGYEIEFTFGIPLDPSRNYTAEEKIFAQRLMRYWANFAKTG	460
ACES_MOUSE	PQASDLAAEAVALVHTDMLHEPDPARLREALSDVGDHNVCPVQAOLAGLAAQG--VYAVVEHRASTLSWPLMGMVPHGYEIEFTFGIPLDPSRNYTAEEKIFAQRLMRYWANFAKTG	450
CHLE_HUMAN	PGVSEFGKESILFHTDWDVDDQRPENYREALGDVGDYNFICPALEFTKKFSEWG--AFFYFFEHRSKSLPWPWMGMVHGYEIEFVFGPLPERRDNYTKAEEILSRSTVKRWANFAKTG	440
CHLE_MOUSE	PGVSEFGKESILFHTDWDVDDQRPENYREALGDVGDYNFICPALEFTKKFSEWG--AFFYFFEHRSKSLPWPWMGMVHGYEIEFVFGPLPERRDNYTKAEEILSRSTVKRWANFAKTG	430
Q675X9	ASAKAAKAVLAASLLEAEVEGEKTYFDLYNAELPASDFELKSFACNGETCDVEGDILIKYENEAVDATWKALANSEGVPLVYLLHGGGNGHYDMVVEQNVVSVAYRLGMFAFLL	420
Q5UR02	GN-AEYYNDLAPLYSTEYNS-NVTYFGQGFISRVDDIWACNTRRMNIYQOQSKK--AHSWYFDSAPDTHIYPSWTKVFHESDVYVYARECDGLW--LTCQODNLGKTWNIYVNGAIRAA	410
Q6MG12	TMLYENPNASICPKMGCWRG--QAGSVYGMRYMCPGLYNDAFDNYDQYSKGT--AYRWNVEDRDQMSG--LGVPHVVELNALFGPANWYVY--GATNAAAVQVMQSTVWVSFIRTF	400
Q872U5	PD--VTNPHSSNPFYRVPVG--NGAQWARLDAAYSHYAVICPVLTQAHFMSQAG--VHVYVFAARGNWDVADAPVVAHDMGFFRSFGPPRSK-----GLRKVADGMNAANGRFISGE	390
ACES_TORCA	NPNEPHSOESKWPFLTTEKQKFDLNTPEPMKHQRLVQMCVFWNQFLKLNATACDGLSSSGTSSSGKGIIFVVLFSILYLIF	380
ACES_DROME	NP-----GEWPNFSKEDPVYIIFSTDD--KLARGPLAARCSFWNDYLPKVSAG--TCDG-GSAS-----	370
ACES_HUMAN	DPNEPRDPKAWPPVYTAGAQYVSLDLRPLEVRRLRAQACAFWNRFLPKLLSATDTLDEAERQ-----	
ACES_MOUSE	DPNDPRDSKQWPPYTTAAQYVSLNKLPLEVRRLRAQACAFWNRFLPKLLSATDTLDEAERQ-----	
CHLE_HUMAN	NP-NETQNNSSWPVKSTEQKYLTLNTESTRIMTKLRAQCQRFWSFFPKVLEMTGNIDEAEWE-----	
CHLE_MOUSE	HP-NCTQGNMWPVFTSTEQKYLTLNTEKSKYKSLRAPQCQFWRFLFPKLEMTGDIIDEQE-----	
Q675X9	LP-WWHTVLESWPFFKVNVMCMGVNNAVSTTKLVLYQCCDTIDCLQYSEEIRDAANGTSRH-----	
Q5UR02	SLK--LRDVVWPQYKQNEVVMHFTAVGENVLFSIISADGDYQYQRCQKIDRVRAEYVLDPE-----	
Q6MG12	NP-CCGGEVNAWKSGDEASAOHQHLLPFTGTGDEGLRCVAGSAWALNSRIIGLAVPRFTYGDGP-----	
Q872U5	KIGKKSGKRYWPLFRTPFGDGDSELGRGDRNTERRWSSSPLWEOSSGDDVVKPPGEGTIVFGE-----	

^aSequences were aligned using BioEdit version 7.0.1 software interface (Hall, 1999).

TABLE 2. Elements of ChE Primary Structures Critical for Catalytic Activity as Found in Alignment of 125 ChE Structures^a

Sequence			Oxyanion hole			Active serine			Catalytic triad																			
ID	SwissProt code		91	95	116	120	201	195	200	205	226	327	440															
AM	ACBS_BOVIN		S	E	D	C	L	Y	G	G	F	A	T	L	F	G	E	S	A	G	A	A	S	S	E	H		
AM	ACBS_FELCA		S	E	D	C	L	Y	G	G	F	A	T	L	F	G	E	S	A	G	A	A	S	S	E	H		
AM	ACBS_HUMAN		S	E	D	C	L	Y	G	G	F	A	T	L	F	G	E	S	A	G	A	A	S	S	E	H		
AM	ACBS_MOUSE		S	E	D	C	L	Y	G	G	F	A	T	L	F	G	E	S	A	G	A	A	S	S	E	H		
AM	ACBS_RABIT		S	E	D	C	L	Y	G	G	F	A	T	L	F	G	E	S	A	G	A	A	S	S	E	H		
AM	ACBS_RAT		S	E	D	C	L	Y	G	G	F	A	T	L	F	G	E	S	A	G	A	A	S	S	E	H		
AMHUMAN2	Q86YX9		S	E	D	C	L	Y	G	G	F	A	T	L	F	G	E	S	A	G	A	A	S	S	-	H		
AMHUMANyt	Q86TM9		S	E	D	C	L	Y	G	G	F	A	T	L	F	G	E	S	A	G	A	A	S	S	E	H		
AMONKEY	Q67BC1		S	E	D	C	L	Y	G	G	F	A	T	L	F	G	E	S	A	G	A	A	S	S	E	H		
AMONKEY	Q67BC2		S	E	D	C	L	Y	G	G	F	A	T	L	F	G	E	S	A	G	A	A	S	S	E	H		
ABCHICK	ACBS_CHICK		S	E	D	C	L	Y	G	G	F	A	T	L	F	G	E	S	A	G	A	A	S	S	E	H		
ACBRIGSAE	ACE4_CAEBR		S	E	D	C	L	F	G	G	F	A	S	V	F	G	Q	S	A	G	A	A	S	S	E	H		
ACBRIGSAE	Q9NDG9		S	E	D	C	L	F	G	G	F	A	S	S	L	V	G	E	S	A	G	A	A	S	S	E	H	
ACELEGANS	061459		S	E	D	C	L	F	G	G	F	A	S	S	L	V	G	E	S	A	G	A	A	S	S	E	H	
ACELEGANS	061372		S	E	D	C	L	F	G	G	F	A	S	A	V	F	G	Q	S	A	G	A	A	S	S	E	H	
AF	ACBS_TORCA		S	E	D	C	L	Y	G	G	F	A	T	I	F	G	E	S	A	G	A	A	S	S	E	H		
AF	ACBS_BRARE		S	E	D	C	L	Y	G	G	F	A	T	I	F	G	E	S	A	G	A	A	S	S	E	H		
AF	ACBS_ELEEL		S	E	D	C	L	Y	G	G	F	A	T	I	F	G	E	S	A	G	A	A	S	S	E	H		
AF	ACBS_TORMA		S	E	D	C	L	Y	G	G	F	A	T	I	F	G	E	S	A	G	A	A	S	S	E	H		
AF	ACBS_MYXGL		-	-	-	-	-	F	G	G	F	A	T	L	F	G	E	S	A	G	A	A	S	S	-	H		
AHAGFISH	ACBS_MUNFA		S	E	D	C	L	Y	G	G	F	A	T	V	F	G	E	S	A	G	A	A	S	S	E	H		
ASNAKE	Q86CZ4		D	E	D	C	L	Y	G	G	F	A	T	I	F	G	E	S	A	G	A	A	S	S	E	H		
ASPIDER	Q97110		S	E	D	C	L	Y	G	G	F	A	T	L	F	G	E	S	A	G	A	A	S	S	E	H		
ASQUID	Q5UR02		S	E	D	C	L	H	G	A	F	A	T	I	V	Q	S	A	G	G	I	S	R	E	E	H		
AVIRUS	Q6KAV3		S	E	D	C	L	F	G	G	F	S	T	L	F	G	E	S	S	G	A	V	S	S	E	H		
AIAPHID	Q6KAV4		S	E	D	C	L	F	G	G	F	A	T	L	F	G	E	S	A	G	A	V	S	S	E	H		
AIAPHID	Q87YU9		S	E	D	C	L	Y	G	G	Y	A	T	L	F	G	E	S	A	G	G	S	S	E	E	H		
AIAPHID	Q65YU0		S	E	D	C	L	Y	G	G	Y	A	T	L	F	G	E	S	A	G	G	S	S	E	E	H		
AIAPHID	Q65Z60		S	E	D	C	L	F	G	G	F	A	T	L	F	G	E	S	A	G	A	V	S	S	E	H		
AIAPHID	Q65Z62		S	E	D	C	L	F	G	G	F	A	T	L	F	G	E	S	A	G	A	V	S	S	E	H		
AIAPHID	Q65Z63		S	E	D	C	L	F	G	G	F	A	T	L	F	G	E	S	A	G	A	V	S	S	E	H		
AIAPHID	Q66S75		S	E	D	C	L	Y	G	G	Y	A	T	L	F	G	E	S	A	G	G	S	S	E	E	H		
AIAPHID	Q66S79		S	E	D	C	L	Y	G	G	Y	A	T	L	F	G	E	S	A	G	G	S	S	E	E	H		
AIAPHID	Q8MV35		S	E	D	C	L	F	G	G	F	A	T	L	F	G	E	S	A	G	A	V	S	S	E	E	H	
AIAPHID	Q6BCH8		S	E	D	C	L	F	G	E	G	F	A	T	L	F	G	E	S	A	G	A	V	S	S	E	E	H
AIAPHID	Q8MV36		S	E	D	C	L	Y	G	G	Y	A	T	L	F	G	E	S	A	G	G	S	S	E	E	H		
AIAPHID	Q6KAV5		S	E	D	C	L	F	G	G	F	A	T	L	F	G	E	S	A	G	A	V	S	S	E	E	H	
AIAPHID	Q9BMJ1		S	E	D	C	L	F	G	G	F	A	T	L	F	G	E	S	A	G	A	V	S	S	E	E	H	
AIAPHID	Q7YZQ0		S	E	D	C	L	Y	G	G	Y	A	T	L	F	G	E	S	A	G	G	S	S	E	E	H		
AIAPHID	Q7YZP9		S	E	D	C	L	Y	G	G	Y	A	T	L	F	G	E	S	A	G	G	S	S	E	E	H		
AIAPHID	Q9GQF7		S	E	D	C	L	Y	G	G	F	A	T	I	F	G	E	S	A	G	G	S	S	E	E	H		
AIABEE	ACBS_LEPDE		S	E	D	C	L	Y	G	G	Y	A	T	L	F	G	E	S	A	G	G	S	S	E	E	H		
AIABEETLE			S	E	D	C	L	Y	G	G	Y	A	T	L	F	G	E	S	A	G	G	S	S	E	E	H		

continues

(continues)

TABLE 2. (continued)

Sequence		Oxyanion hole				Active serine			Catalytic triad		
ID	SwissProt code	91	95	116	120	121	135	140	226	327	440
AIWOLWORM	Q86QW5	S E D C L	S E D C L	Y G G G Y	Y G G G Y	A	T L F G E S A G G G S	E	S	E	H
AIWOLWORM	Q8MX85	S E D C L	S E D C L	Y G G G Y	Y G G G Y	A	T L F G E S A G G G S	E	S	E	H
AIWOLWORM	Q5RIH9	S E D C L	S E D C L	Y G G G Y	Y G G G Y	A	T L F G E S A G G G S	E	S	E	H
AIWOLWORM	Q75VX9	S E D C L	S E D C L	F G G G F	F G G G F	A	T L F G E S A G G G S	E	S	E	H
AIWOLWORM	Q75VY0	S E D C L	S E D C L	Y G G G F	Y G G G F	A	T L F G E S A G G G S	E	S	E	H
AIWOLWORM	P91954	S E D C L	S E D C L	Y G G G F	Y G G G F	A	T L F G E S A G G G S	E	S	E	H
AIWOLWORM	ACES_DROME	S E D C L	S E D C L	Y G G G F	Y G G G F	A	T L F G E S A G G G S	E	S	E	H
AIWOLWORM	Q8MXC4	S E D C L	S E D C L	Y G G G F	Y G G G F	A	T L F G E S A G G G S	E	S	E	H
AIWOLWORM	Q95P20	S E D C L	S E D C L	Y G G G F	Y G G G F	A	T L F G E S A G G G S	E	S	E	H
AIWOLWORM	Q7YZP7	S E D C L	S E D C L	Y G G G F	Y G G G F	A	T L F G E S A G G G S	E	S	E	H
AIWOLWORM	Q8MXC8	S E D C L	S E D C L	Y G G G F	Y G G G F	A	T L F G E S A G G G S	E	S	E	H
AIWOLWORM	Q8MVZ4	S E D C L	S E D C L	Y G G G Y	Y G G G Y	A	T L F G E S A G G G S	E	S	E	H
AIWOLWORM	Q8MXC9	S E D C L	S E D C L	Y G G G F	Y G G G F	S	T L F G E S A G G G S	E	S	E	H
AIWOLWORM	Q95WV7	S E D C L	S E D C L	Y G G G F	Y G G G F	A	T L F G E S A G G G S	E	S	E	H
AIWOLWORM	Q7YVJ9	S E D C L	S E D C L	Y G G G F	Y G G G F	A	T L F G E S A G G G S	E	S	E	H
AIWOLWORM	Q8MU94	S E D C L	S E D C L	Y G G G Y	Y G G G Y	A	T L F G E S A G G G S	E	S	E	H
AIWOLWORM	Q8MXC5	S E D C L	S E D C L	Y G G G Y	Y G G G Y	A	T L F G E S A G G G S	E	S	E	H
AIWOLWORM	Q8MXC6	S E D C L	S E D C L	Y G G G F	Y G G G F	A	T L F G E S A G G G S	E	S	E	H
AIWOLWORM	Q8MXC7	S E D C L	S E D C L	Y G G G F	Y G G G F	A	T L F G E S A G G G S	E	S	E	H
AIWOLWORM	Q7YZP8	S E D C L	S E D C L	Y G G G F	Y G G G F	A	T L F G E S A G G G S	E	S	E	H
AIWOLWORM	Q5WIL0	S E D C L	S E D C L	Y G G G Y	Y G G G Y	A	T L F G E S A G G G S	E	S	E	H
AIWOLWORM	Q9NH6	S E D C L	S E D C L	Y G G G Y	Y G G G Y	A	T L F G E S A G G G S	E	S	E	H
AIWOLWORM	ACES_ANOGA	S E D C L	S E D C L	F G G G F	F G G G F	A	T L F G E S A G G G S	E	S	E	H
AIWOLWORM	ACES_ANOST	S E D C L	S E D C L	F G G G F	F G G G F	A	T L F G E S A G G G S	E	S	E	H
AIWOLWORM	ACES_CULPI	S E D C L	S E D C L	F G G G F	F G G G F	A	T L F G E S A G G G S	E	S	E	H
AIWOLWORM	Q5XL61	S E D C L	S E D C L	F G G G F	F G G G F	A	T L F G E S A G G G S	E	S	E	H
AIWOLWORM	Q6A2E2	S E D C L	S E D C L	F G G G F	F G G G F	A	T L F G E S A G G G S	E	S	E	H
AIWOLWORM	Q7RTL9	S E D C L	S E D C L	Y G G G F	Y G G G F	A	T L F G E S A G G G S	E	S	E	H
AIWOLWORM	Q9TX11	S E D C L	S E D C L	Y G G G F	Y G G G F	A	T L F G E S A G G G S	E	S	E	H
AIWOLWORM	Q7RTM0	S E D C L	S E D C L	Y G G G F	Y G G G F	A	T L F G E S A G G G S	E	S	E	H
AIWOLWORM	Q8MZL2	S E D C L	S E D C L	Y G G G Y	Y G G G Y	A	T L F G E S A G G G S	E	S	E	H
AIWOLWORM	Q5S579	S E D C L	S E D C L	F G G G F	F G G G F	A	T L F G E S A G G G S	E	S	E	H
AIWOLWORM	Q8MZM0	S E D C L	S E D C L	Y G G G F	Y G G G F	A	T L F G E S A G G G S	E	S	E	H
AIWOLWORM	Q61987	S E D C L	S E D C L	Y G G G F	Y G G G F	A	T L F G E S A G G G S	E	S	E	H
AIWOLWORM	Q7RTL6	S E D C L	S E D C L	Y G G S F	Y G G S F	A	T L F G E S A G G G S	E	S	E	H
AIWOLWORM	Q7RTL7	S E D C L	S E D C L	Y G G S Y	Y G G S Y	A	T L F G E S A G G G S	E	S	E	H
AIWOLWORM	Q7LSU5	S E D C L	S E D C L	Y G G S F	Y G G S F	A	T L F G E S A G G G S	E	S	E	H
AIWOLWORM	Q7LSU7	S E D C L	S E D C L	Y G G S F	Y G G S F	A	T L F G E S A G G G S	E	S	E	H
AIWOLWORM	Q86GL8	S E D C L	S E D C L	Y G G S F	Y G G S F	A	T L F G E S A G G G S	E	S	E	H
AIWOLWORM	Q6XR73	S E D C L	S E D C L	Y G G G F	Y G G G F	A	T L F G E S A G G G S	E	S	E	H
AIWOLWORM	Q61864	S E D C L	S E D C L	Y G G G F	Y G G G F	A	T L F G E S A G G G S	E	S	E	H
AIWOLWORM	Q9NFK1	S E D C L	S E D C L	Y G G G F	Y G G G F	A	T L F G E S A G G G S	E	S	E	H
AIWOLWORM	Q6WVH4	S E D C L	S E D C L	Y G G G F	Y G G G F	A	T L F G E S A G G G S	E	S	E	H
AIWOLWORM	Q9NFK4	S E D C L	S E D C L	Y G G G F	Y G G G F	A	T L F G E S A G G G S	E	S	E	H

APTICK	Q9NFK2	- E D C L	Y G G T F A	T L V G Q S A G A I S	S	E	H
APTICK	O45210	S E D C L	H G G G F A	T L F G W S A G G I S	S	E	H
APTICK	Q9NFK3	S E D C L	H G G G F A	T L F G W S A G G I S	S	E	H
APTICK	Q6XR74	S E D C L	H G G G F A	T L F G W S A G G I S	S	E	H
APTICK	Q6XR75	S E D C L	H G G G F A	T L F G W S A G G I S	S	E	H
APTICK	O62563	S E D C L	H G G G F A	T L F G W S A G G I S	S	E	H
AW	ACE1_CAEBR	S E D C L	Y G G G F A	T L F G E S A G A A S	S	E	H
AW	ACE1_CAEBL	S E D C L	Y G G G F A	T L F G E S A G A A S	S	E	H
AW	O61371	S E D C L	Y G G G F A	T L F G E S A G A A S	S	E	H
AW	O61378	S E D C L	Y G G G F A	T L F G E S A G A A S	S	E	H
AW	O61587	S E D C L	Y G G G F A	T L F G E S A G A A S	S	E	H
AW	O96529	S E D C L	Y G G G F A	T L F G E S A G A A S	S	E	H
AW	Q6QDP4	S E D C L	Y G G G F A	T L F G E S A G A A S	S	E	H
AW	Q6QDP5	S E D C L	Y G G G F A	T L F G E S A G A A S	S	E	H
AW	Q6XPY6	S E D C L	Y G G G F A	T L F G E S A G A A S	S	E	H
AW	Q9XYA9	S E D C L	Y G G G F A	T L F G E S A G A A S	S	E	H
AW	Q71JB7	S E D C L	Y G G G F A	T L F G E S A G A A S	S	E	H
AW	Q86GL7	S E D C L	Y G G G F A	T L F G E S A G A A S	S	E	H
AW	Q9U640	S E D C L	Y G G G F A	T L F G E S A G A A S	S	E	H
AW	Q967G8	S E D C L	Y G G G F A	T L F G E S A G A A S	S	E	H
AW	Q8IT86	T E D C L	Y G G G F A	T L F G E S A G A A S	G	E	H
AW	Q9GFL0	S E D C L	Y G G G F A	T L F G E S A G A A S	S	E	H
BAMPHIOXUS	CHL1_BRALA	S E D C L	Y G G G F A	T I F G E S A G A A S	S	E	H
BAMPHIOXUS	CHL2_BRALA	- - -	Y G G G F A	S I F G E S A G A A S	S	E	-
BAMPHIOXUS	O76998	S E D C L	Y G G G F A	T I F G E S A G A A S	S	E	H
BAMPHIOXUS	O76999	S E D C L	Y G G G F A	S I F G E S A G A A S	S	E	H
BBCHICK	Q90ZK8	S E D C L	Y G G G S A	T I F G E S A G A A S	S	E	H
BFUNGUS	Q6MG12	- E D C L	Q G G G F A	V L G G A S A G A A S	S	D	H
BFUNGUS	Q872U5	G E N C L	H G G A F A	T I M G L S A G A H S	S	E	H
EM	CHLE_FELCA	S E D C L	Y G G G F A	T L F G E S A G A A S	S	E	H
EM	CHLE_HORSE	S E D C L	Y G G G F A	T L F G E S A G A A S	S	E	H
EM	CHLE_HUMAN	S E D C L	Y G G G F A	T L F G E S A G A A S	S	E	H
EM	CHLE_MOUSE	S E D C L	Y G G G F A	T I F G E S A G A A S	S	E	H
EM	CHLE_PANTT	S E D C L	Y G G G F A	T L F G E S A G A A S	S	E	H
EM	CHLE_RABIT	S E D C L	Y G G G F A	T L F G E S A G A A S	S	E	H
EMHORSE	Q9NIN9	S E D C L	Y G G G F A	T L F G E S A G A A S	S	E	H
BMP1G	Q9GKJ6	- - -	Y G G G F A	T L F G E S A G A A S	S	E	H
BMRAT	Q9JKC1	S E D C L	Y G G G F A	T L F G E S A G A A S	S	E	H
BOIKOPLURA	Q675X9_t	S E D C L	H G G G F A	S F S A R S S G A E I	N	W	E

*One hundred eighteen AChE sequences are listed first, followed by 17 BuChE sequences. Sequences are roughly clustered as mammals (AM... or BM...), fish (AF...), insects (AL...), pests (AP...), worms (AW...), fungi, and virus. Dashes indicate missing sequence fragments. Sequences were aligned using BioEdit version 7.0.1 software interface (Hall, 1999).

covering the AChE active center gorge (Bücht *et al.*, 1994). Lastly, Ser226 is conserved in 122 of 125 sequences. Located in the spatial vicinity of the active Ser200 and the other two residues of the catalytic triad, it is positioned to be directly involved in catalytic reaction. Its substitution with asparagine, observed in the AChE of embryonic lethals in zebrafish (Behra *et al.*, 2002), rendered zebrafish AChE inactive. Similarly, substitution of this serine with alanine in *Torpedo* and mouse AChEs yielded inactive mutants (Z. Radić, unpublished data). Serine at the homologous position is fully conserved in the structurally related carboxylesterase family and in several lipases (Stok *et al.*, 2004). Ser247Ala and Ser247Gly mutants of rat carboxylesterase ES10, at a position two- and three-dimensionally equivalent to Ser226 of *Torpedo* AChE, were found to be only 5- to 15-fold less active than the wild-type carboxylesterase in hydrolysis of the substrate *p*-nitrophenylacetate (Stok *et al.*, 2004). Rat carboxylesterase ES10 shares 31% identity and 55% amino acid sequence similarity with *Torpedo* AChE.

Most cholinesterase sequences include at least seven cysteines. Six cysteines are usually involved in the formation of three intramolecular disulfide loops, and the seventh one, closest to the C-terminal end, is through intermolecular bond involved in the formation of covalent AChE homodimers (MacPhee-Quigley *et al.*, 1986). Two of three intramolecular cysteine loops have Ω configuration exposed on the protein surface. Their sequence conservation is shown in Table 3. Out of a total of 125 ChE sequences shown in Tables 2 and 3, 120 are fully known in the fragment Cys67–Cys94. All of them contain two cysteines, potentially capable of forming a disulfide loop, whereas in the fragment Cys254–Cys265 117 ChEs out of 125 have the ability to make a disulfide loop. A high degree of conservation of a disulfide bond within fragment Cys67–Cys94, known as the “big Ω loop” or just “ Ω loop,” is consistent with its location on top of the active center gorge, it is the gorge the thinnest of walls that separate from the bulk solvent. Most insects have an additional one or two cysteines located next to Ω loops or between second and third loops that most likely remain unpaired.

Several aromatic residues appear very well conserved in cholinesterases, including tyrosines 148, 420, 421, 130, and 334; phenylalanines 187, 197, 155, 45, 448, and 476; and tryptophanes 179, 114, 84, 233, 432, 435, and 492.

Insects carrying two AChE genes include mosquitoes and aphids, and their sequences are shown in Table 4 in parallel to *T. californica* and *D. melanogaster* sequences. Clearly, two sequences found in each insect appear significantly different. Intraspecies sequence comparisons yield only 36–40% identity, but interspecies comparison of like sequences within each cluster shows larger (60–99%) identity. Both clusters of sequences have approximately 40% identity with *Torpedo* AChE. One of the two clusters (the lower one in the Table 4), however, shares significantly

higher (56–71%) identity with *Drosophila* AChE than the 36–40% identity shared by the other cluster. Worms can carry up to four AChE genes, showing generally similar (approximately 40%) intraspecies identity, with interspecies similarity less pronounced than that observed in insects.

B. Secondary and Tertiary Structure

Several fragments in sequences of cholinesterases are likely to form an α -helical secondary structure, as confirmed by three-dimensional structures of both AChE and BuChE. Obtaining three-dimensional structures of ChEs, AChEs, and BuChEs was not trivial, however. The first studies on the three-dimensional structure of an AChE were done using AChE crystals obtained from protein purified from the electric organ of the freshwater eel (*Electrophorus electricus*) (Chothia and Leuzinger, 1975; Schrag *et al.*, 1988), but insufficient quality of the electron diffraction data prevented its immediate solution. An abundant source of the enzyme and an improved purification scheme proved critical to obtain large (milligram) quantities of the enzyme protein in a state more homogeneous than that possible for *E. electricus* AChE (Taylor *et al.*, 1974) consequently the first successful three-dimensional structure determination was done for AChE of a saltwater fish, *T. californica*, at 2.8 Å resolution (original PDB code, 1ace; Sussman *et al.*, 1991). Several years later, it was realized that in the active center of the solved AChE structure, the inhibitor decamethonium was bound, whose electron density was initially interpreted as an array of water molecules (Raves *et al.*, 1997). Decamethonium, originally used in the purification protocol to elute AChE bound to affinity chromatography column, remained in a complex with AChE despite exhaustive dialysis. This results from a high concentration of AChE in the dialysis bag, exceeding the K_D of decamethonium by several orders of magnitude. This fortunate coincidence was important for the successful solution of the *T. californica* AChE three-dimensional structure and indicated that the structure of a ligand-free AChE would be more difficult to obtain. Accordingly, the determination of crystal structures of mammalian AChEs from mouse (PDB code, 1mah; Bourne *et al.*, 1995) and man (PDB code, 1b41; Kryger *et al.*, 2000) was initially possible only in complex with the potent inhibitor, snake venom toxin fasciculin 2. The first ligand-free AChE structures were obtained later (Raves *et al.*, 1997; Bourne *et al.*, 2004), requiring the use of different inhibitors for enzyme elution. *Drosophila melanogaster* AChE is the only insect AChE with a known three-dimensional structure (Harel *et al.*, 2000).

Because of extensive glycosylation, crystallization of BuChE was more difficult. BuChEs typically have seven to nine N-linked oligosaccharides, instead of the three or four oligosaccharides found in AChEs. Only recombinant-derived, partially deglycosylated BuChE containing five oligosaccharides instead of nine appeared sufficiently

[illegible]

AW 061587
 AW 096529
 AW Q6QDP4
 AW Q6QDP5
 AW Q6QDP6
 AW Q9XTA9
 AW Q7LJB7
 AW Q86GL7
 AW Q9U640
 AW Q967G8
 AW Q8IT86
 AW Q9GFL0

BAMPHIOXUS
 CHL1_BRALA
 CHL2_BRALA
 BAMPHIOXUS 076998
 BAMPHIOXUS 076999
 BBCHICK Q90XK8
 BFUNGUS Q6MG12
 CBFUNGUS Q872U5
 CHLE_FELCA
 CHLE_HORSE
 CHLE_HUMAN
 CHLE_MOUSE
 CHLE_PANTT
 CHLE_RABIT
 Q9NIN9
 BEMORSE Q9GKJ6
 BEMFIG Q9JKC1
 BEMRAT
 BOIKOPIEURA Q675X9_t

C F Q T K D E T Y P G F D G A E M W N P P T E L S E D C
 C V Q S P D T Y F G D F Y G A T M W N S N T P C S E D C
 C F L T I D T S F P P G A E M W N P P N S I G E D C
 C M L T P D T N F G E F P G S E M W N P P E T I S E D C
 C F L T I D T S F P P G A E M W N P P N S I G E D C
 C V Q S P D T Y F G D F Y G A T M W N S N T P C S E D C
 C F F S R D T M F P D F P G A E M W N P P N D I D E D C
 C M L T K D E S F L G F P G S E M W N P P E T I S E D C
 C F Q S K D E T Y P G F D G A E M W N P P T D L S E D C
 C F Q T P D G Y F P G F L G S E M W N A P T E L S E D C
 C F H F P D S K F K G F R G S E M W N P K G N M T E D C
 C M L T P D T N F G E F P G S E M W N P P E S I S E D C

C V E N D A D T I Y E C
 C G N G N M D E V L R C
 C T S K D A S S I H N C
 C V D I D P S A V L E C
 C T S K D A S S I H N C
 C G N G N M D E V L R C
 C S N G A M Q N I V E C
 C A D I D P S A V L E C
 C V E N N V D K I Y E C
 C F D E A V A D I Y R C
 C T K K D P N T V H R C
 C V D I D P S A V L E C
 C S A D D M D V L V A C
 C S T D D I E E T I E C
 C S A E D M D A L V A C
 C S T D D L E E T I E C
 C P T S D E T E L I L C
 C A R S - A A A S L T C
 V D G - D D Q I F D
 C S K E N D T E I I K C
 C S R D N E T E I I K C
 C S R E N E T E I I K C
 C S K E N E M E I I K C
 C S K E N D T E I I K C
 C S T E N E T E I I K C
 C S R D N E T E I I K C
 C S R E N E T E I I K C
 C S K E N E K E I I T C
 P C M F M T D K L G

One hundred eighteen AChE sequences are listed first, followed by 17 BuChE sequences. Sequences are roughly clustered as mammals, fish, insects, pests, worms, fungi, and virus. Only cysteine residues are shown, except within two Ω loops. Dashes indicate missing sequence fragments. Sequences were aligned using BioEdit software interface (Hall, 1999).

TABLE 4. Alignment of AChEs Found in Four Insects Carrying Two AChE Genes Each^a

	10	20	30	40	50	60	70	80	90	100	110	120
<i>Torpedo californica</i>												
<i>Drosophila melanogaster</i>												
<i>Aphis gossypii</i> 2												
<i>Anopheles gambiae</i> 1												
<i>Aedes aegypti</i> 11												
<i>Rhopalosiphum padi</i> 1												
<i>Rhopalosiphum padi</i> 2												
<i>Aphis gossypii</i> 11												
<i>Anopheles gambiae</i> 2												
<i>Aedes aegypti</i> 2												
<i>Torpedo californica</i>												
<i>Drosophila melanogaster</i>												
<i>Aphis gossypii</i> 2												
<i>Anopheles gambiae</i> 1												
<i>Aedes aegypti</i> 11												
<i>Rhopalosiphum padi</i> 1												
<i>Rhopalosiphum padi</i> 2												
<i>Aphis gossypii</i> 11												
<i>Anopheles gambiae</i> 2												
<i>Aedes aegypti</i> 2												
<i>Torpedo californica</i>												
<i>Drosophila melanogaster</i>												
<i>Aphis gossypii</i> 2												
<i>Anopheles gambiae</i> 1												
<i>Aedes aegypti</i> 11												
<i>Rhopalosiphum padi</i> 1												
<i>Rhopalosiphum padi</i> 2												
<i>Aphis gossypii</i> 11												
<i>Anopheles gambiae</i> 2												
<i>Aedes aegypti</i> 2												

<i>Torpedo californica</i>	PHANDLGDAVTLOTTDNDNGIKNRGLDDIVGHRVLCPLMHVFNKTKFNGTLYFENHRASNIWPEWNGVHGVETFEVFGFLPVKELNYTAEELSRIMHYWATPAKTG	480
<i>Drosophila melanogaster</i>	GR--QARE.IIF...S.E--P.YQ.QOQIGRA...FFT..TNEVAQALAE--VHY.Y.T.T.TSL.G....L.D..YF..Q.NMS---RPV.RE.GK.MLSAVIE....	470
<i>Aphys gossypii</i> 2	.N.DAIVKS.IEFE...FNP.DPE...NA..KM...YQFT.VNNE.AH..ALT..--V.M.Y.K..SL.NP..K.T..M..D..SY...D..NENK.G.EI..IE..KKM.R..TN....	460
<i>Anopheles gambiae</i> 1	.YV.GAARQ.IVFE...TEPD.FNS...A..KM...YHFT.VNNE.AOR.AEE--V.M.LYT..SKGNP..R.T..M..D..NY...E..NPT.G..ED.KDF..K.R..SN....	450
<i>Aedes aegypti</i> 11	.YV.GAARQ.IVFE...TEPE.FNS...A..KM...YHFT.VNNE.AOR.AEE--V.M.LYT..SKGNP..R.T..M..D..NY...E..NSD.G.MED.KDF..K.R..SN....	440
<i>Rhopalosiphum padi</i> 1	.N.DAIVKS.IEFE...FSP.DPE...NA..KM...YQFT.VNNE.AH..ALT..--V.M.Y.K..SL.NP..K.T..M..D..SY...D..NENK.R.EI..IE..KKM.R..TN....	430
<i>Rhopalosiphum padi</i> 2	KD--Q.ER..IY..SQ.EKKDDIYS.QKQ.S.V.A.YFV..TNL.A.IVSSR..--V.Y...T..TDSHL.GD...L.D.MQY...H..NMS---N.R.RD..I..EAFTR.SL..	420
<i>Aphys gossypii</i> 1	KD--Q.ER..IY..SQ.EKKDDIYS.QKQ.S.V.A.YFV..TNL.A.IVSSR..--V.Y...T..TDSHL.GD...L.D.MQY...HL.NMS---N.R.RD..I..EAFTR.SL..	410
<i>Anopheles gambiae</i> 2	NK--EPERE.IIF...G.ES--D.YQ.QOQVGRS...FF...TNE.ALGL.ER..--VHY.Y.T.T.TSL.G....L.D.V.YI..Q.NNAS---RQR.RD...MVLSEVSE..R..	400
<i>Aedes aegypti</i> 12	SK--EPERE.IIF...G.ES--D.YQ.QOQVGRS...FF...TNE.ALGLAER..--V.Y.Y.T.T.TSL.G....L.D.V.YI..Q.NMVS---RQR.RD...MVLSEVSE..RS.	390
<i>Torpedo californica</i>	NPNEPHQESKWPFTTKQKIDINTPEMKVHORLEVMCMVFNQFLPKLLNATACDGLSSSGTSSSKGIIFYVLPFSLYLIF	380
<i>Drosophila melanogaster</i>GE..N.SKEDPVYIFS.DD..LARGPLAAR.S...DY...VSW.G.TCDG-G.AS-----	370
<i>Aphys gossypii</i> 2	..EGSWTP...VH.AYKGE.LT.D.NNTSIGVGP.LEQ.A..KNV.D.TAISKMK-SDKN-----	
<i>Anopheles gambiae</i> 1	..-ASSEFP-E..KH.AHGRHYLE.GINTSF.GRGP.LEQ.A..KKY.Q.VA..SN-LPPP.EP-----	
<i>Aedes aegypti</i> 11	..-PNSDFF-E..KH.AHGRHYLE.GINTSF.GRGP.LEQ.A..KKY.Q.VA..SN-LQAP.EP-----	
<i>Rhopalosiphum padi</i> 1	..EGSWTP...VH.AYKGE.LT.D.NNTSIGVGP.LEQ.A..KNV.D.TAISKMK-SDKN-----	
<i>Rhopalosiphum padi</i> 2	T.....DD...YNESKPIYHW.AAE..-GYGP.AAE.Q...G.F..IQALKETSK.DYPD-----	
<i>Aphys gossypii</i> 1	T.....DD...YNESKPIYHW.AAE..-GYGP.AAE.Q...G.F..IQALKETSK.DYPD-----	
<i>Anopheles gambiae</i> 2GH...Y.RENPYIFIF.A.GE.YGRGPMTS.A..D..R.AMSVFLKDDHT-----	
<i>Aedes aegypti</i> 12GH...VY.KENPIYFIF.A.GE.YGRGPMTA.A..D..R.AMSVPPKSI.EOT-----	

^a*Torpedo californica* and *Drosophila melanogaster* sequences were added for comparison. Only residues differing from those found in *Torpedo* sequence are listed by letter. Dashes indicate gaps in sequence. Sequences were aligned using BioEdit version 7.0.1 software interface (Hall, 1999).

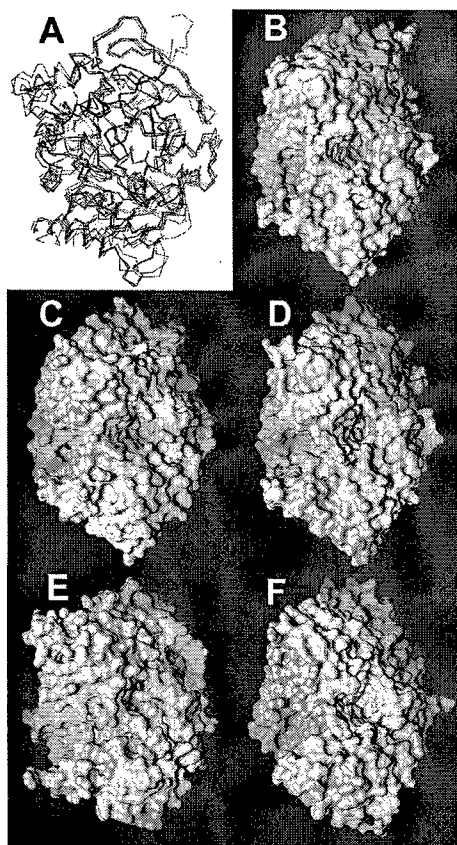


FIG. 1. Three-dimensional structures of five ChEs. (A) Overlay of C α backbone of all five structures. (B–F) Solvent-accessible surfaces of individual enzymes: (B) *Torpedo* AChE, (C) mouse AChE, (D) human AChE, (E) *Drosophila* AChE, and (F) human BuChE. Active center gorge is indentation in the center of each structure. Visualized by WebLabViewer software (Accelrys, San Diego).

homogeneous for crystallization (Nachon *et al.*, 2002; Nicolet *et al.*, 2003). The protein backbones of the five mentioned ChE structures, four AChEs and one BuChE, overlay reasonably well, with only *Drosophila* AChE showing slightly larger deviations (Fig. 1A; Table 5). The common fold includes a twisted β pleated sheet (approximately 10 strands long) in the core of the enzyme molecule, surrounded by more than 12 longer and shorter α -helices. Such unique distribution of elements of the secondary structure was recognized first in ChEs and lipases and then in a number of other proteins, and it was consequently termed the α/β hydrolase fold (Cygler *et al.*, 1993). Catalytically active residues in enzymes belonging to this fold are located almost in the center of a globular protein, at the bottom of a narrow, approximately 20 Å deep active center gorge. The shape and size of the gorge are similar in *Torpedo*, mouse, and human AChEs, but despite similarity in the backbone fold, the respective volumes of gorges in human BuChE and *Drosophila* AChE are approximately 50–100% larger and 50% smaller than in mammalian and fish AChEs (Harel *et al.*, 2000; Saxena *et al.*, 1999). This significant structural difference likely affects the ability of ChEs to effectively hydrolyze ACh (Fig. 2). Hydrolysis appears more efficient in the active center gorges of fish and mammalian AChEs than in either the smaller volume gorge of *Drosophila* AChE or the larger volume gorge of BuChE.

To date, 61 cholinesterase structures have been deposited in the Protein Data Bank. Forty are of *T. californica* AChE, nine of mouse AChE, three of *Drosophila* AChE, two of human AChE, and seven of human BuChE. Overlaying of all *Torpedo* AChE structures reveals exceptional similarity in their protein backbone (Fig. 3A) and even in their side chain conformations (Fig. 3B). The mean value of the root mean square (RMS) deviation of the 40 *Torpedo* AChE structures from the alpha carbon trace of the highest resolution (1.8 Å), unliganded 1ea5 structure is only 0.26 ± 0.10 Å. Twelve

TABLE 5. Structural Pairwise Overlays of Five Unliganded ChE Structures^a

ChE	PDB ID No.	Resolution (Å)	RMS (C α backbone) (Å)					
			<i>Torpedo californica</i> AChE	Mouse AChE		Human AChE	<i>Drosophila melanogaster</i> AChE	Human BuChE
				Chain A	Chain B			
<i>Torpedo californica</i> AChE	1ea5	1.8	0	0.76	0.74	0.87	1.2	0.95
Mouse AChE	1j06	2.4	0.76 (chain A) 0.74 (chain B)	0	0.24	0.56 (chain A) 0.55 (chain B)	1.2 (chain A) 1.2 (chain B)	0.86 (chain A) 0.86 (chain B)
Human AChE	1b41	2.8	0.87	0.56	0.57	0	1.2	0.88
<i>Drosophila melanogaster</i> AChE	1q09	2.7	1.2	1.2	1.2	1.2	0	1.1
Human BuChE	1p0i	2.0	0.95	0.86	0.86	0.88	1.1	0

^aOnly C α backbone atoms were used in pairwise alignments. Sequences were overlaid and RMS was calculated using SwissPDBViewer version 3.7 software interface.

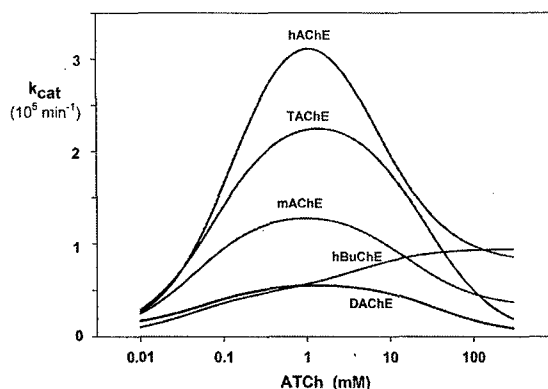


FIG. 2. Activity of ChEs (expressed as k_{cat}) as a function of substrate acetylthiocholine (ATCh) concentration. Curves (except for DAcHE) were calculated using Eq. (1) and literature values of catalytic constants: hAChE and hBuChE from Kaplan *et al.* (2001), TAcHE from Radic *et al.* (1992), and mAChE from Radic *et al.* (1993). The DAcHE curve was calculated using the equation and data from Stojan *et al.* (1998). All constants were determined at room temperature except for hAChE and hBuChE, which were determined at 27 °C, contributing to relatively higher k_{cat} values compared to TAcHE, mAChE, and DAcHE.

unliganded AChEs are only slightly more similar to the 1ca5 with a mean RMS value of 0.20 ± 0.08 Å compared to an RMS of 0.28 ± 0.10 Å for the remaining 28 liganded structures. This is further emphasized in complexes of mouse AChE, in which RMS variation between subunits of the same structure (mean RMS, 0.25 Å) appeared even slightly larger than RMS deviation between the same protein chains of different structures (mean RMS, 0.21 Å), indicating that the effect of packing identical subunits within the same structure perturbed the backbone conformation more than the presence of bound ligand. Even structures containing ligands forming a covalent bond with the AChE active serine did not differ in their RMS from noncovalent ones. The high degree of similarity and small RMS values found also for mouse and *Drosophila* AChEs and human BuChE suggest that binding of ligands to cholinesterases in general is not associated with large conformational changes of the protein backbone. However, dimensions of substrate molecules appear similar to or larger than the size of the AChE gorge that they need to traverse on the way to the active serine at its bottom. The tight entry of a substrate molecule into the narrow site of catalysis in the active center is thus possibly facilitated by a series of fast, small amplitude side chain motions, occurring repeatedly at time intervals far shorter than the catalytic cycle. The absence of structural evidence of large backbone movements in AChE structures may therefore result from evolutionary pressure to achieve and maintain their very fast catalytic turnover. Every AChE molecule (depending on the species) can turn over between 200 and 16,000 molecules of ACh every second or 1 molecule in as short as 63 μ sec (Nolte

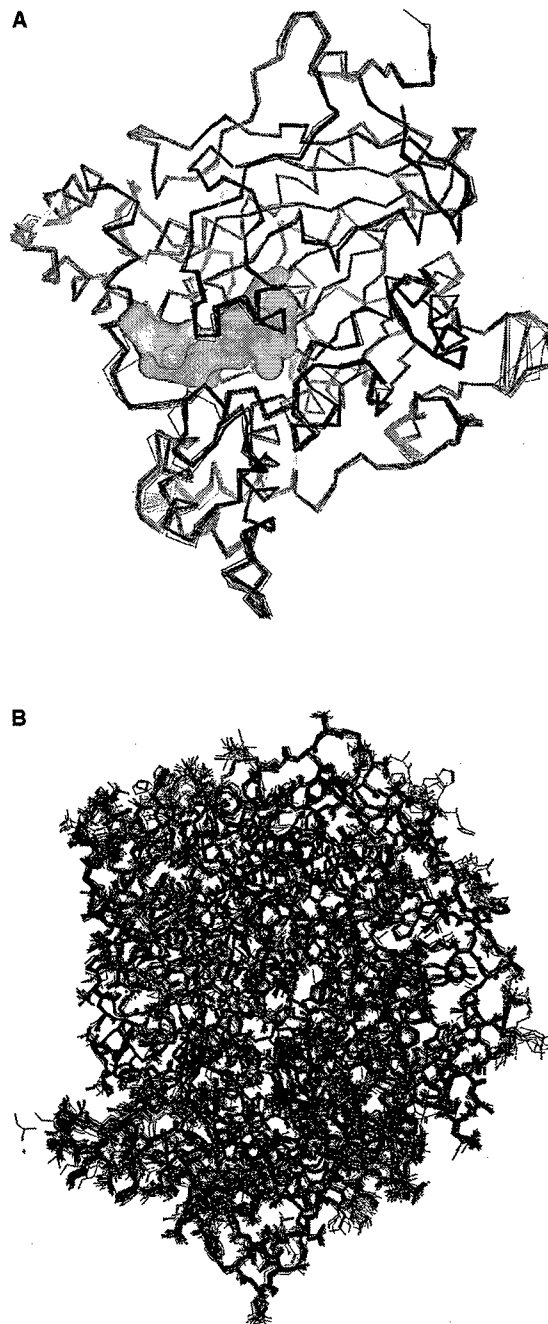


FIG. 3. Overlay of 40 *Torpedo californica* AChE structures using only C α backbone atoms. (A) Trace of C α backbone atoms with combined volume of all ligands found in structures represented as a solvent-accessible surface. (B) Representation of all enzyme atoms found in 40 overlaid structures. Structures were overlaid using SwissPDBViewer software. Visualized by WebLabViewer software (Accelrys, San Diego).



FIG. 4. Topography of binding sites in ChEs represented by selected residue side chains of *Torpedo* AChE structure. A molecule of ACh docked in the active center (taken from PDB entry 2ACE) and shown as solvent-accessible surface is given as a frame of reference. Binding sites are acyl pocket (residues 288 and 290), choline binding site (residues 84 and 330), and peripheral site (residues 70, 72, 121, and 279). Visualized by WebLabViewer software (Accelrys, San Diego).

et al., 1980). Continuous repetition of backbone movements would possibly require both more time and more energy invested per each hydrolytic cycle. These molecular motions have to be fast enough to allow diffusion-limited binding of relatively large ligands. Catalytic turnover of BuChEs is slower despite the much larger opening and larger volume of the active center gorge. Due to the absence of aromatic amino acid side chains lining the AChE gorge, approximately 20 water molecules found in either of the structures or substrate molecules may be retained along the gorge walls by hydrogen bonding and electrostatic interactions. This could inherently slow down catalysis, which may be even slower in the more water-accessible, and thus less hydrophobic, catalytic site of BuChE. Most of the volume of the AChE active center gorge seems to be well accessible to ligand binding judging from the combined volume of all ligands in active center gorges of 40 superimposed *Torpedo* AChE structures totaling approximately 1100 Å³ (Fig. 3A) and filling practically 1000 Å³ of the available gorge space (calculated by CASTp software; Liang *et al.*, 1998).

1. TOPOGRAPHY OF BINDING SITES IN ChEs

In the immediate vicinity of catalytic triad residues at the base of the active center gorge, just above the active serine, is located the electrophilic oxyanion hole, which has the capacity to attract carbonyl oxygen of ACh and other substrates as well as phosphyl oxygen of covalent, OP inhibitors. Three backbone nitrogens well conserved throughout the cholinesterase family (Table 2) form the oxyanion hole, lending their amide protons for the interaction. In oxyanion holes of proteases, only two donor residues are involved. Site-directed mutagenesis of AChEs and use of substrates and inhibitors specific for interaction with either AChE or BuChE helped delineate specific locations of additional ligand binding sites within the enzyme gorge (Shafferman *et al.*, 1992a; Vellom *et al.*, 1993; Ordentlich *et al.*, 1993; Radi *et al.*, 1993). The acyl pocket and the choline binding site are located next to the active serine, at the base of the active center gorge (Fig. 4), controlling the size of ligands that can approach the site of catalysis. The space available for binding is generally smaller in AChEs in which several aromatic residues (14 in fish and mammalian AChEs; Sussman *et al.*, 1991) line the walls of the gorge. In the acyl pocket, in place of phenylalanines Phe288 and Phe290 found in AChEs smaller aliphatic residues are found in BuChEs, whereas in the choline binding site Phe-330 (many AChEs have tyrosine at this position) in BuChEs is replaced by alanine (Table 6). The smaller residues and larger available space in BuChE enable preferential binding of the large substrates butyrylthiocholine and benzoylcholine in the acyl pocket and large inhibitors ethopropazine and isoOMPA in the choline binding site and acyl pocket, respectively. Some mutant insects (mosquitoes and flies) that developed resistance to pesticides have amino acid residues altered in this region in their AChEs, selectively preventing binding of pesticides to active serine while not compromising catalysis (Menozi *et al.*, 2004). In addition to the choline binding site and acyl pocket in the third binding domain of cholinesterases, the peripheral site located at the rim of the gorge, approximately 14 Å from the active serine. Formed by Tyr70, Tyr121, and Trp 279, this aromatic cluster specifically binds cationic and aromatic inhibitors that are too large to enter the gorge, such as propidium, gallamine, or snake toxins fasciculins (Bourne *et al.*, 1995, 2004), or long and slender bisquaternary ligands that extend from the bottom of the gorge, such as BW286c51, decamethonium, and a variety of bifunctional ligands including *bis*-tacrine, *bis*-hyperzines, and very high-affinity triazoles (Lewis *et al.*, 2002; Bourne *et al.*, 2004). In the vicinity of the aromatic cluster is Asp72, a specifically located anionic residue lending its stabilizing contribution to ligands binding to the ~6 Å proximal peripheral site and/or ~8 Å distal choline binding site. Devoid of an aromatic cluster in the peripheral site, BuChEs bind most bisquaternary and bifunctional inhibitors with three or four orders of magnitude lower

TABLE 6. Elements of ChE Primary Structures Involved in Ligand Binding as Found in Alignment of 125 ChE Structures^a

Sequence		Peripheral site						Choline binding site			Acyl pocket			
ID	SwissProt code	70	72	121	279	333	334	84	330	331	233	288	289	290
AM	ACES_BOVIN	Y	D	Y	W	V	Y	W	Y	F	W	F	R	F
AM	ACES_FELCA	Y	D	Y	W	V	Y	W	Y	F	W	F	R	F
AM	ACES_HUMAN	Y	D	Y	W	V	Y	W	Y	F	W	F	R	F
AM	ACES_MOUSE	Y	D	Y	W	V	Y	W	Y	F	W	F	R	F
AM	ACES_RABIT	Y	D	Y	W	V	Y	W	Y	F	W	F	R	F
AM	ACES_RAT	Y	D	Y	W	V	Y	W	Y	F	W	F	R	F
AMHUMAN2	Q86YX9	Y	D	Y	W	-	-	W	-	-	W	F	R	F
AMHUMANyt	Q86TM9	Y	D	Y	W	V	Y	W	Y	F	W	F	R	F
AMONKEY	Q67BC1	Y	D	Y	W	V	Y	W	Y	F	W	F	R	F
AMONKEY	Q67BC2	Y	D	Y	W	V	Y	W	Y	F	W	F	R	F
ABCHICK	ACES_CHICK	M	D	T	G	V	Y	W	Y	F	W	F	R	F
ACBRIGSAE	ACE4_CAEBR	T	D	Y	W	I	Y	W	Y	W	W	L	E	F
ACBRIGSAE	Q9NDG9	G	D	W	W	I	Y	W	F	W	W	L	E	F
ACELEGANS	O61459	G	D	W	W	I	Y	W	F	W	W	L	E	F
ACELEGANS	O61372	T	D	Y	W	I	Y	W	Y	W	W	L	E	F
AF	ACES_TORCA	Y	D	Y	W	L	Y	W	F	F	W	F	R	F
AF	ACES_BRARE	F	D	Y	W	L	Y	W	Y	F	W	F	R	F
AF	ACES_ELEEL	Y	D	Y	W	I	Y	W	Y	F	W	F	R	F
AF	ACES_TORMA	Y	D	Y	W	L	Y	W	F	F	W	F	R	F
AHAGFISH	ACES_MYXGL	-	-	A	G	I	Y	-	F	F	W	F	R	F
ASNAKE	ACES_BUNFA	M	D	Y	W	I	Y	W	Y	F	W	F	R	F
ASPIDER	Q86CZ4	V	D	W	E	V	Y	W	Y	F	W	V	E	F
ASQUID	O97110	G	D	Y	W	T	Y	W	Y	F	W	S	Q	F
AVIRUS	Q5UR02	E	K	I	T	Y	N	V	F	V	Y	G	I	N
AIAPHID	Q6KAV3	I	D	Y	W	F	Y	W	Y	F	W	C	F	F
AIAPHID	Q6KAV4	I	D	Y	W	F	Y	W	Y	F	W	C	F	F
AIAPHID	Q8T7U9	E	Y	M	W	L	Y	W	Y	F	W	L	G	F
AIAPHID	Q65YU0	E	Y	M	W	L	Y	W	Y	F	W	L	G	F
AIAPHID	Q65Z60	I	D	Y	W	F	Y	W	Y	F	W	C	F	F
AIAPHID	Q65Z62	I	D	Y	W	F	Y	W	Y	S	W	C	F	F
AIAPHID	Q65Z63	I	D	Y	W	F	Y	W	Y	F	W	C	F	F
AIAPHID	Q66S75	E	Y	M	W	L	Y	W	Y	F	W	L	G	F
AIAPHID	Q66S79	E	Y	M	W	L	Y	W	Y	F	W	L	G	F
AIAPHID	Q8MV35	I	D	Y	W	F	Y	W	Y	F	W	C	F	F
AIAPHID	Q6BCH8	I	D	Y	W	F	Y	W	Y	S	W	C	F	F
AIAPHID	Q8MV36	E	Y	M	W	L	Y	W	Y	F	W	L	G	F
AIAPHID	Q6KAV5	I	D	Y	W	F	Y	W	Y	S	W	C	F	F
AIAPHID	Q9BMJ1	I	D	Y	W	F	Y	W	Y	S	W	C	F	F
AIAPHID	Q7YZQ0	E	Y	M	W	L	Y	W	Y	F	W	L	G	F
AIAPHID	Q7YZP9	-	-	M	W	L	Y	-	Y	F	W	L	G	F
AIBEE	Q9GQP7	E	Y	M	W	L	Y	W	Y	F	W	L	G	F
AIBEETLE	ACES_LEPDE	E	Y	M	W	L	Y	W	Y	F	W	L	G	F
AIBOLLWORM	Q86QW5	E	Y	M	W	L	Y	W	Y	F	W	L	G	F
AIBOLLWORM	Q8MX85	E	Y	M	W	L	Y	W	Y	F	W	L	G	F
AIBUDWORM	Q5RLH9	E	Y	M	W	L	Y	W	Y	F	W	L	G	F
AICULEX	Q75VX9	I	D	Y	W	I	Y	W	Y	F	W	C	E	F
AICULEX	Q75VY0	E	Y	M	W	L	Y	W	Y	F	W	L	G	F
AIFLY	P91954	E	Y	M	W	L	Y	W	Y	F	W	L	S	F
AIFLY	ACES_DROME	E	Y	M	W	L	Y	W	Y	F	W	L	S	F
AIFLY	Q8MXC4	E	Y	M	W	L	Y	W	Y	F	W	L	S	F
AIFLY	Q95P20	E	Y	M	W	L	Y	W	Y	F	W	L	S	F
AIFLY	Q7YZP7	E	Y	M	W	L	Y	W	Y	F	W	L	S	F
AIFLY	Q8MXC8	E	Y	M	W	L	Y	W	Y	F	W	L	S	Y
AIFLY	Q8MVZ4	E	Y	M	W	L	Y	W	Y	F	W	L	G	F

(continues)

TABLE 6. (continued)

Sequence		Peripheral site						Choline binding site			Acyl pocket			
ID	SwissProt code	70	72	121	279	333	334	84	330	331	233	288	289	290
AIFLY	Q8MXC9	E	Y	M	W	L	Y	W	Y	F	W	L	S	Y
AIFLY	Q95WV7	E	Y	M	W	L	Y	W	Y	F	W	L	S	Y
AIFLY	Q7XWJ9	E	Y	M	W	L	Y	W	Y	F	W	L	S	Y
AIFLY	Q8MU94	E	Y	M	W	L	Y	W	Y	F	W	L	S	Y
AIFLY	Q8MXC5	E	Y	M	W	L	Y	W	Y	F	W	L	G	F
AIFLY	Q8MXC6	E	Y	M	W	L	Y	W	Y	F	W	L	S	X
AIFLY	Q8MXC7	E	Y	M	W	L	Y	W	Y	F	W	L	S	F
AIFLY	Q7YZP8	E	Y	M	W	L	Y	W	Y	F	W	L	S	X
AIHOPPER	Q5W1L0	E	Y	M	W	L	Y	W	Y	F	W	L	G	F
AIHOPPER	Q9NJH6	E	Y	M	W	L	Y	W	Y	F	W	L	G	F
AIMOSQTO	ACE1_ANOGA	I	D	Y	W	I	Y	W	Y	F	W	C	E	F
AIMOSQTO	ACES_ANOST	I	D	Y	W	I	Y	W	Y	F	W	C	E	F
AIMOSQTO	ACES_CULPI	I	D	Y	W	I	Y	W	Y	F	W	C	E	F
AIMOSQTO	Q5XL61	I	D	Y	W	I	Y	W	Y	F	W	C	E	F
AIMOSQTO	Q6A2E2	I	D	Y	W	I	Y	W	Y	F	W	C	E	F
AIMOSQTO	Q7RTL9	E	Y	M	W	L	Y	W	Y	F	W	L	G	F
AIMOSQTO	Q9TX11	E	Y	M	W	L	Y	W	Y	F	W	L	G	F
AIMOSQTO	Q7RTM0	E	Y	M	W	L	Y	W	Y	F	W	L	G	F
AIMOTH	Q8MZL2	E	Y	M	W	L	Y	W	Y	F	W	L	G	F
AIMOTH	Q5S579	I	D	Y	W	L	Y	W	Y	F	W	C	E	F
AIMOTH	Q8MZM0	E	Y	M	W	L	Y	W	Y	F	W	L	G	F
APBOOPHILUS	O61987	V	D	Y	T	Q	Y	W	W	F	W	V	D	F
APCIONA	Q7RTL6	I	D	Y	W	L	Y	W	Y	F	W	F	D	F
APCIONA	Q7RTL7	E	D	Y	W	I	Y	W	Y	F	W	F	D	F
APFLUKE	Q71SU5	P	D	Y	D	L	Y	W	Y	F	W	F	S	V
APFLUKE	Q71SU7	P	D	Y	D	L	Y	W	Y	F	W	F	S	V
APFLUKE	Q86GL8	P	D	Y	D	L	Y	W	Y	F	W	F	S	V
APTICK	Q6XR73	L	D	Y	P	Q	Y	W	W	F	W	V	D	F
APTICK	O61864	V	D	Y	T	Q	Y	W	W	F	W	V	D	F
APTICK	Q9NFK1	V	D	Y	T	Q	Y	W	W	F	W	V	D	F
APTICK	Q6WVH4	V	D	Y	T	Q	Y	W	W	F	W	V	D	F
APTICK	Q9NFK4	V	D	Y	T	Q	Y	W	W	F	W	V	D	F
APTICK	Q9NFK2	C	Q	S	N	F	Y	P	Y	F	I	H	A	L
APTICK	O45210	G	V	Q	A	Y	T	W	N	I	G	-	-	-
APTICK	Q9NFK3	G	V	Q	A	Y	T	W	N	I	G	-	-	-
APTICK	Q6XR74	G	V	Q	A	Y	T	W	N	I	G	-	-	-
APTICK	Q6XR75	G	V	Q	A	Y	T	W	N	I	G	-	-	-
APTICK	O62563	G	V	Q	A	Y	T	W	N	I	G	-	-	-
AW	ACE1_CAEBR	S	D	W	W	T	Y	W	Y	F	W	G	D	F
AW	ACE1_CAEEEL	S	D	W	W	T	Y	W	Y	F	W	G	D	F
AW	O61371	T	D	F	D	P	Y	W	Y	W	W	M	T	F
AW	O61378	T	D	F	D	P	Y	W	Y	W	W	M	T	F
AW	O61587	T	D	F	N	P	Y	W	F	W	W	M	E	W
AW	O96529	S	D	W	W	V	Y	W	Y	F	W	A	D	F
AW	Q6QDP4	T	D	F	D	P	Y	W	Y	W	W	M	T	F
AW	Q6QDP5	T	D	F	G	P	Y	W	F	W	W	M	S	F
AW	Q6XPY6	T	D	F	D	P	Y	W	Y	W	W	M	T	F
AW	Q9XYA9	S	D	W	W	V	Y	W	Y	F	W	A	D	F
AW	Q71JB7	S	D	Y	D	P	Y	W	Y	W	W	M	D	F
AW	Q86GL7	T	D	F	S	P	Y	W	F	W	W	M	S	F
AW	Q9U640	S	D	F	N	P	Y	W	F	W	W	M	E	W
AW	Q967G8	T	D	F	I	P	Y	W	F	W	W	M	E	W
AW	Q8IT86	F	D	F	A	P	Y	W	F	F	W	L	T	F

(continues)

TABLE 6. (continued)

Sequence		Peripheral site						Choline binding site			Acyl pocket			
ID	SwissProt code	70	72	121	279	333	334	84	330	331	233	288	289	290
AW	Q9GPL0	T	D	F	Y	P	Y	W	F	W	W	M	S	F
BAMPHIOXUS	CHL1_BRALA	-	-	F	W	V	Y	-	F	W	W	A	D	I
BAMPHIOXUS	CHL2_BRALA	-	-	M	W	L	Y	-	Y	F	W	C	Q	F
BAMPHYOXUS	O76998	A	D	F	W	V	Y	W	F	W	W	A	D	I
BAMPHYOXUS	O76999	L	D	M	W	L	Y	W	Y	F	W	C	Q	F
BBCHICK	Q90ZK8	L	D	E	V	V	Y	W	S	F	W	L	H	I
BFUNGUS	Q6MGI2	Q	A	N	G	G	F	G	G	G	-	P	I	Y
BFUNGUS	Q872U5	D	D	N	K	P	R	C	M	F	A	V	T	W
BM	CHLE_FELCA	N	D	Q	L	V	Y	W	A	F	W	L	S	V
BM	CHLE_HORSE	N	D	Q	V	V	Y	W	A	F	W	L	S	V
BM	CHLE_HUMAN	N	D	Q	A	V	Y	W	A	F	W	L	S	V
BM	CHLE_MOUSE	N	D	Q	R	V	Y	W	A	F	W	L	S	I
BM	CHLE_PANTT	N	D	Q	L	V	Y	W	A	F	W	L	S	V
BM	CHLE_RABIT	N	D	Q	V	V	Y	W	A	F	W	L	S	V
BMHORSE	Q9N1N9	N	D	Q	V	V	Y	W	A	F	W	L	S	V
BMPIG	Q9GKJ6	-	-	Q	V	V	Y	-	A	F	W	L	S	V
BMRAT	Q9JKC1	N	D	Q	K	V	Y	W	A	F	W	R	S	I
BOIKOPEURA	Q675X9	G	T	N	Y	T	G	Q	Y	F	Y	A	N	Y

"One hundred eighteen AChE sequences are listed first, followed by 17 BuChE sequences. Sequences are roughly clustered as mammals, fish, insects, pests, worms, fungi, and virus. Dashes indicate missing sequence fragments. Sequences were aligned using BioEdit software interface (Hall, 1999).

affinity than AChEs (Radić *et al.*, 1993), whereas the affinity of fasciculins is up to eight orders of magnitude weaker than in corresponding AChEs (Radić *et al.*, 1994). The absence of the aromatic cluster does not critically influence ACh hydrolysis in BuChEs, and its substitution with aliphatic residues in AChEs does not seem to affect catalytic parameters; however, substitution of Asp72 has a pronounced effect on substrate K_m in both AChEs and BuChEs (Shafferman *et al.*, 1992b; Radić *et al.*, 1993; McGuire *et al.*, 1989; Masson *et al.*, 1997). The BuChE variant containing Asp70Gly substitution (corresponding to the Asp72 position in *Torpedo* AChE) is naturally occurring in the human population. Individuals with Asp70Gly mutation appear unable to hydrolyze the muscle relaxant succinylcholine efficiently and thus experience life-threatening apnea lasting from a few minutes to several hours.

Binding of ligands to the various sites in *Torpedo* and mouse AChEs seems to have a comparatively small effect on the overall fold of the enzyme structure (Figs. 5A and 5B), the exception is the largest peripheral site ligands — fasciculin that consistently cause the largest RMS deviations of the Ca fold (Figs. 6A and 6B) due to more than a 1100 Å² contact area in the complex. The increased RMS was thus the cumulative result of a larger number of small, sub-Ångstrom shifts associated with residues of the large Ω loop (Cys67–Cys94). The loop was slightly, but noticeably (Figs. 5A and 5B), pressured by fasciculin into the space of the active center gorge. The Phe330 of the active center choline binding site, however, consistently and sig-

nificantly changes its side chain conformation in all structures recorded to date, both in *Torpedo* and mouse AChEs (in which it is replaced by Tyr). Its unique position at the base of the gorge allows it to regulate available space for ligand binding by rotating around its Cα–Cβ bond (Figs. 5C and 5D). Tacrine and its derivatives in *Torpedo*, mouse, and *Drosophila* structures are stabilized by an aromatic "sandwich" between Trp84, which is always fixed in the same conformation at the very bottom of the gorge, and Phe330 (or its Tyr equivalents in mouse and *Drosophila*). The latter residue assumes conformation roughly parallel to Trp84, thereby closing access to the lower part of the gorge. When bisquaternary ligands, decamethonium and BW286c51 are bound, the position of the Phe330 ring is nearly perpendicular to Trp84, thus opening the full length of the gorge. In the immediate vicinity of Phe330 lies catalytic triad His440. It has been implicated that this histidine might be "mobile" during catalytic reaction — that is, that it can repetitively revert between two or more conformational states during catalysis. The structural evidence of one of these hypothetical states is given in the three-dimensional structure of the "aged" VX phosphonylated *T. californica* AChE with the nerve agent VX (Millard *et al.*, 1999) (Fig. 7A). The analogous crystal structure solved with VX phosphonylated and aged human BuChE, however, did not reveal any movements in the His of the catalytic triad (Nachon *et al.*, 2005). The largest conformational change in the peripheral site was observed in the complex of the tightest binding triazole, the femtomolar

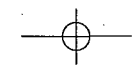
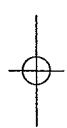


FIG. 6. Quantitative representation of variations in C α traces represented as RMS values of (A) 42 *Torpedo* AChEs using the unliganded 1EA5 structure as a frame of reference and (B) 18 mouse AChEs using the 1J06 chain as a frame of reference. Structures were overlaid and RMS deviations calculated using SwissPDBViewer software. Bar patterns represent the type of ligand found in each structure.

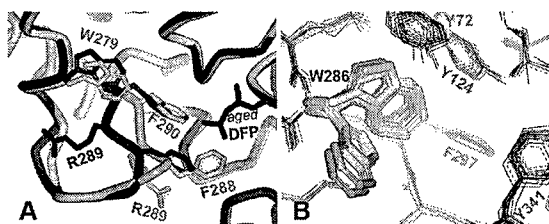


FIG. 7. Conformational changes of AChEs found in (A) *Torpedo* AChE-DFP aged adduct. DFP is covalently attached to the active Ser200. The gray ribbon and selected side chain sticks represent unliganded *Torpedo* AChE structure. Aged DFP-AChE adduct is shown as black ribbon and sticks. (B) Mouse AChE conformations of Trp286 found in the peripheral sites of triazole *syn*-TZ2PA6 liganded (two conformations) and unliganded or liganded with other ligands (16 conformations). Visualized by WebLabViewer software (Accelrys, San Diego).

inhibitor *syn*-TZ2PA6 and mouse AChE (Bourne *et al.*, 2004). Trp286 (Trp279 in *Torpedo*) flips in that structure by approximately 120° (Fig. 7B) to enable a tight fit of the phenantridinium moiety of *syn*-TZ2PA6 in another “aromatic” sandwich between Trp286 and Tyr72 (Tyr70 in *Torpedo*). A substantial change in the backbone conformation has been reported in only two AChE structures, in both cases on the same acyl pocket loop (Trp279–Ser291). In the structure of *Torpedo* AChE phosphorylated by diisopropyl fluorophosphate (DFP) (Millard *et al.*, 1999), and then aged, DFP is partially dealkylated, having only one of two isopropoxy groups bound to phosphorus. To fit between two phenylalanines of the AChE acyl pocket (Phe288 and Phe290), the remaining isopropoxy group had to distort its backbone, causing the extended cationic side chain of Arg289 to flip by almost 90° (Fig. 7A), facing the entrance of the gorge and incoming ligands. An even larger acyl pocket loop conformational change was reported for the complex between *Torpedo* AChE and a bifunctional galanthamine derivative (Greenblatt *et al.*, 2004). Positioning of the ligand in this complex caused the acyl pocket loop (Trp279–Ser291) to assume a severely disordered and poorly defined conformation that was not included in the crystal structure coordinates.

C. Quaternary Structure

Genetic information encoding AChE protein as documented for variety of species is contained in one gene, except for some insects and worms, carrying multiple genes for AChEs of BuChEs. The myriad of molecular forms includes covalent homodimers, either soluble or through a glycopospholipidinositol anchor attached covalently to mostly erythrocyte membranes; homotetramers formed as noncovalent dimers of covalent

dimers; and “readthrough” monomers expressed only during development and in mouse brain under stress as well as heteromeric associations of tetramers with structural peptides ColQ and PRIMA found in mammalian muscle and brain, respectively (Massoulie *et al.*, 1993; Taylor and Radić, 1994; Massoulie, 2002). All molecular forms contain identical catalytic subunits. Slightly different are C-terminal sequences that dictate oligomerization and cellular disposition of subunits. Sequence divergence of C-terminal end is achieved through 3′ alternative splicing of mRNA (Gibney *et al.*, 1988). Additional alternative splicing at the mRNAs 5′ end was reported in tick AChEs (Baxter and Barker, 1998; Xu *et al.*, 2003) but without affecting the sequence of the mature protein. In the vertebrate nervous system, AChE is found in tetrameric form associated through C-terminal peptides forming a four-helix amphipathic bundle around ColQ or PRIMA peptides. The regularly spaced Trp residues at the C-terminal (WAT domain) intercalate between Pro residues of PRAD (proline-rich amphipathic domain) and ColQ or PRIMA as described in a structural study on the WAT/PRAD tetramerization domain (Dvir *et al.*, 2004) showing four parallel helices of WAT supercoiled around the antiparallel helix of PRAD. The naturally occurring monomeric form of fetal bovine serum AChE, unlike the naturally occurring tetrameric form of fetal bovine serum, has a modified C-terminal end sequence, thus compromising its formation of tetramers (Saxena *et al.*, 2003).

III. ChE VARIANTS IN THE HUMAN POPULATION

Numerous structural variants of BuChE in humans consisting of one amino acid substitutions or frameshift mutations have been well documented in the literature (Kalow, 2004). Individuals carrying structural variants of very low or no BuChE activity in their tissues appear normal and are at risk only if given the muscle relaxant succinylcholine in preparation for surgery. On the other hand, variability of AChE structure in the human population is only starting to be discovered. To date, only approximately 13 single nucleotide polymorphisms (SNPs) have been identified in the AChE encoding DNA in the human population (Hasin *et al.*, 2004). Eight are synonymous and they do not alter the protein sequence, and five cause amino acid substitutions in mature AChE protein. Substitutions are positioned on the AChE surface (Fig. 8) and are not likely to affect its catalytic function, but the ability of monomers to associate with other molecules may be influenced. In particular, SNP resulting in substitution located close to the C-terminal end (Pro561Arg in the mature human AChE sequence) could influence tetramerization of AChE and its anchoring in nervous tissue.

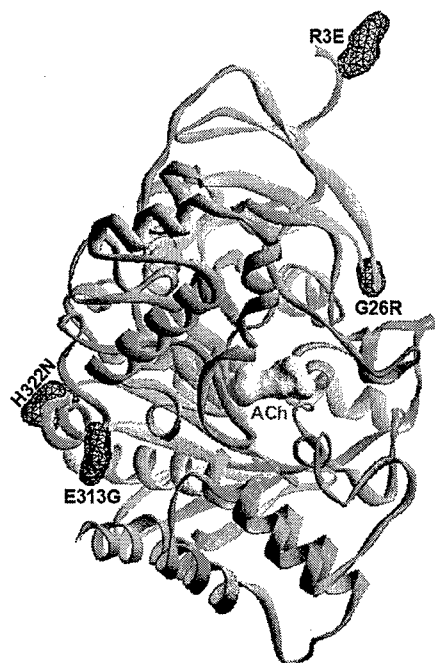
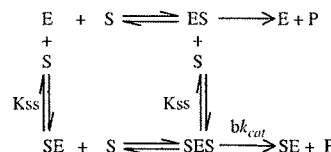


FIG. 8. Variants of AChE structure, resulting in amino acid substitutions of the mature protein, found in the human population (data from Hasin *et al.*, 2004). Sites and types of substitutions are labeled on the gray ribbon, with a molecule of ACh shown as a gray surface, docked in the active center. The fifth identified substitution, Pro561Arg located at the very C-terminal end, is not shown because the known three-dimensional structure extends only through residue 542. Visualized by WebLabViewer software (Accelrys, San Diego).

A. Reaction of Cholinesterases with Substrates

The kinetics of substrate hydrolysis by both AChEs and BuChEs deviates from Michaelis–Menten kinetics. As implicated in Fig. 2 for acetylthiocholine, only at substrate concentrations lower than 1 mM does the rise in enzyme activity follow Michaelis–Menten kinetics. At higher concentrations, AChE activity decreases, inhibited by the excess substrate, whereas BuChE activity increases, activated by the excess substrate. Hence, the terms substrate inhibition and substrate activation are respective hallmarks of catalysis by AChE and BuChE. Both phenomena can be simply described as a consequence of the formation of a ternary complex between the enzyme and two substrate molecules and thus as an allosteric phenomenon. The ternary complex in AChE has reduced or no activity compared to the Michaelis–Menten complex, whereas it appears more active in BuChE hydrolysis. It is important to emphasize that this is a substrate-specific phenomenon. Not all AChE and BuChE substrates exhibit substrate inhibition and sub-

strate activation, respectively. A unique and simple reaction scheme can describe both kinds of interactions:



where E and S stand for the free enzyme and substrate molecules respectively; ES is the Michaelis-Menten complex; SE is substrate bound to an allosteric, peripheral site on the enzyme; and SES is the ternary complex having one substrate molecule bound to the active center and the other to the allosteric, peripheral site. K_{ss} is the dissociation constant for substrate bound to an allosteric, peripheral site, and k_{cat} and bk_{cat} are turnover numbers for the Michaelis-Menten complex and the ternary complex, respectively.

K_{ss} constants for ChEs are always larger than K_m . Thus, the previous reaction scheme differs from the simple Michaelis–Menten scheme in the assumption that S can bind to more than one site on the enzyme, influencing the enzyme turnover by the factor b . When $b = 1$, the reaction kinetics is indistinguishable from Michaelis–Menten kinetics and binding of S to the allosteric, peripheral site appears kinetically “silent.” When $b < 1$, the enzyme is inhibited by excess substrate as most frequently found for hydrolysis of ACh or acetylthiocholine by AChEs. The relationship between enzyme activity and the log of the substrate concentration (Fig. 2) a bell-shaped, indicating substrate inhibition. When $b > 1$, the enzyme activity is increased by excess substrate, as found for hydrolysis of ACh or acetylthiocholine by BuChEs, and the relationship between enzyme activity and the log of the substrate concentration appears as a double sigmoidal substrate activation curve (Fig. 2). The kinetic equation derived from the previous scheme summarizes these relationships as follows (CF. Radić *et al.*, 1993):

$$v = V(1 + b[S]/K_{ss}) / [(1 + [S]/K_{ss})(1 + K_m/[S])] \quad (1)$$

where v is the enzyme activity at concentration of substrate $[S]$, V is maximal activity of the enzyme, K_m is the Michaelis–Menten constant, and K_{ss} is the dissociation constant for substrate bound to the allosteric, peripheral site of the enzyme.

Although the previous relationships hold for most ChEs, there are exceptions. *Drosophila* AChE, for example, exhibits slightly more complex catalytic behavior in which some substrate activation is observed at low substrate concentrations in addition to substrate inhibition observed at millimolar substrate concentrations (Fig. 2) in the same reaction profile. In order to describe the reaction mechanism more precisely in that case, a more complex reaction

mechanism has to be assumed (Stojan *et al.*, 1998, 2004). The molecular basis for this complexity is likely related to the fact that the geometry of the active center gorge in *Drosophila* AChE differs significantly from the gorge geometries of other AChEs and BuChEs.

B. Reaction of Cholinesterases with Inhibitors

The vast majority of molecules that inhibit ChE activity are either reversible inhibitors or “progressive,” “irreversible” covalent inhibitors.

1. REVERSIBLE INHIBITORS

Reversible inhibitors form noncovalent complexes with the enzyme at the bottom of the active center gorge, at the peripheral site at its rim, or they span between the two sites. Association rates of most reversible inhibitors with ChEs are diffusion limited, and traversing the path leading to the base of the enzyme active center gorge does not slow down their entry. The binding equilibrium for those complexes is established rapidly, and only the magnitude of their dissociation rates controls their binding affinity, with dissociation constants usually found in the micromolar to nanomolar range (Radić and Taylor, 2001).

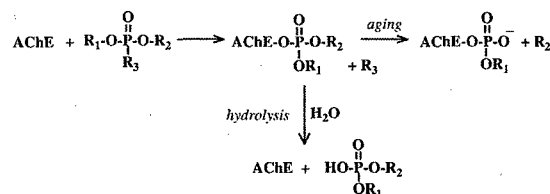
A separate group of reversible ChE inhibitors — fasciculins, triazoles, and trifluoroacetophenones — dissociate from enzyme very slowly (requiring hours, days, or weeks for complete dissociation) while maintaining very fast, diffusion-limited association rates. Affinities of these tight binding inhibitors are exceptionally high, with K_D constants in the low pM and fM range. Fasciculins are a family of peptidic toxins from snake venom (Fasciculin1, Fasciculin2, and Fasciculin3) (Marchot *et al.*, 1993), 61 amino acids long with a characteristic three-finger shape. The central finger enters halfway into the AChE active center gorge, blocking access to the active serine, whereas the bulk of the toxin molecule resides at the enzyme peripheral site (Bourne *et al.*, 1995; Harel *et al.*, 1995). The mechanism of inhibition combines steric blockade with allosteric components (Rosenberry *et al.*, 1999; Radić and Taylor, 2001).

Triazoles are a family of small molecule inhibitors designed by the “*in situ*” cycloaddition reaction between azide and acetylene building blocks in the AChE active center gorge (Lewis *et al.*, 2002; Krasinski *et al.*, 2005; Manetsch *et al.*, 2004). The enzyme is exposed to a library of building blocks, and the tightest binding products predominate in the gorge. This exceptional strategy for the design of high-affinity ligands yielded multiple inhibitors with femtomolar K_D in a single round of screening from a small library of building blocks having high nanomolar to micromolar K_d s. The triazole inhibitors are bifunctional, spanning the peripheral site and the active center (Bourne *et al.*, 2004), but the triazole ring, formed in the cycloaddition reaction, contributes to binding affinity as a separate pharmacophore as well (Manetsch *et al.*, 2004).

In contrast to the previously discussed noncovalent but slowly dissociating inhibitors, trifluoroacetophenones are reversible ChE inhibitors that covalently bind to the active serine but maintain the same structure upon dissociation from the enzyme (Nair *et al.*, 1994). Their structure resembles “extended” reactive conformation of ACh, mimicking the transition state in its reaction with ChEs. Trifluoroacetophenones share three points of stabilization with the enzyme. In addition to the formation of a covalent bond between the active serine and carbonyl carbon of a trifluoroacetophenone, its carbonyl oxygen is stabilized in the oxyanion hole and the positive charge of quaternary nitrogen is stabilized through cation- π interactions by aromatic residues of the choline binding site (Harel *et al.*, 1996).

2. PROGRESSIVE, IRREVERSIBLE ChE INHIBITORS

These inhibitors are substrates of ChEs that deacylate extremely slowly from the active serine, thus causing prolonged occupation of the enzyme active center and its inability to hydrolyze acetylcholine (Aldridge and Reiner, 1972). OPs and CMs are common irreversible inhibitors of ChEs and are frequently used as pesticides (Taylor, 2005). In some pesticides, such as malathion and parathion, specificity of inhibition of insect AChE is achieved by *in vivo* oxidation of the pesticide by cytochrome P450 forming the active oxon (malaoxon and paraoxon). Some OPs are also used as nerve warfare agents. Similar to pesticides, nerve agents are usually small neutral esters of organophosphoric or organophosphonic acid that are prone to be volatile and efficiently penetrate tissues. Upon initial phosphorylation or phosphonylation of the active serine, many OPs undergo an additional reaction called aging (Barak *et al.*, 2000). Aging is a loss of an additional alkyl substituent group of an OP-inhibited enzyme that renders inhibitory OP moiety negatively charged (Aldridge and Reiner, 1972):



Although catalytic activity of phosphorylated or phosphonylated enzymes can be restored by spontaneous deacylation in water or by using nucleophiles stronger than water, such as oximes, means of reactivating aged enzyme have not been demonstrated. Aging of nerve agents such as soman is very fast and occurs in minutes, whereas aging of pesticides such as paraoxon or ethyldichlorvos can take days to complete (Nachon *et al.*, 2005; Aldridge and Reiner, 1972).

Intensive and repeated application of pesticides can lead to the development of pesticide resistance in some insects, as documented for mosquitoes and flies (Hemingway *et al.*,



FIG. 9. Locations of residue substitutions found in insecticide-resistant insect strains mapped onto *Drosophila* AChE structure. Eleven side chain positions (compiled by Menozzi *et al.*, 2004) are given as black surface contours. A molecule of ACh docked in the active center is shown as a gray surface. Visualized by WebLabViewer software (Accelrys, San Diego).

2004; Menozzi *et al.*, 2004). One of the mechanisms involved in this process is the alteration of the insect AChE structure in such a way so as to preserve its ability to hydrolyze ACh but minimize its ability to react with OPs (Fig. 9). This is possible since planar geometry around the carbonyl carbon of ACh and tetrahedral geometry around phosphorus are sufficiently different, as are the overall sizes of pesticide and ACh molecules.

IV. CONCLUSIONS

This chapter summarizes the latest structural information on the cholinesterase family of enzymes and discusses their catalytic properties. Alignment of 125 full-length or nearly full-length ChE sequences demonstrates a high degree of similarity conserved in the family from fungal and viral enzymes to man. Sixty-one reported three-dimensional structures are analyzed herein, illustrating the high degree of similarity in protein fold conformation irrespective of the presence of bound ligands, and this argues for the absence of large conformational changes in the protein interaction with both inhibitors and substrates. At the same time, a plentitude of small-amplitude backbone and selected side chain movements illustrate that rapid fluctuations in conformational states of ChEs prevail in solution and ligands have the capacity to select those conferring higher affinity and lower energy of the respective complex.

References

- Adler, M., Manley, H. A., Purcell, A. L., Deshpande, S. S., Hamilton, T. A., Kan, R. K., Oyler, G., Lockridge, O., Duysen, E. G., and Sheridan, R. E. (2004). Reduced acetylcholine receptor density, morphological remodeling, and butyrylcholinesterase activity can sustain muscle function in acetylcholinesterase knockout mice. *Muscle Nerve* **30**, 317–327.
- Aldridge, W. N., and Reiner, E. (1969). Acetylcholinesterase. Two types of inhibition by an organophosphorus compound: One the formation of phosphorylated enzyme and the other analogous to inhibition by substrate. *Biochem. J.* **115**, 147–162.
- Aldridge, W. N., and Reiner, E. (1972). *Enzyme Inhibitors as Substrates*. North Holland, Amsterdam.
- Barak, D., Ordentlich, A., Kaplan, D., Barak, R., Mizrahi, D., Kronman, C., Segall, Y., Velan, B., and Shafferman, A. (2000). Evidence for P–N bond scission in phosphoroamidate nerve agent adducts of human acetylcholinesterase. *Biochemistry* **39**, 1156–1161.
- Baxter, G. D., and Barker, S. C. (1998). Acetylcholinesterase cDNA of the cattle tick, *Boophilus microplus*: Characterization and role in organophosphate resistance. *Insect. Biochem. Mol. Biol.* **28**, 581–589.
- Behra, M., Cousin, X., Bertrand, C., Vonesch, J. L., Biellmann, D., Chatonnet, A., and Strahle, U. (2002). Acetylcholinesterase is required for neuronal and muscular development in the zebrafish embryo. *Nat. Neurosci.* **5**, 111–118.
- Bourne, Y., Taylor, P., and Marchot, P. (1995). Acetylcholinesterase inhibition by fasciculin: Crystal structure of the complex. *Cell* **83**, 503–512.
- Bourne, Y., Kolb, H. C., Radi, Z., Sharpless, K. B., Taylor, P., and Marchot, P. (2004). Freeze-frame inhibitor captures acetylcholinesterase in a unique conformation. *Proc. Natl. Acad. Sci. USA* **101**, 1449–1454.
- Bücht, G., Haggstrom, B., Radic, Z., Osterman, A., and Hjalmarsson, K. (1994). Residues important for folding and dimerisation of recombinant *Torpedo californica* acetylcholinesterase. *Biochim. Biophys. Acta* **1209**, 265–273.
- Changeux, J. P. (1966). Responses of acetylcholinesterase from *Torpedo marmorata* to salts and curarizing drugs. *Mol. Pharmacol.* **2**, 369–392.
- Chothia, C., and Leuzinger, W. (1975). Acetylcholinesterase: The structure of crystals of a globular form from electric eel. *J. Mol. Biol.* **97**, 55–60.
- Cygler, M., Schrag, J. D., Sussman, J. L., Harel, M., Silman, I., Gentry, M. K., and Doctor, B. P. (1993). Relationship between sequence conservation and three-dimensional structure in a large family of esterases, lipases, and related proteins. *Protein Sci.* **2**, 366–382.
- Dale, H. H. (1914). The action of certain esters of choline and their relation to muscarine. *J. Pharmacol. Exp. Ther.* **6**, 147–190.
- Dvir, H., Harel, M., Bon, S., Liu, W. Q., Vidal, M., Garbay, C., Sussman, J. L., Massoulié, J., and Silman, I. (2004). The synaptic acetylcholinesterase tetramer assembles around a polyproline II helix. *EMBO J.* **23**, 4394–4405.
- Fletcher, S. P., Geyer, B. C., Smith, A., Evron, T., Joshi, L., Soreq, H., and Mor, T. S. (2004). Tissue distribution of cholinesterases and anticholinesterases in native and transgenic tomato plants. *Plant. Mol. Biol.* **55**, 33–43.

- Galagan, J. E., Calvo, S. E., Borkovich, K. A., *et al.* (2003). The genome sequence of the filamentous fungus *Neurospora crassa*. *Nature* **422**, 821–822.
- Gibney, G., MacPhee-Quigley, K., Thompson, B., Vedvick, T., Low, M. G., Taylor, S. S., and Taylor, P. (1988). Divergence in primary structure between the molecular forms of acetylcholinesterase. *J. Biol. Chem.* **263**, 1140–1145.
- Gibney, G., Camp, S., Dionne, M., MacPhee-Quigley, K., and Taylor, P. (1990). Mutagenesis of essential functional residues in acetylcholinesterase. *Proc. Natl. Acad. Sci. USA* **87**, 7546–7550.
- Greenblatt, H. M., Guillou, C., Guenard, D., Argaman, A., Botti, S., Badet, B., Thal, C., Silman, I., and Sussman, J. L. (2004). The complex of a bivalent derivative of galanthamine with torpedo acetylcholinesterase displays drastic deformation of the active-site gorge: Implications for structure-based drug design. *J. Am. Chem. Soc.* **126**, 15405–15411.
- Greenspan, R. J., Finn, J. A., Jr., and Hall, J. C. (1980). Acetylcholinesterase mutants in *Drosophila* and their effects on the structure and function of the central nervous system. *J. Comp. Neurol.* **189**, 741–774.
- Gupta, A., and Gupta, R. (1997). A survey of plants for presence of cholinesterase activity. *Phytochemistry* **46**, 827–831.
- Gupta, A., Vijayaraghavan, M. R., and Gupta, R. (1998). The presence of cholinesterase in marine algae. *Phytochemistry* **49**, 1875–1877.
- Hall, T. A. (1999). BioEdit: A user-friendly biological sequence alignment editor and analysis program for Windows 95/98/NT. *Nucl. Acids Symp. Ser.* **41**, 95–98.
- Harel, M., Kleywegt, G. J., Ravelli, R. B., Silman, I., and Sussman, J. L. (1995). Crystal structure of an acetylcholinesterase-fasciculin complex: Interaction of a three-fingered toxin from snake venom with its target. *Structure* **3**, 1355–1366.
- Harel, M., Quinn, D. M., Nair, H. K., Silman, I., and Sussman, J. L. (1996). The X-ray structure of a transition state analog complex reveals the molecular origins of the catalytic power and substrate specificity of acetylcholinesterase. *J. Am. Chem. Soc.* **118**, 2340–2346.
- Harel, M., Kryger, G., Rosenberry, T. L., Mallender, W. D., Lewis, T., Fletcher, R. J., Guss, J. M., Silman, I., and Sussman, J. L. (2000). Three-dimensional structures of *Drosophila melanogaster* acetylcholinesterase and of its complexes with two potent inhibitors. *Protein Sci.* **9**, 1063–1072.
- Hasin, Y., Avidan, N., Bercovich, D., Korczyn, A., Silman, I., Beckmann, J. S., and Sussman, J. L. (2004). A paradigm for single nucleotide polymorphism analysis: The case of the acetylcholinesterase gene. *Hum. Mutat.* **24**, 408–416.
- Hemingway, J., Hawkes, N. J., McCarroll, L., and Ranson, H. (2004). The molecular basis of insecticide resistance in mosquitoes. *Insect. Biochem. Mol. Biol.* **34**, 653–665.
- Kalow, W. (2004). Human pharmacogenomics: The development of a science. *Hum. Genom.* **1**, 375–380.
- Kaplan, D., Ordentlich, A., Barak, D., Ariel, N., Kronman, C., Velan, B., and Shafferman, A. (2001). Does “butyrylization” of acetylcholinesterase through substitution of the six divergent aromatic amino acids in the active center gorge generate an enzyme mimic of butyrylcholinesterase? *Biochemistry* **40**, 7433–7445.
- Krasinski, A., Radi, Z., Manetsch, R., Raushel, J., Taylor, P., Sharpless, K. B., and Kolb, H. C. (2005). In situ selection of lead compounds by click chemistry: Target-guided optimization of acetylcholinesterase inhibitors. *J. Am. Chem. Soc.* **127**, 6686–6692.
- Kryger, G., Harel, M., Giles, K., Toker, L., Velan, B., Lazar, A., Kronman, C., Barak, D., Ariel, N., Shafferman, A., Silman, I., and Sussman, J. L. (2000). Structures of recombinant native and E202Q mutant human acetylcholinesterase complexed with the snake-venom toxin fasciculin-II. *Acta Crystallogr. D Biol. Crystallogr.* **56**, 1385–1394.
- Lewis, W. G., Green, L. G., Grynspan, F., Radi, Z., Carlier, P. R., Taylor, P., Finn, M. G., and Sharpless, K. B. (2002). Click chemistry in situ: Acetylcholinesterase as a reaction vessel for the selective assembly of a femtomolar inhibitor from an array of building blocks. *Angew. Chem. Int. Ed. Engl.* **41**, 1053–1057.
- Liang, J., Edelsbrunner, H., and Woodward, C. (1998). Anatomy of protein pockets and cavities: Measurement of binding site geometry and implications for ligand design. *Protein Sci.* **7**, 1884–1897.
- Lockridge, O., Bartels, C. F., Vaughan, T. A., Wong, C. K., Norton, S. E., and Johnson, L. L. (1987). Complete amino acid sequence of human serum cholinesterase. *J. Biol. Chem.* **262**, 549–257.
- MacPhee-Quigley, K., Vedvick, T. S., Taylor, P., and Taylor, S. S. (1986). Profile of the disulfide bonds in acetylcholinesterase. *J. Biol. Chem.* **261**, 13565–13570.
- Manetsch, R., Krasinski, A., Radi, Z., Raushel, J., Taylor, P., Sharpless, K. B., and Kolb, H. C. (2004). In situ click chemistry: Enzyme inhibitors made to their own specifications. *J. Am. Chem. Soc.* **126**, 12809–12818.
- Marchot, P., Khelif, A., Ji, Y. H., Mansuelle, P., and Bougis, P. E. (1993). Binding of 125I-fasciculin to rat brain acetylcholinesterase. The complex still binds diisopropyl fluorophosphate. *J. Biol. Chem.* **268**, 12458–12467.
- Masson, P., Legrand, P., Bartels, C. F., Froment, M. T., Schopfer, L. M., and Lockridge, O. (1997). Role of aspartate 70 and tryptophan 82 in binding of succinylthiocholine to human butyrylcholinesterase. *Biochemistry* **36**, 2266–2277.
- Massoulie, J. (2002). The origin of the molecular diversity and functional anchoring of cholinesterases. *Neurosignals* **11**, 130–143.
- Massoulie, J., Pezzementi, L., Bon, S., Krejci, E., and Vallette, F. M. (1993). Molecular and cellular biology of cholinesterases. *Prog. Neurobiol.* **41**, 31–91.
- McGuire, M. C., Nogueira, C. P., Bartels, C. F., Lightstone, H., Hajra, A., Van der Spek, A. F., Lockridge, O., and La Du, B. N. (1989). Identification of the structural mutation responsible for the dibucaine-resistant (atypical) variant form of human serum cholinesterase. *Proc. Natl. Acad. Sci. USA* **86**, 953–957.
- Menozzi, P., Shi, M. A., Lougarre, A., Tang, Z. H., and Fournier, D. (2004). Mutations of acetylcholinesterase which confer insecticide resistance in *Drosophila melanogaster* populations. *BMC Evol. Biol.* **4**, 4.
- Millard, C. B., Kryger, G., Ordentlich, A., Greenblatt, H. M., Harel, M., Raves, M. L., Segall, Y., Barak, D., Shafferman, A., Silman, I., and Sussman, J. L. (1999). Crystal structures of aged phosphorylated acetylcholinesterase: Nerve agent reaction products at the atomic level. *Biochemistry* **38**, 7032–7039.
- Nachon, F., Nicolet, Y., Viguie, N., Masson, P., Fontecilla-Camps, J. C., and Lockridge, O. (2002). Engineering of a monomeric

- and low-glycosylated form of human butyrylcholinesterase: Expression, purification, characterization and crystallization. *Eur. J. Biochem.* **269**, 630–637.
- Nachon, F., Asojo, O. A., Borgstahl, G. E., Masson, P., and Lockridge, O. (2005). Role of water in aging of human butyrylcholinesterase inhibited by echothiophate: The crystal structure suggests two alternative mechanisms of aging. *Biochemistry* **44**, 1154–1162.
- Nair, H. K., Seravalli, J., Arbuckle, T., and Quinn, D. M. (1994). Molecular recognition in acetylcholinesterase catalysis: Free-energy correlations for substrate turnover and inhibition by trifluoro ketone transition-state analogs. *Biochemistry* **33**, 8566–8576.
- Nicolet, Y., Lockridge, O., Masson, P., Fontecilla-Camps, J. C., and Nachon, F. (2003). Crystal structure of human butyrylcholinesterase and of its complexes with substrate and products. *J. Biol. Chem.* **278**, 41141–41147.
- Nolte, H. J., Rosenberry, T. L., and Neumann, E. (1980). Effective charge on acetylcholinesterase active sites determined from the ionic strength dependence of association rate constants with cationic ligands. *Biochemistry* **19**, 3705–3711.
- Ordentlich, A., Barak, D., Kronman, C., Flashner, Y., Leitner, M., Segall, Y., Ariel, N., Cohen, S., Velan, B., and Shafferman, A. (1993). Dissection of the human acetylcholinesterase active center determinants of substrate specificity. Identification of residues constituting the anionic site, the hydrophobic site, and the acyl pocket. *J. Biol. Chem.* **268**, 17083–17095.
- Radi, Z., and Taylor, P. (2001). Interaction kinetics of reversible inhibitors and substrates with acetylcholinesterase and its fasciculin 2 complex. *J. Biol. Chem.* **276**, 4622–4633.
- Radi, Z., Gibney, G., Kawamoto, S., MacPhee-Quigley, K., Bongiorno, C., and Taylor, P. (1992). Expression of recombinant acetylcholinesterase in a baculovirus system: Kinetic properties of glutamate 199 mutants. *Biochemistry* **31**, 9760–9767.
- Radi, Z., Pickering, N. A., Vellom, D. C., Camp, S., and Taylor, P. (1993). Three distinct domains in the cholinesterase molecule confer selectivity for acetyl- and butyrylcholinesterase inhibitors. *Biochemistry* **32**, 12074–12084.
- Radi, Z., Duran, R., Vellom, D. C., Li, Y., Cervenansky, C., and Taylor, P. (1994). Site of fasciculin interaction with acetylcholinesterase. *J. Biol. Chem.* **269**, 11233–11239.
- Raoult, D., Audic, S., Robert, C., Abergel, C., Renesto, P., Ogata, H., La Scola, B., Suzan, M., and Claverie, J. M. (2004). The 1.2-megabase genome sequence of Mimivirus. *Science* **306**, 1344–1350.
- Raves, M. L., Harel, M., Pang, Y. P., Silman, I., Kozikowski, A. P., and Sussman, J. L. (1997). Structure of acetylcholinesterase complexed with the nootropic alkaloid, (-)-huperzine A. *Nat. Struct. Biol.* **4**, 57–63.
- Rosenberry, T. L., Mallender, W. D., Thomas, P. J., and Szegletes, T. (1999). A steric blockade model for inhibition of acetylcholinesterase by peripheral site ligands and substrate. *Chem.-Biol. Interact.* **119–120**, 85–97.
- Saxena, A., Redman, A. M. G., Jiang, X., Lockridge, O., and Doctor, B. P. (1999). Differences in active-site gorge dimensions of cholinesterases revealed by binding of inhibitors to human butyrylcholinesterase. *Chem.-Biol. Interact.* **119–120**, 61–69.
- Saxena, A., Hur, R. S., Luo, C., and Doctor, B. P. (2003). Natural monomeric form of fetal bovine serum acetylcholinesterase lacks the C-terminal tetramerization domain. *Biochemistry* **42**, 15292–15299.
- Schrag, J. D., Schmid, M. F., Morgan, D. G., Phillips, G. N., Jr., Chiu, W., and Tang, L. (1988). Crystallization and preliminary X-ray diffraction analysis of 11 S acetylcholinesterase. *J. Biol. Chem.* **263**, 9795–9800.
- Schumacher, M., Camp, S., Maulet, Y., Newton, M., MacPhee-Quigley, K., Taylor, S. S., Friedmann, T., and Taylor, P. (1986). Primary structure of *Torpedo californica* acetylcholinesterase deduced from its cDNA sequence. *Nature* **319**, 407–409.
- Shafferman, A., Kronman, C., Flashner, Y., Leitner, M., Grosfeld, H., Ordentlich, A., Gozes, Y., Cohen, S., Ariel, N., Barak, D., Harel, M., Silman, I., Sussman, J., and Velan, B. (1992a). Mutagenesis of human acetylcholinesterase. Identification of residues involved in catalytic activity and in polypeptide folding. *J. Biol. Chem.* **267**, 17640–17648.
- Shafferman, A., Velan, B., Ordentlich, A., Kronman, C., Grosfeld, H., Leitner, M., Flashner, Y., Cohen, S., Barak, D., and Ariel, N. (1992b). Substrate inhibition of acetylcholinesterase: Residues affecting signal transduction from the surface to the catalytic center. *EMBO J.* **11**, 3561–3568.
- Stojan, J., Marcel, V., Estrada-Mondaca, S., Klæbe, A., Masson, P., and Fournier, D. (1998). A putative kinetic model for substrate metabolism by *Drosophila* acetylcholinesterase. *FEBS Lett.* **440**, 85–88.
- Stojan, J., Golcink, M., and Fournier, D. (2004). Rational polynomial equation as an unbiased approach for the kinetic studies of *Drosophila melanogaster* acetylcholinesterase reaction mechanism. *Biochim. Biophys. Acta* **1703**, 53–61.
- Stok, J. E., Goloshchapov, A., Song, C., Wheelock, C. E., Derbel, M. B., Morisseau, C., and Hammock, B. D. (2004). Investigation of the role of a second conserved serine in carboxylesterases via site-directed mutagenesis. *Arch. Biochem. Biophys.* **430**, 247–255.
- Sussman, J. L., Harel, M., Frolow, F., Oefner, C., Goldman, A., Toker, L., and Silman, I. (1991). Atomic structure of acetylcholinesterase from *Torpedo californica*: A prototypic acetylcholine-binding protein. *Science* **253**, 872–879.
- Taylor, P. (2005). Anticholinesterase agents. In *The Pharmacological Basis of Therapeutics* (J. G. Hardman and L. E. Limbird, Eds.), 10th ed., pp. 161–176. McGraw-Hill, New York.
- Taylor, P., and Lappi, S. (1975). Interaction of fluorescence probes with acetylcholinesterase. The site and specificity of propidium binding. *Biochemistry* **14**, 1989–1997.
- Taylor, P., and Radi, Z. (1994). The cholinesterases: From genes to proteins. *Annu. Rev. Pharmacol. Toxicol.* **34**, 281–320.
- Taylor, P., Jones, J. W., and Jacobs, N. M. (1974). Acetylcholinesterase from *Torpedo*: Characterization of an enzyme species isolated by lytic procedures. *Mol. Pharmacol.* **10**, 78–92.
- Vellom, D. C., Radic, Z., Li, Y., Pickering, N. A., Camp, S., and Taylor, P. (1993). Amino acid residues controlling acetylcholinesterase and butyrylcholinesterase specificity. *Biochemistry* **32**, 12–17.
- Xu, G., Fang, Q. Q., Keirans, J. E., and Durden, L. A. (2003). Cloning and sequencing of putative acetylcholinesterase cDNAs from the American dog tick, *Dermacentor variabilis*, and the brown dog tick, *Rhipicephalus sanguineus* (Acari: Ixodidae). *J. Med. Entomol.* **40**, 890–896.